THE SEPARATION OF SECONDARY OIL-WATER DISPERSIONS IN PARTICULATE BEDS

SABAH YASSIN IBRAHIM

Doctor of Philosophy

THE UNIVERSITY OF ASTON IN BIRMINGHAM

September 1986

THE UNIVERSITY OF ASTON IN BIRMINGHAM

THE SEPARATION OF SECONDARY OIL-WATER DIPSERSIONS IN PARTICULATE BEDS

SABAH YASSIN IBRAHIM Doctor of Philosophy 1986

SUMMARY

The literature relating to haze formation, methods of separation, coalescence mechanisms, and models by which droplets <100 μm are collected, coalesced and transferred, have been reviewed with particular reference to particulate bed coalescers.

The separation of secondary oil-water dispersions was studied experimentally using packed beds of monosized glass ballotini particles. The variables investigated were superficial velocity, bed depth, particle size, and the phase ratio and drop size distribution of inlet secondary dispersion. A modified pump loop was used to generate secondary dispersions of toluene or Clairsol 350 in water with phase ratios between 0.5-6.0 v/v%. Inlet drop size distributions were determined using a Malvern Particle Size Analyser; effluent, coalesced droplets were sized by photography.

Single phase flow pressure drop data were correlated by means of a Carman-Kozeny type equation. Correlations were obtained relating single and two phase pressure drops, as

$$(\Delta P_2/\mu_c)/(\Delta P_1/\mu_d) = k_P\, U^a\, L^b\, d_c^c\, d_p^d\, C_{in}^e$$

A flow equation was derived to correlate the two phase pressure drop data as,

$$\Delta P_2/(\rho_c U^2) = 8.64\times10^7\, [dc/D]^{-0.27}\, [L/D]^{0.71}\, [dp/D]^{-0.17}\, [N_{Re}]^{1.5}\, [e_1]^{-0.14}\, [C_{in}]^{0.26}$$

In a comparison between functions to characterise the inlet drop size distributions a modification of the Weibull function provided the best fit of experimental data. The general mean drop diameter was correlated by:

$$\frac{d_{qP}}{d_{fr}^{q-P}} = d^{q-P} \cdot \alpha^{P-q/\beta} \cdot \frac{\Gamma((q-3/\beta)+1)}{\Gamma((P-3/\beta+1)}$$

The measured and predicted mean inlet drop diameters agreed within ±15%.

Secondary dispersion separation depends largely upon drop capture within a bed. A theoretical analysis of drop capture mechanisms in this work indicated that indirect interception and London-van der Waal's mechanisms predominate.

Mathematical models of dispersed phase concentration in the bed were developed by considering drop motion to be analogous to molecular diffusion. The number of possible channels in a bed was predicted from a model in which the pores comprised randomly-interconnected passage-ways between adjacent packing elements and axial flow occured in cylinders on an equilateral triangular pitch. An expression was derived for length of service channels in a queuing system leading to the prediction of filter coefficients.

The insight provided into the mechanisms of drop collection and travel, and the correlations of operating parameters, should assist design of industrial particulate bed coalescers.

Key Words: Secondary Dispersions, Particulate Bed Coalescers, Pressure Drops, Mechanisms of Coalescence.

I dedicate this thesis to

my Parents and my Wife

ACKNOWLEDGEMENTS

The author wishes to thank the following:

Professor GV Jeffreys for his encouragement and supervision.

Dr CJ Mumford for his invaluable help, supervision and constructive criticism.

The Ministry of Higher Education and Scientific Research for their financial support.

Members of the Technical and Photographic Staff of the Department of Chemical Engineering for their assistance in fabricating the equipment and the photographic work.

Sue for her diligence in typing this thesis.

LIST OF CONTENTS

LIST OF TABLES

LIST OF FIGURES

LIST OF PLATES

CHAPTER ONE

INTRODUCTION

The separation of fine liquid-liquid dispersions plays an important role in various chemical engineering and scientific fields, particularly in those purification processes where secondary hazes are generated.

Coalescence, and similar methods of phase separation are for example used in numerous industrial and engineering applications, eg in the treatment of aqueous wastes containing finely-suspended oils, the de-watering of petroleum and aviation fuels, prevention of product contamination in liquid-liquid extraction processes, the removal of dispersed oils and other organics from waste waters prior to discharge into receiving water, and processes to prevent shore pollution by sea-borne contamination.

Generally, dispersions are characterised as 'primary' or 'secondary' depending upon the mean drop size of the dispersed phase. Primary dispersions are arbitrarily characterised as containing droplets of mean diameter > 100μm which, in the absence of agitation and given sufficient time, can be separated under gravity due to buoyancy forces. Secondary dispersions are cloudy in appearance and are often referred to as hazes. Conventionally they are classified as a dispersion with a mean droplet diameter < 100μm, and may contain drops as small as 1μm. These dispersions are not easily separated by buoyancy forces and separation by gravity settling is very slow, and may take days or even weeks. For example, on the basis of Stokes' Law,

$$V_S = \frac{g\, d_p^{\,2} (\rho_c - \rho_d)}{18\, \mu_c} \qquad 1.1$$

Hence the settling velocity V_S is proportional to the square of the drop diameter d_p so that a 20μm drop settles 100 times slower than a 200μm drop. Therefore, gravity

separation becomes proportionately less effective with drops of smaller size and settler designs become very inefficient when the droplet diameter falls below 100μm.

The two types of secondary dispersion are oil-in-water (ie o/w) and water-in-oil (ie w/o), where the oil is an immiscible or partially miscible liquid. Some dispersions are stabilised, eg due to the presence of surfactants, and separation by mechanical means is then inefficient.

Secondary dispersions may result from powerful agitation by a mixer in an attempt to increase interfacial area in a mass transfer operation, or by pumps, or in a variety of other ways, eg critical temperature emulsification, super-saturated vapour condensation, or alternate heating and cooling where one liquid phase is present in a minority. Such dispersions may result in loss in solvent extraction process efficiency or pollution problems. Their efficient separation is therefore of considerable importance in present-day technology whether it be in solvent extraction, effluent treatment, or the purification of fuels or chemicals.

Many separation methods are available for droplet dispersions. In all these operations rapid and efficient separation of the two phases is advantageous. Such methods which include the addition of chemical coagulants, use of electrical fields and centrifugation are often expensive and inefficient. However coalescence can often be induced by flow through an inexpensive, porous medium consisting of fibrous or particulate packing.

The attractions of secondary dispersions separation by passage through a porous packing are that it can be highly efficient, inexpensive and continuous. The packed bed usually operates under steady-state conditions because the drops are not permanently retained. However design for a specific duty tends currently to be based on a trial-and-error procedure because the hydrodynamics of two phase flow through packed beds, and the mechanisms of droplet collection and coalescence are not fully understood.

The present work was concerned with the separation of secondary oil-in-water dispersions and the mechanisms by which droplets are collected and held in particulate beds where they grow by coalescence until a critical size is reached at which they are released to settle rapidly under gravity. The droplet behaviour and mechanisms of the coalescence process inside the particulate bed were also investigated to provide a better understanding of secondary dispersions coalescence applicable to practical separator design and operation. Finally mathematical models were derived of dispersed phase concentration inside a packed bed, and a mathematical description of the bed was proposed considering the pores as randomly-interconnected passage-ways formed between adjacent particles. Expressions were derived for queue length and filter coefficient in order to provide a theoretical explanation for the coalescence behaviour of a secondary dispersion within a particulate bed.

CHAPTER TWO

FORMATION OF SECONDARY DISPERSIONS

Liquid-liquid dispersions comprise one or more immiscible, or partially miscible, liquids distributed as discrete drops in a bulk liquid continuum [1]. Even in the absence of surface active contaminants, such a dispersion can exhibit widely-differing physical and chemical properties depending mainly upon the droplet size of the dispersed phase.

Therefore, liquid-liquid systems are classified as primary dispersions, secondary dispersions or colloids, although there is no precise definition of the respective drop size ranges. Indeed any arbitrary definition of a 'secondary dispersion' would involve over-simplification, especially when a theoretical description of the phenomenon of coalescence is attempted since prior to coalescence the dispersion may behave as a colloidal system and coalescence produces a primary dispersion.

The present work is concerned with secondary liquid-liquid dispersions and only their characteristics will be described in detail.

2.1 The Nature of Secondary Dispersions

Any dispersion contains at least two liquids, of which one is commonly aqueous. The other liquid is usually designated as "oil", which is immiscible, or poorly miscible, with water. If "oil" is the dispersed phase, an oil/water (o/w) dispersion is present; when water forms the drops, the dispersion is of the water/oil (w/o) type. This is of practical importance with primary dispersions since a water/oil mixture will generally coalesce more rapidly and, of course, the design of the settler and the positions of the phase inlet depend upon whether droplets rise or fall to the bulk interface.

In principle, if a layer of water and a layer of oil are agitated together, either an o/w or a w/o system may emerge. The result depends on several factors including the

relative volumes, ie the phase ratio of the two phases, their position in relation to the agitator, and the nature and concentration of any emulsifying agent [2]. The tendency is for a two-phase liquid mixture to form an o/w dispersion, when the volume of oil is smaller than that of water and a w/o dispersion, when an excess of oil is present. In the experimentation involved in the present study the phase present in 'trace' amounts to eg $\leq 6\%$ by volume always constituted the dispersed phase.

2.1.1 Properties of o/w and w/o Dispersions

The properties of o/w and w/o dispersions depend greatly upon whether or not an emulsifying agent (eg a surfactant or inadvertant contamination) is present. Such agents tend to 'stabilise' the dispersion, ie prevent the constituent droplets from coalescing.

It has been suggested that the nature of the oil phase in an o/w 'unstablised' dispersion will affect the properties of the resultant interfacial film. Furthermore, the properties of the oil influence the ease of dispersion formation. Properties such as oil viscosity and density are considered to be important. Oil polarity also has an adverse effect on dispersion formation. However, the interfacial tension of liquid-liquid dispersions may be the most important factor in cases where very rapid emulsification is required [3], in which the rate of coalescence is related to the ability of the two phases to penetrate the interfacial film formed and the strength of the interfacial film may be assessed by measurement of the interfacial viscosity [4]. Since oil is not electrically-conducting, o/w dispersions tend to have much higher electrical conductivities than w/o dispersions.

The type and concentration of emulsifying agent is the main factor determining the kind of 'stabilised' dispersion produced (eg sodium soaps generally promote formation of o/w systems, whilst calcium and magnesium soaps favour the w/o type)[2].

Davies and Smith [5] found that the main factors affecting the droplet stability of o/w dispersions were the viscosity, surface charge and the type of additive. The

electrical conductivity of a dispersion frequently depends above all on the nature and concentration of the surface active substance present.

Bennett et al [6] studied the viscosity and conductivity of o/w secondary dispersions in which brine solution constituted the continuous phase and found that dispersion viscosity went through two maxima as salinity was increased. Electrical conductivity data agree remarkably well with predictions based on a model for a random interspersion of conducting and non-conducting material. This model predicts three structural regimes, discontinuous oil-in-brine, bicontinuous oil-in-brine, and discontinuous brine-in-oil [6].

The mechanical properties of the 'unstabilised' and 'stabilised' dispersions differ from those of true solutions because deformation of a dispersion will generally cause deviation of the droplets from the spherical shape, ie an increase in interfacial energy. Therefore, the viscosity of a dispersion, especially if the phase ratio is high, depends on the rate of shear or velocity gradients. Light-scattering is often used for calculation of drop dimensions because the refractive index of the oil phase always differs from that of the aqueous phase [2].

Finally, other properties of dispersions may be of equal practical importance to those mentioned above. An o/w dispersion presents a smaller fire hazard, reduced toxicity, and an advantage in price, as compared with a solution of oil in an organic solvent or with a w/o dispersion.

2.1.2 Identification Methods for Secondary Dispersions

The following methods are commonly used to identify the dispersion type.

a. The dispersion is studied under a microscope. The identification of the continuous phase can then be determined by measuring the respective refractive indices.
b. The dispersion is diluted with water. If water is the continuous phase, mixing proceeds smoothly. If mixing does not occur immediately the continuous phase comprises oil.

c. The dispersion is divided into two parts. One part is sprinkled with a water- soluble dye, and the other with an oil-soluble pigment. If the first powder dissolves, the dispersion medium is 'water'. If the second dye dissolves, the dispersion medium is 'oil'.

d. The electric conductance of the dispersion is measured. Generally the conductivity of o/w systems is greater than that of w/o systems [2].

2.2 Stability of Secondary Dispersions

Secondary dispersions are thermodynamically unstable systems [1]. An increase in entropy occurs, together with an increase in free surface energy, when the degree of dispersion becomes higher. The total free energy of a disperse system may be reduced with decrease of mean droplet radius as a result of entropy increase [7].

To establish the possibility of the existence of a two phase disperse system at thermodynamic equilibrium, it is necessary to analyse the dependence of the system's free energy, F, on the degree of dispersion of the system. It is also necessary to calculate the value of the free energy, F, of the whole ensemble of droplets. A large number of monodisperse systems should be considered in such calculations to determine the distribution corresponding to the minimum of F [7].

The entropy of an ideal disperse system consisting of n droplets and N molecules of the dispersion medium (N >> n) may be represented by the relationship:

$$\Delta S = K' \left[n \ln \frac{N+n}{n} + N \ln \frac{N+n}{N} \right] \quad \ldots. 2.1$$

where ΔS is the entropy and K' is the Boltzmann constant. The expression for the free energy ΔF in the case of spherical droplets is

$$\Delta F = E - K'T \left[n \ln \frac{N+n}{n} + N \ln \frac{N+n}{n} \right] + 4 \pi r^2 \sigma n \quad \ldots. 2.2$$

where E is the internal energy of the system, r is the radius, σ is the interfacial tension,

and T is the temperature. Analysis of these equations shows that free energy as a function of the degree of dispersion has only one extreme point [7].

A dispersion may exhibit instability in three ways: by breaking, by creaming and by flocculation. "Breaking" is the spontaneous joining of small droplets to form larger ones (coalescence), leading ultimately to two separate liquid layers. This is familiar from the temporary mixtures formed by shaking together two pure immiscible liquids. "Creaming" refers to the rise of dispersed droplets under the action of gravity, the droplets remaining separate when they touch. This is bound to occur in any dilute dispersion if the phases are not exactly equal in density and if the dispersion medium is truly fluid. Finally, "flocculation" refers to the sticking-together of droplets in the formation of three-dimensional clusters without coalescence of the individual droplets, as in the curdling of milk by fruit juice. The distinction between these processes provides the main point of interest in the theory of stability [8].

Lissant [9] found that the slow sedimentation of emulsified droplets produced a high internal phase ratio dispersion in which they packed together as some transitional form between spheres and polyhedra. However, the drops remain separate during contact unlike primary drops which undergo coalescence as dispersion bands are formed [10].

A further consideration in any discussion of instability of a dispersion is the time scale and conditions of treatment concerned [8]. Therefore, the stability is determined from the rate of decrease in the number of droplets in each cm^3 of dispersion with time; the droplets are counted microscopically at intervals in a known volume of a known diluted dispersion [5].

Conversely stabilised dispersons may show no perceptible breaking for hours, days or months as the droplets are capable of touching without actual contact occuring between the liquid interiors of the droplets. Evidently, the emulsifying agent forms a molecular barrier between the liquids which is capable of withstanding a certain

amount of pressure [8]. In fact, the addition of small quantities of additive to the disperse phase can have a profound effect on dispersion stability. For example, unstable emulsions of hexane and benzene can be stabilised by an added long chain alkane or alkanol [5].

Other factors affect the stability of secondary dispersions such as interfacial tension, viscosity, density and polarity of the disperse phase [5, 14], the quantity and quality of additive or surfactant agents [3, 11, 12, 13, 14]; pH of dispersion [12, 14] and traces of impurities [13]. In conclusion, the majority of interest relating to the stability of dispersions concerns protection of dispersed droplets against coalescence, and most fundamental research has dealt with this aspect. Less is known about the factors controlling the strength of interfacial films produced by macromolecular emulsifying agents.

2.3 Theory of Dispersion Formation

Fundamental work on the theory of dispersion formation has examined how far the theory of colloid stability goes towards explaining the properties of dispersions. A colloid is a system in which a significant proportion of the dispersed phase molecules lie in, or are associated with, interfacial regions. The basis of the theory is the concept that dispersed particles are subject to two kinds of force namely [8]:

I. The London van der Waals force of attraction.

II. The electrostatic repulsion between electrical double layers of like sign.

As these forces are of entirely independent origin, they can be evaluated separately. The net interaction between particles is obtained by summing the forces for each distance between them. If I exceeds II at all distances, the dispersion will be unstable and will coagulate as fast as the particles can diffuse together. If II exceeds I, an energy barrier opposes actual collision. If the height of this energy barrier is comparable with the kinetic energy of colloid particles then coagulation will be slowed down, but not stopped. If the energy barrier is very much greater than the kinetic

energy, the rate of coagulation will be practically zero [8].

It is usual to evaluate interaction energy curves rather than force curves because the height of the energy barrier is the parameter of interest. The energy is also modified by interactions between the surfaces and the phase. Depending on the magnitude of the energy associated with such interactions, the dispersed colloid may remain unstable with respect to the bulk phase or may become thermodynamically stable. Therefore the state of the dispersed colloids is characterised by the excess free energy [15]. The energy is proportional to the size of the droplets, and it does not decay very sharply with distance between them [8].

The energy barrier, which has to be surmounted before two droplets can adhere, is clearly a function of the distance of separation between them, decreasing as the distance increases. Usually, negative potential energies will be associated with attraction and positive potential energies with repulsion. This convention permits reference to the "height" of energy barriers and the "depth" of energy minima. The implications of the energy curves shown in figure 2.1, a qualitative sketch of potential energy curves which result in a repulsive and an attractive component, can be considered as follows:

In case (I), the associated kinetic energy is sufficient to carry the system over the height of the energy barrier (P) into the primary minimum (M_1). Then collision will result in association of the droplets, ie flocculation or coagulation occurs. If the potential energy barrier is high in comparison with thermal kinetic energies, the particles will repulse one another and the dispersion will remain stable indefinitely.

In case II, another possibility arises in which the two droplets may become associated in a state represented by a secondary minimum (M_2). Flocculation occurs at the secondary minimum, but the flocs in this case will clearly be much more easily disrupted than those formed by flocculation at the primary minimum. Two droplets associated with the primary minimum may remain in this state or may coalesce to form a larger droplet of lower surface energy, as when a dispersion breaks [15, 16].

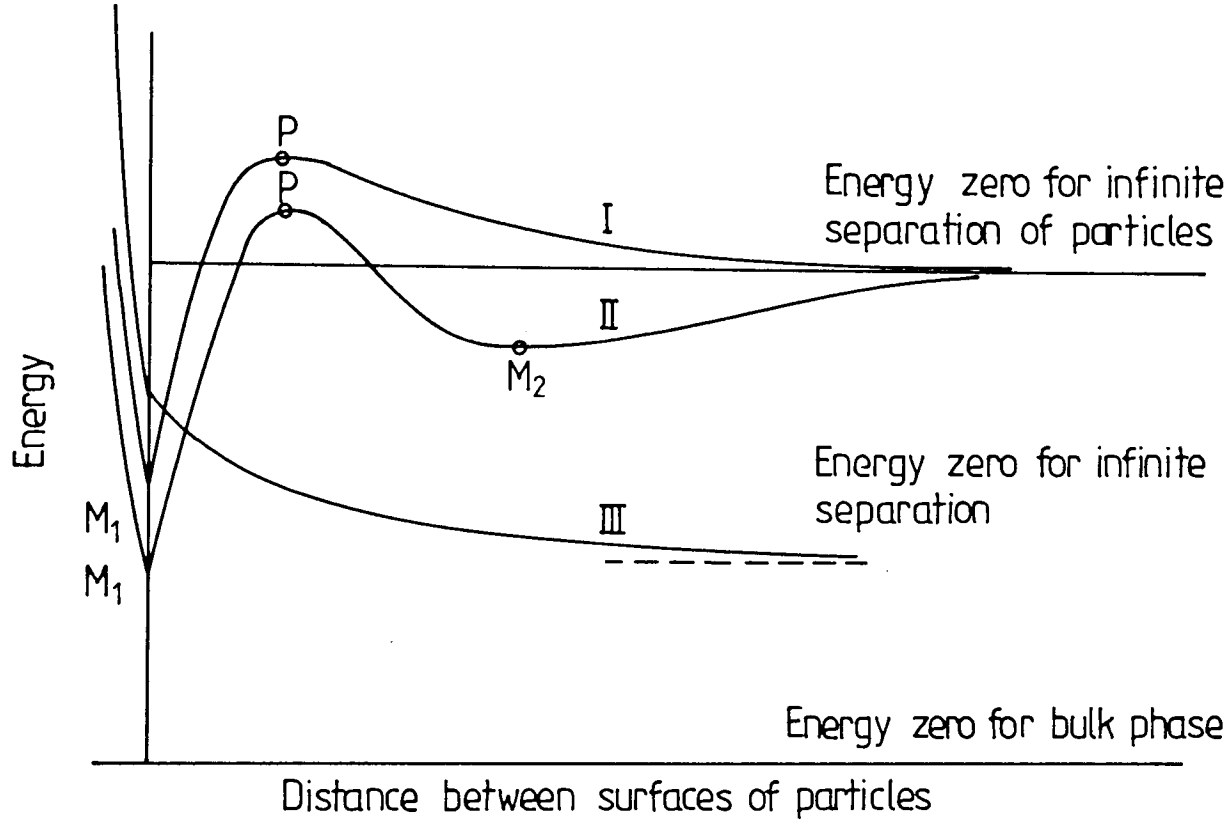

Figure 2.1 Mutual potential energy of two colloidal particles as a function of the distance of separation between their surfaces:

I. curve with primary maximum P and primary minimum M_1

II. curve with primary maximum P , primary minimum M_1 and secondary minimum M_2

III. curve for spontaneous (unactivated) dispersion

In case III, the dispersed state is stable, at constant particle size, so that dispersion of the droplets occurs spontaneously [15, 16].

The form of the curves in figure 2.1 depends upon the size of the drops involved. Therefore, to represent different monodisperse systems a three-dimensional surface, shown schematically in figure 2.2, is used. However the shapes and characteristics of such surfaces depend on many other parameters besides size [15]. Continuous phase properties, dispersed phase concentration, structure and chemical state of the dispersed phase, the presence of adsorbed films at the interface, and electrical state of the interface are among the more important factors.

The phase which separates out may have various forms depending on the type of system considered. With reference to figure 2.2 if the secondary minimum (M_2) is sufficiently deep, an associated stage with a loose open structure is formed. This stage is termed 'flocculation'. The height of the primary maximum controls the rate at which droplets transfer to the primary minimum. If the activation energy for this process is not too high, the aggregated state may transform to a more compact structure by coagulation. Whether flocculation is an intermediate stage in the overall coagulation process depends on the relative positions of the secondary minimum and primary maximum points. This is represented by the path $CM_2\ P_1\ M_1B$ on figure 2.2 [15].

However, the surface illustrated in figure 2.2 is only one three-dimensional section of a multi-dimensional hyper-surface. It is useful for a basic description of the dispersion and coalescence phenomena. Secondary dispersions may be formed either [16]:

a. By mechanically breaking-down a bulk phase to colloidal dimensions and dispersing the particles as formed, or

b. By building up colloidal particles from molecular units.

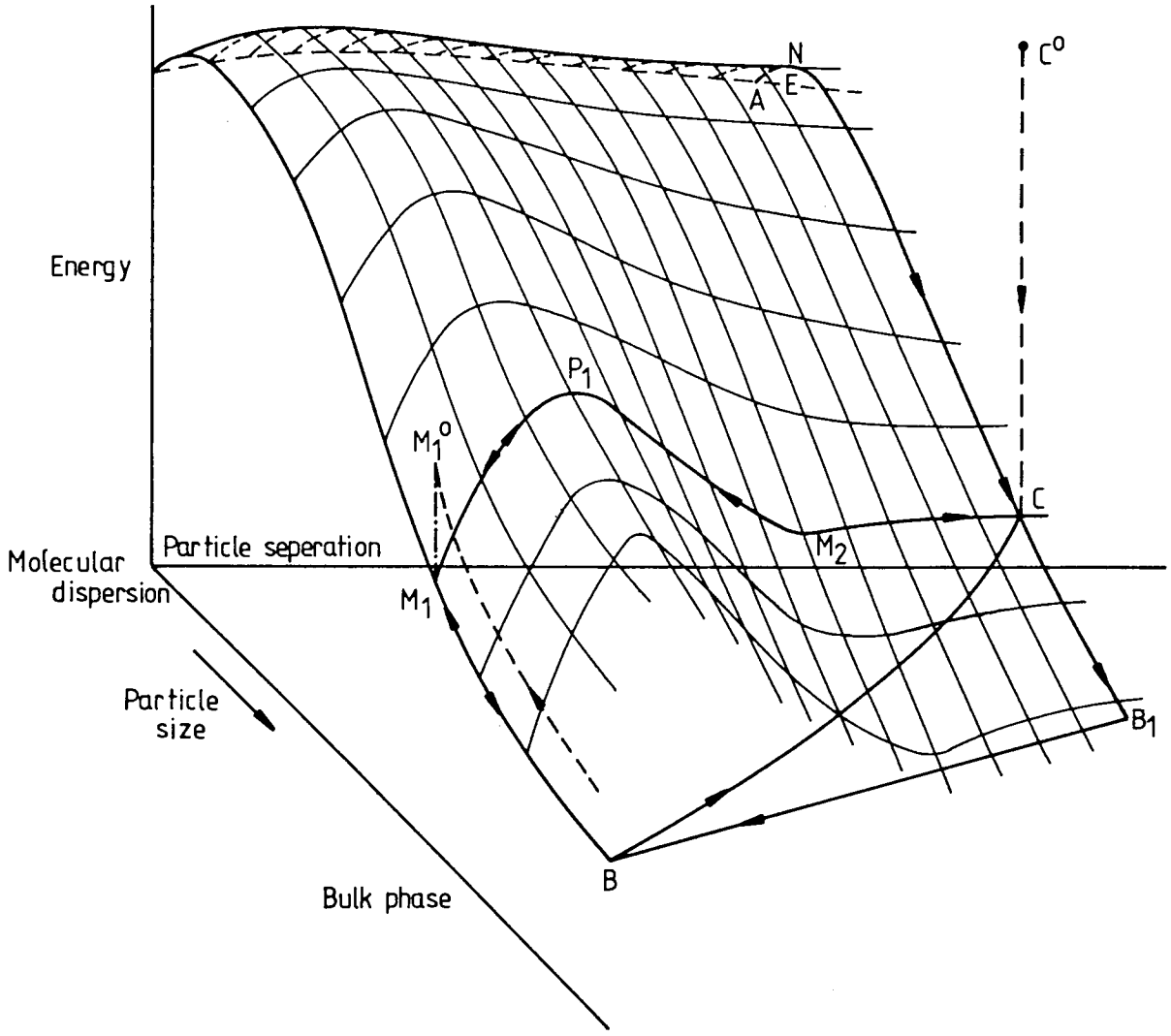

Figure 2.2 Mutual potential energy surface of two colloid particles of a lyophobic colloid in a liquid medium as function of distance of seperation and size of particles, showing routes by which colloid state C can be reached by (i) comminution, routes BC or $BM_1P_1M_2C$ or (ii) by nucleation and growth, ANC; and routes by which coagulation can occur (i) CB_1B and (ii) $CM_2P_1M_1B$. Note that the reverse route CNA in which a colloid would disperse to the molecular state does not in general occur spontaneously. (The short range repulsion "cliff" adjacent to the left hand face of the diagram is omitted for clarity). M_1^0 and C^0 are points representing energies in a vacuum environment.

2.3.1 Subdivision of Bulk Phase

A liquid phase can be subdivided into droplets of colloidal size by mechanical means, i.e emulsification. This process may be represented schematically in figure 2.2 by route B-C when the drops are already dispersed in the continuous phase and by route $BM_1\ P_1\ M_2\ C$ when the dispersed phase is introduced as a continuum into the continuous phase. In fact, if the activation energy for the path of the system from M_1 over P_1 is sufficiently low, thermal motions or mechanical disturbance, eg shearing by an agitator, will take the system to the dispersed state C and generate droplets [16].

2.3.2 Formation by Nucleation and Growth

The formation of an embryo, at E, of new phase in an existing bulk phase involves an increase in energy, which when the embryo reaches a critical size (termed a nucleus at N), passes through a maximum. This process may be represented schematically in figure 2.2 by path AENC when the build-up of colloidal particles (C) from atomic or molecular units (A) involves following the route A-C.

The decrease in surface energy which accompanies growth acts as the driving force for spontaneous growth of the nucleus. However, if a large number of nuclei are present and the bulk phase is of limited extent, then growth involves the depletion of the bulk phase of the components of the growing particles, whose ultimate size (at C) is thus limited by the amount of material available.

Since not all nuclei are formed simultaneously, they will have been growing for different times when growth ceases and consequently the final dispersion will be polydisperse. Therefore, a high degree of dispersion can be obtained when the rate of nucleation is high and the rate of growth is low [15].

2.4 Preparation Methods for Secondary Dispersions

The parameters affecting formation of secondary dispersions are reviewed since,

a. An understanding of drop break-up mechanisms assists the design of coalescers in that reformation of secondary dispersions should be avoided.
b. The operations yielding secondary dispersions give some indication of where packed bed coalescers are likely to be applicable [16].

The important factors controlling dispersion formation are the relative volumes of the two phases, dispersed phase physical properties, continuous phase physical properties, dispersed phase concentration, electrical state of the interface structure, chemical state of the dispersed phase, presence of adsorbed films at the interface, type of the emulsifying agent (if present), mode of adding the emulsifier, mode of adding the two phases, time of emulsification, intensity of emulsification, and temperature [2, 8, 13, 14, 18, 19, 20].

The classification of formation methods of dispersions may be based upon the energy changes and mechanisms of their formation. This is discussed briefly below.

2.4.1 Critical Emulsification

If two liquids are partially miscible at room temperature and completely miscible above an "upper critical dissolution temperature" T_1, then warming a mixture of the two liquids to the vicinity of T_1 often causes appearance of critical opalescence due to formation of a dispersion. The interfacial tension and the density difference are the two most important causes of destruction of a dispersion. When the two liquids near T_1 have similar compositions, then the interfacial tension and the density difference are small so that droplets may exist for a long time before they dissolve in the dispersion

medium. This dispersion is reversible since an increase of temperature beyond T_1 causes their destruction (ie molecular mixing) but cooling of the system to the vicinity of T_1 gives rise to a dispersion very similar to that observed initially [2].

Some systems also exhibit a "lower critical dissolution temperature" T_2, when cooling from room temperature is required to achieve partial miscibility. Such dispersions are fairly stable at the critical temperature due to the similarity in densities and interfacial tensions of the dispersed and continuous phases [16].

2.4.2 Emulsification by Mechanical Dispersion

Mechanical dispersion is by far the most common method of emulsification. It is based on a two-stage mechanism. In the first stage, a drop is extended to form a cylinder, which becomes unstable as soon as its length exceeds its circumference and ruptures to form two spherical drops. If the cylinder extends beyond its stability limit, it will tend to break-down into many droplets [2]. The second stage of spontaneous break-up then results in the formation of a number of smaller drops. This emulsification may be delayed when external forces are continuously acting on the deformed drops during agitation [2, 16]. The advantage of interrupting agitation is employed in Brigg's method of preparing dispersions and the dispersion is obtained more rapidly, and after fewer shakes, then when the agitation continues without interruption [2]. Ford and Furmidge [3] applied this technique to the study of oil-soluble emulsifiers. There are many variants in this method such as mixing, colloid milling and homogenizing [8] as illustrated in figure 2.3.

Many mechanical dispersion methods have been used to generate secondary dispersions covering a wide range of capacities, from small laboratory models to large industrial units. These methods are as follows:

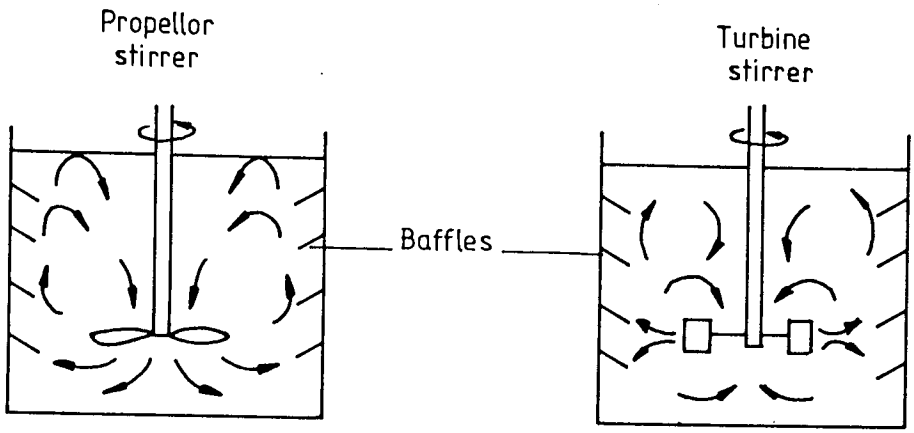

(a) Mixer

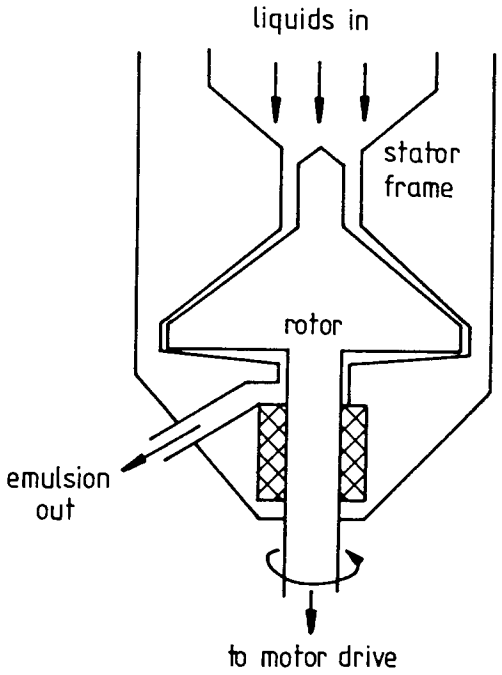

(b) Colloid mill

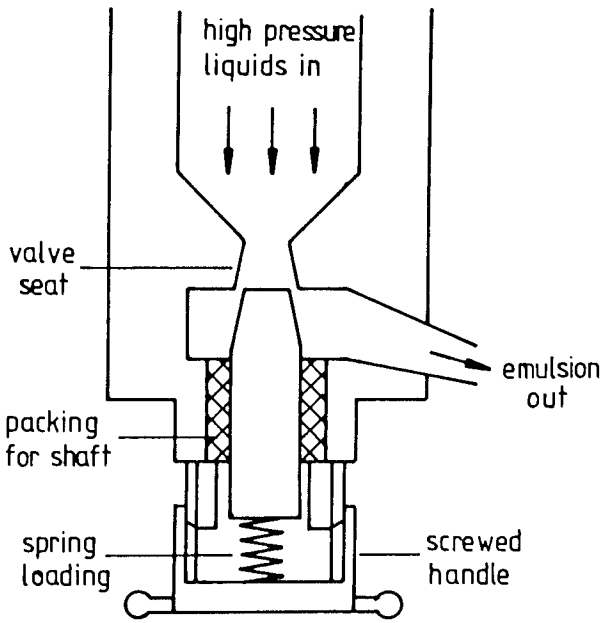

(c) Homogeniser

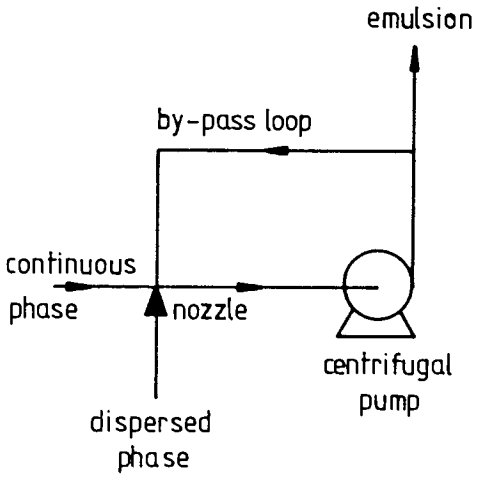

(d) Centrifugal phase pump

Figure 2.3 Mechanical methods of emulsification

2.4.2.1 *Mixing*

Two types of technique have been used,

i. *Use of a standard mixer:*

In this technique the liquids are set in rotation using a simple paddle in a large cylindrical vessel as shown in figure 2.3a. The swirling motion often results in stratification rather than in mixing, especially in large tanks. Therefore, the mixing is best accomplished when there are lateral and vertical flows which distribute the materials rapidly to all parts of the tank. An efficient, and convenient, way to achieve such mixing is to install vertical baffles near the walls. Furthermore, the use of a propeller-shaped stirrer impels the liquids axially up, or down, and contributes to the mixing [8].

Many variants of the basic design are possible to give greater shear flow, which tends to produce finer dispersions. The simple mixers are well-suited for producing low or medium viscosity dispersions, the turbine mixers tolerating somewhat higher viscosities than propellers.

ii. *Orifice mixing*

The orifice mixing technique involves acceleration of one liquid to form the dispersed phase, into a continuum of the other. Either a nozzle or a perforated plate may be used for liquid injection [21].

Richardson [22] investigated the break-up of a liquid jet under the combined action of the interfacial tension and the relative viscosity of the fluids. He also examined the conditions of the two types of droplet break-up near the nozzles, which were arranged in the form of drawn-out capillary tubes, and defined the critical velocity (V_o) from a nozzle of diameter dn [17]:

$$\frac{\mu_1}{(\rho_1 \gamma dn)^{1/2}} = 2000 \left(\frac{\mu_1}{V_o \rho_1 dn} \right)^{4/3} \qquad \text{.... 2.3}$$

It has been found that the action of an ultrasonic generator on the nozzle is to

cause a finer break-up without the necessity of increasing the velocity of efflux [22].

In most commercial injection processes the critical velocity is greatly exceeded, so that the following empirical formula:

$$\left(\frac{V_o\, d_n\, \rho_d}{100\, \mu_d}\right)^{1.25} = 100 \left(\frac{\mu_c\, \rho_d}{\mu_d \rho_c}\right) \qquad \ldots. 2.4$$

can be used to find the velocity of injection which should be used to produce a dispersion of given mean drop size [22].

2.4.2.2 *High Shear*

Formation at high shear involves flow of the liquid-liquid system through a narrow gap between a high speed rotor and a stator surface, e.g in a colloid mill or blender [8].

Rumscheidt and Mason [23] described the formation and breaking-up of fluid drops in shear and plane hyperbolic flow. The shear flows have also been measured for a large number of fluid pairs covering a wide range of viscosity ratio. Taylor [24] formulated a relationship between the radii of droplets formed under conditions of high shear and such parameters as the rate of shear, interfacial tension, and the viscosities of two phases. This was supported by photographic studies of oil drops suspended in syrup under stress. A major aspect of the studies of Rumscheidt and Mason [23] and Taylor [24] was the dependence of the breakage pattern of droplets upon the system parameters such as viscosity ratio. This led to a linear relationship between the Reynold's number and the ratio $\mu_c\, \rho_d / \mu_d\, \rho_c$ for a number of systems when plotted logarithmically.

Gupta et al [25] developed a simple model for the breakage frequency of solid aggregates in a suspension under shear. This model was used to simulate the

aggregation-disaggregation behaviour of dispersions.

Colloid mills may be modified to suit different conditions. For example, the rotor and stator surfaces may either be smooth or roughened with a series of notches or serrations. Homogenizers are devices in which liquid dispersions are achieved by forcing the mixture through a small orifice under very high pressure. These machines are available in a wide range of capacities and designs and have provision for recycling the dispersion. One important application is to reduce the size of fat globules in milk [8]. These methods have been illustrated in figure 2.3 b and c.

2.4.2.3 *Centrifugal Pumps*

A simple, but effective, method of producing secondary dispersions continuously is to pass the bulk phases through a centrifugal pump with a by-pass circuit [16, 17, 27, 57], as shown in Figure 2.3d. Polichronakis [26] has investigated the characteristics of dispersions formed in this manner which typically produce a mean drop size of about 20 μm diameter.

Several workers have recently used centrifugal pumps to generate secondary dispersions for the study of coalescence of emulsions [16, 17, 27, 57, 104].

2.4.3 Emulsification Produced by Condensation

Emulsification by condensation is achieved by nucleation and growth, as described in section 2.3.2. The nuclei may be natural specks of dust and/or smoke, or may be ions, or other seeds, that are artificially introduced. The nuclei may alternatively be formed spontaneously by the aggregation of molecules into very tiny droplets [8].

The condensation technique has been employed extensively in the laboratory for the evaluation of dispersion stabilisers [19, 28]. The method is extremely sensitive to temperature and the geometry and materials, of equipment used. There are two basic types of emulsification by condensation namely vapour injection and the freeze-heat

technique as shown in figure 2.4.

2.4.3.1 *Vapour Injection*

This method involves injection of supersaturated vapour of the liquid to comprise the dispersed phase into a continuous phase containing a suitable emulsifier using a submerged jet orifice. The vapour becomes supersaturated and condenses as micron-sized droplets which are stabilised in the external liquid by the emulsifier. The liquid to be dispersed is pre-heated in a separate vessel and, by controlling the heat input, the temperature and pressure of the vapour are controlled at the desired values. The pressure of injected vapour, the diameter of the jet orifice, and the emulsifier added to the external phase are the principal factors affecting the size of the droplets, as illustrated in figure 2.4 a.

2.4.3.2 *Freeze-Heat Technique or Precipitation*

Meisner and Chertow [29] developed a freeze-heat technique for emulsification which relies upon the temperature dependence of mutual solubility of two liquid phases. This technique involves varying the temperature of an agitated mixture of the organic and aqueous phases in a sealed system containing an emulsifier until condensation occurs. The method is extremely sensitive to temperature changes which may affect the characteristics of the dispersion formed [21].

Condensation methods have not progressed beyond the stage of laboratory development due to the complexity of the equipment required to adequately control the conditions of formation. This method is illustrated in figure 2.4 b.

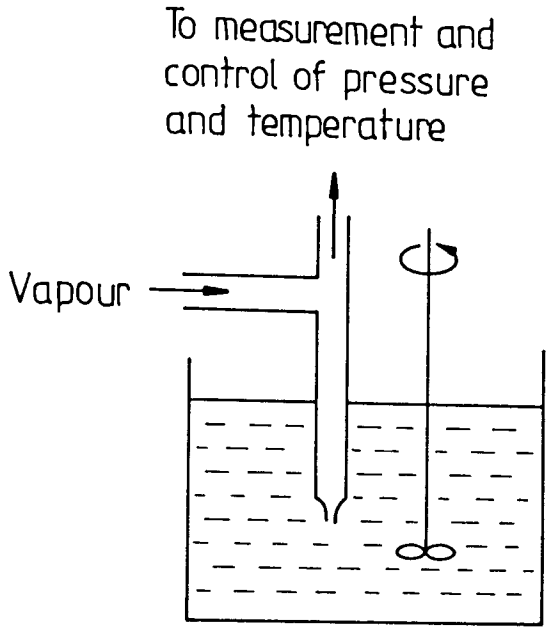

(a) Vapour injection

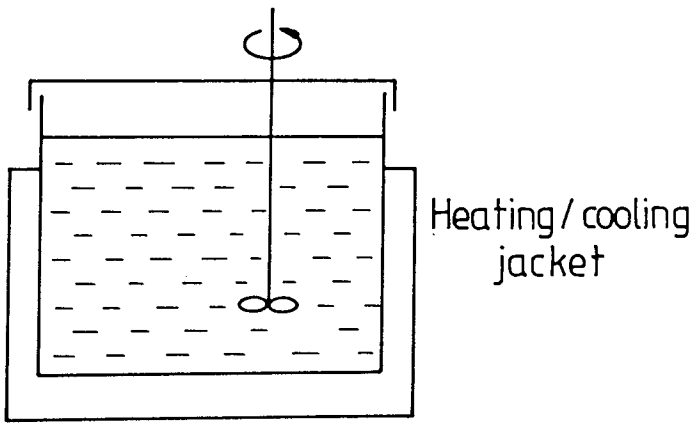

(b) Freeze-heat technique

Figure 2.4 Emulsification by condensation.

2.4.4 Recently-Developed Techniques

Secondary dispersions may also be produced in the following ways.

2.4.4.1 *Sonic and Ultrasonic Techniques*

In sonic and ultrasonic methods of emulsification, electrical energy is converted into mechanical vibrations in the audio or radio frequency range by the use of electro-mechanical transducers as illustrated in figure 2.5 a.

Wood and Loomis [30] investigated the effects obtained with sound-waves of high frequency and great intensity generated in an oil-bath by a piezo-electric oscillator of quartz operated at 50 000 volts and vibrating 300 000 times per second. When the waves were passed across the boundary separating two liquids, such as oil and water or mercury and water, stable secondary dispersions were formed.

In summary for any liquid-liquid system, sonic methods are capable of giving as good an emulsion as can be obtained by any other method. Ultrasonic methods have one special feature, namely the possibility of obtaining a concentrated (30%) highly-dispersed, dispersion without the use of any surface-active agent [8]. However, the disadvantage is that the method is most efficient at the lower frequencies in the audio range.

2.4.4.2 *Electric Dispersion Method*

An electric dispersion method may be employed for production of high concentration, monodisperse secondary dispersions on a laboratory scale. The basic equipment provides for the application of an appropriate high voltage (about 8KV) between the bulk dispersed and continuous phases to produce an aerosol of the dispersed phase which passes into the bulk continuous phase [16, 27] as shown in figure 2.5 b. The advantage of this method is the uniformity of droplet size produced [8].

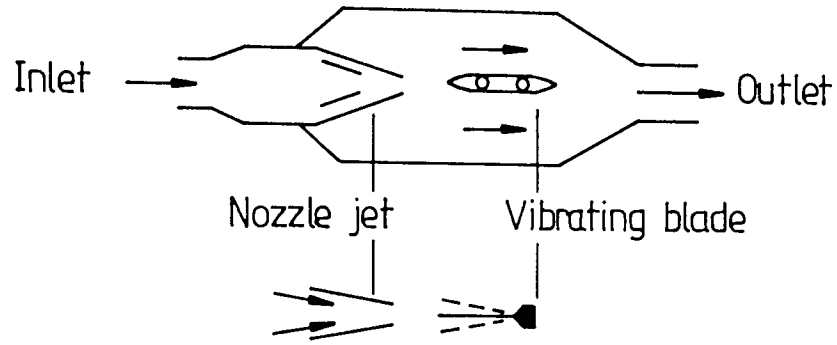

(a) Sonic emulsification

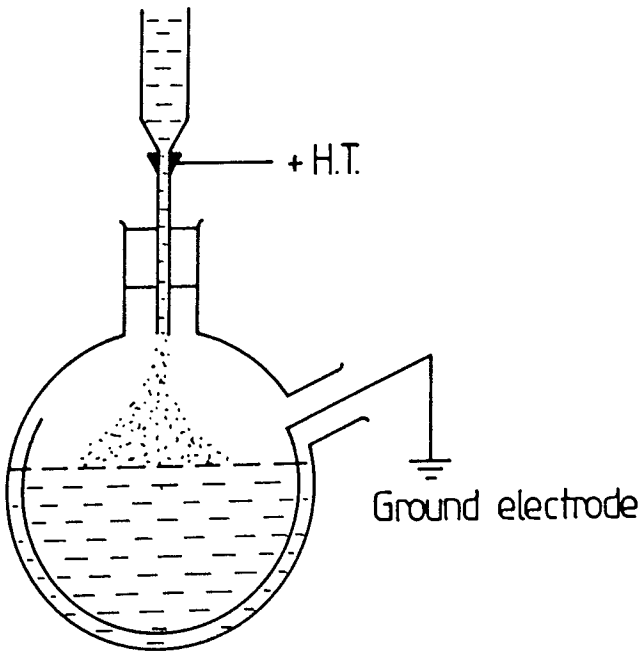

(b) Electric dispersion of liquids

Figure 2.5 Emulsification using electromagnetic transducers

There are some limitations related to the electric dispersion method. Emulsification becomes difficult if the viscosity of either phase is high. Further, there are some difficulties with controlling the properties of such dispersions.

2.5 Industrial Occurrence of Secondary Dispersions

The undesirable economic and ecological consequences of uncontrolled dispersion-formation in industry has resulted in the initiation of numerous research investigations. In this section the principal sources of undesirable emulsion formation will be briefly described.

2.5.1 The Petroleum Industry

Following the accelerated increase in oil prices in the 1970's, consumers endeavoured to make savings by reducing oil consumption and/or using cheaper grades of oil [31]. Low quality crudes usually contain inorganic salts dissolved in both free and emulsified water. The presence of such salts in crude is highly undesirable because it results in corrosion of refining equipment and scaling of heat transfer surfaces. The Pan American Refining Corporation therefore investigated the use of glass fibres as a contacting agent in the solid contact method of desalting crude oil [32].

The Petroleum Industry has co-operated to study mutual pollution problems. Refineries were of necessity located near a water supply, and the common water supply tended to receive waste oil dispersions and even some oil fractions. This pollution constituted a real problem, since refinery effluent waste water may be cleaned to the point where the oil concentration is too low to show iridescence on the surface. Usually oil in effluent water is removed by a specially-designed, gravity separator making use of the principles of low-velocity uniform distribution, film rupture and coalescence, and continuous-skimming of oil [33].

Petroleum refinery waste water systems generally handle four types of contaminated water namely, oil-free water, cooling water, process water, and sanitary

and other waste water. The greatest volume of water circulated is for cooling processes [34]. The basis unit for recovering oil is the gravity type oil-water separator which is in general use throughout the petroleum industry [35]. Recently however, Bloess [36] improved the performance of a gravel bed separator and sand filter by passing the oil from the stripping step through a series of heat exchangers to reduce its temperature before passage through a sand-bed coalescing vessel. The water droplets collected and coalesced in the beds of sand, and the dewatered oil was passed through a heat exchanger to increase its temperature prior to storage.

2.5.2 In Liquids Fuels

Water is a critical contaminant in aviation fuels, since corrosion and microbiological growth can be controlled by the removal of free water. In addition, the presence of water may cause icing problems with low-temperature operations [37]. When jet powered aircraft began to replace piston engine aircraft as primary airline equipment [38], the removal of water droplets became more difficult as the fuel became heavier [37]. Therefore, fuel filtration equipment was introduced to remove droplets of water from the aircraft fuels [39]. The filter/separator has been applied successfully for several years for separation of water-in-oil dispersions. Operation depends upon coalescence of fine droplets inside the filter [40].

Water droplets in diesel oil fractions are generally coalesced by passage through a ceramic filter (pore radius 65 μm) [41]. Although most studies have been carried out in the context of removing water from jet fuel, many of the basic concepts developed may be applied to the removal of water droplets from other fuels or organic liquids, and to the removal of dispersed organic liquids from a continuous aqueous phase [40, 41].

2.5.3 Effluents

Oil effluents can be of two varieties, either a true emulsion, in which the oil and water phases are mixed and the oil has been made soluble by the addition of emulsifying agents, or in with oil the form of discrete droplets. The latter type of effluent arises from most industrial operations which use oil as a lubricant or process material [42]. It also arises from ships ballast, i.e the practice of filling fuel tanks with water to compensate for the weight of fuel used. In order to refuel, this oil-contaminated water has to be pumped-out into the oceans, seas and rivers. All oil-industries and ships employing this procedure are now obliged to process the effluent in some form of oil/water separator before discharge [43].

A recent problem of much concern to the US Navy is the contamination of aviation kerosene with Navy Special Fuel Oil (NSFO), and residual fuel oil on aircraft carriers. Although the aviation kerosene and residual fuel oil are stored in separate tanks, contamination can occur by seepage through cracks in a common bulkhead [44].

Gabriel and Parry [45] suggested that the main causes of oil pollution of the seas are collision, or grounding of, a vessel at sea causing the escape of oil from cargo; the discharge of cargo tank washings and oil contaminated engine room bilge water directly overboard without prior treatment; accidental discharge of oil overboard during loading or refuelling; and coastal oil-drilling operations.

A number of dispersive forces act upon the floating oil contamination. Low-molecular-weight and water-soluble components are lost from the sea surface by dissolution and evaporation. Other substances are returned to the sea by bacteriological attack and the chemically-unsaturated components are readily attacked by ultraviolet radiation. In spite of this, there is an immediate need for oil dispersion and control techniques in coastal areas, estuaries, and rivers where extensive petroleum pollution can be economically and aesthetically harmful. Recent approaches to effluent treatment have followed two general paths, physical and chemical [46]. In either case the equipment is required to alleviate discharge of large amounts of crude oil dispersion.

2.5.4 Miscellaneous Effluents

In many other industries, oil contamination of aqueous effluents is due to accidental spillage or the use of the sewerage system for disposal of waste oils. Oil-in-water dispersions arise from most industrial operations which use oil as a lubricant or process material. The steel and motor industries are particularly prone to this type of problem. In the textile industry, high-powered centrifuges have been frequently used for the recovery of wool greases and oil from their secondary dispersions [42]. In solvent extraction operations, the coalescence of primary dispersions by the stage-wise mechanism is often responsible for the formation of smaller drops which result in secondary fogs.

Hence temporary dispersions may be encountered industrially in liquid-liquid extraction processes and in steam distillation [29]; they may result when one liquid phase is dispersed in another in the absence of a stabiliser or after the emulsifying agent has been destroyed, or otherwise removed, from a stabilised dispersion [47].

In conclusion, this section illustrates that the separation of secondary dispersions, whether for recovery, treatment or to avoid pollution, is a problem that has to be faced in a wide variety of fields, from metal extraction, solvent extraction, petro-chemical and chemical processing, to tank washing and waste-water treatment.

CHAPTER THREE

SEPARATION METHODS FOR SECONDARY DISPERSIONS AND DROPLET COALESCENCE IN PACKED BEDS

3.1 Methods of Separation

Many methods have been applied to coalesce secondary dispersions into larger droplets so that the dispersed phase can be separated easily by gravity settling. These separation methods are discussed in detail below.

3.1.1 Centrifugation and Hydrocycloning

If settling of an unstable emulsion is slow due to a small density difference, high viscosity of the continuous phase or a small drop size, a centrifuge may be used to increase the rate of separation. Alternatively a stable emulsion may be concentrated rather than 'broken' by centrifugation. The force in a centrifuge results in a liquid pressure which may be expressed as,

$$P_L = \frac{\rho_L}{2g_c} w^2 (r_2^2 - r_1^2) \qquad \ldots. 3.1$$

The pressure of light liquid (L) between the inner discharge lip and the interface must also be equal to the pressure of the heavy liquid (H) at the interface (r_n). The position of the interface can be controlled simply by altering the radius of the discharge weir in the centrifuge [48].

The centrifugation of dispersions has been used to provide a measure of their stability by observing the separation of coalesced phase as a function of time [5]. A centrifugal separation is basically a settling pond, in which gravitational force is magnified several thousand times owing to centrifugal force [31].

Three main types are available

a. The hollow-bowl centrifuge has the advantage of simplicity and ease of cleaning. It may be built in the form of a long tube with a relatively small diameter to obtain large centrifugal forces together with a high ratio of travel to settling distances [48].

b. The disc-bowl centrifuge for which there are a number of different constructions to provide disc-bowls with shallow settling spaces, eg concentric cylinders, spiral leaves or conical discs. The majority of centrifuges use conical discs with thin spacer caulks to obtain a shallow settling space with a long path of travel. The discs are usually smaller than the diameter of the bowl to allow for the collection of sediment [48]. The disc-type separator bowl is widely used because of its high efficiency and because it permits the feeding and discharging of the liquids at the top of the bowl, which is an advantage from a mechanical view point [49].

c. The hermetic or pressure separator is fitted with back-pressure control valve on the light phase discharge, which provides a means of adjusting the zone of separation between the light and heavy phases whilst separation is in progress. Because of the closed pressure bowl and its high efficiency, flammable solvents such as light hydrocarbons can be separated safely and economically. This design is claimed to have all the advantages of the disc bowl and, in addition, operates under positive pressure [50].

In a hydrocyclone, separation is accomplished by a centrifugal force caused by the vortex motion of the dispersion. When the flow of dispersion through the hydrocyclone is increased, this centrifugal force is also increased. However, hydrocycloning has not proved very efficient for the separation of emulsified oil from water because the turbulence created by the high flow rate tends to shear and break the dispersed oil phase into a still finer dispersion [51].

3.1.2 Electrical Coalescers

The petroleum industry relies on electrostatic coalescers, such as the type shown in figure 3.1, to purify crude petroleum from connate sediments and corrosion-inducing salts, and thereby reduce corrosion and fouling of distillation equipment. Electrical coalescence has been applied extensively to the separation of emulsions generated during the desalting of crude oil [52].

Electrical methods of inducing coalescence are based on either of two mechanisms:

a. Forces between particles (solid or liquid) resulting from their acquiring induced dipoles in an a.c or d.c field, termed dipole coalescence, or
b. Forces that result from the interactions between a unidirectional applied field and particles having a net charge, termed electrofining. The first mechanism is the more general since it results from the application of either an alternating or a unidirectional field [52].

Generally, for two liquid spheres in an oil, the force of attraction F_a is

$$F_a = 6\,(\varepsilon/\varepsilon')\,E^2\,r^2\,(r/d_s)^4 \qquad \ldots. \; 3.2$$

where, r is the radius of a drop and d_s is the distance between centres of two drops. The quantity $(r/d_s)^3$ is proportional to the concentration of the dispersed phase, and is almost independent of the particle sizes so that, for a specific dispersion, the factors $(r/d_s)^4$ and $(\varepsilon/\varepsilon')$ remain nearly constant until partial phase separation has occurred. Thus, the rate of separation is proportional to $E^2\,r^2$ [8].

Electro-filtration of conventional fuels using electrostatic precipitators has not progressed significantly in recent years. A filter, which has been tested, is a non-ionizing electrostatic precipitator designed as a self-contained filtration device for the purification of petroleum-based oils or solvents. However limited tests were conducted

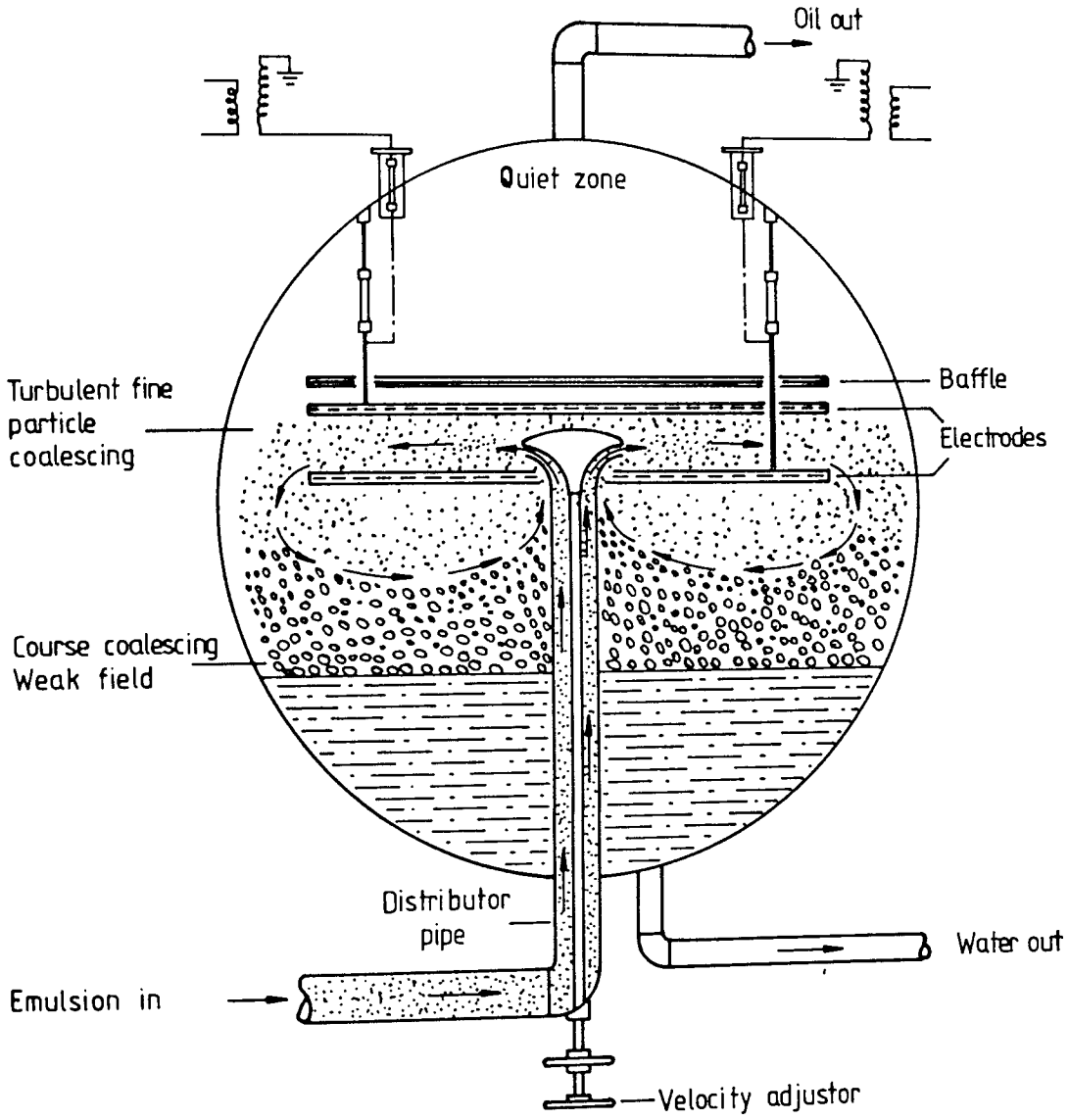

Figure 3.1 Internal circulation and electrical field in an electrical coalescer.

on an electro-filter using heavily-contaminated fuel derived from shale oil [53]. It has been proved analytically, and by experiment, that coalescence of droplets in uniform electrical fields is only possible up to a certain field strength [54].

Recently, electro-static methods have been successfully applied for the recovery of copper from an aqueous solution. The droplet size of the disperse phase of the dispersion was in the range 0.3-10μm with the majority of droplets being between 0.8-3μm [55].

3.1.3 Chemical Coagulation

Chemical coagulation is probably the most widely-used technique for 'breaking' dispersions. It depends upon the removal of barriers that hinder coalescence. The de-emulsifiers counteract the influence of the protective films that surround the dispersed drops and the double layer forces [8].

The separation of oil-in-water emulsions can be achieved by suitable chemical treatment to inactivate the emulsifying substance. Inactivation may be accomplished by the use of chemical coagulation agents such as aluminium, ferric, calcium, and sodium salts [51,56]. The use of organic polyelectrolytes, such as polyvalent salts and acids, is also widely recognised as a practical and efficient technique [8, 51].

Such chemical additions may assist in any of the following ways [57]:

a. by inversion of the phases;

b. by neutralisation of surface charges; or

c. by dissolution of the protective film surrounding each droplet.

Coagulation may be promoted by reducing repulsive electrical charges between oil droplets and by the addition of compounds which bridge and link the oil droplets. Hydrolysing metal salts destabilise oil droplets by bridging between them as well as by neutralising the charge on negatively-charged oil droplets [58].

3.1.4 Gravity Settlers

Gravity settlers may be classified into two main groups according to whether they are to separate the unstable primary dispersions commonly-encountered in liquid extraction, or the more stable secondary dispersions that often remain after the first break has occurred. Secondary gravity settlers may be of the coalescence or membrane type [48]. The dynamics of settling particles can be classified into three categories according to their respective concentration ranges:

a. Dilute systems in which the settling rate is constant with time.
b. Intermediate systems in which the settling rate passes through a maximum and aggregates settle as a coherent network.
c. Concentrated systems in which a compressive settling mechanism results in a monotonically decreasing rate of settling with time [59].

Mathematical models for the settling of particle clouds are limited and generally involve application of some correlation factor to Stokes Law (equation 1.1). With increasing volumetric concentration, settling is hindered by inter-particle interaction [59].

Gravity settlers are simple to construct and to operate but they have slow response characteristics; they require a large ground space and have a large liquid hold-up [60].

3.1.5 Heating, Evaporation or Distillation

Oil-in-water emulsions can be de-emulsified by heating since raising the temperature of a dispersion increases the settling rate by reducing the continuous phase viscosity and possibly changing the density difference, since $\Delta\rho$ depends on density vs temperature for each liquid [42].

Heat treatment is economically feasible because of the value of oil that can be recovered for re-use. Conversely evaporation or distillation are generally considered to be unfavourable economically for the separation of oil-in-water dispersions since a large

amount of energy is needed for heating, pumping or providing a reduced pressure to vaporise the water before the oil can be removed [51].

There are two techniques in heat treatments [61]:

a. Heating at atmospheric pressure is usually used in the separation of o/w dispersions.
b. Heating at elevated pressure is used for a few w/o dispersions in which high temperature may affect the properties and the nature of the oil.

Therefore, heat treatment is usually used in conjunction with chemical coagulation [42] because it increases the reaction rate of the demulsifying agents.

3.1.6 Air Flotation

Separation by air flotation depends on the injection of fine air bubbles to which oil drops adhere and are removed by being carried to the water surface. The air can be added in a dispersed form or be generated from dissolved substances [51].

Flotation processes operate more efficiently when the dispersion is pretreated with flocculating agents. Luthy et al [58] studied dissolved air flotation (DAF) using the appropriate coagulant and controlling pH to remove emulsified oil from waste water.

The best results were obtained when the polyelectrolyte was mixed as quickly as possible with the wastewater and some preliminary flocculation time was necessary. Rohlich [62] reported that under conditions of 50% recycle and the use of 28.13 litres of air to 567.75 litres of water, an average oil removal of 62% was achieved. Addition of 25mg/l of alum as the precipitant increased the removal efficiency to 94%.

There are two different air flotation techniques: precipitate flotation in which the flotation process efficiency has been increased by adding aluminium sulphate to the o/w dispersion to form a gelatinous precipitate, and adsorption flotation which involves the addition of powdered activated carbon to the flotation unit to adsorb the oily and dissolved pollutants in the waste water. Both techniques have found extensive application in the treatment of oily-wastes from refineries, petrochemical plants and steel mills [51, 63]. For oil and grease removal the advantages of air flotation over other

systems of sedimentation are the smaller space requirement due to the higher feed flow rate, the reduced residence time, and the higher separation efficiency [64].

3.1.7 Magnetisation

Kaiser et al [65] performed experiments to demonstrate the feasibility of recovering oil from fine, stable oil-in-water dispersions by magnetic means. Dispersions, in which the oil phase was rendered magnetically responsive by the addition of a ferrofluid, were passed through packed beds (containing magnetic particles or screens) and placed in a magnetic field. Removal of droplets with diameters as small as one micron was obtained with packed beds of magnetic materials several inches deep, using air-gap fields of several thousand oersteds, oil phase magnetisation from about 2 to 10 gauss, and superficial velocity as high as 0.7cm/sec [51].

3.1.8 Solid Surface Coalescers

In solid surface coalescing, the continuous phase passes through the porous material while the dispersed liquid contaminant remains on the surface, coalesces and falls away from the porous material [66]. Operation of these coalescers sometimes referred to as 'Interfacial Tension Separators', depends upon the interfacial tension, the size of opening in the porous membrane, the pressure drop across the membrane, and the degree of wetting. The main requirements for this type of membrane filtration are a high surface area, a thin cross-sectional area, and the membrane should have a good mechanical strength and chemical resistance [57, 67].

The main factors affecting the overall performance are the surface properties of the liquid system and the solid packing, the system hydrodynamics, inlet drop size and packing geometry i.e surface/volume ratio [68].

The use of layer filtration for removing the emulsified oil from water has been investigated by the Calspan Corporation using powdered, activated carbon as the filter medium [51]. However, this techique is still in the development stage.

Reverse osmosis has been applied to the treatment of petrochemical process effluent waste waters. However, this membrane-filtration technique requires proper matching of the membrane to the material to be separated and its use for oil-water separation is still in the development stage [51].

3.1.9 Crystallisation or Freezing Techniques

The separation of o/w dispersions by crystallisation or freezing techniques are generally considered economically infeasible, except on a small scale, because of the need for complex refrigeration equipment and relatively large supplies of energy [69]. However sufficient information is not available for a full assessment [51].

3.1.10 Filtration-Extraction-Filtration Method

In 1971 Wolfe [70] developed a novel method for removing emulsified oil from water. The basic unit processes are sand filtration, solvent extraction, and filtration. The waste water is first passed through a packing medium consisting of sand and gravel and then through a solvent which is insoluble in water. The solvent used may by acetylene tetrabromide, acetylene tetrachloride or xylene. After passing through the solvent, the waste water is then purified by letting it pass through a semiporous mass which is permeable to water but not to the solvent and oil. The cost effectiveness of this process is not well-established.

3.1.11 Cartridge-Type Coalescers

Three basic types of cartridge coalescer, which are shown in figure 3.2, are used in chemical processing. They work on the same principle as separation by depth coalescence with a different design. They comprise single-stage, two-stage and three-stage units wherein one, two or three types of cartridge are provided. The configuration of each design varies with the process application and efficiency requirements. The coalescer cartridge is made up of one or more layers of media. This

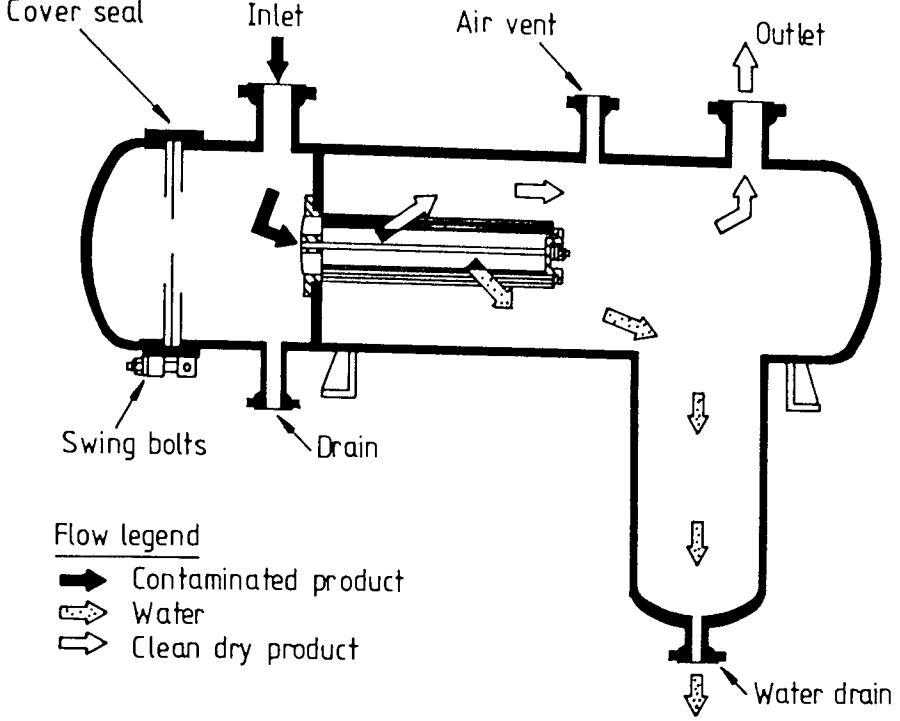

(a) A typical single-stage coalescer

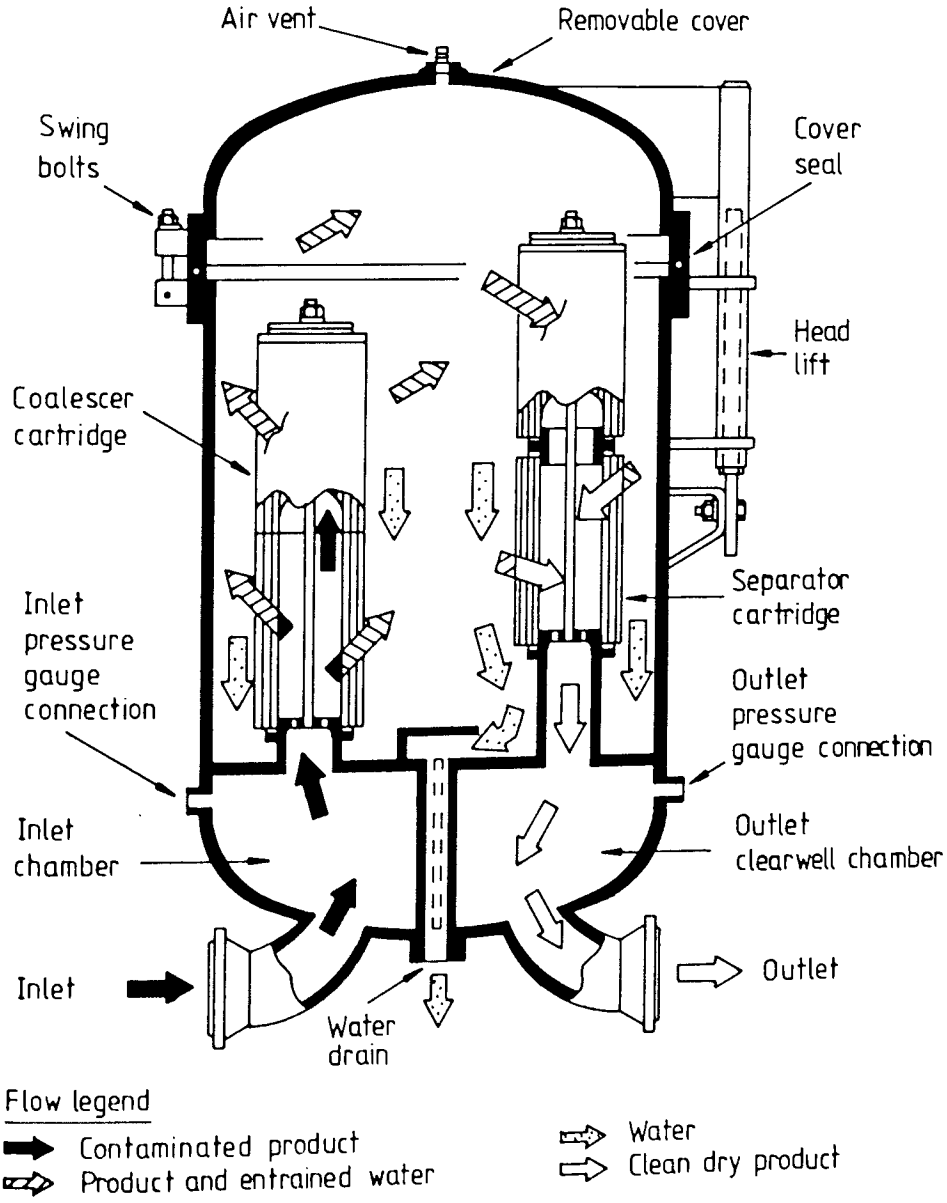

(b) A typical two-stage vertical coalescer

Figure 3.2 Single and two-stage cartridge-type coalescers

media is primarily a porous membrane which retains its dimensional stability by the use of thermo-setting resins or binders. To ensure that separation of the dispersed phase is complete, the media must possess an infinite number of irregular continuous passages of very small diameter. The interfacial tension between the continuous and dispersed phase is an important factor in application of cartridge coalescers to a fluid process stream. Below values of 20 dyne/cm, the size of the droplets in the dispersed phase become progressively smaller and coalescence becomes more difficult [71].

The coalescer and stripper cartridges used in multi-element systems usually have an outside diameter of 0.15m and vary in length from 0.29m to 0.85m. The emulsified fuel first meets a pleated assembly of media comprising a combination of glass-fibre, asbestos paper, and phenolic resin-impregnated paper in that order. The pleated configuration is used to obtain the optimum area consistent with maximum dirt-retention capacity and efficiency [72].

Cartridge-type coalescers have been successfully applied in water removal from aircraft jet fuel, diesel engine fuel, and steam turbine lubricating oil. Nowadays, the two stage coalescer cartridge type, illustrated in figure 3.2b, with a semi-permanent stripper stage, is finding favour, mainly on account of reduced replacement and servicing costs. Further work is directed towards the use of man-made fibres and plastics in the manufacture of cartridge-type coalescers [71, 72].

3.1.12 Depth Coalescers

Coalescence may be induced by causing a dispersion to flow through a bed packed with a substance possessing a large ratio of surface to volume. The mechanism probably involves two factors; preferential wetting of the bed by dispersed phase, causing the drops to collect in the bed, and coalesce, and mechanical destruction of any surface film that may be present, allowing the dispersed phase more freedom of

to the down-stream face of the packing where 0.5-2mm diameter drops are released to be separated from the effluent by gravity [66, 72].

A fibrous bed was used as early as 1949 to separate primary dispersions in commercial processes. Subsequently a wide variety of porous media have been investigated including ungraded gravel beds and stainless steel gauzes [43]. Wilkinson et al [73] used glass ballotini particles and Thomas and Mumford [74] used knitted mesh packing to separate primary dispersions and studied the hydrodynamic behaviour and coalescence mechanisms of primary drops.

Recently, fibrous beds have been used for separation of a secondary oil/water dispersion by passing it through a depth coalescing unit at relatively high pressure (165 KN/m^2 gauge) and at a temperature of 10°C [66]. Fibrous beds have also been used to remove secondary oil drops from water [75] and secondary water drops from aviation fuel [37, 39, 72].

Polymeric materials have also been used in the form of an open-pored and non-woven structure to separate secondary dispersions in commercial depth coalescing designs [45, 76].

3.2 Disadvantages of Separation Methods

Each of the above methods suffers from certain disadvantages. Centrifugation involves high capital and operating costs, and difficulties may arise in cleaning and maintenance due to the number and weight of the components. Therefore, centrifuges tend to be limited in application to the separation of secondary dispersions where a very short time of contact is essential. The use of centrifuges for dispersion separation has been restricted to military applications such as the removal of water from aviation fuel and those cases where the value of the product is exceptional. Hydrocycloning has not proved very efficient in separating oil-in-water emulsions since the operating flow rate tends to break the dispersed oil phase into a stable and finer dispersion.

Electrical coalescers involve high capital and operating costs. They are

unsuitable for applications where high separation efficiencies are required. The chemical coagulation method suffers from the disadvantage of high costs and technical and practical limitations because chemical additions may result in unacceptable contamination of the liquid system. Therefore, care is needed in both the choice of chemical(s) and the level of addition.

Additives which are surface active will reduce the interfacial tension between the liquids leading to reduced efficiency. Furthermore where coagulation and filtration are used in combination, the chemical additive could harm the filter or coalescer element by forming surface coatings on them. Consequently, chemical coagulation is more often employed in conjunction with flotation processes when recovery of the dispersed phase is not mandatory. The separation efficiency has been found to vary dependent upon traces of impurities, the quantity of air bubbles drawn into the system, and with the variation in intensity of agitation. Therefore reproducibility of the rate of separation can only be obtained with a very high degree of control, whereas regulation of all the variables is difficult in industrial scale operation.

Gravity settlers are simple to construct and operate but they are very inefficient for the separation of secondary dispersions and require large ground areas. The time and space required are the major limitations and therefore gravity settling represents the most expensive approach to separating oil from water.

The high energy consumption may make heating, evaporation and distillation techniques uneconomical for the treatment of large quantities of dispersions. Air flotation processes operate more efficiently when the effluent is pretreated with flocculating agents. However, the dissolved air flotation technique is more common due to its simplicity and high capacity, when it is not necessary to recover the dispersed phase from the float which may be contaminated by the addition of chemical coagulants.

The use of magnetisation, membrane filtration, crystallisation or freezing, and filtration-extraction-filtration techniques for the separation of oil-in-water secondary dispersions still remains in the development stages.

Recently, there has been considerable interest in the coalescence of secondary dispersions by using fibrous, porous media, or particulate bed coalescers as they are relatively inexpensive, efficient, small and simple to operate. These are discussed in detail in the following section.

3.3. Coalescence of Secondary Dispersions in Packed Beds

Packed bed coalescers can be divided into three categories as follows:

3.3.1 Coalescence in Fibrous Packings

Passage of an o/w, or w/o, secondary dispersion through a fibrous packed bed, which has randomly-arranged matrices usually consisting of layers of fine woven fibres or meshes, is widely-used for the coalescence of fine drops. Many workers [16, 17, 37, 57, 62, 66, 72, 75, 77 - 90, 111] have therefore studied the coalescence of secondary dispersions in different types of fibrous material using different coalescer designs. It is generally accepted that the fibre beds should have a high voidage, be closely-packed and possess a high ratio of surface area to volume. Langdon [91] considered the separation performance of a packing to be mainly determined by its wetting properties. However Sareen [81] concluded that preferential wetting was not the controlling factor, but that the relative surface roughness of the fibres was important. A similar conclusion was reached by Davies and Jeffreys [92]. Hazlett [93] also suggested that the wetting properties of fibres are unimportant for the collection of small water droplets.

The capture efficiency increases with the depth of the packing and with the interfacial area per unit volume of packing. However, there is an optimum packed depth above which break-up of drops takes place [90]. Fibre roughness and fibre diameter are also considered to be important factors affecting the coalescence efficiency [94]. Sareen *et al* [81] confirmed that the coalescer performance improved with decrease in fibre diameter and increase in bed depth, but an optimum existed between bed depth and the

pressure drop across the packing. Coalescence rates have been found to increase with decreasing fibre diameter and increasing surface roughness. In this respect, cotton fibres have been successfully applied to the coalescence of secondary dispersions, but tend to become compressed [95].

The manner by which surfactants may poison coalescer elements has been studied. Osterman *et al* [96] suggested there was adherence of the surfactant to the media thus allowing the dispersion to pass through unaffected due to the change in fibre wettability. However, Lindenhofen [44] disproved this proposal experimentally and considered that the surfactant film at the oil-water interface presents a mechanical, or electrical, barrier to the coalescence of water droplets in the media. Hazlett [84] confirmed that such an additive did not affect the approach and attachment processes but only affected droplet release.

Shalhoub [57] studied the coalescence of secondary dispersions in phenol-formaldehyde bonded, glass fibre beds and concluded that exit drop size was independent of inlet drop size distribution and phase ratio but was a function of superficial velocity and packing thickness. Average bed hold-up was independent of inlet drop size distribution and phase ratio, but decreased with increase in superficial velocity. The hold-up remained constant throughout the glass fibre bed until the exit plane, where it increased. Attarzadeh [17] prepared fibrous packing from pure glass wool and devised a novel technique to study drops within the packing by matching the refractive indices of the packing, its holder and the continuous and dispersed phases. This rendered the packing transparent and a soluble phototropic dye was used to colour the drops by illumination with ultraviolet light. A technique was also developed using ultrasonic probes to detect drop collection and coalescence within the packing. Observation of drop collection, coalescence and travel within the packing indicated that captured drops moved along the fibres and coalesced at intersections. Six different mechanisms of droplet release were identified namely drip-point, jetting, pointing, graping, foaming and chaining; these are discussed later in section 4.1.4.

Finally, Austin [16] used woven micro-meshes of stainless steel, nylon or polyester in packed bed coalescers to separate secondary o/w dispersions. Statistical analysis of two phase pressure drop data produced a correlation relating pressure drop to superficial velocity and bed depth for each mesh tested. A theoretical equation for drop capture efficiency, discussed in section 4.1.1, was used to predict the initial and local drop capture rates in a coalescer. This analysis indicated that direct and indirect interception mechanisms were predominant. A mathematical description of the saturation profiles was formulated and verified by average saturation data. Good agreement was obtained between experimental pressure drop data and model predictions. Further details are given in section 4.2.7.

The majority of mathematical equations and theoretical models developed for coalescence of secondary dispersions within fibrous packed beds, relate to specific systems and experimental arrangements. However, these equations and models are not necessarily suitable for general use in design. Further studies are likely to be needed to improve and/or develop mathematical descriptions of secondary dispersions separation for practical design applications.

3.3.2 Flow Through Porous Media

Any porous medium generally comprises an extremely complicated, network of channels and obstructions. It is usually described statistically and in some average sense. The number of holes or pores is usually sufficiently large that a volume average is necessary in order to calculate the bed porosity, channeling and wettability properties [97].

Coalescence of secondary dispersions induced by flow through porous media has proved effective in removal of oil droplets prior to discharge of effluent into receiving water [126, 98]. Krueger [99] used porous materials, preferably webs of microfibre in which the pores at least approached capillary size, as a coalescing media for separation of water containing 394 ppm of petroleum at a flow rate of 36.30 litre/min.

Pontello [100] used clay filters as a porous medium to remove the secondary water drops from jet fuel.

Spielman and Goren [77, 85] investigated the separation of oil-in-water secondary dispersions using thin glass fibre mats. The upstream and downstream drop size distributions, pressure drops across the mats, and total oil hold-ups were reported for steady-state conditions. However, the measured values of oil saturation were unreliable since the dispersion flow had to be stopped to dismantle the mats and this permitted spontaneous adhesion of oil by capillary action.

Bartle [72] reported the use of multi-element systems for separation of oil-in-water dispersions. The secondary dispersions flowed through a pleated assembly of media comprising a combination of fibreglass, asbestos, paper and phenolic resin-impregnated paper. Initial coalescence took place in the pleated assembly and was completed on passage through the cylindrical wrap of glass fibre.

The major factors affecting coalescence and flow through porous media have been well-documented by previous workers [101-103]. They are:

i. surface tension and viscosity of liquid-liquid system;

ii. contact angle of the dispersed phase on the packing; and

iii. capillary pressure.

However, the application of theory to practical problems is often limited by the complicated geometry associated with porous solids [98].

3.3.3 Flow Through Particulate Beds

Packed beds of granular material such as sand, pebbles, quartz, gravel and polymeric materials (eg polyethylene chips) have been used to coalesce secondary dispersions [27, 35, 42, 104-107].

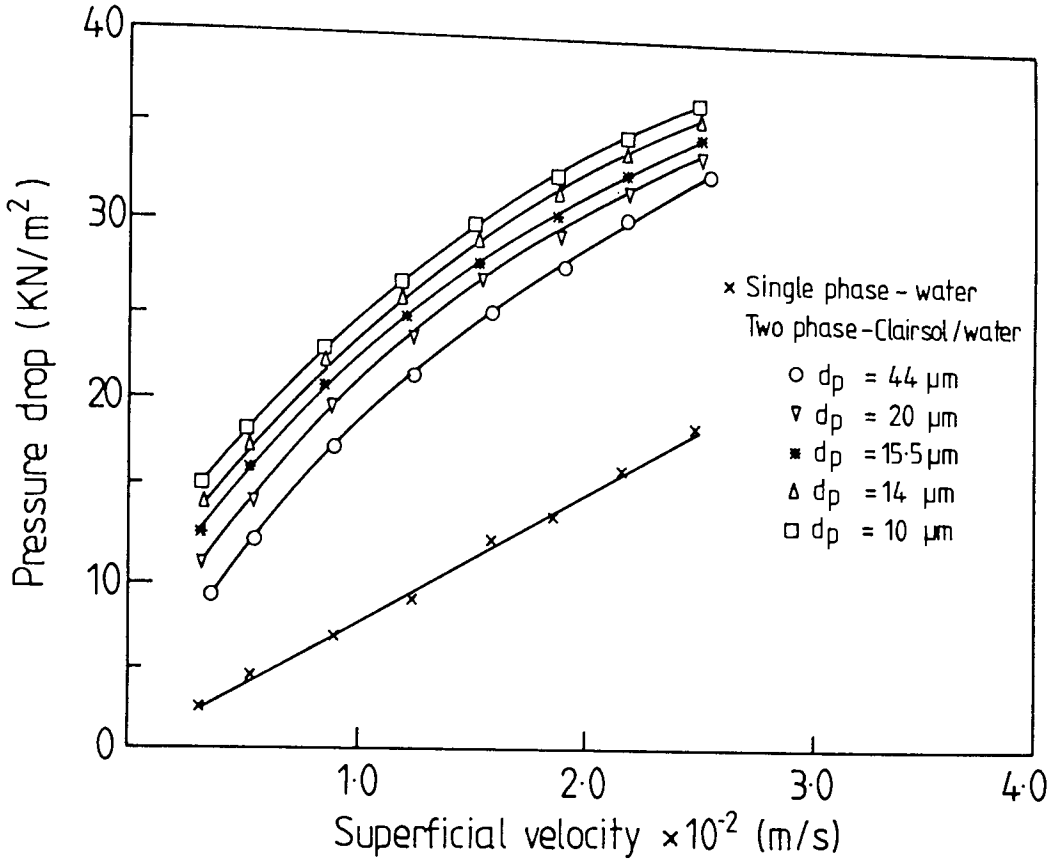

(a) Sand bed depth = 20×10^{-3} m, Sand particle diameter = 250 μm

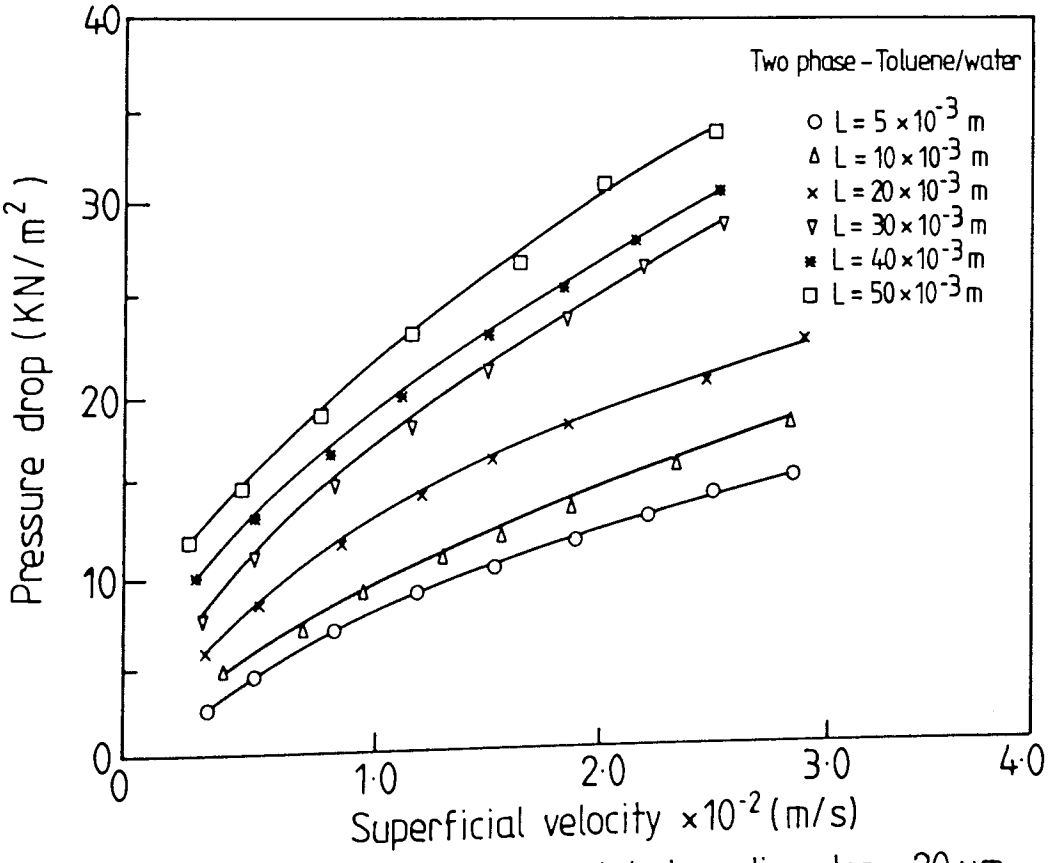

(b) Sand particle diameter = 250 μm, Mean inlet drop diameter = 20 μm

Figure 3·3 Variation of pressure drop with superficial velocity (Data of Ibrahim[104])

Douglas and Elliot [108] reported that particulate beds performed 'acceptably' when coalescing oil-in-water dispersions. However, their investigation was mainly concerned with industrial usage and very little quantitative analysis was reported. Heidenreich et al [109] used plastic rings in a packed bed to separate diesel oil and water secondary dispersions. The efficiency was improved by either gas injection and/or by using composite beds made up of different packings. Smith [35] compared the performance of a number of coalescing materials using a laboratory scale separator. Polyethylene chips were considered a suitable material for a practical coalescing bed. A full-scale gravel bed separator was also described and a method proposed for scaling-up the laboratory data to the design of a full-size particulate bed separator.

Ibrahim [104] investigated the separation of toluene or Clairsol 350-in-water secondary dispersions in packed beds of ordinary building sand. Statistical analysis of single and two phase flow data, as shown in figure 3.3, produced a correlation relating the pressure drop to superficial velocity and bed depth,

$$\left[\frac{\Delta P_2}{\Delta P_1}\right]\left[\frac{\mu_c}{\mu_d}\right] = cU^bL^d \qquad \ldots. 3.3$$

This covered three mean inlet drop diameters i.e 20, 14 and 9μm in beds of optimum sand particle diameter of 250μm. Constant, c and the exponents, b and d were determined by multiple linear regression analysis of the data [78]. Performance, hold-up and pressure drop data were summarised for different sand particle sizes, i.e 210, 250, 530 and 710μm and different bed depths i.e 5, 10, 20, 30, 40 and 50 x 10^{-3}m as shown in figure 3.3b.

Beaz Poleo [27] studied the coalescence of o/w secondary dispersions in beds of glass ballotini. The main variables investigated were superficial velocity, bed depth, ballotini size and oil-saturation. A mathematical description of the oil-saturation data, as shown in figure 3.4, was formulated and verified by oil-saturation data obtained by relative permeability, based on the Carman-Kozeny equation (see chapter 7). Al-Meshan

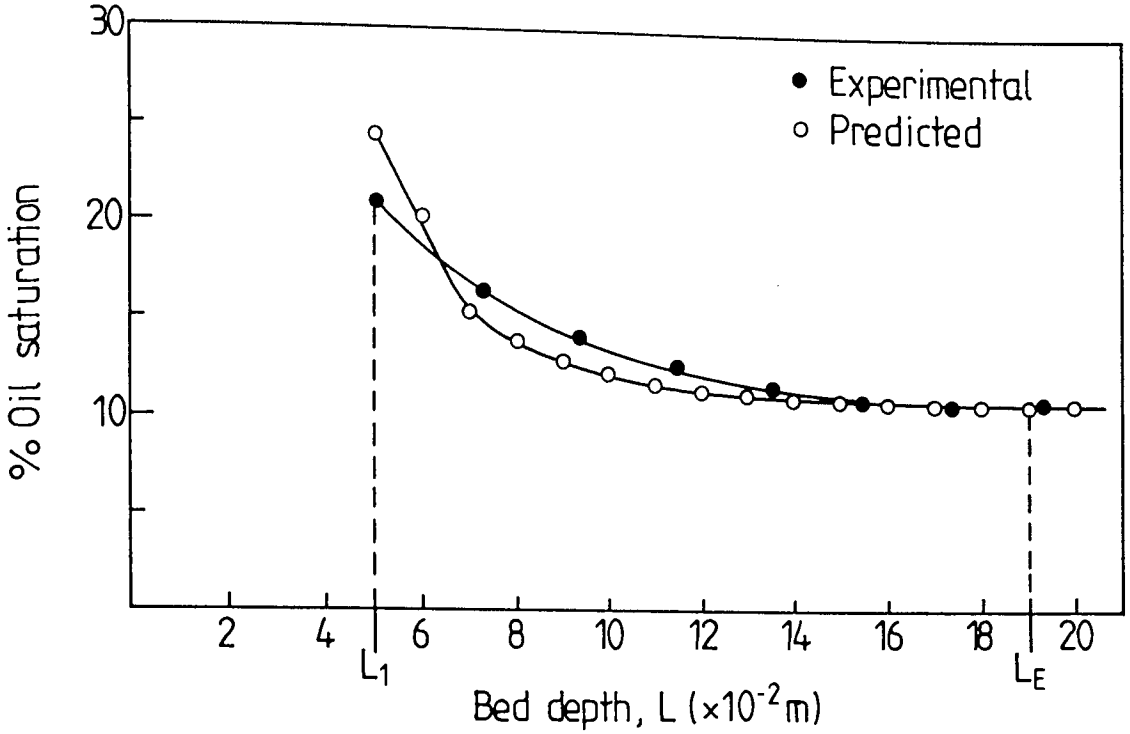

(a) Bed depth = 20×10^{-2}m, Ballotini particle diameter = 486 μm
Velocity = $5{\cdot}0 \times 10^{-2}$m/s, Dispersed phase concentration = 0·1% v/v

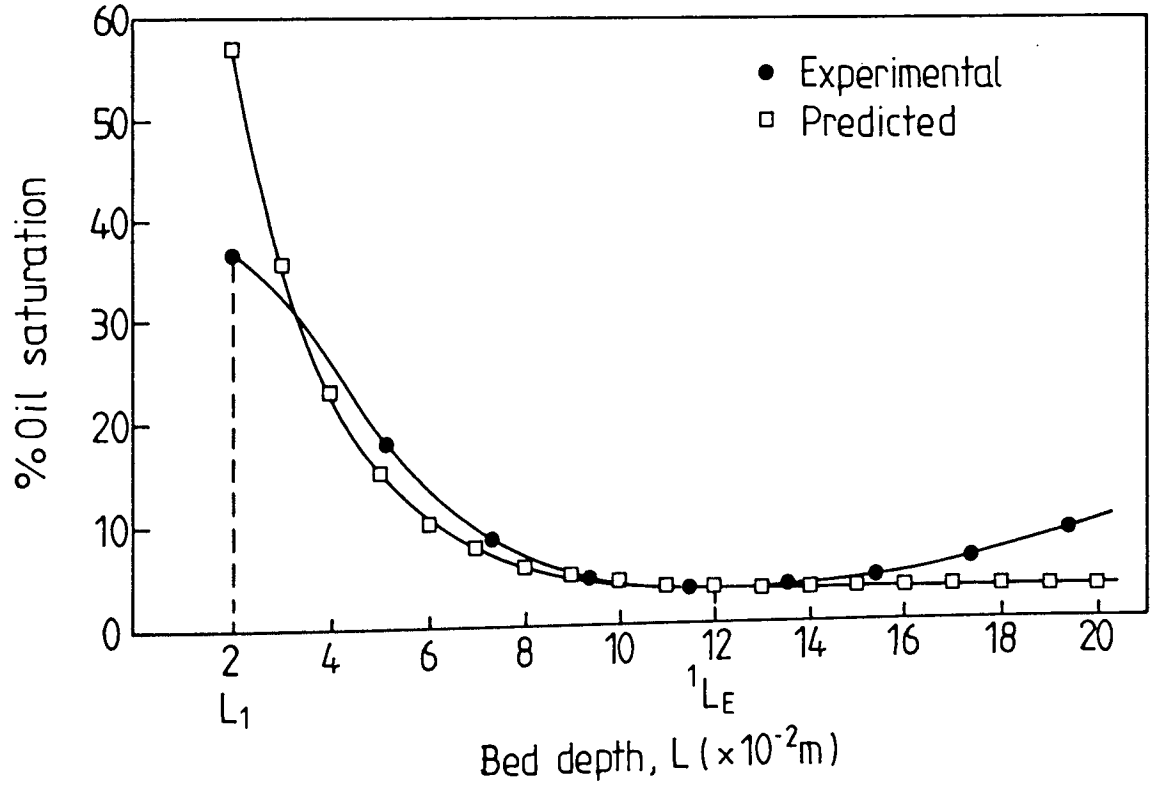

(b) Bed depth = 20×10^{-2}m, Ballotini particle diameter = 486 μm
Velocity = $0{\cdot}3 \times 10^{-2}$m/s, Dispersed phase concentration = 0·2% v/v

Figure 3·4 Experimental and predicted phase saturation vs. bed depth (Data of Baez Poleo [27])

[106] studied the mechanisms of coalescence of o/w secondary liquid dispersions in particulate beds of different sizes and heights of glass ballotini. The effect of packed height and packing size upon critical velocity, pressure drop and coalescence efficiency were investigated. Two phase pressure drop was correlated by two equations, one for large ballotini sizes (i.e 267 and 367μm).

$$\Delta P_2 = \frac{252\,\mu_c\,U}{e_1^{3}} \left[\int_{L}^{L_i} f(s)\,dl + \int_{L_i}^{L} f(s)\,dl \right] \qquad \ldots. 3.4$$

the other for small ballotini sizes (i.e 93μm and 147.4μm);

$$\Delta P_2 = \frac{81.36\,\mu_c\,U}{e_1^{3}} \left[\int_{L}^{L_i} f(s)\,dl + \int_{L_i}^{L} f(s)\,dl \right] \qquad \ldots. 3.5$$

The packings were efficient coalescers up to critical velocities of 3 x 10^{-2}m/s to 5 x 10^{-2}m/s.

In conclusion, particulate bed coalescers allow a much larger operating period and, in the less-frequent event of excessive solids build-up, they can be periodically cleaned by fluidisation. Materials such as sand, pebbles, ballotini and plastic particles or grains are also less-expensive than manufactured synthetic fibres and porous materials. Hence, whilst the complete economics are not yet clear, it appears that granular or particulate media are likely to play an increasingly-important role in certain separation schemes, particularly those involving oily waste water treatment.

3.4 Basic Requirements of Packed Bed Coalescers

The requirements of a packed bed coalescer with regard to operating conditions and packing characteristics are,

a. The bed should be closely-packed and possess a high surface to volume ratio [77, 110].

b. The bed must be chemically-inert and mechanically-strong [57, 110].

c. The bed should be preferentially wetted by the dispersed phase [17, 57, 67, 110]. This is disputed by some authors [43, 75, 81] and is discussed in section 3.5.4.

d. Increased temperature promotes coalescence [78, 83].

e. Coalescence efficiency increases with bed depth [83], but an optimum exists between bed depth and pressure drop across the packing [16, 81]. Surface roughness is an important factor affecting the fundamental drop collection process [67, 81, 111]. Also, fine packings with high surface roughness are more efficient [66].

f. A high interfacial tension system is more easily-coalesced than one of low interfacial tension [57, 62, 77, 81, 111]. The presence of surfactants at high viscosities of either phase tends to significantly reduce coalescence, but this can be alleviated by operation at high temperatures [75, 81]. This is discussed in more detail in section 3.5.3.

g. The superficial velocity should be maintained between certain minima and maxima for a given packing [17, 78, 83, 110]. The minimum velocity places a practical limitation on coalescer area whereas the permissible maximum velocity increases with bed depth, as does capture efficiency [81]. However, there is an optimum thickness for each application since excessive bed depth causes redispersion of the coalesced drops [16, 110]. Operation at high velocities is also associated with high pressure drops and reduction in exit drop sizes, imposing higher limits on settler design [17]. Break- through of the secondary dispersion occurs if the critical separation velocity is exceeded. This is discussed in more detail in section 3.5.1.

h. For more efficient separation, especially for decontamination of jet fuels, a multi-element separator has been designed incorporating both a depth coalescer and a surface coalescer. Vessels have also been designed which contained two or more stage separators in a vertical or horizontal arrangement [66, 71, 72, 76].

3.5 Operating Parameters in the Coalescence of Dispersions in Packed Beds

Previous studies of secondary dispersions coalescence using some form of solid packing will now be discussed to establish the preferred features of a coalescing bed and the optimum operating conditions.

3.5.1 Superficial Velocity

Superficial velocity is simply the volumetric flow rate of the complete dispersion divided by the surface area across the empty coalescer cell, i.e it is the average linear velocity the fluid would have in the column if no packing were present [80].

The performance of a coalescer is usually assessed both by its efficiency in coalescing small drops and its ability to operate at a high superficial velocity with the lowest possible pressure drop [17].

The feasibility of glass fibre coalescers for crude oil desalting was studied by Burtis and Kirkbride [78]. They found that exit effluent concentration of secondary dispersion was reduced from 2.5% to 1% by weight by decreasing superficial velocity in the range 0.66×10^{-2} to 0.027×10^{-2} ms^{-1}. Bitten and Fochtman [112] studied the effects of liquid velocity on the distribution of water inside a fibreglass bed coalescing free water from a fuel/water emulsion. An increase in dispersion velocity always resulted in an increased amount of water at the influent face of the fibre bed and a decrease in the amount of water in the middle of the bed.

The separation of w/o secondary dispersion is only achieved using fibrous packings below a certain critical velocity [82, 83]. Below this velocity coalescence depends upon total contacting surface rather than on pore size [83].

In a previous investigation into the coalescence of o/w dispersions using sand beds, the author found that channelling phenomena occurred when the superficial velocity was higher than the flooding velocity [104]. Scheele and Clark [113] studied the coalescence of tetrachloroethylene drops at a plane organic-water interface for

velocities from 3 to 8cm/s. They found that the critical velocity decreased with continuous phase viscosity. Sareen *et al* [81] observed visually the performance of mixed fibres in coalescing different o/w dispersions. The superficial velocity was varied from 0.1×10^{-2} ms^{-1} and dispersed phase concentration was in the range 2% to 5% by volume. A critical separation velocity was identified above which retained drops were carried away before attaining the equilibrium size.

3.5.2 Pressure Drop

The pressure drop across a coalescer is a function of the dispersed phase hold-up or bed saturation, prevailing at the operating velocity [17]. Thus pressure drop has been used as an indication of stability of the flow conditions prior to taking samples of the effluent for either oil concentration or droplet size distribution measurement [35].

Langdon *et al* [75] used phenol-formaldehyde, coated glass fibres to separate an effluent of oil in water and found that the pressure drop during the runs increased from 13.8×10^3 to 172.4×10^3 Nm^{-2}. This was due to oil accumulation in the bed and, to a lesser extent, to mechanical degradation of the fibres.

Spielman and Goren [77] studied coalescence efficiency and pressure drop during the separation of oil-in-water secondary dispersions using glass fibre beds. Steady-state pressure drops for flow of prefiltered distilled water through the beds were found to obey Darcy's law [114]:

$$U = \frac{B}{\mu_c} \frac{\Delta P_1}{L} \qquad \ldots. 3.6$$

where B, the permeability coefficient for the bed, depends only on the properties of the bed. Therefore, the pressure drop across the packing increases linearly with increasing dispersion flow rate. Shak [115] used commercial glass fibres, bound together into a rigid structure by application of isobutyl methacrylate resin and subsequent heat treatment, to study pressure drop-vs-flow rate. The study was performed under

unsteady-state conditions, not the usual mode of operation of coalescers. As a result the pressure drop increased during operation.

The pressure drop associated with single phase flow through packed beds could be correlated by a Blake-Kozeny type equations such as [114]:

$$\frac{\Delta P_1}{L} = \frac{Ka^2 (1 - e_1)^2 \mu_c U}{e_1^3} \quad \ldots\ldots 3.7$$

where K is the Kozeny constant, and depends on the material and shape of packing used in the operation. This parameter is discussed in more detail in chapter 7.

3.5.3 System Characteristics and Properties

The physical properties of the phases (e.g interfacial tension, viscosity and density) and the properties of the system (e.g drop size, temperature, concentration etc) must be considered in the coalescence operation [72, 81, 105, 116, 117]. The rate of flocculation of droplets was determined by properties such as density difference between the phases, continuous phase viscosity and drop size distribution [116].

The important effect of system interfacial tension upon coalescence, and hence the performance of liquid-liquid dispersion separation in packed beds has been investigated [72, 81, 117]. Bartle [72] suggested that systems with interfacial tension as low as 20 x 10^{-3} Nm^{-1} can be separated satisfactorily; below this, separation becomes increasingly difficult. Vinson [117] observed little effect of interfacial tension; but when it was varied above 30 x 10^{-3} Nm^{-1} the performance of packing elements was found to decrease rapidly. Conversely Sareen *et al* [81] found that the higher the system interfacial tension, the easier it was to achieve a separation. With interfacial tension approximately equal to 20 x 10^{-3} Nm^{-1}, separation became difficult. However the interfacial tension was usually lowered by using surfactants during separation of oil-in-water dispersions hence introducing extraneous effects.

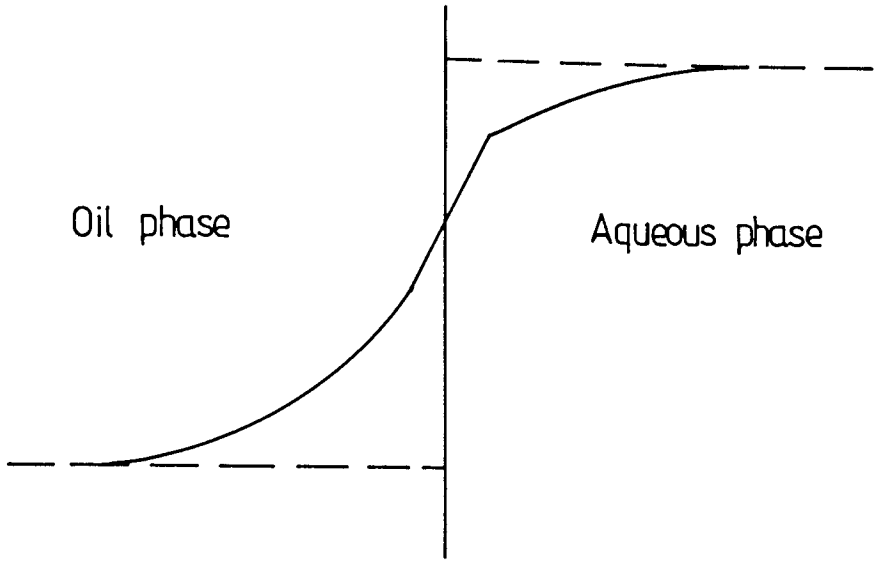

(a) No surfactant - main potential difference in oil phase

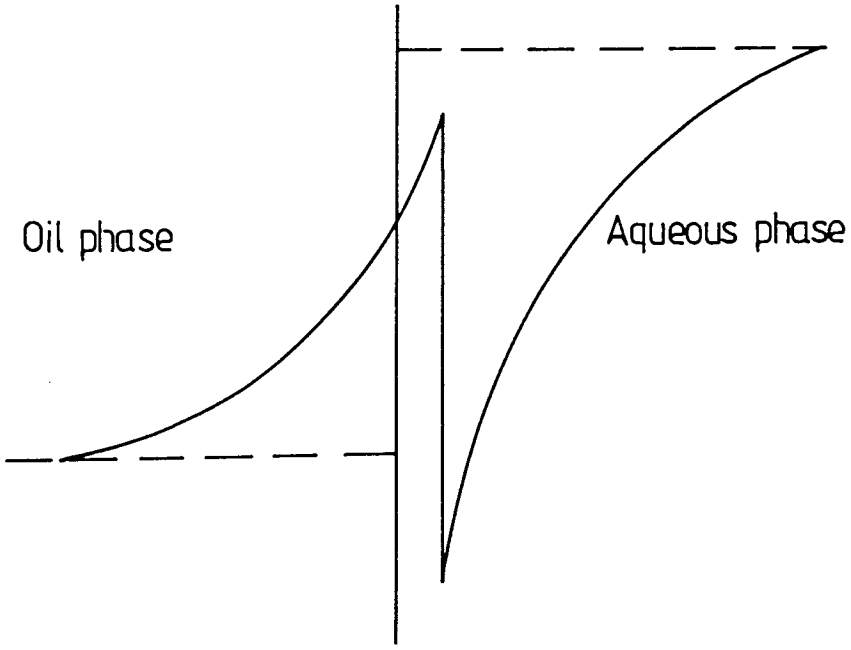

(b) Surfactant present - large potential difference now in aqueous phase

Figure 3.5 Effect of surfactants on the potential profile across the interface

Figure 3.5(b) represents a situation in which the formerly small potential drop in the aqueous phase (Fig 3.5(a)) has become very large, due to the high surface charge of adsorbed surfactant molecules, and the subsequent rearrangement of ions to preserve the electrical neutrality. This is for an ionic surfactant, which may be used as a stabiliser for oil-water emulsions. For a non-ionic surfactant, this mechanism is inapplicable, since there is no surface charge due to adsorbed ions [105].

Belk [40] studied the effects of organic compounds on the surface free energy of water and found that surfactants caused the most drastic decreases in the efficiencies of commercial filter/separators. Several theories have been presented as to how surfactants poison coalescer elements. Bartle [72] suggested adsorption of the surfactant by the element. Osterman [38, 96] suggested there was adherence on the media thus allowing the emulsion to pass through unaffected due to the change in fibre wettability. Lindenhofen [44] disagreed with the above theory and suggested that the surfactant film at the oil-water interface may present a mechanical or electrical barrier to the coalescence of water droplets in the media. More recently, Lindenhofen [118] suggested that commercial coalescers, which have a cotton outer wrapping, may malfunction because of the adsorption of surfactant from the continuous phase. These results confirm the theory, first presented by Hazlett [84], that poisoning is caused by interference with the detachment process at the points of release of drops.

From the above review, it is apparent that due to the effects of a surfactant on the packing and its performance, it is not scientific to study the effects of variation of system interfacial tension by adding surface active agents; it is preferable to use pure systems with other physical properties which are approximately similar.

High viscosities of either phase tend to significantly reduce coalescence efficiency but may be alleviated by operation at higher temperatures [119]. In the impingement mechanism of coalescence the viscous drag forces will increase with increase in continuous phase viscosity so that lower droplet sizes will break-away from the fibres attracting them [72]. Continuous phase viscosity will also afect the settling

velocity according to the Stoke's equation (equation 1.1).

Gutkowski et al [120] studied the influence of oil viscosity on the degree and saturation profile of a coalescer bed using o/w dispersions. The saturation profile depends upon oil viscosity. Spielman and Goren [77] separated two oils of different viscosity in oil-in-water dispersions using packed beds of glass fibre mats and found that the filter coefficient was independent of oil viscosity. Sareen [85] also suggested that viscosity had no effect on the critical separation velocity for velocities in the ranges 76.2 cm/min to 3.96 cm/min. Davies and Jeffreys [121] observed a decrease in critical velocity for dispersions in a glass fibre coalescer when the viscosity of the dispersed phase was increased. Hsu and Kintner [122] showed that when the surfactant concentration is high, the surface active molecules not only reduce the interfacial tension but also increase the viscosity of the continuous phase.

Density difference is an important consideration affecting positioning of the coalescence element and in the design of the after-settler [16, 17]. According to Stoke's equation 1.1 the direction in which the drop will move depends on the relative values of densities and the higher the difference in density between the liquid phases the higher the rate of settling and hence the smaller the settler required.

Doxastakis and Sherman [123] studied the rate of drop coalescence in concentrated corn oil-in-water dispersions stabilised with sodium caseinate. Both pH and the monoglyceride/diglyceride ratio influenced coalescence rate. Overall, the lowest coalescence rate was at pH 5.5 using 1% caseinate and 1% glycerides in the ratio of 5:2. However pH value is of less importance with regard to the coalescence mechanism. Nielsen et al [14] suggested that in nearly all cases, increasing the temperature decreases the lifetime of drops at an oil-in-water interface. The o/w interface was bowed upwards for oil drops or downwards for water drops. Hence, the interface always tended to 'curve around' the drops and to maximise their lifetimes.

Finally, Burtis and Kirkbride [78] studied the coalescence of crude oil using fibre glass coalescers and found that the coalescence efficiency was improved by,

i. Decreasing the phase ratio in the range 0.3:1 to 0.2:1 water/oil.

ii. Increasing packing density from 140 to 240 kg/m^3. Densities above 240 kg/m^3 were undesirable because of the high pressure required in operation.

iii. Increasing the temperature, 408K was found to be the optimum temperature, since operation above 450K was impractical due to the high pressure required to prevent vaporisation.

iv. Increasing bed depth, e.g up to 12.7 x 10^{-2}m was capable of reducing the concentration of salt in crude oil to 30 ppm. Hayes et al [32] confirmed these results and concluded that desalting of crude oil by glass fibre beds was commercially attractive.

3.4.4 Wettability

Wettability plays important roles in any multiphase flow through porous materials [124]. Qualitatively, wettability denotes the ease with which a fluid can displace other fluids. When two fluids A and B are in equilibrium on a solid surface S, as shown in Figure 3.6, interfacial tension (forces) γ_{S-B}, γ_{S-A} and σ_{A-B} will act along the three interfaces S-B, S-A and A-B respectively. Under static equilibrium, these forces will be interpreted according to the Dupre-Young equation:

$$\gamma_{S-B} = \gamma_{S-A} + \gamma_{A-B} \cos\theta \qquad \ldots. 3.8$$

where θ is the contact angle, i.e the angle between the solid surface and the liquid-liquid interface as measured through the liquid phase A. This angle is one of the most widely-used indices of wettability [1, 91, 124, 125]. Wenzel [126] suggested that the roughness of the solid surface may affect wettability. In addition, it has been predicted theoretically [127] and observed experimentally [128], that under dynamic conditions the contact angle depends upon the flow rate and hence will differ from the static contact angle. If θ is $< 90^\circ$, as shown in figure 3.6, the liquid phase (A) is said to wet the solid surface; likewise, a contact angle $> 90^\circ$ as illustrated in Figure 3.7, implies that the liquid

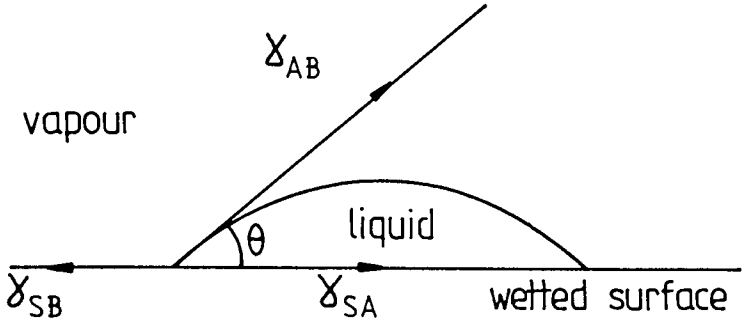

A contact angle $\theta < 90°$

Figure 3.6 Behaviour of a liquid drop at a wetted solid surface placed in vapour

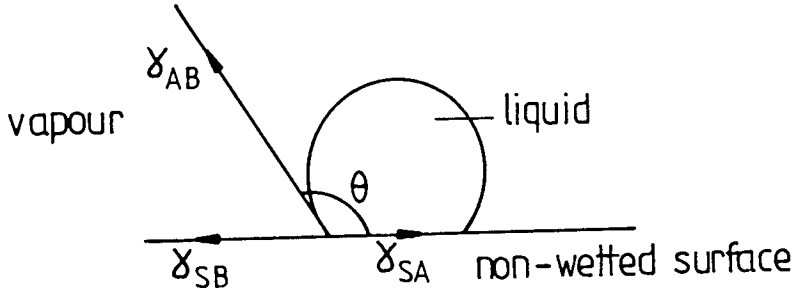

A contact angle $\theta > 90°$

Figure 3.7 Behaviour of a liquid drop at a non-wetted solid surface placed in vapour

phase (A) is non-wetting to the solid surface [124]. If $\theta = 0$ then the surface is completely-wetted by the dispered phase; $\theta = 180°$, which is rarely encountered in practice, corresponds to complete non-wetting [67]. For the water-air system $\theta = 0$ has been reported at a fresh soda-lime glass surface [129].

The contact angle provides information about solid surface energies, surface roughness, and the surface heterogenity. It is also a sensitive measure of surface contamination.

The main factors affecting the contact angle are:

a. Surface Roughness

Surface roughness is defined in terms of the average height to which asperities rise above the horizontal surface plane and the mean angle of inclination of the sides of asperities with respect to the horizontal plane of the solid surface [130]. Wenzel [126] investigated surface roughness and suggested a modified form of Young's equation:

$$r (\gamma_{SL} - \gamma_{SV}) = \gamma_{LV} \cos \theta' \quad \text{.... 3.9}$$

where 'r' is the ratio of the actual surface area to the geometrical surface area and is always > 1.0 except on an ideally-smooth surface when its value is unity, $\theta'$is the contact angle on the rough surface. Therefore, if the contact angle on a smooth surface is < 90°, roughening the surface would decrease the observed angle and vice versa.

b. Temperature

Since the physical properties of a system vary with temperature, the stability of a liquid drop is also temperature dependent. However, although contact angle varies with temperature, the variations observed are very small. Davies and Rideal [131] investigated the effect of temperature on contact angle values and found that $d\theta/dT$ for a high energy surface was -0.06 degree/degree C. Fowkes and Harkins [132] noted that the contact angle of water drops on low energy surfaces increased by 0.06 degree/ degree C.

c. Time

Borgin [133] studied contact angle variation with time for the system water-cellulose-air. Initially the angle was 30° but fell to 11° after a period of 24 hours. The initial decrease in the contact angle could be attributed to the fact that water penetrated into the cellulose mass so that the results are specific to this system.

d. Hysteresis

The term hysteresis applies to a contact angle which exhibits an increase or decrease from a previously determined value with time. Several theories have been proposed to explain hysteresis, for example it has been suggested that the degree of adsorption at a solid-liquid-liquid interface is different for the advancing and the receeding angle [134]. Other theories relate to the change in orientation of the polar groups [135]. Some workers consider that hysteresis can be avoided by careful experimental techniques but others assert that it is a fundamental phenomena [136].

e. Experimental Techniques

A wide variation has been found in the values of the contact angle of a sessile drop for a given system. Some of the variation is undoubtedly due to the use of different system specifications, e.g variation in contact angles on a glass surface may result from differences in the compositions of the glass. The composition of a solid surface is also altered by the treatment given to it [137]. Different surface treatments have been favoured by different workers, e.g cleaning the packings with an acid, such as chromic acid, exposes a fresh surface whereas cleaning with surfactant removes all the surface active compounds from the surface, which after washing with deionised water and finally drying in an oven at 120°C, could be treated by a preferential wetting technique [74].

Sareen *et al* [81] using a photomicrographic technique, concluded that preferential wetting was not the controlling factor since drops that adhered to the packing did not wet it. A similar conclusion was reached by Davies and Jeffreys [92].

Bascom and Singleterry [138] studied the effect of polar and non-polar solutes on the contact angles exhibited by water drops on packing surfaces submerged in organic solutions and found that a parabolic relation exists between cos θ and the oil-water interfacial tension. Voyutskii [83] studied water-in-oil secondary dispersions separation with varying relative wettability. Burtis and Kirkbride [78] concluded that the packing must be preferentially wetted by the dispersed phase. Hazlett [84] accepted this principle to explain the attachment mechanism. Farley and Valentin [43] concluded that water-wetted packings were far superior to oil-wetted ones for the separation of oil from water. Langdon *et al* [75] considered the separation performance of a packing to be mainly determined by its wetting properties. Recently, Najmi [67] suggested that the behaviour of primary drops impinging upon a solid-liquid interface, is immediately dependent upon the wetting or non-wetting nature of the surface (i.e upon the surface characteristics).

In conclusion, although droplets in secondary dispersions tend to retain their sphericity when retained upon a packing surface, wettability is recognised as important in coalescence of primary dispersions. Therefore, since secondary dispersion drops coalesce to primary-sized drops at some stage within the packing neglecting consideration of wetting properties of packing for secondary dispersions could be misleading.

CHAPTER FOUR

COALESCENCE MECHANISMS AND MODELS OF THE BEHAVIOUR OF DROPLET COALESCENCE IN PACKED BEDS

4.1 Mechanisms of Capture, Coalescence, Flow and Release in Packed Beds

Both primary and secondary dispersions may co-exist during coalescence in a packed bed. Therefore discussion of the mechanisms, whatever the drop sizes, will be combined. The coalescence process will be considered in three basic stages, namely droplet capture, drop coalescence and flow of the bulk phase through the packing, and finally release of the coalesced drops. This approach is convenient because most previous workers have defined three stages of capture, flow and release although they have either disagreed as to the mechanisms postulated or found them inapplicable to the specific system under consideration.

4.1.1 Drop Capture

Any coalescer designed to treat a secondary dispersion must first be able to capture the drops then retain them in close proximity with others. The capture of a drop suspended in a flowing continuous phase is theoretically possible by one or more of the following occurrences:

1. Collision with another drop suspended in the dispersion.
2. Collision with an obstruction in the packing structure.
3. Collision with another drop which has been captured and is attached to the packing structure.

Sareen *et al* [81] reported that the probability of the first occurrence is very low. Although collisions with the packing structure are important, especially during the initial transient operation of a coalescer; the drop collection rate is considerably enhanced by the presence of drops held within the interstices and attached to the packing structure.

Bitten [139] observed growth of drops attached to fibres due to coalescence with drops captured from a flowing dispersion. This significant role of retained drops in contributing to capture is also confirmed by the experimental data of Ghosh and Brown [140]. Sherony and Kintner [111] derived a theoretical model of a fibrous bed coalescer which related the collision efficiency between drops and fibres to the overall coalescence efficiency. This model took into account the mean inlet drop size, mean fibre size, degree of saturation, bed length and superficial velocity through the bed, and this approach was further modified by Rosenfeld and Wasan [141] by inclusion of an effective fibre diameter.

Modelling drop capture processes is inherently difficult due to the complex interfaces which exist between the dispersed and continuous phases and the solid surfaces of the packing. A convenient way of analysing the collection mechanisms is to consider the behaviour of a drop or particle as it approaches a collector. Cylindrical collectors describe the geometry of fibrous beds and spherical collectors characterise granular media.

To describe and compare possible drop capture mechanisms, the geometrical model illustrated by figure 4.1 is proposed which represents drops approaching either a cylindrical or spherical collector [142].

4.1.1.1 *Indirect Interception*

The diameter of the collector may be comparable to the drop diameter. Under these conditions, the finite size of the drops cannot be neglected and interception between the drop and collector becomes significant [16]. This mechanism is characterised by the value of the interception number $N_R = \frac{d_p}{d_c}$. The capture efficiency is defined as the number of drops captured to the number of drops approaching within the projected area of the collector per unit time. The Reynolds number, N_{Re}, based on the diameter of the collector, is included because of its influence on the streamlines [143].

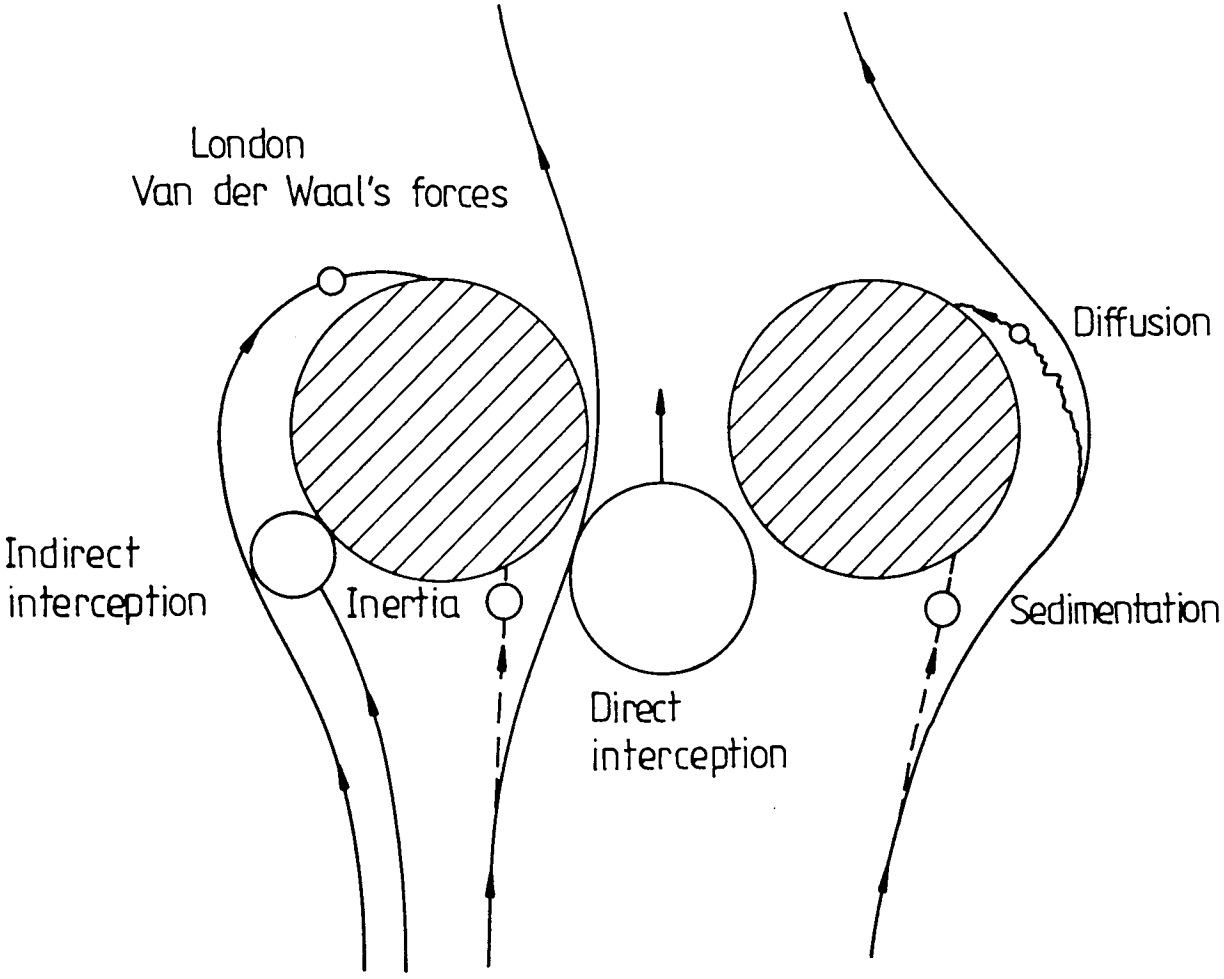

Figure 4.1 Depiction of drop capture mechanisms

Hazlett [84], and Rosenfeld and Wasan [141] proposed the use of an equation developed by Langmuir [144] to evaluate the interception mechanism. The decrease in filter coefficient as the superficial velocity increases may not be due to a decrease in drop capture efficiency since Davies and Jeffreys [92] concluded that an optimum velocity exists for a given packing.

For a spherical collector, Rajogopalan and Tien [145] described the efficiency due to indirect interception by the following equation:

$$\eta_I = 1.5\, N_R^2 \qquad \ldots. 4.1$$

This equation shows the increasing influence of indirect interception for increasing values of N_R.

4.1.1.2 *Direct Interception*

Interception by pore catchment occurs when an approaching drop is arrested by a pore through which it cannot pass (see figure 4.1). The drop is hence captured and subsequently coalesced with a retained drop [72]. Wilkinson et al [73] suggested that for primary-dispersion sized drops the coalescence rate is very low when the drop diameter is less than the equivalent diameter of the packing interstice, even when the dispersed phase wets the packing. Direct interception of a drop may be characterised by a second interception number $N_{Rd} = \frac{d_p}{d_a}$. Inspection of N_{Rd} shows that pore catchment will contribute significantly to the capture rate when either drop diameter increases by coalescence, or when the equivalent diameter of the interstices, d_a is significantly decreased [16]. The value of η_{DI} equals to 1.0 at $N_{Rd} \geq 1.0$ and it equals zero at $N_{Rd} < 1.0$ [27].

Recently, Soo and Radke [146] suggested that re-entrainment of interception-captured drops may take place in several different ways. When a repulsive

hydrodynamic force on the drops overcomes London Van der Waals and electrostatic attraction forces between the drops and the sand grains used in a packed coalescer, the captured drops may re-entrain. Alternatively when flow is interrupted, drops in the recirculation eddies may re-enter the flow stream. In addition, at high velocities and with a low interfacial tension system, captured drops may break-up. They also concluded that at low velocities with drops sizes smaller than pore sizes, drops are captured in crevices or trapped in caverns where flow is almost stagnant. The drops captured at the critical re-entrainment velocity can be re-entrained into the flowing stream and drops squeeze through pore constrictions. Therefore those trapped in crevices or in caverns re-entrain only when flow conditions are disturbed.

4.1.1.3 *Inertial Impaction*

When the density of the dispersed phase exceeds that of the continuous phase, the trajectory of a drop as it approaches a collector, may not coincide with the fluid streamlines due to the inertia of the drop. This mechanism is important in filtration where the density difference is high and the viscosity of the continuous phase is low [147].

Sareen *et al* [81] reported that if a droplet has the same relative mass as the field phase, it will usually follow the fluid streamlines around any obstruction in the stream, and if the flow is turbulent and if vortices occur, the drop can be brought to a fluid interface even if the density difference is low. However Redman's [148] opinion, was that low density difference systems are extremely difficult to coalesce and that if the drop density is less than that of the field liquid, the inertial impaction mechanism will act to prevent drops approaching the fibre or other drop surface.

Hazlett [37] and Sherony and Kintner [111] considered this mechanism relevant to coalescence in fibrous beds and characterised its contribution by the magnitude of the Stokes number

$$N_{stk} = \frac{d_p^2 \rho_c U}{9 \mu_c d_c} \quad \text{.... 4.2}$$

Impaction becomes significant when N_{stk} exceeds a critical value which depends on the Reynolds number. Langmuir [144] determined N_{stk} critical to be 0.063. The latter value was applied by Sherony and Kintner [86] for viscous flow conditions which would have overestimated the significance of impaction. For a spherical collector, the efficiency due to inertial impactions could be calculated by the following equation [27]:

$$\eta_{II} = N_{stk}^3/(N_{stk}^3 + 0.77\, N_{stk}^2 + 0.22) \quad \text{.... 4.3}$$

4.1.1.4 *Sedimentation*

The density difference between dispersed and continuous phases also causes the drop trajectories to deviate from the fluid streamlines due to buoyancy forces. Their magnitude is characterised by the Gravity number [145],

$$N_G = \frac{d_p^2 (\rho_d - \rho_c) g_c}{18 \mu_c U} \quad \text{.... 4.4}$$

which is the ratio of the drop terminal velocity assuming a viscous flow condition, to the superficial velocity of the dispersion flowing through the bed. Rajagopolan and Tien [145] showed that the capture efficiency is equal to the value of the Gravity number,

$$\eta_G = N_G \; ; \; N_G > 10^{-3} \quad \text{.... 4.5}$$

and that the contribution due to sedimentation is negligible for $N_G < 10^{-3}$.

With reference to figure 4.1, it should be emphasised that gravity forces aid drop capture upstream of the collector but oppose collection on the downstream side [16].

4.1.1.5 *London Van der Waal's Forces*

As the drop approaches the collector London van der Waal's dispersion forces increase rapidly to overcome the hydrodynamic retardation effects or to offset any double layer interaction [149, 150]. The London dispersion forces arise from the interaction of fluctuating electrical dipoles with induced dipoles in neighbouring atoms or molecules. These forces therefore depend upon the electrical properties of the volume elements involved and the distance between them, but are independent of temperature [151, 152]. Sherony and Kintner [153] concluded that Van der Waal's repulsions as well as attractions are also possible and, in a system in which the dispersed and continuous phases are of the same chemical structure, both are probable.

Spielman and Fitzpatrick [150] described the attraction between a liquid-liquid system and a plane surface by the equation:

$$\text{Adhesion Number, } N_{Ad} = \frac{4\,Q}{9\,\pi\,N_R^2\,\mu_c\,A_s\,U\,d_p^2} \qquad \ldots. \; 4.6$$

Adhesion Number also represents a measure of the London dispersion forces which may exist in the coalescence of a secondary dispersion in a packed bed. For a spherical collector, Spielman and Fitzpatrick [150] described the capture efficiency due to London Van der Waal's forces by following equation:

$$\eta_L = 2\,A_s\,N_R^2\,(9/5\,N_{Ad})^{0.333} \qquad \ldots. \; 4.7$$

where As is a function of bed voids. Happel's [155] model for flow around a characteristic spherical grain gave:

$$A_s = 2\,(1-\gamma_s^5)/(2 - 3\gamma_s + 3\gamma_s^5 - 2\gamma_s^6) \qquad \ldots. \; 4.11$$

with $$\gamma_s = (1 - e_1)^{0.333} \qquad \ldots. \; 4.12$$

4.1.1.6 *Diffusion*

Brownian motion, due to bombardment of suspended drops by continuous phase molecules may contribute to the capture efficiency. Prieve and Ruckenstein [154] have demonstrated that separate treatment of this mechanism is adequate. Sherony [165] and Shalhoub [57] evaluated a theoretical collision frequency due to coagulation using the hydraulic diameter of the interstices as a first estimate for the size of large scale turbulence. Their calculations indicate a negligible contribution from a diffusion mechanism.

$$\text{The Peclet number, } N_{pe} = \frac{d_c U}{D_{BM}} = \frac{3 \pi_c d_p d_c U}{K'T} \qquad \ldots. \ 4.8$$

is often introduced to characterise diffusion and is a measure of the ratio of transport by convective forces to transport by molecular diffusion [145]. Some workers investigating diffusion for low Reynold's numbers employed the Sherwood number [16],

$$N_{sh} = \frac{I}{\pi d_c D_{BM} C_a} \qquad 4.9$$

as a measure of the mass transfer or deposition rate. This approach is useful for correlation of results for different collector geometries. For a cylindrical collector, the Sherwood number is related to capture efficiency by

$$N_{sh} = \eta_D N_{\rho e} \qquad \ldots. \ 4.10$$

The equations developed in several investigations of diffusional transport of drops have been rearranged using equation 4.10 and are presented in table 4.1. Examination of these modified forms shows a common relationship between capture efficiency and Peclet number, with slightly differing dependency on Reynolds number. Any of these equations may be applied without incurring significant errors since the capture efficiency due to diffusion alone is relatively small.

Table 4.1

Comparison of Equations Describing Drop Capture by Diffusion

Investigator	Proposed Equation for Travel Through Bed	Diffusion Capture Efficiency
Langmuir [144]	$\eta_D = 2.16(2A)^{-1/3}N_{Pe}^{-2/3}$	$2.16(2A)^{-1/3}\ N_{Pe}^{-2/3}$
Natanson [156]	$N_{Sh} = 1.17\pi(2A)^{-1/3}N_{Pe}^{1/3}$	$3.68(2A)^{-1/3}N_{Pe}^{-2/3}$
Friedlander [157]	$N_{Sh} = 1.035\pi(2A)^{-1/3}N_{Pe}^{1/3}$	$3.25(2A)^{-1/3}N_{Pe}^{-2/3}$
Ranz [156]	$\eta_D = \frac{\pi}{N_{Pe}}(1/\pi + 0.55N_{Sc}^{1/3}N_{Pe}^{1/2})$	$N_{Pe}^{-1} + 1.727N_{Re}^{1/6}N_{Pe}^{-2/3}$
Emi [143]	$\eta_D = 6\ N_{Re}^{1/6}N_{Pe}^{-2/3}$	$6N_{Re}^{1/6}\ N_{Pe}^{-2/3}$
Rajagopalan [145]	$\eta_D = 4.04\ N_{Pe}^{-2/3}$	$4.04\ N_{Pe}^{-2/3}$
Prieve [154]	$N_{Sh} = 0.995\ N_{Pe}^{1/3}$	$3.98\ N_{Pe}^{-2/3}$
Spielman [150]	$\eta_D = 2.3(2As)^{-1/3}N_{Pe}^{-2/3}$	$2.3(2As)^{-1/3}N_{Pe}^{-2/3}$

where $A = 2 - \ln N_{Re}$

4.1.2 Coalescence Processes

4.1.2.1 *Coalescence Sites*

Drops captured within a packed bed will continue to grow by further capture and coalescence until hydrodynamic forces cause their detachment from the coalescence site. Figure 4.2a demonstrates that when the drops are small compared with the collector and aperture diameter, coalescence may take place between adjacent drops located on the collector surface. Bitten [139] reported that this was a slow process for the coalescence of drops on single fibres compared to growth by acquisition of the dispersed phase from the flowing dispersion (figure 4.2b).

Davies and Jeffreys [92] proposed that the coalescence of a drop into a liquid film, which either adheres to the collector surface or occupies the packing void, is the predominant mechanism for primary dispersions when the dispersed phase wets the packing (figures 4.2c and 4.2d). For the converse situation, coalescence may occur between two freely-moving drops (figure 4.2e); this may be important for primary dispersions but experimental observations refute this possibility for secondary dispersions coalescence [81, 111]. Alternatively, drops captured by direct interception and retained by the collectors, may then trap other approaching drops and subsequently coalesce with them (figure 4.2f). The drops increase in volume by coalescence until the buoyancy forces exceed the restraining interfacial tension forces, deformation of the drop then occurs as it is squeezed through the aperture [95].

4.1.2.2 *Drop Passage Through Interstices*

Drops which simultaneously approach a pore are likely to jostle for priority before one of them passes through it (figures 4.2g and 4.2h). However important differences exist between the conditions under which secondary and primary coalescers operate. Secondary dispersion drops possess more surface energy per unit mass due to their size and also buoyancy forces are usually negligible. Therefore drop deformation, and drainage of the intervening continuous phase film prior to coalescence, is less-easily

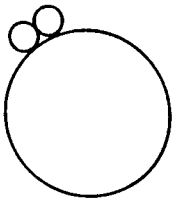

Small
Drop : Collector
Diameter Ratio

(a) Adjacent drops (both in contact with collector)

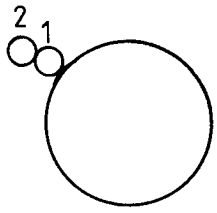

(b) Adjacent drops (drop 2 captured by and coalesced with 1)

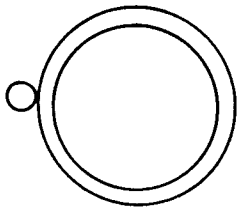

Wetted
Packings

(c) Coalescence with film of dispersed phase adhering to collector

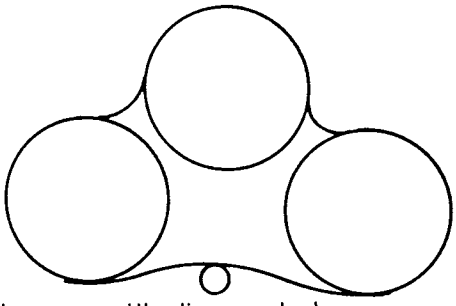

(d) Coalescence with dispersed phase retained in packing void

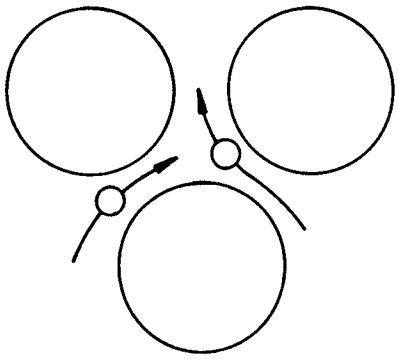

Non - wetted
Packings

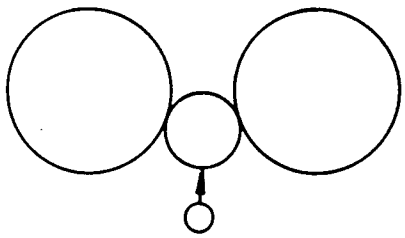

(e) Interdrop coalescence between freely moving drops

(f) Interdrop coalescence between one moving drop and another retained by collectors

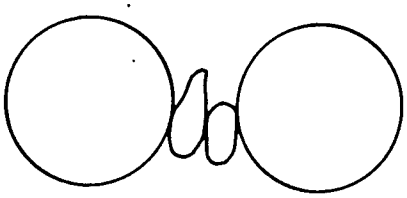

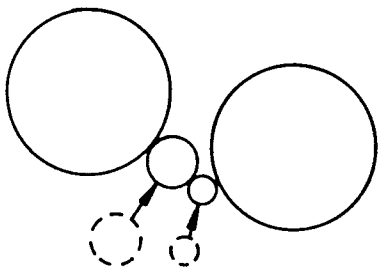

(g) Deformation as drops jostle for position which causes drainage of the intervening film causing coalescence

(h) Coalescence after one drop has gained priority

(i) Coalescence of a locally formed dispersion band upstream of a blocked pore

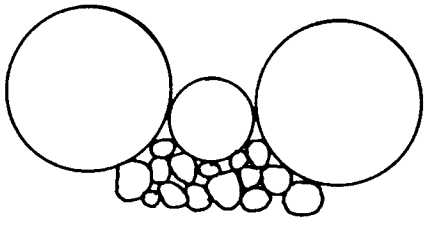

Figure 4.2 Coalescence mechanisms in a Packed Bed

accomplished. For that reason the retention-impact-release mechanism is unlikely to be important for secondary dispersions [16].

The drops attaining a critical diameter for release from a collector are likely to be immediately recaptured by direct interception (see section 4.1.1.2). This provides evidence that pores may become blocked by large drops, or by simultaneous approach of smaller ones. If blockage happens frequently fewer channels are available for flow of the dispersion and the pressure gradient per unit length of the bed will increase. As more flow paths become blocked, the increasing pressure gradient will eventually be sufficient to force coalesced drops through the pores. This proposed mechanism is illustrated in figure 4.2i.

An experimental study of collisions and coalescence of drops on single fibres showed that capture efficiency is unlikely to be affected by whether or not the fibre is wetted [139].

Recently Soo and Radke [146] studied velocity effects in emulsion flow through porous media. They proposed that when a drop lodges in a small pore, it may be re-entrained into the flowing stream if the flow velocity is increased enough to provide a local dynamic pressure drop larger than the capillary resistance. As the pressure rises, at larger flow rates the drops may squeeze through successively smaller pore constrictions until, at very large velocities, they undulate through the entire porous medium. Although the process appears continuous, it is actually a capture event followed by a re-entrainment event. In the case of deformable droplets, the retention profiles are strongly coupled to the local pressure drop.

4.1.3 Flow Through the Bed

Drops, which have been collected and reside in the packing interstices until they are coalesced, act as potential collectors for other drops entering the bed.

4.1.3.1 *Droplet Break-Up or Redispersion*

After coalescence by one of the mechanisms described in the previous section, movement of the coalesced dispersed phase may occur by release of the drop from the packing when the drag forces exceed adhesive and London attractive forces.

Vinson and Churchill [82] states that cohesive failure results when only part of the drop is detachable. Also the cohesion mechanism involves formation of threads which subsequently break-up into smaller drops which are then redispersed into the flowing continuous phase. The size of these drops depends on attenuation of the liquid threads which is suggested to be a function of viscosity ratio $\frac{\mu d}{\mu_c}$ [85].

There exists a critical velocity above which redispersion occurs which considerably reduces separation efficiency due to both redispersion and the drops moving too fast for capture. However values of reported critical velocity vary over two orders of magnitude [17]. These values are of little use in practical coalescer design because they were specific to the liquid and packing properties.

In addition to cohesive failure, redispersion may also be attributed to secondary drop formation during the coalescence process [158].

4.1.3.2 *The Travelling Drop Hypothesis*

Sherony and Kintner [153] and Rosenfeld and Wasan [86, 141] have proposed that drop release is by adhesion failure after which the large drops travel through the pores of the medium. Hazett [37] reported that channeling behaviour occurred when threads of dispersed phase were observed in a fibrous bed during the coalescence of a water-in-fuel dispersion. Whilst saturations in the region of 20% are typical for high porosity bed [149], if the dispersed phase flows in a small number of channels, a low saturation does not necessarily imply the absence of a continuum.

4.1.3.3. *Critical Drop Diameter*

The travelling drop models also assume that when drops are detached from packing elements, their passage through the bed to the exit face remains unimpeded; their diameters should therefore be less than the pore diameters [16]. Individual fibres were reported to retain drops having diameters many times greater than those of the fibres without re-entrainment for velocities up to 2×10^{-2}m/s [153].

Rosenfeld [159] developed an equation to calculate the critical drop diameter for release but this predicted unrealistically large values. There is no evidence to support this, and calculations performed for both high and low porosity beds using maximum values of saturation and superficial velocity yield minimum critical diameters several times larger than the pore sizes [16].

4.1.4 Exit Drop Release

Various observed drop release patterns are illustrated in figure 4.3.

4.1.4.1 *Ballooning*

The balloon-shaped drops grow until the hydrodynamic buoyancy forces exceed the interfacial tension forces. Rupture then occurs at the neck of the drop whose size, when released, depends on the flow velocity and interfacial tension [16, 78, 144].

For the non-wetting situation, Hazlett [84] derived an expression to predict the size of released drops,

$$d_{Pe} = \frac{0.55\, d_c^{0.71}\, \gamma^{0.71}}{\Delta U\, \rho_c^{0.29}\, \mu_c^{0.43}} \qquad \ldots. 4.13$$

For $dc < 0.1\, d_{Pe}$, and $0.3 < N_{Re} < 1000$ where $N_{Re} = d_p\, \rho_c\, U / \mu_c$

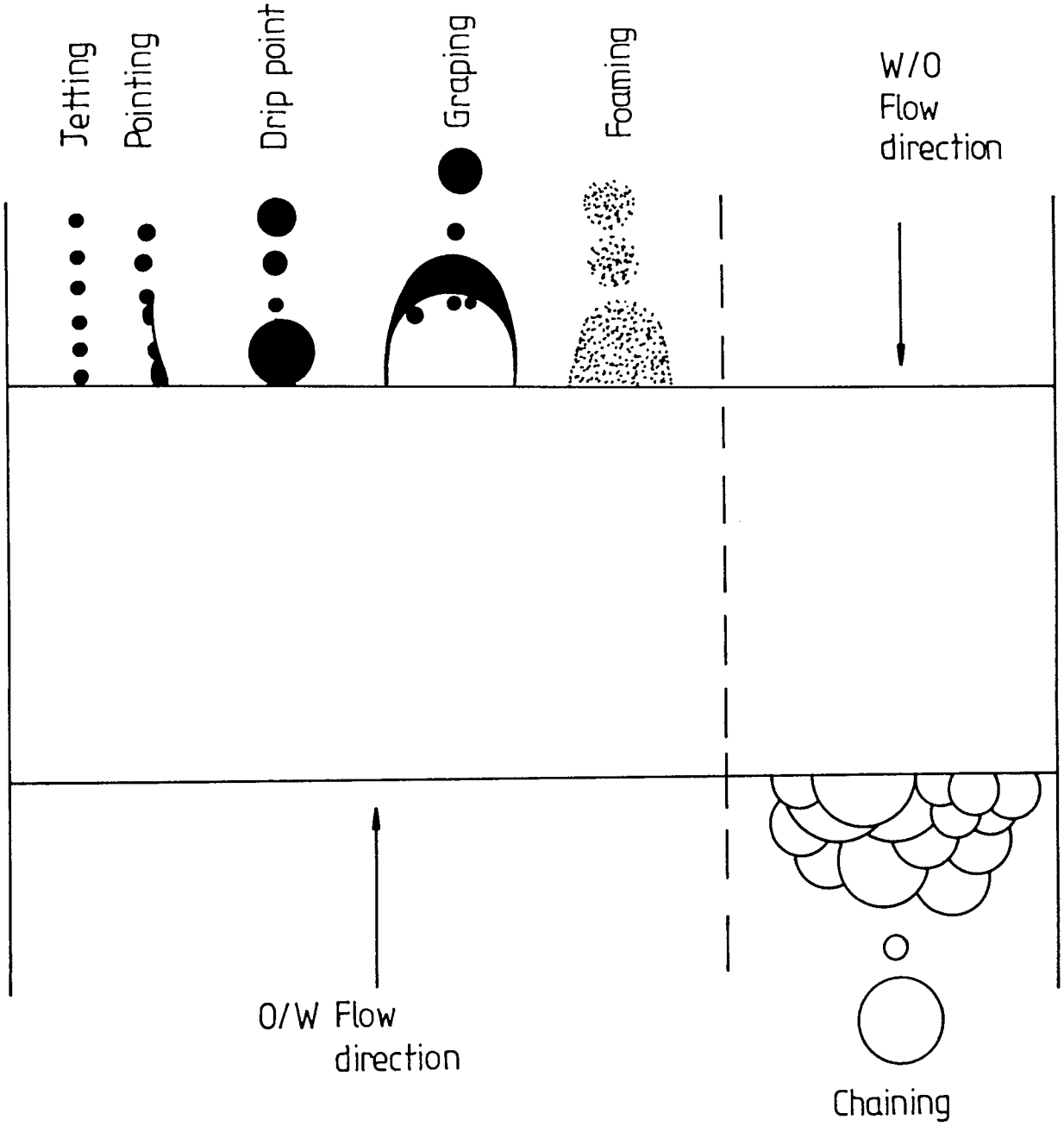

Figure 4.3 Various types of mechanisms of release

4.1.4.2 *Pointing*

In pointing 'fingers' of collected drops project beyond the exit face. These 'fingers' taper to a point, vibrate and kick small drops from the tip [16]. The size has been reported to range from 0.2 x 10^{-3}m to 0.5 x 10^{-3}m depending on the packing diameter, bed depth and superficial velocity [16, 17].

4.1.4.3 *Jetting*

In this mechanism a droplet with a high velocity enters a pore at the exit surface and passes through without any retention on the surface. Many correlations are available for prediction of drop sizes produced by a jetting mechanism but they only strictly apply when the continuous phase is stationary [95].

4.1.4.4 *Graping*

Graping occurs when the film of dispersed phase blocks some of the outlet pores and continuous phase pushes this film to form a 'grape' filled with continuous phase [16, 17, 57, 104]. When the drop is sufficiently thick the buoyancy and drag forces cause it to break away giving one or two satellite drops. The size of grape is dependent on the velocity of flow.

Langdon [91] and Linderhofen [44] reported that a graping release pattern is encouraged when the phase ratio is high, or when the dispersed phase wets the packing. Shalhoub [57] and Attarzadeh [17] observed that satellite drops in the size range 1.5 x 10^{-3} to 2.5 x 10^{-3}m in diameter were released from the top of the grape, but in the final stage, the grape ruptured yielding one large drop of about 4 x 10^{-3} to 5 x 10^{-3}m in diameter and several very small drops.

4.1.4.5 *Foaming*

This release mechanism, observed at low bed depths in low voidage packings

is defined here as 'flooding' of the packing [17]. Ibrahim [104] observed that with a packing of 250μm mean sand particle diameter compressed to a depth of 10×10^{-3}m a foam- like dispersion was formed at the exit face of the coalescer.

4.1.4.6 *Chaining*

Attarzadeh [17, 106] reported that 'chaining' was only observed with water/ oil dispersions. Drops grew on the exit surface of the packing and adhered together to form a large bunch of drops. Ultimate release of the drops by this mechanism produced primary drops so that, unlike foaming, this type of release is acceptable. However release of the drops caused some disturbance of the exit flow so that this kind of release is not ideal.

Austin [16], Ibrahim [104], and Baez Poleo [27] all observed that when the bed consisted of random packings drop formation takes place by a combination of all the mechanisms described above.

However formation predominantly by the ballooning mechanism is desirable, since it produces large drops that require short residence times in the subsequent settler.

4.2 Models of the Coalescence of Dispersions

The design of coalescing devices was until 1969 largely empirical. Some mathematical models were later derived to assist in the design of coalescers. These are reviewed below.

4.2.1 Emi and Okuyama's Model

Emi and Okuyama [143] reported that the separation efficiency of an isolated fibre due to the combination of four mechanisms was as follows:

1. Indirect interception (η_I)

The interception efficiency for the viscous flow region had been expressed by

Langmuir [144] as:

$$\eta_I = \frac{1}{2\,(2 - \ln N_{Re})}\left[2\,(1 + N_R)\ln(1 + N_R) - (1 - N_R) + \frac{1}{1 + N_R}\right]$$

.... 4.14

2. Inertial - interception (η_{II})

Efficiency of inertia-interception has been obtained as a function of three parameters, N_{Re}, ψ and N_R. In experimental work both N_{Re} and ψ were varied simultaneously and an attempt was made to represent the efficiency by two parameters for convenience, using the relation:

$$\psi = K_m N_{Re} N_R^2 \qquad \text{.... 4.15}$$

Values of K_m depend only on the properties of the secondary dispersion but the range of values was narrow; hence K_m can be regarded as nearly constant, e.g $K_m = 53.5$ [143].

3. Diffusion (η_D)

Friedlander [160] proposed a semi-empirical equation for diffusion efficiency from his experimental work. It was expressed in the following form:

$$\eta_D = 6\, N_{Re}^{1/6}\, D_c^{2/3} \qquad \text{.... 4.16}$$

where

$$D_c = 1/N_{Pe}$$

4. Settling-interception (η_{GI})

Individual droplets have a certain sedimentation velocity due to gravity. The expression for collection efficiency in such a case involving vertical downward flow was:

$$\eta_{GI} = \frac{1 + N_R}{1 + N_G}\left[\frac{1}{2(2 - \ln N_{Rc})}\left\{\frac{1}{(1 + N_R)^2} - 1 + \ln (1 + N_R)^2\right\} + N_G\right] \quad \text{.... 4.18}$$

When the direction of flow was horizontal, the equation derived was:

$$\eta_{GI} = \left[\frac{1 + N_R}{\sqrt{(1 + N_G^2)\,[1 + \{N_R^2/(2 - \ln N_{Rc})\, N_G\}^2]}}\right]$$

$$\left[\frac{N_R^2\,\{1/(1 + N_R)^2 - 1 + 2 \ln (1 + N_R\}}{2\,(2 - \ln N_{Re})^2\, N_G} + N_G\right] \quad \text{4.19}$$

However, there was only a small difference between η_{GI} values in equations 4.18 and 4.13. When neglecting the effect of interception ($N_R = 0$), equations 4.18 and 4.19 reduced to equations 4.20 and 4.21 respectively

$$\eta_G = N_G/(1 + N_G) \quad \text{for vertical downward flow} \quad \text{..... 4.20}$$

$$\eta_G = N_G/\sqrt{1 + N_G} \quad \text{for horizontal flow} \quad \text{.... 4.21}$$

Finally, the total efficiency of an isolated fibre could be predicted from the expression,

$$\eta_{GTID} = \eta_{GTI} + \eta_D \quad \text{.... 4.22}$$

where $\eta_{GTI} = \eta_{GI} + (\eta_{TI} - \eta_I)$ for $\eta_{GI} > \eta_{TI}$

$$\eta_{GTI} = \eta_{GI} + (\eta_{GI} - \eta_I) \text{ for } \eta_{GI} > \eta_{TI} \quad \text{.... 4.23}$$

4.2.2 Hazlett's Model

Hazlett [37, 84] based his model on three main steps:

a. Approach of a droplet to a fibre or to a droplet attached to a fibre;

b. Passage of collected liquid through the bed;

c. Release of an enlarged droplet from a bed surface.

The approach of a droplet to a fibre could occur by one, or more, of the following

mechanisms:

i. Interception

In evaluating the interception mechanism, under laminar flow, the equation developed by Langmuir (ie equation 4.14) was useful.

ii. Diffusion

A particle moving within a fluid would tend to depart from the flow streamlines. The most important mechanism affecting this departure was the random transverse motion due to diffusion.

Langmuir [144] related the efficiency of the diffusion mechanism for a single, isolated fibre to the diffusion coefficient of an aerosol particle at low velocities by,

$$Es = 2.16\left[\frac{1}{2\,(2 - \ln N_R)}\right]^{1/3}\left[\frac{D_c}{V d_f}\right]^{2/3} \quad \ldots. 4.24$$

where $D_c = \dfrac{3.0 \times 10^{-13}}{dp}$; V = flow velocity of fuel (cm/s)

The efficiency decreases with an increase in flow velocity, increase in particle size, or increase in fibre size. However, diffusion would be important only for droplets less than 1 micron in diameter and then only if the fibre diameter were less than 1 micron [84].

iii. Inertial Impaction

In aerosol filtration, inertial impaction was a significant mechanism for particles removal [161]. Because of the low viscosity and density of air, inertial impaction was the most important mechanism at high flow velocities. Since the density of jet fuel was close to that of water, and the viscosity of a liquid was much higher than that of a gas, the significance of inertial impaction was deduced to be less important for water-in-fuel secondary dispersion separation than for aerosols [84]. To evaluate the contribution of this mechanism to coalescence, the inertial parameter, K_a, of aerosol

technology was calculated for various conditions using the equation [162]:

$$K_a = \frac{(\rho_{H20} - \rho_F)\, U\, (d_p)^2}{9\, \mu\, d_f} \qquad \ldots. 4.25$$

where ρ_F = density of fuel (gm/cm^3)

The value of K_a increased with velocity and with water drop size. It decreased, however, as the fibre diameter (d_f) increased [84].

The application of the inertial parameter to efficiency calculations was based on an empirical basis. Landahl and Hermann [163] used the formula:

$$Es = \frac{K_a^3}{K_a^3 + 1.54\, K_a^2 + 1.76} \qquad \ldots. 4.26$$

to determine filtration efficiencies for aerosols at high Reynolds numbers > 10. The efficiency of inertial impaction fell rapidly as K_a decreased and this mechanism was therefore inefficient in most fibrous bed coalescers. Moreover, the velocity must be high and drop size large to attain a significant efficiency [84].

The release mechanism was considered to involve coalesced droplets forming threads through the bed until released as individual drops from the exit face. The size of the released drop was evaluated by:

$$dp = \frac{0.90\, do^{0.71}\, \gamma^{0.71}}{(\Delta V)\, \rho_F^{0.29}\, \mu^{0.43}} \qquad \ldots. 4.27$$

For a viscosity in the range 0.5 to 1.0 C.P., which is typical of the water-jet fuel system, the elongation of a thread was proportional to a dimensionless number F*:

$$F^* = \frac{2\, G\, \mu\, (dp/2)}{\gamma} \qquad \ldots. 4.28$$

where G is the shear rate.

The elongation became more sensitive to an increase in F* at distortions near

those where rupture took place. The rupture of the extended thread produced a series of drops of uniform but smaller size. The effect of interfacial tension on elongation is apparent in equation 4.28 [84].

4.2.3 Vinson and Churchill's Model

Vinson and Churchill [82] proposed a model on the assumption that the probability of a drop colliding with a filter was normally large compared with the probability that it would collide and coalesce with another drop in the flowing stream. It was further assumed that the approach of a drop to a filament was due to direct interception and that Brownian movement was negligible, since it was only effective for sub-micron size drops.

The phenomena of drop-filament approach, film thinning, adhesion and disengagement could be described by seven independent dimensionless groups as in Table 4.2.

An equation was given to represent the separation performance of a filter. However, it was not based on any theoretical model; it was obtained by fitting experimental data for the system studied using three layers of nickel screen treated with octade- cylamine to simulate a filter bed:

$$f_i = -0.089 + 0.128\,(U_o\, d_f\, \mu_c)^{-0.4} \qquad 4.29$$

or,

$$\lambda_c = -\log_e [-0.089 + 0.128\,(U_o\, d_f\, \mu_c)^{-0.4}]/L \qquad 4.30$$

where f_i = fraction of drops removed, and

λ_c = filter coefficient

Table 4.2

Dimensionless Groups Which Characterise Drop Removal on Porous Screens

No	Name	Expression of dimensionless group
1	Drop interception	d_p/d_f
2	Drop interception	d_p/D
3	Drop inertia	$\sqrt{\dfrac{\rho_c U_o d_p^2}{\mu_c d_f}}$
4	Film thinning by London van der Waal's attraction	$\dfrac{A d_f}{U_o/\mu_c d_p^3}$
5	Adhesion	$\dfrac{\gamma^*}{\mu_c U_o}$
6	Cohesion	γ_{CD}/γ^*
7	Viscosity ratio	μ_d/μ_c

4.2.4 Sherony and Kintner's Model

Sherony and Kintner [80, 111, 153] were the first to develop a model for fibrous bed coalescence and to use it to derive a design equation.

Coalescence was assumed to occur between a drop in the stream and a drop attached to the fibre. There was deduced to be a population of drops adhering to the fibre, and the size distribution of drops was some subset of the size distribution in the stream [80].

The steps in the coalescence process, by analogy between fibrous bed coalescence and aerosol filtration, were described as,

a. Impaction

The first step in the coalescence process is impaction. It occurs when a droplet in the stream collides with a droplet attached to a fibre and a coalescence results. It may be subdivided into two mechanisms, impaction by inertial transport of the drop in the stream to the fibre; and impaction by interception of the drop with the fibre [80]. The following model for the coagulation frequency is based upon a combined impaction-interception concept.

$$K_I \mu_o \phi_o = \left[\frac{\text{collision frequency}}{\text{unit volume, unit time}}\right]\left[\frac{\text{coalescence frequency}}{\text{collision frequency}}\right] \quad \ldots. 4.31$$

The collision frequency in the above expression represents collisions between drops in the stream and drops on the fibre.

b. Brownian Diffusion

This can occur between two drops in the stream, or between a drop in the stream, and a drop on the fibre.

The Brownian diffusion coefficient was given as:

$$K_B = \frac{2\,K'T}{3\mu_c} \quad \ldots. 4.32$$

c. Gradient Coagulation

Under this mechanism, drops can cross steamlines due to the gradient shear. Levich [164] gave the following expression for the collision frequency by this mechanism:

$$K_G = \frac{4}{3} d_{10}^3 G \qquad \text{.... 4.33}$$

where G is the shear rate.

d. Turbulent Coagulation

In this mechanism, drops which have associated in pairs are squeezed through the capillary passage of the bed and eventually coalesce. In a photomicrographic study [165] of coalescence in a fibrous bed, it was found that these doublets were formed by eddies created by the presence of the fibres. It was apparent that small drops would vortex in large capillaries of the bed or pinwheel around larger drops.

Levich [164] proposed the following expression for the coagulation frequency

$$K_T \mu_o^2 = \frac{d_{10}^3 U^{3/2}}{8\sqrt{\frac{\mu_c}{\rho_c}}\,\gamma_o} \mu_o^2 \qquad \text{.... 4.34}$$

where γ_o is the size of large scale turbulence.

The final equation for the filtration coefficient for a coalescer λ_c, was,

$$\lambda_c = \frac{3}{4} \frac{S_m}{(1 - S_m)} \cdot \frac{(1 - e_1)(1 + d_p/d_f)}{d_f} \eta_c \qquad \text{.... 4.35}$$

If S_m and η_c are constant over the bed length.

$$Y = \frac{\mu_o (L)}{\mu_o (0)} = \exp (-\lambda_c L) \qquad \text{.... 4.36}$$

This model shows that the performance of coalescer will increase with:

i. decrease in fibre diameter,

ii. larger mean inlet drop size,

iii. increase in packing thickness, in agreement with experimental results [111].

Furthermore, the overall coalescence efficiency η_c was defined as:

$$\eta_c = \alpha\beta \qquad \text{.... 4.37}$$

Experimentally the average value of β was 0.41 [86] but this clearly depends upon the system properties and superficial velocity; a model for α was based upon the efficiency of an aerosol filter. However, it was found that the degree of coalescence increased with increasing saturation, inlet drop size and bed depth and decreased with increasing velocity.

4.2.5 Rosenfeld and Wasan's Model

The following assumptions were made to derive a design equation [86],

1. The droplets were small and the dispersed phase is dilute. These requirements would ensure that the suspended drops did not affect the flow of the continuous phase.
2. The saturation in the bed was sufficiently small so that a continuum of the dispersed phase did not exist.
3. The drops approach a fibre by the mechanism of interception. The effect of London forces in the capture of the drops had been shown to be negligible.
4. When a drop struck a fibre, or a held drop, the probability that it would remain on the fibre or coalesce with the held drop, was a constant for one particular system.

5. A drop on a fibre grew by coalescing with drops from the free stream, and there was essentially no coalescence between two drops in the free stream.
6. The drop remained attached to the fibre until it had attained a certain size. This had been observed in photomicrographic studies [81, 105].
7. Each drop could be considered independently of the overall distribution. Spielman and Goren [85] observed that if the volume fraction of dispered phase in the inlet was very small, the coalescence efficiency for any given size drop, whilst dependent upon that drop size, was independent of the size distribution.

After formulation, determination and solution of a set of equations, the final theoretical design equation was:

$$\lambda_c = \left[\frac{8\,\beta\,(1 - e_1)}{\pi^2\, e_1\, (1 - S_d)\, d_f^2}\right] \cdot \left[\frac{2\, d_{fe} + d_p}{d_{fe} + d_p}\right] \qquad \ldots. 4.38$$

where

$$d_{fe} = d_f \left[\frac{(1 - e_1)\,(1 - S_d)}{1 - e_1}\right]^{1/2} \qquad \ldots. 4.39$$

and, β = number of effective collisions/total number of collisions, and hence an adjustable parameter which varies between 0 and 1 [85]. A typical valueof β was determined by Sherony and Kintner [111], to be 0.41. Spielman [94] measured the filter coefficient for a system of silicone oils and his data was best fitted by a β value of 0.24. The range of β values was from 0.158 to 0.348 for each drop diameter in each separate run. The classical interception mechanism was used to formulate the following equation.

$$\eta = 2\, A_F\, (d_p/d_f)^2 \qquad \ldots. 4.40$$

where A_F is a parameter which characterises the influence of a neighbouring fibre on the flow field near an individual fibre. A purely empirical extension of the above equation is

$$\lambda_c = \left[\frac{8\,\beta\,(1 - e_1)}{\pi^2\, e_1\,(1 - S_d)\, d_f^2}\right] \cdot \left[\frac{U_{cr}}{U}\right]^{1/2} \cdot \left[\frac{2\,d_f + d_p}{d_f + d_p}\right] \qquad \ldots. \; 4.41$$

where, U_{cr} = critical superficial velocity m/sec.

4.2.6 Spielman and Goren's Model

Spielman and Goren [77, 85, 98, 149, 166, 167] assumed that two readily-distinguished, regimes of the coalesced oil phase exist within the pores. One regime consisted of microdroplets suspended in the non-coalescing water; the other was coalesced oil held-up within the pores and assumed to form a network of channels sufficiently well-connected to support viscous flow of oil by capillary-conduction. This latter regime was consistent with established ideas from petroleum reservoir science about immiscible fluid flow through porous media. Furthermore, this second regime was taken to be in local capillary-equilibrium with the solid and water phases. The drop capture step was assumed to be rate-controlling, with subsequent coalescence and interfacial adjustment of the held-up oil considered to be so rapid as to prevent appreciable build-up of captured droplets which had not coalesced into the capillary-conducted regime. With this physical picture Spielman and Goren [161] formulated a set of equations and boundary conditions which they solved with appropriate simplications [126]. Their scheme of equations relates the local drop size distribution, phase pressures and held-up oil through four fundamental coefficients, the relative permeabilities of two phases, the capillary pressure and the filter coefficient, all of which are functions of S.

It was observed experimentally [77] that the dependence of the filter coefficient λ on drop diameter, fibre diameter, bed depth, flow rate, oil viscosity, was in contradiction of the classical interception theory which predicts:

$$\lambda \propto d_f^{-3}\, d_p^{\,2}\, U \qquad \ldots. \; 4.42$$

This led them to re-examine the concepts underlying the theory of collection

by interception and to develop a rigorous treatment of collection by convection and London van der Waal's attraction. The dimensionless filter coefficient ($\lambda\, d_f^3/d_p^2$) is expected to be a function of a single dimensionless group ($N_{Ad} = 4Q\, d_f^2 / 9\mu\, U d_p^4\, A_f$) termed the adhesion number. The Hamaker constant Q has been taken arbitrarily as $Q = 10^{-14}$ erg. However, it would be interesting to vary Q experimentally also.

The final equations developed were

a. For non-wetted beds.

$$\lambda = 0.29 \frac{d_p^2}{d_f^3} (N_{Ad})^{0.25} \qquad \text{.... 4.43}$$

b. In making the adjustment, it was assumed that λ would vary as the first power of filter volume fraction α. This gave the following modified equation:

$$\lambda = 5.3\ \alpha \frac{d_p^2}{d_f^3} (N_{Ad})^{0.25} \qquad \text{.... 4.44}$$

c. For oil-wetted beds:

$$\lambda = 0.08\ \alpha \frac{d_p^2}{d_f^3} (N_{Ad})^{0.2} \qquad \text{.... 4.45}$$

The constants and exponents were determined from the data.

Their equations were not based on the model but upon the capture of a drop by a filter rather than by other coalesced drops. Also, since a considerable amount of data were required to determine the exponent, these equations were of limited help in designing a coalescer.

4.2.7 Austin's Model

Austin [16] considered the previous models for describing single phase flow in porous media and found that his experimental data from micromesh beds were best represented by Keller's equation, which was based on a physical model similar to the internal structure of the meshes.

The flow parameter evaluated from the single phase model was incorporated into a theoretical comparison of drop capture mechanisms which indicated that direct and indirect interception are predominant. A mathematical description of the saturation profiles was formulated using average saturation data, the Blake-Kozeny equation. This was also used to determine the effective voidage of the packing during coalescence as:

$$\frac{\Delta P_2}{\Delta P_1} = \frac{e_1^3 (1 - e_2)^2}{e_2^3 (1 - e_1)^2} \qquad \ldots. 4.46$$

The dispersed phase saturation was then calculated by:

$$S_m = 1 - (e_2 / e_1) \qquad \ldots. 4.47$$

Drop capture efficiency due to interception, London van der Waal's forces, diffusion and sedimentation were determined employing a basic set of parameters, relevant to the experimental work. The equations for evaluation of the individual mechanisms were discussed in section 4.1.1. and are summarised in table 4.1. The overall efficiency is therefore [142]:

$$\eta_T = \eta_I + \eta_D + \eta_G + \eta_L \qquad \ldots. 4.48$$

The following assumptions were introduced in order to derive a new model of coalescence:

i. Poisson arrival distribution of mean arrival rate, λ

ii. Exponential service distribution of mean service rate, μ

iii. Queue discipline is on a first-come first-served basis

iv. No simultaneous arrivals or service, which eliminates terms of second order in t

v. There are M channels having an identical service rate

vi. Under steady-state conditions, the number in the system exceeds the number of service channels, ie $n \geq M$ and there are no constraints governing the queue length "Lq".

The filter coefficient may therefore be related to the fraction of "customers" which undergo 'balking'. For steady state conditions;

$$f_{Lq} = \gamma^{2Lq} \; ; \text{ when } n = Lq \qquad \ldots. \; 4.49$$

Now, the filter coefficient, λc is given by;

$$\lambda c = \frac{-\log_e (1 - f_{Lq})}{L} \qquad \ldots. \; 4.50$$

Substituting for f_{Lq} from equation 4.43 and bed depth L,

$$\lambda c = \frac{-\log_e (1 - \gamma^{2Lq})}{2 d_c N_L} \qquad \ldots. \; 4.51$$

where, the length of the "queue" Lq, was given by:

$$Lq = \frac{\sum_{n=1}^{\infty} n\rho^n \gamma^n (n-1)}{\sum_{n=1}^{\infty} \rho^n \gamma^n (n-1)} \qquad \ldots. \; 4.52$$

Then, the experimental filter coefficient λe was determined as,

$$\lambda e = \frac{-\log_e \left[(1 - \eta_s) \left[\frac{dp_{in}}{dp_{out}} \right]^3 \right]}{L} \qquad \ldots. \; 4.53$$

where η_s is the fractional separation efficiency, and if 'dp'may be taken as the mean linear diameter of the inlet dispersion, the Lq was given by:

$$Lq = \frac{3\, e_1\, dc\, D^2\, S_d\, N_L}{dp^2} \qquad \ldots. 4.54$$

In conclusion, few generally applicable principles have been established to assist in the design and scale-up of liquid-liquid coalescers. The data are mainly confined to the measurement of operating parameters for each individual case. Thus trial and error still tends to be used to select the appropriate liquid-liquid coalescer for any particular duty.

CHAPTER FIVE

EXPERIMENTAL INVESTIGATION

5.1 Introduction

Experimental work on the coalescence of secondary dispersions in packed beds necessitates the use of chemically-inert and mechanically-strong materials. In this investigation the packings used comprised ordinary ballotini glass spherical particles. The ballotini were supported in a simple, specially-designed glass holder which was then inserted into equipment capable of producing oil-in-water dispersions. These dispersions were pumped through the packing vertically in one direction.

5.2 Materials of Construction

To minimise contamination of the oil-in-water system, the materials of construction were restricted to glass, stainless steel and ptfe.

5.3 General Arrangement

A flow diagram of the equipment is shown in figure 5.1 and the general arrangement is illustrated in plate 5.1.

The equipment was installed in a hardboard cabinet to exclude draughts and light. Temperature control by cooling, was found to be necessary because of the energy input from the centrifugal pumps. The temperature was controlled by a parallel tube heat exchanger in the emulsification loop as shown in plate 5.3. This facilitated temperature control within $\pm$ 0.5°C.

Pressure drop across the coalescer was determined by means of an inter-changeable, one meter long, U tube mercury manometer. Manometer readings were checked using two pressure gauges in the range zero to 2.1 x 10^5 Nm^{-2} at the high

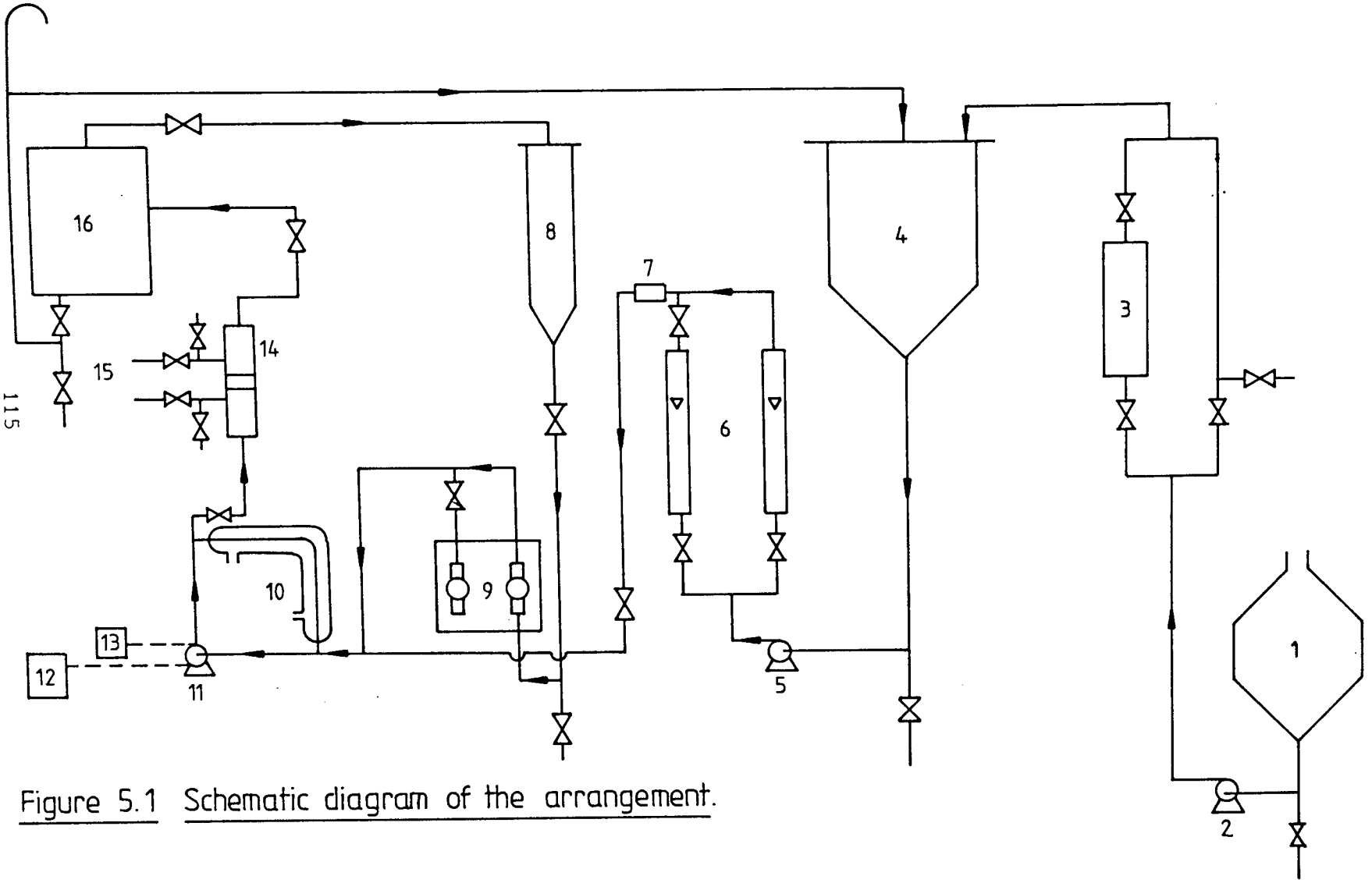

1 FEED RESERVOIR
2 CENTRIFUGAL PUMP
3 FILTER
4 CONTINUOUS PHASE RESERVOIR
5 CENTRIFUGAL PUMP
6 ROTAMETERS
7 FILTER
8 DISPERSED PHASE
9 METERING PUMP
10 EMULSIFICATION LOOP
11 CENTRIFUGAL PUMP WITH DC MOTOR
12 VOLTAGE REGULATOR
13 DIGITAL ELECTRONIC TACHOMETER
14 COALESER CELL
15 TO PRESSURE MANOMETER AND GAUGES
16 SETTLER

Figure 5.1 Schematic diagram of the arrangement.

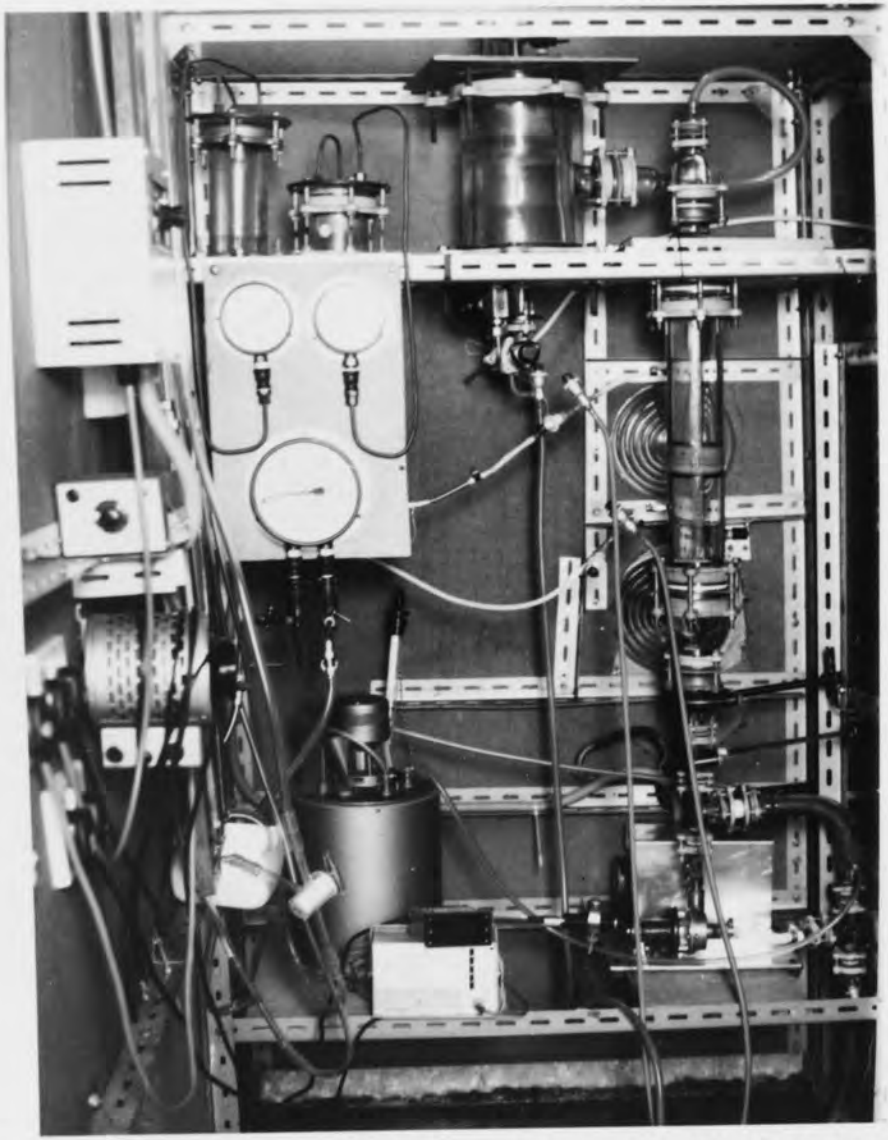

a LEFT SIDE, DISPERSION GENERATION LOOP, COALESCER CELL AND SETTLER. (Emulsification loop, coalescer and settler sections.)

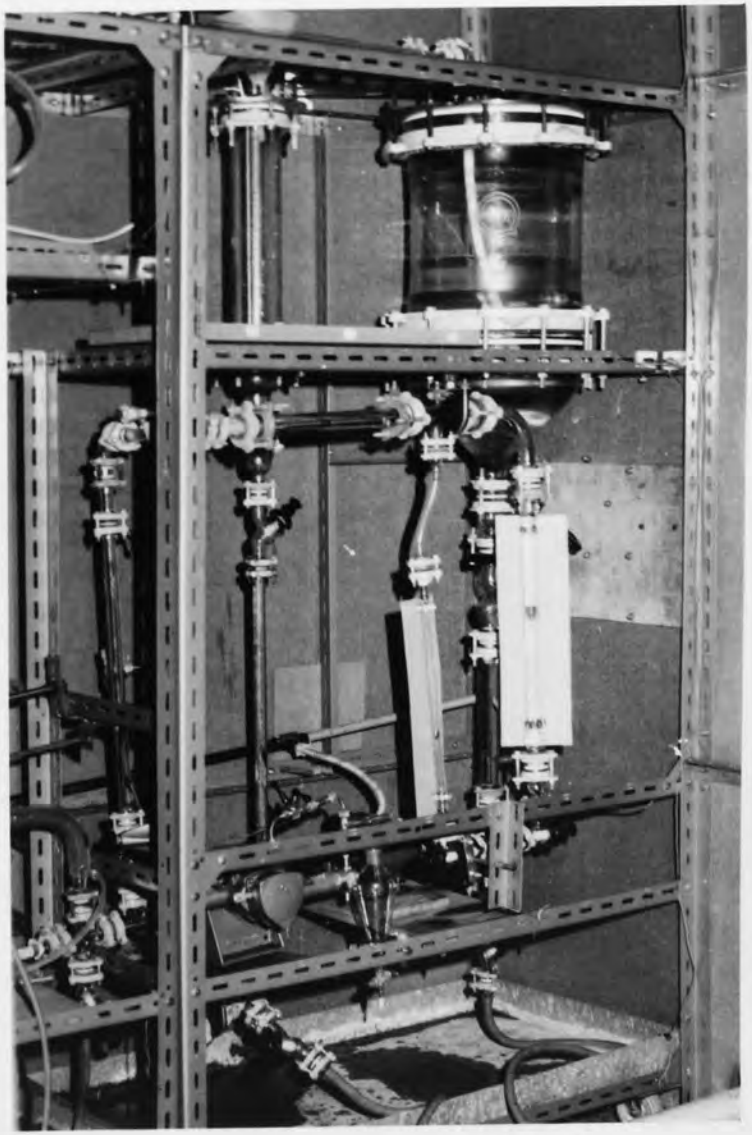

b RIGHT SIDE, PHASE RESERVOIRS AND TRANSFER PUMPS. (Continuous phase and dispersed phase sections.)

PLATE 5.1 GENERAL ARRANGEMENT OF EQUIPMENT

pressure end, and zero to 3.4 x 10^4 m^{-2} at the low pressure end. A further check was made using a differential pressure gauge in the range zero to 1.03 x 10^5 Nm^{-2}. These instruments were connected via two reservoirs which prevented the process liquid entering the manometer and/or gauges and served to damp-out minor fluctuations and give stable readings. The main sections of the equipment are described below.

5.3.1 Feed Section

The feed section, plate 5.2, consisted of a 1.5 x 10^{-2} m^3 capacity container, constructed from two QVF industrial glass reducers, connected to a Stuart Turner no. 12 centrifugal pump.

The feed was pumped through a fibrous glass cartridge filter with a stainless steel jacket which served to retain any solid particles > 1μm in diameter.

5.3.2 Continuous Phase Section

The continuous phase section is shown on the right (b) of plate 5.1. The continuous phase reservoir consisted of a 30 x 10^{-2}m diameter QVF glass container covered with a stainless steel plate; it had a capacity of 50 litres. Continuous phase was pumped via a Stuart Turner no. 12 stainless steel centrifugal pump with Viton seals and capable of transferring a maximum flow rate of 54.1 litre/m. The rate was controlled by two QVF industrial glass valves and flow was measured by two K14 and K7 rotometers with Koronite and stainless steel floats respectively; these covered a range of zero to 56 x 10^{-6} m^3s^{-1}. The continuous phase was filtered further by passage through a specially-designed, pure fibrous-glass packing, comprising several layers of knitted fibrous glass placed in a 2.5 x 10^{-2}m inside diameter glass pipe section.

This filter eliminated any residual particulate matter which may have introduced experimental errors, or caused blockage of the pores of the test coalescers.

PLATE 5.2 FEED SECTION ARRANGEMENT

(Feed reservoir, transfer pump and filter)

5.3.3 Dispersed Phase Section

The dispersed phase section is illustrated on the right (b) of plate 5.1, to the left of the continuous phase section. The dispersed phase reservoir comprised a 5 x $10^{-3}m^3$ capacity QVF glass container. The dispersed phase was metered by a Micro Metering Series II type pump, manufactured by Metering Pumps Ltd. This had two units, one large-stroke and one short-stroke, each with stainless steel pump heads. The ranges of flow rate were zero to 8.7 x $10^{-7}m^3\ s^{-1}$ and zero to 2.6 x $10^{-7}m^3\ s^{-1}$ respectively. These ranges were reduced in the ratio of 5 to 1 by means of a reduction capsule gear when required. The pump delivery lines were also provided with,

a. Two stainless steel back-pressure valves, one for each pump head.

b. A safety relief valve, and

c. Two outlet points to facilitate direct calibration of flow rates versus vernier setting on the pump stroke.

Each of the dispersed and continuous phase reservoirs were connected via a QVF "T" piece section to the emulsification loop.

5.3.4 The Emulsification Loop

Secondary dispersions generation under high shear conditions has been used previously by many investigators. Vinson [117] produced secondary dispersions by using a homogeniser, that is by forcing the mixture of liquids through a small orifice under very high pressure; Sherony [165] used an agitation technique with varying speeds.

Previous work by Shalhoub [57], Attarzadeh [17], Austin [16], Ibrahim [104] and Baez Poleo [27] had confirmed the practicality, reliability and validity of reproducible- emulsion production by circulation in a loop using a centrifugal pump. This technique was therefore adopted in this work.

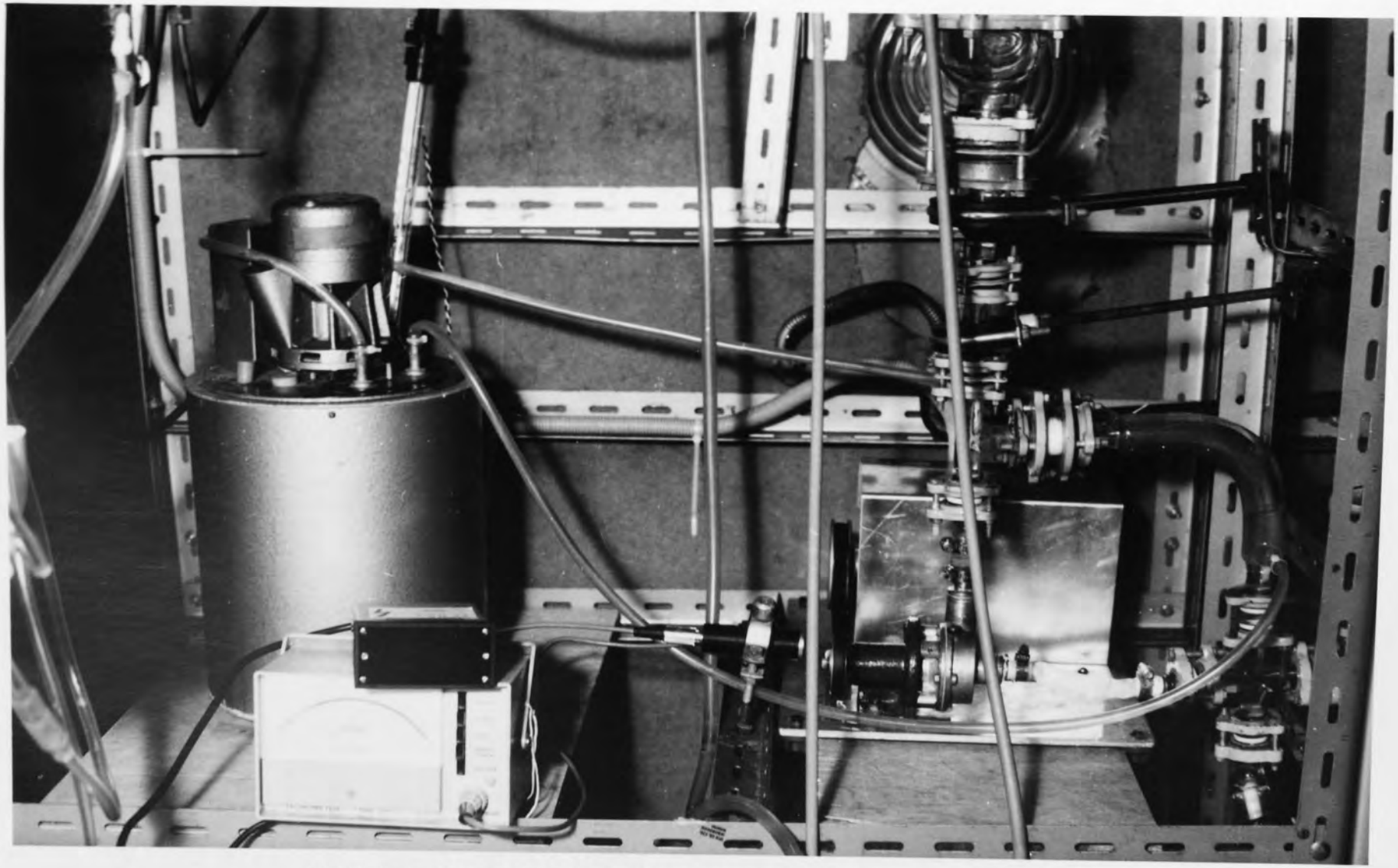

PLATE 5.3 ARRANGEMENT OF THE EMULSIFICATION LOOP

(Emulsification loop on right and water circulation on left.)

The emulsification loop, shown in plate 5.3, incorporated a Stuart Turner No 12, V-belt driven, centrifugal pump provided with a digital electronic tachometer. This tachometer was activated by reflection of light from a line painted on the pump shaft. The pump speed was varied in the range of 500 rpm to 5000 rpm and the drop size distribution variation with pump speed recorded (see section 8.8). For close speed control the centrifugal pump was fitted with a DC motor controlled by a GEC Industrial Controls (GEMINI) controller (i.e voltage regulator).

5.3.5 Coalescer and Settler Section

The coalescer and settler section are illustrated on the left (a) of plate 5.1. The coalescer consisted of packings supported in a specially designed glass holder (see section 5.4). The secondary dispersions, produced in the emulsification loop, were made to flow vertically upwards through the packings. The settler comprised a 15.24 x 10^{-2}m (6 inches) diameter QVF industrial glass pipe section with stainless steel end plates. Provision was made for continuous phase recycle from either the top or the bottom dependent upon its relative density.

5.4 Coalescer Design

The coalescer design is illustrated in plates 5.4 and 5.5. Each coalescer cell consisted of a QVF glass pipe section, 7.62cm (3 inches) inside diameter and 30cm high. Two pressure tapping points were provided in the glass wall approximately 6.5cm from each end. These tubes were connected to a manometer and pressure gauges (see section 5.3). The coalescer was made-up as follows:

a. A section of steel mesh, supported by plastic mesh of 0.2cm hole size supported by a ptfe ring, 7.00cm (2.75 inches) outside diameter, 5.08cm (2 inches) inside diameter, and 1.27cm ($^1/_2$ inch) thick. Two sections of this supported steel mesh were placed at the top and bottom of a ptfe plastic cup as shown in plate 5.4a.

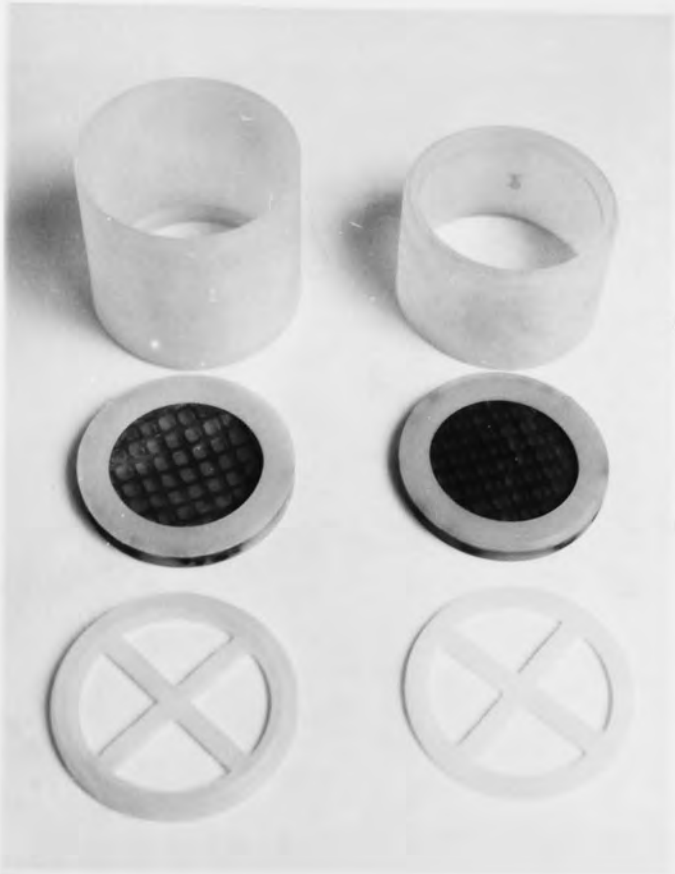

a PLASTIC CUP

(P.t.f.e plastic cylinder with two 85µm stainless steel meshes supported by polyethylene 2 mm size meshes, fixed in a p.t.f.e plastic ring; with two p.t.f.e plastic covers).

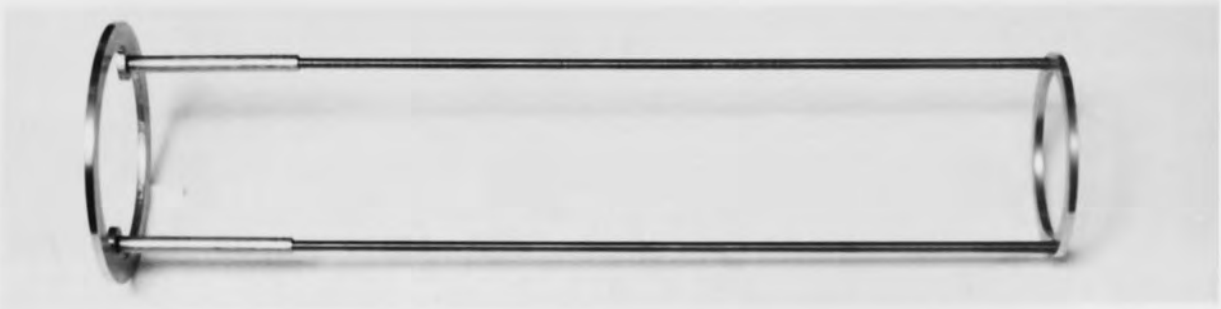

b STEEL HOLDER

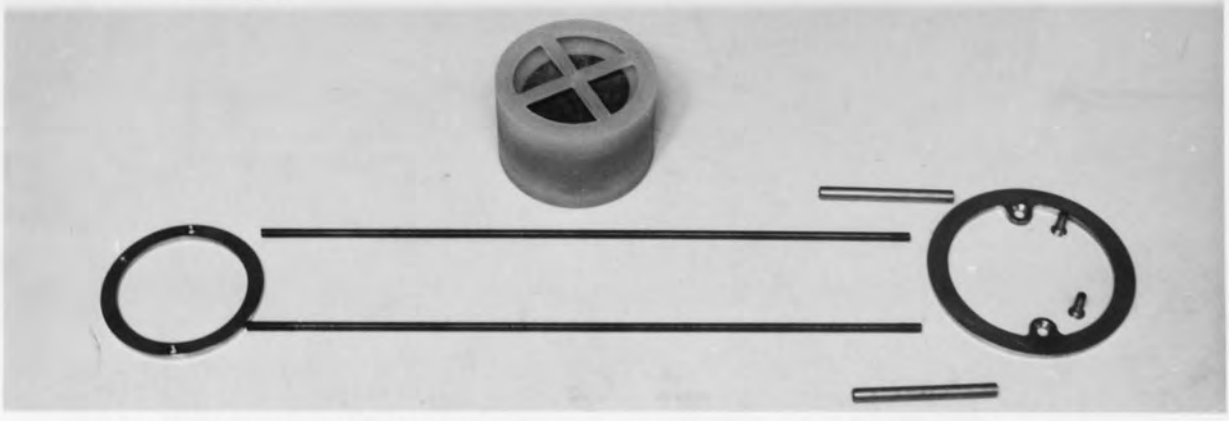

c COALESCER CELL AFTER ASSEMBLY AND STEEL HOLDER PARTS

PLATE 5.4 COALESCER CELL DESIGN

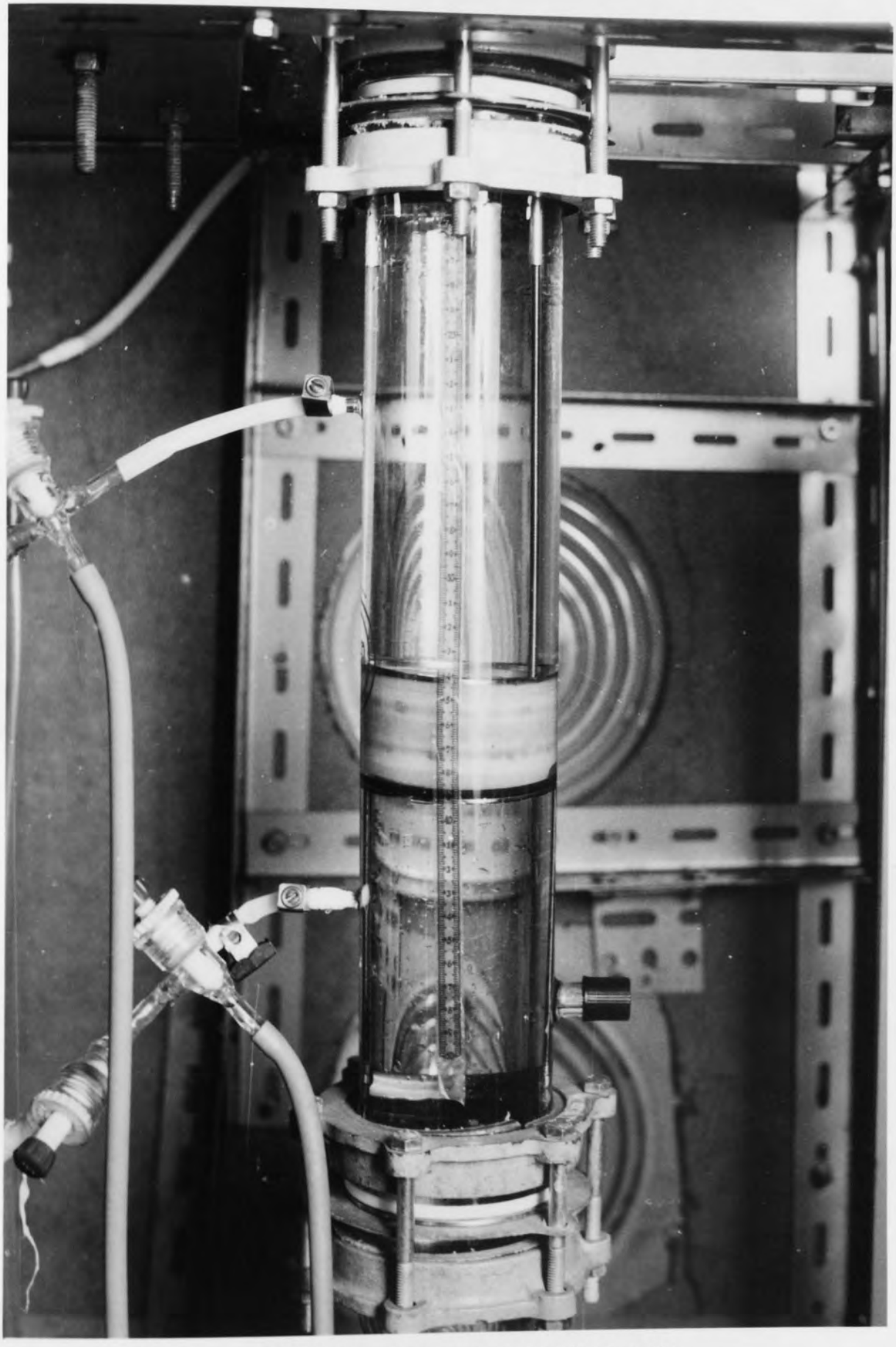

PLATE 5.5 ARRANGEMENT OF THE COALESCER CELL

(20 mm depth, 256 μm ballotini particle size, 7.6 cm coalescer cell diameter and 105 μm stainless steel mesh size)

b. The particles (ballotini) were poured in and uniformly distributed by adding distilled water to the plastic cup after fixing the steel mesh ptfe ring at the bottom. The particles were compressed by fixing the top steel mesh ptfe ring in place as shown in plate 5.4c.

c. A special plastic cup holder was designed and care was taken to ensure that no obstructions existed inside the packing, to avoid variation in flow conditions across the bed. The stainless steel holder is shown in plate 5.4b.

The plastic cup containing the particulate packing was secured between two 7.6cm outside diameter, 6.3cm inside diameter, and 0.32cm thick stainless steel rings, thereby preventing changes in bed thickness and position inside the glass pipe holder during experimentation. The holder was constructed from two threaded rods of 0.47cm diameter with a thread pitch of 0.081cm, 2BA screw thread, and 8.0cm outside diameter 0.32cm thickness a stainless steel ring, as shown in plate 5.5. Two of these stainless steel holders were used to locate the bed between the two pressure tappings at approximately the middle of the glass section holder. This enabled beds of different thickness to be studied. The outside ring served to prevent the liquid at high flow rates from displacing the holder out of position.

5.4.1 Packing Selection

The coalescer beds comprised non-porous pure glass ballotini obtained from Englas, English Glass Company Limited. Their properties are listed in Table 5.1. The overall range of glass ballotini diameter was 146-615μm, measured by a Stereoscan Electron Microscope, as shown in plate 5.6. The stainless steel meshes (plate 5.7) were supplied by Begg Cousland Ltd with an approximate thickness of 0.1cm.

Particles had been previously used to study capillary pressure in packing [168], to coalesce a primary dispersion of oil-in-water [95], and in the form of building sand [104] or glass ballotini [27, 106] to coalesce secondary oil-in-water dispersions.

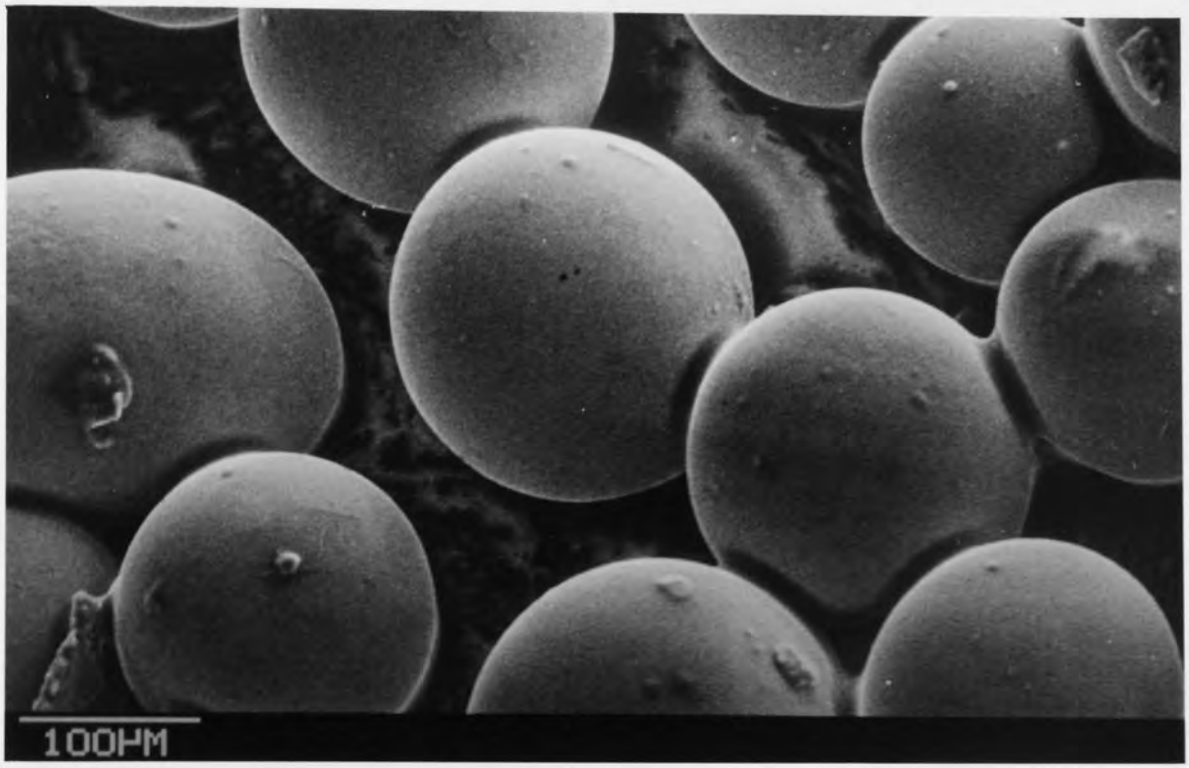

a SPHERICAL BALLOTINI PARTICLES

(Normal particle size = 146 µm, the junctions between particles are due to the method of mounting for steroscan electron microscopy)

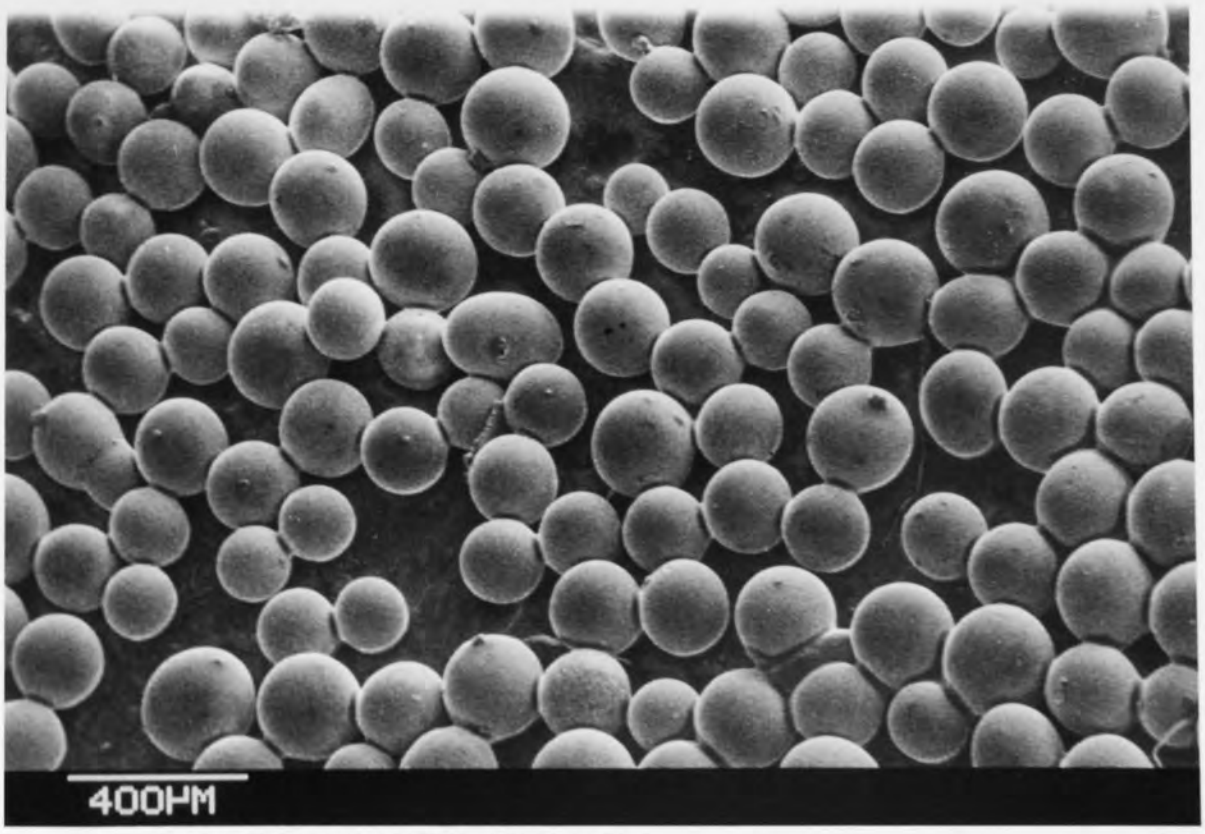

b SPHERICAL BALLOTINI PARTICLES

(Calculated mean diameter = 146 µm)

PLATE 5.6 ELECTRONMICROGRAPHS OF BALLOTINI PARTICLES

Table 5.1

Properties of Ballotini Particles

Composition: Lead glass

Physical Properties:

Specific gravity (approx)	2.95
Refractive index	1.6
Thermal conductivity at 20 °C (Kal./m.hr.degree C)	0.0018
Specific heat between 20 and 100 °C (cal/gm.degree C)	0.156
Hardness (Moh's scale)	5.7
Linear coefficient at expansion (between 0 °C to 300 °C x 10^{-6}/°C)	9 x 10^{-6}
Maximum working temperature °C	350
Softening point °C	470

Diameter range μm	Test Sieves B.S.410: 1969 pass	retain	Approximate density Kg/m^3
0.045 - 0.070	63	53	1740
0.060 - 0.095	50	63	1720
0.210 - 0.325	300	250	1780
0.440 - 0.530	500	425	1840

Approximately 85% in "Diameter Range" specified. Less than 5% irregular shapes as shown in Plate 5.6.

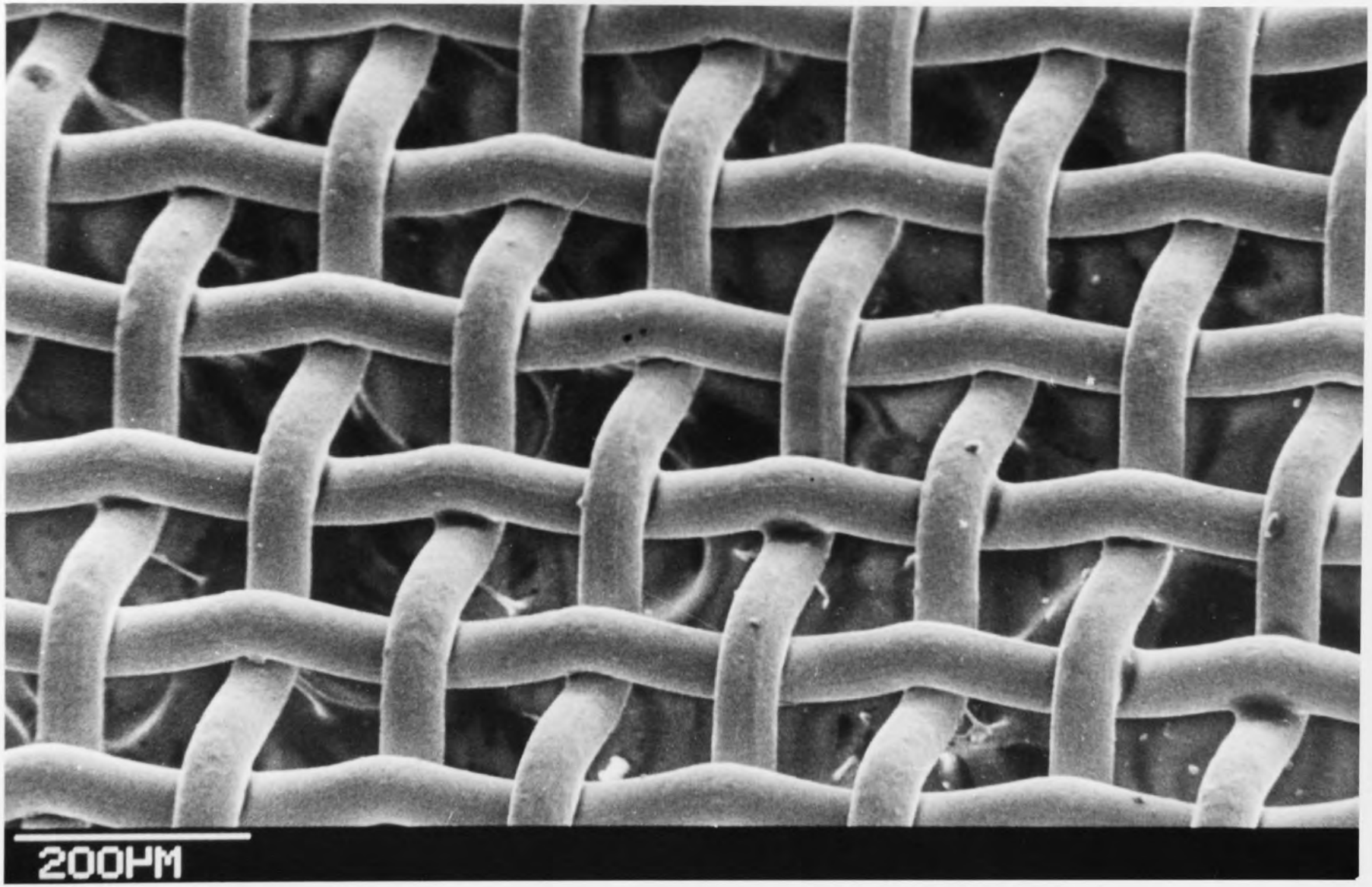

PLATE 5.7 PHOTOMICROGRAPH OF STAINLESS STEEL MESH

(85 µm aperture mesh size)

They were however selected here to determine their effectiveness for secondary dispersions coalescence. Stainless steel meshes with specific pore size of 105 and 250μm were used to support and retain particles in the coalescer during operation. The mesh size used was the largest which would retain the granular material for each particular experiment. This minimised any coalescence effects at the inlet and minimised the pressure drop across the support. These packing materials contained no binder which eliminated potential contamination of the liquid-liquid systems. They were also chemically inert, mechanically strong, and closely packed.

Glass was favoured as packing material because it is relatively inexpensive, is resistant to the extreme thermal and chemical environment used in cleaning procedures, and its wetting properties may be modified by the attachment of silicone groups to the surface of the glass material [124, 169].

Packings of various geometries have been related to that of a sphere by a shape factor, where a sphere has a shape factor 1.0. Therefore, the use of spheres as a packing may facilitate the use of a shape factor to equate the effect of surface area to volume ratios on the coalescence efficiency of different packings. The theory, and measurements of the packing arrangments of spheres, have been widely reported [119, 170, 171]. Co-ordination numbers and voidage relationships have been evaluated from both regular and random packing of spheres. Pore sizes and channel diameter variations have been evaluated from a theoretical standpoint [170]. Therefore, from these properties, it is possible to quantify the packing geometry and its effects on coalescence.

Furthermore, Ridgeway and Tarburk [119] investigated local voidage variation of spheres in cylindrical columns. In that study the ratio of column diameter to grain diameter was always greater than 35:1. Thus, wall effects were virtually eliminated.

The present study of coalescence mechanisms and droplet hydrodynamics was restricted to the coalescence process in a non-wetted packing. Glass, having a high

surface energy was thus well suited when organic liquids were used as the dispersed phase.

5.4.2 Preparation of Packing Materials

Circular pieces of stainless steel mesh 6.8cm in diameter, were prepared from sheets using a specially-designed, punch which was a hollow cylinder manufactured from high carbon steel and had circular sharp edge of 6.8cm in diameter. After cutting the meshes were washed carefully for more than five minutes with distilled water. The stainless steel meshes were dried in the oven at 70°C and fixed in the ptfe rings. Microscopic examination of the meshes confirmed that the relevant dimensions were both consistent and accurate to the manufacturer's specifications as shown in plate 5.7.

The ballotini particles were cleaned with distilled water, dried in the oven at 70°C and separated into the required size range fractions using test sieves made by Endecotts Filters Ltd; the size ranges of these sieves are listed in table 5.2. The particulate packing to be inserted into the coalescence devices was subjected to the preferential wetting treatment devised by Thomas and Mumford [74], and previously used successfully by Wilkinson [95], Austin [16], Baez Poleo [27] and Al-Meshan [144] to ensure that all the packing had a uniformly reproducible surface. The clean, dry ballotini particles were first soaked in chromic acid for 24 hours and then thoroughly washed with distilled water, after which they were dried for 8 hours at > 150°C. The dried particles were stored in sealed polyethylene containers for subsequent use. The effect of surface renewal by acid etching and the thorough drying proved to be a suitable method of producing a highly active surface. If the dried ballotini particles were then immersed in either organic or aqueous phase they would be preferentially wetted by the liquid which first came into contact with it. Thomas and Mumford [74] stated that this effect was possible irrespective of the solid surface free energy. Therefore glass, which has a high surface free energy and is normally wetted by water, could be rendered wettable by the organic phase. However, in this study, surfaces wetted by the

Table 5.2

Packing Arrangements

Packing Arrangement	Bottom steel mesh aperture diameter (m)	Ballotini particles mean diameter (m)	Top steel mesh aperture diameter (m)
A	105×10^{-6}	146×10^{-6}	105×10^{-6}
B	105×10^{-6}	266×10^{-6}	105×10^{-6}
C	105×10^{-6}	364×10^{-6}	105×10^{-6}
D	105×10^{-6}	487×10^{-6}	250×10^{-6}
E	105×10^{-6}	615×10^{-6}	250×10^{-6}

continuous aqueous phase were in all cases produced by immersion in distilled water. Microscopic examination of the glass ballotini particles confirmed that the relevant dimensions were both consistent and accurate to the manufacturer's specifications. However the glass ballotini sizes measured by Stereoscan micro- photography for several ballotini sizes at several magnifications, revealed the presence of 2 to 5 per cent of smaller and irregular shapes of ballotini particles within the samples, as illustrated in plate 5.6. The stereoscan photographs also confirmed the smoothness and regular sphericity of the glass particles. The packing general arrangements are summarised in Table 5.2.

5.5 Selection and Preparation of Liquid-Liquid Systems

The organic systems selected covered a range of relevant physical properties. Interfacial tension values were in the range 29 x 10^{-3} to 39 x 10^{-3} Nm^{-1}. Viscosity values were in the range 0.58 x 10^{-3} to 1.85 x 10^{-3} kg $s^{-1}m^{-1}$ and density differences were in the range 0.78 x 10^{3} to 0.86 x $10^{3}kgm^{-3}$. The organic liquids and their physical properties are listed in Appendix A.1 and A.2. In all experiments the continuous phase comprised filtered, de-ionised, distilled water. These systems were all convenient to use; all being relatively non-toxic, non-corrosive and available to a fixed specification at low cost.

Prior to use, the organic liquids (i.e Analar grade toluene and GPR grade Clairsol-350) saturated with distilled water were stored in clean, sealed dark glass containers to eliminate the possibility of deterioration due to exposure to sunlight. Any effects due to the mutual solubility of organic liquids and water were minimised by allowing the two phases to attain mutual saturation by contact for over 48 hours before use. Mass transfer effects could be completely eliminated, since the organic-in-water systems were saturated and temperature control was achieved using the cooling system, described in section 5.3. The physical properties of the systems were therefore

determined at 20 ± 0.5°C only.

Distilled water was produced by a standard laboratory distillation column. This water was first continuously passed through a filter to retain all particles >10μm; it was then de-ionised and distilled. Distillation was at a rate of 8 litres per hour with collection in a special sealed container of 40 litres capacity.

5.6 Cleaning Procedure

Great care was taken in cleaning the apparatus. The following procedure was adopted to clean all parts of the equipment in contact with the liquid phases.

Before each set of experiments the equipment was flushed through with hot distilled water. It was then filled with a solution of 2% Decon 90 in distilled water and allowed to soak for two days with periodic recirculation of the cleaning solution. After soaking, the equipment was drained and rinsed with distilled water several times to eliminate any residual surface-active compound or any of the detergent solution remaining in the equipment. The equipment was finally washed through with distilled water and then allowed to stand full of distilled water for one day. Upon completion of cleaning, the coalescence packing cell was placed in position, the continuous and dispersed phase reservoirs filled and the equipment operated as described below.

5.7 Operating Procedure

Following assembly, the equipment was operated with recycle of the continuous phase only. The continuous phase was first pumped through the coalescence cell at a superficial velocity of $3 \times 10^{-3} ms^{-1}$ and allowed to recirculate for thirty minutes. This removed any air bubbles trapped in the bed. The continuous phase flow rate was then varied and single phase pressure drops across the packing were determined for incremental increases in flow rate.

The dispersed phase flow rate was metered in at a rate to give the required

phase ratio (concentration) in the range from 0.5 to 6% since secondary dispersions seldom arise in higher concentrations. The mixture passed into the emulsification, temperature-controlled loop, containing the variable speed centrifugal pump. For each value of phase ratio (concentration) the emulsification pump speed was increased incrementally and a sample of the dispersion collected for inlet drop size and phase ratio or concentration analysis as described in Chapter 6. Samples were also collected from the exit stream for experimental efficiency analysis as described in section 6.5. This procedure was repeated for several coalescer depths, different inlet drop sizes, different phase ratios (concentrations), several ballotini particle sizes, and different liquid-liquid systems.

Each dispersion, produced by operating the recirculation pump at a speed preset to achieve the required drop size distribution, was passed through the coalescence cell until steady-state was attained. Steady-state conditions were judged to have been achieved when the pressure drop and mean exit drop size remained constant with time. Photographs were taken of droplets leaving the exit side of the bed for size analysis, as described in section 6.2. Samples were also taken from the outlet to determine whether any secondary dispersion was present and to determine the efficiency of each coalescer cell. The pressure drop across the packing was also recorded. Experiments were repeated for different flow rates at constant phase ratio (concentration) and constant inlet drop size distribution i.e constant emulsification pump speed. The experimental procedure was repeated for several inlet drop sizes.

The same operating procedure was used with cells having different packing heights but with a constant voidage. Two different liquid-liquid systems were used. The mechanisms of outlet droplet release with each packing and liquid-liquid system were carefully observed and photographed over the complete range of operating parameters.

In this study, the aim was to obtain large exit drop diameters and high separation efficiency with low pressure drop and high superficial velocity. Therefore

experiments were carried out to determine the optimum variables at which a high separation efficiency could be achieved. Therefore a set of experiments was devised whereby the changes in ballotini size, bed depth, superficial velocity, phase ratio or dispersed phase concentration, and inlet drop size were measured as changes in the pressure drop, exit drop size, and separation efficiency.

CHAPTER SIX

INVESTIGATION TECHNIQUES

A knowledge of the drop size distribution, in addition to the mean drop size, is necessary in order to characterise a dispersion. Furthermore, the capture efficiency for any drop flowing through a packed bed depends upon its diameter. The dispersion produced by the centrifugal pump was analysed at regular intervals during an experiment to ascertain the drop size distribution and to check that the feed to the coalescer was consistent. Outlet dispersions from the coalescence cell were also monitored to measure the exit drop size and coalescence efficiency.

In this chapter new techniques or techniques which were developed for use, are briefly discussed below:

6.1 Analytical Methods of Inlet Drop Size Distribution

The determination of droplet sizes is an important step in the study of micro-dispersions. In all practical cases however, the dispersion is polydisperse, and must be characterised in terms of a drop size distribution. Various methods are available for measurement of the drop size distribution [16, 172, 175, 176, 178]. Those used in this study are reviewed below:

6.1.1 Coulter Counter

The Coulter Counter is a particle size analyser capable of measuring the size distribution of solid particles or immiscible droplets in a dispersion containing varying amounts of emulsifier at various time intervals [172]. Unfortunately its application was limited to oil-in-water emulsions since the sample must be diluted with an electrolyte before examination. The diluted dispersion was stirred throughout the course of the test to ensure that the oil droplets were uniformly-dispersed; it was also 'stabilised' to avoid

distribution changes due to coalescence. The electrolytes used include 1% sodium chloride solution and 2% calcium chloride solution [173]. The Coulter Counter was a model ZB, supplied by Coulter Electronics Ltd and had an access for a model M2 volume converter, through the use of a Timer Circuit and a Divider Circuit. The Coulter Counter had a facility for analysing samples over the range 0.6×10^{-6} to 300×10^{-6} in particle diameter.

Lycopodium powder particles of 28×10^{-6}m diameter were used to calibrate the device before commencing analyses of the samples. Samples for inlet drop size analysis were taken via the sampling valve positioned just before the point at which dispersion entered the packing. Each sample was immediately stabilised, to avoid coalescence prior to analysis; by direct transfer into a specially-prepared solution of 1% sodium chloride and 2% calcium chloride, and surfactant i.e 3-5 drops of Hyamine 2389. This electrically-conductive solution was then analysed using the Coulter Counter. This method was considered most suitable since a large number of drops could be counted to give an accurate size distribution with minimum statistical error.

The lowest range of application for the Coulter Counter has been the subject of many investigations. Matthews [174] claimed that the working range was between 2.8×10^{-6} to 56.0×10^{-6}m particle diameter; whereas Allen [175] found the lower limit to be 0.8×10^{-6}m. Clearly the Coulter Counter cannot size all of the droplets in a dispersion, and its application is limited to oil-in-water emulsions [17, 27, 106]. Errors could arise in counting due to coincidence of particles or droplets in the aperture and from losses resulting from the inability of the pulse-height analyser to process electronic pulses occurring in too rapid succession. This method was more complicated and more time-consuming than microscopy and laser techniques. Therefore the alternative techniques were adapted for drop size distribution of oil-in-water emulsions in this work.

6.1.2 Optical Microscopy

Microscopy is the simplest but the most tedious method for drop size analysis. A stabilised, diluted sample of the secondary dispersion was placed on a glass slide under an optical microscope. The various size ranges were then determined by matching against a calibrated graticule situated in the eye-piece. Photographs could also be taken for subsequent sizing. Only one sample was required for analysis for each set of conditions. The use of the microscope was most effective in the range of 0.25 x 10^{-6}m to 20 x 10^{-6}m. Obviously the sample had to be representative i.e care had to be taken that small droplets were not carried away. Furthermore the method of slide mounting was critical since in a supension larger droplets may settle rapidly and not be in focus, as shown in plate 6.1, thus giving an uneven droplet count. Accuracy was dependent on rigourousness of counting and sizing; the number of droplets counted depends on the total number representative of the mother sample. In practice, as shown in plate 6.1, errors in counting could arise due to the overlap of drop images, large drops may settle rapidly and not be in focus, and the tedium of visual counting (i.e more than 300 drops per sample were counted in order to obtain statistically valid results for a poly-dispersion [176]). Therefore the Laser Particle Size Analyser was eventually adopted in this study to measure the inlet drop size distributions of oil-in-water secondary dispersions.

6.1.3 Holography

Holography is a method of recording an image of an object using the entire content of light reflected, or transmitted, by that object. The light source used must be coherent and lasers are therefore employed to provide a source of monochromatic, coherent light to satisfy this requirement. There are two general types of holography systems, "off-axis" and "in-line" holography, as shown in figure 6.1. These two basic types differ according to the relative paths of the signal and reference beam before they coincide at the recording plan [177]. The interference field produced by diffraction from

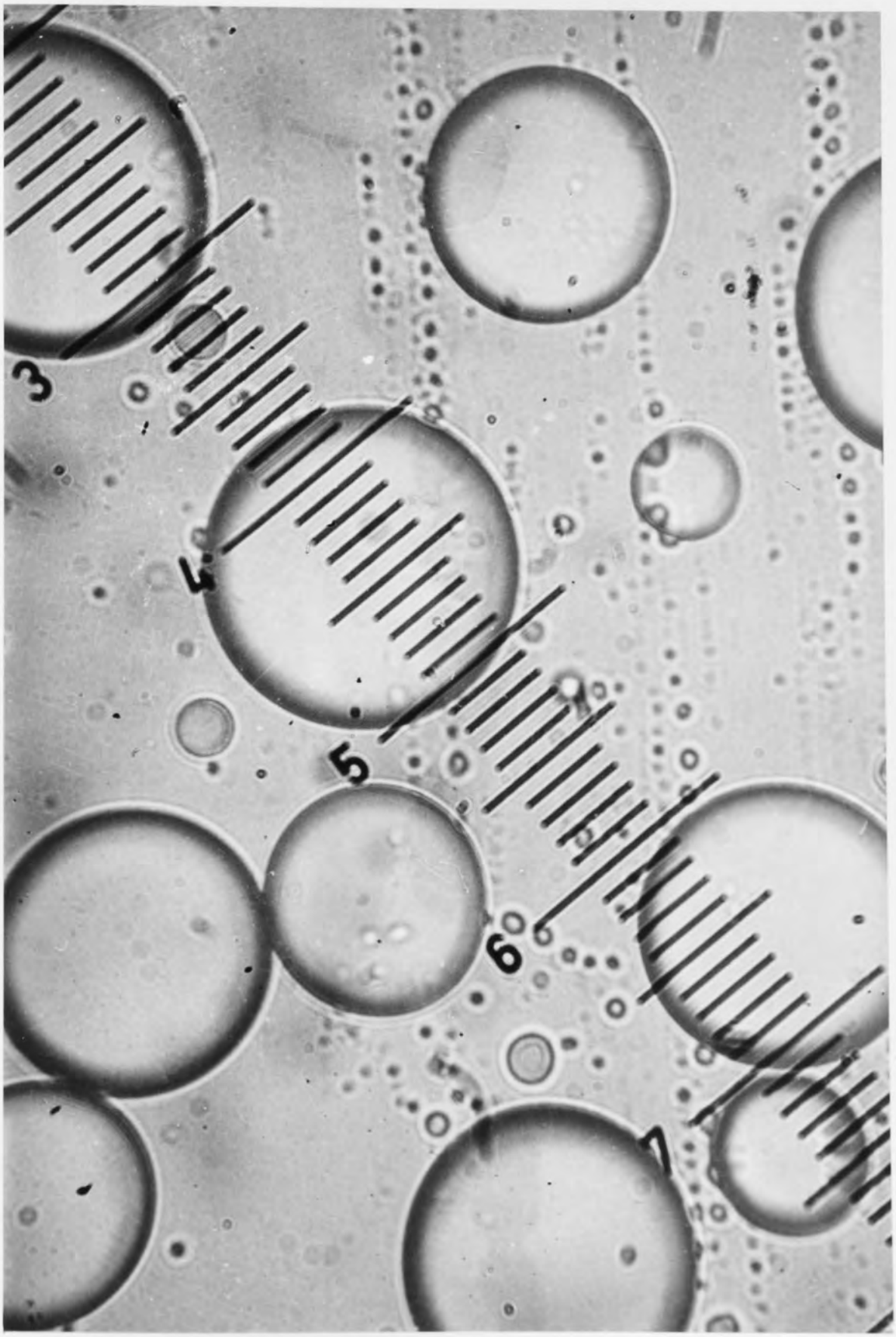

EMULSIFICATION PUMP SPEED = 3000 rpm

PLATE 6.1 PHOTOMICROGRAPH OF INLET DROPLETS

Superficial velocity = 1.85×10^{-2} m/s

Dispersed phase concentration = 0.5%

System = Toluene/Water

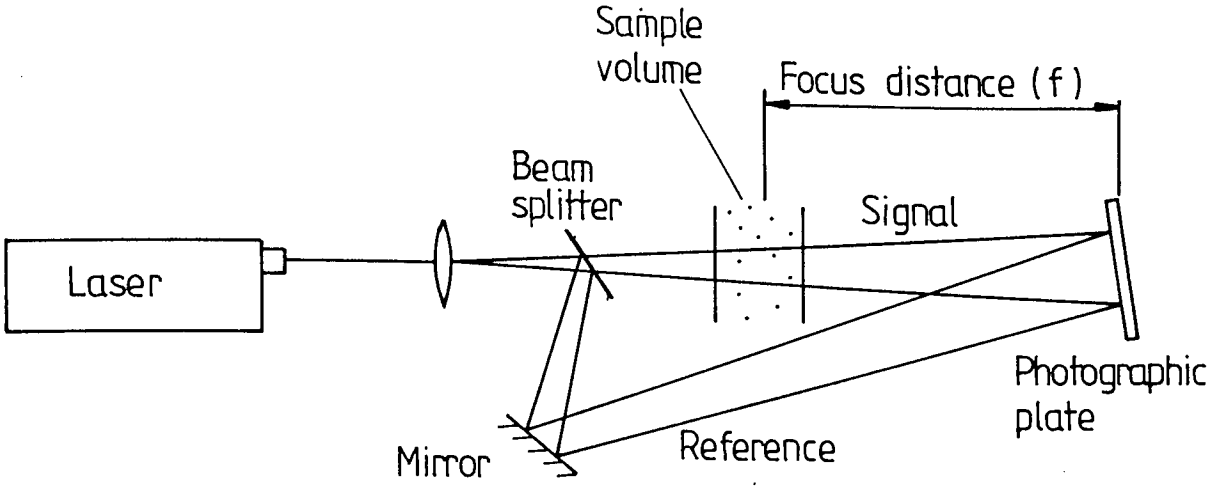

(a) 'Off-axis' holography

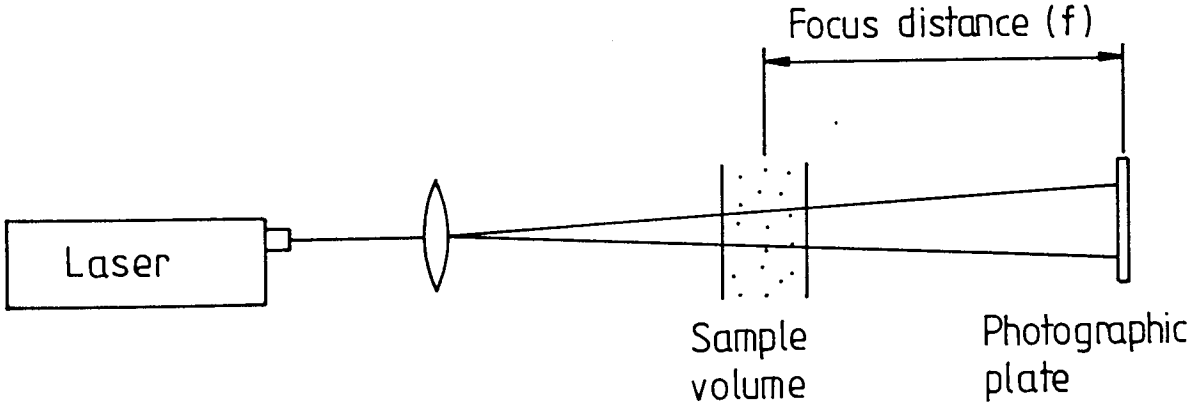

(b) 'In-line' holography

Figure 6.1 Types of holography systems

the drops and the reference beam is called a Fraunhofer Pattern [178]. Fraunhofer holograms consist of a series of concentric circular fringes, with a central maximum, associated with each drop. Fraunhofer holography was originally developed as a technique to monitor the size distribution of naturally occurring fog droplet [179], which led later to the design of laser hologram camera [180]. Similar techniques and designs were used by Thompson [178] to study glass fibre production, by Austin [16] to measure the micro-droplet size distribution of secondary dispersions; and by Bachalo [181] to measure particles in the range of 0.5 to 25μm and the flow velocity in fuel-gas pipes.

6.1.4 Laser Particle Size Analyser

The Malvern 2200 Laser Size Analyser, which was used in this work, consisted of He/Ne laser emitter and laser receiver and lenses. When a laser beam of light falls on to a spherical or non-circular droplet, a diffraction pattern is formed whereby some of the light is deflected (or diffracted) by an amount dependent upon the size of the droplet. If a suitable Fourier Transform Lens is placed in the light path behind the droplet, and a detector placed at the focal point to the lens, then light not diffracted by the droplet is brought to a point of focus on the axis. Light diffracted by the particles is concentrated concentrically at a distance from the axis, this distance being a direct function of the droplet diameter. If droplets of different diameter are sampled in the beam, then a series of concentric light rings are generated at various radii, as shown in figure 6.2, each being a function of a particular droplet size. Since the concentric rings are obtained from parallel rays of light, a far field pattern is produced and this technique is known as Fraunhafer Diffraction. For any group of droplets their combined diffraction pattern is uniquely related to their particle size and independent of droplet motion or position [181].

In the Malvern Size Analyser, as shown in figure 6.3, high energy is extracted

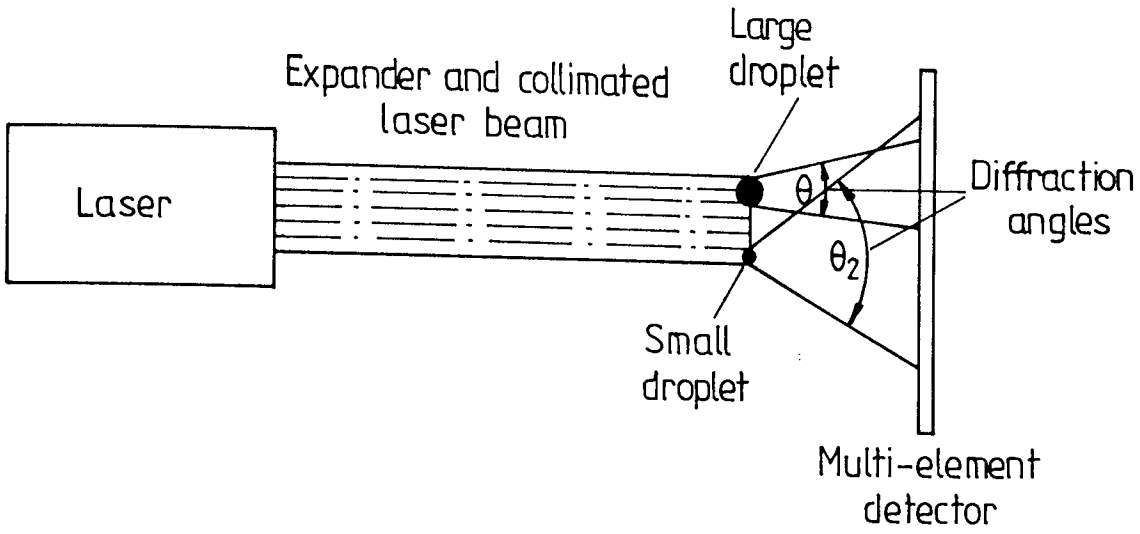

Figure 6.2 Principle of operation

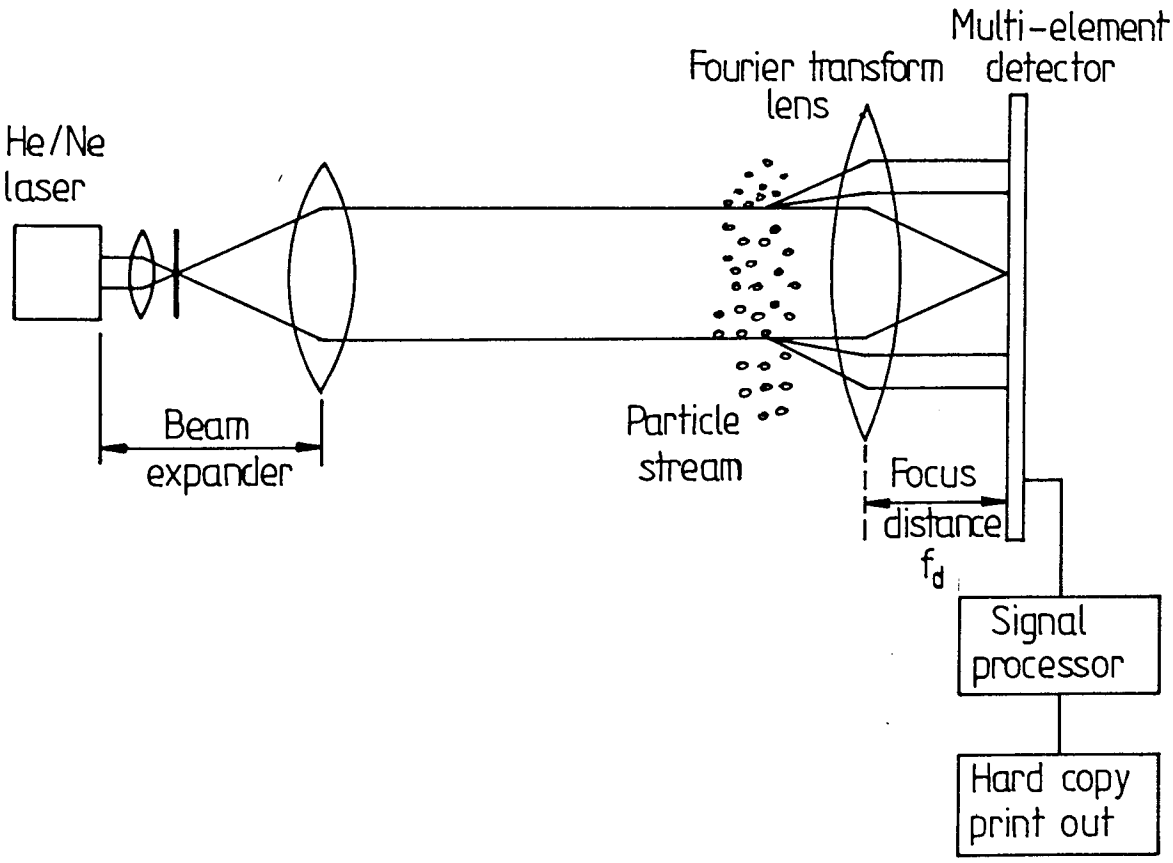

Figure 6.3 Schematic of Malvern Particle Sizer

from the droplet diffraction pattern by a specially developed, large-scale solid state detector, which consists of 31 concentric semi-conductor photo-sensitive rings, surrounding a central quadrant, each ring being most sensitive to one particular droplet diameter. The electrical output from the rings is scanned and amplified, and the analysis of light energy distribution into particle size carried out in the computer. The optimum resolution of a particular range of particle sizes, within the total instrument size range of 1-1800 microns, is achieved by a simple lens change [182].

6.1.4.1 *Construction and Operation*

In this work a Malvern 2200 Particle Size Analyser was fixed directly to the experimental equipment by using the "circulate" cell as shown in plate 6.2. It comprised the component sub-system illustrated in figure 6.4.

1. He/Ne laster emitter.
2. Optical processing unit.
3. Sample cell (i.e recirculation cell in this work).
4. Electronic measurement technique.
5. Desk-top computer system.
6. Application software package.
7. High speed line printer.

This particle sizer comprised a small safe laser transmitter mounted at one end of a rigid aluminium beam. At the opposite end of the beam the detector, lens and electronics were contained in a suitable housing, as shown in plate 6.3. The transmitter and receiver were typically separated by approximately 60cm; although this could be increased if required [182].

It was only necessary for droplets to be measured to pass through the laser beam; all measurement functions were then automatic. Results were computed in the micro-computer and presented on the VDU/CRT display in both numerical and histogram forms, together with a hard copy for long-term retention of results. The desk-

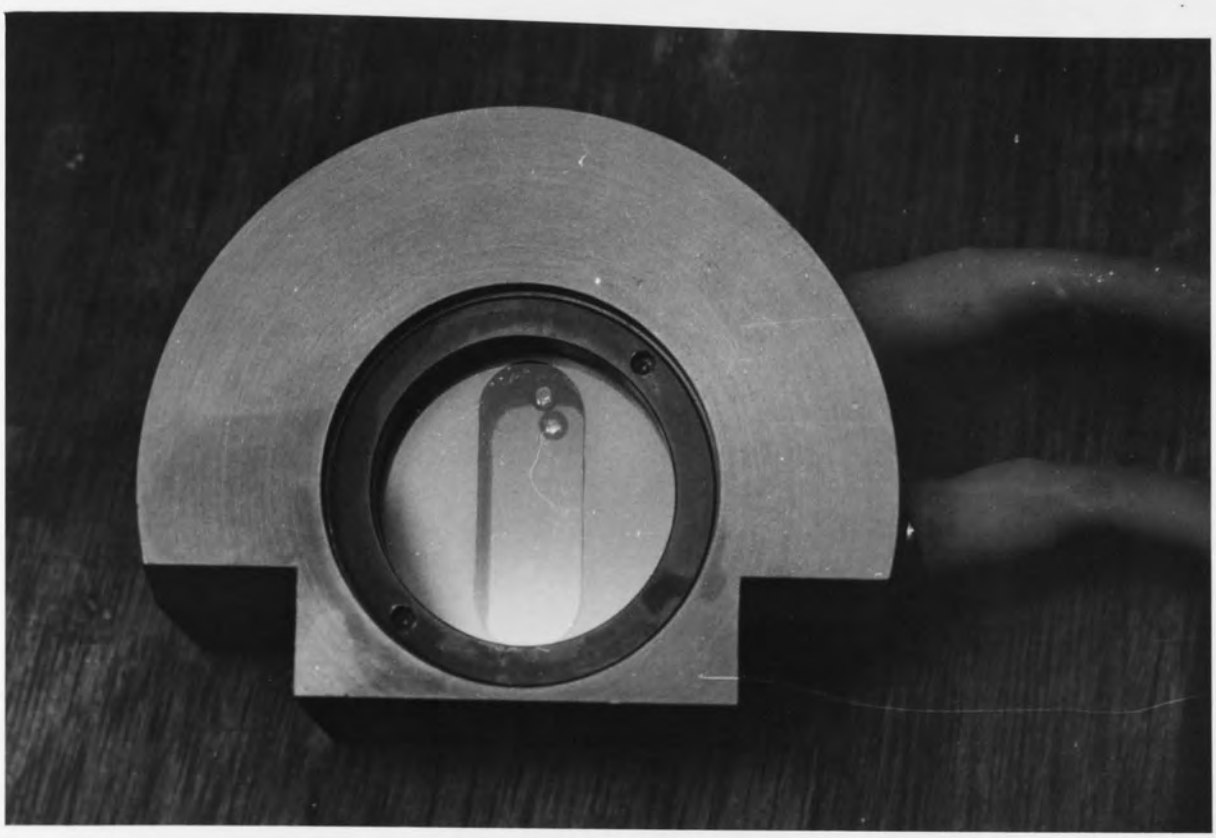

a CIRCULATED SAMPLE CELL

b ARRANGEMENT OF SAMPLE CELL

PLATE 6.2 CIRCULATED SAMPLE CELL OF MALVERN PARTICLE SIZE ANALYSER

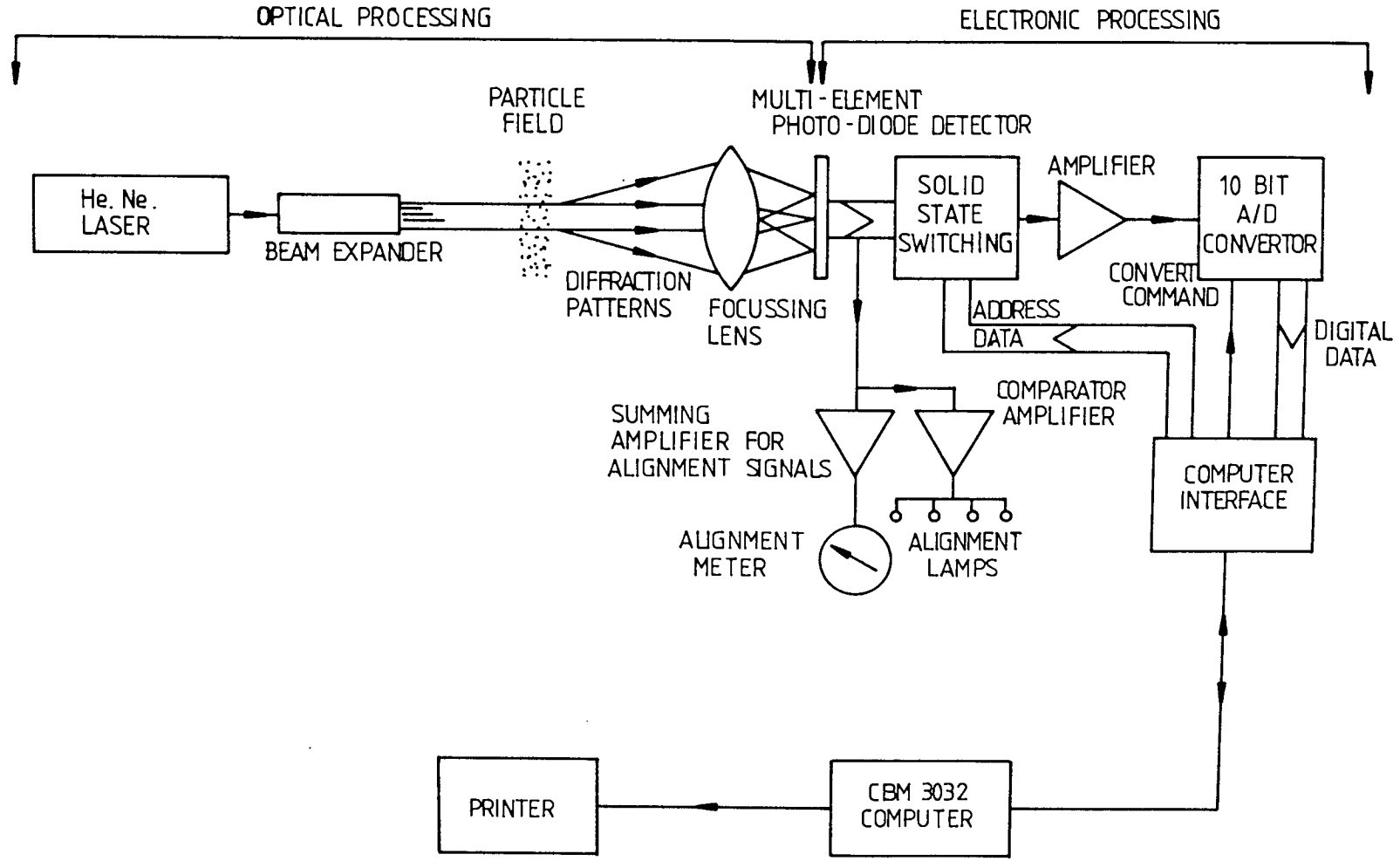

Figure 6.4 Basic opto-electronic system to obtain particle size and distribution.

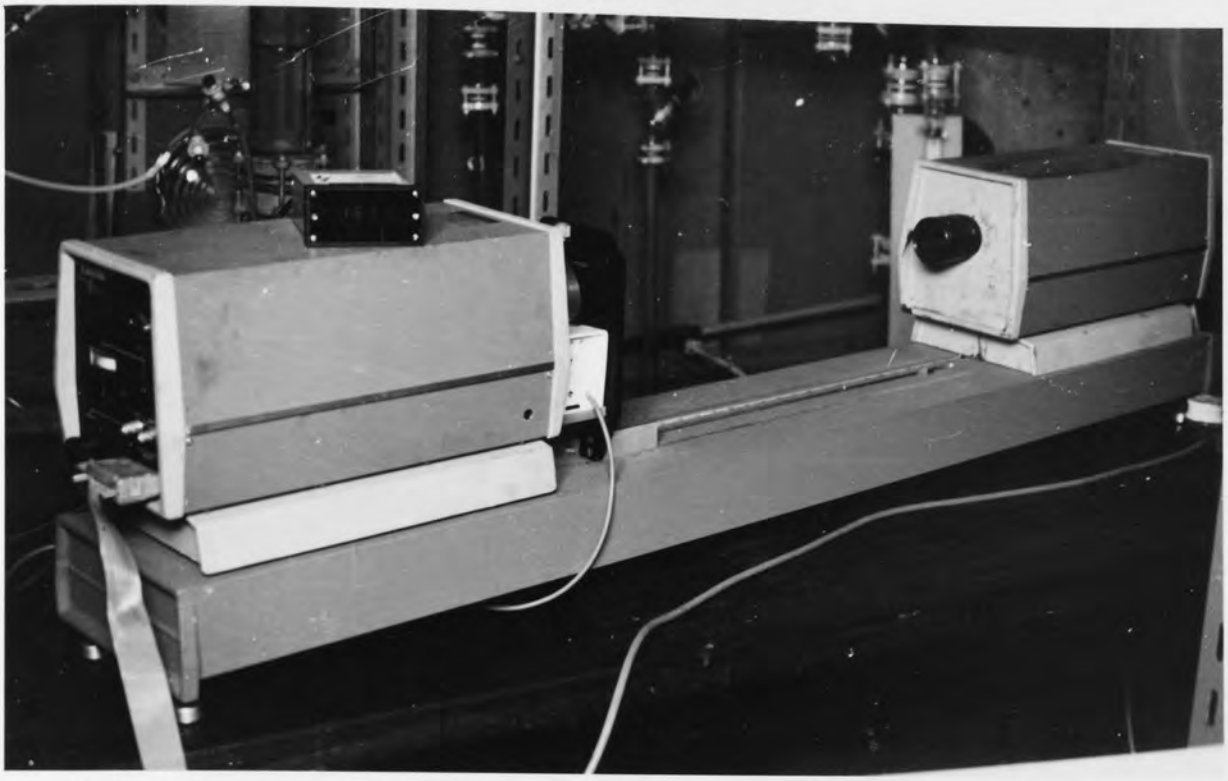

a OPTICAL MEASUREMENT UNITS

(He/Ne Laser emitter and electronic processing unit-receiver)

b CBM 3032 DESK-TOP COMPUTER SYSTEM WITH HIGH SPEED LINE PRINTER

PLATE 6.3 GENERAL ARRANGEMENT OF MALVERN 2200 PARTICLE SIZE ANALYSER CONNECTED DIRECTLY TO THE EQUIPMENT

top computer was a modified CBM 3032. The printer was a standard CBM tracer feed line printer. The application programme consisted both of an operation system relaying information to and from the user, and the data processing and results presentation [182]. Measurement could be taken as rapidly as at intervals of 40 micro seconds, and up to 32 consecutive measurements could be stored in the tape recorder. The time intervals were under user control.

6.1.4.2 *Measurement Procedure*

The Malvern 2200 Particle Sizer was aligned in the normal way to get all four lights flashing. This was done with the measurement cell unclipped from its holder and moved out of the beam. The reflected lights spot was seen just above the aperture in the beam expander. This prevented the reflections from the glass cell interfering with the main beam. Using only the control knobs protruding from the side and top of the receiver housing, the system was then re-aligned for all four lights flashing. Final small adjustments were made using the horizontal and vertical controls on the receiver rear panel.

The potentiometer was adjusted for a reading of 10 with the system primed with clean fluid with the "circulate" valve open and the flow running slowly inside the "circulate cell". A background reading was then taken. All background data in the output list had to be <30. An example of background reading is shown in figure 6.5.

The sample to be measured was next introduced into the "circulate cell" by re-opening the valve and letting the dispersed flow run slowly inside the cell. After the sample was circulating and fully dispersed, 10 seconds were allowed before taking a measurement using an EL command. A minimum of 1000 sweeps was advisable to ensure representative sampling. (This should be increased for large size droplets since there will be fewer of them in the cell at any one time; but < 1000 sweeps is acceptable if the droplets are very small as in this study). The supply flow rate was regulated and the dispersed sample flow was constant [182].

PRINTING INPUT DATA

RUN NO.	TIME	OBSCURATION
3	00-25-40	1.00

INDEX	SIGNAL	BACKGROUND	DATA
1.00	0.00	27.02	- 14.91
2.00	0.00	27.85	- 16.81
3.00	0.00	15.72	- 9.94
4.00	0.00	12.29	- 8.25
5.00	0.00	11.73	- 8.16
6.00	0.00	11.14	- 7.31
7.00	0.00	12.36	- 8.50
8.00	0.00	11.28	- 8.09
9.00	0.00	10.84	- 8.09
10.00	0.00	11.75	- 9.06
11.00	0.00	11.32	- 8.97
12.00	0.00	11.24	- 9.09
13.00	0.00	10.81	- 8.94
14.00	0.00	11.00	- 9.22
15.00	0.00	11.85	- 10.06
16.00	0.00	13.93	- 11.97
17.00	0.00	15.16	- 13.09
18.00	0.00	16.24	- 14.06
19.00	0.00	20.54	- 17.94
20.00	0.00	23.98	- 21.22
21.00	0.00	21.72	- 19.41
22.00	0.00	24.74	- 22.28
23.00	0.00	26.53	- 24.09
24.00	0.00	23.44	- 21.50
25.00	0.00	21.97	- 20.38
26.00	0.00	18.62	- 17.47
27.00	0.00	17.78	- 16.53
28.00	0.00	16.44	- 15.56
29.00	0.00	15.76	- 15.28
30.00	0.00	14.76	- 14.72

Figure 6·5 Malvern 2200 Particle Sizer Background Reading Printout

The results of the analysis, a size distribution of the sample by weight, could be displayed graphically on the VDU screen of the computer or printed as a hard copy on the line printer. The size distribution could be presented as the weight in size bands, the cumulative weight below a size, and the cumulative weight above a size. When a size distribution of the dispersion was made, the log error for the two parameter programmes was required to be < 5 to establish that the independent model was an adequate fit of the sample data.

The results of an E and a BL command were two data sets which were combined to give a "derived data" set that was used in further analysis. The derived data was automatically placed into a "Block Memory" of the system. The software had 32 "Block Memories" each of which could hold a complete experiment's data for analysis. Thus it was possible for the machine to perform 32 experiments and hold all the data for subsequent analysis. At any time the current block memory was identified by a Block Pointer.

A print output of a sample analysis using the independent model are shown in figures 6.6 to 6.8. Further details on this technique and the mode of operation are to be found in the Malvern 2200 Particle Sizer Handbook [182].

6.2 Exit Drop Size Analysis

Photography has previously been used successfully to analyse the effluent primary dispersion leaving a coalescer [16, 17, 27, 47, 57, 75, 95, 104-106]. Despite the inherently-tedious nature of drop size distribution analysis using manual counting methods, photography was selected in this study because of its simplicity and reliability. Photographs of drops leaving the coalescer were taken on Kodak Trix-Pan 35mm, 400 ASA film using a Nikkormat still camera fitted with an f3.5, 55m Nikon lens. A shutter speed of 1/5000 second was used to "freeze" the drops. Illumination was provided from the rear of the column by light uniformly diffused through a 2mm polypropylene sheet.

The negatives were enlarged to give an overall magnification of the true drop

PRINTING VARIABLES

FOCUS	LENGTH	RI SAMPLE	RI MEDIUM
63	14.30	1.50	1.33

PRINTING DATA BLOCK 24

RUN NO.	TIME	OBSCURATION
33	01-13-00	0.21

INDEX	DATA
1	61.03
2	66.28
3	90.03
4	112.31
5	133.22
6	147.25
7	176.59
8	182.22
9	187.94
10	223.13
11	223.50
12	225.91
13	214.78
14	197.22
15	181.91
16	167.69
17	157.59
18	154.47
19	152.81
20	159.50
21	166.50
22	178.44
23	198.66
24	223.38
25	254.75
26	292.84
27	327.94
28	378.47
29	440.59
30	486.41

Figure 6·6 Malvern 2200 Particle Sizer "derived data" Printout

PAGE 1.

DATA BLOCK 24

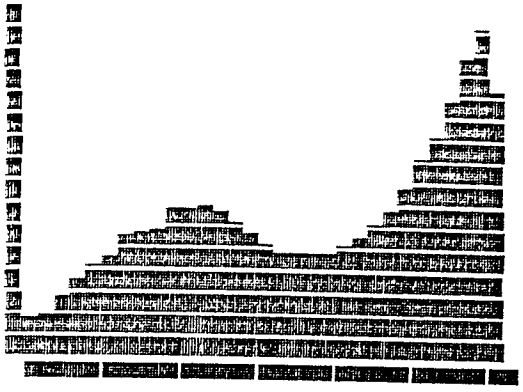

DETECTOR RING NO. (5/DIV)

MALVERN 2200/3300 PARTICLE SIZER V3.1

MALVERN INSTRUMENTS LTD, SPRING LANE, MALVERN, ENGLAND.

PRINTING RESULTS FROM DATA BLOCK 24

TIME 01-13-00 RUN NO. 33 LOG ERROR = 3.84

SAMPLE CONCENTRATION = 0.0029 % BY VOLUME
OBSCURATION = 0.21

SIZE BAND UPPER	SIZE BAND LOWER	CUMULATIVE WT BELOW	WEIGHT IN BAND	CUMULATIVE WT ABOVE	LIGHT ENERGY COMPUTED	LIGHT ENERGY MEASURED
118.4	54.9	99.3	0.7	0.0	266	281
54.9	33.7	94.9	4.4	0.7	422	447
33.7	23.7	80.3	14.6	5.1	583	619
23.7	17.7	54.1	26.2	19.7	734	792
17.7	13.6	35.7	18.4	45.9	868	908
13.6	10.5	23.2	12.5	64.3	914	992
10.5	8.2	16.1	7.1	76.8	867	910
8.2	6.4	16.1	0.0	83.9	746	772
6.4	5.0	14.0	2.1	83.9	660	689
5.0	3.9	14.0	0.0	86.0	636	690
3.9	3.0	14.0	0.0	86.0	742	762
3.0	2.4	14.0	0.0	86.0	946	932
2.4	1.9	14.0	0.0	86.0	1215	1209
1.9	1.5	11.4	2.6	86.0	1608	1560
1.5	1.2	7.8	3.6	88.6	2047	2047

Figure 6.7 Malvern 2200 Particle Sizer sample analysis Printout

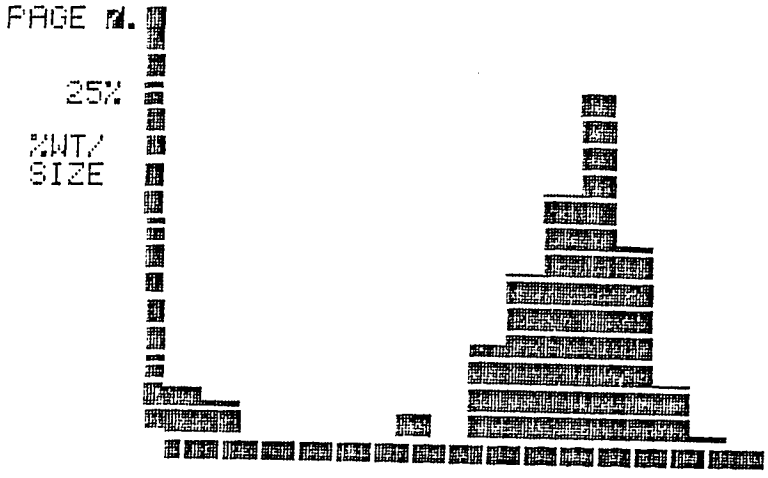

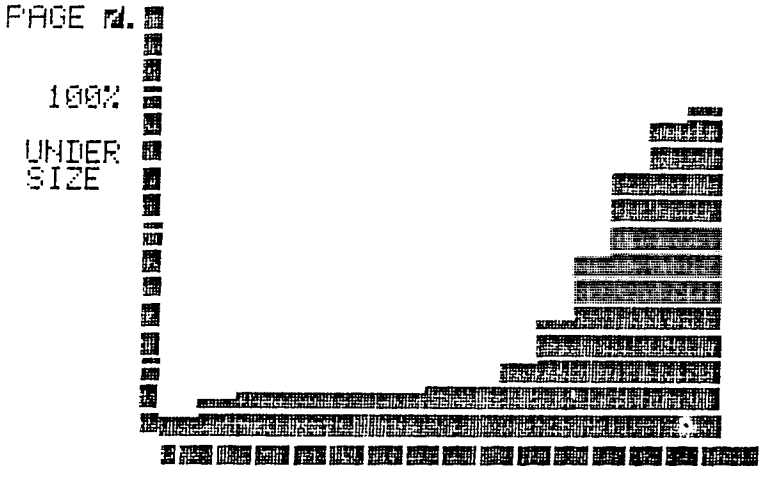

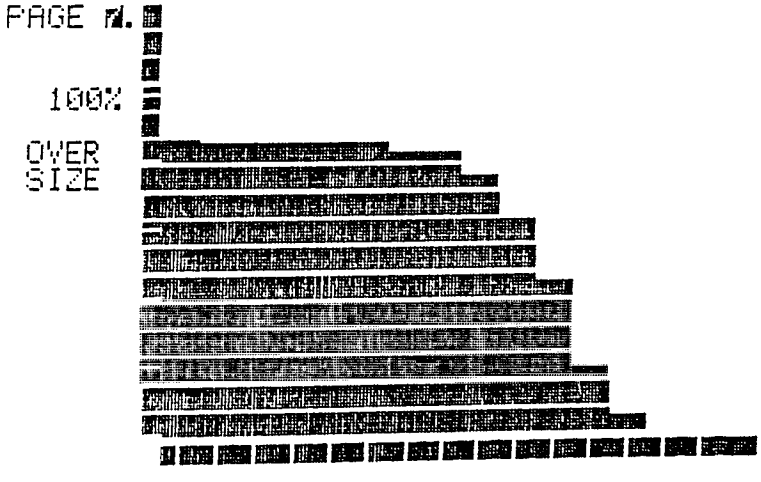

Figure 6·8 Malvern 2200 Particle Sizer Sample Analysis Graphical Printout represented in Histogram form

size of about 3 times and were printed on grade 4 'Bromesko' paper. This gave sufficient magnification and contrast for counting. Calibration of the counting technique was performed by photographing a graduated millimetre scale on the outer wall of the coalescer column. The enlarged photograph of the scale was then compared with the reading on the counter.

Manual counting of drops recorded on the photographs was accomplished by a Zeiss TG3 particle counter to identify and record linear drop dimensions.

6.3 The Stereoscan Electron Microscope

The Stereoscan electron microscope produced three-dimensional photographs of the sample under observation. It had a wide magnification range, from 20,000 to 100,000x, although the image began to blur above 20,000x. This broad magnification range, together with the ease of changing magnification made it possible to zoom from a gross image of the object to an image showing fine details.

Inspection of the nature of packing material surfaces (i.e surface roughness) and microscopic examination of the relevant dimensions of meshes was by studying the micro-photographs taken by this technique.

6.4 Bed Voidage Determination

The single phase initial bed voidage was determined using a displacement method. Distilled water was pumped through the particulate bed at high flow rate, for twenty minutes to displace all air bubbles. Some of the water was then drained down the bed to a predetermined level 15cm above the packing. A measured volume, 200×10^{-6} m^3 of water was removed from the column and the distance the water level dropped was measured. This procedure was repeated until the water level was about one centimetre above the packing. These initial measurements were used to obtain an average value for the water level drop per $200 \times 10^{-6} m^3$ since the column diameter could not be assumed

uniform because of the addition of the pressure taps. Following this, 200 x $10^{-6}m^3$ were collected and the water level reduced to beneath the packing. This reduction in the water level was measured; from this value together with packing thickness, packing bulk volume and the initial average value recorded, the bed voidage was calculated as shown in Appendix C. This was an average voidage determined over the whole bed. Voidages in the range 0.238 to 0.428 were utilised in this study.

6.5 Measurement of Proportion of Residual Dispersion in the Outlet Stream

Smith [35] measured small quantities of oil in water by extracting the oil with carbon tetrachloride followed by evaporation of the solvent at 70°C in a current of air. Approximately 1 litre samples of effluent were taken for this process and about 8 hours was needed for evaporation before the oil residue was weighed. This method did not give accurate results because some of the oil residue could evaporate and be lost during the 8 hours evaporation process. Furthermore, it was time-consuming.

Therefore, in this study, the ultraviolet absorbance of liquid technique [183] was used to measure the concentration of residual dispersion in the exit stream. This technique was also used to check the inlet concentration of dispersions before coalescence in the particulate beds.

The procedure for measurement of concentration of any dispersion was as follows:

i. Samples of dispersion were taken from the inlet and outlet streams by using the tap on the bottom and on the top of the coalescer respectively. The sample of the outlet stream was settled for about 3 minutes in a clean beaker to allow for separation of any large primary droplets. 10 ml volume samples were then taken from several positions in the sampling beaker.

ii. The oil present in each 10 ml sample was extracted with carbon tetrachloride (eg 50

ml). The solvent was then separated from water at room temperature using a separation funnel.

iii. The ultraviolet absorptivity of the solvent sample was determined by measuring the absorbance, at specified wave length (e.g for toluene 269μm [184]), in a cell of known path-length.

iv. A graph was plotted between concentration of toluene in the solvent (i.e carbon tetrachloride) and absorbance of liquid. A calibration graph was also plotted for concentrations of toluene in samples, as shown in Appendix B6-B8. Hence from the reading of absorbance values, the oil concentration in the secondary dispersions could be read directly from these graphs.

CHAPTER SEVEN

ANALYSIS OF PRESSURE DROP DATA

Steady-state and unsteady-state operation of ballotini bed coalescers were studied for the separation of oil-in-water secondary dispersions at constant temperature, 20 ^{o}C. The parameters and variables are listed in Table 7.1.

7.1 Single Phase Flow Pressure Drop

A study was made of pressure drop during single phase flow to determine the pressure drop characteristic of the porous media (ie particulate beds) for coalescence. It also served to check the reproducibility of the packing technique , and to detect any foreign particulate matter or re-arrangement of the individual particles in the coalescer bed. Furthermore the data provided a basis for comparison with that during two-phase flow with coalescence.

The individual experimental work on single-phase flow pressure drop was carried out by Darcy [114]. The relationship obtained, termed Darcy's Law, showed the average velocity to be directly proportional to the driving pressure and inversely proportional to the thickness of the bed. This relation can be written [114]

$$U = K_f \frac{\Delta P}{L} = B \frac{\Delta P_1}{\mu_c L} \qquad \ldots. 7.1$$

where K_f is a constant depending on the physical properties of the bed and fluid and B is the permeability coefficient of the bed, which depends only on the properties of the bed. The value of B is frequently used to give an indication of the ease of passing a fluid through a bed of particles. The linear relationship between the rate of flow and pressure drop is charateristic of streamline flow; therefore the value of B only applies to the

Table 7.1

List of Parameters and Variables

General variables	1	Inlet drop size (pump speed)
	2	Superficial velocity
	3	Phase ratio
	4	Liquid-liquid system (o/w)
		a) interficial tension
		b) Viscosity
Bed variables	1	Particle diameter
	2	Bed depth
	3	Bed materials. Packing arrangment
	4	bed voidage or porosity
	5	Sphericity or shape of particles
Measured variables	1	Exit drop size and size distribution
	2	One phase and two phase pressure drop
	3	Mechanisms of coalescence
	4	Coalescence efficiency
	5	Average saturation (hold-up)
	6	Friction factor
	7	Wettability (liquid and packing material properties)
System parameters	1	Surface tension
	2	Dispersed and continuous phase viscosities
	3	Dispersed and continuous phase densities
	4	Temperature
	5	Diameter of coalescers

laminar flow regime. For flow through industrial packed columns Ergun [185] obtained a semi-empirical correlation for pressure drop,

$$\frac{\Delta P_1}{L} = 150 \frac{(1-e_1)^2}{e_1^3} \frac{\mu_c U}{dc^2} + 1.75 \frac{(1-e_1)}{e_1^3} \frac{\rho_c U^2}{dc} \qquad \text{.... 7.2}$$

For low values of Reynolds number, ie

$$N'_{Re} = \frac{dc\rho_c U}{\mu_c (1-e_1)} < 10 \qquad \text{.... 7.3}$$

the second term on the rightside is negligible and equation 7.2 reduces to the Blake-Kozeny equation. The value of the constant, 150 is equal to the product of Kozeny constant K and another constant which relates the characteristic particle diameter, dc to the specific surface area, a:

$$\text{for spheres, } dc = \frac{6}{a} \text{ or } dc^2 = \frac{36}{a^2}, \qquad \text{.... 7.4}$$

The calculated value of Kozeny constant, K is $\frac{150}{36} = 4.17$. For cylinders the value of the constant should be taken as 16K (ie assuming the height of a cylinder is equal to the radius of the base $h = \frac{d}{2}$; $dc^2 = \frac{16}{a^2}$) and so on.

Macdonald et al [186] modified the Ergun equation as follows:

$$\frac{\Delta P_1}{L} = \frac{180\,\mu_c U (1-e_1)^2}{dc^2 e_1^3} + \frac{1.8\,\rho_c U^2 (1-e_1)}{dc\ e_1^3} \qquad \text{.... 7.5}$$

which reduces to the Carman-Kozeny equation for low Reynolds numbers (ie $N'_{Re} <$ 10). The constant, 180, is equal to the product of Kozeny constant, K and another constant relating the characteristic particle diameter to the specific surface. The

commonly-accepted value for the Kozeny constant is 5.0 however, as will be shown in section 7.4. K depends on, among other factors, the structure of the bed, voidage fraction, and particle shape.

7.2 Single Fluid Phase Flow Equations

Fluid flowing through a bed of particles or other porous medium as distinct from a conduit, flows through passages between the particles of the bed. The dimensions of these passages depend upon porosity of the bed, diameter of the particles, sphericity or shape of the particles, orientation or spacing arrangement of the particles, roughness of the particles and the superficial velocity.

As discussed in section 5.4.1, monosized ballotini glass spheres were selected as the packing media since their internal geometry would be known. For the case of beds of particles there are different model approaches for the treatment of single phase flow. Two fundamentally different approaches can be distinguished:

i) The flow around solid objects immersed in the fluid is considered; or

ii) the flow inside conduits is analysed.

For low and intermediate porosities the conduit flow approach is more appropriate, whereas for very high porosities the first approach is more suitable.

The empirical correlations obtained , often aided by dimensional analysis and theoretical considerations, have been termed "phenomenological models" [187]. This approach is independent of considerations pertaining to conduit flow or flow around submerged objects. Phenomenological models have proved to be paticularly useful in the case of packs of fairly uniform and isometric particles.

Rumpf and Gupte [188] proposed the following relationship among the dimensionless parameters,

$$\frac{\Delta P_1}{\rho_c U^2} = f\,(U\,dc/\nu,\ L/dc,\ e_1,\ \emptyset_i,\ \text{structure}) \qquad \ldots. 7.6$$

The various parameters that characterise particle shape and packing structure may be very difficult to evaluate in the general case. For random packs consisting of various distributions of spherical particles over a wide range of voidages the expression proposed for the permeability was [188],

$$B = \frac{dcs^2 \, e_1^{5.5}}{5.6 \, K_1} \qquad \text{.... 7.7}$$

where dcs is the "surface average" sphere diameter and the value of the constant K_1 depends on the particle size distribution parameters, particle shape and packing structure.

The Carman-Kozeny model [189, 190] often called the "hydraulic radius theory", is sometimes regarded as a phenomenological approach. The porous medium was assumed to be equivalent to a conduit, the cross-section of which has an extremely complicated shape but, on the average, a constant area., The value of the permeability, when the Carman-Kozeny model is related to Darcy's Law equation, can be obtained by this equation:

$$B = e_1 \, d_H^2 / 16Ko \, (Le/L)^2 \qquad \text{.... 7.8}$$

The hydraulic diameter", d_H, can be expressed as,

$$d_H = 4e_1 / a(1-e_1) \qquad \text{.... 7.9}$$

where a is the specific surface area based on the solid's volume. By combining equations 7.8 and 7.9, the usual form of the Carman-Kozeny equation for the permeability is obtained:

$$B = e_1^3 \, / Ko \, (Le/L)^2 \, (1-e_1)^2 \, a^2 \qquad \text{.... 7.10}$$

where (Le/L) is the tortuosity (Te). According to Carman [189], the best numerical value of the combined factor $K = Ko \, (Le/L)^2$ to fit most experimental data on packed beds is 5, where K is the "Kozeny constant". Defining the mean particle diamter dc as the diameter of the hypothetical sphere with the same specific surface (ie dc = 6/a) the

final equation for permeability becomes:

$$B = \left[\frac{dc^2}{180}\right] \cdot \left[\frac{e_1^2}{(1-e_1)^2}\right] \qquad \text{.... 7.11}$$

Scheidegger [191] distinguished straight-, and parallel-type capillaric models which were based on the geometric arrangement of the packings and their voidages. The first of these consists of a bundle of parallel capilliaries of equal length and the same diameter d. For this model, the following expression was obtained for the permeablity:

$$B = e_1 \, d^2 / 32 \qquad \text{.... 7.12}$$

In the "parallel-type" model the right hand side of equation 7.12 is divided by three, since 1/3 of the capillaries should be pointing in each of three spatial directions, and the mean square diameter is evaluated according to some pore size distribution function. Therefore the permability of Scheideggers's parallel-type capillary model becomes:

$$B = (e_1 /96) \cdot \int_0^\infty d^2 \, \phi(d) \, dd \qquad \text{.... 7.13}$$

where $\phi(d)$ is a "pore size distribution" function.

In the "serial type" capillaric model, the pore network is approximated by three indentical sets of tortuosity channels. Hence, the expression for the permeability for this model is:

$$B = \frac{e_1}{96Te} \cdot \frac{\{\int_0^\infty f(d) \, dd/d^2\}^2}{\int_0^\infty f(d) \, dd/d^6} \qquad \text{.... 7.14}$$

The factor 96 was again introduced on the grounds that 1/3 of the total capillaries point in

each spatial direction.

Millington and Quirk [192] obtained the following expression for the permeability

$$B = \frac{2\, e_1^{4/3}}{32} \int_0^{\infty} f(de)\, dde \,.\, \int_0^{de} (de)^2 \,.\, f(de)\, dde \qquad \ldots. 7.15$$

Here, the pores in the solid matrix are assumed to be distributed at random so that their chance of overlap is governed by random probability. This expression has been modified by Marshall [193] by using e_1^2, as the voidage function. A different way of expressing the resistance of the porous medium to flow involves a friction factor, f,

$$f = \frac{dc}{\rho_c\, U^2} \,.\, \frac{\Delta P_1}{L} \qquad \ldots. 7.16$$

as a function of the superficial Reynolds number, N_{Re},

$$N_{Re} = \frac{dc\, U\, \rho_c}{\mu_c} \qquad \ldots. 7.17$$

The different models have been presented in terms of friction factor by many workers. Morcom [194] proposed for spheres and irregular broken materials the expression:

$$f = \frac{800}{N_{Re}} + 14 \qquad \ldots. 7.18$$

and for flat-ended cylinders,

$$f = \frac{1750}{N_{Re}} + 28 \qquad \ldots. 7.19$$

Chilton and Colburn [195] suggested that for low rates of flow ($N_{Re} < 40$)

$$2f = 850 / N_{Re} \quad \text{.... 7.20}$$

and for high rates of flow

$$2f = 38 / (N_{Re})^{0.15} \quad \text{.... 7.21}$$

For laminar flow the equation may be used to predict friction loss through spherical particulate beds as [196],

$$f = 64 / N_{Re} \quad \text{.... 7.22}$$

At flow rates outside the range of validity of Darcy's Law, the two best-known relationships are, for intermediate values of $N_{Re} < 10^3$, the Ergun [185] equation:

$$f = \frac{(150/N_{Re})\,(1-e_1) + 1.75}{\{e_1^3 / (1-e_1)\}} \quad \text{.... 7.23}$$

and, for higher values of N_{Re}, the Burke Plumer equation:

$$f = \frac{1.75}{\{e_1^3 / (1-e_1)\}} \quad \text{.... 7.24}$$

Macdonald [186] developed the Ergun equation, using more data than previously and found that the following relations gave the best fit to all the data:

Smooth particles: $$f = \frac{(180 / N_{Re})\,(1-e_1) + 1.8}{\{e_1^3 / (1-e_1)\}} \quad \text{.... 7.25}$$

Roughest particles: $$f = \frac{(180 / N_{Re})\,(1-e_1) + 40}{\{e_1^3 / (1-e_1)\}} \quad \text{.... 7.26}$$

For intermediate surface roughness, the value of the second term, the inertia parameter lies between 1.8 to 4.0.

Shape , or sphericity, of the particle, ψ, is defined as the surface area of a sphere having a volume equal to that of the particles divided by the surface area of the

particle.

The sphericity of a particle composed of agglomerated spheres is $N_S^{-1/3}$, where N_S is the number of spheres in the agglomerate. Most granular particles or crystals may be expected to have a sphericity varying from 0.7 to 0.8.

Orientation is an important variable in special cases. Pressure drops were determined for different arrangements of stacked spheres by Martin [197], as indicated in Figure 7.1.

In order to correlate the friction losses with Reynolds number, it was found necessary to draw a separate curve for each particular geometric orientation, as indicated in Figure 7.2. Such variations in orientation do not occur with the random packing generally encountered in industrial practice, although oriented beds are used in some absorbers and for other applications where the packing is stacked by hand.

7.3 Analysis of Single Phase Pressure Drop Data

Of the many equations used to describe single phase flow in packed beds, the Ergun equation [185], equation 7.3, is the most - frequently applied. For low values of Reynolds number, $N_{Ré} < 10$, the second term on the right-hand side is negligible and equation (7.3) reduces to the Blake-Kozeny equation,

$$\Delta P_1 = \frac{150\,\mu_c\,(1-e_1)^2}{e_1^3} \cdot \frac{L}{dc^2} \cdot U \qquad \ldots\ 7.27$$

In this work, depending on superficial velocity ballotini particle diameter and bed depth, 10 to 15 minutes were required for a packing to reach its equilibrium pressure drop, that is for the bed hold-up to reach a steady-state value.

Graphs of pressure drop versus single phase (water) flow are shown in Figures 7.3 and 7.4. These plots demonstrate linear relationships and the slopes are dependent

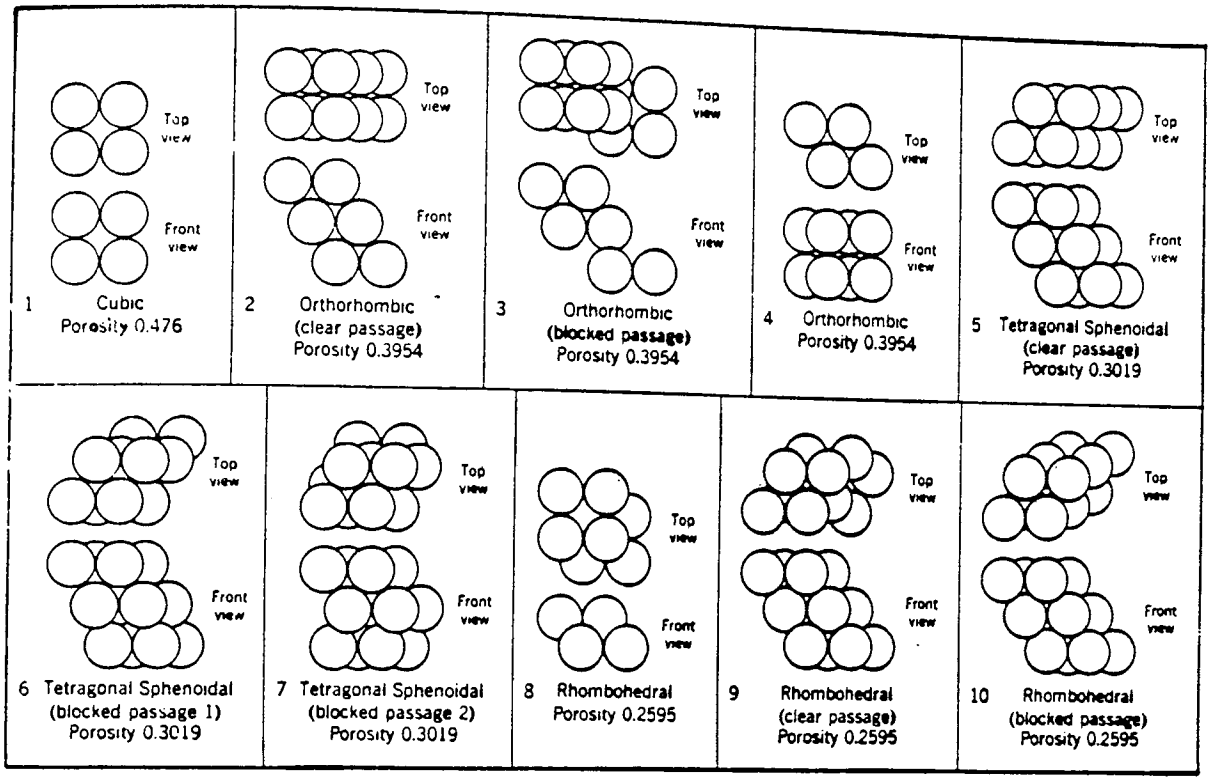

Figure 7.1 Systematic arrangement of spheres and their porosities.

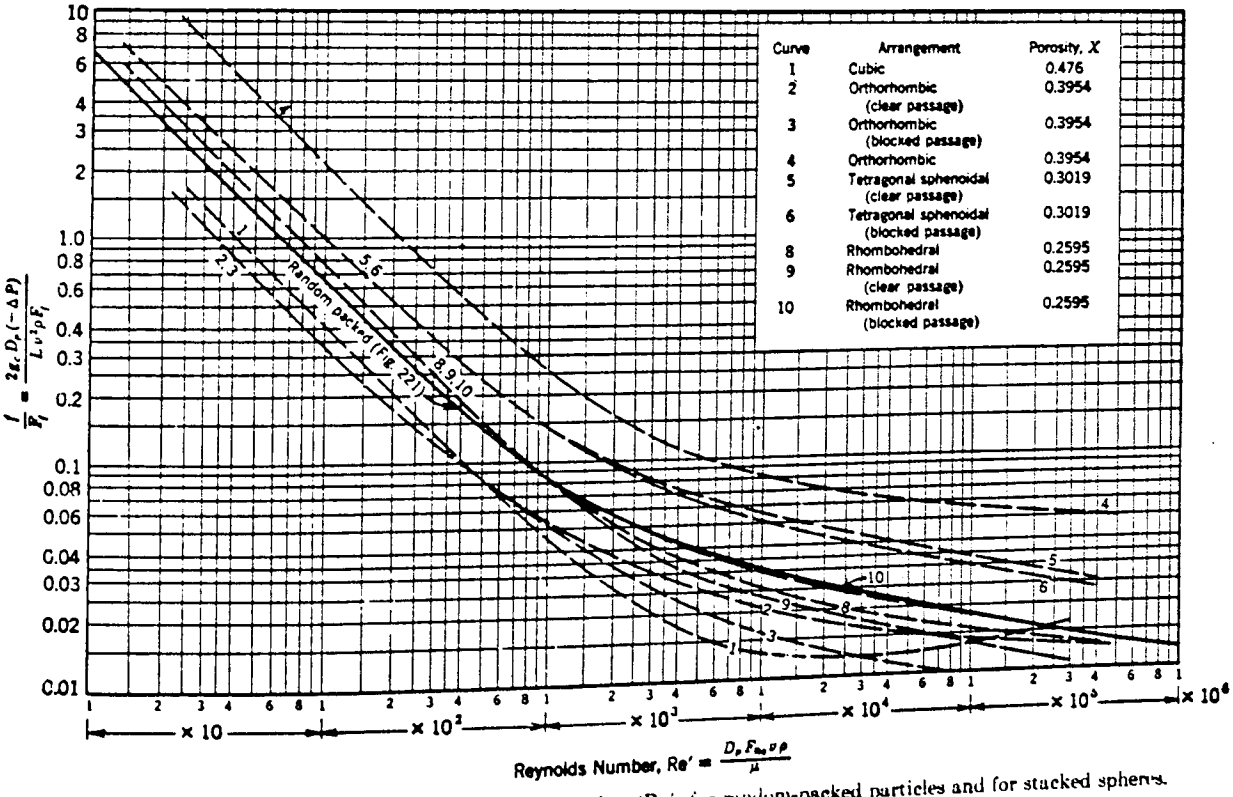

Figure 7.2 Friction factor (f/F_f) versus Reynolds number (Re') for random-packed particles and for stacked spheres.

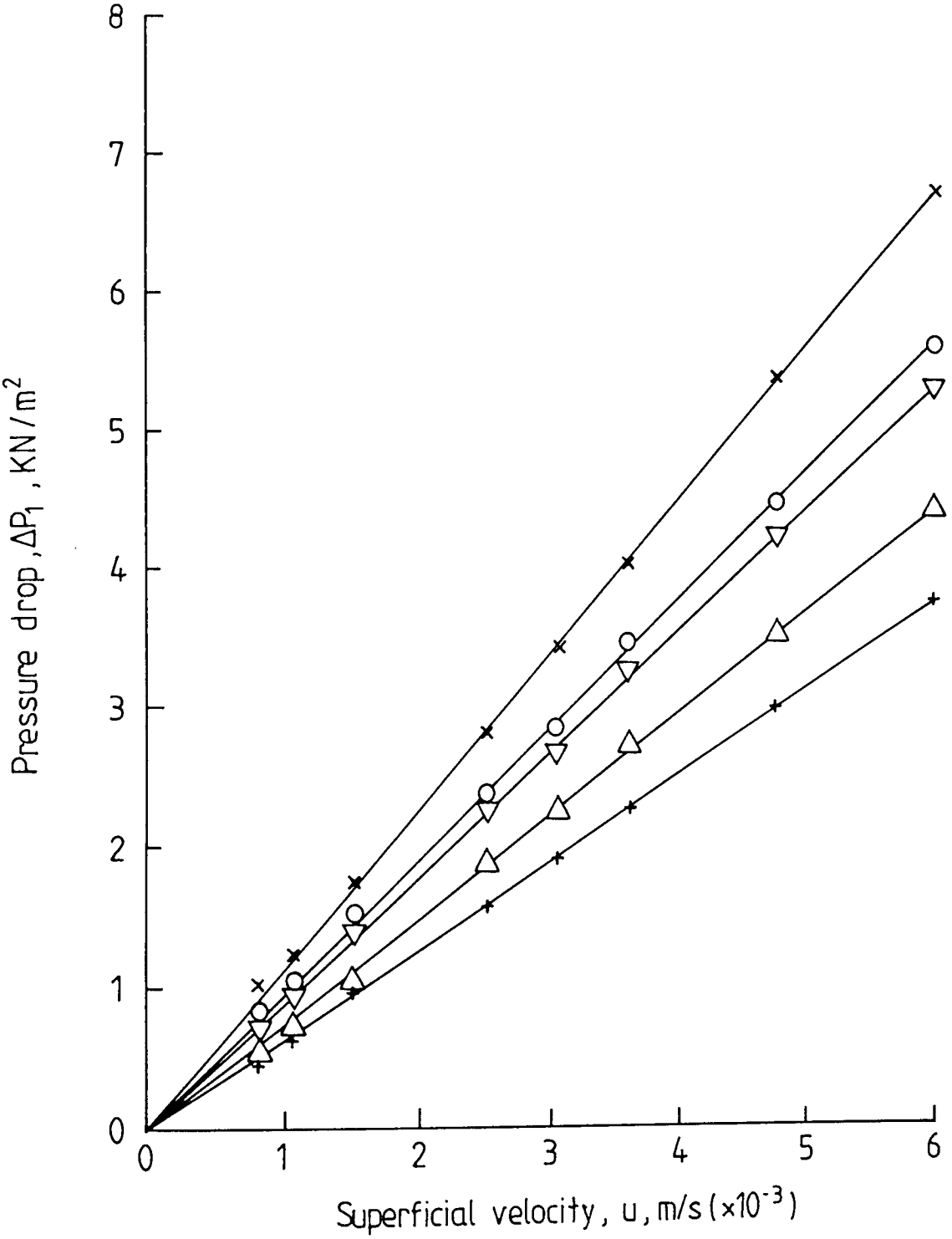

Figure 7·3 Pressure drop vs. superficial velocity for single phase flow (water) at different ballotini particle sizes.

Ballotini particle sizes, d_c, μm

× 146
○ 266
▽ 364
△ 487
\+ 615

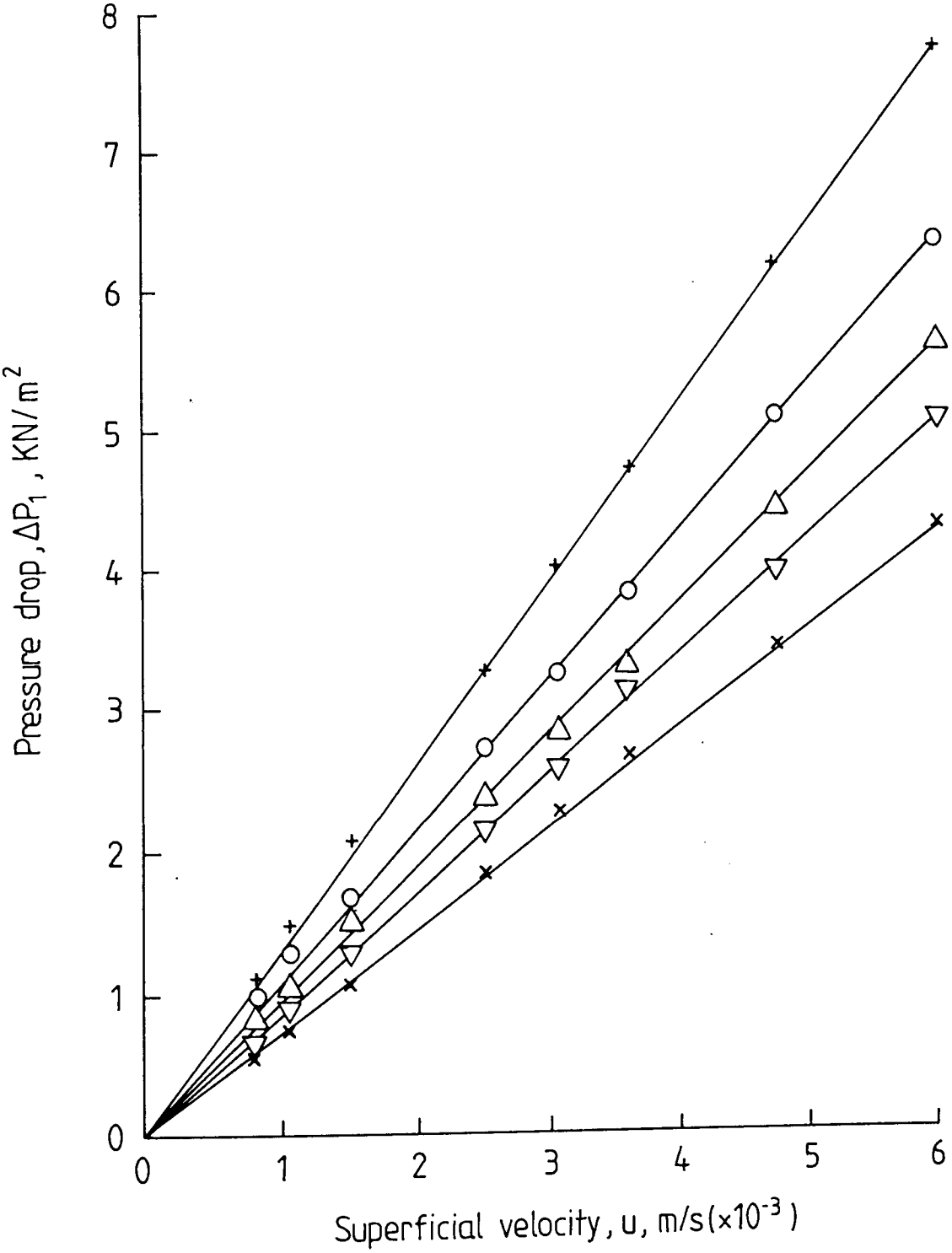

Figure 7·4 Pressure drop vs. superficial velocity for single phase flow (water) at different bed depths.

Bed depths, L, mm

× 10
▽ 20
△ 30
○ 40
+ 50

upon the ballotini particles diameter and bed depths.

7.4 Carman-Kozeny Constant

The modified Ergun equation, equation 7.5, proposed by Macdonald et al [186] was used to correlate the experimental results. The maximum value of the Reynolds number $N_{Ré}$, defined in section 7.1 was always ≤10 for the range of variables investigated. Therefore the second term involving U^2 could be neglected and equation 7.5 reduced to the Carman-Kozeny form.

$$\frac{\Delta P_1}{L} = \frac{180\,\mu_c\,U\,(1-e_1)^2}{dc^2\,e_1^3} \qquad \ldots. 7.28$$

For spherical particles, rearrangement of equation 7.28 gives,

$$\left[\frac{\Delta P_1}{\mu_c}\right]\left[\frac{e_1\,dc^2}{36\,L\,(1-e_1)^2}\right] = K\,.\,U \qquad \ldots. 7.29$$

The second term embodies all the properties of the packing which were evaluated experimentally.

The single phase pressure drop data was correlated against superficial velocity by linear regression analysis using equation 7.29, see Appendix G. The correlations obtained for different ballotini sizes and bed depths are illustrated in Figures 7.5and 7.6 respectively, where the slope of the best fit line is equal to the Carman-Kozeny constant. The results are shown in Table 7.2. Despite the care taken to ensure reproducibility during data acquisition, the Carman-Kozeny constant exhibits some variation.

The main factors which affect the value of the Carman-Kozeny constant are:

a) Effects of voidage:

The Carman-Kozeny equation has been tested with spherical particles over a

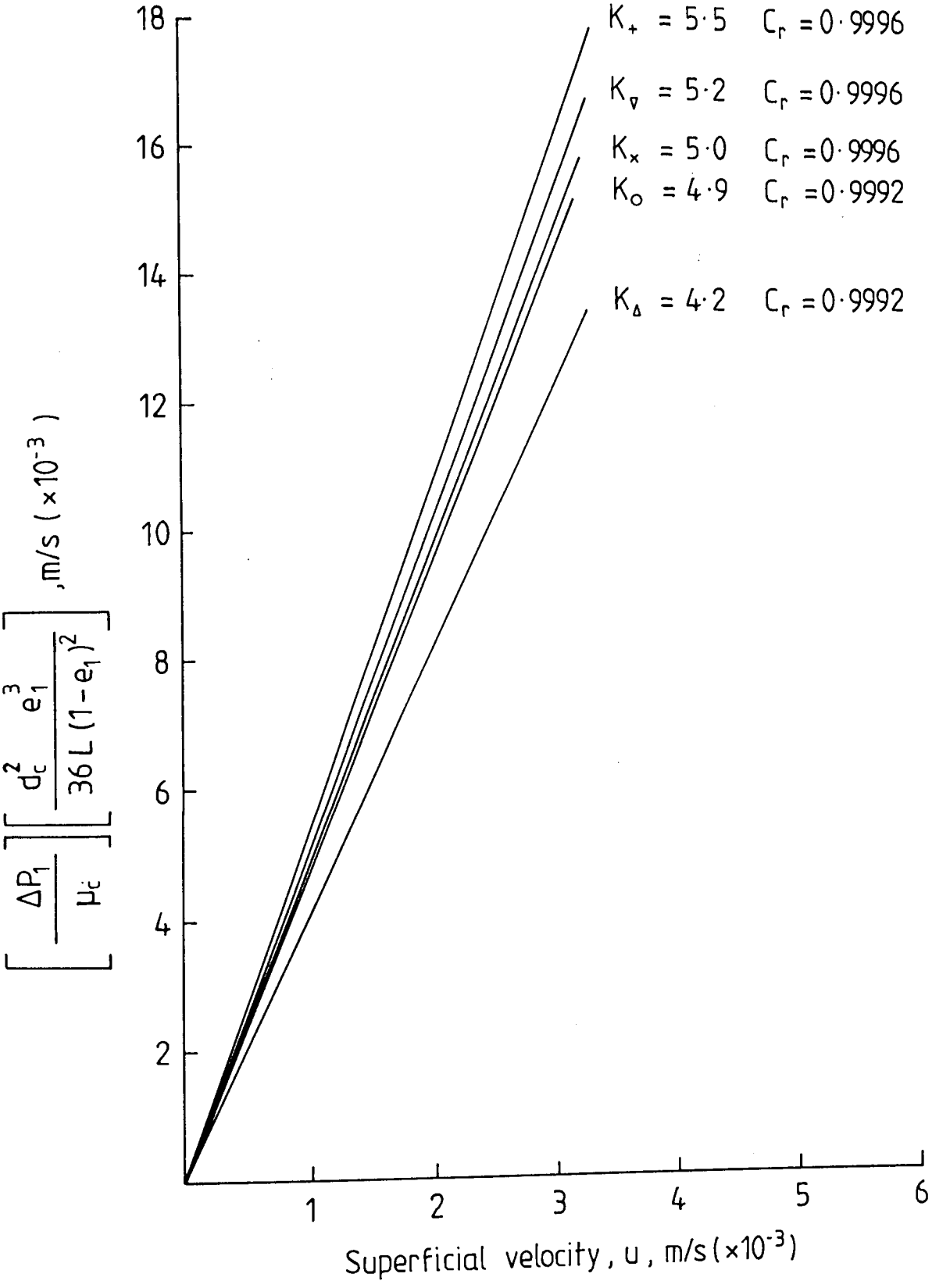

Figure 7·5 Correlation of single phase pressure drop at different ballotini particle sizes for 30 mm bed depth.

Ballotini particle sizes, d_c , μm

×	146
+	266
△	364
○	487
▽	615

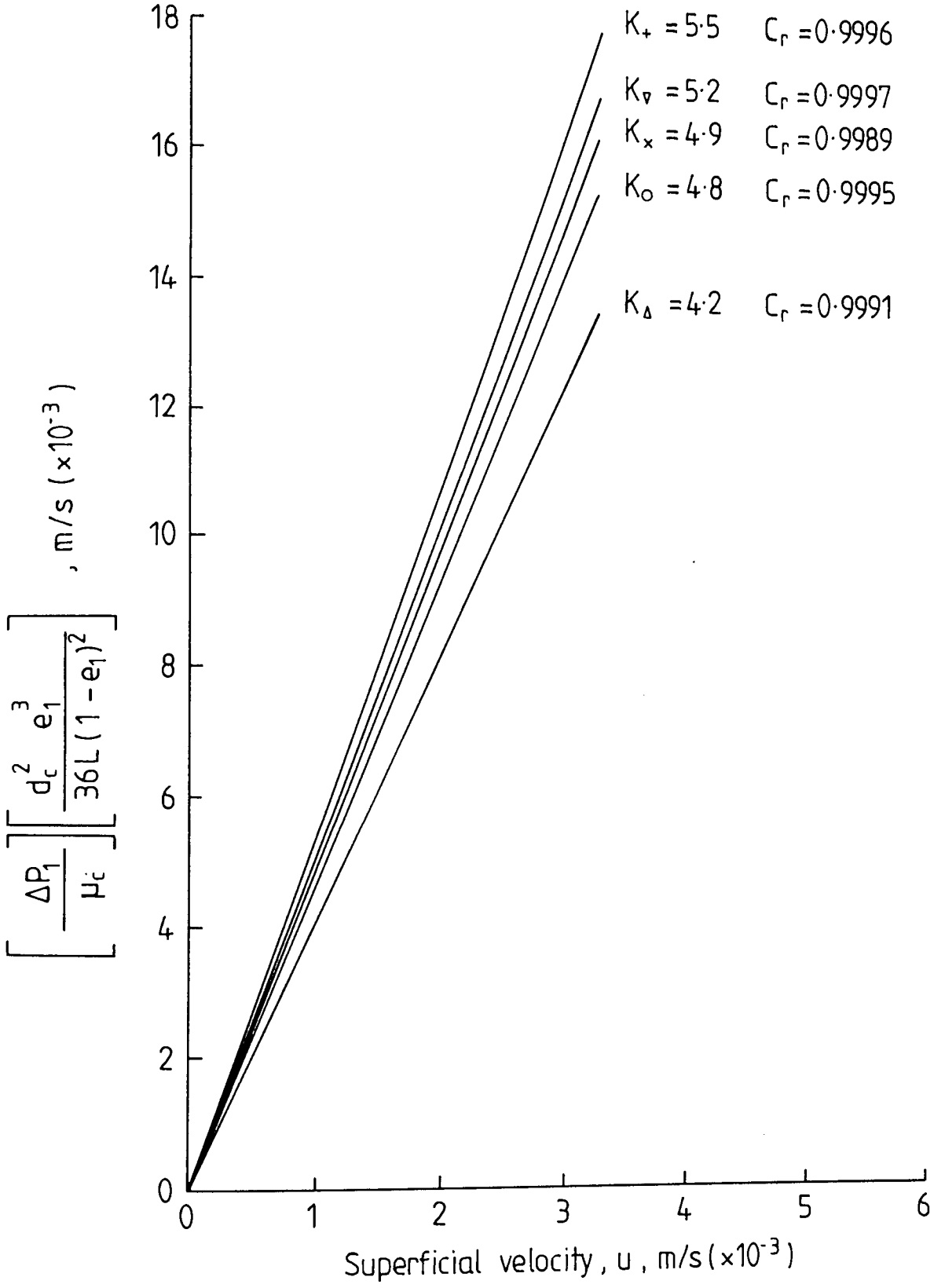

Figure 7·6 Correlation of single phase pressure drop at different bed depths for 266 μm ballotini particle size.

Bed depths, L, m ($\times 10^{-3}$)

×	10
▽	20
+	30
△	40
○	50

Table 7.2

Single Phase Pressure Drop Correlation

Ballotini Particle Size $dc_1 \mu m$	Bed Depth L, mm	Voidage e_1	Kozeny Constant K	Correlation Coefficient C_r	Run Number
146	20	0.407	5.6	0.9995	1A
	30	0.421	5.0	0.9995	2A
	40	0.428	4.5	0.9995	3A
266	10	0.264	4.9	0.9989	4A
	20	0.307	5.2	0.9997	5A
	30	0.338	5.5	0.9996	6A
	40	0.328	4.2	0.9991	7A
	50	0.342	4.8	0.9995	8A
364	20	0.457	4.7	0.9995	9A
	30	0.271	4.2	0.9992	10A
	40	0.303	5.5	0.9995	11A
487	30	0.254	4.9	0.9992	12A
615	30	0.238	5.2	0.996	13A

wide range of sizes and under many different experimental conditions [194, 198, 199, 200] and the Kozeny constant, K, has been found to ≈ 4.8 ± 0.3 in the streamline region. Different arrangements of spheres and their voidages are given on figure 7.1.

From equations 7.23 and 7.25 for low Reynolds numbers, the term $e_1^3/(1-e_1)^2$ could be considered the voidage function $f(e_1)$. For the Blake-Kozeny or Carman-Kozeny equations, the value of the constant in the various equations depends on the form of $f(e_1)$ used. For example the Blake-Kozeny equation gives a value of 150 and the Carman-Kozeny equation gives 180. The two "best values" of the constant differ by as much as 20%.

b) Shape Factor and Tortuosity:

According to Carman [189] the constant, K, can be written in the form:

$$K = Ko \left(\frac{Le}{L}\right)^2 \qquad \text{.... 7.30}$$

where $\left(\frac{Le}{L} = T_e\right)$ is the tortuosity and is a measure of fluid path length through the bed compared with the actual depth of the bed; Ko is a factor which depends on the shape of the cross-section of the channel through which fluid passes, as illustrated in Table 7.3, Le is the actual average effective length of fluid flow in a porous medium; and L is the geometrical length of the medium in the direction of macroscopic flow. Carman [189] listed values of Ko for many cross-sections; all lie within the range 2.0 to 3.0 with a probable average value of 2.5.

The value to be assigned to K is still controversial. From equation 7.30, if Ko is approximately 2.5, the magnitude of the Kozeny constant, K, would always be about 5.0. The work of Coulson [201], however, strongly indicates that even in the restricted void fraction range of 30% to 40%, K, is significantly dependent upon bed voidage and particle shape.

Table 7.3

Variation of Ko for Streamline Flow in Various Cross Sections

	Shape	K_o
1	Circle	2.0
2	Ellipses	
	a) Major Axis = twice minor axis	2.13
	b) Major axis = 10 times minor axis	2.15
3	Rectangles	
	a) length = breadth	1.78
	b) length = 2 by breadth	1.94
	c) length = 10 by breadth	2.65
	d) length = infinite	3.0
4	Equilateral Triangle	1.57
5	Pipes and Cores	
	a) Core set concentrically	2.0 - 3.0
	b) Core set eccentrically eccentricity < 0.7	1.7-3.0
	c) Core set eccentrically eccentricity < 0.7	1.2-2.0

Bartell and Osterhof [202] arrived at the Carman-Kozeny equation by regarding the equivalent capillaries as circular, that is Ko = 2.0, and with the aid of Hitchcock's [203] assumption that Le/L = $\pi/2$. This gives K = 2 $(\pi/2)^2$ = 4.9, in good agreement with their experimental value. It is difficult to explain why K≈ 5.0 for many different beds but one possibility is that changes in tortuosity from one bed to another have been compensated for by changes in Ko in the opposite direction.

c) Wall effect:

In a packed bed the particles do not pack as closely in the regions near the wall as in the centre of the bed; therefore the actual resistance to flow in a bed of small diameter is less than it would be in an infinite container for the same flow rate per unit area of bed cross-section. Coulson [201] determined experimentally a correction factor (fw) for this effect,

$$fw = (1 + 1/2 \ \frac{a_c}{a})^2 \qquad \text{.... 7.31}$$

where a_c is the surface of the container per unit volume of bed.

The effect of the ratio of the diameter of the container, D, to that of the particle, d_c, has been studied in many different systems. Carman [189] concluded that the wall effect is locally negligible if D/d_c >10 and Rose and Rizk [204] stated that it was negligible if D/d_c > 40. Therefore, it was not necessary in this study to correct the experimental data for wall effects, as the ratio of D / dc for the largest size ballotini used was > 123. Smooth monosized glass spheres, with ψ = 1, were used as packing media. Although different arrangements of stacked spheres are possible (Figure 7.1), such variations in orientation do not occur with random packings as encountered in ordinary industrial practice.

7.5 Transient Two Phase Flow Pressure Drop

The pressure drop across the coalescer was recorded for different bed depths, phase ratios, ballotini particle sizes, average inlet droplet sizes and superficial velocities at regular intervals after the dispersion was introduced to the inlet face. Typical examples of observed transient behaviour, prior to attainment of steady-state conditions, are illustrated in Figures 7.7 to 7.11.

The dispersed phase in the system existed as discrete drops. Also the phase ratio never exceeded 6%. Therefore the majority of the hydrodynamic forces contributing to the pressure drop should have been due to the continuous phase.

Figure 7.11 shows the effect of superficial velocity on transient two-phase pressure drop. As expected, pressure drop increased with an increase in superficial velocity. In all cases, it initially increased rapidly and then remained almost constant through-out the remainder of an experiment.

To determine true steady state pressure drops it was necessary to eliminate any factors responsible for short term fluctuations:

i Temperature changes

ii Experimental errors in measurement of superficial velocity and pressure drop

iii Pseudo-steady state processes occuring within the bed, ie accumulation and release of dispersed phase.

The first factor was eliminated by controlling the temperature by means of a parallel tube heat exchanger in the emulsification loop as described in Section 5.3.4. Flow distriburbances during the measurement of velocity and pressure drop were minimised by careful operation. Pseudo-steady state processes only appeared to be manifested as pressure drop changes at low velocities when they were readily recognisable.

The transient pressure drop data were analysed to find the time to steady state

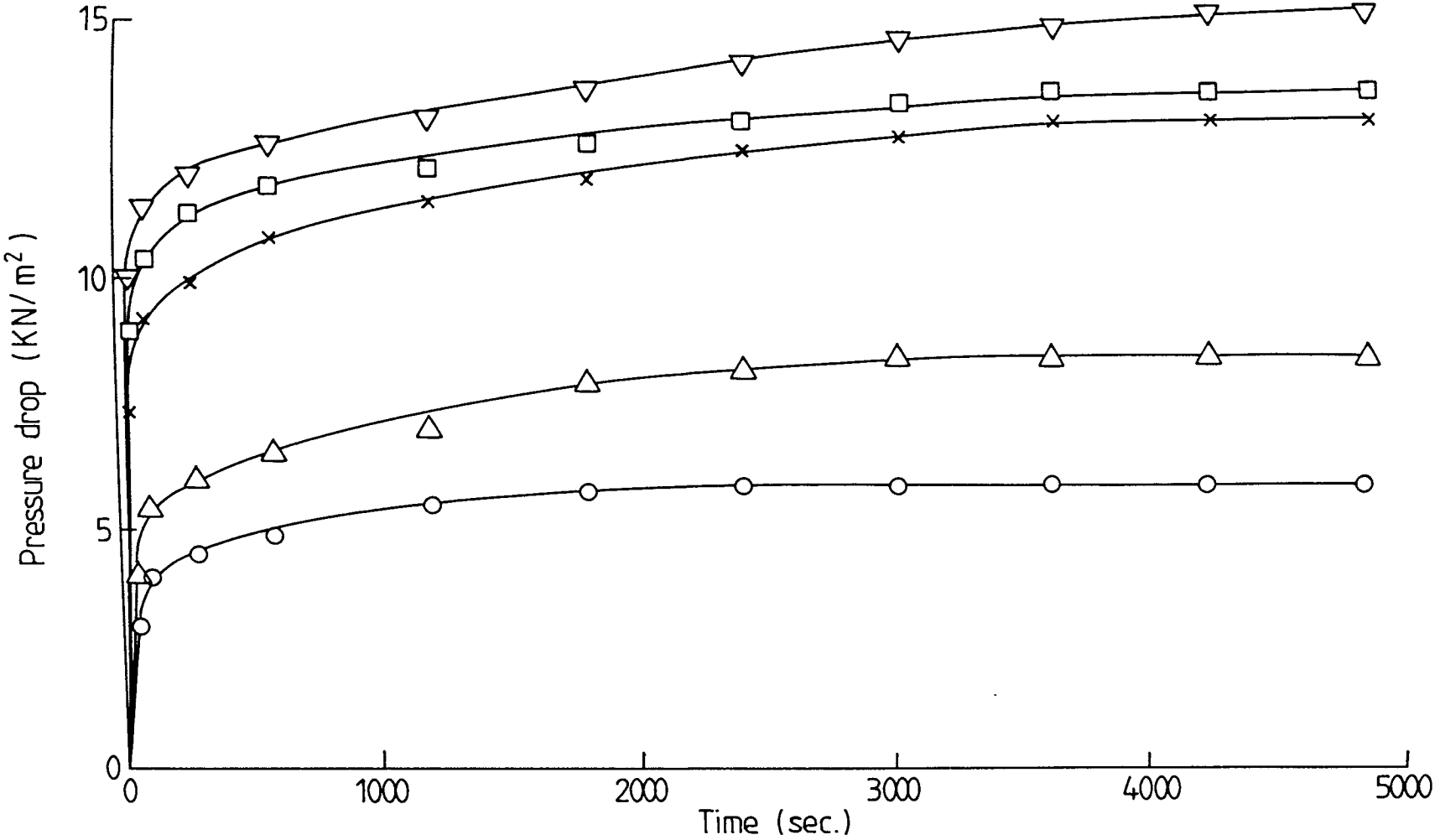

Figure 7·7 Transient two phase pressure drop vs. time for $3{\cdot}05 \times 10^{-3}$ m/s velocity, 266 μm ballotini size, 27 μm inlet drop size and 2% phase ratio.
Bed depth, L, (mm)
○ 10, △ 20, × 30, □ 40, ▽ 50.

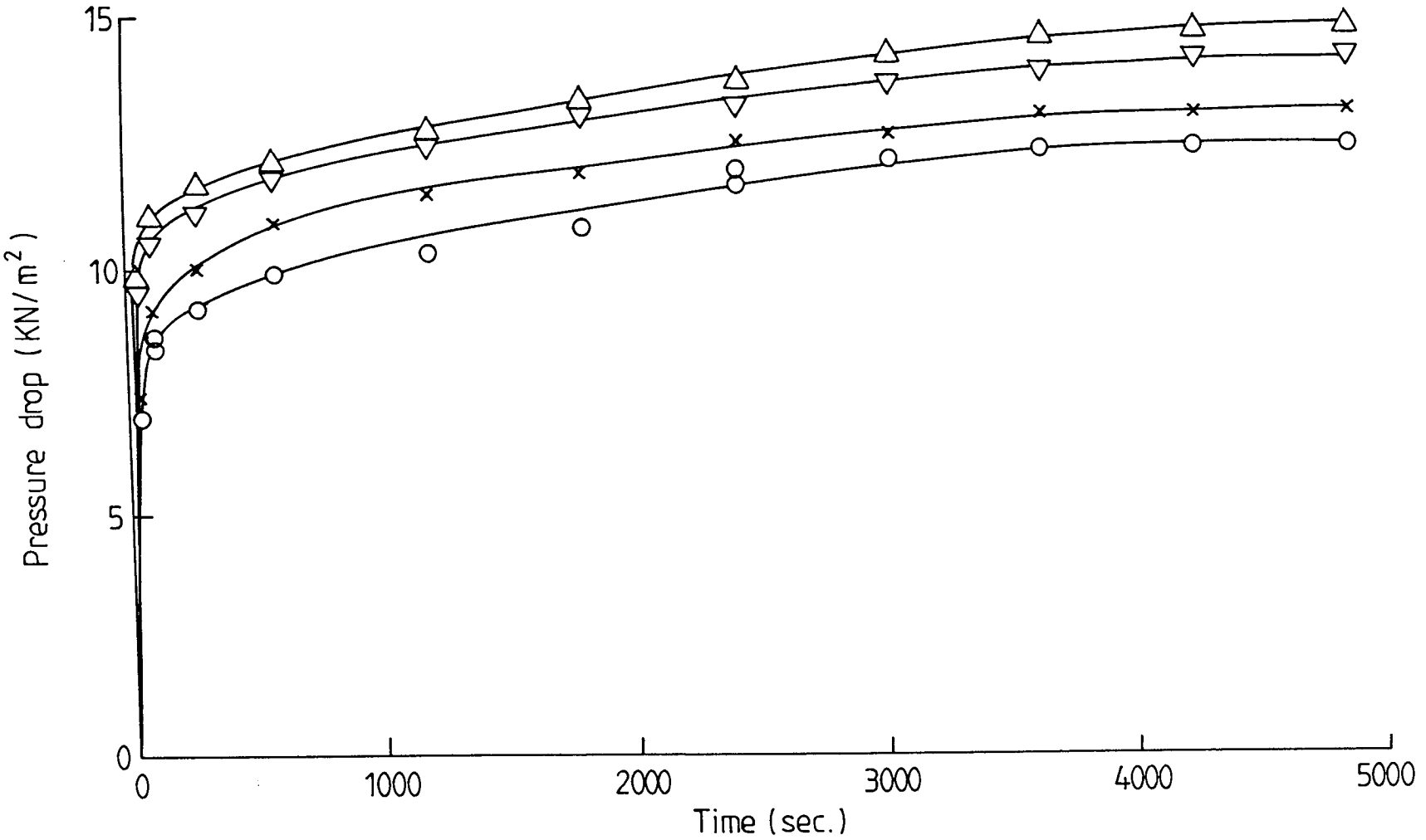

Figure 7·8 Transient two pressure drop vs. time for $3{\cdot}05 \times 10^{-3}$ m/s superficial velocity, 266 μm ballotini size, 30 mm bed depth and 27 μm inlet drop size.
Phase ratio, %, v/v
○ 0·5 &1·0, × 2, ▽ 4, △ 6.

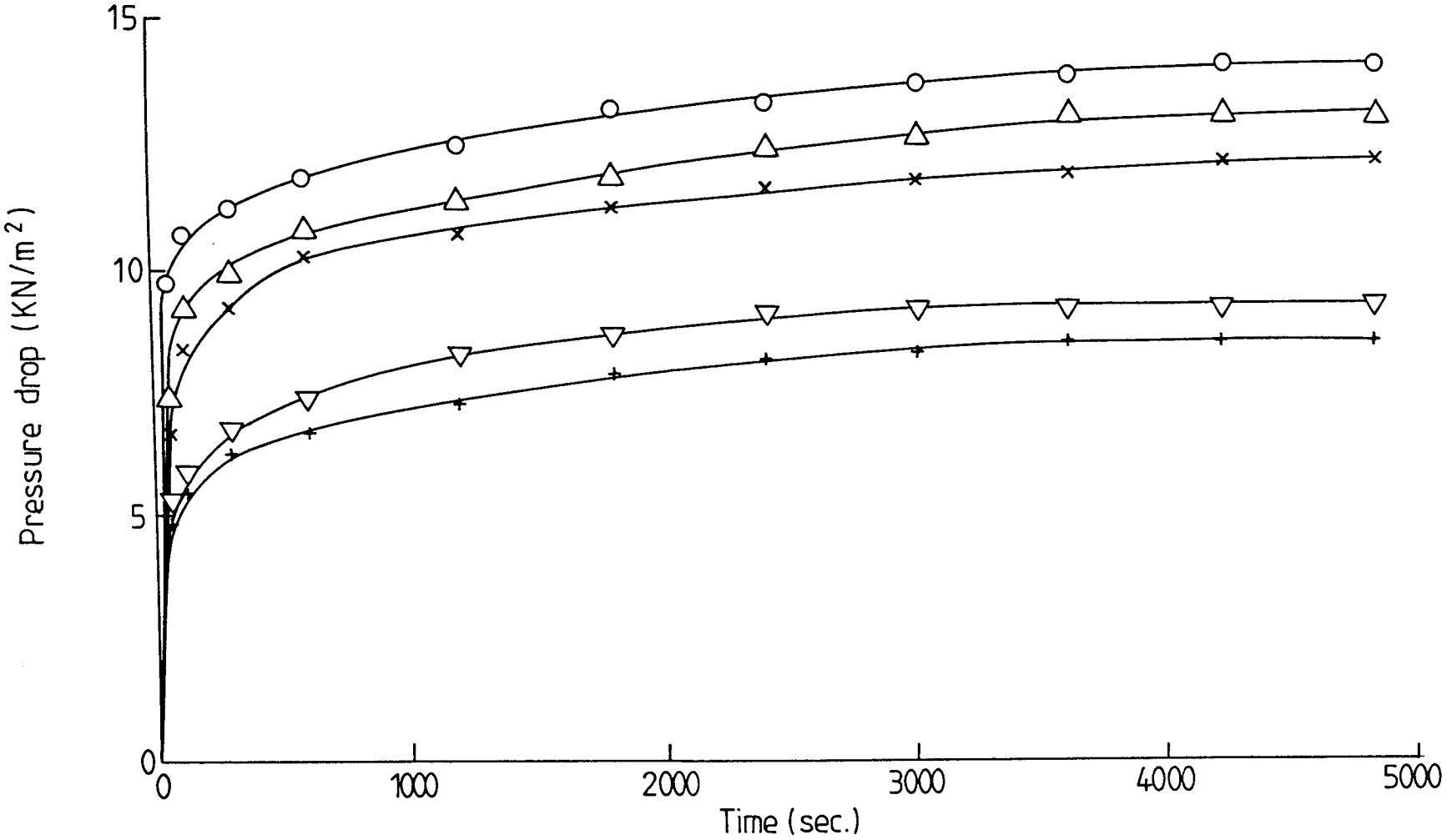

Figure 7·9 Transient two phase pressure drop vs. time for $3{\cdot}05 \times 10^{-3}$ m/s superficial velocity, 27 μm mean inlet drop size, 30 mm bed depth and 2% phase ratio
Ballotini particle sizes, d_c, μm
○ 146, △ 266, × 364, ▽ 487, + 615.

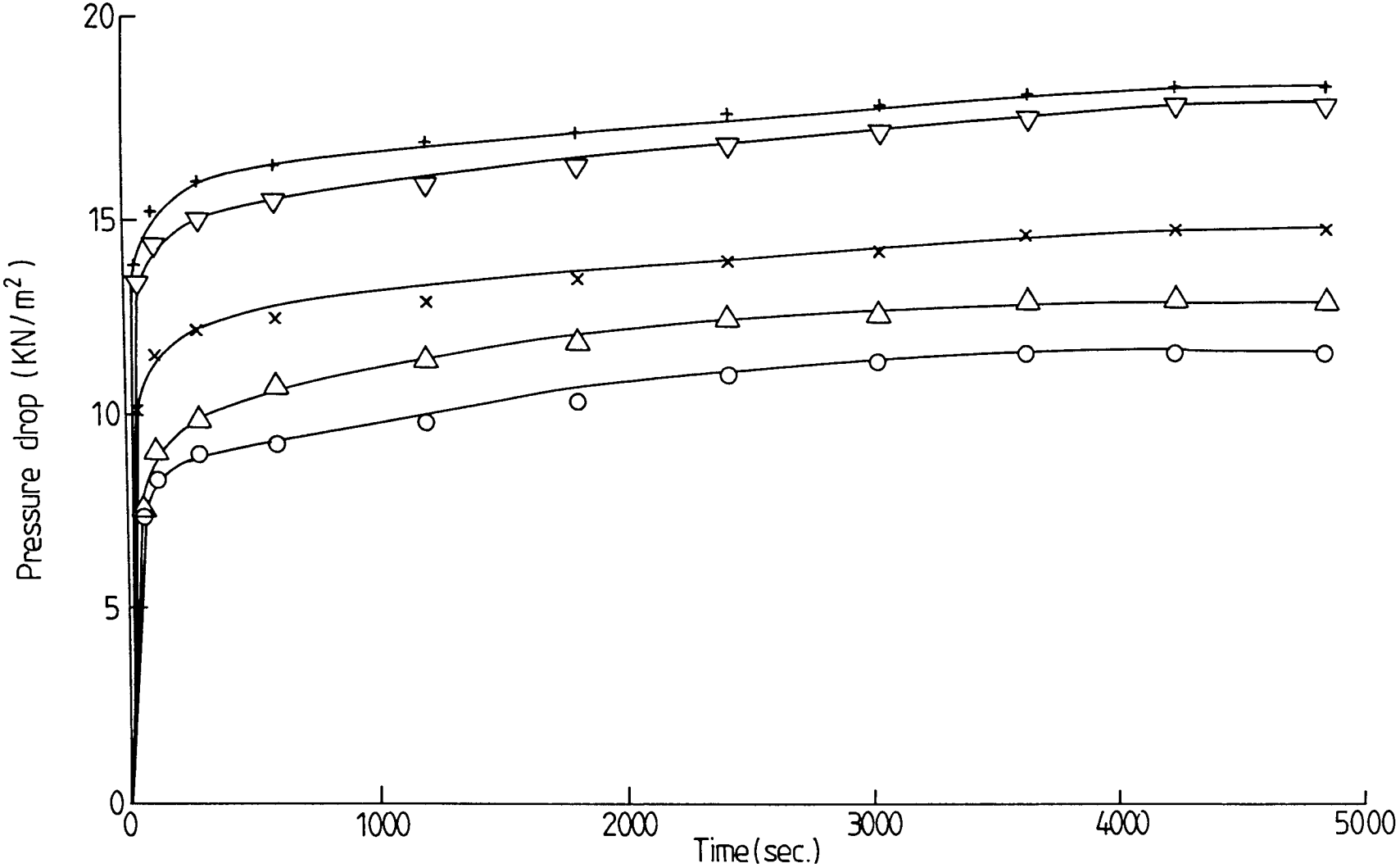

Figure 7·10 Transient two phase pressure drop vs. time for $3{\cdot}05\times10^{-3}$ m/s superficial velocity, 266 µm ballotini particle size, 30 mm bed depth and 2% v/v phase ratio.

Mean inlet drop size, d_{21}, µm ; + 13, ▽ 17, × 22, △ 27, ○ 42.

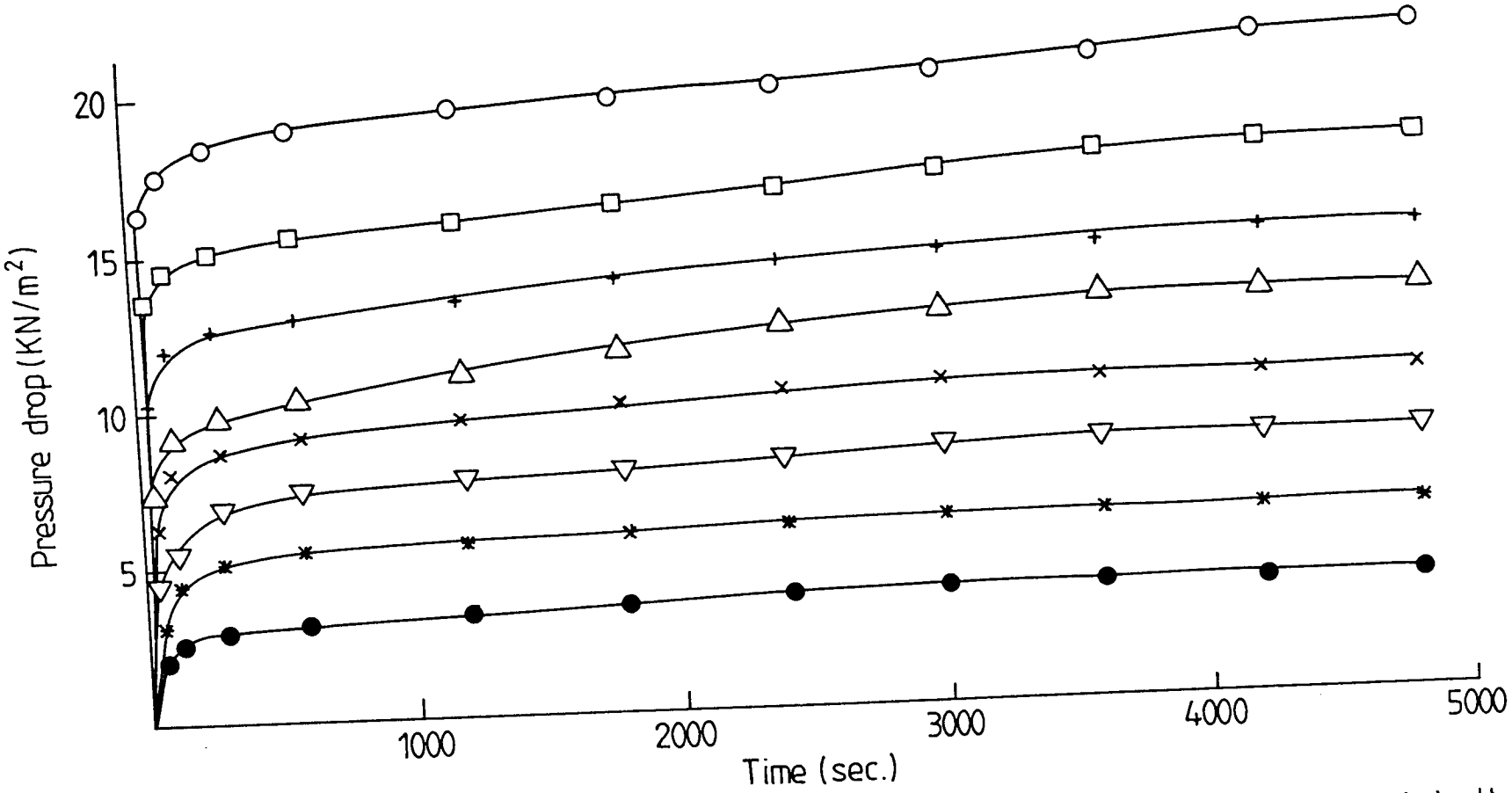

Figure 7·11 Transient two phase pressure drop vs. time for 266μm ballotini particle size, 30mm bed depth, 2% phase ratio and 27 μm mean inlet drop size

Superficial velocity, u, m/s ($\times 10^{-3}$)

● 0·8, × 2·5, □ 4·75
✱ 1·03, △ 3·05, ○ 6·0
▽ 1·5 + 3·6

from figures 7.7 to 7.11. The systems reached steady state when the rate of change of pressure drop gradually decreased to approach the final value. 3000 to 4200 seconds were required to reach their steady-state pressure drop.

7.6 Steady-state Two Phase Flow Pressure Drop

Steady state two-phase flow pressure drop was determined as a function of superficial velocity at different mean inlet drop diameters, different phase ratios, different bed depths and different ballotini particle diameters. Two different oil-in-water systems were used, i.e.toluene-water and Clairsol-water. Sixty to seventy minutes were required for a packing to reach its equilibrium pressure drop, that is for the bed hold-up to reach a steady state value. This was also observed by Austin [16] ,Beaz Poleo [27] and Spielman [94] who found that the pressure drop increased when the dispersed phase accumulated in the bed.Clearly, the effective voidage is reduced until the equilibrium hold-up is reached.

Graphs of two-phase flow pressure drop against superficial velocity for the two oil / water dispersions are shown in figures 7.12 to 7.15. These plots illustrate non - linear relationships and the shapes of the curves are dependent on the bed depth , ballotini particle size, phase ratio and inlet drop size. These graphs also show that pressure drop increased with increase in bed depth and phase ratio, since the level of dispersed phase saturation in the packing increase more rapidly as more dispersed phase was injected into the system over the same period of time. The pressure drops also increased with decrease in ballotini particle size.

The local slopes for two phase flow differ for a different mean inlet drop size.This suggests that pressure drop is a function of the number of pores, or micro-channels, occupied by drops. In addition, passage of some large drops (i.e >100 mm) was restricted by the fine pore size (i.e < 100 mm) of the bed resulting in low superficial velocity.Such large inlet drops were broken down to smaller drops or, at high superficial velocity, caused channelling phenomena in the beds.

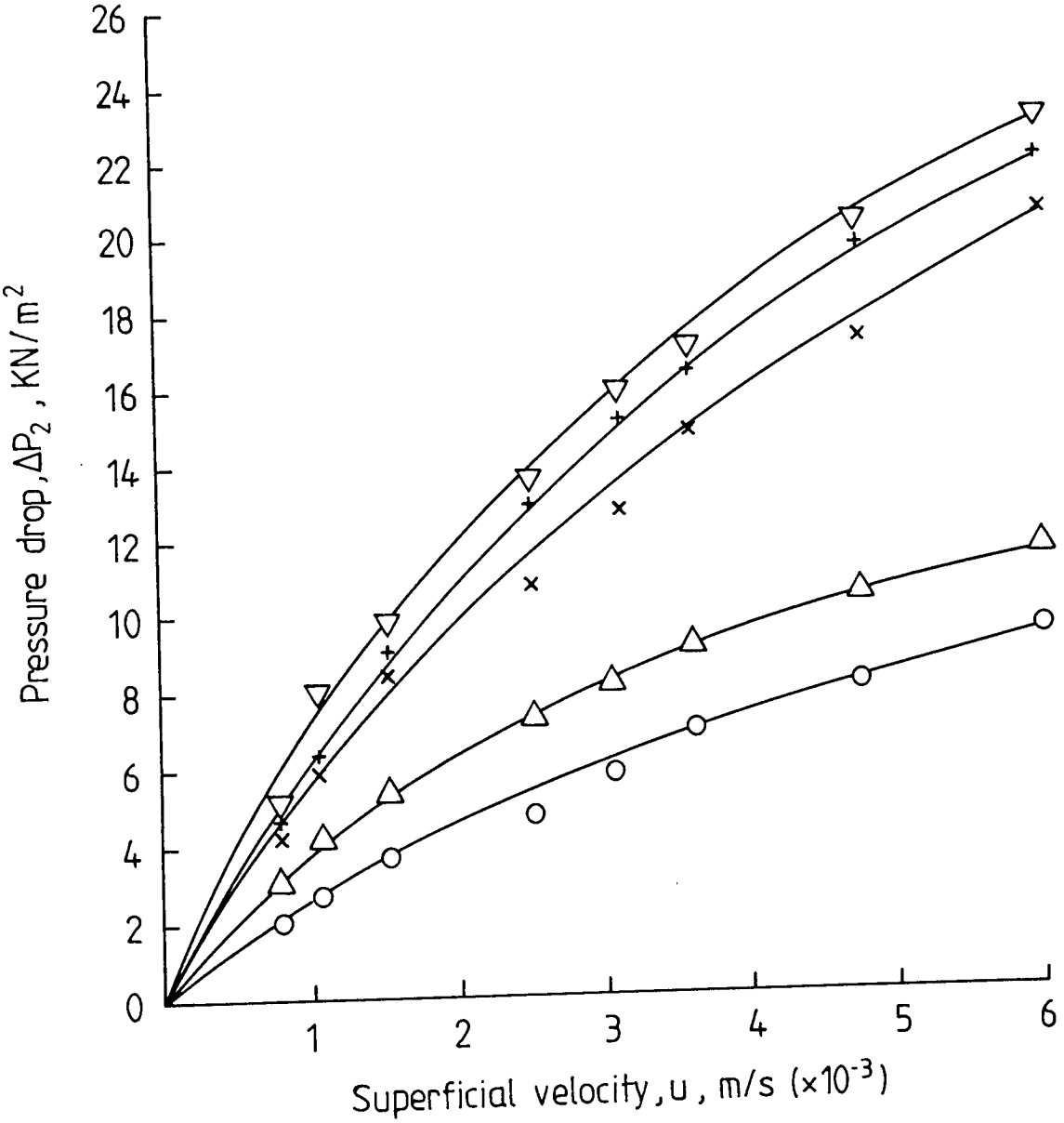

Figure 7·12 Variation of two phase pressure drop with superficial velocity for 266 µm ballotini particle size, 2% v/v phase ratio, 27 µm mean inlet drop size and toluene - water liquid system.

Bed depth, L, mm

○	10
△	20
×	30
+	40
▽	50

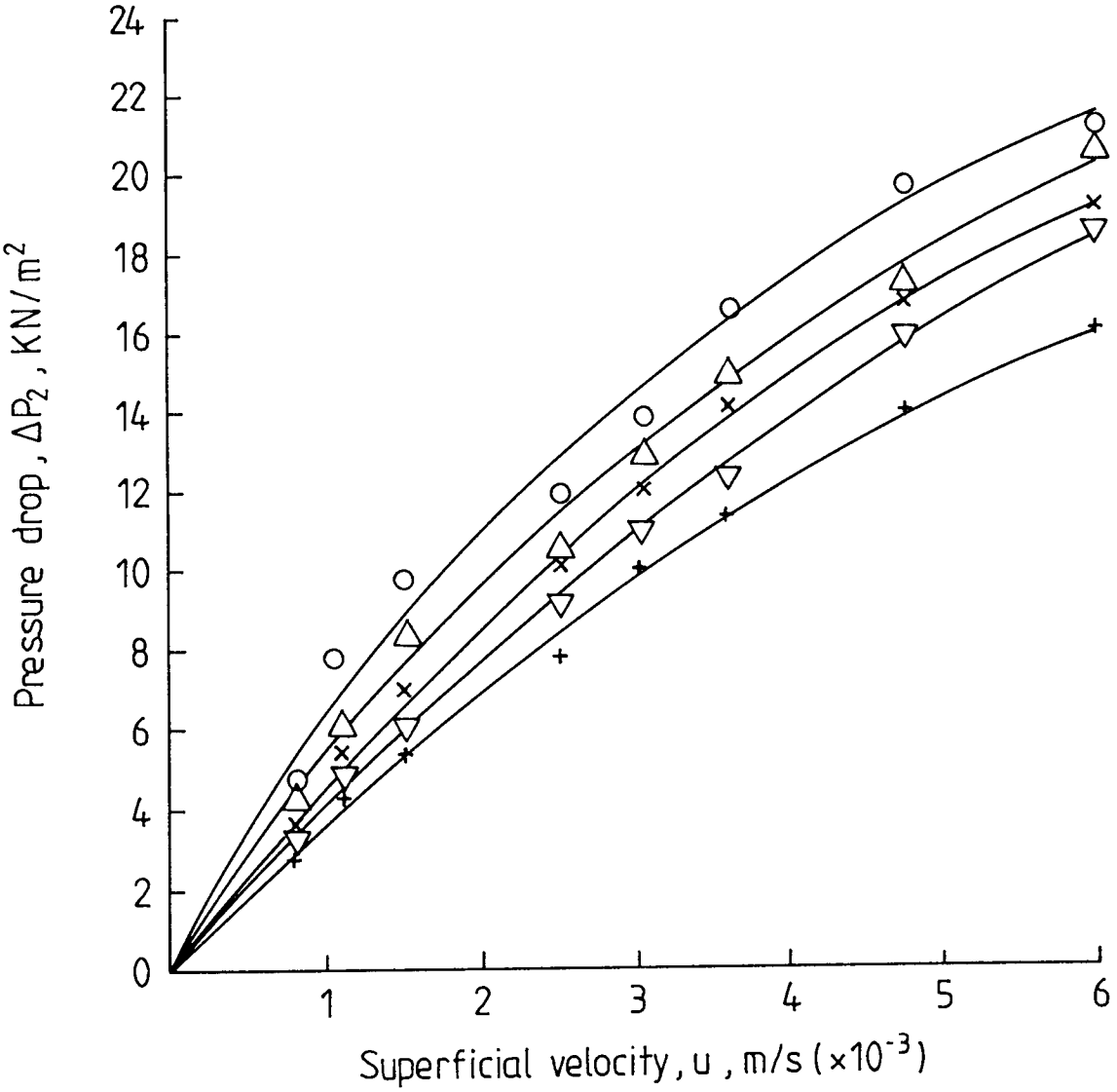

Figure 7·13 Variation of two phase pressure drop with superficial velocity for 30 mm bed depth, 2 % phase ratio, 27 μm mean inlet drop size and toluene - water liquid system.

Ballotini particle sizes, d_c, μm

○	146
△	266
×	364
▽	487
+	615

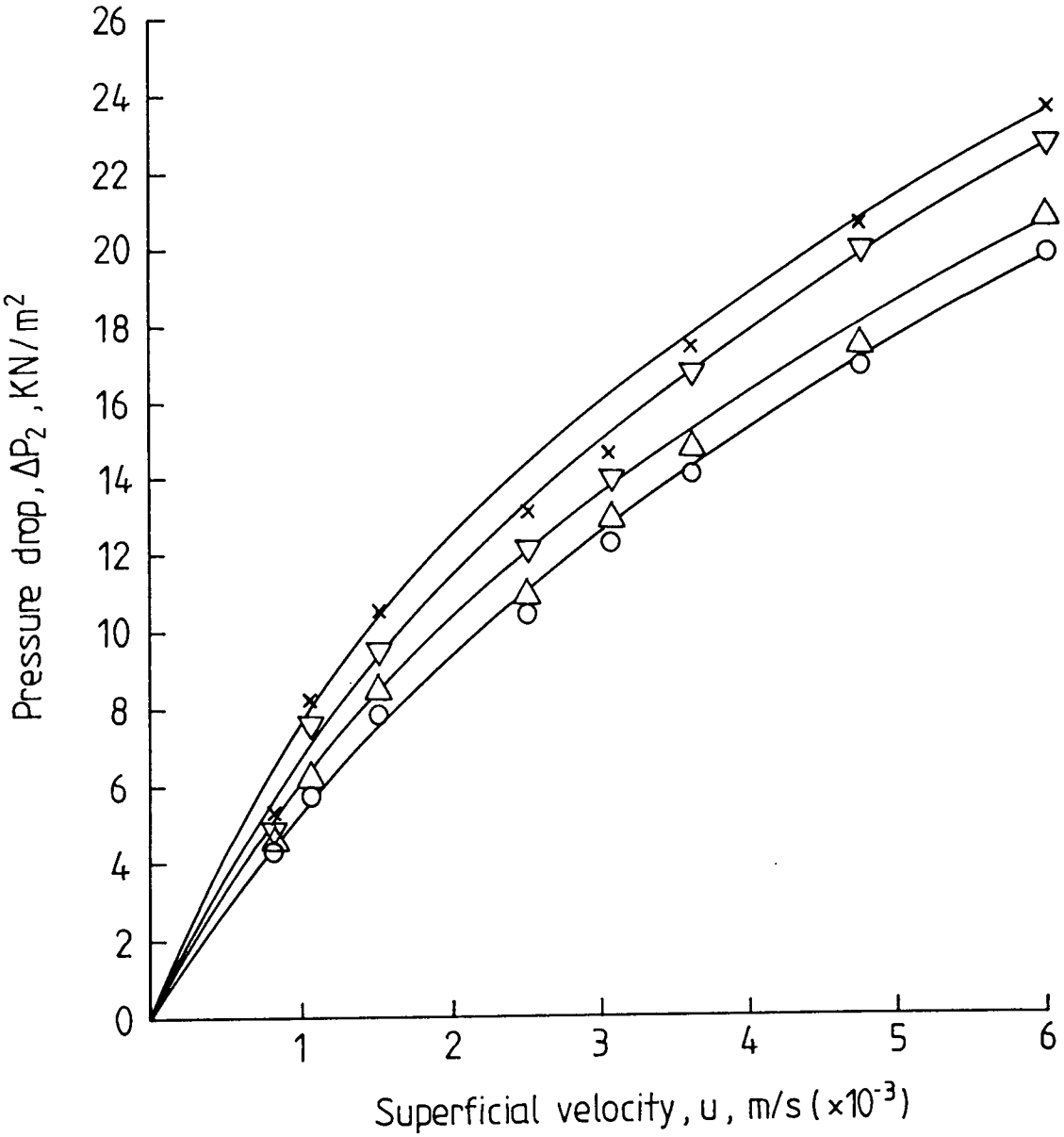

Figure 7·14 Variation of two phase pressure drop with superficial velocity for 30mm bed depth, 266μm ballotini particle size, 27μm mean inlet drop size and toluene - water liquid system.

Phase ratios, %, v/v

○	0·5 & 1·0
△	2
▽	4
×	6

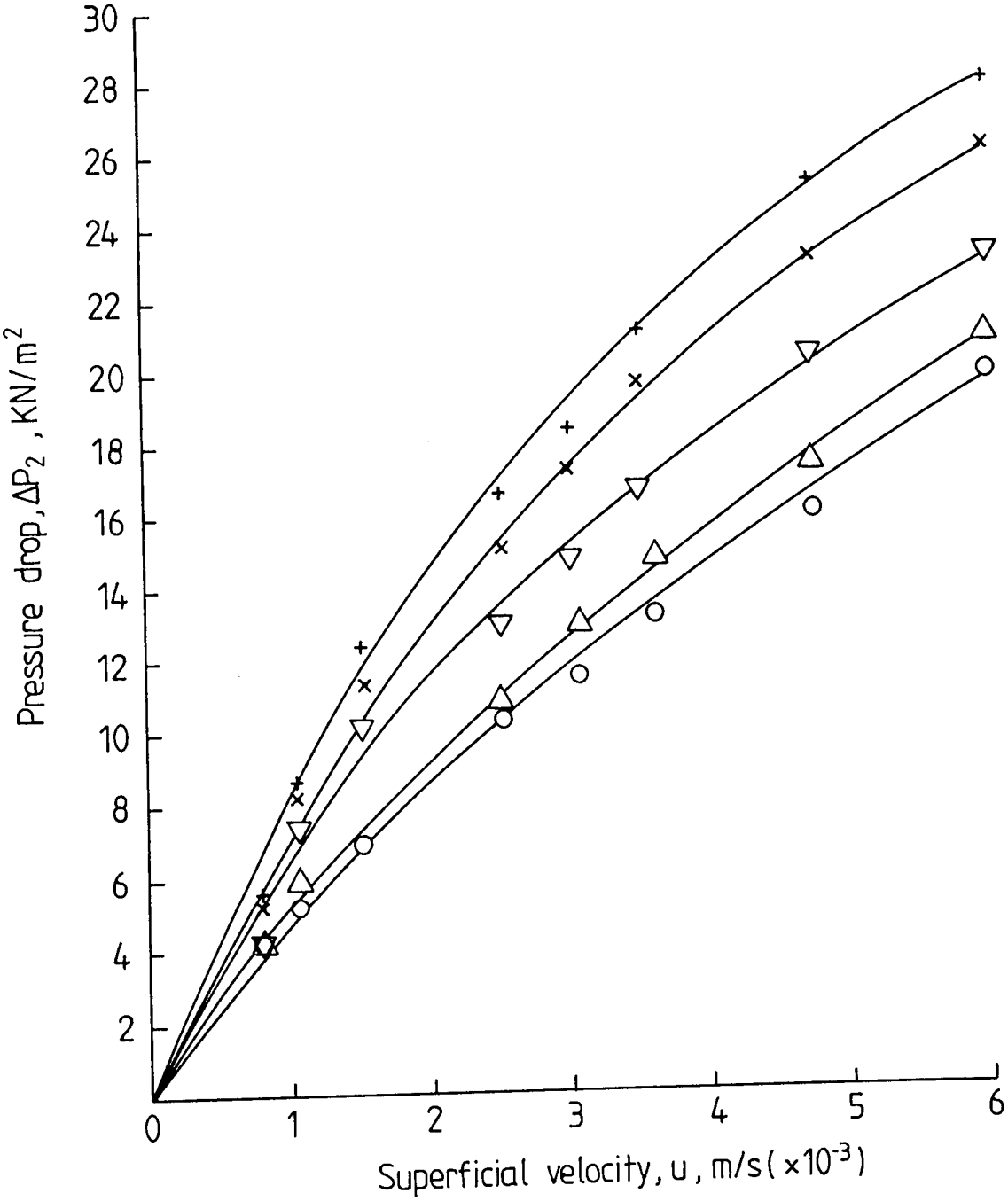

Figure 7·15 Variation of two phase pressure drop with superficial velocity for 30mm bed depth, 266 μm ballotini particle size, 2% v/v phase ratio and toluene - water liquid system.

Mean inlet drop sizes, d_{21}, μm

○	42
△	27
▽	22
×	17
+	13

7.7 Comparison Between Single Phase And Steady State Two Phase Pressure Drop Data:-

Two phase pressure drop at any particular superficial velocity differs from that for single phase flow because the effective voidage, ie. e_2, of the packing is decreased due to hold-up of the dispersed phase within the packing.

Previous workers [16, 17, 27, 57, 111] used the Blake-Kozeny or Carman-Kozeny equation to determine the effective voidage of the packing during coalescence. This involved substitution of the experimental value of the two phase flow which was then solved numerically to find the voidage as;

$$\frac{\Delta P_2}{\Delta P_1} = \frac{e_1^3 (1-e_2)^2}{e_2^3 (1-e_1)^2} \qquad \text{.... 7.32}$$

In this work, graphs of single phase and two phase flow pressure drop against superficial velocity were plotted, as shown in Figures 7.3 and 7.13 and Figures 7.4 and 7.12. These plots illustrate that the value of pressure drop was dependent on the bed depth, particle size, mean inlet drop size, phase ratio, and superficial velocity at constant coalescer diameter and operating temperature.

Generally, the pressure drop for either single phase or two phase flow increased steadily with increase in superficial velocity as shown in Figures 7.3 and 7.4, and 7.12 to 7.15, and with increase in the bed depth as shown in Figures 7.4 and 7.12, and with decrease in the ballotini particle size as shown in Figure 7.3 and 7.13.

7.8 Variables Affecting Pressure Drop Data:

The main variables affecting pressure drop studied in this work were:

1 Bed Depth:-

Five different ballotini bed depths in the range 10×10^{-3} to 50×10^{-3} m were

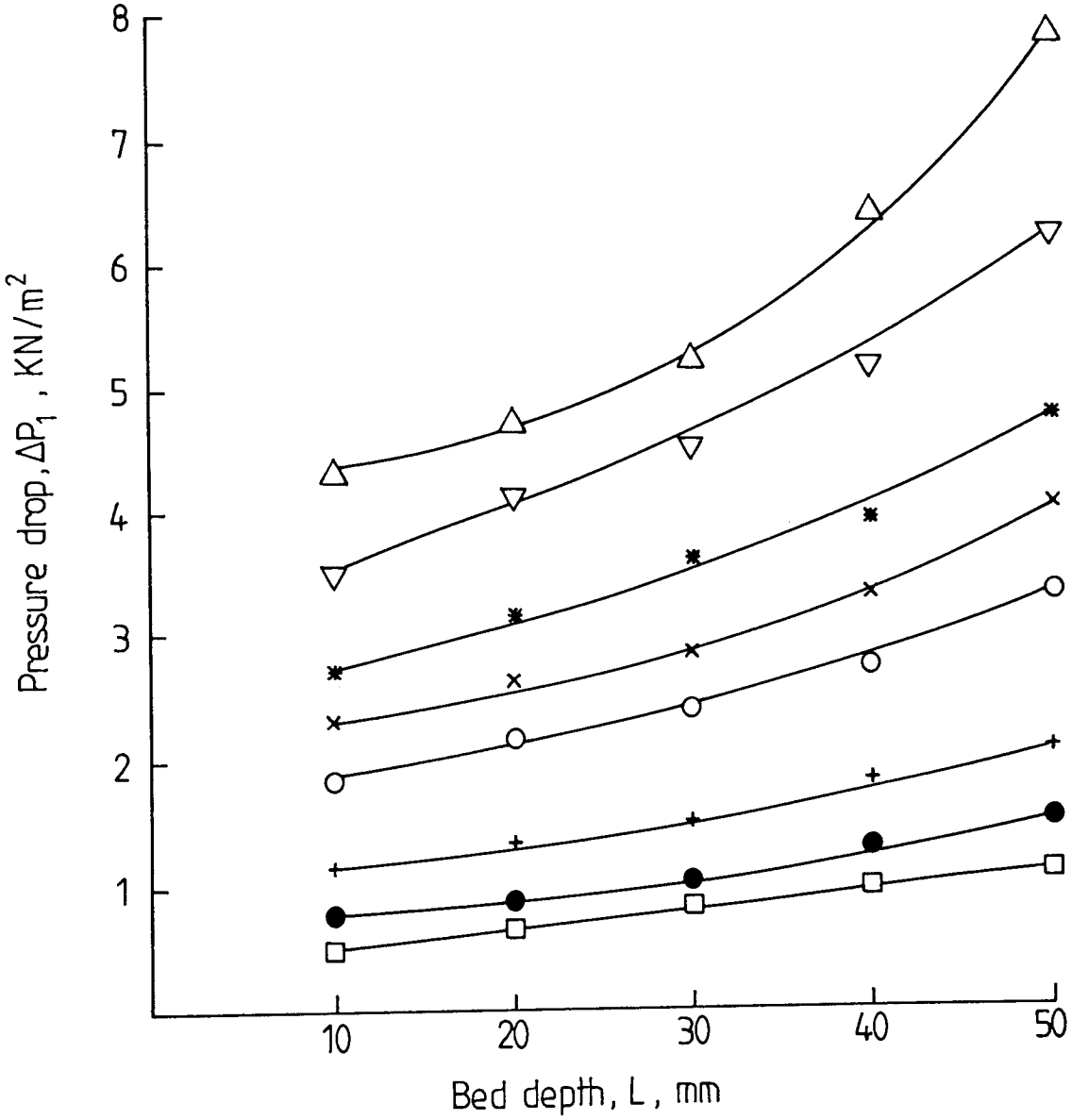

Figure 7·16 Variation of single phase pressure drop with bed depth for 266 μm ballotini particle size.

Superficial velocity, u, m/s ($\times 10^{-3}$)

- □ 0·8
- ● 1·03
- \+ 1·5
- ○ 2·5
- × 3·05
- ✱ 3·6
- ▽ 4·75
- △ 6·0

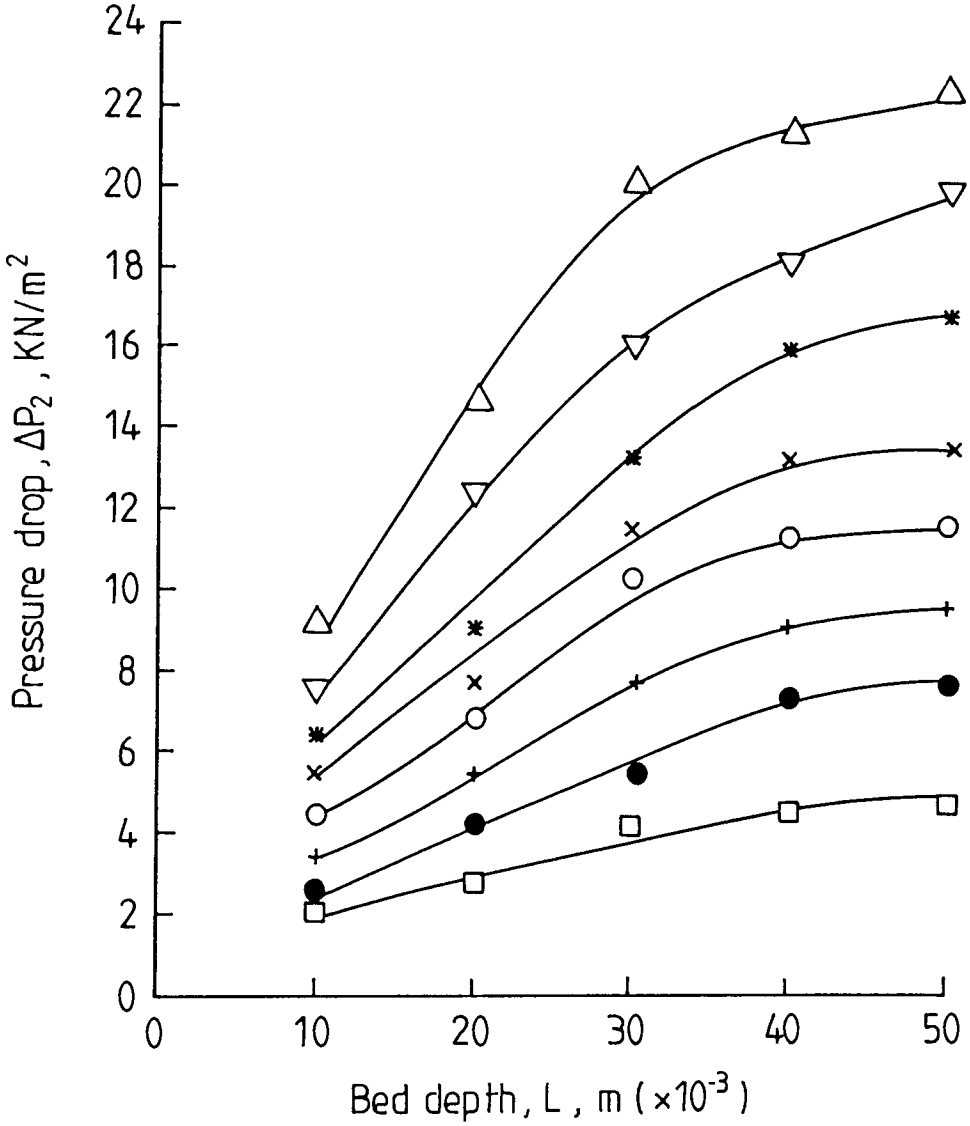

Figure 7·17 Variation of two phase pressure drop with bed depth for 266 µm ballotini particle size, 2% phase ratio, 42 µm mean inlet drop size and toluene-water liquid system.

Superficial velocity, u, m/s ($\times 10^{-3}$)

□	0·8
●	1·03
+	1·5
○	2·5
×	3·05
✱	3·6
▽	4·75
△	6·0

investigated with constant ballotini particle size and phase ratio. An increase in bed depth led to an increase in pressure drop at any given superficial velocity as shown in Figure 7.16 for single phase flow and in Figure 7.17 for two phase flow.However, there was an optimum bed depth which could be used before a secondary haze appeared at the coalescer outlet stream as described in Chapter 9. Therefore a greater bed depth is required at smaller mean inlet drop size in order for coalescence to take place. For both the toluene-water and Clairsol-water systems the optimum bed depth in this study was 30×10^{-3}m.

2 Ballotini particle size:-

Five different ballotini particle sizes in the range 146 to 615 μm were investigated with a constant bed depth of 30×10^{-3} m. An increase in ballotini particle diameter led to a decrease in pressure drop at any given superficial velocity as shown in Figure 7.18 for single phase flow and Figure 7.19 for two phase flow. However, there was an optimum particle size, dependent on the value of inlet drop size generated by centrifugal pump, before the haze of secondary dispersion appeared over the coalscer as described in Chapter 9. For toluene-water and Clairsol-water systems the optimum ballotini particle diameter in this work was about 266 μm.

3 Phase ratio or concentration of dispersed phase in continuous phase:-

Phase ratio in the range of 0.5 to 6 v/v were investigated with constant bed depth, particle size and superficial velocity. The changed phase ratio in the range of 0.5 to 1 v/v% had a very small effect on pressure drop. However, at steady state conditions and at different inlet drop sizes, the pressure drops increased, with increase in phase ratio in the range of 2 to 6% v/v% as shown in figure 7.20.

4 Inlet drop size

The determination of inlet drop size distribution will be described in Chapter 8.

The effect of inlet drop size on the pressure drop was described in section 7.6.

Generally, pressure drop increased slightly with a decrease of mean inlet drop size as shown in Figure 7.21. In fact, the mean drop size of a secondary dispersion produced by a centrifugal pump with by-pass loop depends on the pump speed, as described in Section 8.7.

5 Superficial velocity

Superficial velocities were investigated in the range of 0.8 to 6.0 x 10^{-3}m/s. The effects of superficial velocity were described in section 7.6 and illustrated in Figures 7.12 to 7.15 previously.

Any increase in superficial velocity in either single phase or two-phase systems caused an immediate increase in the presssure drop. However, for any particular system and packing there was a maximum dispersion superficial velocity flow above which either direct passage through bed, or redispersion of drops held within it , or a combination of both occurred. This velocity is termed the "critical" superficial velocity, ie. the velocity for a specific system and packing arrangement, above which secondary drops started to appear clearly in the exit flow. The "critical" superficial velocities usually occur at values near to the flooding velocity values [17, 104]. Therefore, the "critical" superficial velocity did not occur in this study because the ranges of superficial velocity were less than the flooding velocity for each packing and system used. However, it is important to study the relation between critical velocity and flooding velocity in the coalescence of secondary dispersions in packed beds in the future.

6 Liquid-liquid system

The variation of pressure drop with superficial velocity for different values of bed depth, particle diameter, phase ratio and inlet drop size for two different liquid-liquid systems are shown in Figures 7.22 to 7.25.

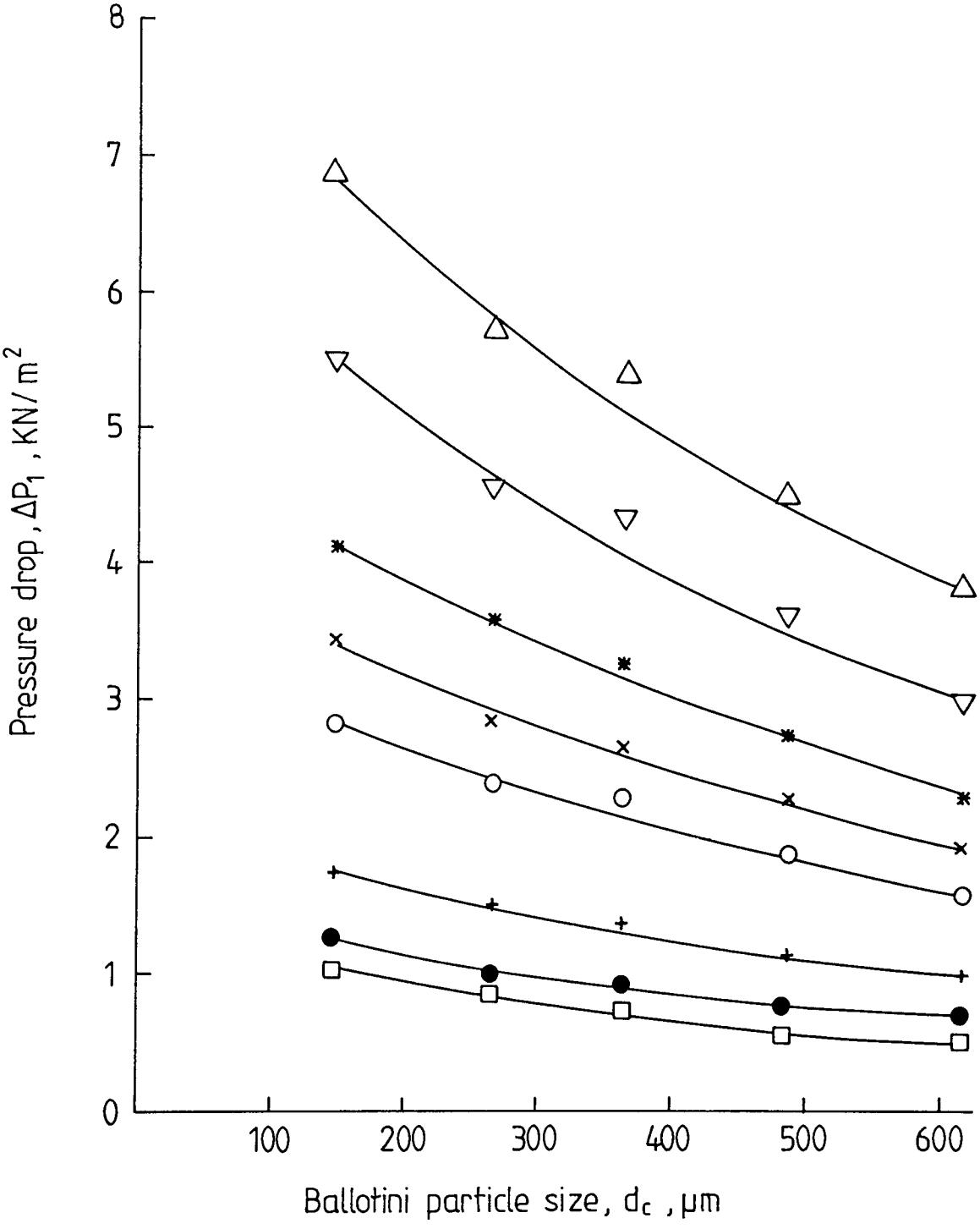

Figure 7·18 Variation of single phase pressure drop with ballotini particle size for 30 mm bed depth.

Superficial velocity, u, m/s ($\times 10^{-3}$)

- □ 0·8
- ● 1·03
- \+ 1·5
- ○ 2·5
- × 3·05
- ✱ 3·6
- ▽ 4·75
- △ 6·0

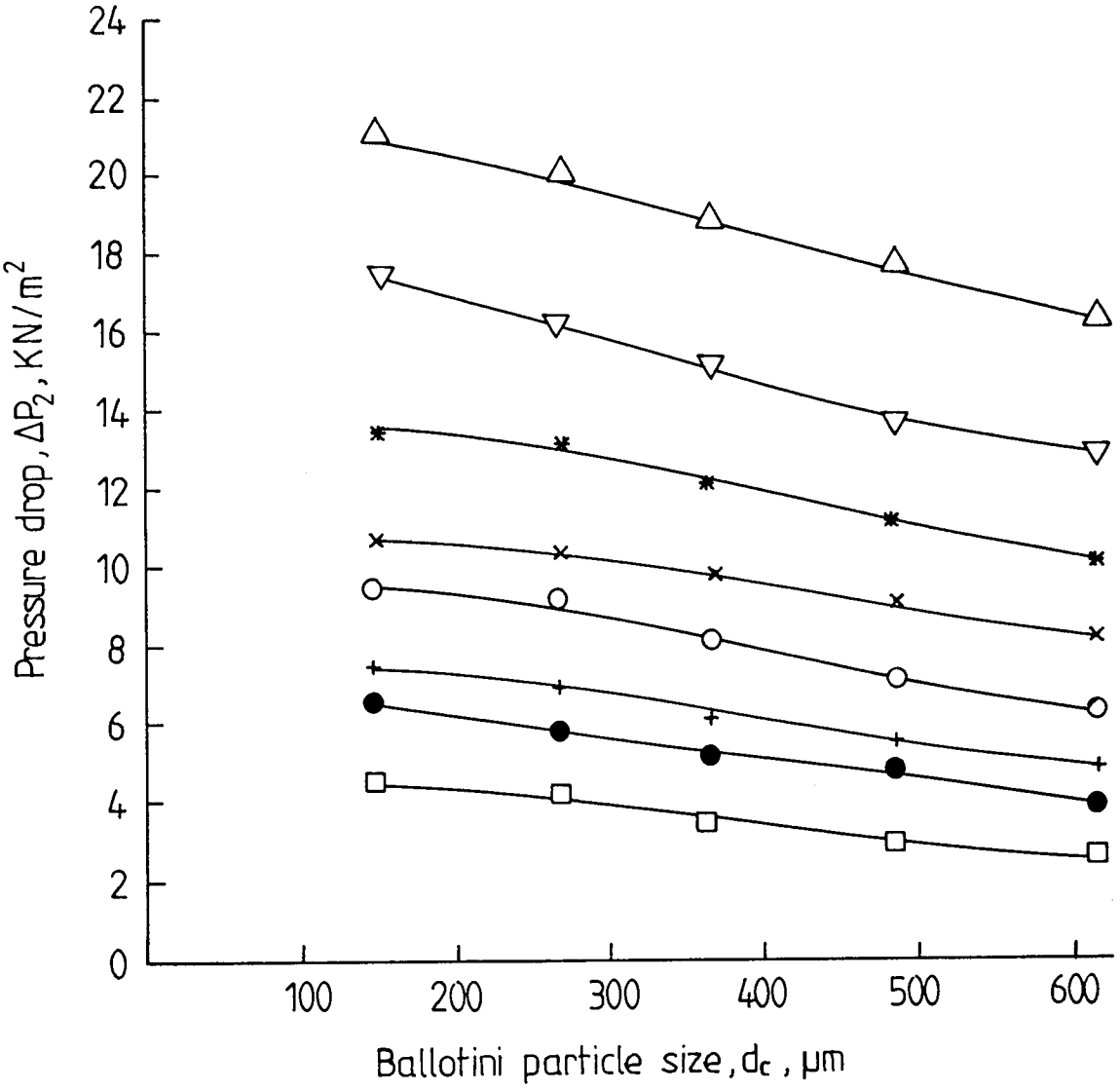

Figure 7·19 Variation of two phase pressure drop with ballotini particle size for 30 mm bed depth, 2% v v phase ratio, 42 μm mean inlet drop size and toluene-water liquid system.

Superficial velocity, u, m/s ($\times 10^{-3}$)

- □ 0·8
- ● 1·03
- \+ 1·5
- ○ 2·5
- × 3·05
- ✱ 3·6
- ▽ 4·75
- △ 6·0

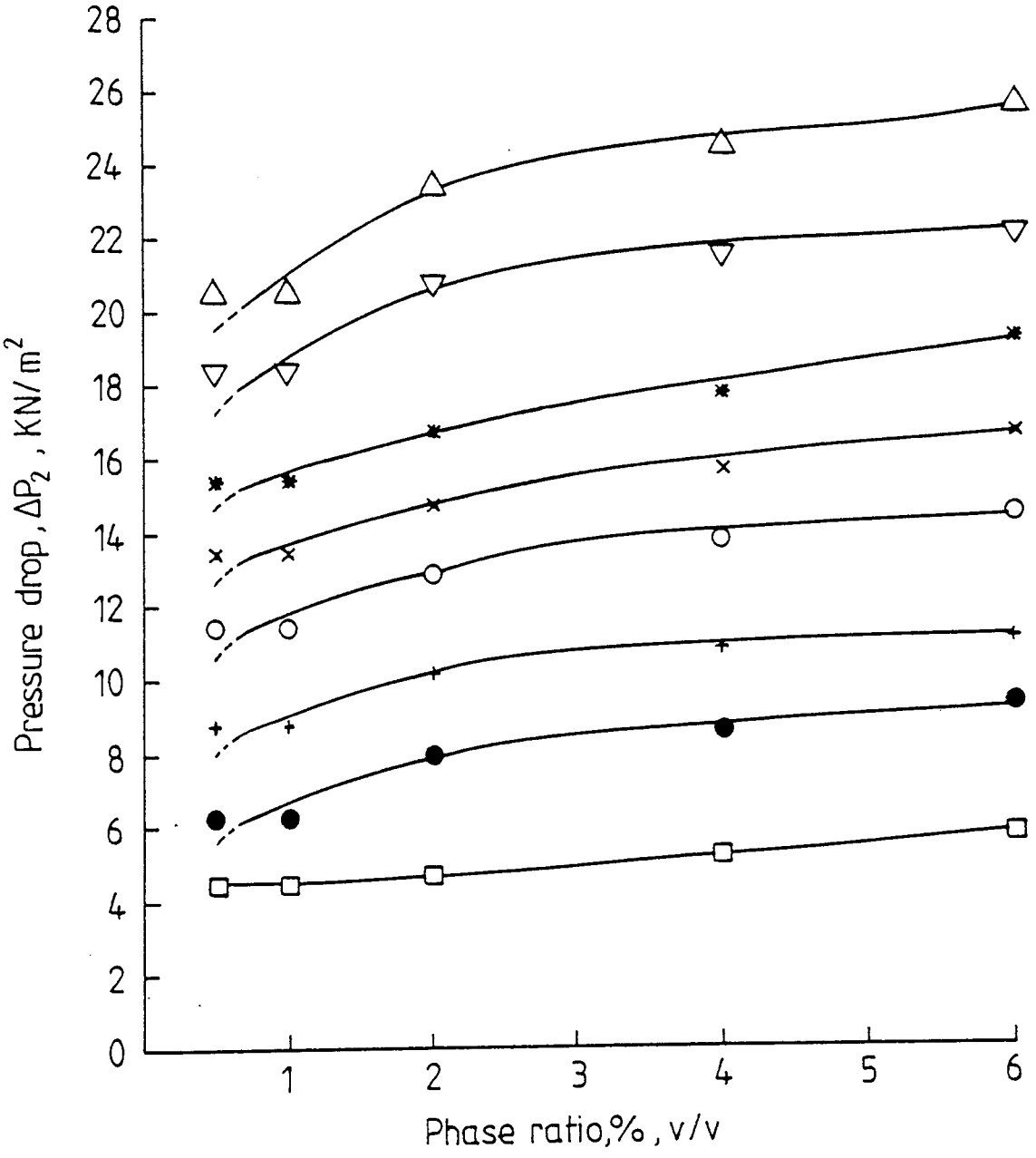

Figure 7·20 Variation of two phase pressure drop with phase ratio for 266 µm ballotini particle size, 30 mm bed depth, 22 µm mean inlet drop size and toluene - water liquid system

Superficial velocity, u, m/s ($\times 10^{-3}$)

- □ 0·8
- ● 1·03
- \+ 1·5
- ○ 2·5
- × 3·05
- ✱ 3·6
- ▽ 4·75
- △ 6·0

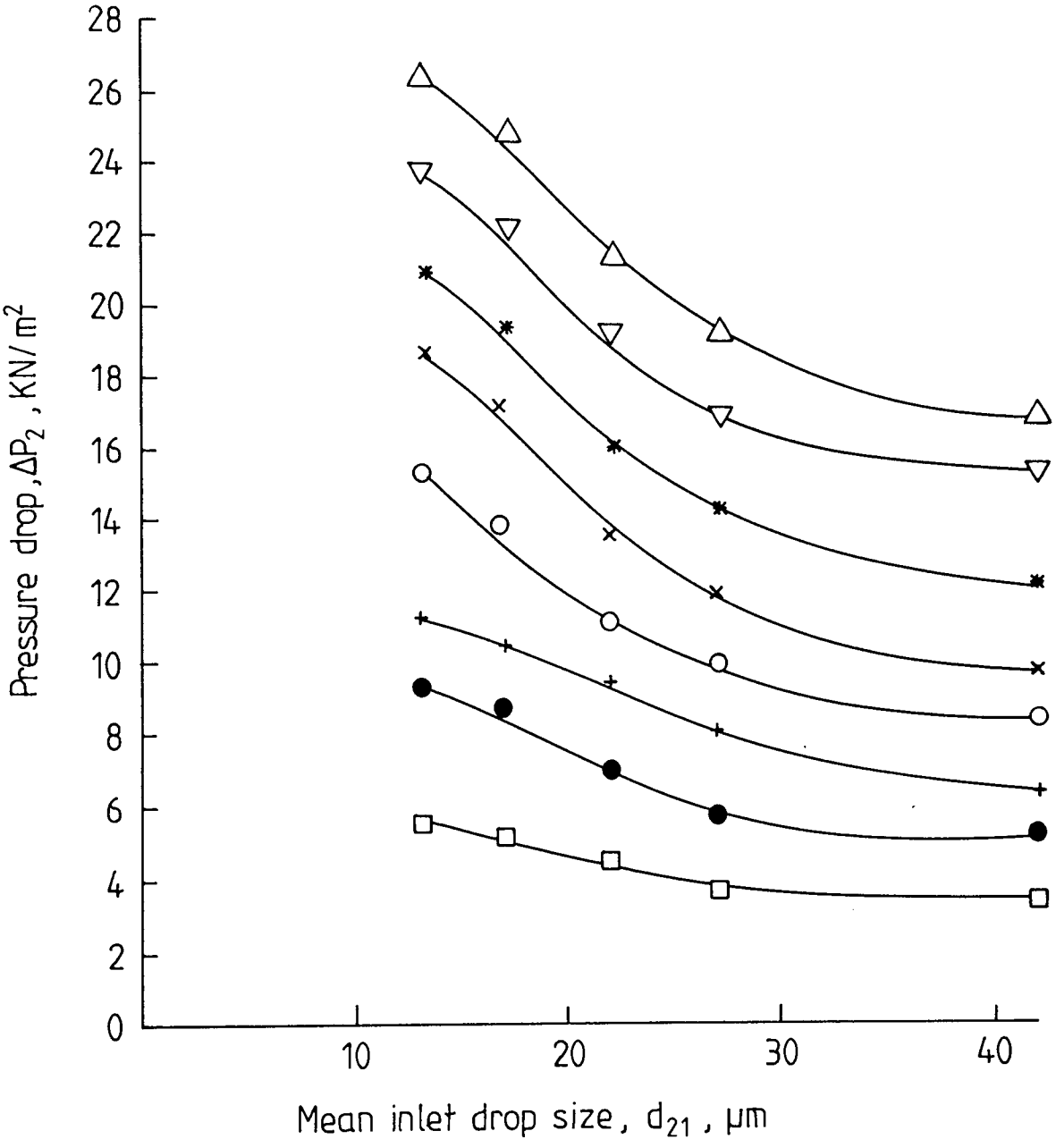

Figure 7·21 Variation of two phase pressure drop with mean inlet drop size for 364 μm ballotini size, 30mm bed depth, 2% v/v phase ratio and toluene-water liquid system.

Superficial velocity, u, m/s($\times 10^{-3}$)

□	0·8
●	1·03
+	1·5
○	2·5
×	3·05
✱	3·6
▽	4·75
△	6·0

The pressure drop was, as expected, higher with the dispersed liquid (ie Clairsol 350) with a higher viscosity. Other properties of the liquid-liquid system, eg interfacial tension, or the presence of surfactants would be likely to affect both coalescence performance and pressure drop; further study would be necessary to correlate these effects.

7.9 Quantitative Analysis of Pressure Drop Data

To account for variations in packing technique and operating temperature , the two phase pressure drop is presented in the quantitative analysis of data as the ratio,

$$\left[\frac{\Delta P_2}{\Delta P_1}\right].\left[\frac{\mu_c}{\mu_d}\right]$$

According to the previous section; the relations between pressure drop ratio, bed depths; particle diameter, phase ratio, mean inlet drop size and superficial velocity suggested that the results might be correlated by equations of the form.

$$\left[\frac{\Delta P_2}{\Delta P_1}\right]\left[\frac{\mu_c}{\mu_d}\right] = k_p\ U^a\ L^b\ dc^c\ dp^d\ Cin^{\,e} \qquad \ldots\ 7.33$$

By taking logarithms of each term the constant, k_p and exponents a, b, c, d and e were determined by multiple linear regression analysis of the data.

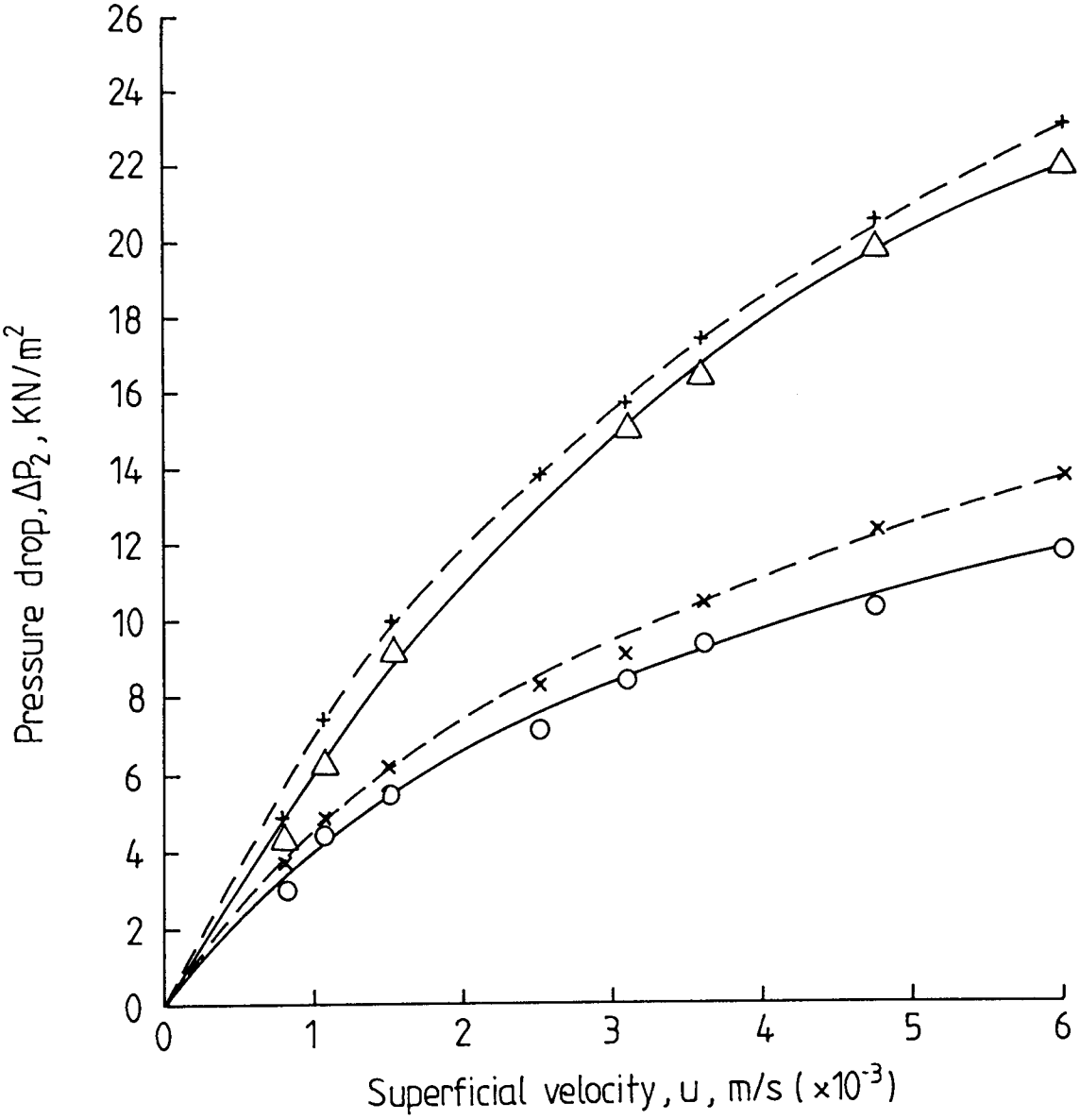

Figure 7·22 Variation of two phase pressure drop with superficial velocity at different bed depths.

——— toluene - water

– – – – – Clairsol - water

○ , × 20mm bed depth

△ , + 40mm bed depth

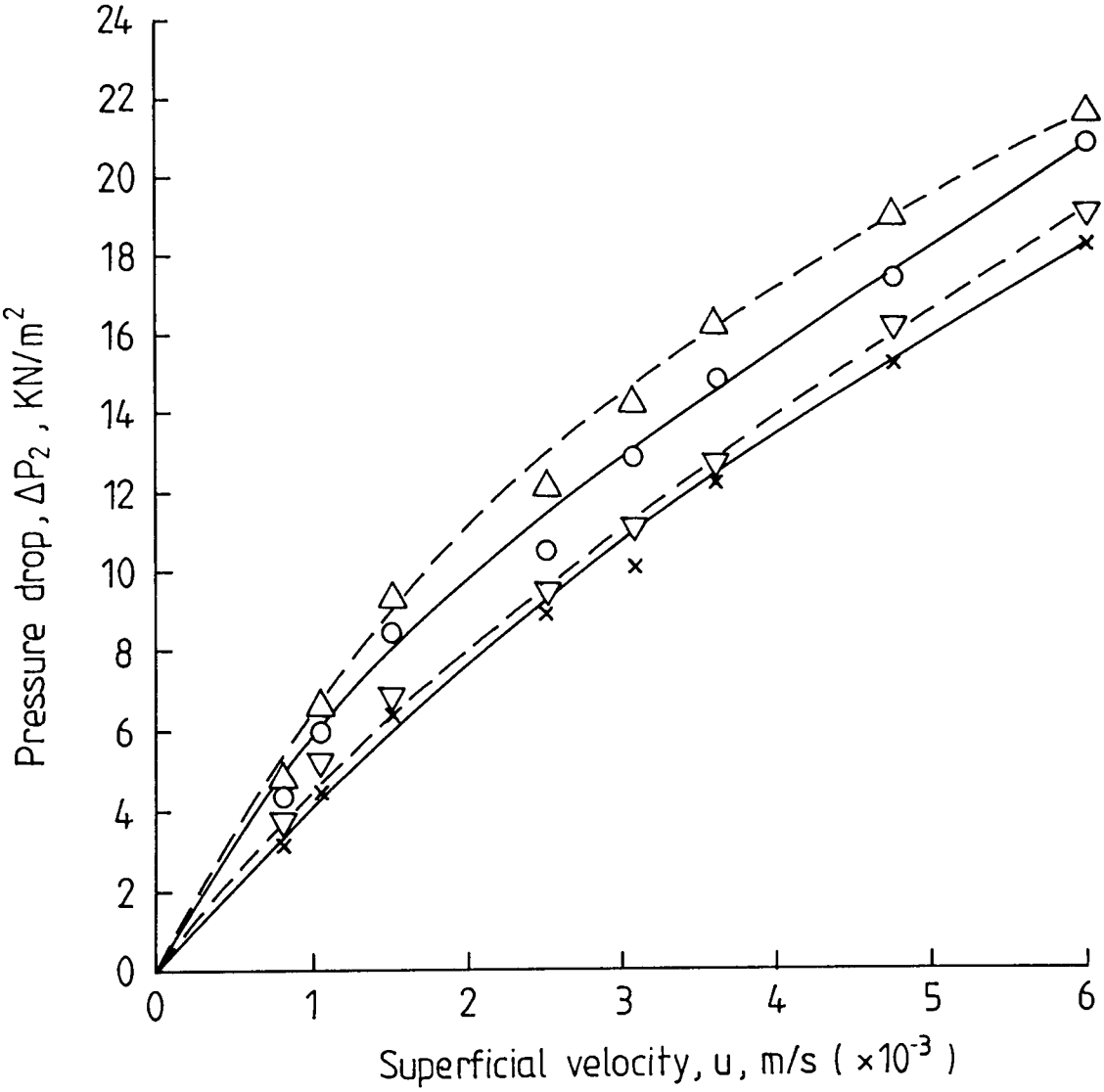

Figure 7·23 Variation of two phase pressure drop with superficial velocity at different ballotini particle sizes.

——— toluene - water

– – – – – Clairsol - water

× , ▽ 615 μm ballotini particle size

○ , △ 266 μm ballotini particle size

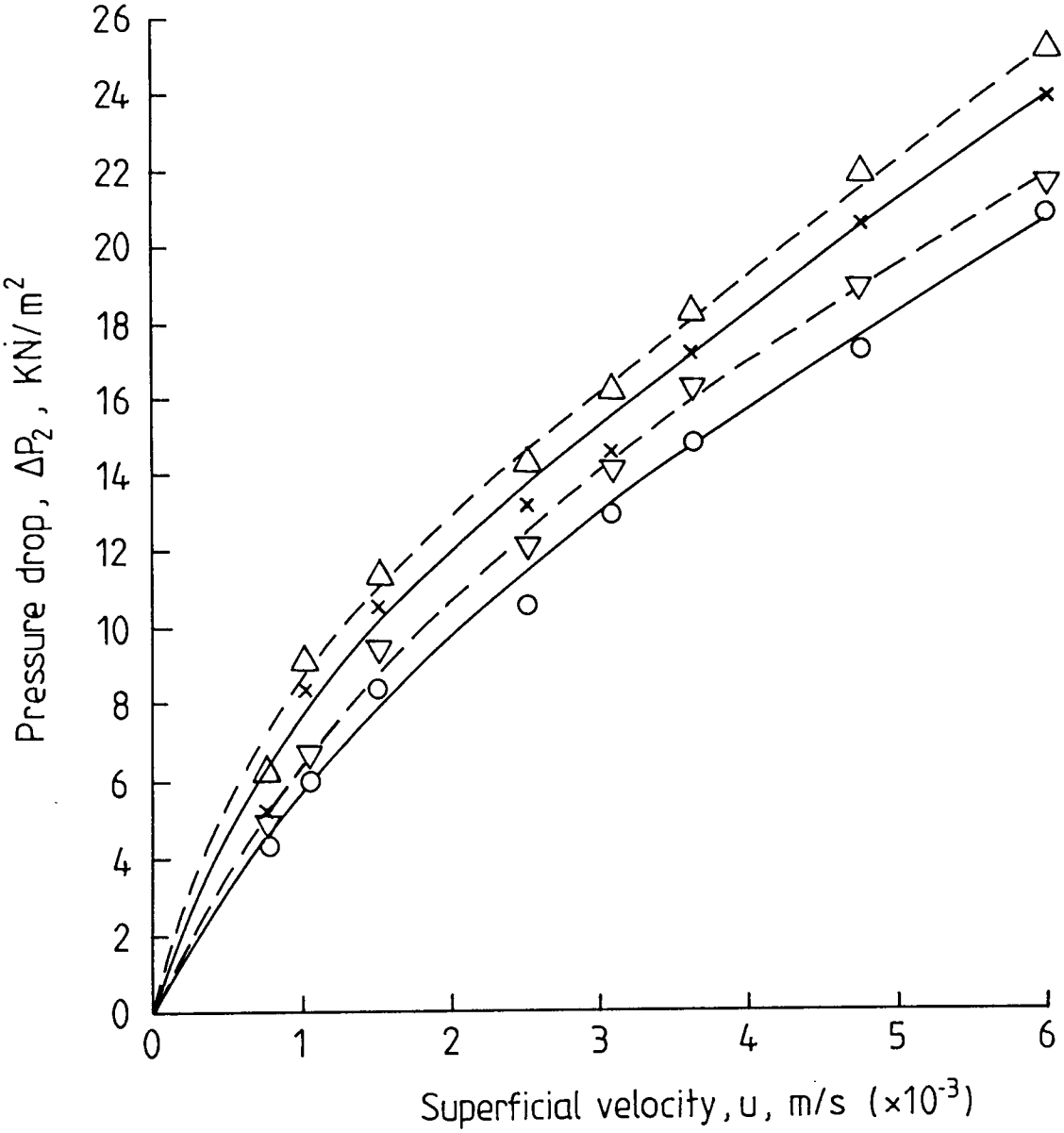

Figure 7·24 Variation of two phase pressure drop with superficial velocity at different phase ratios.

——— toluene - water

– – – – Clairsol - water

○ , ▽ 2 % v/v phase ratio

× , △ 6 % v v phase ratio

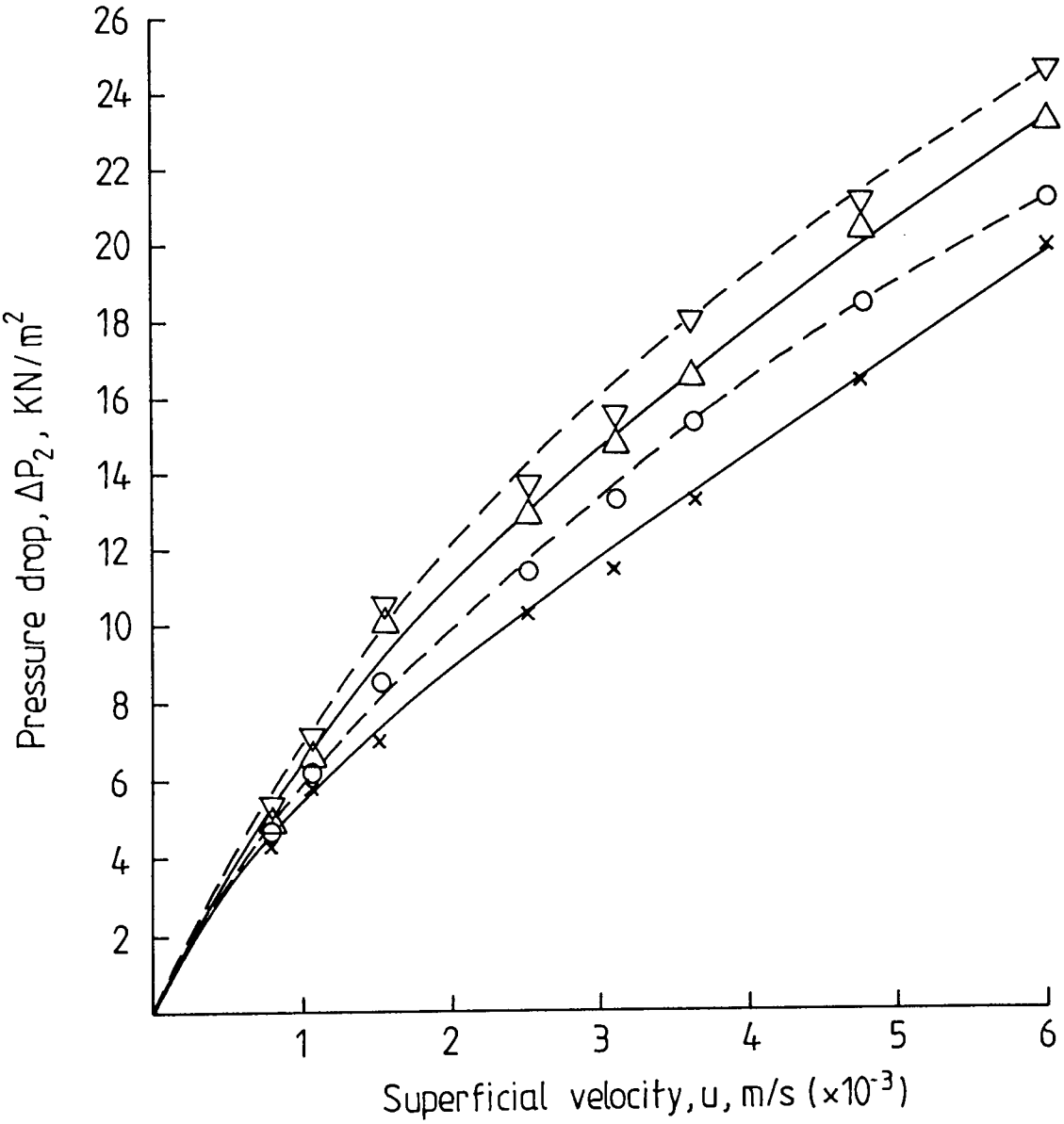

Figure 7·25 Variation of two phase pressure drop with superficial velocity at different mean inlet drop sizes.

——— toluene - water

– – – – – Clairsol - water

× , ○ 42·0 μm mean inlet drop size

△ , ▽ 22·0 μm mean inlet drop size

$$\log_e\left[\frac{\Delta p_2}{\Delta p_1}\cdot\frac{\mu_c}{\mu_d}\right] = \log_e k_p + a \log_e U + b \log_e L + c \log_e d_c +$$

$$d \log_e dp + e \log C_{in} \qquad \text{.... 7.34}$$

The results of this analysis, which were generated using the computer program given in Appendix T are presented in Table 7.4.

Table 7.4

Correlations of Pressure Drop Results by Multiple Linear Regression

Constant and Exponents for Eqn 7.33	Toluene-water liquid system	Clairsol-water liquid system
k_p	1.241	2.531
a	0.200	0.337
b	0.281	0.093
c	0.131	0.138
d	-0.327	-0.297
e	-0.255	-0.292
Multiple Correlation Coefficient*	0.625	0.698

* See Appendix T

CHAPTER EIGHT

INLET DROP SIZE DISTRIBUTION ANALYSIS AND MODELLING

8.1 Introduction

The method used to generate a secondary dispersion in this study produced a polydispersion, as described in Chapter 5, but very few dispersions encountered in industrial processes are monodisperse. The inlet drop size distribution was measured by Malvern Particle Size Analyser as described in Chapter 6.

A knowledge of the drop size distribution, in addition to the mean drop size, is necessary in order to characterise a dispersion. Furthermore, the capture efficiency depends upon drop diameter. The dispersion produced by the centrifugal pump was analysed at regular intervals during an experiment to ensure that the drop size distribution fed to the coalescer was consistent. The analysis and discussion of the experimental data, development of a distribution model, and derivation of the theoretical mean drop diameter are described in this Chapter.

8.2 Methods of Data Presentation

There are two basic forms of presentation available to express the characteristics of size and size distribution; these forms are summarized below:-

8.2.1 Tabular Form

This is the general method of presenting drop size data, as shown in Appendix U. Tables may show a listing of size against one or more ways of expressing their distribution, eg. size frequency or size cumulation, as illustrated in Appendix U. However, large amounts of data can result in the table becoming unwieldy and difficult to interpret [205].

8.2.2 Graphical Form

The use of graphs offers many advantages in spite of the accuracy of tabular presentations. However, there are several important reasons for presenting droplet size distribution graphically. Graphs present data in such a form that approximate values of the deviation and skewness of the data from the mean, and the location of the mean, can be visually obtained. Graphs are also more concise than long tables of measurements in their original form. In some cases, graphs yield specific numerical values of constant which describe the size distributions, eg. the mean and the median and the relationship of a size distribution to a certain mathematical function can readily be observed from graphical presentation [205]. Three types of graphical forms are used in this study, to present the data as:

1 *Histogram*

A histogram is the simplest way of representing the size distribution of droplets . It is a plot of the frequency of occurrence (ie percentage of droplets) in a given size range (ie size increment). It gives an immediate indication of the droplet size distribution, as illustrated in Figure 8.1.

2 *Size-frequency curves*

Curves are more practical when a large number of size increments are used to express the size distribution. Size frequency curves represent a smoothed-out histogram. The frequency curve is expressed as [205]:

$$\int_{d_{min}}^{d_{max}} fn\,(d)\,d(d) = 100\% \qquad \ldots\ldots\ 8.1$$

In general, the area between any interval on the abscissa and the curve above that interval is equal to the probability that a droplet chosen at random

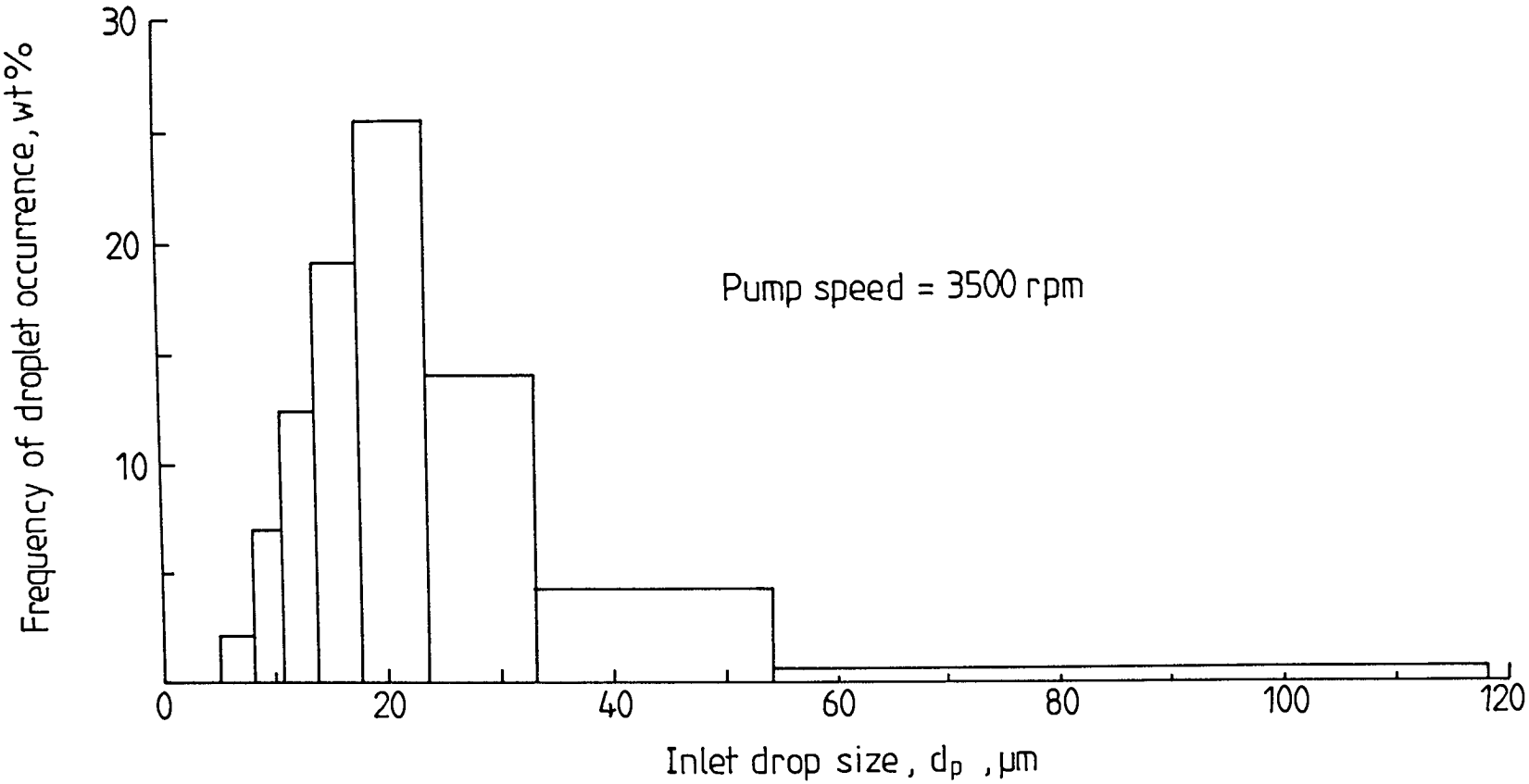

Figure 8·1 Frequency of droplet occurrence vs. inlet drop size. Drop size distribution represented in histogram form.

from the whole data will have a droplet size within that interval. This graphical type is shown in Figure 8.2.

3 *Cumulative plot*

A cumulative plot is obtained by plotting the percent of droplets > or < a given droplet size against the droplet size. Thus the limiting values of the ordinate vary form zero to 100%. The ordinate can represent total surface, external surface, weight, number of droplets, or any other basis [206]. This graphical type is shown in Figure 8.3 based upon weight percentage.

8.2.3 Mathematical Forms

There are many different mathematical forms to represent secondary dispersion drop size data. the results of all the forms are presented in Appendix U.

8.2.3.1 *Mean Diameter*

Mean diameter can be calculated on the basis of length, area, volume or weight. The general equation for mean diameter is (205)

$$(d_{pq})^{q-p} = \frac{\Sigma d^q \cdot f_n(d)}{\Sigma d^p \cdot f_n(d)} \qquad \ldots\ldots 8.2$$

where d_{pq} is the mean diameter, q and p are integers or zero, and $f_n(d)$ is the number frequency or percentage of the droplets in each size interval.

a) *Most frequent diameter or Mode (d_{fr})*: This can be seen from tabular results. When represented graphically (d_{fr}) corresponds to the highest value on the frequency curve. It also appears as the point of inflection for data represented on a cumulative curve.

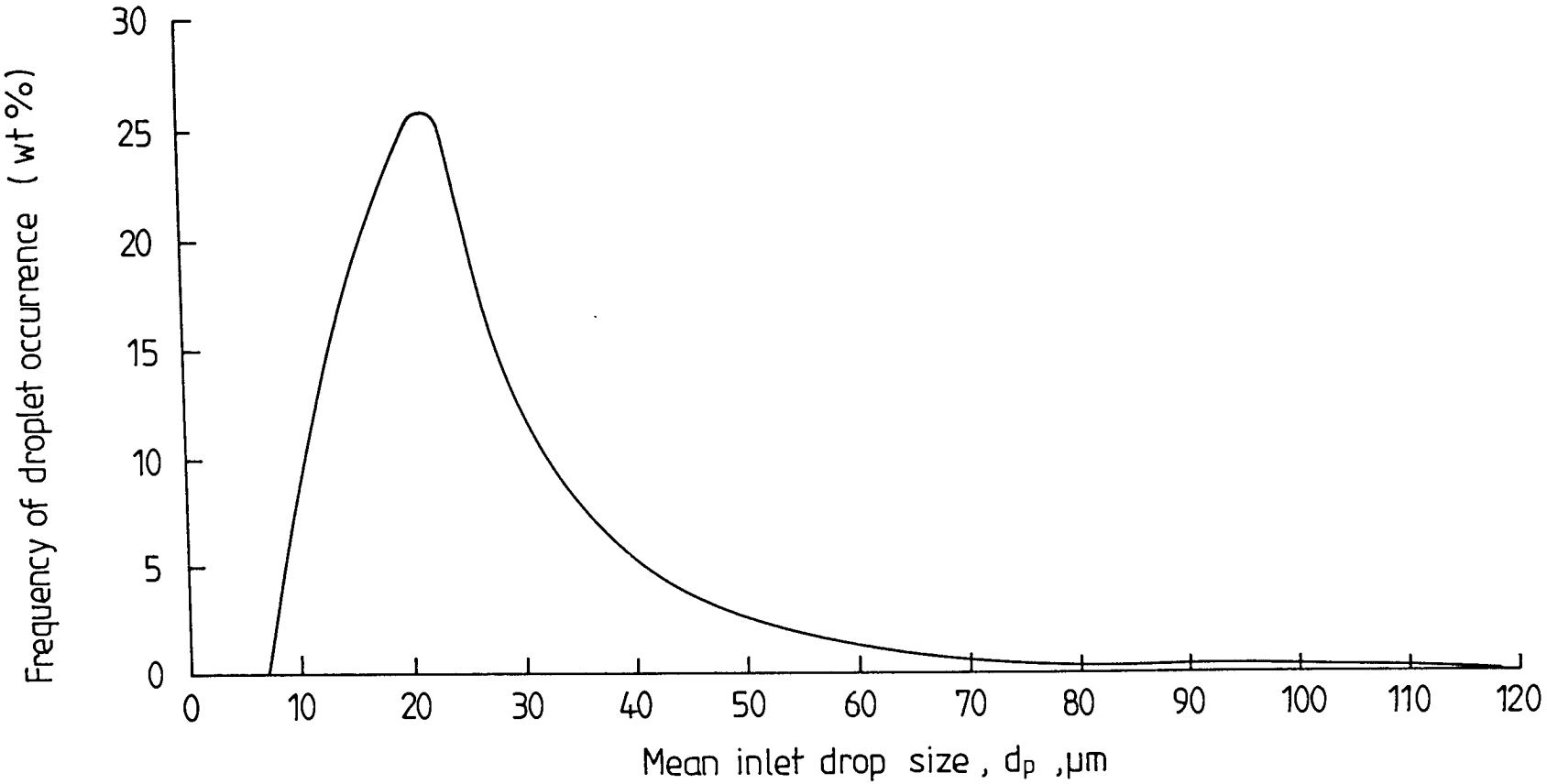

Figure 8·2 Frequency of droplet occurrence vs. mean inlet drop size. This frequency curve shows mean inlet drop size data from Particle Size Analyser at 3500 rpm pump speed.

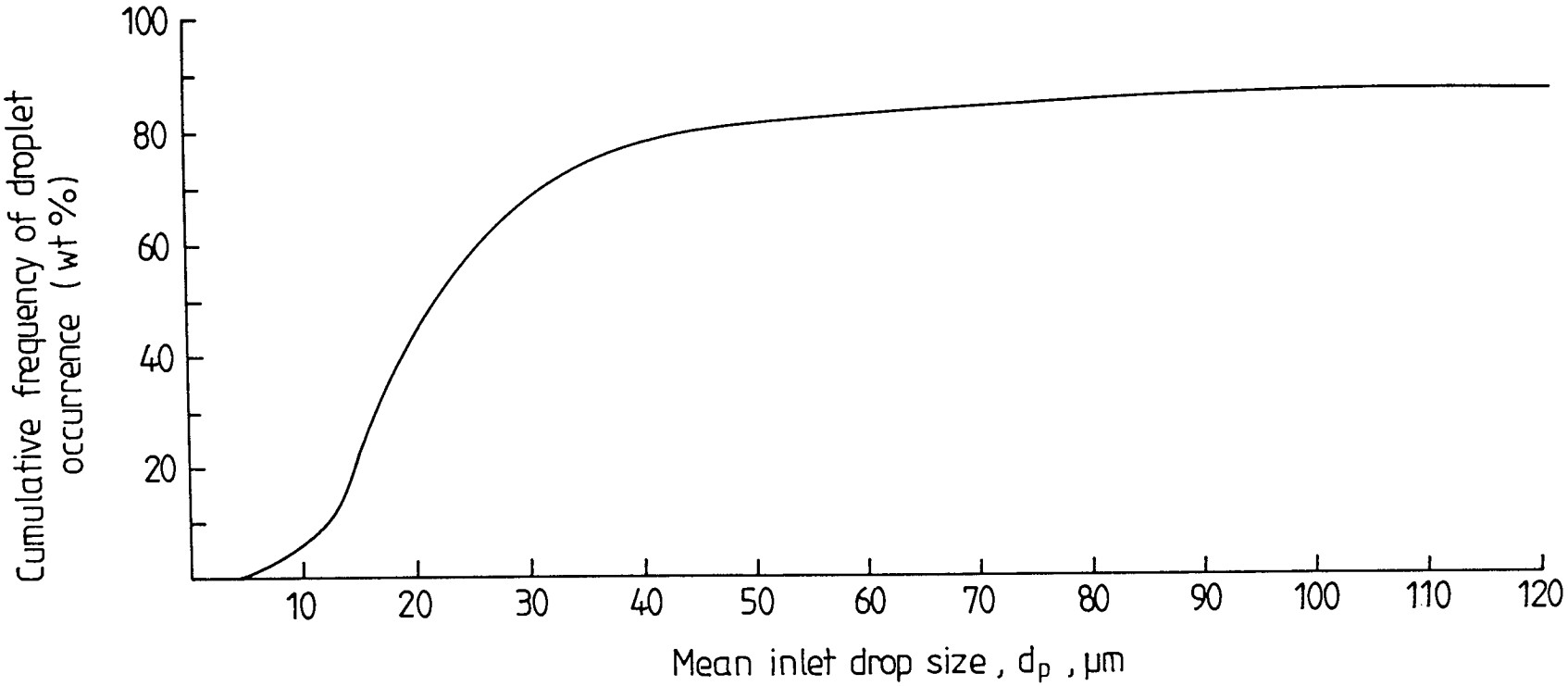

Figure 8·3 Cumulative frequency of droplet occurrence vs. mean inlet drop size. This cumulative curve shows mean inlet drop sizes data from Particle Size Analyser at 3500 rpm pump speed.

b) *Arithmetic mean diameter (dam)*: The arithmetic mean diameter is the sum of the diameters of droplets divided by the number of droplets.

A general equation for (dam) based on the number of droplets , is [205]:

$$dam = 1/100 \int_{d_{min}}^{d_{max}} d.\, fn\,(d).\, d\,(d) \qquad \ldots. \ 8.3$$

d_{am} can also be calculated from the sampling data as an arithmetic mean based on weight frequency [206, 208]:

$$d_{am} = \frac{\Sigma d.\, fw(d)}{\Sigma fw(d)} \qquad \ldots. \ 8.4$$

where fw(d) is the weight frequency or percentage of droplets in each size interval.

This mean diameter is most significant when the droplet size distribution is not overbalanced by either very large or very small droplets.

c) *Geometric mean diameter (dgm)*: The dgm is defined as the nth root of the product of the diameters of the n drop diameters analysed. d_{gm} is always smaller than d_{am} and is represented by [205]:

$$dgm = \sqrt[100]{d_1^{fw(d1)}\ d_2^{fw(d2)} \ldots\ldots d_N^{fw(dn)}} \qquad \ldots. \ 8.5$$

It is also defined in terms of logarithm weight basis as:

$$Log\ dgm = \frac{\Sigma\ fw(d)\ .\ (Log(d))}{100} \qquad \ldots. \ 8.6$$

or where $\Sigma fw(d) = 100$

$$\text{Log } d_{gm} = \frac{\Sigma fw(d) \,.\, (\text{Log } (d))}{\Sigma fw(d)} \qquad \ldots. \; 8.7$$

d) Harmonic mean diameter (d_{hm}): (d_{hm}) is defined on the basis of weight percentages of droplet diameter intervals as,

$$d_{hm} = \frac{100}{\Sigma \, fw(d)/d} \qquad \ldots. \; 8.8$$

or where $\Sigma fw(d) = 100$

$$d_{hm} = \frac{\Sigma fw(d)}{\Sigma fw(d)/d} \qquad \ldots. \; 8.9$$

The harmonic mean diameter is always smaller than d_{gm}. It is also related to specific surface, and is of value where surface area is the important process characteristic.

e) *Median diameter (dm)*: dm is defined as the diameter above, or below, which 50% of the droplets lie. The median diameter divides the area under the frequency curve into two equal parts. In general:

$$d_{hm} \leq d_m \leq d_{am} \qquad \ldots. \; 8.10$$

However, the relationship between the mean diameters follows no definite rule, as any relation depends upon the skewness of the distribution.

The median diameter is especially useful, when an excessive number or frequency percentage of very large and very small droplets are present. In this study, median

diameter (dm) was calculated using Lagrange's Interpolation Formula described in Appendix F.

f) *Equivalent Projected Diameter (d_{PJ}):* The projected diameter of the droplet is the diameter of a circle having the same area as the projected image of the droplet when viewed in the direction perpendicular to the plane of greatest stability [209]. The equivalent projected diameter (d_{PJ}), the diameter of a sphere having the same volume as the droplet, may be used as a standard of comparison [209]. The two types of (d_{PJ}) depend on the shape factor as follows:

(i) Equivalent projected diameter by using a surface factor. The shape factor may be defined by the equations [209].

$$\text{Average surface of droplet} = \alpha_s d_{am}^2 \quad \text{.... 8.11}$$

$$\text{Then, } \pi d_{PJs}^2 = \alpha_s d_{am}^2 \quad \text{.... 8.12}$$

$$d_{PJs} = d_{am} \sqrt{\frac{\alpha_s}{\pi}} \quad \text{.... 8.13}$$

where as is the surface shape factor, equal to 3.14 for a sphere [208].

(ii) Equivalent projected diameter by using a volume factor (d_{PJv}): the shape factor may be defined by [209]:

$$\text{Average volume of droplet} = \alpha_c d_{am}^3 \quad \text{.... 8.14}$$

$$\text{Then, } \pi/6\ d_{PJv}^3 = \alpha_v d_{am}^3 \quad \text{.... 8.15}$$

$$d_{PJv} = d_{am}\sqrt{\frac{\alpha_v}{\pi}} \qquad \text{.... 8.16}$$

where α_v is the volumetric shape factor, equal to 0.52 for sphere [208].

8.2.3.2 *Mean Diameter Based Upon Number, Surface,Volume and Weight*

The other mathematical forms can be derived from equation 8.2 by using different q, p integer numbers or zero.

The weight fraction of droplets can be represented in terms of the number of droplets present in the fraction and their size, as [206].

$$fw(d) = fn(d).Kv.\rho.d^3 \qquad \text{.... 8.17}$$

where Kv is volume coefficient, fw(d) is weight fraction of droplet in size d, and fn(d) is number fraction of droplet in size d. Substituting equation 8.17 in equation 8.2 yields:

$$d_{qP}^{q-P} = \frac{\sum d^{q-3} \cdot fw(d)}{\sum d^{P-3} \cdot fw(d)} \qquad \text{.... 8.18}$$

This equation and equation 8.2 are used to represent the mean diameters based upon number, surface, volume and weight, as shown in Table 8.1. These average diameters could in some cases be used to describe the drop size distribution.

8.3 Size Distribution Functions

Many mathematical relationships have been derived to represent size distributions. The use of varying forms to describe drop size distributions illustrates that no one mathematical distribution fits the size range in all circumstances. The more common distributions are given below:

Table 8.1

Mean Diameter Based Upon Number, Surface, Volume or Weight With Respect to Number Fraction or Weight Fraction

Name of Mean Diameter	Symbol	Number fraction Basis	Weight fraction Basis	Field of Application
Linear mean	d_{10}	$\frac{\Sigma d.fn(d)}{\Sigma fn(d)}$	$\frac{\Sigma d^{-2}fw(d)}{\Sigma d^{-3}fw(d)}$	comparisons, evaporation
Mean surface	d_{20}	$\sqrt{\frac{\Sigma d^2.fn(d)}{\Sigma fn(d)}}$	$\sqrt{\frac{\Sigma d^{-1}.fw(d)}{\Sigma d^{-3}.fw(d)}}$	surface area controlling, eg adsorption
Mean volume	d_{30}	$\sqrt[3]{\frac{\Sigma d^3.fn(d)}{\Sigma d.fn(d)}}$	$\sqrt[3]{\frac{\Sigma fw(d)}{\Sigma d^{-3}.fw(d)}}$	volume controlling eg hydrology
Volume-linear mean	d_{31}	$\sqrt{\frac{\Sigma d^3.fn(d)}{\Sigma d.fn(d)}}$	$\sqrt{\frac{\Sigma fw(d)}{\Sigma d^2.fw(d)}}$	Evaporation, molecular diffusion
Volume-surface or Sauter	d_{32}	$\frac{\Sigma d^3.fn(d)}{\Sigma d^2.fn(d)}$	$\frac{\Sigma fw(d)}{\Sigma d^{-1}.fw(d)}$	Efficiency studies, mass transfer, reaction
Surface-linear mean	d_{21}	$\frac{\Sigma d^2.fn(d)}{\Sigma d.fn(d)}$	$\frac{\Sigma d^{-1}.fw(d)}{\Sigma d^{-2}.fw(d)}$	Adsorption
Moment-Weight	d_{43}	$\frac{\Sigma d^4.fn(d)}{\Sigma d^3.fn(d)}$	$\frac{\Sigma d.fw(d)}{\Sigma fw(d)}$	Combustion equilibrium

a) Normal (or Gaussian) distribution: the most familiar distribution function is the normal distribution defined by [209, 210, 211],

$$fw(d) = \frac{1}{S_N \sqrt{2\pi}} \exp\left[-\frac{1}{2}\left(\frac{d - d_{am}}{S_N}\right)^2\right] \quad \ldots. 8.19$$

where, standard deviation $S_N = \sqrt{\sum_{o}^{\infty} \frac{(d - d_{am})^2}{M - 1}}$ 8.20

and M is number of drop diameters measured.

Normal distributions are generally symmetrical about the arithmetic mean and thus have the propoerty that mode, median, and arithmetic mean are identical [209].

b) Log-normal distribution: The lognormal distribution function is applicable to drop distributions formed in some chemical processes such as spray-drying and mass transfer in agitated liquid-liquid systems [209, 210]. The log-normal distribution is defined by [182]:

$$fw(d) = \frac{1}{\text{Log } S_G \cdot \sqrt{2\pi}} \exp\left[-\frac{1}{2}\left(\frac{\text{Log } d - \text{Log } d_{gm}}{\text{Log } S_G}\right)\right] \quad \ldots. 8.21$$

The geometric standard deviation (S_G) is the size ratio at the corresponding oversize values of 50% and 15.9%, or the size ratio of the corresponding undersize values of 84.1% and 50% [205]. The log-normal distribution permits determination of geometric mean diameter (d_{gm}) and geometric deviation (S_G). This is possible since the nature of the log-normal distribution law means the geometric standard deviation on number and weight bases are equal.

c) Square root normal distributions: This type of distribution is similar in form to the

log-normal distribution because both distributions have a mean and standard deviation. The square root of d, d_{gm} and S_G merely replaces Log d, Log d_{gm} and Log S_G. The square root normal distribution is defined by:

$$fw(d) = \frac{1}{\sqrt{2\pi\, S_G}} \exp\left[-\frac{1}{2}\left(\frac{\sqrt{d} - \sqrt{d_{gm}}}{\sqrt{S_G}}\right)^2\right] \quad \ldots. \ 8.22$$

This distribution function is used with centrifugal pressure nozzles, as the distribution often represents spray-size data with greater accuracy than the log normal distribution [205].

d) Rosin-Rammler distribution: The Rosin-Rammler distribution is widely-quoted to express droplet size distribution especially from nozzle sprays. It is empirical and relates the volume, or weight, percent oversize (V or W) to droplet diameter (d). The mathematical form is :

$$\text{Log}\frac{100}{W} = \left(\frac{d}{d_R}\right)^{\gamma_c} \quad \ldots. \ 8.23$$

or,

$$\text{Log}\left(\text{Log}\frac{100}{W}\right) = \gamma_c \text{Log}\left(\frac{d}{d_R}\right) \quad \ldots. \ 8.24$$

The plot of log (100/w) against (d) will give a straight line on log-log paper. The slope represents the dispersion coefficient (γ_c). In this study, the slope has been calculated mathematically by using a linear regression method, ie linear least square method, described in Appendix G. The higher the value of γ_c, the more uniform the distribution.

The Rosin-Rammler mean (d_R) can be obtained directly from the curve as it is the droplet diameter above which lies 36.8% of the entire volume, or weight, percent oversize. Also, in this work the mathematical formula, ie Lagrange's interpolation formula, has been used to predict the value of (d_R), as described in Appendix F.

e) Upper Limit function: This is a developed function from the log-normal distrbution function. This distribution is defined by:

$$fw(d) = \frac{1}{\text{Log } S_G \sqrt{2\pi}} \cdot \exp\left[{}^1/_2 \cdot \left(\frac{\text{Log } ((d_{max} - d)/d_{gm})^2}{\text{Log } S_G{}^2}\right)\right] \quad \ldots. \ 8.25$$

The upper limit distribution places practical limits on the minimum and maximum droplet sizes because it contains a third parameter dmax (maximum droplet diameter) unlike the square root distribution which gives meaningless values in the maximum size range [205]. The results of thse distribution functions are presented in Appendix U.

8.4 Developed Distribution Function

The Weibull distribution function has been used extensively in recent years to deal with complicated modern technology systems. The Weibull distribution function is defined by [212]:

$$f(t) = \alpha\beta(t).^{B-1} \exp(-\alpha t^{\beta}) \text{ at } t > 0$$
$$= 0 \qquad \text{elsewhere} \qquad \ldots. \ 8.26$$

where, parameters α and β are both > 0.

The curves of this function change considerably in shape for different values

of the parameters particularly the parameter β, as shown in Figure 8.4. Moreover, the, mean of the Weibull distribution is stated in the following theroretical equation [212]:

$$\text{Mean} = \alpha^{-1/\beta}\,\Gamma\,(1 + 1/\beta) \qquad \ldots. \ 8.27$$

The following logical developments were introduced into the Weibull distribution function to make it suitable for fitting the inlet drop size distribution data, calculated by the computer program in Appendix U:-

1 The values of d are divided by d_{fr} (ie most frequent diameter) to generalise equation 8.26 because the value of fw(d) is a maximum at the value of $d = d_{fr}$. Therfore, the Weibull distribution function can be re-written with respect to d instead of t as:

$$fw(d) = \alpha\,\beta\,\left(\frac{d}{d_{fr}}\right)^{\beta-1} \cdot \exp\left(-\alpha\left(\frac{d}{d_{fr}}\right)^{\beta}\right) \qquad \ldots. \ 8.28$$

2 The constant (Z) is introduced into equation 8.28, but equals the value of fw(d) when d/dfr = 1.0. Then this constant (Z) equals:

$$Z = \alpha\,\beta\,\exp(-\alpha) \qquad \ldots. \ 8.29$$

This constant is introduced to estimate more accurate theoretical values of fw(d). Therefore equation 8.28 becomes:

$$fw(d) = \left[\frac{\alpha\,\beta}{Z}\right]\left[\frac{d}{d_{fr}}\right]^{\beta-1} \cdot \exp\left[-\alpha\left[\frac{d}{d_{fr}}\right]^{\beta}\right] \qquad \ldots \ 8.30$$

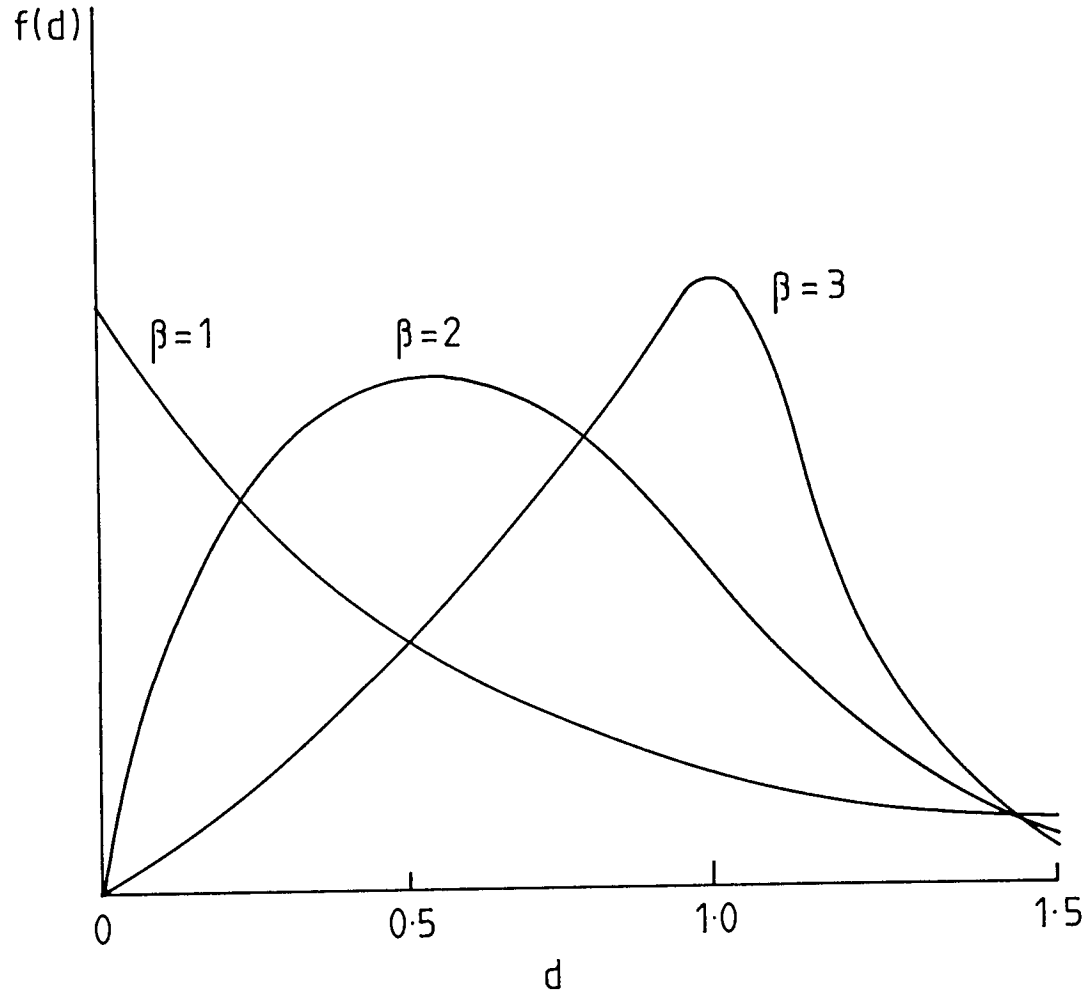

Figure 8.4 Weibull Distributions ($\alpha = 1$)

3 The values of fw(d) in equation 8.30 are a fraction of the maximum value of fw(d). Therefore equation 8.30 should be multiplied by the maximum value of fw(d) (ie $fw(d)_{max}$). The final formula of the developed distribution function is:-

$$fw(d) = \frac{fw(d)_{max}}{Z} \alpha \beta \left[\frac{d}{d_{fr}}\right]^{\beta-1} \exp\left[-\alpha\left[\frac{d}{d_{fr}}\right]^{\beta}\right] \quad \text{.... 8.31}$$

where, β and α = distribution coefficients, dfr = most frequent diameter (or Mode), $fw(d)_{max}$ = maximum value of frequency or percentage occurrence of drop sizes.

8.5 The calculation of α and β Distribution Coefficients

To apply the Weibull distribution to reliability theory, the reliability of a component or product is defined as the probability that it will function properly for at least a specified time under specified experimental conditions. By analogy in the present analysis [212],

$$R(d) = Pr\,(D > d) \quad \text{.... 8.32}$$

$$R(d) = \int_{d}^{\infty} fw(d)\, d(d) \quad \text{.... 8.33}$$

$$R(d) = 1 - Fw(d) \quad \text{.... 8.34}$$

where Fw(d) is the cumulative distribution of diameter (d). Then, by using equations 8.28, 8.33 and 8.34, the following equation is formed,

$$R(d) = 1 - Fw(d) = 1 - \int_{o}^{d} \alpha \beta \left[\frac{d}{d_{fr}}\right]^{\beta-1} \exp\left[-\alpha\left[\frac{d}{d_{fr}}\right]^{\beta}\right] d(d) \quad \text{.... 8.35}$$

$$R(d) = 1 + \int_{o}^{d} d \exp\left[-\alpha\left[\frac{d}{d_{fr}}\right]^{\beta}\right] \quad \text{.... 8.36}$$

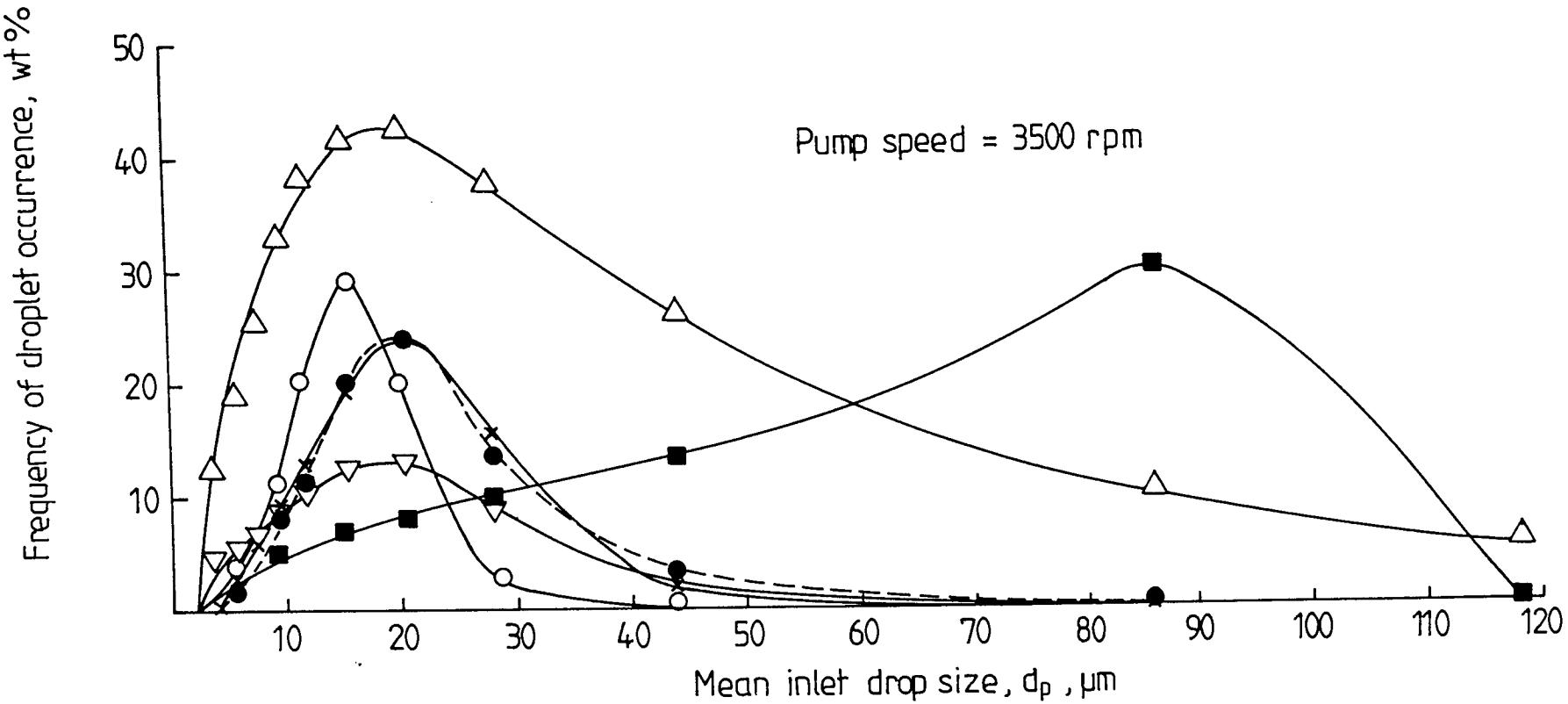

Figure 8·5 Comparison of distribution functions with experimental data of mean inlet drop sizes.

---- ● Experimental data
——— × Theoretical distribution model
■ Upper limit distribution function
▽ Square root normal distribution function
○ Rosin-Rammler distribution function
△ Log-normal distribution function

$$R(d) = \exp\left[-\alpha\left[\frac{d}{d_{fr}}\right]^{\beta}\right] \quad \text{.... 8.37}$$

or, $$\ln(R(d)) = \ln(1 - Fw(d)) = -\alpha\left(\frac{d}{d_{fr}}\right)^{\beta} \quad \text{.... 8.38}$$

To linearize equation 8.38:

$$\ln . \ln\left[\frac{1}{1 - Fw(d)}\right] = \ln(\alpha) + \beta \ln\left(\frac{d}{d_{fr}}\right) \quad \text{.... 8.39}$$

This represents $\ln \ln \frac{1}{1 - Fw(d)}$ as a linear function of $\ln(d/d_{fr})$, some set of data which gives a particularly good fit to a straight line when plotted on this basis, or by using the library package (G02 CAF) from the NAGIO of the Computer Centre Library, as described in Appendix G.

The last method gives the slope, intercept and correlation coefficient. The value of slope equals b. The value of α is

$$\alpha = \exp(\text{Intercept value}) \quad \text{.... 8.40}$$

and the correlation coefficient represents the linear relationship between the two variables (ie $\ln \ln\left[\frac{1}{1 - Fw(d)}\right]$ and $\ln(d/d_{fr})$). Thus a value of correlation coefficient equal to (+1) implies a perfect linear relationship with positive slope, whilst a value of correlation coefficient equal to (-1) results from a perfect linear relationship with negative slope [212].

The results of Malvern Particle Size analyses presented in Appendix U, shows that the best fit of the developed distribution function to the experimental data was obtained when the values of $0.5 \leq \alpha \leq 1.0$, as shown in the computer program and results in Appendix U. Therefore, if $\alpha < 0.5$, it was taken as 0.5 and β was multiplied

by 1.15; if $\alpha > 1.0$, it was taken as 1.0 and β was multiplied by 1.35 to give the best fit of the rest of experimental data by the developed distribution function, as illustrated in Figure 8.5.

8.6 Derivation of the Theoretical Mean Diameter

For the purpose of this work, the developed distribution function of fw(d) can be used to derive theoretical mean diameter equations as follows. The two basic equations are equation 8.31 and,

$$d_{qP}^{q-P} = \frac{\Sigma d^{q-3} fw(d)}{\Sigma d^{P-3} fw(d)} \quad \text{.... 8.42}$$

The linear diameter, d_{10} can be calculated from this equation [213],

$$d_{10} = \Sigma d \,.\, fn(d) \,/\, \Sigma\, fn(d) \quad \text{.... 8.43}$$

for a smooth distribution curve, equation 8.43 can be rewritten as:

$$d_{10} \int_{d_o}^{d_{max}} fn(d)\, d(d) = \int_{d_o}^{d_{max}} d.f_n(d).d(d) \quad \text{.... 8.44}$$

Consider two functions of droplet diameter which are compared, and let their orders be q and p. Then the relevant mean, dqp, is defined by:

$$d_{qP}^{q-P} \int_{do}^{d_{max}} d^P.f_n(d)\, d(d) = \int_{do}^{d_{max_q}} d^q.f_n(d).d(d) \quad \text{.... 8.45}$$

The Gamma function which appears in the Weibull mean equation (8.27) is defined as [213]

$$\Gamma(n) = \int_0^\infty u^{n-1} C^{-u} \delta u \qquad \text{.... 8.46}$$

More information about the Gamma function is given in Appendix J.

Assuming, (i) the distribution of drop diameters is uniform; (ii) $d_o = O$ and $d_{max} = \infty$ represent end points of the curve, which implies that for the "smallest" and "largest" droplets in the inlet drop sample, dfw(d)/d(d) may be taken as infinitesimal or zero beyond the actual d_o and d_{max}.

Equation 8.45 can be written in weight percentage or frequency basis as,

$$d_{qP}^{q-P} = \frac{\int_0^\infty d^{q-3} \cdot fw(d)\, d(d)}{\int_0^\infty d^{P-3} \cdot fw(d)\, d(d)} \qquad \text{.... 8.47}$$

the integrations of $\int_0^\infty d^{q-3} \cdot fw(d)\, d(d)$ and $\int_0^\infty d^{p-3} \cdot fw(d).d(d)$ have the following steps:

$$\int_0^\infty d^{q-3} \cdot fw(d)\, d(d) = \int_0^\infty d^{q-3} \cdot \frac{fw(d)_{max}}{Z} \cdot \alpha \cdot \beta \left(\frac{d}{d_{fr}}\right)^{\beta-1} \cdot \exp\left[-\alpha \left(\frac{d}{d_{fr}}\right)^{\beta}\right] \cdot d(d) \qquad \text{.... 8.48}$$

$$\text{let:} \quad H = \frac{fw(d)_{max}}{Z}; \text{ and } x = \frac{d}{d_{fr}} \qquad \text{.... 8.49}$$

Then equation 8.48 becomes:

$$\int_0^\infty d^{q-3} \cdot fw(d)\, d(d) = H \int_0^\infty \alpha\beta\, {}_{fr}^{(q-3)} \cdot \alpha^{(q+\beta-4)} \cdot \exp[-\alpha x^\beta] \cdot dx \qquad \text{.... 8.50}$$

or

$$\int_0^\infty d^{q-3} \cdot fw(d)\, d(d) = H\, \alpha\beta d_{fr}^{q-3} \int_0^\infty x^{q+\beta-4} \cdot \exp(-\alpha x^\beta) \cdot dx \qquad \text{.... 8.51}$$

The integration of equation 8.51 has been solved by comparing equation 8.51 with equation 8.52, listed in the special integration table in reference [214], ie

$$\int_0^\infty x^m \exp(-a x^2) \cdot \delta x = \frac{\Gamma((m+1)/2)}{2\, a^{(m+1)/2}} \qquad \text{.... 8.52}$$

Therefore, equation 8.51 becomes:

$$= H\, \alpha\, \beta\, d_{fr}^{q-3} \cdot \frac{\Gamma((q+\beta-4+1)/\beta)}{\beta \cdot \alpha^{(q+\beta-4+1)/\beta}} \qquad \text{.... 8.53}$$

$$= H \cdot d_{fr}^{q-3} \cdot \alpha \cdot \frac{1}{\alpha^{(q+\beta-3)/\beta}} \cdot \Gamma\left(\frac{q+\beta-3}{\beta}\right) \qquad \text{.... 8.54}$$

$$= H \cdot d_{fr}^{q-3} \cdot \frac{1}{\alpha^{(q-3)/\beta}} \cdot \Gamma\left(\frac{q-3}{\beta} + 1\right) \qquad \text{.... 8.55}$$

A similar result arises from solving $\int_0^\infty d^{P-3} \cdot fw(d) \cdot d(d)$ using the same steps:

$$\int_0^\infty d^{P-3} \cdot fw(d) \cdot d(d) = H \cdot d_{fr}^{P-3} \frac{1}{\alpha^{(P-3)/\beta}} \cdot \Gamma\left(\frac{P-3}{\beta} + 1\right) \qquad \text{.... 8.56}$$

Therefore, equation 4.47 becomes:

$$d_{qP}^{q-P} = \frac{H \cdot d_{fr}^{q-3}\ \alpha^{1/(q-3/\beta)}\ .\ \Gamma((q-3/\beta)+1)}{H \cdot d_{fr}^{q-3} \cdot \alpha^{1/(P-3/\beta)} \cdot \Gamma((P-3/\beta)+1)} \qquad \ldots. 8.57$$

Therefore, the new general equation derived for mean diameter is:

$$d_{qP}^{q-P} = d_{fr}^{q-P} \cdot \alpha^{P-q/\beta} \cdot \frac{\Gamma((q-3/\beta)+1)}{\Gamma((q-3/\beta)+1)} \qquad \ldots. 8.58$$

For example, d_{21} mean diameter equals:

$$d_{21} = d_{fr} \cdot \left[\alpha\right]^{-1/\beta} \cdot \left[\frac{\Gamma(-(1/\beta)+1)}{\Gamma(-(2/\beta)+1)}\right] \qquad \ldots.8.59$$

where, (see Appendix J)

$$\Gamma(y) = y^{y} \cdot e^{-y} \cdot \sqrt{\frac{2\pi}{y}} \cdot \left[1 + \frac{1}{12y} + \frac{1}{288y^2} - \frac{139}{51840y^3} - \frac{571}{2488320y^4} + ..\right] \qquad \ldots. 8.60$$

y is positive value.

8.7 Analysis of Mean Diameter of Inlet Drops

Sets of experimental and predicted results of mean diameters of inlet drops for different values of centrifugal pump speed (ie rpm) are presented in Appendix U. The computer program presented in Appendix U, was used to evaluate the experimental data and predicted results. A comparison between experimental and predicted data is shown in Figure 8.6, ie the difference ranges between -15% to +15% indicative of the experimental data being well represented by the derived model.

This approach was developed further by calculating the mean inlet drop sizes for different pump speeds using the polynomial regreasion analysis technique described by the computer program in Appendix V. The results of this approach are plotted in

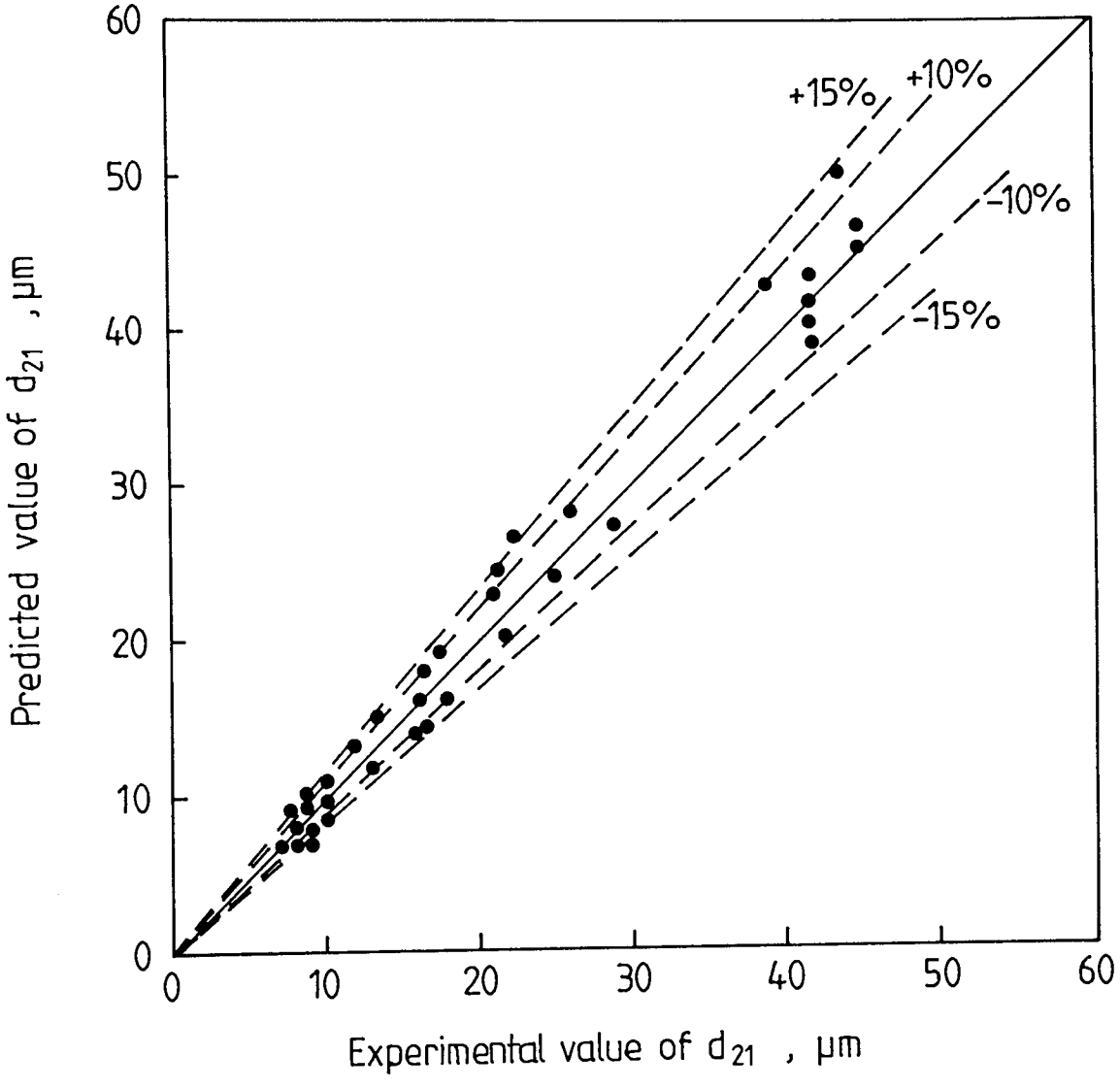

Figure. 8·6 Correlation of experimental d_{21} data with equation 8·60

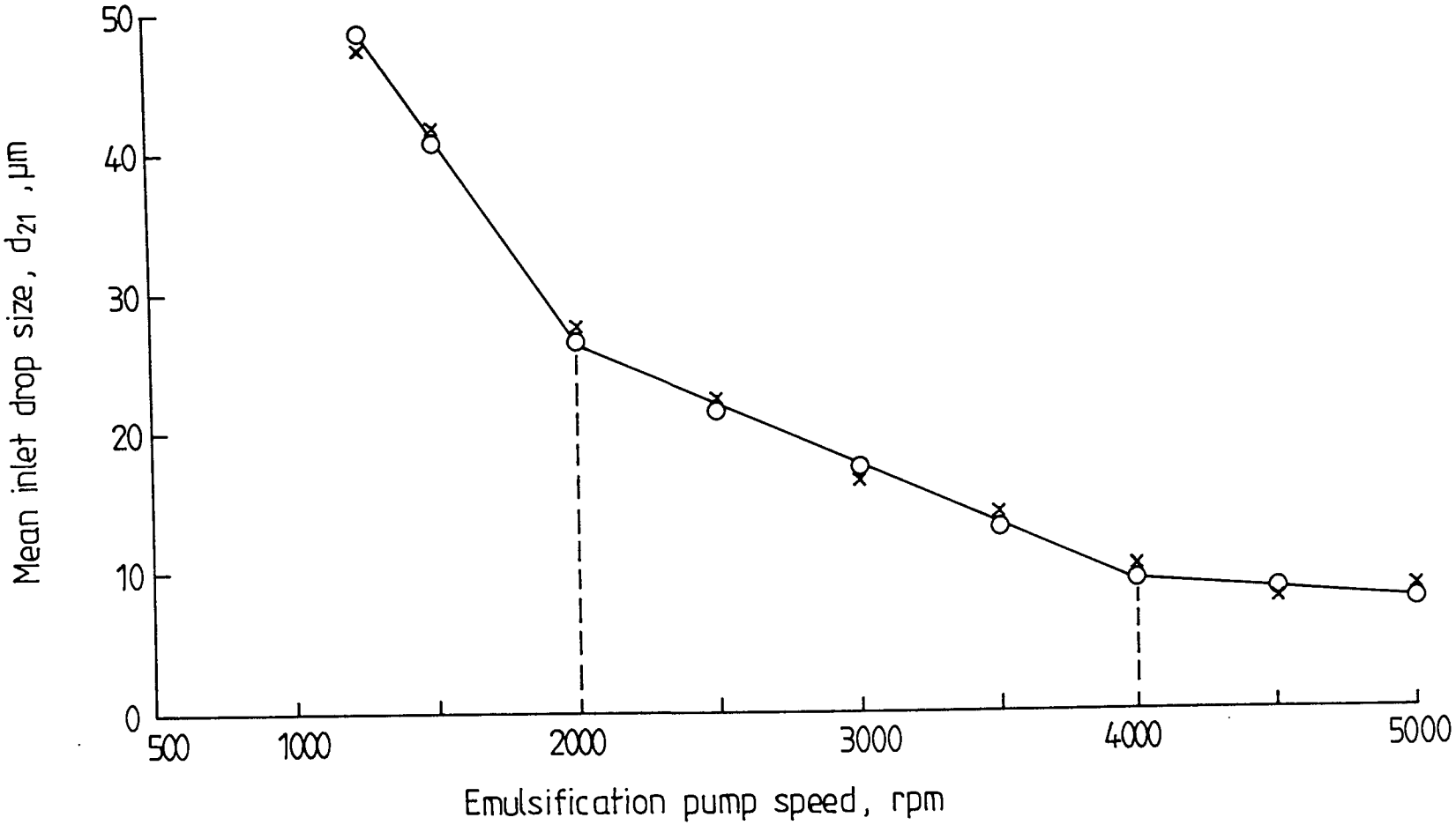

Figure 8·7 Mean inlet drop size vs. emulsification pump speed. Correlation of experimental d_{21} data with polynomial regression.
(× , Experimental d_{21} data. o , Regression value of d_{21} .)

$$d_{21} = 82.531 - 0.027 \text{ . Ps at } 1000 \leq Ps < 2000 \quad \text{.... 8.62}$$

$$d_{21} = 43.329 - 0.0084 \text{ . Ps at } 2000 \leq Ps < 4000 \quad \text{.... 8.63}$$

$$d_{21} = 17.95 - 0.002 \text{ . Ps at } 4000 \leq Ps < 5000 \quad \text{.... 8.64}$$

where d_{21} is the surface-linear mean drop diameter, and Ps is pump speed (rpm).

Figure 8.7 demonstrates that all the data points are very well represented by the equations 8.62 to 8.64.

CHAPTER NINE

ANALYSIS AND DISCUSSION OF EXPERIMENTAL RESULTS

9.1 Exit Drop Size

Mean exit drop size was found to depend upon the precise mechanism of release at the exit side of the packing as well as other factors, such as superficial velocity, phase ratio, bed depth, particle size, and inlet drop size [17, 104]. The individual release mechanisms were discussed in Section 4.1.4.

The mean size of exit drops, determined as the mean linear diameter, was found to decrease with an increase in superficial velocity as shown in Figure 9.1. This is in agreement with the results of other workers (16, 17, 27, 57, 81, 94, 104, 106), who found experimentally that the mean exit drop size decreased with increase in superficial velocity.

Typical photographs of exit drops for the toluene-water system, shown in Plates 9.1 to 9.3, indicate that different exit drop sizes result from different mechanisms of coalescence and release.

For any particular flow velocity the exit drop size distributions were dependent upon the mean inlet drop size (d_{21}) for the range investigated [8-47 μm]. This was because the growth of each captured drop on a packing element increased until the drag and buoyancy forces overcame the surface forces.

Under steady-state conditions, the mean drop size was independent of phase ratio, within the range 0.5% v/v to 1% v/v. This indicated that the degree of coalescence was independent of ratio of dispersed phase entering the bed. This is in agreement with other workers (17, 27, 104, 106). However, a slight increase of mean exit drop size was apparent with an increase in phase ratio within the range 2% v/v to 6% v/v, as

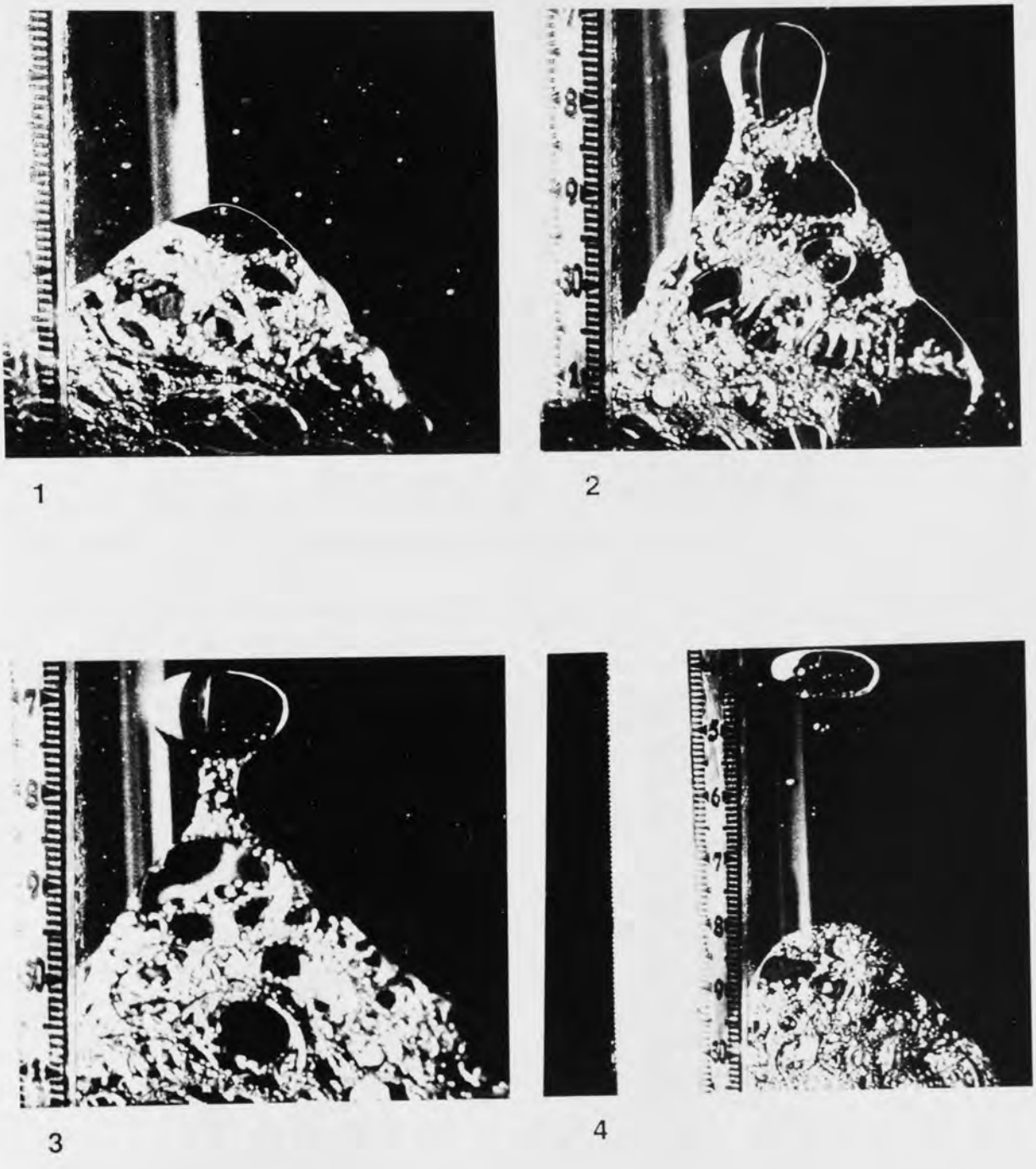

Plate 9.1 Drops Released by Graping Mechanism

System: toluene/water
Phase ratio = 2% v/v
Ballotini size = 266 μm

Superficial Velocity = 2.05×10^{-3} m/s
Bed depth = 30 mm
Mean inlet drop size = 27.0 μm

Plate 9.2 Drops Released by Ballooning Mechanism

System: toluene/water
Phase ratio = 1% v/v
Ballotini size = 266 μm

Superficial Velocity = 1.50×10^{-3} m/s
Bed depth = 30 mm
Mean inlet drop size = 22.0 μm

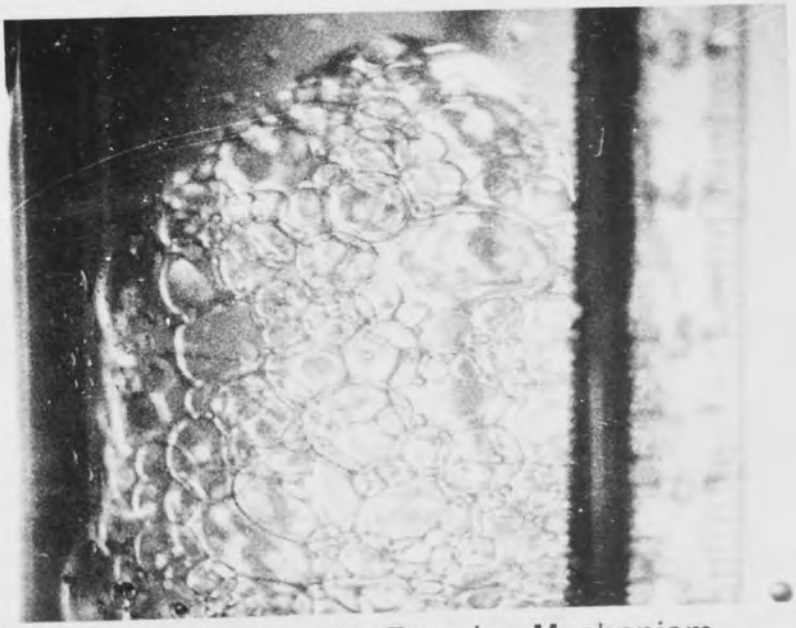

Plate 9.3 Drops Released by Foaming Mechanism

System: toluene/water
Phase ratio = 2% v/v
Ballotini size = 266 μm

Velocity = 3.05×10^{-3} m/s
Bed depth = 30 mm
Mean inlet drop size = 27.0 μm

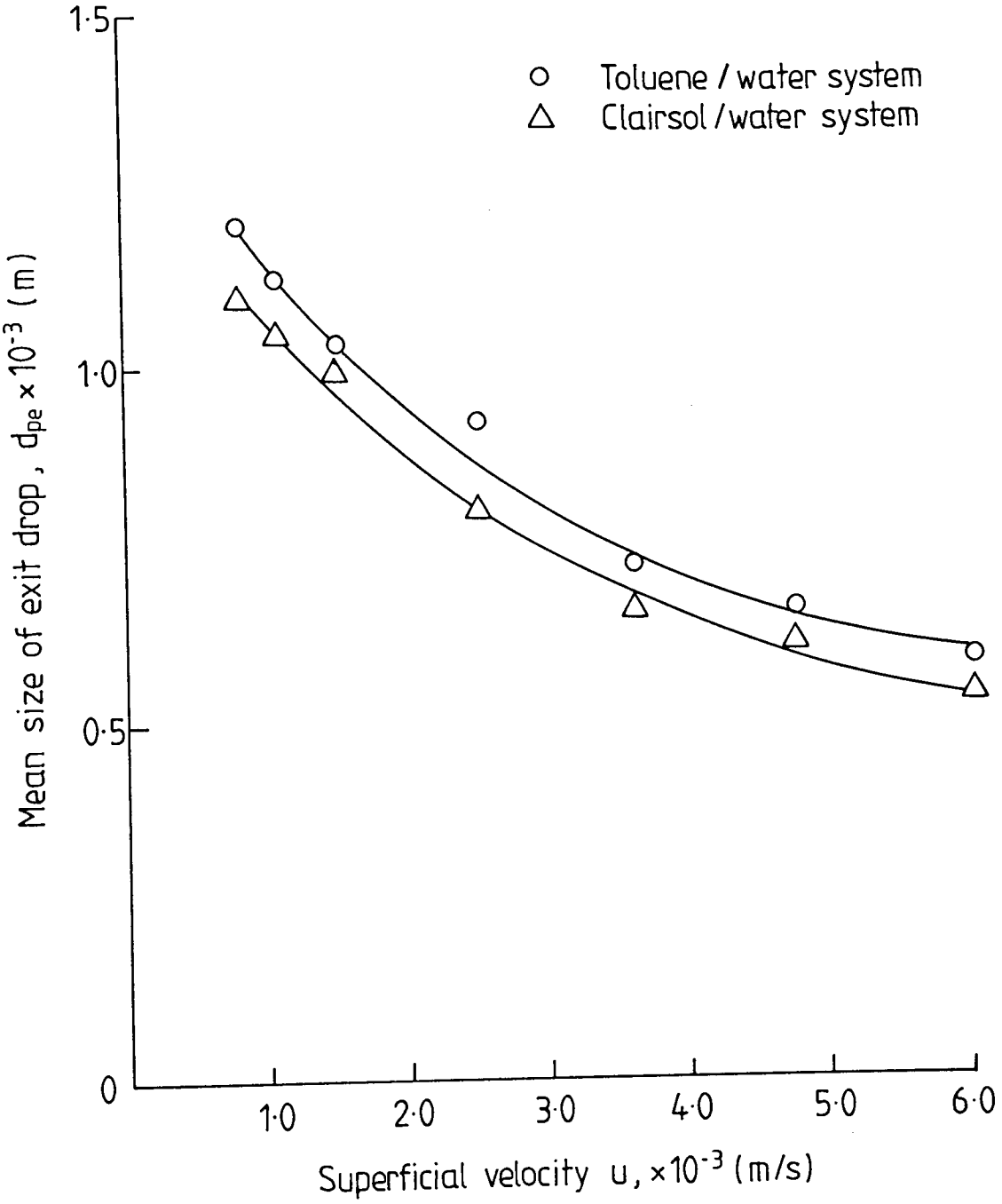

Figure 9.1 Mean size of exit drop vs. superficial velocity for 30 mm bed depth, 266 μm ballotini particle size, 2% v/v phase ratio; 27 μm mean inlet drop size.

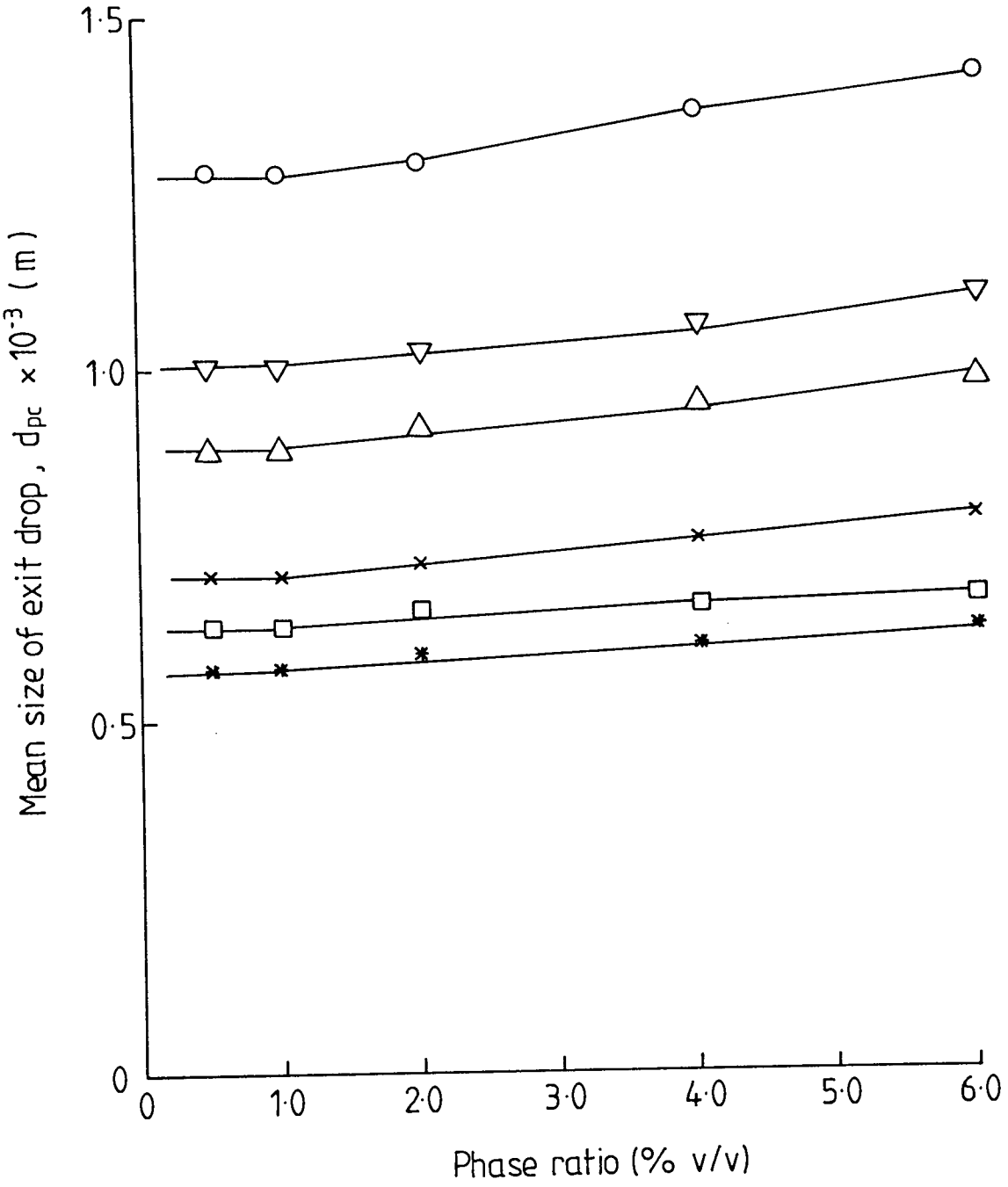

Figure 9·2 Mean size of exit drop vs. phase ratio for 30 mm bed depth, 266 μm ballotini particle size, 27 μm mean inlet drop size; toluene-water system.

Superficial velocity u, $\times 10^{-3}$ (m/s)

- ○ 0·8
- ▽ 1·5
- △ 2·5
- × 3·6
- □ 4·75
- ✱ 6·0

shown in Figure 9.2. Although phase ratios less than 0.5% were not studied in this work, there is no reason in theory why, once steady-state is attained, these packings should not function satisfactorily at very low phase ratios, eg 0.01% v/v.

Five different packing thicknesses in the range 10×10^{-3} to 50×10^{-3} m, with a constant particle diameter, were investigated. Any increase in bed depth led to an increase in exit drop size as shown in Figure 9.3 but there appeared to be an optimum bed thickness after which any increase in thickness did not result in a corresponding increase in mean exit drop size. This was in complete agreement with the observations of many workers (17, 27, 57, 104, 106). This optimum thickness existed for each application because the velocity of any droplet within the packing decreased as it travelled through the bed until after some distance the retention time was sufficient for dispersed phase drainage to occur and hence for adherance of the droplet on a particle.

Figure 9.3 shows that the optimum bed depth was approximately 30×10^{-3} m.

An increase in ballotini particle size resulted in an increase in the average exit drop size, as shown in Figure 9.4. This arises because, for any random packing of spheres, the mean void diameter will increase as the particle size is increased. However, total coalescence efficiency depends on drop capture efficiency so that the smallest size ballotini, with the smallest average void diameter, should be most effective in capturing the smallest drops.

The deep beds may induce drop redispersion and hence reduce the separation efficiency. Therefore, an optimum ballotini particle size exists and the largest exit drop size was actually obtained with the coalescer constructed from ballotini of 266 μm mean particle diameter at a bed depth of 30×10^{-3}m. For all practical purposes however, provided exit drops were > 0.2 mm, and preferably > 0.5 mm, so that they settled fairly rapidly under gravity, the precise mean linear diameter was not considered a measure of bed efficiency. Rather it was the ability to coalesce drops without secondary haze

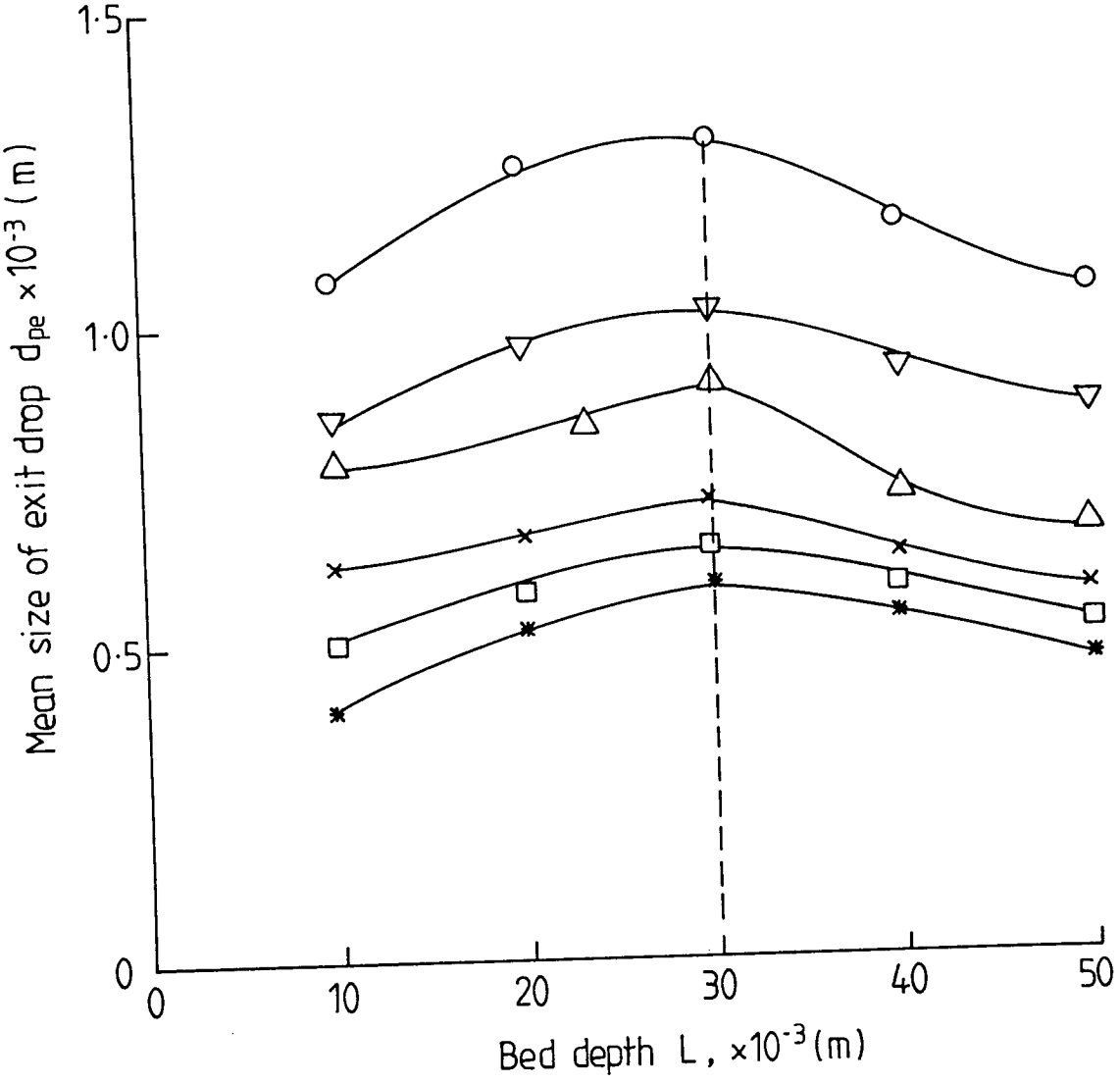

Figure 9·3 Mean size of exit drop vs. bed depth for 266 μm ballotini particle size, 2% phase ratio, 27 μm mean inlet drop size; toluene / water system.

Superficial velocity u, $\times 10^{-3}$ (m/s)

○	0·8
▽	1·5
△	2·5
×	3·6
□	4·75
✱	6·0

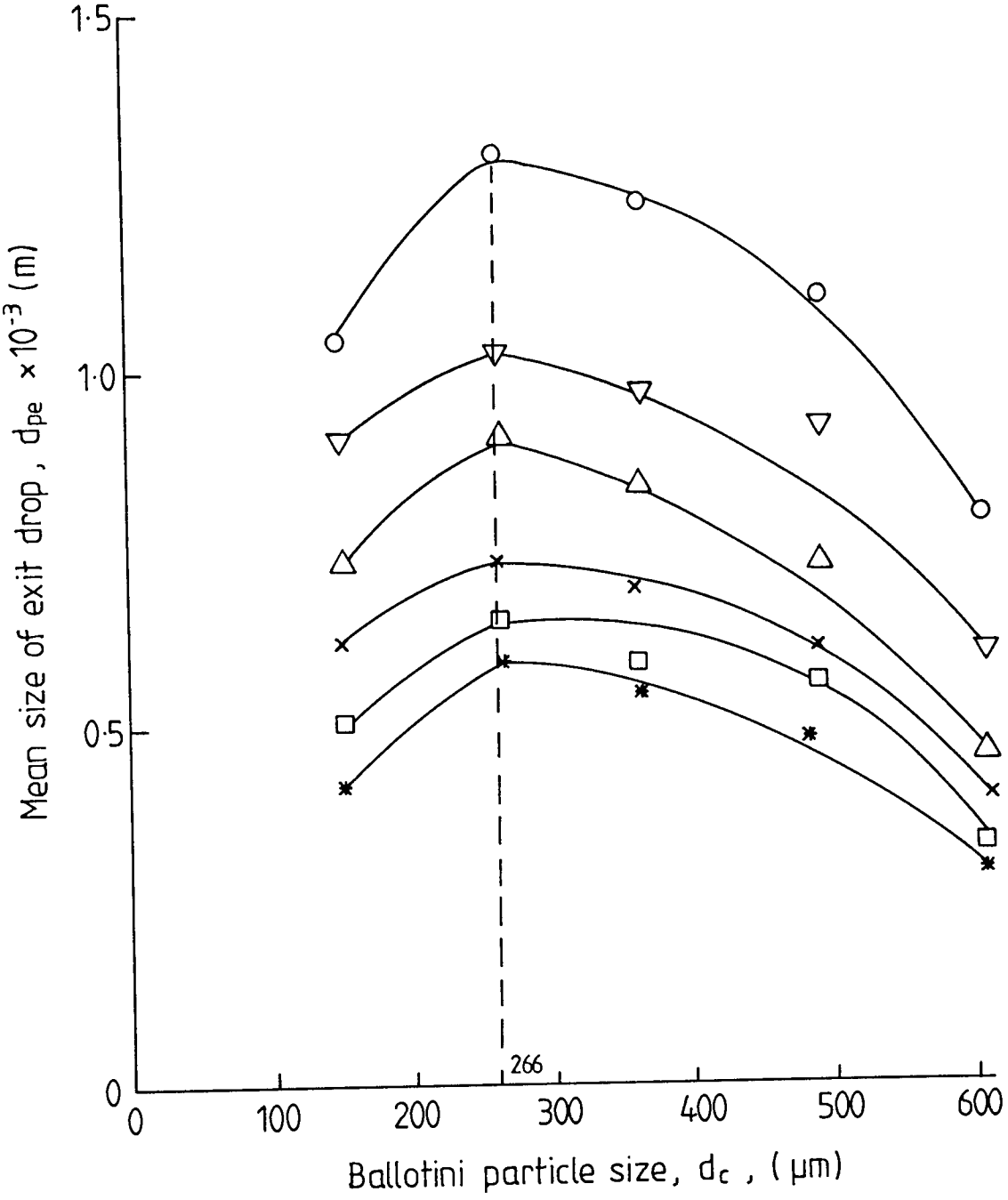

Figure 9·4 Mean size of exit drop vs. ballotini particle size for 30 mm bed depth, 2% phase ratio, 27 μm mean inlet drop size; Toluene - water system.

Superficial velocity, u, $\times 10^{-3}$ (m/s)

- ○ 0·8
- ▽ 1·5
- △ 2·5
- × 3·6
- □ 4·75
- ✱ 6·0

break-through which was important.

9.2 Separation Efficiency

The separation efficiency of the coalescer, determined by a material balance over the bed, is presented in Figures 9.5 to 9.10, as a function of factors such as superficial velocity, inlet drop size, phase ratio, ballotini particle size and bed depth.

In Figures 9.5 and 9.6 separation efficiency decreases with increased superficial velocity to almost a constant value. The separation efficiency decreased with a decrease of inlet drop size because greater hydrodynamic forces entrain the smaller drops downstream out of the coalescer with the effluent without capture by the packing element as shown in Figure 9.6.

An increase in dispersed phase ratio resulted in an increase in the separation efficiency, as shown in Figure 9.7.

Either a decrease in the ballotini particle size or an increase in the bed depth led to an increase in the seapration efficiency, until optimum values were reached after which they had no effect or actually resulted in a decrease in the separation efficiency, as presented in Figures 9.8 and 9.9. From these Figures the optimum ballotini particle size was 255 μm and the optimum bed depth was about 30×10^{-3} m.

Also, as Figure 9.10 illustrates, as the ballotini size in the bed was increased, the optimum effective height also increased. Thus at a ballotini size 146 μm the optimum bed depth was approximately 20×10^{-3} m, for ballotini size 266 μm, it was about 30×10^{-3} m, and for 364 μm ballotini particle size it was approximately 40×10^{-3} m.

Finally, for any given experimental condition, there was a maximum limit to the separation efficiency which remained almost constant regardless of the operating time.

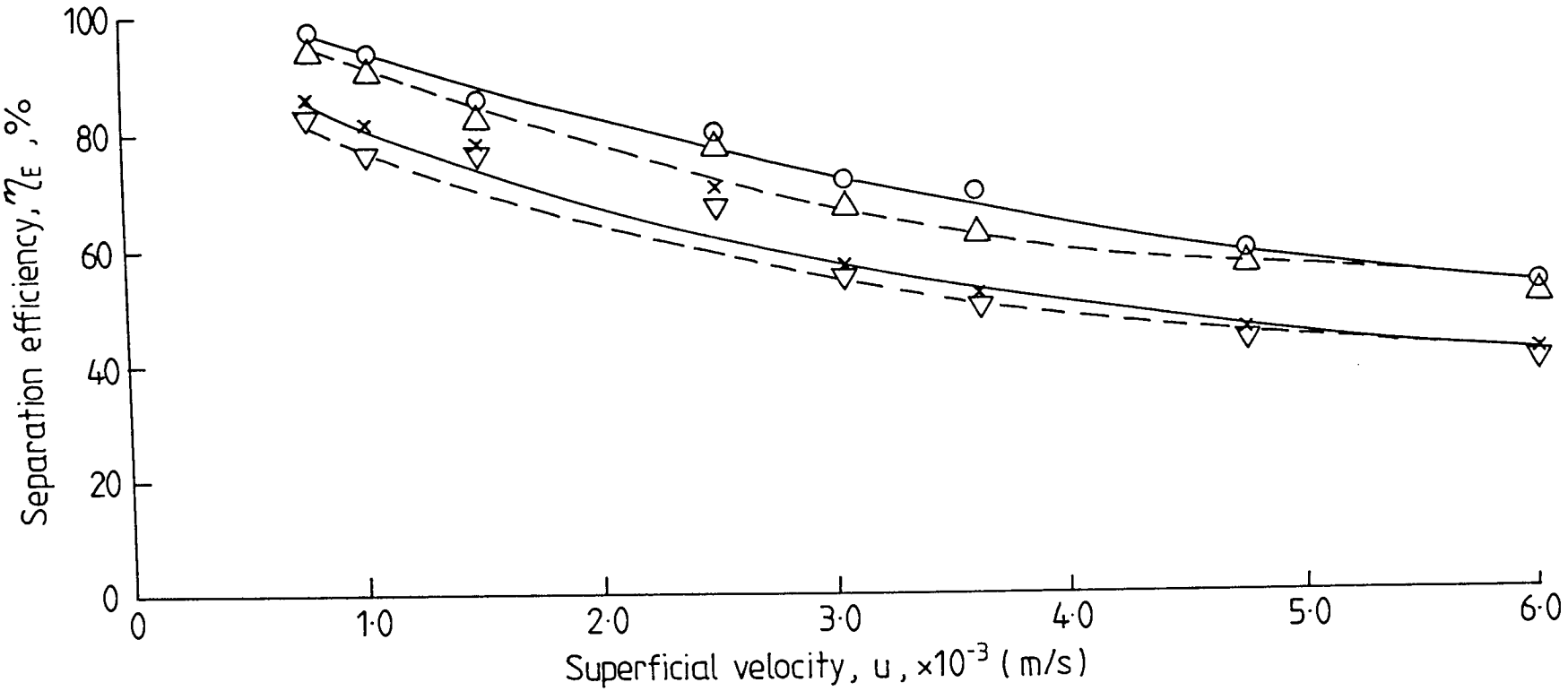

Figure 9·5 Variation of separation efficiency with superficial velocity for 30mm bed depth, 2% phase ratio; 27 μm mean inlet drop size.

KEY.
——— toluene-water system
○ 266 μm ballotini size
× 487 μm ballotini size
– – – – – Clairsol-water system
△ 266 μm ballotini size
▽ 487 μm ballotini size

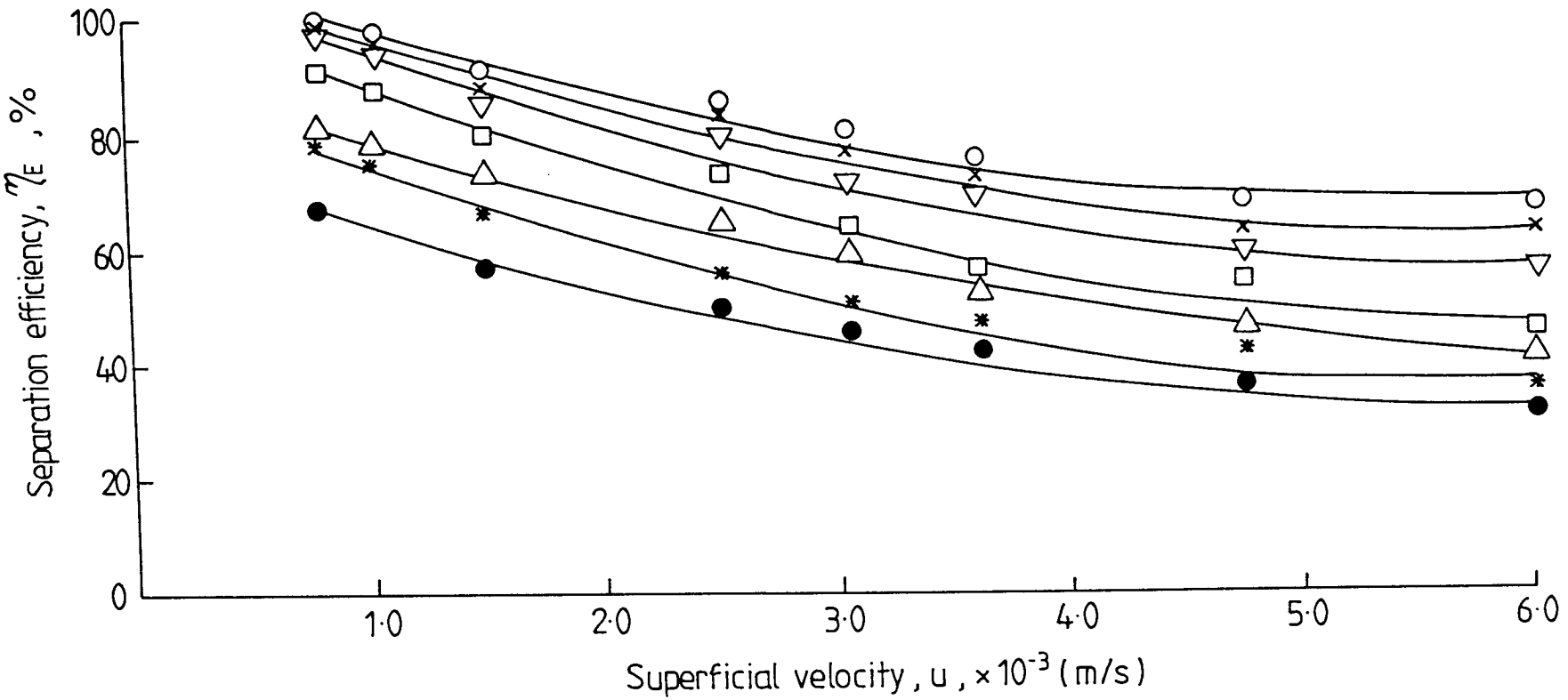

Figure 9·6 Variation of separation efficiency with superficial velocity for 30mm bed depth, 266 μm ballotini size, 2% v/v phase ratio ; toluene - water system

Inlet drop size, d_c , μm

○ 47 , △ 17
× 42 , ✱ 13
▽ 27 , ● 10
□ 22

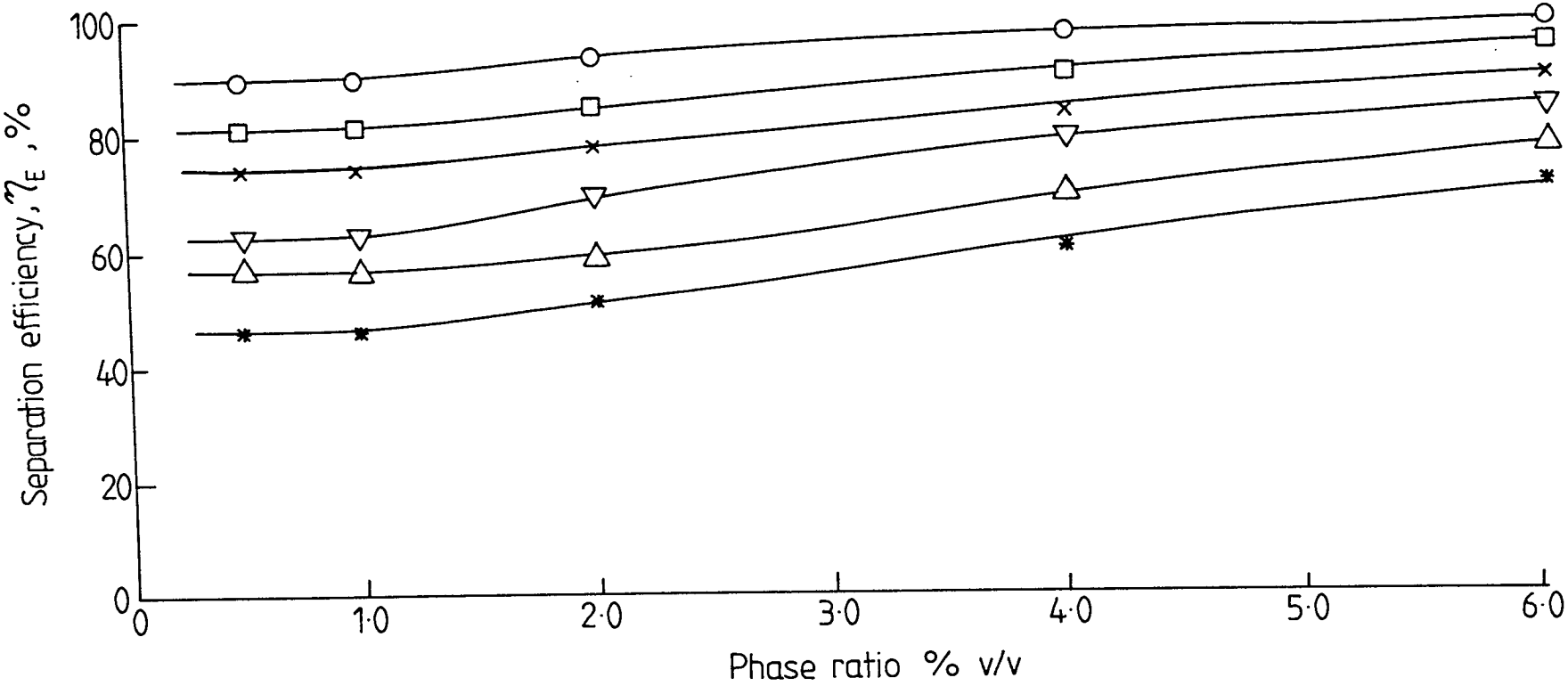

Figure 9·7 Variation of separation efficiency with phase ratio for 266 µm ballotini particle size, 30 mm bed depth, 27 µm mean inlet drop size; toluene - water system.

Superficial velocity, u, $\times 10^{-3}$ (m/s)

- ○ 1·03, ▽ 3·60
- □ 2·50, △ 4·75
- × 3·05, ✱ 6·00

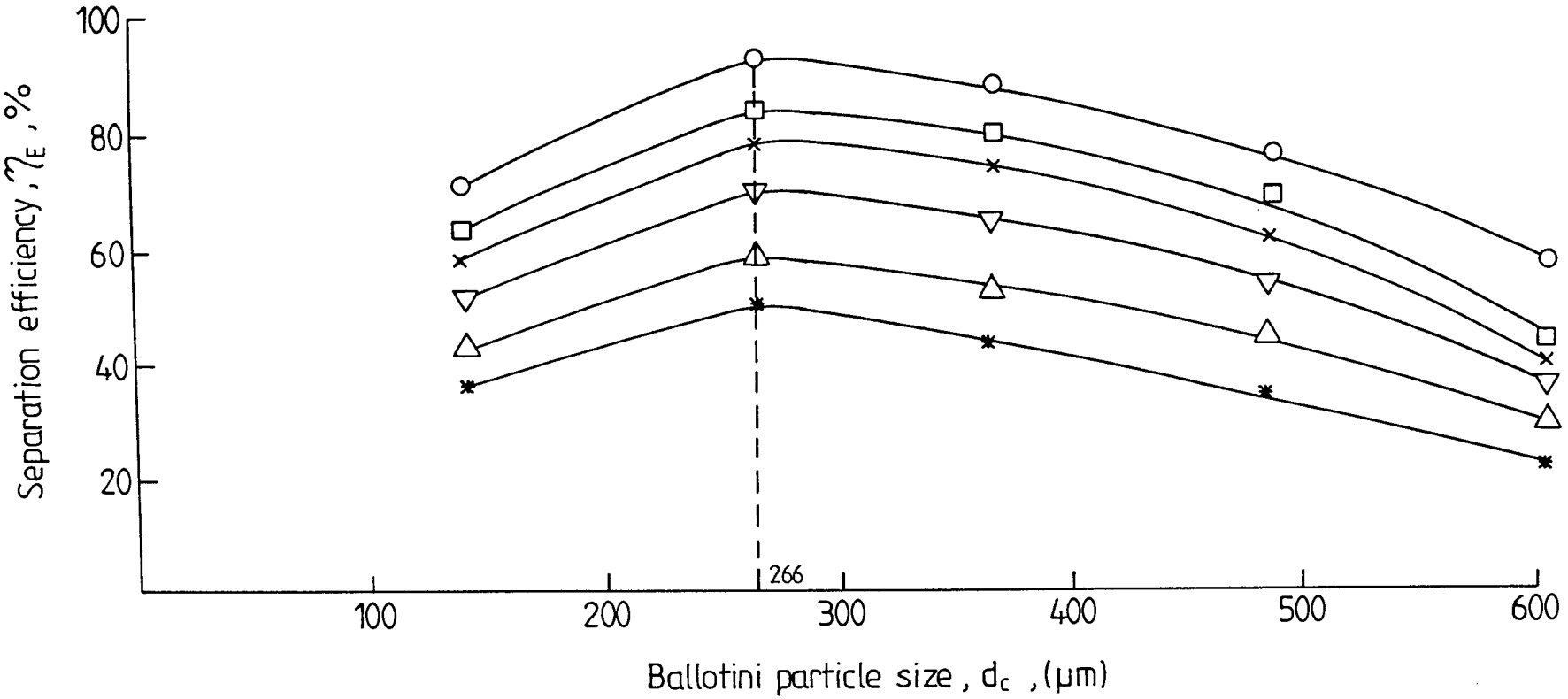

Figure 9·8 Variation of separation efficiency with ballotini particle size for 30 mm bed depth, 2 % phase ratio, 27 μm mean inlet drop size; toluene-water system.

Superficial velocity, u, $\times 10^{-3}$ (m/s)

○ 1·03, ▽ 3·60
□ 2·50, △ 4·75
× 3·05, ✱ 6·00

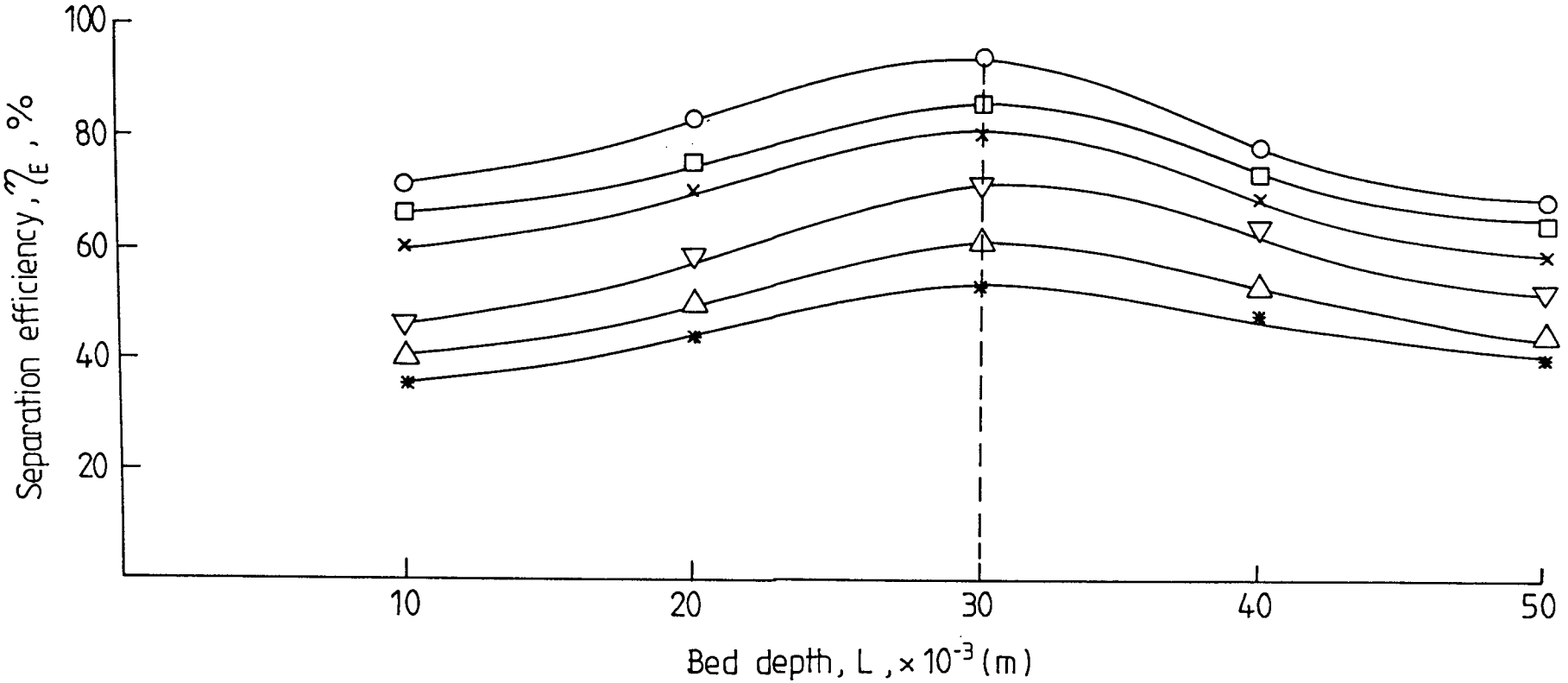

Figure 9·9 Variation of separation efficiency with bed depth for 266 μm ballotini particle size, 2 % phase ratio, 27 μm mean inlet drop size; toluene - water system.

Superficial velocity, u, $\times 10^{-3}$ (m/s)

○ 1·03, ▽ 3·60
□ 2·50, △ 4·75
× 3·05, ✱ 6·00

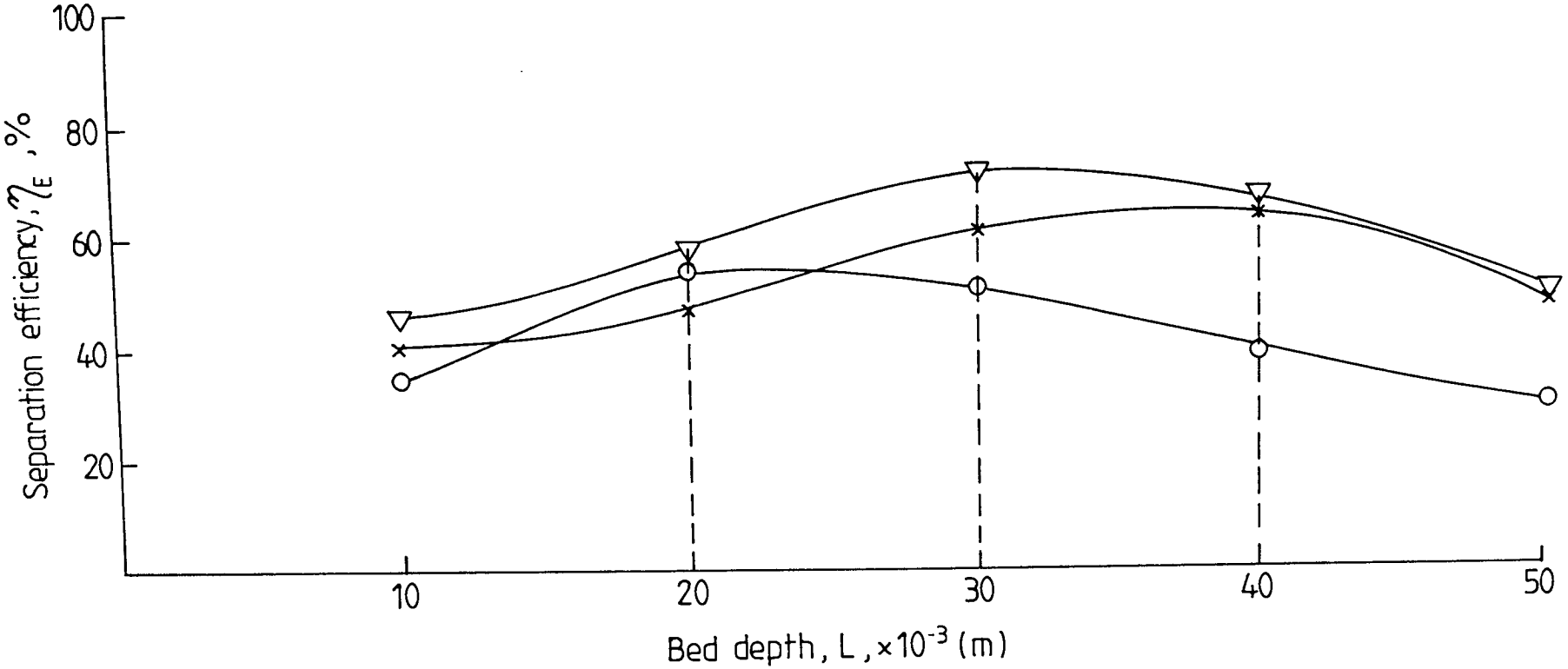

Figure 9·10 Variation of separation efficiency with bed depth for 3·60 m/s superficial velocity, 2% phase ratio, 27 μm mean inlet drop size; toluene - water system.

Ballotini particle size, d_c, μm

▽ 266
× 364
○ 146

9.3 Saturation Determination

The degree of saturation, ie the fraction of pore space of the bed occupied by the dispersed phase influenced both pressure drop and coalescence efficiency. Both have been observed to increase as deposited oil accumulates during the approach to steady-state from an initial oil-free condition (16, 27, 94). Various means have been developed to measure the oil or water-saturation and used for measuring two-phase and three-phase permeabilities or average saturation in porous media. These include electrical resistance, gamma ray adsorption, neutron bombardment, radioactive tracers, x-ray adsorption and nuclear magnetic resonance [215, 216].

The measurement of relative permeability consists, essentially, of the determination of two-phase flow rates under a given pressure drop. The relative permeability data have been correlated with the continuous or dispersed phase saturations [217] as:

$$\frac{B_d}{K_o} = (1 - 1.11\ Sc)^2 = (1.11\ Sd - 0.11)^2 \qquad \text{.... 9.1}$$

$$\frac{B_c}{K_o} = Sc^3 = (1\text{-}Sd)^3 \qquad \text{.... 9.2}$$

The permeability to the water-phase or two-phase flow through a column of porous medium with uniform cross-section may be defined as:

$$Bc = \frac{U_2 \mu_{c2} \Delta L}{\Delta P_2} \qquad \text{.... 9.3}$$

where ΔL is the depth of the porous medium, ΔP_2 is the total pressure drop within the aqueous phase, and U_2 is the superficial velocity of the aqueous phase.

The permeability of the medium to a single (water) phase is defined by Darcy's

Law as:

$$Ko = \frac{U_1 \mu_{c1} \Delta L}{\Delta P_1} \qquad \text{.... 9.4}$$

where ΔP_1 is the total pressure drop. If the superficial velocity U_1 is adjusted to equal the value of U_2, the ratio $\Delta P_1/\Delta P_2$ is equal to Bc/Ko. Therefore, the relative permeability can be calculated from the ratio $\Delta P_1/\Delta P_2$ for each ΔL of the packed bed. It was proposed that division of the single phase and two phase pressure drop by the fluid viscosity provides adequate compensation for temperature changes [16], so,

$$\frac{Bc}{K_o} = \left(\frac{\Delta P_1}{\Delta P_2} \; \frac{\mu_{c2}}{\mu_{c1}}\right) = (1\text{-}Sd)^3 \qquad \text{.... 9.5}$$

The theoretical permeability can be calculated by using the Carman-Kozeny equation as:

$$Ko = \frac{dc^2 \; e_1^3}{180 \; (1\text{-}e_1)^3} \qquad \text{.... 9.6}$$

from which the theoretical value for the permeability of the medium can be calculated. Therefore the Darcy's Law and Carman-Kozeny equations can be used to predict the single phase flow permeability of the system [27].

The method employed by Sherony and Kintner [111] can be applied in which the dispersed phase saturation was then calculated by

$$S_m = 1 - \frac{e_2}{e_1} \qquad \text{.... 9.7}$$

Unfortunately, the result from this equation can only be regarded as approximate since

this method has a number of shortcomings. The integrated average superficial linear velocity "U" for the fluid wetting the walls of particles may be related to the quantity of this fluid flowing per total cross section of the conduit in terms of the dispersed phase saturation Sd as follows [27]:

$$U = \frac{g_c \, d_c \, S_d \, \Delta P_2}{3\,2\,L\,\mu_c} \qquad \ldots. \; 9.8$$

However, the results of this equation can only be regarded as approximations in other cases [196].

In Figures 9.11 to 9.14 examples are presented of the dispersed phase saturation (S_d) obtained by the relative permeability method of calculation (ie equation 9.5).

As shown in Figure 9.11 to 9.13, the average saturation Sd is highest for the highest superficial velocities. This suggests that the coalesced drops are carried more easily and faster by hydrodynamic forces associated with continuous phase flow at high superficial velocity.

Figure 9.12 shows the variation of average oil saturation with bed depth. The highest value of oil saturation was obtained for a coalescer constructed from ballotini of 266 μm particle diameter at a bed depth of 30×10^{-3} m. This confirms that the highest separation efficiency is likely to occur in the system with highest average oil saturation. Also the average oil saturation increases with an increase in bed depth until an optimum value is reached.

Figure 9.13 shows the variation of average saturation with phase ratio; an increase in phase ratio obviously increases the average saturation.

Finally, the average saturation under unsteady state conditions depends upon time. The average saturation increases rapidly with time until the system reaches the steady-state condition, as shown in Figure 9.14. During unsteady state operation, the average saturation profile is predominantly caused by deposition of captured oil droplets.

During the early stages the coalesced oil droplets tend to remain where they are captured until they coalesce with neighbouring, or incoming, drops to form continuous channels for flow. With time the saturation inside the bed reaches the critical value and capillary pressure resists further increase of local oil saturation and forces the coalesced oil droplets to flow towards the exit face of the bed.

9.4 Voidage, Hold-up and Effective Saturation Determination:

9.4.1 Voidage Determination

The single phase (initial) bed voidage e_1 was determined experimentally as described in Section 6.4 and Appendix C.

The calculated values of single phase bed voidage can also be obtained by using the Blake-Kozeny equation (ie equation 7.27). However, particles of different diameters were found, experimentally and theoretically, to have different single phase water voidages, as shown in Table 7.2.

Under two-phase flow conditions a finite amount of the dispersed phase was retained in the bed thus decreasing its initial voidage. The two-phase flow voidages of the coalescer were found using equation 7.32 and are tabulated in Tables 9.1 and 9.2. Generally the voidage increased with an increase of superficial velocity of two-phase flow as shown in Tables 9.1 and 9.2.

9.4.2 Hold-up Determination

Hold up is the volume of liquid held per unit volume of solid,

$$\emptyset_H = \frac{e_1 - e_2}{1 - e_1} \qquad \text{.... 9.9}$$

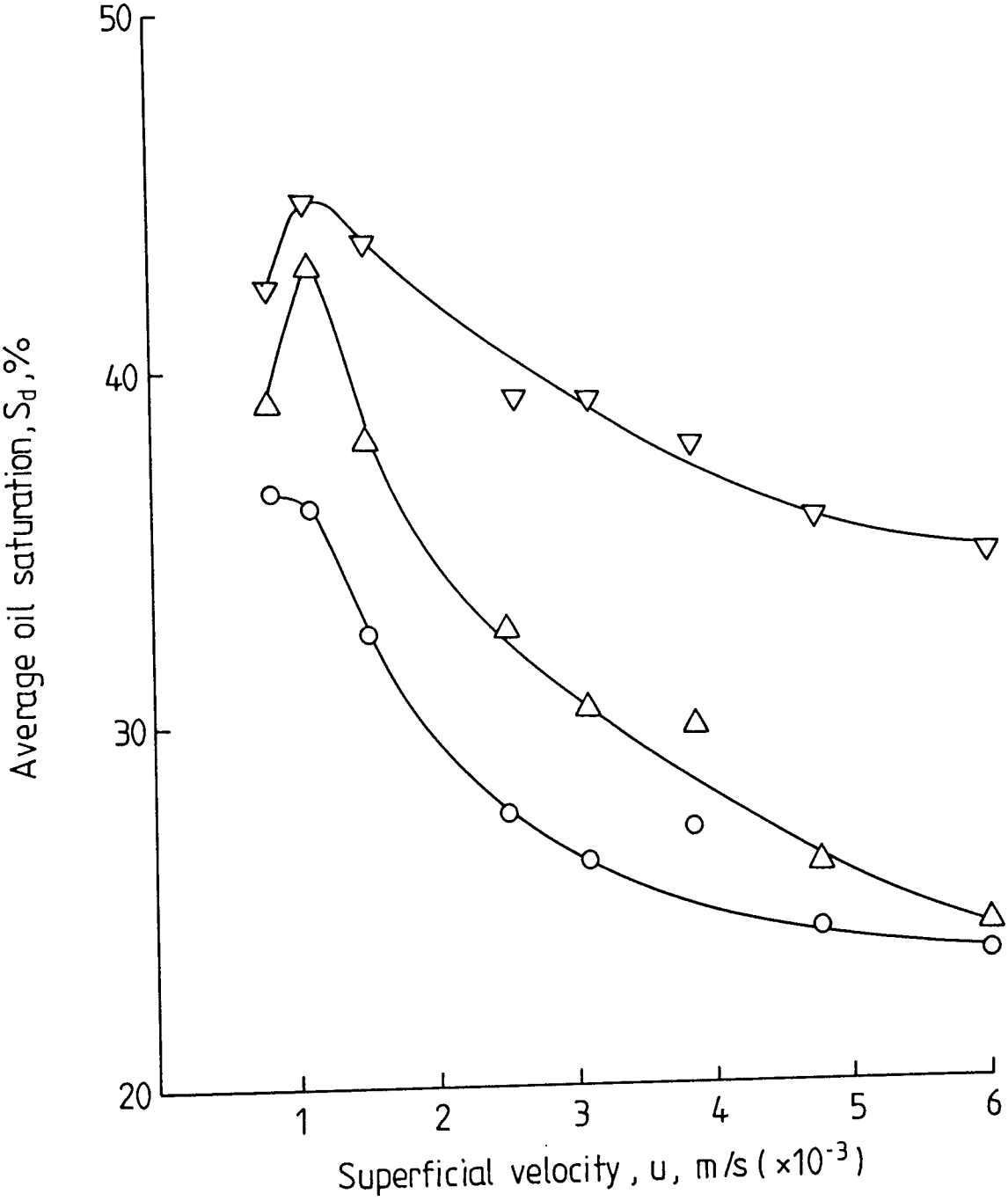

Figure 9·11 Variation of average oil saturation with superficial velocity for 266 μm ballotini particle size, 2% v/v phase ratio and 27 μm mean inlet drop size.

Bed depth, L, mm

- ○ 10
- △ 20
- ▽ 30

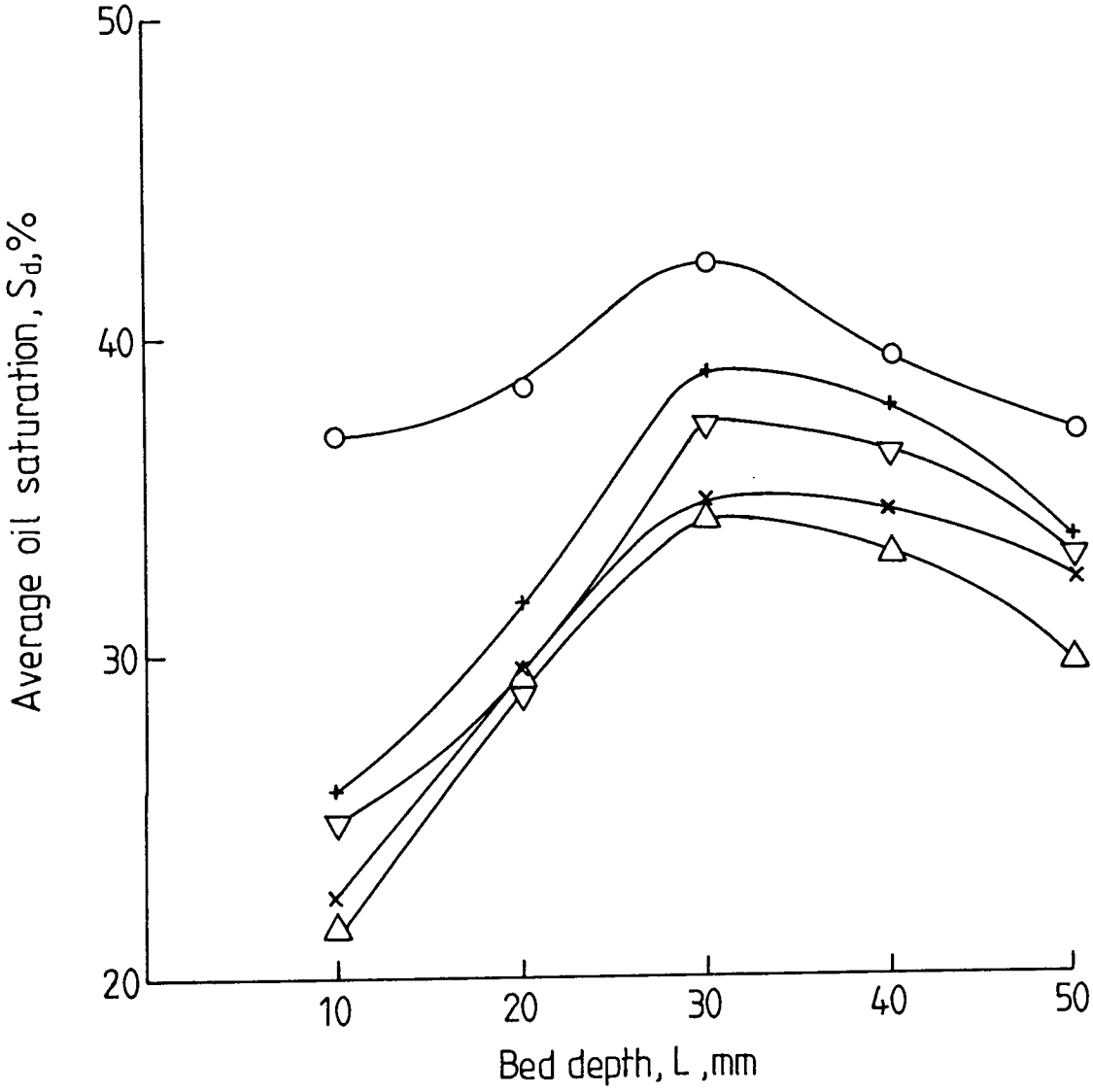

Figure 9·12 Variation of average oil saturation with bed depth for 266 μm ballotini particle size, 42 μm mean inlet drop size and 2% v/v phase ratio.

Superficial velocity, u , m/s ($\times 10^{-3}$)

○	0·8
+	2·5
▽	3·05
×	4·75
△	6·0

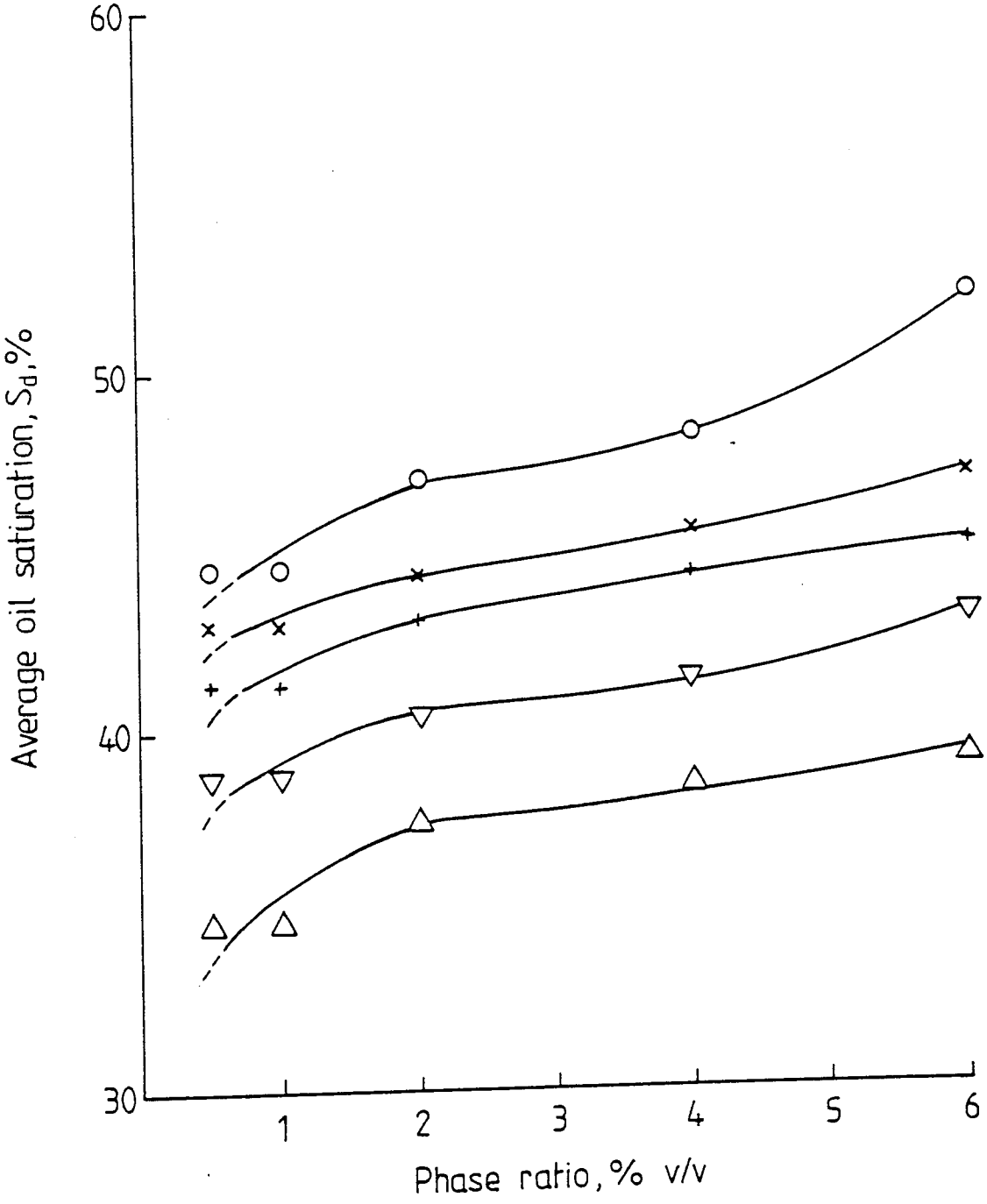

Figure 9·13 Variation of average oil saturation with phase ratio for 266 μm ballotini particle size, 22 μm mean inlet drop size and 30 mm bed depth.

Superficial velocity, u, m/s ($\times 10^{-3}$)

○	1·5
×	0·8
+	2·5
▽	3·6
△	6·0

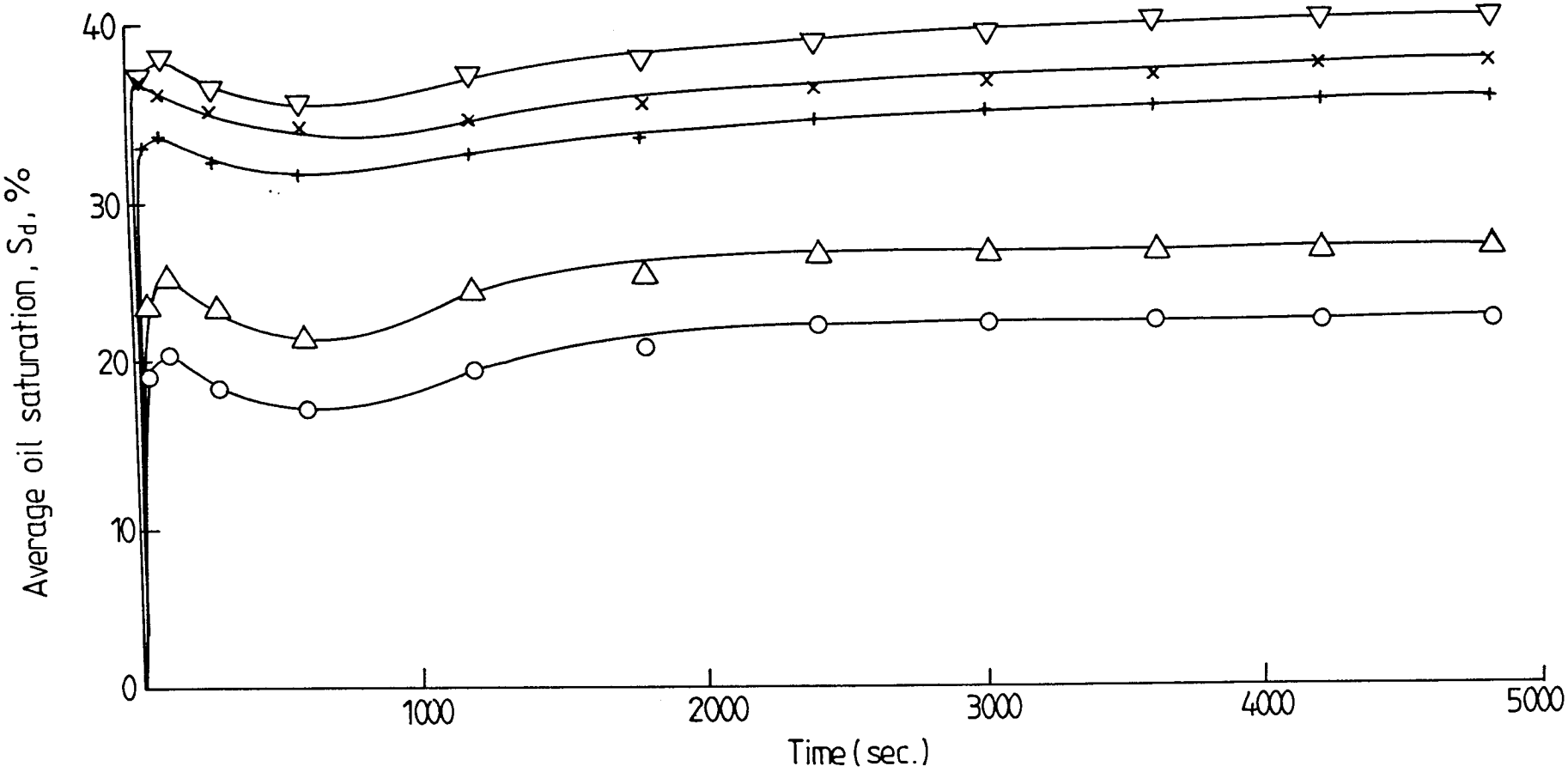

Figure 9·14 Variation of average oil saturation with time at unsteady state conditions for 266 μm ballotini particle size, 2% v/v phase ratio, 3·05 m/s superficial velocity and 27 μm mean inlet drop size.

Bed depths, L, mm

△ 10, ▽ 30, + 50

○ 20, × 40,

Calculated values, presented in Tables 9.1 and 9.2, indicate that bed hold-up varied with superficial velocity. This is in agreement with the work of Sherony and Kintner [111], in which hold-up was concluded to decrease with increase in superficial velocity, contrary to the results of some other workers [16, 17, 57].

9.4.3 Effective Saturation Determination

The degree of saturation, defined as the fraction of pore space of the bed occupied by the dispersed phase, influenced both pressure drop and coalescence performance. The method employed by Sherony and Kintner [111] can be applied for determination of average saturation.

However, the results of this method can only be regarded as approximation in most cases.

Average saturation, S_m, can be defined as:

$$Sm = \frac{\text{Volume of voids filled with wetting fluid}}{\text{Total volume of voids}} = 1 - e_2/e_1 \qquad \ldots. 9.10$$

and the residual saturation, S_r, is defined as the maximum volume of wetting-fluid eliminated from flow per total volume of voids. The residual saturation, Sr, could be calculated from [191],

$$S_r = \frac{1}{86.3} \left[\frac{B\,\Delta P2}{g_c\,\gamma \cos\theta} \right]^{-0.264} \qquad \ldots. 9.11$$

Where B is the permeability and θ is the contact angle measured through the more dense phase. In many cases cos θ is taken as unity [196].

Table 9.1

Effect of Superficial Velocity on Two-Phase Voidage, Saturation and Hold-up Determination for 266μm Ballotini Particle Size, Toluene/Water System

Bed Depth L, mm	e_2 Sm $Ø_H$	Superficial Velocity, U, m/s (x 10^{-3})							
		0.8	1.03	1.5	2.5	3.05	3.6	4.75	6.00
10	e_2	0.215	0.205	0.213	0.239	0.229	0.228	0.236	0.241
	S_m	0.186	0.222	0.195	0.132	0.131	0.137	0.106	0.086
	$Ø_H$	0.067	0.080	0.070	0.047	0.047	0.046	0.038	0.031
20	e_2	0.186	0.175	0.190	0.206	0.210	0.214	0.227	0.233
	S_m	0.394	0.430	0.383	90.329	0.316	0.303	0.261	0.241
	$Ø_H$	0.175	0.190	0.169	0.146	0.140	0.134	0.116	0.107
30	e_2	0.195	0.186	0.190	0.205	0.204	0.209	0.215	0.219
	S_m	0.423	0.450	0.439	0.394	0.396	0.382	0.364	0.352
	$Ø_H$	0.216	0.230	0.224	0.201	0.202	0.195	0.186	0.180
40	e_2	0.196	0.195	0.186	0.194	0.204	0.205	0.209	0.216
	S_m	0.402	0.405	0.433	0.408	0.378	0.376	0.361	0.341
	$Ø_H$	0.196	0.198	0.212	0.199	0.184	0.184	0.176	0.167
50	e_2	0.211	0.196	0.207	0.214	0.219	0.226	0.231	0.238
	S_m	0.384	0.428	0.396	0.375	0.359	0.240	0.324	0.305
	$Ø_H$	0.200	0.222	0.206	0.195	0.185	0.177	0.169	0.159

Table 9.2

Effect of Superficial Velocity on Two-Phase Voidage, Saturation and Hold-up Determination for 266μm Ballotini Particle Size, Clairsol350/Water System

Bed Depth L, mm	e_2 Sm $Ø_H$	Superficial Velocity, U, m/s (x 10^{-3})							
		0.8	1.03	1.5	2.5	3.05	3.6	4.75	6.00
20	e_2	0.183	0.171	0.184	0.197	0.203	0.206	0.213	0.221
	S_m	0.405	0.443	0.400	0.357	0.337	0.329	0.307	0.280
	$Ø_H$	0.179	0.196	0.177	0.158	0.149	0.146	0.136	0.124
30	e_2	0.188	0.181	0.183	0.196	0.198	0.202	0.209	0.216
	S_m	0.443	0.464	0.459	0.421	0.415	0.402	0.381	0.360
	$Ø_H$	0.226	0.237	0.235	0.215	0.212	0.205	0.195	0.184
40	e_2	0.194	0.183	0.181	0.189	0.195	0.201	0.207	0.213
	S_m	0.409	0.442	0.450	0.422	0.403	0.387	0.368	0.351
	$Ø_H$	0.199	0.216	0.219	0.206	0.197	0.189	0.180	0.171

The fixed saturation eliminated from flow S_f, is defined as the ratio of the volume of wetting fluid held stationary by capillary forces to the total volume of voids. The fixed saturation can be calculated from :

$$S_f = \frac{(1\text{-}Sm)\, S_r}{(1\text{-}S_r)} \qquad \text{.... 9.12}$$

The effective saturation is S_e, defined as the ratio of voids containing wetting fluid active in flow to voids containing both fluids in flow. The effective saturation could be calculated from [191],

$$S_e = \frac{Sm - S_f}{Sm - S_f + 1 - Sm} = \frac{Sm - S_r}{1\text{-}2S_r + Sm\, S_r} \qquad \text{.... 9.13}$$

Calculated values of the effective saturation, S_e, are presented in Tables 9.3 and 9.4.

The equivalent voidage or two-phase flow voidage (e_2) can also be calculated by

$$e_2 = \frac{(1\text{-}Sm)\, e_1}{1\text{-}S_r} \qquad \text{.... 9.14}$$

9.5 Dimensional Analysis of Two-Phase Pressure Drop Data

In this work, dimensional analysis was used to derive a flow equation of two-phase pressure drop experimental data in which the two-phase pressure drop (ΔP_2) across a packed bed was described as a function of a number of dimensionless groups raised to a power by using Rayleigh's method [218] as described in Appendix I. The equation is:

Table 9.3

Effect of Superficial Velocity on Effective Two-Phase Voidage, Saturation and Hold-up Determination for 266μm Ballotini Particle Size, Toluene/Water System

Bed Depth L, mm	e_2 S_e $\emptyset_H$	Superficial Velocity, U, m/s (x 10^{-3})							
		0.8	1.03	1.5	2.5	3.05	3.6	4.75	6.00
10	e_2	0.109	0.109	0.117	0.131	0.134	0.135	0.143	0.148
	S_e	0.419	0.429	0.409	0.368	0.362	0.361	0.339	0.324
	$\emptyset_H$	0.211	0.210	0.200	0.181	0.177	0.175	0.65	0.157
20	e_2	0.113	0.111	0.122	0.136	0.140	0.145	0.154	0.161
	S_e	0.510	0.528	0.494	0.453	0.442	0.431	0.402	0.386
	$\emptyset_H$	0.279	0.282	0.267	0.247	0.240	0.234	0.220	0.211
30	e_2	0.126	0.124	0.130	0.144	0.146	0.150	0.156	0.161
	S_e	0.521	0.535	0.523	0.487	0.485	0.474	0.458	0.446
	$\emptyset_H$	0.321	0.232	0.314	0.294	0.291	0.284	0.274	0.267
40	e_2	0.128	0.131	0.130	0.140	0.148	0.150	0.155	0.162
	S_e	0.504	0.503	0.516	0.492	0.469	0.466	0.452	0.435
	$\emptyset_H$	0.297	0.293	0.294	0.280	0.268	0.265	0.257	0.247
50	e_2	0.140	0.135	0l.145	0.155	0.160	0.166	0.172	0.179
	S_e	0.490	0.514	0.488	0.467	0.453	0.439	0.424	0.407
	$\emptyset_H$	0.308	0.315	0.299	0.285	0.276	0.268	0.258	0.248

Table 9.4

Effect of Superficial Velocity on Effective Two-Phase Voidage, Saturation and Hold-up for 266μm Ballotini Particle Size, Clairsol350/Water System

Bed Depth L, mm	e_2 / S_e / $\emptyset_H$	Superficial Velocity, U, m/s (x 10^{-3})							
		0.8	1.03	1.5	2.5	3.05	3.6	4.75	6.00
20	e_2	0.109	0.106	0.116	0.128	0.134	0.137	0.144	0.151
	S_e	0.521	0.540	0.508	0.475	0.460	0.452	0.434	0.414
	$\emptyset_H$	0.286	0.289	0.275	0.258	0.250	0.246	0.236	0.225
30	e_2	0.19	0.119	0.123	0.136	0.1349	0.143	0.150	0.156
	S_e	0.538	0.548	0.540	0.508	0.502	0.491	0.474	0.456
	$\emptyset_H$	0.331	0.332	0.324	0.306	0.301	0.295	0.284	0.274
40	e_2	0.124	0.122	0.124	0.134	0.140	0.145	0.151	0.157
	S_e	0.513	0.530	0.530	0.506	0.490	0.477	0.461	0.446
	$\emptyset_H$	0.304	0.307	0.303	0.288	0.280	0.273	0.263	0.255

$$\frac{\Delta P_2}{\rho_c U^2} = k_D \left[\frac{dc}{D}\right]^a \left[\frac{L}{D}\right]^b \left[\frac{dp}{D}\right]^c \left[\frac{U\rho_c D}{\mu c}\right]^{-f} \left[e_2\right]^g \left[C_{in}\right]^h \quad \text{.... 9.16}$$

By taking logarithms of each dimensionless group, constant k_D and the exponents a, b, c, f, g and h were determined by multiple linear regression analysis of the data.

This analysis, using a computer program (see Appendix T) yielded,

$$\frac{\Delta P_2}{\rho_c U^2} = 8.64 \times 10^7 \left[\frac{dc}{D}\right]^{-0.27} \left[\frac{L}{D}\right]^{0.71} \left[\frac{dp}{D}\right]^{-0.17} \left[\frac{U\rho_c D}{\mu_c}\right]^{1.5} \left[e_1\right]^{-0.14} \left[C_{in}\right]^{0.26} \quad \text{.... 9.17}$$

Comparison between experimental and predicted data showed an average difference of 25%.

CHAPTER TEN

APPLICATION OF MODELS AND MECHANISMS OF DISPERSION COALESENCE

10.1 Prediction of Filter Coefficient

The majority of models for fibrous bed coalescers attempt to predict the filter coefficient . The equations developed were reviewed in Section 4.2. A comparison is possible between λc for particulate beds of the type used in this study and the fibrous beds used by Austin [16]. The parameters, used in the prediction of filter coefficient, are presented in Table 10.1

(a) *Vinson and Churchill's equation*

For a ballotini bed depth of 30 x 10^{-3} m used to coalesce a toluene/water dispersion at 3.05 x 10^{-3} ms^{-1}, equation 4.30 predicts λc = 210.568 m^{-1}. This equation is not based on any theoretical model but was simply obtained by fitting experimental data for the system studied using fibrous screens to simulate fibrous beds.

(b) *Sherony and Kintner's equation*

This equation was based on the 'travelling drop' model discussed in Section 4.2 and drop capture was assumed to occur by interception and inertial impaction.

From the correlation given by Sherony and Kintner [111], using the data of Table 10.1, ηc = 0.0263 also for a mean saturation of 0.394, equation 4.35 gives λc = 35.156 m^{-1}.

(c) *Rosenfeld and Wasan's equation*

This equation also advocated the 'travelling drop' hypothesis but, unlike Sherony's model, did not assume that when a drop detaches from a fibre, it is replaced by an identical one and that detachment occurs after a single coalescence event. Rosenfeld and Wasan [141] introduced an effective collector diameter, d_{ce}, to account for retained drops and introduced a factor, β, to relate the collision frequency to

Table 10.1

Basic Set of Parameters Used in Comparison of Filter Coefficients

Parameter	Symbol	Value
Ballotini Particle size	d_c	266 (μm)
Bed Depth	L	30 (mm)
Mean inlet Drop Size	d_p	27 (μm)
Phase ratio	C_{in}	2% (v/v)
Dispersed Phase Density	ρ_d	860.0 (kg/m^3)
Continuous Phase Density	ρ_c	1000.0 (kg/m^3)
Dispersed Phase Viscosity	μ_d	0.58 c 10^{-3} (NS/m^2)
Continuous Phase Viscosity	μ_c	1.0 x 10^{-3} (NS/m^2)
Average Saturation	Sm	0.394 (-)
Boltzman's Velocity	K'	3.05 x 10^{-3} (J/K_o)
Superficial Velocity	U	3.05 x 10^{-3} (m/s)
Absolute Temperature	T	2-3 (K^o)
Capture Efficiency	η_c	0.0263 (-)
Hamaker Constant*	Q	0.401 x 10^{-20} (J)
Single Phase Voidage	e_1	0.338 (-)
Hydrodynamic Function (Function of bed voidage)	A_s	57.088 (-)

* See Appendix E

coalescence efficiency. A typical value of β was determined by Sherony and Kintner [111] to be 0.41 which produces a filter coefficient, $\lambda c = 785.785\ m^{-1}$ by using equations 4.38 and 4.39.

(d) *Spielman and Goren's equation*

Spielman and Goren [85, 94, 150, 166] assumed that the immiscible liquids flowed within fixed microscopic channels with the none-wetting liquid flowing inside; each channel being described by Darcy's Law. They suggested that London-van der Waal's forces are of sufficient magnitude to overcome any hydrodynamic retardation effects. Their equation 4.43 predicts $\lambda c = 1.292\ m^{-1}$ for similar conditions to those described in (a), and for a mean inlet drop diameter, dp = 27 μm. This equation is of limited use in coalecer design since it was not based on the model but was obtained by correlation of experimental data. Therefore, to cover different systems a considerable amount of data is required to determine values for the constant and exponent.

(e) *Austin's equation*

Values of queue length (Lq) calculated using equation 4.52 and hence $Log_e\gamma$ were evaluated from the abscissa of Figure B-9 in Appendix B. The filter coefficient was then calculated using equation 4.51 for steady-state conditions. For a ballotini bed depth of 30×10^{-3} m used to coalesce a toluene/water system at $3.05 \times 10^{-3}\ ms^{-1}$, equation 4.50 predicted $\lambda c = 5037.629\ m^{-1}$.

Calculated values of filter coefficient using the above five equations were found to vary over five orders of magnitude for the same operating conditions, as shown in Table 10.2, whilst this indicates short comings in the models, it is not surprising in view of possible interactions between packing and operating parameters in the extremely complex coalescence process. The filter coefficient depends on the saturation and capture mechanisms in the bed. Estimation of capture mechanisms by theoretical or experimental methods is dealt with in the following sections.

Table 10.2

Comparison Between This Work's Results and Previous Results for Filter Coefficients (λc)

Model Equation	Austin λc [16]	Ibrahim λc [104]	Baez-Poleo λc [27]	This Work λc
Vinson and Churchill	19 m^{-1}	285.0 m^{-1}	19.19 m^{-1}	210.563 m^{-1}
Spielman and Goren	195 m^{-1}	10.5 m^{-1}	0.266 m^{-1}	1.292 m^{-1}
Sherony and Kintner	672 m^{-1}	280.0 m^{-1}	154.37 m^{-1}	35.156 m^{-1}
Rosenfeld and Wasan	8486 m^{-1}	1264.0 m^{-1}	147.65 m^{-1}	785.785 m^{-1}
Austin	9310 m^{-1}	3550.0 m^{-1}	—	5037.629 m^{-1}

10.2 Theoretical Comparison of Capture Mechanisms

Many mechanisms were proposed in section 4.1 for drop capture. It is desirable to determine their relative contributions to the overall capture efficiency under practical operating conditions in order to produce an equation for estimation of the rate of drop capture in a coalescer.

The variables investigated in this experimental study included drop size, superficial velocity and particle size which affect theoretical capture efficiency. Drop capture efficiencies due to interception, London Van der Waal's forces, diffusion and sedimentation were determined employing a basic set of parameters, relevant to the experimental work presented in Table 10.1. The equations for evaluation of the individual mechanisms were discussed in Section 4.1 and are summarised in Table 10.3. The calculations were performed for a range of values of drop diameter and superficial velocity using a computer program listed with the output in Appendix W.

Direct interception was not included in the analysis since the efficiencies can not be compared directly and this mechanism only becomes significant when the drop size exceeds the effective aperture diameter. Inertial impaction and sedimentation were also excluded since the drop density was less than the continuous phase density. Therefore, the overall efficiency is,

$$\eta_T = \eta_I + \eta_D + \eta_L \qquad \ldots. \ 10.1$$

and the calculated values of η_T are presented in Table 10.4. The domain associated with each mechanism is also expressed quantitatively in Table 10.5, where its significance is recorded if its contribution is greater than 1% of the total efficiency.

Figure 10.1 shows that the overall efficiency, decreases gradually to an almost constant value over the range studied. Figures 10.2 and 10.3 indicate that London-van der Waal and indirect interception are the most important mechanisms in the velocity range studied. Table 10.5 also shows a minimum efficiency, since diffusion becomes significant for small drops, ie less than 10 μm. The significance of London Van der

Table 10.3

Dimensionless Groups and Equations Used in Capture Mechanisms Evaluation

Mechanism	Characteristic Dimensionless Group	Equation for Capture Efficiency
Indirect Interception	Interception No., N_R	$\eta_I = 1.5\ N_R 2$
Direct Interception	Direct Interception No., N_{Rd}	$\eta_{DI} = 1.0\ (N_{Rd} \geq 1.0)$; $\eta_{DI} = 0 (N_R \leq 1.0)$
Inertial Impaction	Stoke's Number, N_{stk}	$\eta_{II} = \dfrac{N_{stk}^3}{N_{stk}^3 + 0.77\ N_{stk}^3 + 0.22}$
Sedimentation	Gravity Number, N_G	$\eta_G = N_G = \dfrac{d_p^2\ (\rho_d - \rho_c)\ g}{18\ \mu_c\ U\ A_s}$
London-van der Waal's Forces	Adhesion Number, N_{Ad}	$\eta_L = 2A_s\ N_R^2 \left[1.8\ .\ N_{Ad}\right]^{0.333}$
Diffusion	Peclet Number, N_{Pe}	$\eta_D = 4.04\ N_{Pe}^{-2/3}$

Table 10.4

Total Capture Efficiency for the Range of Velocities and Mean Inlet Drop Sizes Encountered in Secondary Dispersion Coalescence for 30 mm Bed Depth and266 μm Ballotini Particle Size

Mean Inlet Drop size d_{21} d(μm)	Superficial Velocity, U, m/s (x 10^{-3})							
	0.8	1.03	1.5	2.5	3.05	3.6	4.75	6.00
47	0.074	0.069	0.066	0.063	0.062	0.061	0.060	0.059
42	0.060	0.058	0.055	0.053	0.052	0.051	0.050	0.049
27	0.032	0.031	0.029	0.027	0.026	0.025	0.024	0.024
22	0.025	0.023	0.022	0.020	0.129	0.019	0.018	0.017
17	0.018	0.017	0.016	0.014	0.014	0.013	0.013	0.012
13	0.014	0.013	0.012	0.010	0.010	0.009	0.009	0.008
10	0.011	0.010	0.009	0.008	0.007	0.007	0.007	0.006
8	0.009	0.008	0.007	0.006	0.006	0.006	0.005	0.005

Table 10.5

Significance of Different Capture Mechanisms at 1% Contribution Level for Range of Velocities and Mean Inlet Drop sizes Encountered in Secondary Dispersion Coalescence for 30 mm Bed Depth and 266 μm Ballotini Particle Size

Mean Inlet Drop size	Superficial Velocity, U, m/s (x 10^{-3})							
	0.8	1.03	1.5	2.5	3.05	3.6	4.75	6.00
47	IL	IL	IL	IL	IL	IL	IL	IL
42	IL	IL	IL	IL	IL	IL	IL	IL
27	IL	IL	IL	IL	IL	IL	IL	IL
22	IL	IL	IL	IL	IL	IL	IL	IL
17	IL	IL	IL	IL	IL	IL	IL	IL
13	IL	IL	IL	IL	IL	IL	IL	IL
10	ILD	ILD	IL	IL	IL	IL	IL	IL
8	ILD	ILD	ILD	ILD	ILD	IL	IL	IL

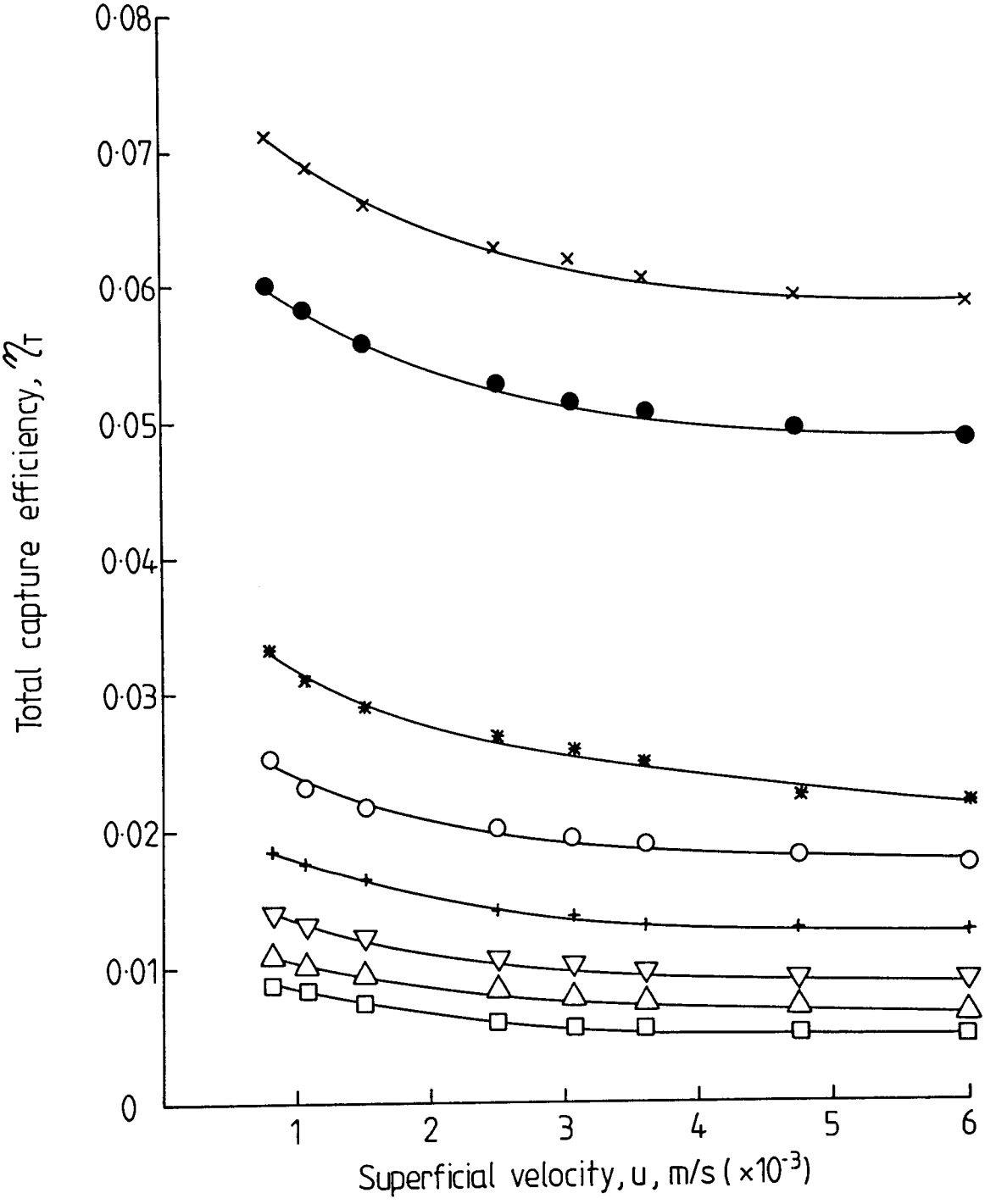

Figure 10·1 Variation of total capture efficiency with superficial velocity at 266 μm ballotini particle size and 30 mm bed depth for different mean inlet drop sizes.

Mean inlet drop sizes, d_{21}, μm

×	47,	+	17
●	42,	▽	13
✱	27,	△	10
○	22,	□	8

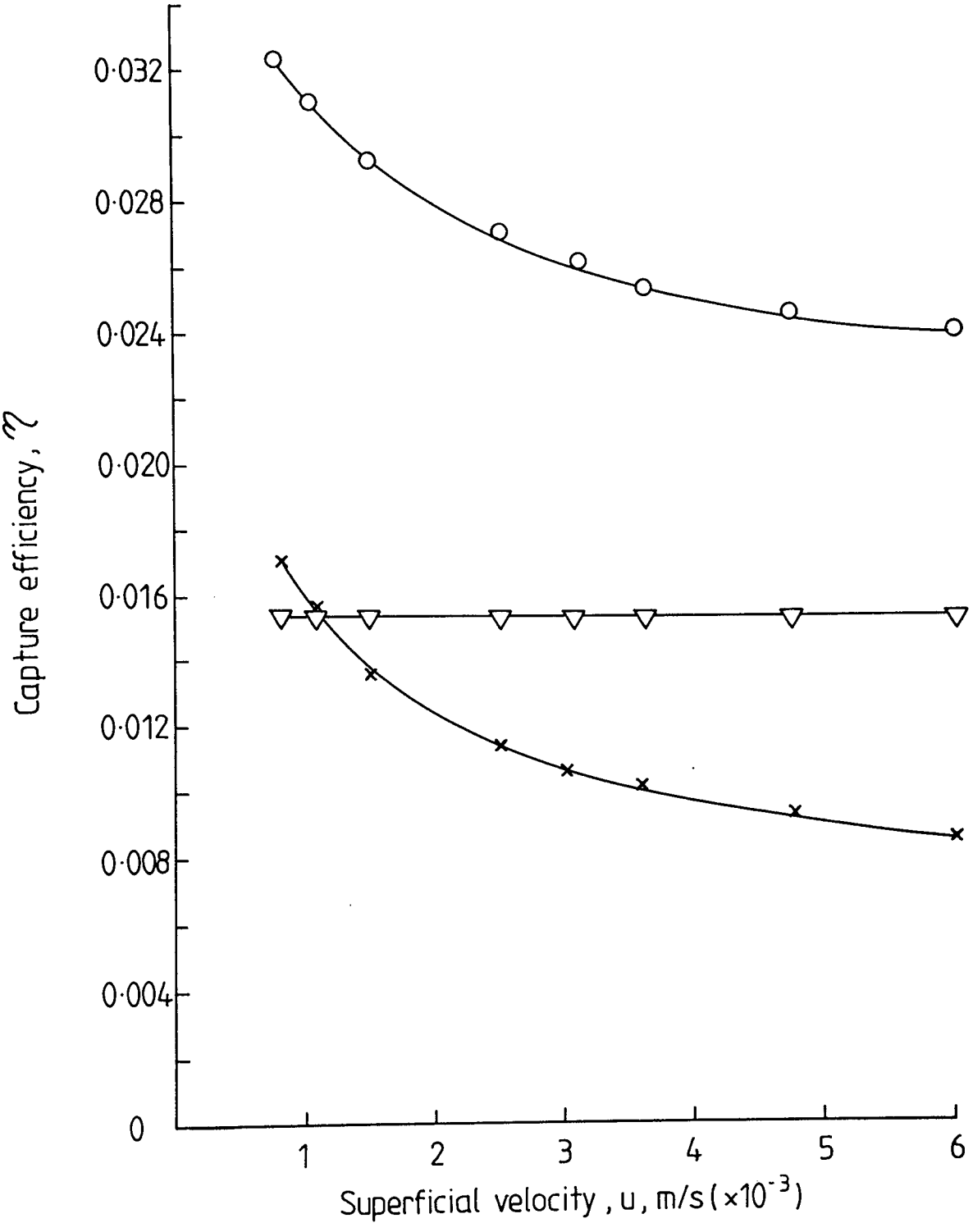

Figure 10·2 Variation of capture efficiency with superficial velocity at 27 μm mean inlet drop size, 266 μm ballotini particle size and 30mm bed depth.

× η_I = Indirect interception capture efficiency

▽ η_L = London - Van der Waal capture efficiency

○ η_T = Total capture efficiency

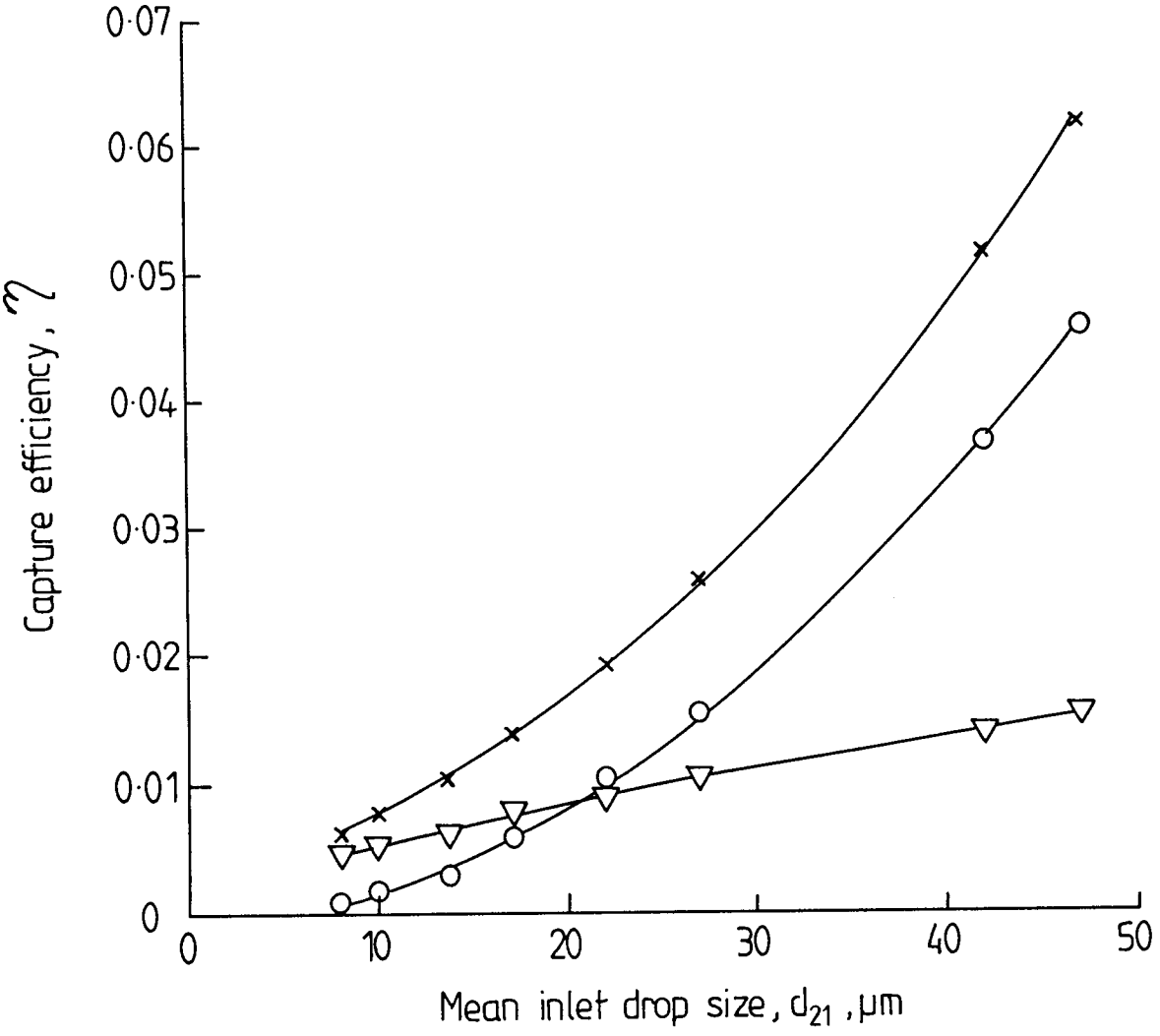

Figure 10·3 Variation of capture efficiency with mean inlet drop size at $3{\cdot}05 \times 10^{-3}$ m/s superficial velocity, 266 μm ballotini particle size and 30 mm bed depth.

o η_I = Indirect interception capture efficiency

▽ η_L = London - Van der Waal capture efficiency

× η_T = Total capture efficiency

Waal's mechanism increases as the inlet drop size increases, and its contribution to drop capture increases as the particle size is decreased, as shown in Figures 10.4 and 10.5.

Different formulae have been proposed, when more than one capture mechanism is important in predicting the total capture efficiency. For the case of interception and gravity settling, Prieve and Ruckenstein [154] suggested that the combined effects of sedimentation and interception may be represented by,

$$\eta_{GI} = \eta_G + \eta_I \qquad \text{.... 10.2}$$

Emi [219] derived analytically the equation

$$\eta_{GI} = \frac{1+N_R}{1+N_G}\left[\frac{1}{2A}\left[\frac{1}{(1+N_R)^2} - 1 + \log_e (1+N_R)^2 + N_G\right] + N_G\right] \qquad \text{.... 10.3}$$

where the hydrodynamic function $A = 2\text{-}\log_e N_{Re}$ [219]. Equation 10.3 has been proposed to account for the sedimentation and interception mechanisms where the direction of flow and gravity forces coincide.

Pich [156] investigated the variation of capture efficiency by gravity forces with angular position of a particle relative to a collector and suggested an alternative form:

$$\eta_{GI} = \eta_I + \eta_G + N_R N_G \qquad \text{.... 10.4}$$

The combination of interception and sedimentation as implied in equations 10.2, 10.3 and 10.4 will not be considered because sedimentation is predicted to only be a significant mechanism for large drop diameters (ie more than 250 μm) and low velocities (ie laminar flow).

Friedlander [157] proposed the removal efficiency formula,

$$\eta_{ID}\, N_R\ N_{Pe} = f\,(A_s^{0.333}\, N_R\, N_{Pe}^{0.333}) \qquad \ldots. 10.5$$

from a study of the case of simultaneous interception and diffusion for both cylindrical and spherical collectors using dimensional analysis. Equation 10.5 is for particles or droplets of finite diameter but much smaller than the diameter of the collecting sphere.

Spielman and Goren [149] have also shown that the collection efficiency by interception and diffusion is of the form:

$$\eta_{ID}\, N_R\, N_{Pe} = f\,(N_{Ad},\, A_s\, U\, a_p^3/D_{BM} r_c^2) \qquad \ldots. 10.6$$

if retardation is neglected. After substitution of $D_{BM} = K'T/6\pi\mu_c r_p$. Then:

$$\frac{A_s U r_p^3}{\Delta_{BM}\, r_c^2} = \frac{6\pi\mu_c U A_s r_p^4}{K'T\, r_c^2} = \frac{2}{3}\ \frac{Q}{K'T}\ \frac{1}{N_{Ad}} \qquad \ldots. 10.7$$

and

$$A_s\, N_R^3\, N_{Pe} = A_s\, \frac{r_p^2}{r_c^3}\left(\frac{2 r_c U}{D_{BM}}\right) = \frac{4}{3}\ \frac{Q}{K'T}\ \frac{1}{N_{Ad}} \qquad \ldots. 10.8$$

Equations 10.5 and 10.7 give the expression:

$$\eta_{ID}\, N_R\ N_{Pc} = f\,(N_{Ad},\, K'T/Q) \qquad \ldots. 10.9$$

The group (K'T/Q) is very nearly constant in most experimental studies, so that the group ($\eta_{ID}\, N_R\, N_{Pc}$) should depend on N_{Ad} along even when diffusion is significant.

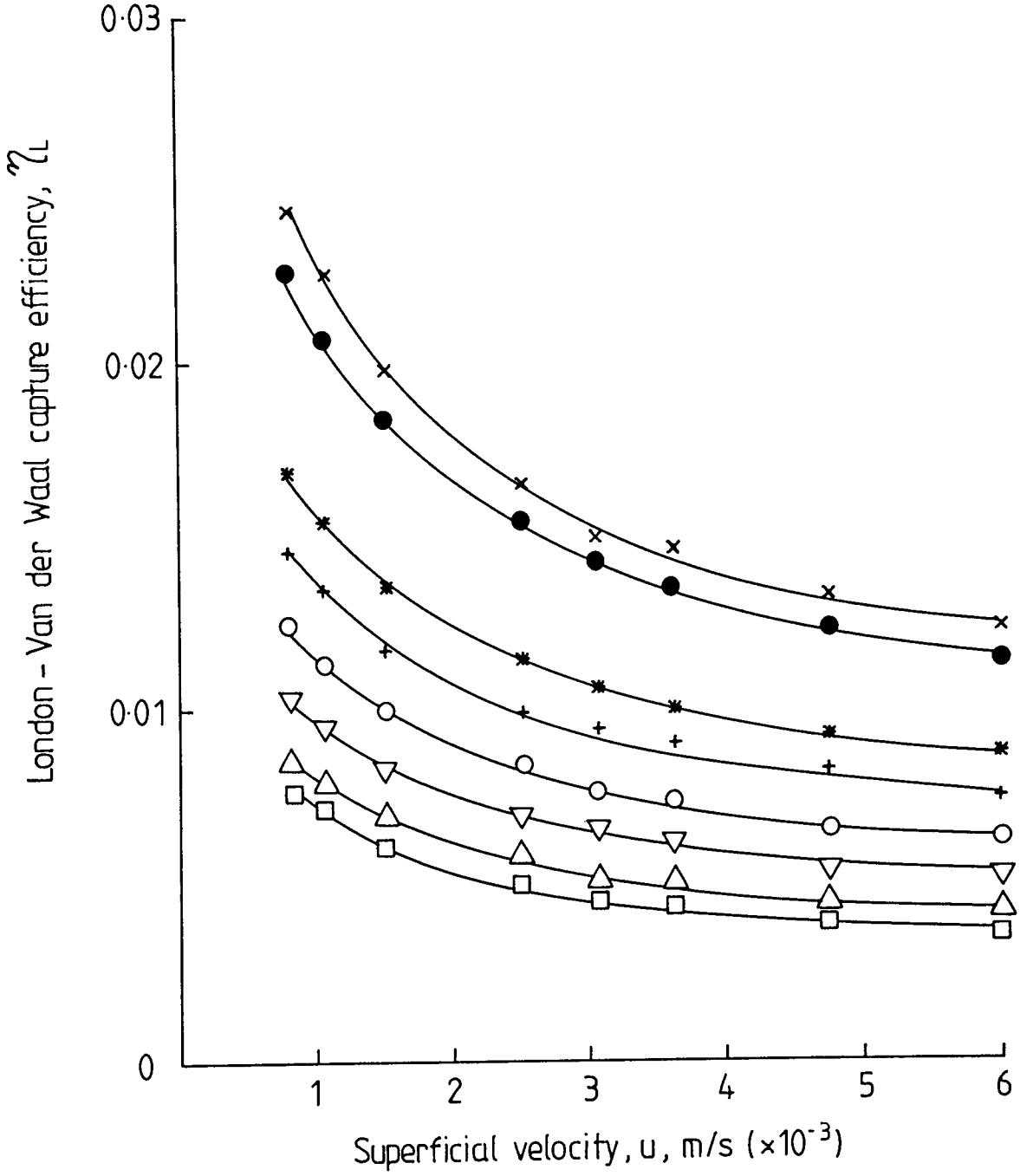

Figure 10·4 Variation of London-Van der Waal capture efficiency with superficial velocity at 266 μm ballotini particle size and 30 mm bed depth for different mean inlet drop sizes.

Mean inlet drop sizes, d_{21}, μm

×	47,	○	17
●	42,	▽	13
✱	27,	△	10
+	22,	□	8

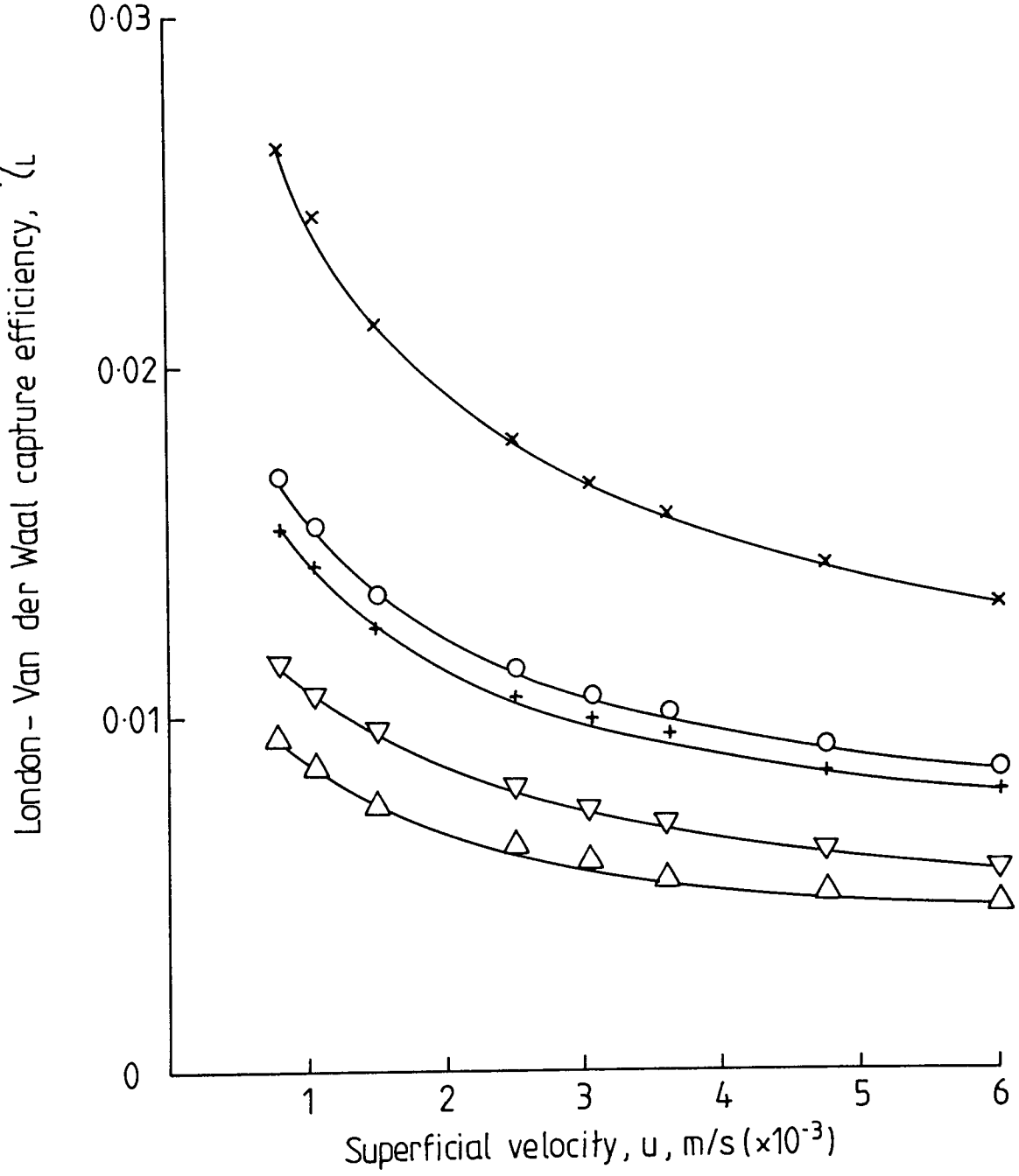

Figure 10·5 Variation of London- Van der Waal capture efficiency with superficial velocity at 27 μm mean inlet drop size and 30 mm bed depth for different ballotini particle sizes.

Ballotini particle sizes, d_c, μm

× 146
○ 266
\+ 364
▽ 487
△ 615

The dimensionless collection efficiency is then

$$\frac{\eta_{ID}}{\eta_I} = \frac{\eta_I}{\eta_I} + \frac{\eta_D}{\eta_I} + 1 + 2.223\ A_s^{0.667}\ (K'T/Q)^{0.667}\ (N_{Ad})^{0.667}$$

$$= 1 + 2.223\ [A_s \cdot N_{Ad} \cdot (K'T/Q)]^{0.667} \qquad \text{.... 10.10}$$

Equation 10.10 is a useful method for correlating experimental data by plotting. If the collection efficiency by London attraction and diffusion can be approximated by the sum of their respective efficiencies, then

$$\frac{\eta_{LD}}{1.5N_R^2} = \frac{\eta_L}{1.5N_R^2} + \frac{\eta_D}{1.5N_R^2} \qquad \text{.... 10.11}$$

or

$$\frac{\eta_{LD}}{\eta_I} = 1.622\ A_s\ (N_{Ad})^{0.333} + 2.223\ [A_s \cdot N_{Ad} \cdot (K'T/Q)]^{0.667} \qquad \text{.... 10.12}$$

Similarly, the theoretical collection efficiency for interception, London forces and diffusion is approximated by their sum as:

$$\frac{\eta_{ILD}}{1.5\ N_R^2} = \frac{\eta_I}{1.5\ N_R^2} + \frac{\eta_L}{1.5\ N_R^2} + \frac{\eta_D}{1.5\ N_R^2} \qquad \text{.... 10.13}$$

therefore,

$$\frac{\eta_{ILD}}{\eta_I} = 1 + 1.622\ A_s\ (N_{Ad})^{0.333} + 2.223[A_s \cdot N_{Ad} \cdot (K'T/Q)]^{0.667}$$

.... 10.14

When (K'T/Q) = 0, the capture efficiency is due to indirect interception and London forces alone, or pure direct interception if the London forces are not being considered.

Table 10.6

Total Capture Efficiency for Different Superficial Velocities for 266 μm Ballotini Particle Size, 27.0 μm Mean Inlet Drop Size and 30 mm Bed Depth

Superficial Velocity U, m/s ($x10^{-3}$)	Experimental η_T/η_I	Theoretical * η_{ILD}/η_I	Difference %
0.8	2.10	2.09	0.57
1.03	2.01	1.98	1.2
1.5	1.88	1.86	1.5
2.5	1.75	1.73	0.96
3.05	1.70	1.68	0.94
3.6	1.66	1.62	2.5
4.75	1.60	1.54	3.8
6.00	1.55	1.54	0.96

* Obtained from Equation 10.14

Table 10.7

Total Capture Efficiency for Different Mean Inlet Drop Sizes for 266μm Ballotini Particle Size, 30 mm Bed Depth and 3.05×10^{-3} m/s Superficial Velocity

Mean Inlet Drop Size (d_2) μm	Experimental η_T/η_I	Theoretical * η_{ILD}/η_I	Difference %
47	1.33	1.33	0.00
42	1.39	1.38	0.14
27	1.70	1.68	0.94
22	1.92	1.89	1.25
17	2.30	2.29	0.30
13	2.87	2.86	0.27
10	3.67	3.65	0.62
8	4.56	4.59	-0.56

* obtained from equation 10.14

In this work, the different values for equation 10.14 are presented in Table 10.6 and 10.7, for the Hamaker constant Q calculated in Appendix E. The results obtained for the total efficiency, η_T, using equation 10.1 show close agreement with the results obtained using equation 10.14, as shown in Tables 10.6 and 10.7.

Tables 10.6 and 10.7 also show that the difference in values between the two methods is <3%. Therefore, the drop capture efficiency can be predicted from either method.

10.3 Rate of Drop Capture

For any capture mechanism, the relationship between the dimensionless filter coefficient and dimensionless efficiency is obtained by equating the difference in droplet concentration entering and leaving the bed. The filter coefficient λ is defined as:

$$-\frac{dn}{dl} = \lambda n \qquad \text{.... 10.15}$$

For a bed of uniform, spherical particles perpendicular to the flow , a suspended droplet balance over a differential depth of bed dl gives for the differential change dn in suspended droplet number concentration [27]:

$$-\frac{dn}{dl} = \frac{j}{U}\left(\frac{\alpha_1}{4/3\,\pi\, r_c^3}\right) \qquad \text{.... 10.16}$$

where α_1 is the volume fraction of solid and j is the average rate of droplet capture per spherical collector.

The dimensionless spherical particle collection efficiency is defined as [27]

$$\eta = \frac{j}{\pi\, r_c^2\, U\, n} \qquad \text{.... 10.17}$$

The relationship between λ and η may then be obtained by substituting equation

10.16 and 10.17 into 10.15 as:

$$\lambda = \frac{3}{4}\frac{\alpha_1}{r_c}\eta \qquad \text{.... 10.18}$$

Integration of equation 10.15 over a depth of bed 0 to L gives [27]:

$$\lambda = \frac{-\log_e (n_1/n_o)}{L} \qquad \text{.... 10.19}$$

where n_o and n_1 are the inlet and outlet drop density numbers entering and leaving a depth of bed L. Substituting and rearranging for n_1 in equation 10.18 gives:

$$n_1 = n_o . \text{Exp}\left[-\frac{3}{4}\frac{\alpha_1}{r_c}\eta L\right] \qquad \text{.... 10.20}$$

In this study, the inlet drop size distribution was fitted to a distribution function by polynomial regression (see Section 8.7) and the resulting expression used to calculate the number of drops in each drop diameter interval (2 μm). The total capture efficiency, η_T, for a given superficial velocity was calculated by application of equations 10.1 or 10.14, as explained in Section 10.2, to each size interval.

For a given bed depth, l_1, between 0 - L the number of drops, n, leaving the bed interval was obtained from equation 10.20. Assuming no drop redispersion this was used as the input of suspended drops to the next interval of bed depth l_2 and a new value of n_1 was obtained.

This calculation procedure was repeated, for a bed consisting of 30 x 10^{-3} m bed depth using the computer program given in Appendix X. Figure 10.6, was plotted from the program output, and shows the removal rate of drops as a function of bed depth.

This shows that increasing the superficial velocity decreases the rate of drop capture to a minimum after which, any further increase in velocity no longer results in a decrease in drop capture. The shape of this profile exhibits a marked resemblance to the experimental data of Section 6.5 under steady-state conditions (Figure 10.7).

The theoretical results were determined for operation of the coalescer after a period of 1 second from an intially dispersed phase free condition. Due to rapid accumulation of the dispersed phase, this analysis cannot be applied to a coalescer which has been operating even for a few seconds because:

i) the presence of drops affects the flow of continuous phase over the collectors;

ii) held drops effectively reduce the aperture diameter so that capture by direct interception, which does not feature in equation 10.1 or 10.14, increases rapidly as the local saturation increases.

However, this theoretical approach is useful because the drop capture rate depends on local saturation and therefore the drop capture saturation and hence the drop capture efficiency would not be expected to change significantly.

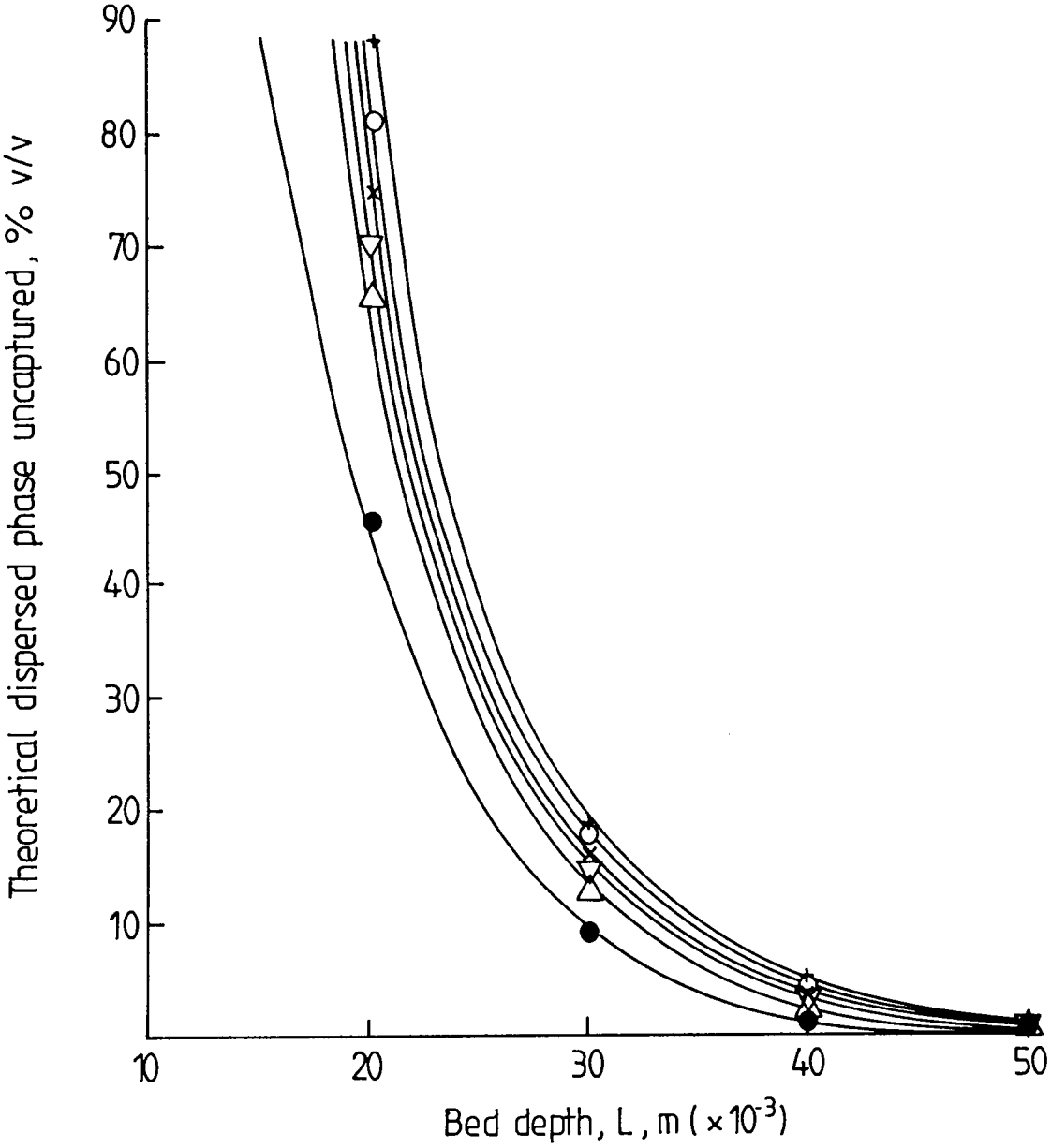

Figure 10·6 Variation of theoretical volume fraction of dispersed phase uncaptured with bed depth at 266 μm ballotini particle size and 2% v/v phase ratio for different superficial velocities.

Superficial velocities, u, m/s (×10⁻³)

●	1·03,	×	3·6
△	2·5,	○	4·75
▽	3·05,	+	6·0

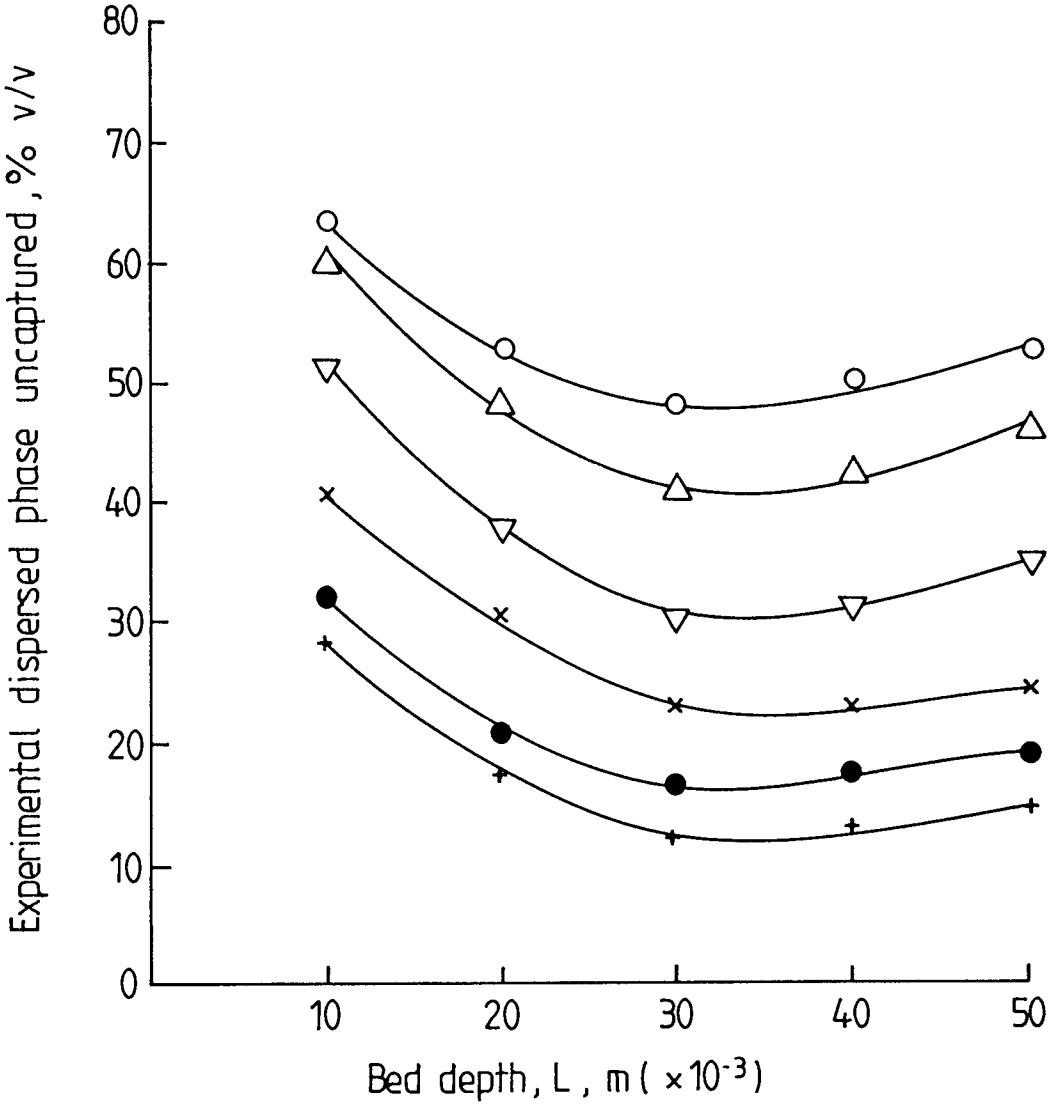

Figure 10·7 Variation of experimental volume fraction of dispersed phase uncaptured with bed depth at 266 μm ballotini particle size and 2% phase ratio for different superficial velocities.

Superficial velocities, u, m/s ($\times 10^{-3}$)

+	1·03
●	2·5
×	3·05
▽	3·6
△	4·75
○	6·0

CHAPTER ELEVEN

NEW PROPOSALS FOR THEORETICAL MODELS FOR DISPERSION CONCENTRATION, QUEUEING AND FILTER COEFFICIENT

11.1 The Concentration of Dispersion in Flow in Packed Beds

When a fluid flows through a packed bed, dispersion of fluid occurs as a result of the combined effects of molecular diffusion and mixing in the voids. Thus, in using a packed bed as a coalescer, allowance must be made for the fact that the flow deviates somewhat from plug flow. In general, the dispersion coefficient in the longitudinal direction is greater than in the radial direction. New proposals for theoretical models for dispersion concentration in the packed bed were derived as follows:

11.1.1 Assumptions

The following assumptions are proposed to derive the models of dispersion concentration in the packed bed.

a) The flow within the bed is plug-flow with constant flow velocity "U"

b) Drops of secondary dispersions behave like molecules because these drops are very small; so the material diffusion in these dispersions is similar to that in molecular diffusion with, of course, different coefficients.

c) The new coefficient has been called the secondary dispersion coefficient (E). There are two types of this coefficient as follows:

i Secondary dispersion coefficient in a longitudinal direction termed the Axial Secondary Dispersion Coefficient (Ea)

ii Secondary dispersion coefficient in a Radial direction termed the Radial Secondary Dispersion Coefficient (Er).

d) The combined effects of micro-drop diffusion (ie molecular diffusion) and mixing in the flow spaces occurs when a secondary dispersion fluid flows through a

packed bed.

e) No leaks or evaporation in the system.

f) No heat transfer occurs and the temperature is constant.

g) Density and viscosity are constant.

h) Voidage in the bed equals e which is constant for specific packed bed.

i) A cylindrical element has been considered inside the bed because the packed bed coalescer usually has a cylindrical shape.

The element dimensions are:

δl = height

r = inner radius

$r + \delta r$ = outer radius

c = concentration of dispersed liquid (vol. of dispersed/total vol. of flow)

l = axial position

t = time

R = radius of packed bed

L = thickness of packed bed

11.1.2 Fick's Laws

Fick's first law of diffusion (ie rate of mass transfer through unit cross section area) [220] is

$$F = - A_C D_F (dc/dx) \quad \text{.... 11.1}$$

where F is the rate of mass transfer, A_C is cross section area, c is concentration and x is space co-ordinate.

Fick's second law of diffusion (ie diffusion inside the element) [220] is:

$$\frac{dF}{dx}\delta x = -A_C \frac{d^2c}{dx^2}\delta x \cdot D_F \qquad \text{.... 11.2}$$

and,

$$\frac{dc}{dt} = -\frac{dF}{dx} = A_C D_F \frac{d^2c}{dx^2} \qquad \text{.... 11.3}$$

11.1.3 Material Balance

Under unsteady state conditions the material balance due to diffusion from boundaries in axial diffusion (as illustrated in Figure 11.1) are represented by the following equations:

$$\text{Input rate of mass transfer} = -(2\pi r\, \delta re)\, Ea\, (dc/dl) \qquad \text{.... 11.4}$$

$$\text{Output rate of mass transfer} = -(2\pi r\, \delta re)\, Ea \left(\frac{dc}{dl} + \frac{d^2c}{dl^2}\delta l\right) \qquad \text{.... 11.5}$$

Accumulation rate due to diffusion from boundaries in a radial direction

$$= -(2\pi r\, \delta le)\, Er\, (dc/dr) \qquad \text{.... 11.6}$$

$$\text{Output rate of mass transfer} = -[2\pi (r + \delta r)\, \delta le]\, Er \left(\frac{dc}{dr} + \frac{d^2c}{dr^2}\delta r\right) \qquad \text{.... 11.7}$$

$$\text{Accumulation rate due to flow in an axial direction} = -U (2\pi r\, \delta r) \frac{dc}{dl}\delta l \qquad \text{.... 11.8}$$

$$\text{Total accumulation rate} = (2\pi r\, \delta r\, \delta l)\, e \frac{dc}{dt} \qquad \text{.... 11.9}$$

Total accumulation = Input - Output

Then,

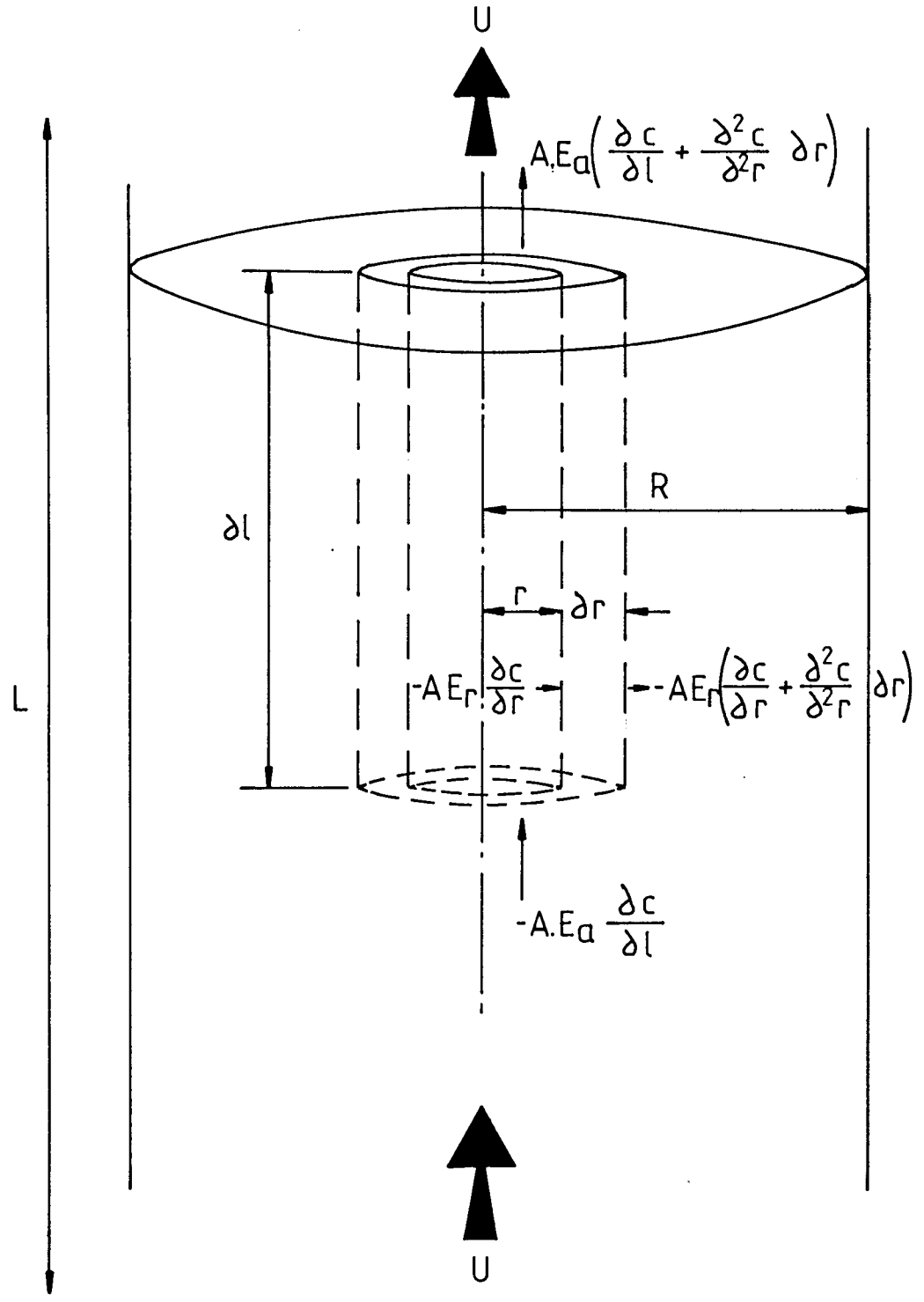

Figure 11.1 The cylindrical element inside the packed bed coalescer

$$(2\pi r\,\delta r\,\delta l)\,e\frac{dc}{dt} = -U(2\pi r\,\delta r)\frac{dc}{dl}\delta l - [2\pi r\,\delta le]\,Er\frac{dc}{dr} - (2\pi r\,\delta re)\,Ea\frac{dc}{dl} - \Big[$$

$$-2\pi(r+\delta r)\,\delta le \cdot Er\left[\frac{dc}{dr} + \frac{d^2C}{dr^2}\delta r\right] - (2\pi r\,\delta re)\,Ea\left[\frac{dc}{dl} + \frac{d^2c}{dl^2}\delta l\right]\Big]$$

.... 11.10

$$2\pi r\,\delta r\,\delta le\frac{dc}{dt} = -U(2\pi r\,\delta r)\frac{dc}{dl}\delta l$$

$$- (2\pi r\,\delta le)\,Er\frac{dc}{dr} - (2\pi r\,\delta re)\,Ea\frac{dc}{dl}$$

$$+ (2\pi r\,\delta le)\,Er\frac{dc}{dr} + (2\pi\delta r\,\delta le)\,Er\frac{dc}{dr}$$

$$+ (2\pi r\,\delta le)\,Er\frac{d^2c}{dr^2}\delta r + (2\pi\,\delta le)\,Er\frac{d^2c}{dr^2}\delta r^2$$

$$+ (2\pi r\,\delta re)\,Ea\frac{dc}{dl} + (2\pi r\,\delta re)\,Ea\frac{d^2c}{dl^2}\delta l$$

.... 11.11

The value of the term $(2\pi\delta le\,Er\frac{d^2c}{dr^2}\delta r^2)$ is very small and hence it can be ignored.

Therefore equation 11.11 becomes

$$2\pi r\,\delta r\,\delta le\frac{dc}{dt} = -e\frac{1}{e}U(2\pi r\,\delta r)\frac{dc}{dl}\delta l + \frac{1}{r}(2\pi r\,\delta r\,\delta le)\,Er\frac{dc}{dr} + (2\pi r\,\delta le)$$

$$Er\frac{d^2c}{dr^2}\delta r + (2\pi r\,\delta re)\,Ea\frac{d^2c}{dl^2}\delta l$$

.... 11.12

then,

$$\frac{dc}{dt} = -\frac{U}{e}\frac{dc}{dl} + \frac{Er}{r}\frac{dc}{dr} + Er\frac{d^2c}{dr^2} + Ea\frac{d^2c}{dl^2} \qquad \text{.... 11.13}$$

or

$$\frac{dc}{dt} = -\frac{U}{e}\frac{dc}{dl} + Er\,\frac{1}{r}\left[\frac{dc}{dr} + r\frac{d^2c}{dr^2}\right] + Ea\frac{d^2c}{dl^2} \qquad \text{.... 11.14}$$

Finally, equation (11.14) becomes in the general form,

$$\frac{dc}{dt} = \frac{Ea}{e}\frac{d^2c}{dl^2} - \frac{U}{e}\frac{dc}{dl} + \frac{Er}{r}\frac{d}{dr}\left(r\frac{dc}{dr}\right) \qquad \text{.... 11.15}$$

11.1.4 Solution of Axial Secondary Dispersion Diffusion Equations for Unsteady-State and Steady State Conditions

Equation 11.15 is the general equation for secondary dispersion diffusion inside the packed bed.

a) For the case of unsteady state and high velocity (high NRe, ie $N_{Re} \geq 10$) inside the packing, the rate of diffusion in the radial direction becomes very small. Therefore dc/dr approximates to zero. then, equation 11.15 reduces to

$$\frac{dc}{dt} = Ea\frac{d^2c}{dl^2} - \frac{U}{e}\frac{dc}{dl} \qquad \text{.... 11.16}$$

Equation 11.16 represents the axial dispersion diffusion only. This equation has been solved as described in Appendix (K). The analytical solution is:

$$\frac{C_1 - C}{C_1 - C_o} = \frac{2}{\pi} \sum_{n=1}^{\infty} \frac{1 - (-1)^n}{n} \left[\text{Exp} \left(- \frac{n^2 \pi^2 \, Ea \, t}{L^2} \right) . \text{Sin} \left(\frac{n \pi (le - ut)}{e.L} \right) \right]$$

.... 11.17

b) For the case of steady state and high velocity ($N_{Re} > 10$), the value of dc/dt = 0 and equation 11.16 becomes:

$$Ea \frac{d^2c}{dl^2} - \frac{U}{e} \frac{dc}{dl} = 0 \qquad \text{.... 11.18}$$

Equation 11.18 represents the axial dispersion diffusion under steady state conditions. This equation is solved as described in Appendix L. The analytical solution is:

$$C = A + B \ \text{Exp} \left(\frac{U}{e \, Ea} \right) \qquad \text{.... 11.19}$$

where A and B are arbitrary constants.

c) For the case of axial secondary dispersion diffusion from an instantaneous point source under unsteady state conditions:-

This method of calculation can be used to obtain the value of axial secondary dispersion diffusion coefficient (Ea). A definite quantity Q_M of dispersion injected at input of the bed and left to diffuse into it.

Then equation 11.16 becomes:

$$Ea \frac{d^2c}{dl^2} = \frac{dc}{dt} \qquad \text{.... 11.20}$$

The boundary conditions are:

$c = f(l)$ when $t=0$ 11.20a

$c = f(l, t)$ when $t > 0$ 11.20b

Suppose that in the infinite solids there exists initially a concentration $c = c_o$ between the

solid layers

ie $\lim_{l \to \infty} C(l,t) = 0 \quad t > 0$ 11.21

also, $Q_M = \pi r^2 e \int_{-\infty}^{\infty} c\,(l, t)\, dl$ 11.22

Then, the solution of equation 11.20 as presented in reference [221]:

$$C\,(l,t) = \frac{Q_M}{2\pi r^2 e \sqrt{\pi E a t}} . \text{Exp}\,[\, - l^2/4Eat] \qquad \text{.... 11.23}$$

And, when instantaneous source, quantity Q_M, is deposited at l=0 of a semi-infinite solid, the variation of concentration C with time at l=0 is given by

$$C\,(t) = \frac{Q_M}{2\pi r^2 e \sqrt{\pi E a t}} \qquad \text{.... 11.24}$$

Therefore, by putting l=0 in equation 11.23 gives a very simple method of obtaining the value of Ea from equation 11.24.

Carberry and Bretton [222] studied the dispersion mass flow through fixed beds and derived equation 11.23. However they suggested that the time (t_m) was the time at which C_{max} appeared. They proposed the equation for t_m:

$$t_m = L/U - Ea/U^2 \qquad \text{.... 11.25}$$

As L/U is the normal holding time, then as a result of dispersion the dispersed pulse maximum actually arrives at the point of observation earlier than the residence time by an amount governed by E/U^2. This method of calculation could also be used to obtain the value of Ea. However, the first method of calculation is more simple and accurate than the second method.

11.1.5 Solutions of Radial Secondary Dispersion Diffusion Equations for Unsteady-state and Steady-state conditions

(a) In the case of unsteady-state operation with velocity = 0 (ie $N_{Re} = 0$) within a long circular cylinder and with molecular diffusion only in a radial direction (ie dc/dl = 0) the secondary dispersion diffusion general equation (ie equation 11.15) reduces to

$$\frac{dc}{dt} = \frac{Er}{r}\frac{d}{dr}\left(r\frac{dc}{dr}\right) \qquad \text{.... 11.26}$$

this equation was solved as described in Appendix M. The analytical solution is:

$$\frac{C-C_1}{C_o-C_1} = \frac{\sqrt{2\lambda_n\pi}}{r_o}.\left(\frac{\text{Sin}\,(\lambda_n r_o)}{\lambda_n^2} - \frac{r_o\,\text{Cos}\;\lambda_n r_o}{\lambda_n}\right).$$

$$\left(\sum_n \sqrt{\frac{2}{\lambda_n\pi}}.\,\text{Exp}\,(-\,Er\,\lambda_n^2 t).\frac{\text{Sin}\,\lambda_n r}{r}\right) \qquad \text{.... 11.27}$$

(b) In the case of steady-state conditions and velocity = 0 (ie $N_{Re=0}$), dffusion is also considered in a long circular cylinder in which the secondary dispersion diffusion is everywhere radial (ie dc/dt = 0). Therefore the radial secondary dispersion diffusion equation (ie equation 11.26) reduces to:

$$\frac{Er}{r}\frac{d}{dr}\left(r\frac{dc}{dr}\right) = 0 \qquad \text{.... 11.28}$$

At $a < r < b$, the general solution of this equation, as described in Appendix N, is

$$C = A + B\,.\,\ln(r) \qquad \text{.... 11.29}$$

where A and B are constants to be determined from the boundary conditions at r=a and

r=b.

If c at r=a equal to C_1

If c at r=b equal to C_2

Then the solution of equation 11.29 is, as described in Appendix N,

$$C = \frac{C_1 \ln (b/r) + C_2 \ln (r/a)}{\ln (b/a)} \quad \ldots\ 11.30$$

The quantity of diffusing material Q_M which diffuses through unit length of cylinder in time, t is given by [235]

$$Q_M = \frac{2\pi e\, Er.t\, (C_2-C_1)}{\ln (b/a)} \quad \ldots\ 11.31$$

Equation 11.31 can be used to obtain the value of Er by choosing two points in the plane in the packing to check C_1 and C_2 in positions a and b respectively. Then, the following equation can be used to obtain the value of Er at each interval of time;

$$Er = \frac{Q_M \ln (b/a)}{2\pi e\, (C_2-C_1)\, t} \quad \ldots\ 11.32$$

where Q_M is the quantity of dispersed phase, diffused through unit length.

11.2 Model for the Simulation of Channeling in a Random Bed of Spherical Packing

The model proposal is based on beds of random packed, equi-sized spheres, following work on primary coalescence [105]. The spaces or voids between the packing elements are assumed to comprise interconnected parallelopipedon passage-ways.

11.2.1 Assumptions

The following assumptions have been proposed:

(a) The packing is arranged so that each packing element has three neighbours.

(b) The pass length, x, is selected at random between (1-1.414) dc, since the maximum angle of inclination is 45^{o}.

(c) The orientation of packing is random between 0 - π (See Figure 11.3).

(d) Drop collection is by the interception mechanism only.

(e) The bed structure is such that pores formed between adjacent packing elements interconnect randomly to form a continuous path through the bed. Liquid is then assumed to flow through these random pathways.

(f) The pores or passage-ways, in random packing are of complicated cross-section. It is assumed however that the cross-section of such passage-ways approximate to mutually-tangential,. parallel, circular cylinders on an equilateral triangular pitch, as illustrated in Figure 11.2. The passage-ways are then parallelopidea [105].

(g) On average, the co-ordination number is assumed to be 3 with each packing element having three neighbours.

(h) A channel connecting the inlet to the outlet of the bed, is assumed to be formed by a series of passes. Each pass may have a different length and may be

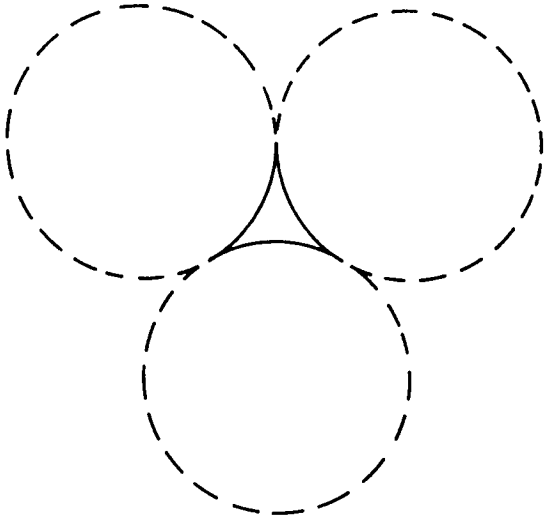

(a) Schematic representation of packing arrangement in media bed.

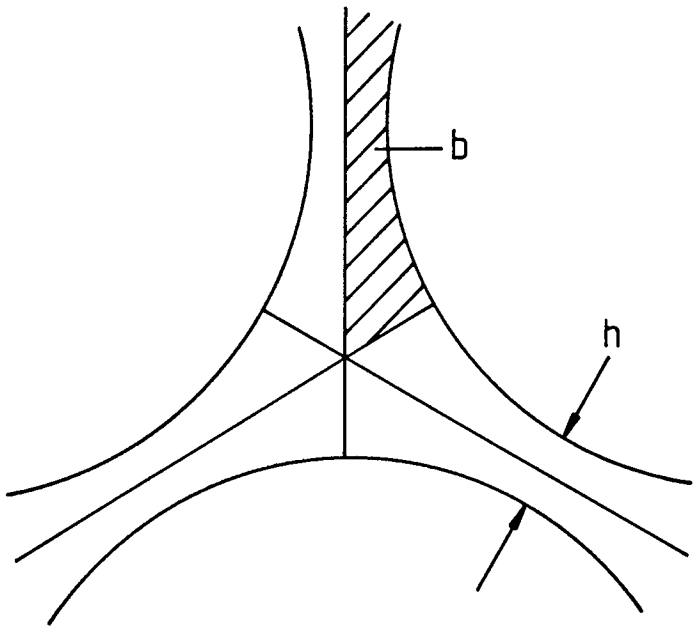

(b) Area for passage flow with sixfold geometry

Figure 11.2 Schematic representation of passage area.

inclined at a different angle to the horizontal [105], as illustrated in Figures 11.3 and 11.4

(i) The length, cross sectional area and angle of inclination of any increment section in an irregular random channel through the packed bed, related to a parallelo-pipedon, will be allowed to vary between fixed values.

11.2.2 Random Simulation of the Networks

The networks to be considered are a series of passes with each pass to be represented as a parallelopipedon. The width of each pass should be related to the packing size. The length of the pass is allowed to vary so that:

$$dc \leq x \leq 1.414\ dc \qquad \ldots\ 11.33$$

where x: is the pass length, and dc : is the packing diameter.

The cross-sectional area of the pass is related to the packing dimension illustrated in Figure 11.2. This shows the void between three packings through which fluid will pass. This cross-section is obviously identical with that of the free space between tangential, parallel, congruent circular cylinders. Although the channels for flow are periodically constricted, it will be assumed that they have constant longitudinal cross-sectional areas as shown in Figure 11.2b. The dispersed phase is compressible and is in steady, longitudinal laminar flow. The area for flow is shown in Figure 11.2b and it has been shown from geometric considerations [27, 224] that,

$$A_c = (3\sqrt{3} - \frac{3\pi}{2})\, b^2 + 3bh + \frac{\sqrt{3}}{4} h^2 \qquad \ldots\ 11.34$$

since b >> h normally, therefore equation 11.34 reduces to,

$$Ac \approx 0.4838\ b^2$$

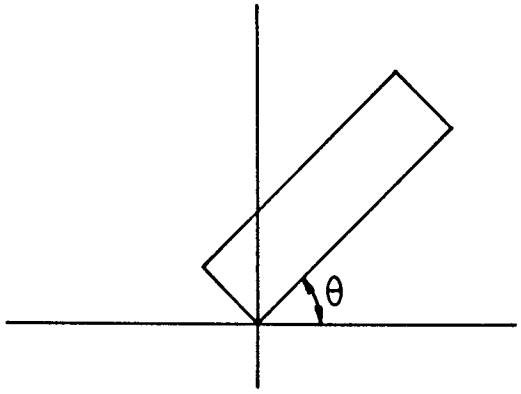

(a) $0 \leq \theta \leq \pi/2$

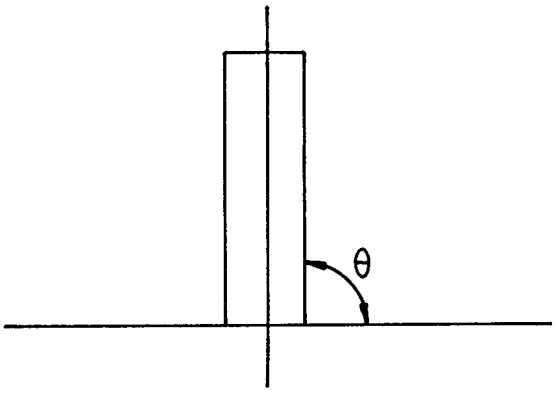

(b) $\theta = \pi/2$

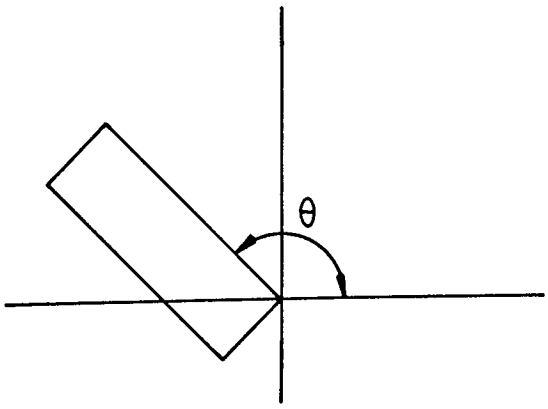

(c) $\pi/2 < \theta \leq \pi$

Figure 11.3 Orientation angle of packing.

or $Ac \approx 0.121\ dc^2$ 11.35

where Ac is the cross-sectional area of the pass, and b is the radius of an equivalent spherical particle.

The inclination of path through the bed is allowed to vary up to 90^o from the axial direction. This determines the angle of inclination of the pore or parallelopipedon of flow passage-ways. This angle, θ, is allowed to vary randomly as shown in figure 11.3 and 11.4 so that:

$$0 \leq \theta \leq \pi \quad \text{.... 11.36}$$

To present the total free volume of the pore the following details of the networks are important .

(a) Flow passage

- i Number of passes in each channel,
- ii Total vertical length of the channel
- iii Vertical pass length
- iv Total number of channels

(b) Porosity of free voidage

- i Pore area of the channel
- ii Volume of the channel
- iii Total channel voidage

11.2.3 Networks Generation

The height and diameter of the coalescer is fixed, so that the cross sectional area (Ac) and the depth are determined. Consider a media bed of a unit cross section and unit total depth. A random network can now be generated to simulate connected pores in the bed.

The procedure (after 105) is as follows, the dimensions of the pore making the

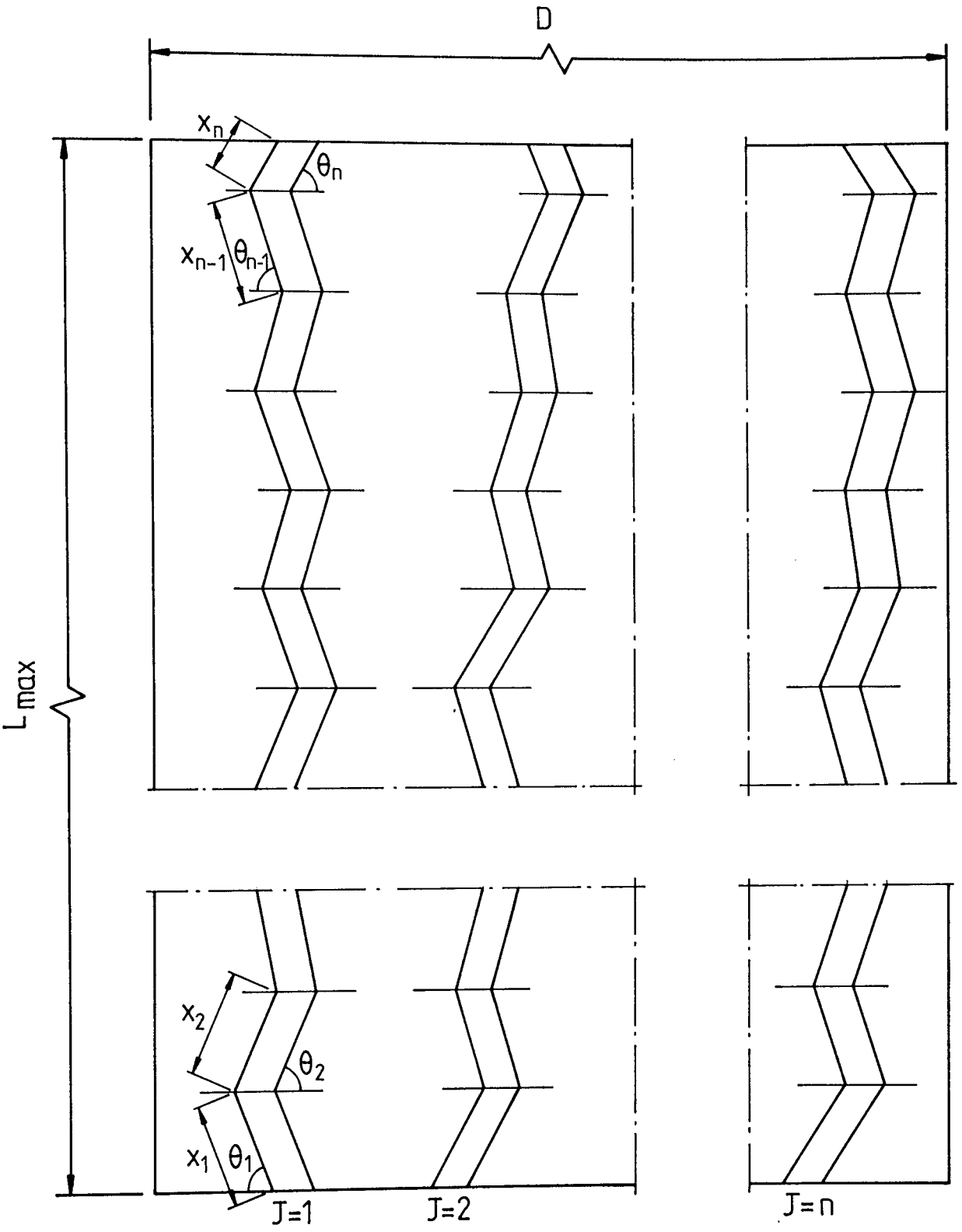

Figure 11.4 Channels distribution in two-dimensional coordinate.

first pass of a channel or continuous flow path through the bed are determined. This requires the length x_1, and the orientation of the pore θ_1, to be defined. The length of the pass is allowed to vary, to simulate the random relative orientation of a packing element at any local position in the bed. The length of the pass will not exceed the total length of the packing element. This therefore defines their upper limit. The minimum length is taken as dc, so that the length of the first pass is determined by selecting at random a value between (1-1.414) dc. The orientation of this pass θ_1, is next determined, again at random, such that $0 \leq \theta_1 \leq \pi$ (Figure 11.3). The value of this pass is then determined from:

$$V_1 = A_c \cdot x_1 \qquad \text{....11.37}$$

The components x_1, θ_1, V_1 are then stored. the procedure is continued by considering the next pass in the channel. Referring to Figure 11.4, this will correspond to the second element in any one of the zigzag paths shown. As before the length, inclination angle and volume are determine, x_2, θ_2, V_2. The cumulative volume $(V_1 + V_2)$ is determined and the total vertical height of the pore is determined as:

$$L = x_1 \cdot \text{Sin}\ \theta_1 + x_2 \cdot \text{Sin}\ \theta_2 \qquad \text{.... 11.38}$$

The procedure is repeated for passes 3, 4, 5, ... i; in each case the parameter x_i, θ_i, and V_i are stored. At each increment, i, of the pass the total cumulative height L of the channel is checked with total height of the bed, L_{max}. When,

$$\sum_{i=1}^{n} x_i \sin\theta i \geq L_{max} \qquad \text{.... 11.39}$$

then the connecting channel from the inlet to the outlet is completed. The total volume of the channel J, is then computed as the free volume of the interconnected passes within the packing. Thus for channel J, the total channel volume, V_J, is:

$$V_J = \sum_{i=1}^{n} V_{iJ} \qquad \text{.... 11.40}$$

If the free volume of the packing computed, from the total volume of the channel divided by the total volume of the bed, is less than the free volume, e,

ie $$\frac{V_J}{V_T} \leq e \qquad \text{.... 11.41}$$

then additional channels must be added by repeating the simulation procedure outlined above. Thus starting at the inlet of the bed, the dimensions of the first pass is selected and the procedure for adding passes followed. Two criteria need now to be tested, these are:

(a) Total vertical depth of the bed is compared with the vertical length of the channel J+1 after each pass is added. The equation used is,

$$\sum_{i=1}^{n} x_{iJ+1} \sin \theta_{iJ+1} \geq L_{max} \qquad \text{.... 11.42}$$

(b) The free volume of the bed is checked from the condition,

$$\frac{\sum_{J=1}^{n} \sum_{i=1}^{n} V_{iJ}}{V_T} \leq e \qquad \text{.... 11.43}$$

When the first condition is attained a further channel must be added J+2. When the second condition is attained, the description of the bed is complete. The computer program, developed [after 105], and the output results are illustrated in Appendix Y.

For interest, it was decided to investigate the structural arrangement of packing by simulating beds of different packing size, as illustrated in Table 11.1 and Appendix Y. These results are compared with the result obtained from a development of Baez Poleo's [27] method of prediction of exit drop sizes shown in Appendices O and P. The development of the equations is as follows. The rate of flow through the channels is [169],

$$U_{cap} = \frac{d_H^2}{2K\mu} \frac{\Delta P}{\Delta L} \quad \text{.... 11.44}$$

where the hydraulic mean diameter, $d_H = 0.177$ dc and K = 6.43. Then the volumetric flowrate $V_f = U_{cap}$. Ac that is:

$$V_f = \frac{0.0038\ dc^4}{12.86} \frac{\Delta P}{\Delta L} \quad \text{.... 11.45}$$

Then,

$$\text{number of channels} = \frac{\text{Total flowrate of dispersed phase}}{\text{Flowrate through channel}}$$

From a knowledge of the velocity through the channel, volumetric flowrate and physical properties of the system it is possible to calculate the number of channels. Typical results are is presented in Appendix O.

The predicted number of channels by using the simulation model vs the number calculated by the development from Baez-Poleo correlations are presented in Table 11.1. The agreement is poor because the Baez-Poleo correlations was deroved apply only to those channels through which drops were actually flowing whereas the present model is

for simulation of the channels and passes inside the particulate bed to predict the total possible parallel channels.

The object of the simulation is to produce a quantitative description of a pore structure of a packed bed in order to predict, theoretically, exit drop size, as described in Appendix P and thus coalescence efficiency for a particular bed through which a secondary liquid-liquid dispersion is flowing.

The residence time could also be obtained and the effective flow path, Le, evaluated. This may aid the modelling of the coalescence process by means of the "queueing theory" approach.

11.3 Queueing Drop Model

11.3.1 Basic Definitions and Notations

A queueing system is defined to include the waiting line (or queue) and the service channels. The number of customers (ie drops) in the system at any one time is the sum of the number in the queue plus the number in service [151]. Figure 11.5 shows the basic elements of a queueing system with parallel servers.

Kendall [225] introduced a useful notation for multiple-server, queueing models which describes the arrival distribution, departure distribution, and number of parallel service channels Lee [226] added the fourth and fifth characteristics to the notation that is, the service discipline and the maximum number in the system. The Kendall-Lee notation is augmented by a sixth characteristic describing the calling source. The complete notation thus appears in the following symbolic form, (a/b/c):(d/e/f) where [225]:

a = arrival (or interarrival) distribution

b = departure (or service time) distribution

c = number of parallel service channels in the system

d = service discipline

e = maximum number allowed in the system

f = calling source.

The following conventional codes are usually used to replace the symbols a, b, and d. For symbols a and b, the G code is used in this work where G is the Poisson arrival or departure distribution. For symbol d, the following codes could be used:

FCFS = first come, first served

LCFS = last come, first served

SIRO = service in random order

GD = general service discipline

The symbol c is replaced by any positive number representing the number of parallel servers. The symbols e and f represent a finite or infinite number in the system and calling source, respectively. In this work, the notation is considered as (G/G/c):(GD/∞/∞). This denotes Poisson arrival (exponential interarrival), Poisson departure (exponential service time), c parallel servers, "general service discipline", maximum allowable number N in the system, and infinite calling source.

11.3.2 Assumptions

The following assumptions are made to derive the queueing drop model:

i Poisson arrival distribution of mean arrival rate, λ, per unit time.

ii Exponential service distribution of mean service rate, μ, per unit time.

iii Queue discipline is on a service in general service discipline basis.

iv No simultaneous arrivals or service, which eliminates terms of second order in time, t.

Table 11.1

Comparison between Model for Simulation of Channeling in a Random Bed of Spherical Packing Results and Developed Baez-Poleo Correlations of Number of Channels Inside Packed Bed: Results for 266 μm Ballotini Particle Size

Bed Depth mm	No. of Channels Using Baez-Poleo Correlations*	No. of Channels using Channeling Simulation Model †	
		Total No. of Channels	Per Unit Area (100 mm^3)
10	186	14879	255
20	372	17352	299
30	558	198151	330
40	744	18692	321
50	930	18441	335

* See Appendix O
† See Appendix Y

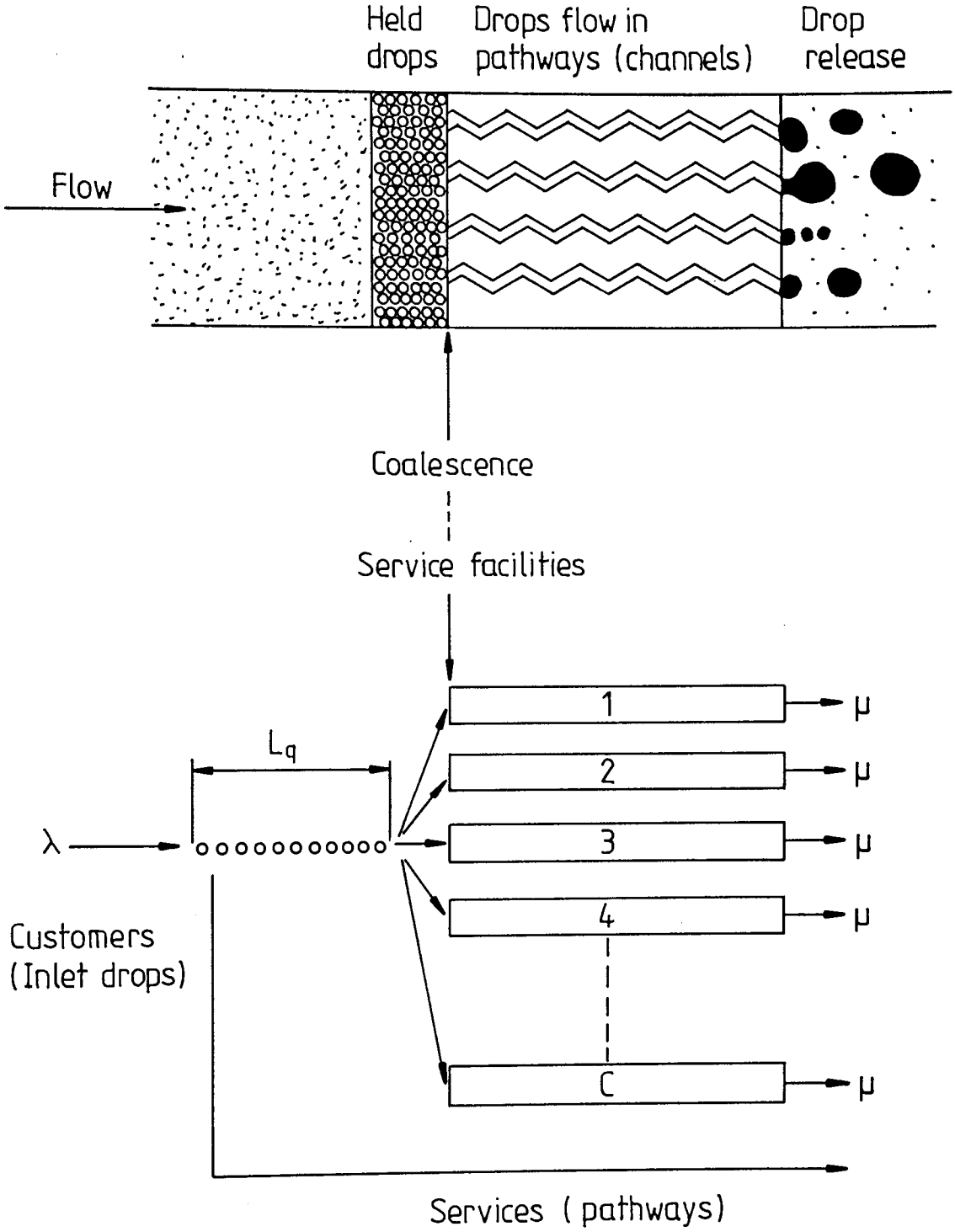

Figure 11·5 Diagramatic representation of analogy between coalescence process and multiple channel queuing system.

v There are c channels having an identical service rate, and all channels have the same (exponential) service distribution.

vi Under steady state conditions, the number in the system exceeds the number of service channels, ie N≥ c and there are no constraints governing the queue length.

11.3.3 Derivation of Queue Length Equation for (G/G/c):(GD/∞/∞) System

In this section, only Poisson queues with c servers have been considered and the model with c parallel servers, where $c \geq 1$, is considered so that c customers may be in service simultaneously. The probability of a service during an instant h is approximatley nμh for n<c and cμh for $n \geq c$ [227]. Thus at unsteady state when h- o, the differential equations are [225].

$$P'_o(t) = \mu P_1(t) - \lambda Po(t) \quad n=o \qquad \ldots. 11.46$$

$$P'_n(t) = \lambda P_{n-1}(t) - (\lambda + n\mu) P_n(t) + (n+1) \mu P_{n+1}(t) \; o < n < c \qquad \ldots. 11.47$$

$$P'_n(t) = \lambda P_{n-1}(t) - (\lambda + c\mu) P_n(t) + c\mu P_{n+1}(t) \quad n \geq c \qquad \ldots. 11.48$$

Asuming the parameters of the system are such that a steady-state solution exists, the steady-state equations are [225]:

$$- \lambda P_o + \mu P_1 = 0 \quad n=o \qquad \ldots. 11.49$$

$$\lambda P_{n-1} - (\lambda + n\mu) P_n + (n+1) \mu P_{n+1} = 0 \quad o<n<c \qquad \ldots. 11.50$$

$$\lambda P_{n-1} - (\lambda + c\mu) P_n + c\mu P_{n+1} = 0 \quad n \geq c \qquad \ldots. 11.51$$

The steady-state solution is then [244]:

$$Pn = \left(\frac{\rho^n}{n!}\right) P_o, \quad o \le n \le c \qquad \text{.... 11.52}$$

$$Pn = \left(\frac{\rho^n}{c^{n-c}.c!}\right) P_o \quad n>c \qquad \text{.... 11.53}$$

$$\text{where } P_o = \left\{ \sum_{n=o}^{c-1} \frac{\rho^n}{n!} + \frac{\rho^c}{c!\,(1-(\rho/c))} \right\}^{-1} \qquad \text{.... 11.54}$$

$$\text{and} \quad \frac{\rho}{c} < 1 \quad \text{or} \quad \frac{\lambda}{\mu c} < 1 \qquad \text{.... 11.55}$$

Also, the solution for queue length equation, which is presented in Appendix (Q), is:

$$Lq = \frac{\rho^{C+1}}{(c-1)!\,(c-\rho)^2} P_o = \left(\frac{c\rho}{(c-\rho)^2}\right) P_c \qquad \text{.... 11.56}$$

$$Ls = Lq + \rho \qquad \text{.... 11.57}$$

$$Wq = Lq/\lambda \qquad \text{.... 11.58}$$

$$Ws = Wq + (1/\mu) \qquad \text{.... 11.59}$$

where,

n = number of customer (ie drops) in the system

$P_n(t)$ = transient state probabilities of exactly n customers in the system at time t assuming the system started operation at time zero.

P_n = steady-state probabilities of exactly n customers in the system.

λ = mean arrival rate (number of customers arriving per unit time)

c = number of parallel services (ie channels)

ρ = λ/μ = traffic intensity

α = ρ/c = utilisation factor for c service (channels) facilities

Ws = expected waiting time per customer (drop) in the system

Wq = expected waiting time per customer (drop) in the queue

Ls = length of service channel in queuing system

Lq = length of queue in queuing system.

The computation associated with this model is presented in Appendix Z; this computer program computes the probabilities and the operating characteristics for Poisson queue length model.

Finally Morse [228] gives two useful approximations for Po and Lq. For ρ much smaller than one.

$$Po \approx 1-\rho \quad \text{and} \quad Lq \approx \frac{\rho^{C+1}}{c^2} \qquad \ldots. 11.60$$

and for α ($=\rho/c$) very close to one,

$$Po \approx \frac{(c-\rho)\,(c-1)!}{c^c} \quad \text{and} \quad Lq \approx \frac{\rho}{c-\rho} \quad \text{and} \quad L_s = \frac{\rho}{c-\rho} + \rho \qquad \ldots. 11.61$$

11.4 Filter Coefficient Model

The function of the queue length model is to predict the filter coefficient using average saturation data. It is based on the hypothesis that drops are captured in the forepart of the bed where they accumulate until coalescence into a dispersed phase continuum occurs. The dispersed phase is then conveyed in discrete channels to release sites at the exit face of the coalescer. As shown in Figure 11.5, this model recognises an analogy between phase continuum and drops as 'customers' queueing at a service facility. This analogy may be pursued further by considering, as Austin [16] proposed,

and 'impatience factor',ϑ, defined as the ratio of the rate of coalescence to the rate of drop capture [111] and it is possible to determine ϑ experimentally. Therefore, the fraction of drop ' customers' which join the queue when there are n drops in the system is given by [16],

$$fn = Exp\ (-\vartheta n/\mu) \qquad \ldots. 11.62$$

The term, fn is easier to manipulate if another term, γ is introduced [16],

$$\gamma = Exp\ (-\vartheta/2\mu) \qquad \ldots. 11.63$$

then,

$$fn = \gamma^{2n} \ ; \quad fn\text{-}1 = \gamma^{2n-2} \qquad \ldots. 11.64$$

For steady-state conditions when n=Ls:

$$f_{Ls} = \gamma^{2Ls} \qquad \ldots. 11.65$$

The filter coefficent λc is given by

$$\lambda c = \frac{-\log\ (1-f_{Ls})}{L} \qquad \ldots. 11.66$$

Substitution for f_{Ls} from equation 11.65 gives

$$\lambda_c = \frac{-\log\ (1-\gamma^{2Ls})}{L} \qquad \ldots. 11.66$$

The filter coefficient λ_c was determined using Austin's filter coefficient model equation 4.20. Table 11.2 lists the values of λc of this work and λe of Austin's model. Whilst the theoretical and experimental filter coefficients are of the same order, and are in fact much closer than achieved by Austin [16] the deviations appear to be random. Therefore more work is required on the model given in Section 12.2

Table 11.2

Comparison Betwen This Work's Theoretical Filter Coefficient Model and Austin's Experimental Filter Coefficient Correlation for 266 μm Ballotini Particle Size and 27.0 μm Mean Inlet Drop size

Superficial Veloicty $x10^{-3}$ (m/s)	Bed Depth $x10^{-3}$ (m)	This Work's Model		Experimental Austin Model
		L_s	λc (m^{-1})	λexp (m^{-1})
1.5	10	6.66	799	1140
	20	13.33	108	624
	30	20.0	68	458
	40	26.66	34	406
	50	32.22	17	229
3.05	10	3.27	1625	1031
	20	6.55	812	544
	30	9.83	161	383
	40	13.11	109	274
	50	16.39	57	203
6.00	10	1.66	2833	859
	20	3.33	1535	475
	30	5.0	283	335
	40	6.66	182	241
	50	8.33	27	182

CHAPTER TWELVE

CONCLUSIONS AND RECOMMENDATIONS

12.1 Conclusions

12.1.1 Main Conclusions

The main conclusions arising from this work are:

1 The pressure drop associated with single phase flow through beds of glass ballotini particles could be correlated by a Carman-Kozeny type equation

$$\Delta P1 = \left[\frac{36\,\mu_c\,L}{dc^2}\right]\left[\frac{(1-e_1)^2}{e_1^3}\right].\ KU \qquad \text{.... 12.1}$$

A value of 5.0 for the Kozeny constant, K, from theoretical considerations, was in good agreement with values obtained experimentally, ie within ± 16%, as described in Section 7.4.

2 Two phase pressure drop data under steady-state conditions were expressed as $\left[\frac{\Delta P_2}{\Delta P_1}\right]\left[\frac{\mu_c}{\mu_d}\right]$ to compensate for temperature and variations in single phase permeability. The data were correlated with superficial velocity, bed depth, ballotini particle diameter, mean inlet drop size and inlet phase ratio by:

$$\left[\frac{\Delta P_2}{\Delta P_1}\right]\left[\frac{\mu_c}{\mu_d}\right] = k_p\,U^a\,L^b\,d_c^{\,c}\,d_p^{\,d}\,C_{in}^{\,e} \qquad \text{.... 12.2}$$

the values of the constant, kp, and exponent a, b, c, d, and e are listed in Table 7.4.

3 Dimensional analysis was used to derive an equation to correlate two phase pressure drop data at steady state,

$$\frac{\Delta P_2}{\rho_c U^2} = 8.64 \times 10^7 \left[\frac{dc}{D}\right]^{-0.27} \left[\frac{L}{D}\right]^{0.71} \left[\frac{dp}{D}\right]^{-0.17} \left[N_{Re}\right]^{1.5} \left[e_2\right]^{-0.14} \left[C_{in}\right]^{0.26} \quad \ldots\ldots 12.3$$

Comparison between the predicted data from equation 12.3 and experimental data showed an average error of 25%.

4 The separation efficiency provided a measure of the overall drop coalescence efficiency of the bed. The results show that the separation efficiency for the optimum glass ballotini coalescer, with a 30×10^{-3} m bed depth of 266 μm ballotini particle diameter, was generally higher than for the other packing systems studied.

5 Droplet release mechanisms of the Hazlett [84] and Attarzadeh [17] types, described in Section 4.1.4, were observed in this work. The major factors affecting the mean size of the outlet drops were the inlet drop size, particle diameter, superficial velocity and bed depth, as described in Section 9.1. The particle diameter and superficial velocity played an important role in the drop release mechanisms, and hence in the sizes of exit droplets.

6 A centrifugal pump with a recirculation loop provided a simple method of preparing a continuous supply of secondary dispersion with a reproducible drop size distribution. The inlet drop size distribution, as determined by a Malvern Particle Size Analyser, decreased with increasing pump speed, as described in Section 8.7.

A newly developed distribution function has been proposed to fit the inlet drop size distributions, as described in Section 8.4. A new theoretical mean drop diamter equation has also been derived and the results predicted from this equation exhibited a maximum error of ±15% from the experimental data. The general theoretical mean diameter equation , as described in section 8.6 is:

$$d_{qp}^{q-P} = d_{fr}^{q-P} \cdot \alpha^{(P-q)/\beta} \cdot \frac{\Gamma(q-3/\beta)}{\Gamma(P-3/b)} \quad \ldots\ 12.4$$

7 A theoretical comparison of drop capture mechanisms demonstrated that indirect interception and London-van der Waal's mechanisms are most significant. The diffusion mechanism may become significant for drops less than 10μm diameter.

The overall capture efficiency can be expressed by η_T/η_I or η_{ILD}/η_I, as described in section 10.2. The drop capture efficiency for beds initially free from dispersed phase, may be estimated by using:

$$\frac{\eta_T}{\eta_I} = 1 + 1.622\, A_S\, (N_{Ad})^{0.333} + 2.223\, [A_S.N_{Ad}.(K'T/Q)]^{0.667} \quad \ldots\ 12.5$$

The results obtained from this equation showed close agreement with the results obtained using equation 10.1, as described in section 10.2.

8 Using an analogy between molecular diffusion and flow of the secondary dispersion inside the packed bed, a general differential equation has been applied to explain the concentration profiles of dispersed phase through the packed bed. This general equation has been solved in two directions, the axial direction and the radial direction, under both unsteady-state and steady-state conditions to describe the concentration profiles of dispersed phase in each direction.

The equations could be used to obtain the values of Ea and Er, as described in

9 A development of a simulation model of channeling in a random bed has been proposed for a bed of random equi-sized, spherical particles, in which networks of interconnected passes make up the pathways through which the liquid flows. The pathways and the free volume are predicted in the simulation.

The number of channels (passage-ways) distributed in the bed was shown to depend upon the packing diameter and bed voidage. The number of channels predicted by this model has been compared with that predicted by the method proposed by Baez Poleo [27], as described in Section 11.2. The agreement was poor, as shown in Table 11.1 because the Baez Poleo correlations were derived originally for droplets actually travelling through the bed and the present model for simulation of the total possible parallel channels inside the bed of the random packed, equi-sized spheres.

10 The filter coefficient derived from the queueing drop model, as described in Sections 11.3 and 11.4, gave reasonable results compared with the Austin Model.

11 Based on the theoretical and experimental studies, a mechanism of coalecence of secondary dispersions is proposed;

Secondary dispersion drops are captured by indirect interception and London-van der Waal's mechanisms, if the size of drops >10 μm. Drops are captured primarily in the forepart of the bed. The drops reside in the packed bed, touching to the packing, where coalescence occurs by collision of two or more drops until they attain a size when hydrodynamic forces exceed the restraining interfacial tension and adhesion forces. These drops are then squeezed-through the fixed channels, in zig-zag fashion.

The primary drops within fixed channels are conveyed to the exit face where drops are formed and released by the mechanisms described in section 4.1.4.

12.1.2 Minor Conclusions

In addition the following minor conclusions arose:

1 The experimental two phase pressure drops increased with an increase in superficial velocity or bed depth and, slightly, with a decrease of inlet drop size. Changes of inlet phase ratio in the range of 0.5 to 1% v/v had a very small effect. However the pressure drop increased with increase in phase ratio in the range of 2 to 6% v/v. The two phase pressure drop decreased with increase in ballotini particle diamter, as described in Section 7.8.

2 The effective saturation had different values with respect to average oil saturation measured by the method described in Section 9.3. The effective saturation gave more accurate value of oil saturation inside the bed, as described in Section 9.4.3

3 Average bed hold-up and the degree of oil saturation were independent of inlet drop size. However, they varied with superficial velocity, particle size, inlet phase ratio and bed depth, as described in Section 9.4.

12.2 Recommendations for Further Work

As a continuation of this work, the following areas appear worth studying.

12.2.1 Experimental Investigations

1 Using the equipment and techniques described in Chapter 5,

a) Study the effect of using a glass mesh holder. This would eliminate any effects on primary drop coalescence and release due to differences in surface energy and roughness between the ballotini packing and the stainless steel mesh surface.

b) Investigate the effects of particle physical properties (ie density, surface roughness, surface energy and voidage) for different types of ballotini and other solid materials (eg plastics and non-corrosive metal particles) ,and of different particle shapes, upon the separation efficiency and upon the exit droplet size. Definition of the optimum operating conditions could result in an improved particulate coalescer for use in industry.

c) Study the coalescence of water in oil systems under similar conditions to those in this work and compare the results on the efficiency of coalscence and pressure drop with the present work.

d) The study of exit drop mechanisms indicated that the roughness and surface energy of the top mesh layer of the packing, ie exit surface, played a major role in the release mechanism. This could be investigated further by choosing different surface energy and roughness materials for the exit layer, ie top mesh layer, of the packed bed.

e) Investigate the effect of additives such as surfactants and solid contaminants with different concentrations on the coalescence efficiency, pressure drop and capture and release mechanisms.

f) Study the separation efficiency of packing consisting of two beds of different ballotini sizes. The smaller size ballotini should be used at the inlet of bed. Use of these larger size ballotini at the outlet may improve the separation efficiency and droplet size released. A study would also be worthwhile with two or more different sizes of ballotini within the bed.

2 An investigation could be made using a similar type of centrifugal pump with a similar emulsification loop but with a different number and capacity of the curved vanes of the impeller and with different types of impeller to generate more uniform drop size distributions. This could be used to formulate a general correlation between pump speed and the mean drop size generated.

3 Operation at increased superficial velocities could be investigated to find the

critical velocities where breakthrough, or redispersion, occurred. Particulate media may be subject to fluidisation; therefore, the superficial velocity should be limited to the fluidisation velocity.

4 More study is necessary to determine how wettability may be characterised for two phase flow in packed beds when coalescence occurs. Chemical treatment of glass ballotini particles could be applied, as described in section 5.4.2, to study the effect of wettability on the coalscence efficiency and two-phase pressure drop.

5 The equations for concentration of secondary dispersion in the bed could be tested using the conductivity measurement technique described in detail in Appendix D, since the electrical conductance of the dispersion will vary with concentration of dispersed phase.

12.2.2 Further Theoretical Studies

Additional theoretical studies would be worthwhile as follows:

1 The general differential equation for the concentration of dispersion in flow in a packed bed (ie equation 11.15) could be solved in a three-dimensional system (ie l, r, t direction or axes) using numerical methods instead of the analytical method used in this study for a two dimensional system (section 11.1).

2 The proposed simulation model represents a pore structure as parallel interconnected passage-ways with triangular cross-sectional area forming channels within the bed. These channels are treated separately and it is assumed that there is not interconnection between them. This is one assumption which needs to be relaxed in further theoretical development work. The geometrical arrangement of particles in fours with a cross-section area approximately equal to a rectangle or square, or any other

geometrical arrangment could also be considered (Section 11.2).

3 Improvements to the queuing model could be useful to cover some of the assumptions from which deviations occur in practice. Only queues of drops of secondary dispersion with c parallel channels which have the same exponential services distribution with constant rate were considered in present work. Therefore, the situation would clearly be more complex in an actual bed and it would be more complex mathematically to describe queues of drops in the bed with parallel-series and interconnection between the channels (services).

APPENDICES

A complete set of Experimental and Derived Data, listed in Appendices S, T, U, W, X, Y and Z, have been depositied in the Department of Chemical Engineering as Unbound Material

APPENDIX A

SPECIFICATION OF ORGANIC LIQUIDS USED FOR EXPERIMENTATION

A.1 Toluene 'Analar'

Density	0.86×10^{3}	kgm^{-3}	at	20 °C
Viscosity	0.58×10^{-3}	$kgm^{-1}s^{-1}$	at	20 °C
Surface Tension	27.96×10^{-3}	Nm^{-1}	at	20 °C
Interfacial Tension for Toluene-Water	29.20×10^{-3}	Nm^{-1}	at	20 °C

Impurities	Maximum Limit %
Acidity	0.012
Alkalinity	0.012
Non-Volatile matter	0.002
Benzene	0.5
Organic impurities	Pass Acid-Wash Test
Sulphur components	0.0003
Thiophen components	0.0002
Water	0.03

A.2 Clairsol - 350

Density	0.78×10^{3}	kgm^{-3}	at	20 °C
Viscosity	1.65×10^{-3}	$kgm^{-1}s^{-1}$	at	20 °C
Surface Tension	27.50×10^{-3}	Nm^{-1}	at	20 °C
Interfacial Tension for Clairsol-water system	39.25×10^{-3}	Nm^{-1}	at	20 °C

APPENDIX B

ROTAMETERS, PUMP AND ULTRAVIOLET ABSORBANCE CALIBRATION GRAPHS; AND QUEUE LENGTH VS DEGREE OF 'BALKING' STANDARD GRAPH

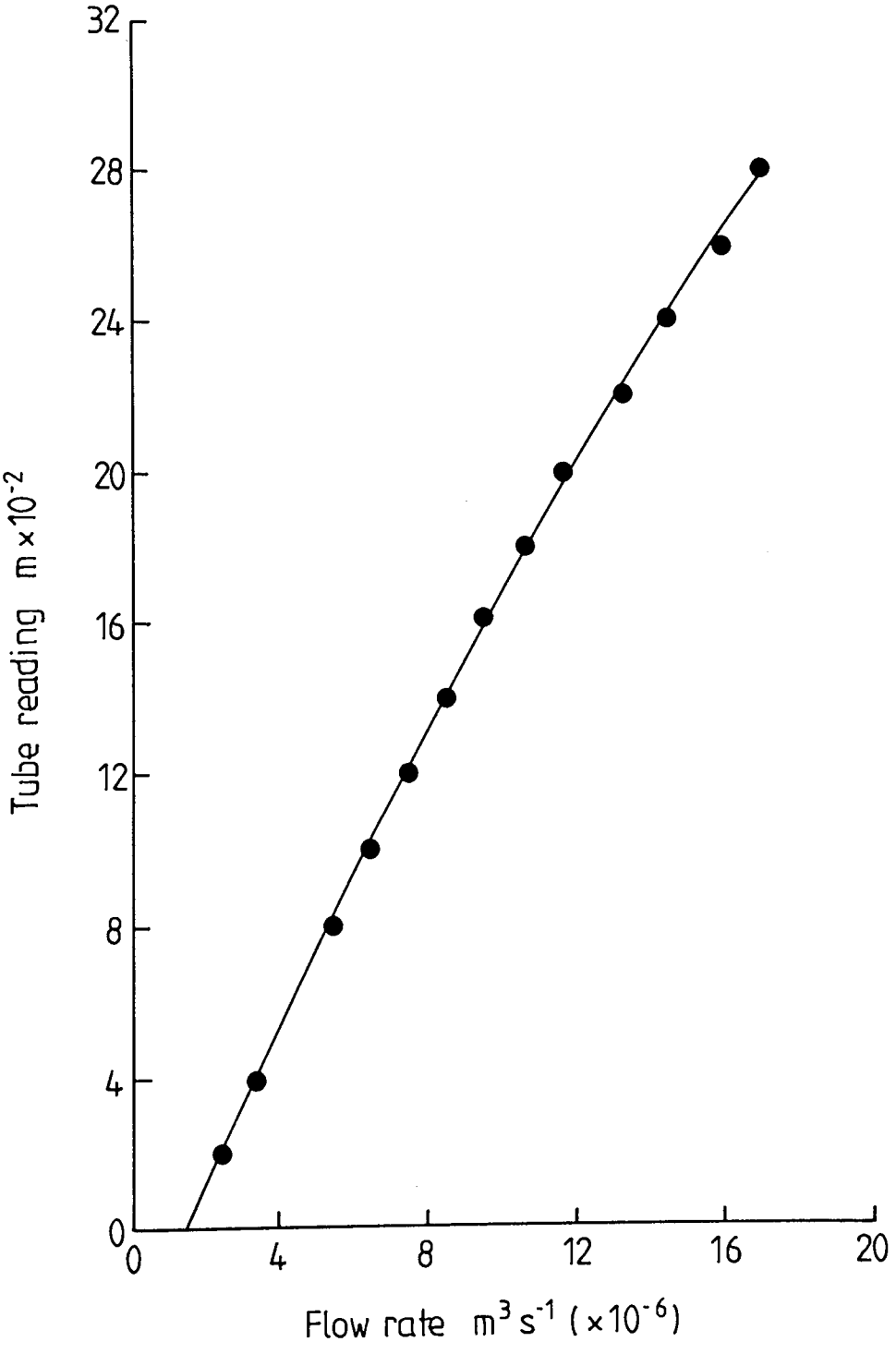

Figure B.1 Metric tube size 7 Rotameter calibration
Water at 20°C

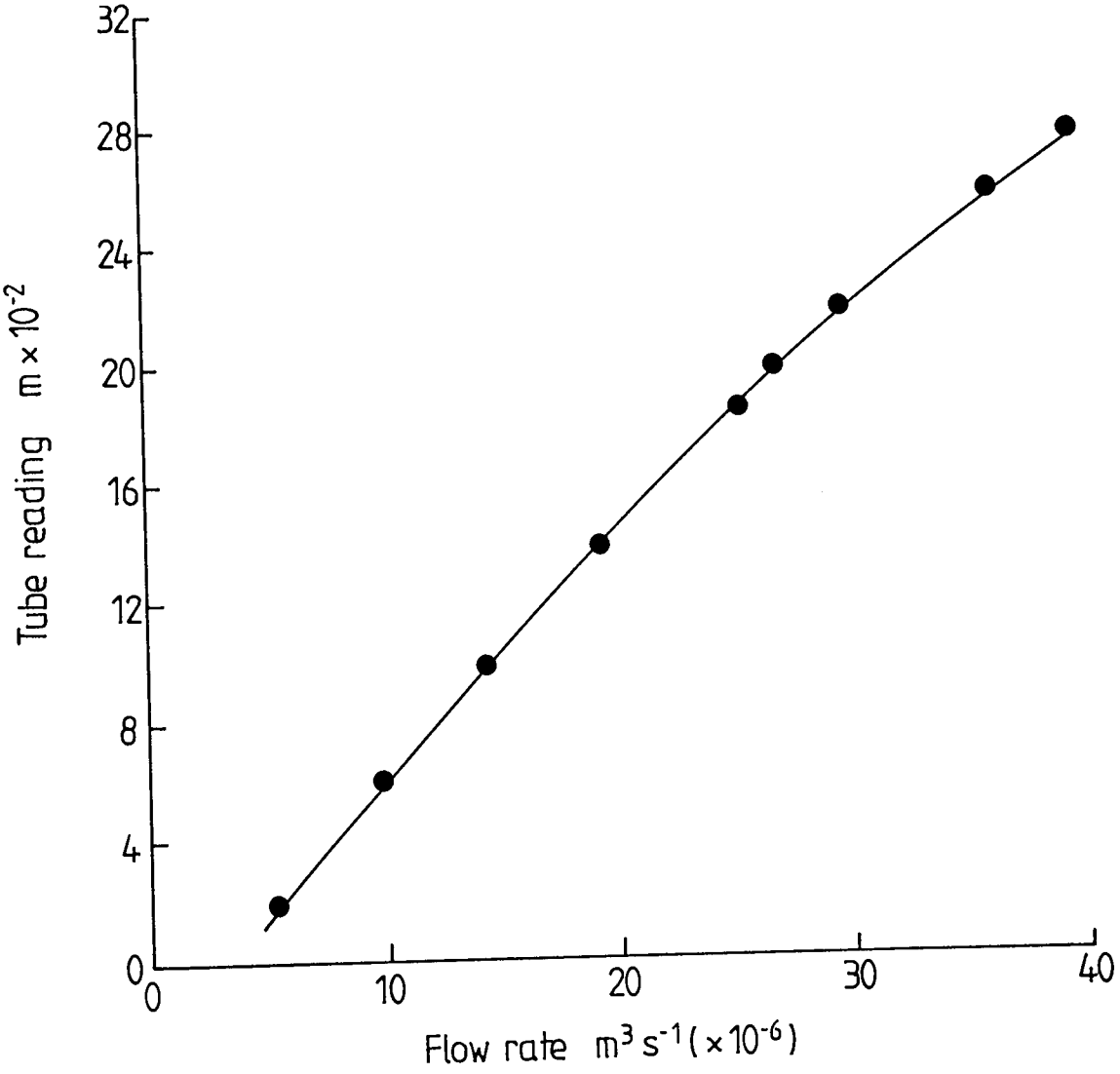

Figure B.2 Metric tube size 14 Rotameter calibration
Water at 20°C

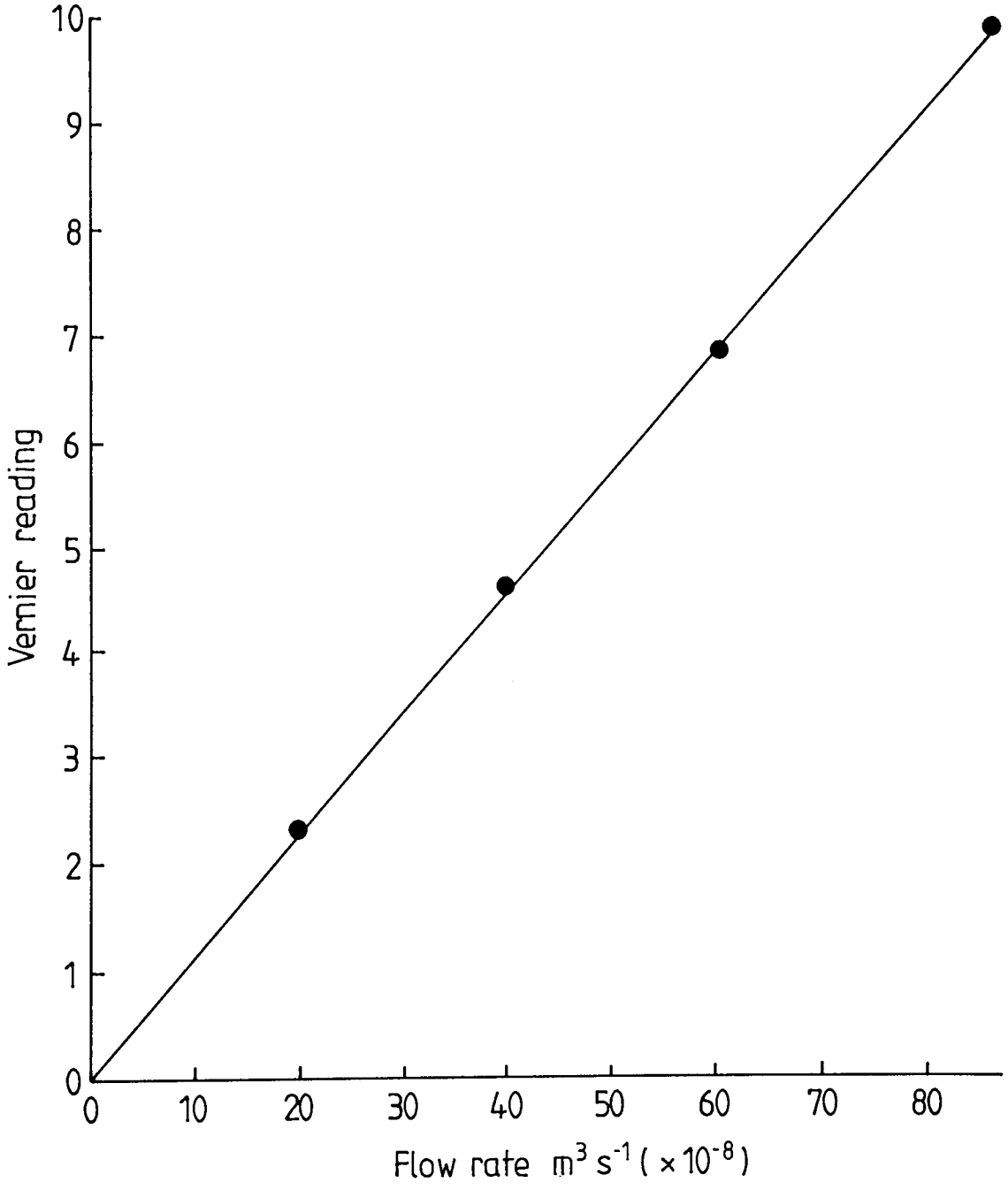

Figure B.3 Metering pump calibration. Long stroke mechanism
Toluene

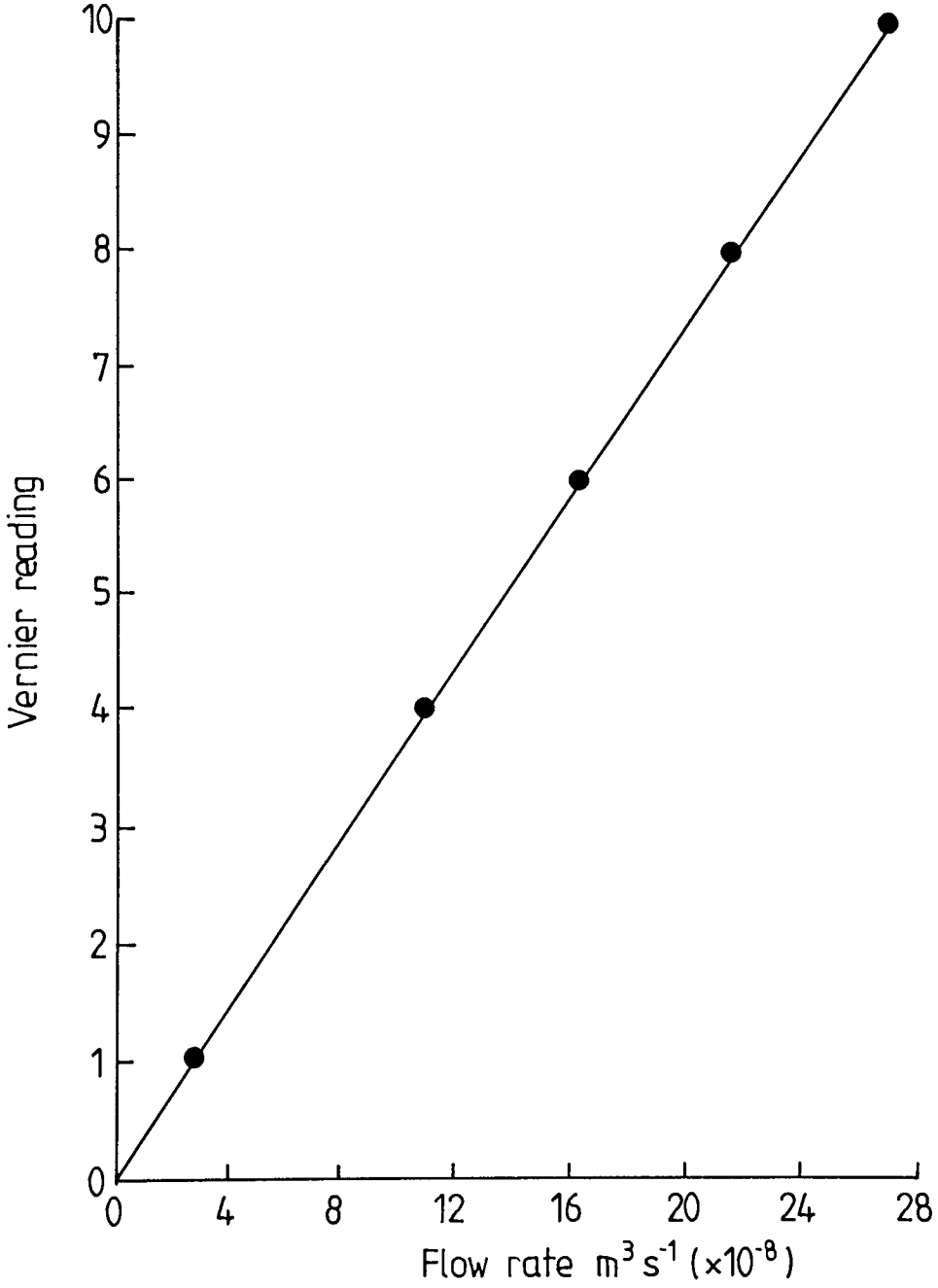

Figure B.4 Metering pump calibration. Short stroke mechanism
Toluene

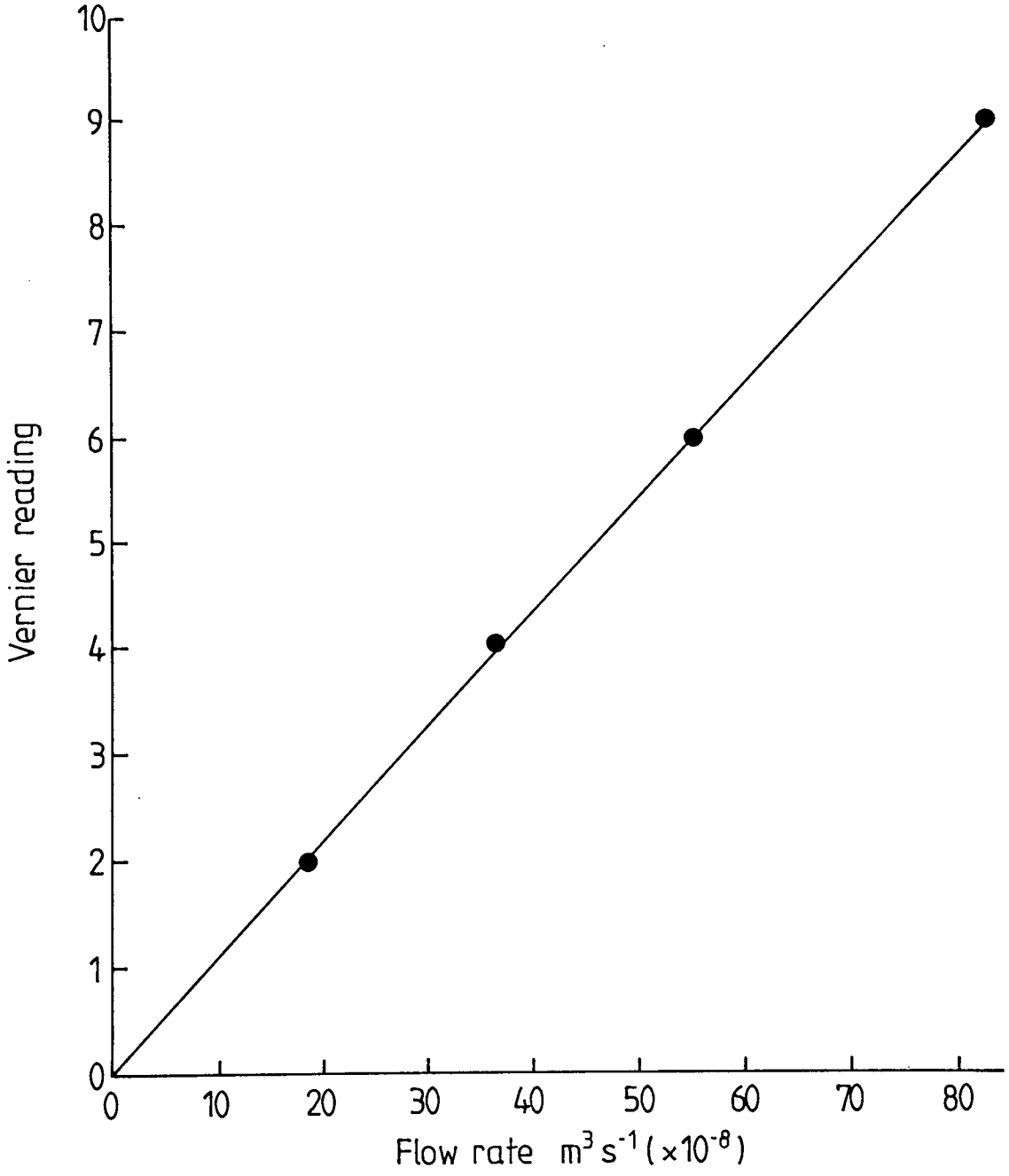

Figure B. 5 Metering pump calibration. Long stroke mechanism
Clairsol - 350

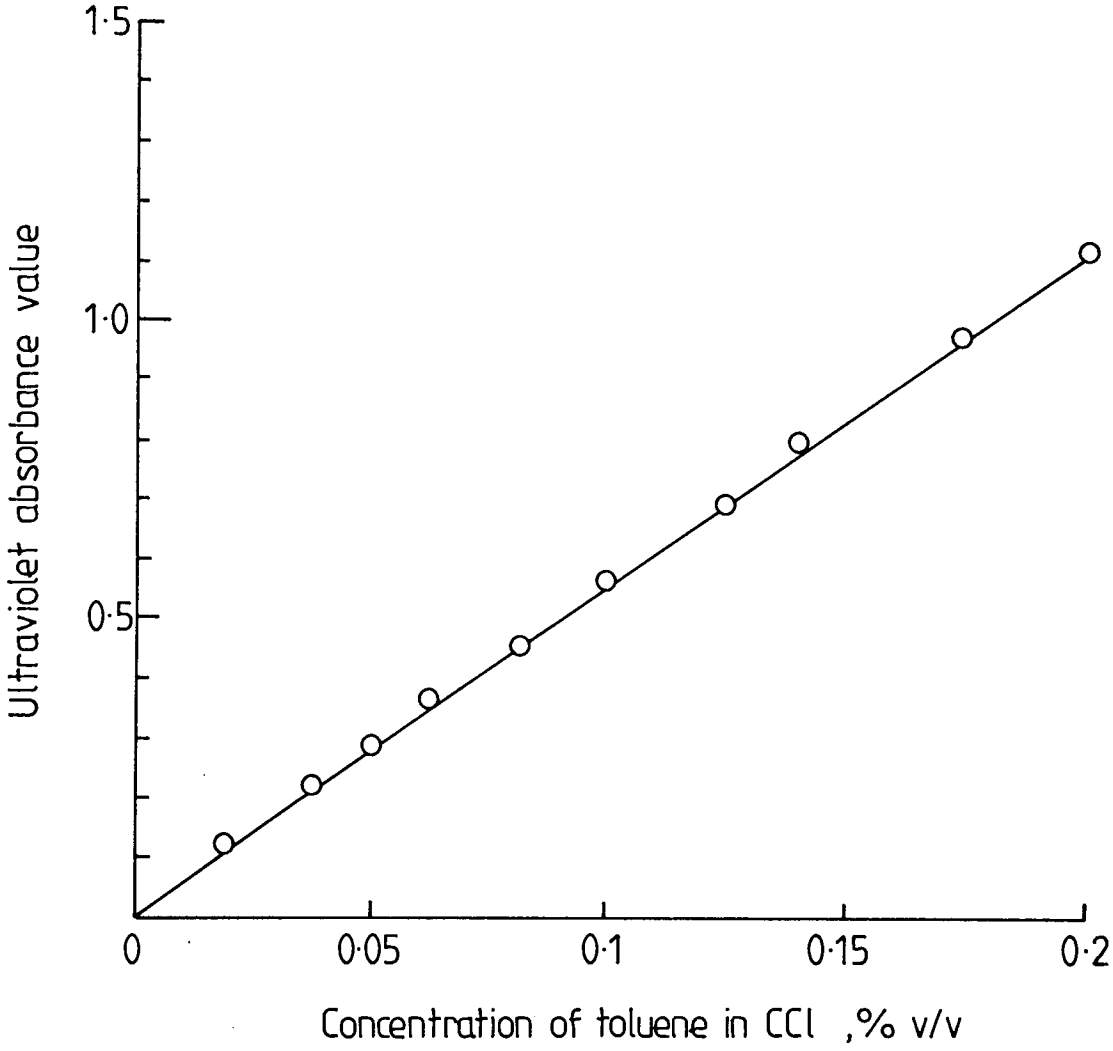

Figure B·6 Ultraviolet absorbance value vs. concentration of toluene in carbon tetrachloride, % v/v

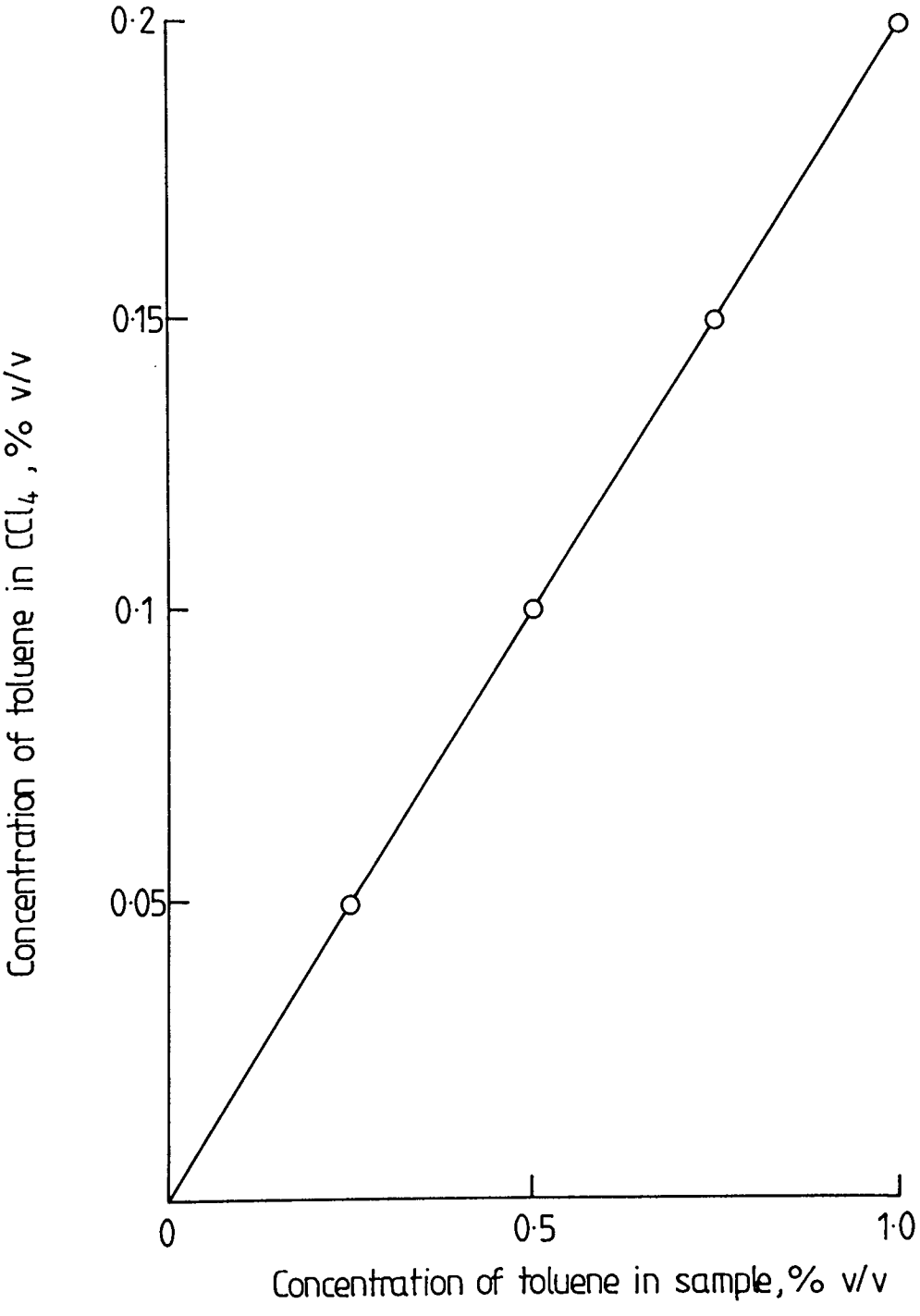

Figure B·7 Concentration of toluene in CCl_4 vs. concentration of toluene in sample.

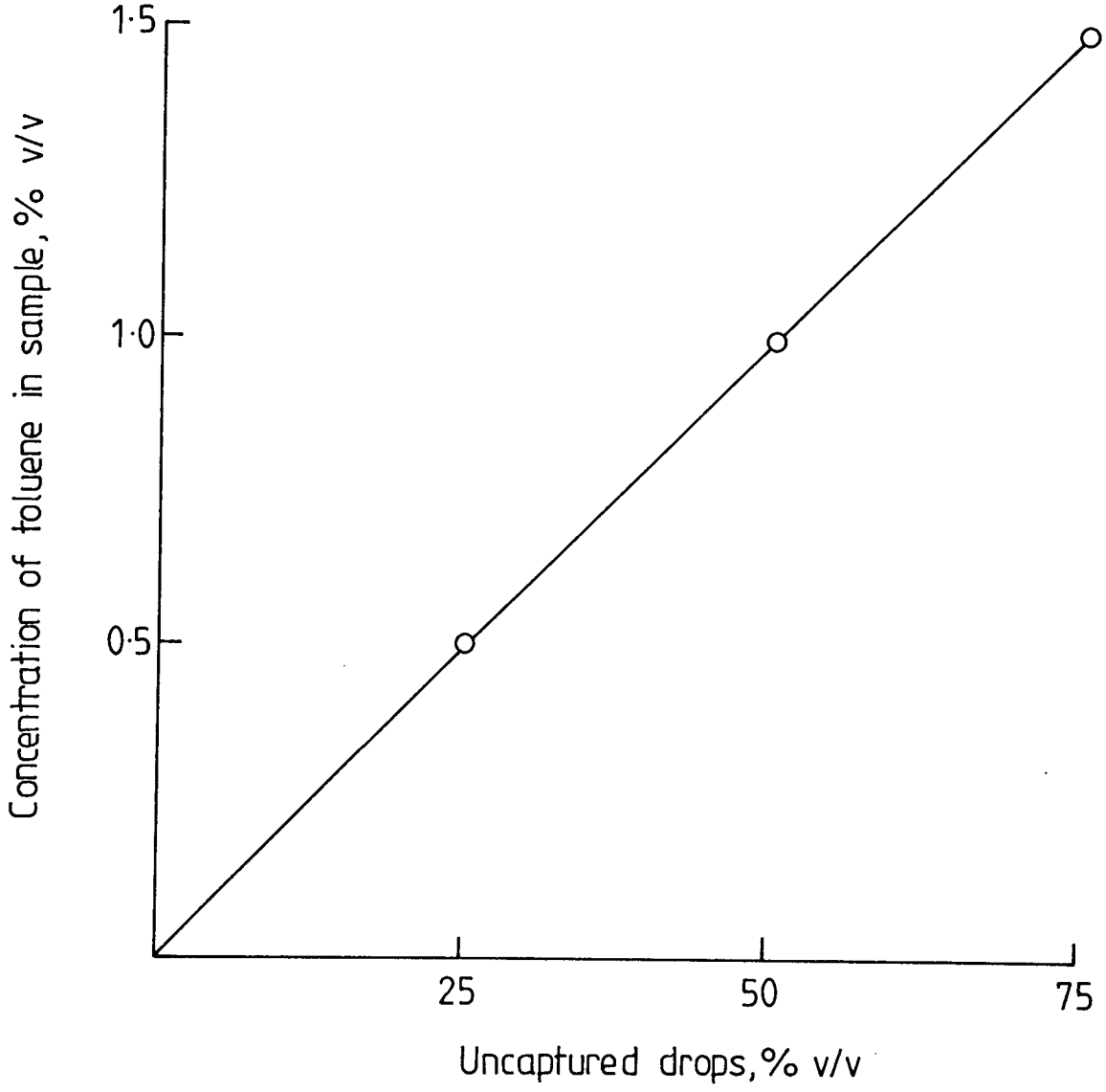

Figure B·8 Concentration of toluene in samples vs. uncaptured drops in outlet stream for 2% inlet phase ratio.

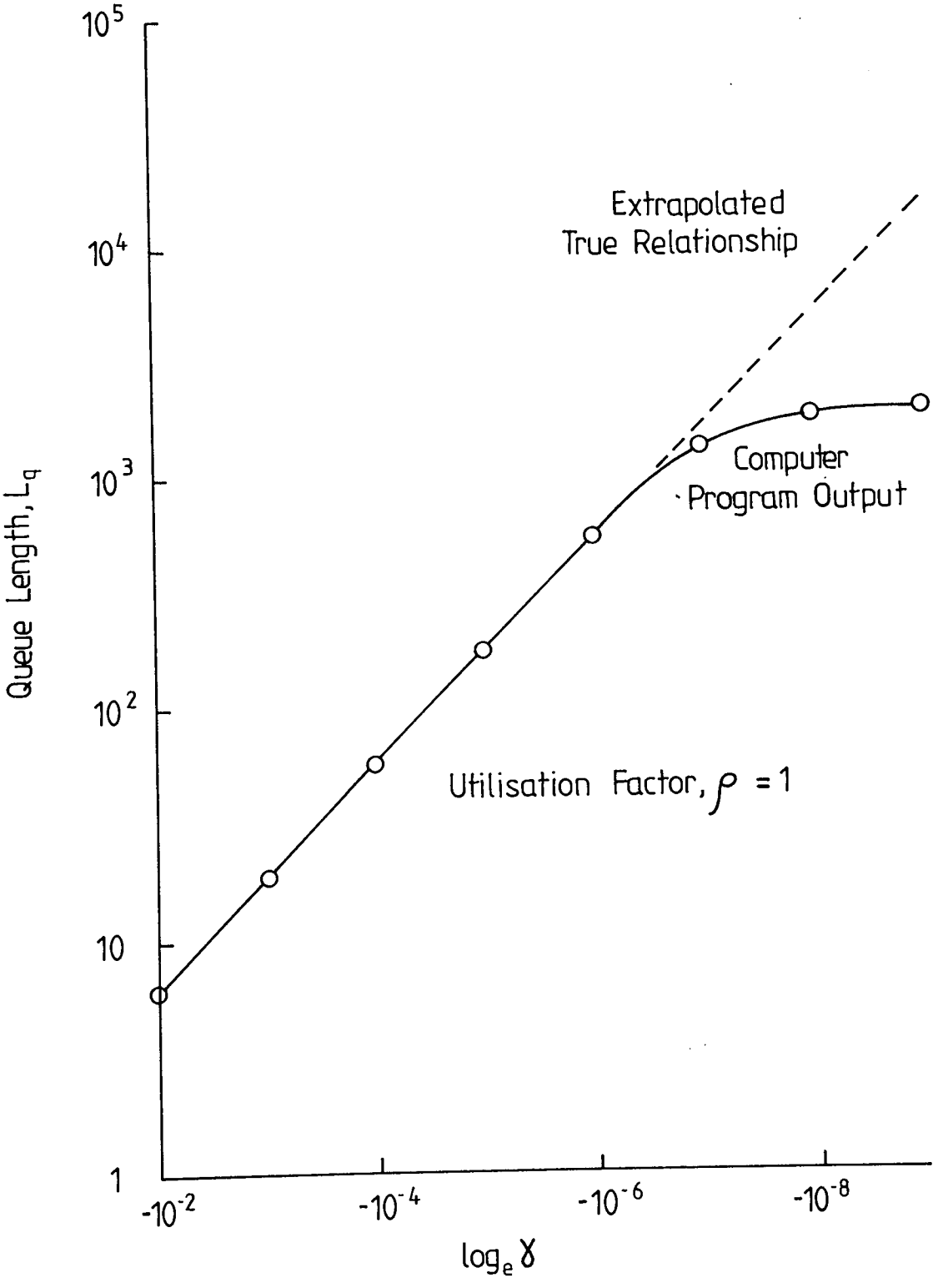

Figure B·9 Variation of Steady State Queue length with degree of 'Balking' [16]

APPENDIX C

BED VOIDAGE DETERMINATION

Packing thickness = 3×10^{-2} m

Datum Reading = 30.4

Volume Collected x 10^{-6} m^3	New Reading x 10^{-2} m	Distance Drop x 10^{-2} m
200	26.1	4.3
200	21.7	4.4
200	17.4	4.3
200	12.9	4.5
200	7.5	5.4

Distance drop per 200 x 10^{-6} m^3 above packing =

$$\frac{4.3 + 4.4 + 4.3 + 4.5}{4} = 4.375 \times 10^{-2} \text{ m}$$

$5.4 \times 10^{-2} - 3.0 \times 10^{-2} = 2.4 \times 10^{-2}$ m. This contains 109.44×10^{-6} m^3 water.

But water collected : 200×10^{-6} m^3

$\therefore$ Hold up of water = $200 \times 10^{-6} - 109.44 \times 10^{-6} = 90.56 \times 10^{-6}$ m^3

Volume of packing = 136.8×10^{-6} m^3

$$\therefore \text{ Packing voidage } e_1 = \frac{136.8 \times 10^{-6} - 90.56 \times 10^{-6}}{136.8 \times 10^{-6}} = 0.338$$

This was repeated three more times with the following results,

$e_1 = 0.305$
$e_1 = 0.338$
$e_1 = 0.371$

$\therefore$ Average value of $e_1 = 0.338$

The same procedure was repeated for each bed depth and ballotini size used. The average voidages obtained are presented in Table 7.2.

APPENDIX D

D: Conductivity Measurement

When operated with single-phase flow all the pores of the packing were occupied by the continuous phase, water. The bed then had a characteristic conductivity. When operated with two phase flow, a number of the pores would be occupied by the oil, thereby changing the conductivity. Since the water formed a continuoum surrounding the fibres increasing the conductivity of the whole, the packing conductivity was greater the higher the proportion of water in the pores. Therefore the difference between the single phase flow conductivity and that with two phase flow could be related to the quantity of oil held-up in the pores of the bed. The greater the difference, the greater the amount of oil retained in the bed.

D-1: Coalescence Device

In a modification of the technique developed by Shalhoub [57], a packing holder with the necessary connections was constructed as shown in plate D-1 and conductivity measurements were taken at different planes in the particulate bed. The holder was constructed from three 4.7×10^{-3} m diameter nylon threaded rods with a thread pitch of 0.8×10^{-3} m , 2BA screw thread, so as to be nonconducting. The five sensing plates were made from copper mesh with 2.0 mm holes. A ptfe insulated silver wire was soldered on each mesh which was sandwiched between two ptfe rings to provide a good seal. A particulate packing was placed between each consecutive pair of meshes, with the wires passing through drilled holes in the glass column. The drilled holes were sealed by a silicone rubber compound which was easily-removable.

D-2 Conductivity Apparatus and Measurement Procedure

The wires from the copper meshes inside the coalescence device were connected

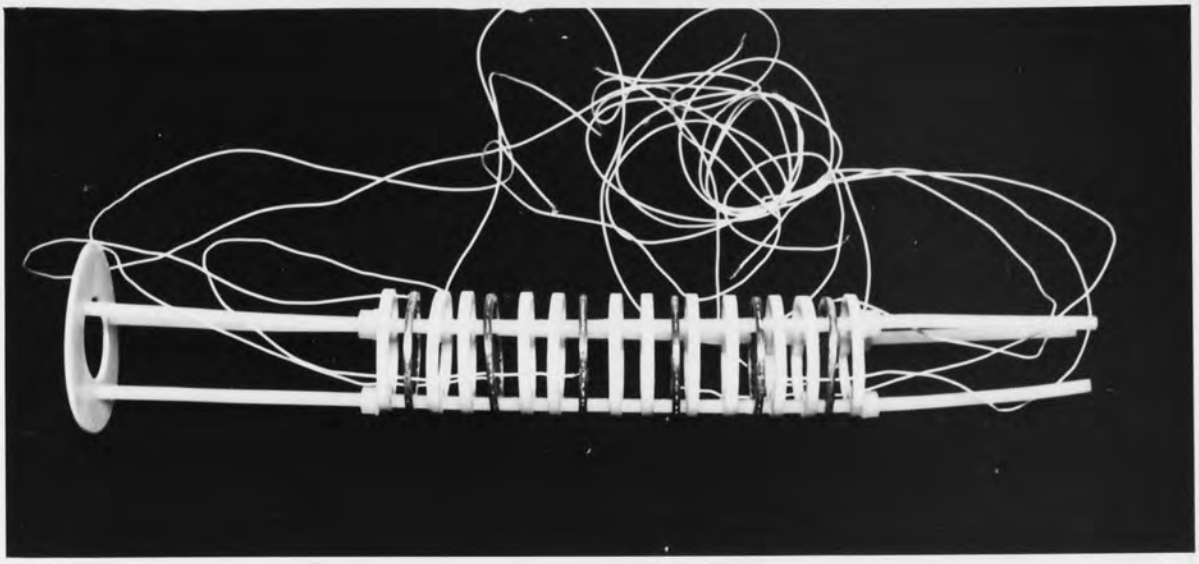

a PACKING HOLDER

(Five copper meshes with 2 mm holes, each one is sandwiched between p.t.f.e rings, three nylon threaded rods and insulated silverwires were soldered onto each copper mesh)

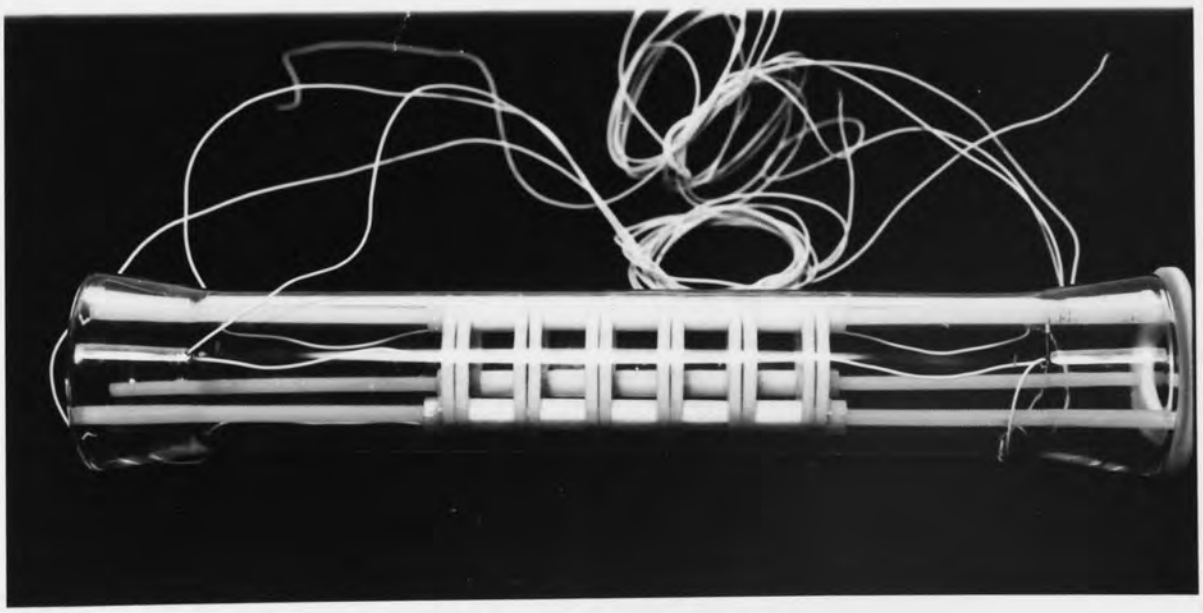

b ARRANGEMENT OF PACKING CELL IN GLASS HOLDER

PLATE D-1 CONDUCTIVITY MEASUREMENT DEVICE

to a junction box possessing a selection switch. The signal was fed into an AC conductivity meter with a range of 0.0 to 10 x 10^6 ohm^{-1} in order to prevent any polarization taking place. From this the conductivity at different planes along the bed could be estimated.

The same operating procedure should be used with the second coalescence device, described in section 5.7. The conductivity values at different planes in the bed could be recorded for both one phase and two phase flow.

The same particulate packing should be used for a set of experiments to examine the effect of inlet drop size, superficial velocity and phase ratio (dispersed phase concentration) on the conductivity values at different planes in the bed. Before starting each experiment, the bed should be washed at high water flow rates to remove any entrapped liquid drops and should be then thoroughly drained.

APPENDIX E

DETERMINATION OF LONDON VAN-DER WAALS CONSTANT

(Hamaker Constant) Q [151, 152, 153]

An equation for the calculation of the London-van-der Waals constant (Hamaker constant) for a system of two immiscible liquids and a solid is presented by Sherony and Kinter [153]. This equation is:

$$Q = 6 \pi r_{22}^2 (\sqrt{\sigma_d^d} - \sqrt{\sigma_c^d}) (\sqrt{\sigma_s^d} - \sqrt{\sigma_c^d}) \quad \text{.... E.1}$$

where r_{22} is the intermolecular distance; σ_c^d, σ_d^d and σ_s^d are London-van der Waals component to the surface tensions of the continuous, dispersed and solid phases, respectively. The terms of equation E.1 were obtained directly from the data of Fowkes [152] for water-hydrocarbon system; $6 \pi r_{22}^2 = 1.44 \times 10^{-18}$ m^2

For water $\sigma_c^d = 0.0218$ N/m

For toluene $\sigma_d^d = 0.0285$ N/m

For example if glass (silica) is used as poacking

glass (silica) $\sigma_s^d = 0.078$ N/m

$\therefore$ The London-van der Waals constant Q:

$Q = 1.44 \times 10^{-18} (\sqrt{0.0285} - \sqrt{0.0218}) (\sqrt{0.078} - \sqrt{0.0213})$

$\therefore$ London Van-der Waals constant $Q = 0.401 \times 10^{-20}$ N

Material (packing)	σ_c^d(N/m)	σ_c^d(N/m)	σ_d^d (N/m)	Q(N)	Liquid-liquid system
Glass	0.078	0.0218	0.0285	0.401×10^{-20}	Toluene/water
Polyethylene	0.053	0.0218	0.0285	0.251×10^{-20}	Toluene/water
Iron	0.108	0.0218	0.0285	0.551×10^{-20}	Toluene/water
Copper	0.060	0.0218	0.0285	0.296×10^{-20}	Toluene/water

APPENDIX F

LAGRANGE'S INTERPOLATION FORMULA [219, 223]

As in the other interpolation methods; it is assumed that the function may be represented by a polynomial, written in the form [219]

$$y = a_1 (x-x_2)(x-x_3)(x-x_4) \ldots (x-x_n)$$
$$+ a_2 (x-x_1)(x-x_3)(x-x_4) \ldots (x-x_n)$$
$$+ a_3 (x-x_1)(x-x_2)(x-x_4) \ldots (x-x_n)$$
$$+ \ldots + a_n (x-x_1)(x-x_2)(x-x_3) \ldots (x-x_{n-1}) \quad \ldots . F.1$$

Substituting y_1, x_1, yields

$$a_1 = \frac{y_1}{(x_1-x_2)(x_1-x_3)(x_1-x_4) \ldots (x_1-x_n)} \quad \ldots . F.2$$

the other constants are obtained by similar substitutions, and:

$$a_n = \frac{y_n}{(x_n-x_1)(x_n-x_2)(x_n-x_3) \ldots (x_n-x_{n-1})} \quad \ldots . F.3$$

Re-writing the polynomial gives:

$$y = y_1 \frac{(x-x_2)(x-x_3)(x-x_4) \ldots (x-x_n)}{(x_1-x_2)(x_1-x_3)(x_1-x_4) \ldots (x_1-x_n)} \quad \ldots . F.4$$

$$+y_2 \frac{(x-x_1)(x-x_3)(x-x_4) \ldots (x-x_n)}{(x_2-x_1)(x_2-x_3)(x_2-x_4) \ldots (x_2-x_n)}$$

$$+ \ldots + y_n \frac{(x-x_1)(x-x_2)(x-x_3) \ldots (x-x_{n-1})}{(x_n-x_1)(x_n-x_2)(x_n-x_3) \ldots (x_n-x_{n-1})} \qquad \ldots \text{F.5}$$

The accuracy of the result naturally depends on how well such an equation fits the data. This must be kept in mind in using Lagrange's formula.

The arithmetic in this method is tedious, therefore, a computer subroutine program in Appendix U implements the method.

APPENDIX G

1 Purpose

GO2CAF performs a simple linear regression with dependent variable y and independent variable x (229)

2 Specification (Fortran only)

```
SUBROUTINE GO2ACAF (N, X, Y, RESULT, IFAIL)
INTEGER N, IFAIL
REAL X(N), Y (N), RESULT (20)
```

3 Description

The routine fits a straight line of the sum:

$$y = a + bx \qquad \text{.... G.1}$$

to the data points:

(x_1, y_1) , (x_2, y_2) .... (x_n, y_n),

such that

$$y_i = a + bx_i + e_i \qquad \text{.... G.2}$$

The routine calculates the regression coefficient, b, the regression constant a, and various other statistical qantities by minimising

$$\sum_{i=1}^{N} e_i^2 \qquad \text{.... G.3}$$

The input data consists of N pairs of observations:

(x_1, y_1), (x_2, y_2) .... (x_n, y_n)

on the independent variable, x, and the dependent variable y, given as two arrays

$[x_i]$, i = 1, 2 .... n

and $[y_i]$, i = 1, 2 .... n

The only quantities calculated for the purpose of this study were,

(a) the regression coefficient, b :-

$$b = \frac{\sum_{i=1}^{N} (x_i - \bar{x})(y_i - \bar{y})}{\sum_{i=1}^{N} (x_i - \bar{x})^2} \qquad \text{.... G.4}$$

Its number in RESULT equals (6). The regression coefficient represents the slope.

(b) The regression constant, a:-

$$a = \bar{y} - b\bar{x} \qquad \text{.... G.5}$$

Its value in RESULT equals (7). The regression constant represents the intercept of the line with the y-axis.

(c) Correlation Coefficient, r:-

$$r = \frac{\sum_{i=1}^{N} (x_i - \bar{x})\ (y_i - \bar{y})}{\sqrt{\sum_{i=1}^{N} (x_i - \bar{x})2 \,.\, \sum_{i=1}^{N} (y_i - \bar{y})^2}} \qquad \text{.... G.6}$$

It s value in RESULT equals (5). The correlation coefficient represents the linearity of the set of points.

4 Parameters

N - integer; N specifies the number of pairs of observations. (N>2). Unchanged on exit.

x - Real array of DIMENSION at least (N)
y - Real array of DIMENSION at least (N)

RESULT - Real array of DIMENSION at least (20) on successful exit.

5 Error Indicators

Errors detected by the routine:-

IFAIL = 1 This indicates that the routine has been enforced with N≤2

IFAIL = 2 This indicates that all N values of at least one of the variables x or y are identical.

APPENDIX H

EVALUATION OF NUMBER OF PARTICLES, NUMBER OF DROPS AND SPECIFIC SURFACE AREA PER UNIT VOLUME OF COALESCER BED

NP = Number of drops per unit volume of bed

surface area = $N_P \pi d_P^2$ H.1

volume = $N_P \pi d_P^3/6$ H.2

Nc = Number of particles per unit volume of bed

surface area = $N_c \pi d_c^2$ H.3

volume = $N_c \pi d_c^3/6$ H.4

e1 = Void fraction of spherical particle

$$Nc = \frac{6(1-e_1)}{\pi d_c^3} \quad \text{..... H.5}$$

e_P = Void fraction of drops

e_2 = Two phase effective voidage

$e_2 = (e_P + e_1) - 1$ H.6

$e_P = (e_2 - e_1) + 1$ H.7

$$N_P = \frac{6(1 - e_P)}{\pi d_P^3} \quad \text{.... H.8}$$

Then,

$$N_P = \frac{6(e_1 - e_2)}{\pi d_P^3} \quad \text{.... H.9}$$

$$\text{specific surface area, } a = \frac{\text{(surface areas of drops) + (surface area of particle)}}{\text{(volume of drops) + (volume of particles)}}$$

.... H.10

$$a = \frac{(6(e_1 - e_2)/d_P) + (6(1 - e_1)/d_c)}{(1 - e_2)} \quad \text{.... H.11}$$

APPENDIX I

RAYLEIGHS METHOD OF DIMENSIONAL ANALYSIS [218]

Rayleighs method of dimensional anaylsis was used to derive a flow equation in which two phase pressure drop across the bed was described as a function of selected variables raised to powers as follows:

$$\Delta P_2 = \emptyset(dc, L, dp, e_1, C_{in}, \mu_c, \rho_c, U, D) \quad \text{.... I.1}$$

For dimensional homogeneity, equation I.1 becomes:

$$\Delta p_2 = k_D\, d_c^{a}\, L^{b}\, d_p^{c}\, e_1^{d}\, C_{in}^{e}\, \mu_c^{f}\, \rho_c^{g}\, U^{h}\, D^{i} \quad \text{.... I.2}$$

where K_D is constant and a, b, c, d, e, f, g, h, and i are the exponents.

Then:

$$\frac{M}{LT^2} = L^a\, L^b\, L^c \left(\frac{L^3}{L^3}\right)^d \left(\frac{L^3}{L^3}\right)^e \left(\frac{M}{LT}\right)^f \left(\frac{M}{L^3}\right)^g \left(\frac{L}{T}\right)^h L^i \quad \text{.... I.3}$$

The individual powers of the fundamental magnitudes L, M, T on the two sides of this relation mst be identical. Three separate equations are therfore obtained.

Equation exponents of L:

$$-1 = a + b + c + 3d - 3d + 3e - 3e - f - 3g + h + i \quad \text{.... I.4}$$

Equation exponents of M: $1 = f + g$ I.5

Equation exponents of T: $-2 = -f - h$ I.6

Then, from equation I.5: $g = 1 - f$ I.7

from equation I.6: $h = 2 - f$ I.8

From equation I.4:

$$a + b + c - f - 3g + h + i = -1 \quad \text{.... I.9}$$

$$i = -1 - a - b - c + f + 3 - 3f - 2 + f \quad \text{.... I.10}$$

$$i = - a - b - c - f \quad \text{.... I.11}$$

Then,

$$\Delta p_2 = k_D\, d_c^{\,a}\, L^b\, d_p^{\,c}\, e_1^{\,d}\, C_{in}^{\,e}\, \mu_c^{\,f}\, \rho_c^{\,1-f}\, U^{2-f}\, D^{-a-b-c-f} \quad \text{.... I.12}$$

or,

$$\Delta p_2 = k_D[\rho_c U^2] \left[\frac{d_c}{D}\right]^a \left[\frac{L}{D}\right]^b \left[\frac{d_p}{D}\right]^c [e_1]^d [C_{in}]^e \left[\frac{\mu_c}{\rho_c UD}\right]^f \quad \text{.... I.13}$$

finally,

$$\left[\frac{\Delta P_2}{\rho_c U^2}\right] = k_D \left[\frac{d_c}{D}\right]^a \left[\frac{L}{D}\right]^b \left[\frac{d_p}{D}\right]^c [e_1]^d [C_{in}]^e \left[\frac{\rho_c UD}{\mu_c}\right]^{-f} \quad \text{.... I.14}$$

or,

$$\left[\frac{\Delta P_2}{\rho_c U^2}\right] = k_D \left[\frac{d_c}{D}\right]^a \left[\frac{L}{D}\right]^b \left[\frac{d_p}{D}\right]^c [e_1]^d [C_{in}]^e [N_{Re}]^{-f} \quad \text{.... I.15}$$

APPENDIX J

THE GAMMA FUNCTION CALCULATION [207]

Definition:

$$\Gamma(n) = \int_0^{\infty} t^{n-1} e^{-t}\, dt \quad n > 0 \qquad \text{.... J.1}$$

$$\Gamma(n) = \frac{\Gamma(n+1)}{n} \text{ at } n < 0 \qquad \text{.... J.2}$$

If n integer:

$$\Gamma(n+1) = n\,\Gamma(n) \qquad \text{.... J.3}$$

and $\Gamma(n) = n!$ if $n = 0, 1, 2, \ldots$ where $0! = 1$ J.4

Also

$$\Gamma(x+1) = \lim_{K \to \infty} \frac{1.2.3 \ldots K}{(x+1)(x+2)\ldots(x+K)} K^x \qquad \text{.... J.5}$$

then

$$\frac{1}{\Gamma(x)} = x\, e^{\gamma x} \prod_{m=1}^{\infty} \{ (1 + \frac{x}{m}) e^{-x/m} \} \qquad \text{.... J.6}$$

This is an infinite product representation for the gamma function where γ is Euler's constant and the equation J.6 becomes:

$$\Gamma(x+1) = \sqrt{2\pi x}\; x^x e^{-x} [\, 1 + \frac{1}{12x} + \frac{1}{288x^2} - \frac{139}{51840x^3} + \ldots\ldots\ldots\ldots]$$

.... J.7

This is termed Stirling's asymptotic series. Letting x = n a positive integer, then a useful approximation for n! where n is large (eg n>10) is given by Stirling's Formula:

$$n! \approx \sqrt{2\pi n}\, n^n\, e^{-n} \qquad \text{.... J.8}$$

For large positive values of x, $\Gamma(x)$ approximates Stirling's asymptotics series is equal:-

$$\Gamma(x) = x^x\, e^{-x} \sqrt{\frac{2\pi}{x}} \left[1 + \frac{1}{12x} + \frac{1}{288x^2} - \frac{139}{51840x^3} - \frac{571}{2488320x^4} + \ldots\ldots \right] \qquad \text{.... J.9}$$

Equation J.9 has been used to calculate the values of gamma function in this work [207].

APPENDIX K

SOLUTION OF AXIAL SECONDARY DISPERSION DIFFUSION EQUATION (ie Equation 11.16) UNDER UNSTEADY STATE CONDITIONS

$$\frac{dc}{dt} = Ea\frac{d^2c}{dl^2} - \frac{U}{e}\frac{dc}{dl} \qquad \text{.... K.1}$$

Equation K.1 could be solved by using the separation of variables technique. This was used by Carberry and Bretton [222] to solve the second order differential equation as follows:

IF $X = 1 - \frac{U}{e}t$ at U and e constant K.2

and $t = t$ K.3

then equation K.1 becomes

$$Ea\frac{d^2c}{dX^2} = \frac{dc}{dt} \qquad \text{.... K.4}$$

Boundary condition:-

$C = Co$	at	$t = 0,$	$x > 0$	.... K.5a
$C = C_1$	at	$t = \infty,$	$x > 0$	.... K.5b
$C = C_1$	at	$x = 0,$	$t > 0$	.... K.5c
$C = C_1$	at	$x = L,$	$t > 0$	.... K.5d

where Co = initial concentration of dispersed phase inside the packing

C_1 = the input concentration of dispersion

To simplify the boundary conditions the change of variable is [223]

$$\emptyset = \frac{C - C_1}{Co - C_1} \qquad \text{.... K.6}$$

Then: equation K.4 becomes:-

$$Ea \frac{d^2\emptyset}{dx^2} = \frac{d\emptyset}{dt} \qquad \text{.... K.7}$$

with boundary conditions as

$$\emptyset = 1 \quad \text{at} \quad t = 0, \quad x > 0 \qquad \text{.... K.8a}$$
$$\emptyset = 0 \quad \text{at} \quad t = \infty, \quad x > 0 \qquad \text{.... K.8b}$$
$$\emptyset = 0 \quad \text{at} \quad x = 0, \quad t > 0 \qquad \text{.... K.8c}$$
$$O = 0 \quad \text{at} \quad x = L, \quad t > 0 \qquad \text{.... K.8d}$$

Partial differential solution of equation K.7

Assume that the solution of equation K.7 is in the form [220, 223, 240],

$$\emptyset = X(x)\, T(t) \qquad \text{.... K.9}$$

where X(x) is a function of x only and T(t) is a function ot t only. When equation K.9 is replaced in equation K.7 there results:

$$X \frac{dT}{dt} = Ea\, T \frac{d^2X}{dx^2} \qquad \text{.... K.10}$$

which may be written :

$$\frac{1}{T} \frac{dT}{dt} = \frac{E_a}{X} \frac{d^2X}{dx^2} \qquad \text{.... K.11}$$

The left hand side of equation K.11 depends upon t, whilst the right-hand side depends only on x. Both sides must therefore be equal to the same constant which, for the sake of the subsequent algebra, is conveniently taken as - χ^2 Ea. This gives two ordinary differential equations [220]

$$\frac{1}{T} \frac{dT}{dt} = -\lambda^2 Ea \qquad \text{.... K.12}$$

and $$\frac{1}{X}\frac{d^2X}{dx^2} = -\lambda^2 \qquad \text{.... K.13}$$

For linear homogeneous equations with constant coefficients; the auxilliary equation gives the general solution, because the solution has two roots of m, which are independent, for second order and one root of m for first order. the solution of equation K.12 is of the form [223]

$$T = e^{mt} \qquad \text{.... K.14}$$

$$\frac{dT}{dt} + \lambda^2 Ea\, T = 0 \qquad \text{.... K.15}$$

$$(m + \lambda^2 Ea)\, e^{mt} = 0 \qquad \text{.... K.16}$$

or,

$$m + \lambda^2 Ea = 0 \qquad \text{.... K.17}$$

Then,

$$m = -\lambda^2 Ea \qquad \text{.... K.18}$$

then $$T = D\, e^{-\lambda^2 Eat} \qquad \text{.... K.19}$$

where D is the integration constant.

The solution of eqution K.13 as follows:

$$\frac{d^2X}{dx^2} + \lambda^2 X = 0 \qquad \text{.... K.20}$$

Here the auxilliary equation is [237]

$$(m^2 + \lambda^2) = 0 \qquad \text{.... K.21}$$

which has roots:-

$$m = \sqrt{\pm \lambda^2} = \pm i\lambda \qquad \text{.... K.22}$$

consequently the general solution of equation K.13

$$X = Ae^{(o+i\lambda)x} + Be^{(o-i\lambda)x} \quad \text{.... K.23}$$

where, as here the roots of the auxillary equation are complex the general solution of equation K.13 may be written in different form as [231]

$$e^{ix} = \cos x + i \sin x \quad (x \text{ real}) \quad \text{.... K.24}$$

then, equation K.23 becomes:

$$X = A \sin \lambda x + B \cos \lambda x \quad \text{.... K.25}$$

The solution of equation K.7 becomes:

$$\emptyset = (A \sin \lambda x + B \cos \lambda x)\, e^{-\lambda^2 Eat} \quad \text{.... K.26}$$

where A, B are arbitrary constants of integration. Since equation K.7 is a linear equation, the most general solution is obtained by summing solutions of type K.25 so that:

$$\emptyset = \sum_{n=1}^{\infty} (A_n \operatorname{Sin} \lambda_n x + B_n \operatorname{Cos} \lambda_n x)\, e^{-\lambda^2 Eat} \quad \text{.... K.27}$$

where A_n, B_n and λ_n are determined by initial and boundary conditions for any particular problem.

Now the boundary condition (K.8b) requires $\emptyset \rightarrow o$, $t \rightarrow \infty$. This will be true only if λ^2 is real and positive; the condition (K.8c) $\emptyset = o$ at $x = o$, requires B_n = zero since Cos o = 1. Then equation K.27 becomes [230, 231]:

$$\emptyset = \sum_{n=1}^{\infty} (A_n \text{ Sin } \lambda_n x)\, e^{-\lambda^2 Eat} \qquad \text{.... K.28}$$

The condition (K.8d) $\emptyset$=o at x + L can be satisfied if:

$$\lambda_n = \frac{n\pi}{L} \qquad \text{.... K.29}$$

where n is a none zero, positive integer.

The solution then has the form:-

$$\emptyset = \sum_{n=1}^{\infty} \left(A_n \text{ Sin } \frac{n\pi}{L} x\right) \text{Exp } [-(n^2\pi^2/L^2)Eat] \qquad \text{.... K.30}$$

which is mean infinite sum of terms having the form of K.30

$$\emptyset = A_1 \text{ Exp } [-(\pi^2/L^2)Eat] \cdot \text{Sin } \frac{\pi x}{L} + A_2 \text{ Exp } [-(4\pi^2 t/L^2)Eat] \cdot \text{Sin } \frac{2\pi x}{L}$$

$$+ A_3 \text{ Exp } [-(9\pi^2 t/L^2)Eat] \cdot \text{Sin } \frac{3\pi x}{L} + ... + A_n \text{ Exp } [-(n^2\pi^2 t/L^2)] \cdot \text{Sin } \frac{n\pi x}{L}$$

.... K.31

The boundary condition (K.8a) then required

$$1 = \sum_{n=1}^{\infty} A_n \sin \frac{n\pi x}{L} \qquad \text{.... K.32}$$

The problem now is to determine the value of An which makes equation K.32 true.

To do this, K.32 is multiplied by (Sin (mπx/L))dx [234], where m is an integer, and the result integrated between O and L [235, 231]:-

$$\int_o^L (\sin (n\pi x/L))dx = \int_o^L (\sin (m\pi x/L)) \left(\sum_{n=1}^{\infty} A_n \text{ Sin } (n\pi x/L)\right) dx \qquad \text{.... K.33}$$

$$\int_o^L (\text{Sin } (n\pi x/L))\, dx = \sum_{n=1}^{\infty} A_n \int_o^L (\text{Sin } (m\pi x/L))\ (\text{Sin } (n\pi x/L))dx$$

Now the integral of each term on the right-hand side of K.34 is zero except when m=n

and

$$\int_0^L \left(\text{Sin}\frac{n\pi x}{L}\right)^2 dx = \frac{L}{2} \qquad \text{....K.35}$$

consequently

$$A_n = \frac{2}{L}\int_0^L \left(\sin\frac{n\pi x}{L}\right) dx = [1-(-1)^n]\frac{2}{n\pi} \qquad \text{.... K.36}$$

The formal solution of the problem is then given by K.30 and K.36. When these two relations are combined, the solution may be written in the form:

$$\emptyset = \sum_{n=1}^{n=\infty} [1-(-1)^n]\frac{2}{n\pi}\cdot \text{Sin}\frac{n\pi}{L}x \cdot \text{Exp}\,[-(n^2\pi^2/L^2)Eat] \qquad \text{.... K.37}$$

But $x = 1 - (U/e)\,t$ K.38

then equation K.37 becomes:

$$\emptyset = \sum_{n=1}^{n=\infty} [1-(-1)^n]\frac{2}{\pi n}[\,\text{sin}\frac{n\pi}{L}(1-(U/e)t]\cdot \text{Exp}\,[-(n^2\pi^2/L^2)Eat]$$

.... K.39

so,

$$\frac{C-C_1}{Co-C_1} = \frac{4}{\pi}(\text{Exp}[-(\pi^2 Eat/L^2)])\cdot \text{Sin}\frac{\pi(1-(U/e)t)}{L} + 0 + 1/3\,(\text{Exp}\,[-(9\pi^2 Eat/L^2)])\cdot$$

$$\text{Sin}\frac{3\pi(1-(U/e)t)}{L} + 0 + 1/5\,(\text{Exp}\,[-(25\pi^2 Eat/L^2)])\cdot \text{Sin}\frac{5\pi(1-(U/e)t)}{L} + \ldots.$$

....K.40

then,

$$\frac{C-C_1}{Co-C_1} = \frac{2}{\pi} \sum_{n=1}^{\infty} \frac{1-(-1)^n}{n} [(\text{Exp}\,[-(n^2\pi^2 Eat/L^2)])\ (\text{Sin}\ \frac{n\pi\,(le-ut)}{e \cdot L})]$$

.... K.41

The analytical solution is then an infinite series.

APPENDIX L

SOLUTION OF AXIAL SECONDARY DIFFUSION EQUATION AT STEADY STATE CONDITION (EQUATION 18):

$$Ea \frac{d^2c}{dl^2} - \frac{U}{e} \frac{dc}{dl} = 0 \qquad \text{.... L.1}$$

when equation 1 is divided by Ea, it becomes:

$$\frac{d^2c}{dl^2} - \frac{U}{e\,E_a} \frac{dc}{dl} \qquad \text{.... L.2}$$

To solve equation 2, it is convenient to introduce the notation of differention operators in which the operation of differentiating C with respect to 1 is written DC. The symbol D thus stands for d/dl, and d^2c/dl is written D^2C. In this notation, Equation 2 becomes:

$$D^2C - \frac{U}{e\,E_a} DC = 0 \qquad \text{.... L.3}$$

or $$D\left(D - \frac{U}{e\,E_a}\right) C = 0 \qquad \text{.... L.4}$$

then, the solution of this equation is [235]

$$C = A + B.\ Exp\ (U/e\,E_a)\cdot \qquad \text{.... L.5}$$

where A and B are arbitrary constants.

APPENDIX M

SOLUTION OF RADIAL SECONDARY DISPERSION DIFFUSION EQUATION (ie Equation 11.26) AT UNSTEADY STATE CONDITION

$$\frac{dc}{dt} = \frac{Er}{r}\frac{d}{dr}\left(r\frac{dc}{dr}\right) \qquad \text{.... M.1}$$

$$\frac{dc}{dt} = \frac{Er}{r}\left[\frac{dc}{dr} + r\frac{d^2c}{dr^2}\right] \qquad \text{.... M.2}$$

$$\frac{dc}{dt} = \frac{Er}{r}\frac{dc}{dr} + Er\frac{d2c}{dr^2} \qquad \text{.... M.3}$$

$$\frac{d^2c}{dr^2} + \frac{1}{r}\frac{dc}{dr} = \frac{1}{Er}\frac{dc}{dt} \qquad \text{.... M.4}$$

Boundary condition:

$C = Co$ at $t = 0$, $r > 0$ M.5a
$C = C1$ at $t = \infty$, $r > 0$ M.5b
$C = Finite$ at $r = 0$, $t > 0$ or alternatively

$$\frac{dc}{dr} = 0 \text{ at } r = 0 \qquad \text{.... M.5c}$$

which is a consequence of the symmetry of the concentration distribution. In the surface condition (220)

$$\left(\frac{dc}{dr}\right)_{r=r_o} + h(C_1 - C) = 0$$

$$\left(\frac{dc}{dr}\right)_{r=r_o} = -h(C_1 - C) \qquad \text{.... M.5d}$$

The solution of (M.4) is somewhat facilitated by "Change of variable", but this is not

necessary and will not be done here. It is now assumed that the solution of (M.4) is of the form (207, 220):

$$C = R(r)\,T(t) \qquad \text{.... M.6}$$

substituting (M.6) into (M.4) as:

$$\frac{R''}{R} + \frac{R'}{rR} = \frac{1}{Er}\,\frac{T'}{T} = -\lambda^2 \qquad \text{.... M.7}$$

where λ is a constant. Two equations result from equation M.7:

$$r^2\,R'' + rR' + \lambda^2 r^2 R = 0 \qquad \text{.... M.8}$$

$$T' + Er\,\lambda^2\,T = 0 \qquad \text{.... M.9}$$

Equation (M.8) is one form of Bessels's equation and has a solution of the form [223]:

$$R = A_1\,r^{1/2}\,J_{1/2}(r)\,\lambda r + A_2\,r^{-1/2}\,J_{-1/2}(r)\,.\,\lambda r \quad \text{at} \quad \lambda \neq 0 \qquad \text{.... M.10a}$$

$$R = A_3 + A_4/_r \quad \text{at} \quad \lambda = 0 \qquad \text{.... M.10b}$$

The solutions of equation M.9 are of the form

$$(m + Er\,\lambda^2)T = 0 \qquad \text{....M.11}$$

If a solution of M.9 is of the form [231]

$$C = e^{mt} \qquad \text{.... M.12}$$

then $$(m + Er\,\lambda^2)\,e^{mt} = 0 \qquad \text{.... M.13}$$

Hence (M.12) is a solution of (M.9) when m is a root of

$$m + Er\,\lambda^2 = 0 \qquad \text{.... M.14}$$

$$m = -\,Er\,\lambda^2 \qquad \text{.... M.15}$$

Then $$T = A_5\, e^{-Er\,\lambda^2 t} \quad \text{at} \quad \lambda \neq 0 \qquad \text{.... M.16a}$$

$$T = A_6 \quad \text{at}\ \lambda = 0 \qquad \text{.... M.16b}$$

However, the Bessel function of half order may be expressed in terms of sines and coses.

Consequently, equation (M.10a) may be written in the form [223]:

$$R = \frac{1}{r}\sqrt{\frac{2}{\lambda\pi}}\,(A_1 \operatorname{Sin}\lambda r + A_2 \operatorname{Cos}\lambda r)$$

Use of (M.10) and (M.16) in (M.6) gives:

$$C = \left(\frac{1}{r}\sqrt{\frac{2}{\lambda\pi}}\right)\left[e^{-Er\lambda^2 t}\,.\,[A \operatorname{Sin}\lambda r + B \operatorname{Cos}\lambda r]\right] + \frac{F}{r} + D \qquad \text{.... M.17}$$

This is a general solution of equation M.1. The boundary condition (M.5b) and M.5c) required

$$B = 0 \text{ and } D = C_1 \qquad \text{.... M.18}$$

Then,

$$C = \sqrt{\frac{2}{\lambda\pi}}\,.\,e^{-Er\lambda^2 t}\,.\,\frac{A}{r}\,.\,(\operatorname{Sin}\lambda r) + C_1 \qquad \text{.... M.19}$$

Differentiation of M.19:

$$\left(\frac{dc}{dr}\right)_{r=ro} = \sqrt{\frac{2}{\lambda\pi}}\,\left(e^{-Er\lambda^2 t}\right)\left(\frac{A\lambda \operatorname{Cos}\lambda r}{r} - \frac{A \sin\lambda r}{r^2}\right) \qquad \text{.... M.20}$$

Substitution of (M.19) and (M.20) into the boundary condition (M.5d) gives,

$$\sqrt{\frac{2}{\lambda\pi}}\, e^{-Er\lambda^2 t}\left(\frac{A\lambda \cos \lambda r}{r} - \frac{A\lambda \sin \lambda r}{r^2}\right) =$$

$$h\sqrt{\frac{2}{\lambda\pi}}\, .\, e^{-Er\lambda^2 t}\, .\, \frac{A}{r} \sin \lambda r \qquad \text{.... M.21}$$

$$\frac{\lambda \cos \lambda r}{r_o} - \frac{\lambda \sin \lambda r}{r_o^2} = h\frac{\sin \lambda r}{r_o} \qquad \text{.... M.22}$$

$$\lambda \cos \lambda r = \sin \lambda r\, .\, (h + \frac{\lambda}{r_o}) \qquad \text{.... M.23}$$

$$\lambda \cos \lambda r = \sin \lambda r.\, (\frac{\lambda + hr_o}{r_o}) \qquad \text{.... M.24}$$

$$\tan \lambda r_o = \frac{\lambda r_o}{\lambda + hr_o} \qquad \text{.... M.25}$$

Equation M.25 is a transenal equation and for specific values of r_o, h an infinte number of values of λ, λ_o λ_1 ... λ_n satisfy equation M.25. Denoting the values of λ which satisfy M.25 by the generic term λ_n then M.19 becomes:

$$C\text{-}C1 = \sqrt{\frac{2}{\lambda_n\pi}}\, e^{-Er\lambda_n^2 t}\, .\, \frac{A \sin \lambda_n r}{r} \qquad \text{.... M.26}$$

The boundary condition M.5a requires:

$$C_o - C_1 = \sqrt{\frac{2}{\lambda_n \pi}} \frac{A \sin \lambda_n r}{r} \qquad \text{.... M.27}$$

Again is is clear that no single value of A will Satisfy M.26 for all values of r and equation M.26 only represents the form of the final solution.

The original differential equation is satisfied by a solution which consists of sum of terms each of the form of M.26. Consequently, the solution is taken as:

$$C - C1 = \sum_n \sqrt{\frac{2}{\lambda_n \pi}} \frac{An \sin \lambda_n r}{r} . e^{-Er\lambda_n^2 t} \qquad \text{.... M.28}$$

Then equation M.27 becomes:

$$C_o - C_1 = \sum_n \sqrt{\frac{2}{\lambda_n \pi}} \frac{A_n \sin \lambda_n r}{r} \qquad \text{....M.29}$$

It remains to be determined if the constant An can be obtained by making use of the properties of orthogonal function:-

Solution of equation M.8 is in form

$$\text{Ø}n(r) = \sqrt{2/\lambda_n \pi}\, [(\sin \lambda_n r)/r] \qquad \text{.... M.30}$$

$f(x) = f(r) = To\text{-}T_1$ which represented by equation M.29 hold over the range $0 \leq r \leq r_o$. At r=o the boundary condition M.5c in form of dc/dr = 0 is equivalent to dr/dr =0 which satisfied the orthogonal function.

At $r=r_o$ in the form as R + b(dR/dr) by virtue of M.19 and M.20 and is equivalent to M.25.

The differential equation M.8 may be compared with orthogonal functions to give [220]:-

$$g_o(r) = r^2,\ g_1(x) = 2r$$

$$g_2(r) = o,\ a = \lambda^2,\ g_c(x) = r^2 \qquad \text{.... M.31}$$

then: $P(r) = e^{\int(2r/r^2)dr} = e^{\ln r^2} = r^2$

$$q(r) = 0$$

$$r(r) = \frac{r^2}{r^2} r^2 = r^2 \qquad \text{.... M.32}$$

So;

$$\text{Øn}(r) = \sqrt{\frac{2}{\lambda_n \pi}} \frac{\text{Sin } \lambda_n r}{r} \qquad \text{.... M.33}$$

and by using this orthogonal function

$$An = \frac{\int_a^b r(x)\, \text{Ø}_n(x)\, f(x)\, dx}{\int_a^b r(x)\, [\text{Ø}_n(x)]^2\, dx} \qquad \text{.... M.34}$$

then,

$$An = \frac{\int_o^{r_o} (r^2) \sqrt{2/\lambda_n \pi}\, [\text{Sin } \lambda_n r/r]\, (C_o - C_1)\, dr}{\int_o^{ro} (r^2)\, (2/\lambda_n \pi)\, [\text{Sin}^2 \lambda_n r/r^2]\, dr} \qquad \text{.... M.35}$$

Finally,

$$An = [Co\text{-}C1] \left[\frac{\sqrt{2\lambda_n \pi}}{r_o}\right] \left(\frac{\text{Sin } \lambda_n r_o}{\lambda_n^2} - r_o \frac{\cos \lambda_n r_o}{\lambda_n}\right) \text{.... M.36}$$

$$\frac{C-C_1}{C_o-C_1} = \frac{\sqrt{2\lambda_n\pi}}{r_o}\left(\frac{\text{Sin}\,\lambda_n r_o}{\lambda_n^2} - r_o\frac{\text{Cos}\,\lambda_n r_o}{\lambda_n}\right)$$

$$\sum_n \sqrt{\frac{2}{\lambda_n \pi}} . e^{-Er\lambda_n^2 t} . \left(\frac{\text{Sin}\,\lambda_n r}{r}\right) \qquad \text{.... M.37}$$

APPENDIX N

SOLUTION OF RADIAL SECONDARY DISPERSION DIFFUSION EQUATION UNDER STEADY STATE CONDITIONS (ie Equation 28)

$$\frac{Er}{r} \cdot \frac{d}{dr}\left(r \frac{dc}{dr}\right) = 0 \qquad \text{.... N.1}$$

The integration of equation (N.1) is

$$\int \frac{d}{dr}\left(r \frac{dc}{dr}\right) = 0 \qquad \text{.... N.2}$$

$$r \frac{dc}{dr} = B \qquad \text{.... N.3}$$

where B is the integration constant. The integration of equation N.3 is:

$$\int \frac{dc}{B} = \int \frac{r}{dr} \qquad \text{.... N.4}$$

then,

$$^1/_B \cdot C = \ln r + F \qquad \text{.... N.5}$$

where F is the integration constant.

or $C = B \ln r + A$ N.6

where A is the integration constant = BF.

IF C at r = a equals to C_1

IF C at r = b equals to C_2

then,

$$C_1 = A + B \ln a \qquad \text{.... N.7}$$

$$C_2 = A + B \ln b \qquad \text{.... N.8}$$

therefore,

$$B = (C_2 - C_1) / \ln (b/a) \qquad \text{.... N.9}$$

and,

$$A = C_1 - \frac{C_2 - C_1}{\ln (b/a)} . \ln a \qquad \text{.... N.10}$$

Then,

$$A = \frac{C_1 \ln b - C_2 \ln a}{\ln (b/a)} \qquad \text{.... N.11}$$

Th solution of equation (N.6) at $a < r < b$ becomes:

$$C = \frac{C_1 \ln b - C_2 \ln a}{\ln (b/a)} + \frac{C_2 - C_1}{\ln b/a} \qquad \text{.... N.12}$$

or

$$C = \frac{C_1 (\ln b - \ln r) + C_2 (\ln r - \ln a)}{\ln (b/a)} \qquad \text{.... N.13}$$

Then,

$$C = \frac{C_1 \ln (b/r) + C_2 \ln (r/a)}{\ln (b/a)} \qquad \text{.... N.14}$$

APPENDIX Q

PREDICTION OF NUMBER OF CAPILLARIES INSIDE THE PACKED BEDS [27]

The following steps were used in the determination of the number of capillaries inside the packed beds by using the equations described in Section 11.2.

The data used is:

$d_c = 266 \times 10^{-6}$ m

$K = 6.43$

$\mu_c = 1.0 \times 10^{-3}$ Nsm^{-2}

$D = 7.62 \times 10^{-2}$ m

$C_{in} =$ 2% v/v

$U = 3.05 \times 10^{-6}$ ms^{-1}

$L = 0.03$ m

The value of ΔP used is the overall value of two-phase pressure drop less the overall single-phase pressure drop, ie $\Delta P = P_2 - P_1$

therefore, $\Delta P = 13001 - 2870 = 10131$ Nm^{-2}

From equation 11.35,

$A_{cap} = 0.121 \times (266 \times 10^{-6})^2 = 0.856 \times 10^{-8}$ m^2

$d_H = 0.177 \times 266 \times 10^{-6} = 47.082 \times 10^{-6}$ m

Equation 11.44 gives,

$$U_{cap} = \frac{d_H^2}{2K\mu_c} \cdot \frac{\Delta P}{\Delta_L} = 5.821 \times 10^{-2} \text{ ms}^{-1}$$

$$Q = \frac{\pi D^2}{4} . C. U = 0.278 \times 10^{-6}$$

$$q = A_{cap} . U_{cap} = 0.856 \times 10^{-8} \times 5.821 \times 10^{-2}$$
$$= 4.983 \times 10^{-10}$$

$$\text{No of capillaries} = \frac{Q}{q} = \frac{0.278 \times 10^{-6}}{4.983 \times 10^{-10}} = 557.896$$

Number of channels inside the bed ≈ 558.

APPENDIX P

PREDICTION OF EXIT DROP SIZE

Scheele andMeister [232] proposed the following correlation to predict the volume of an exit drop from a single nozzle,

$$V_{Pe} = F' \frac{\pi \gamma d_H}{g \Delta \rho} + \frac{4.5\, q^2 d_H^2 \rho_d \gamma^{1/3}}{(g \Delta \rho)^2} - \frac{4 \rho_d q U_{cap}}{3 g \Delta \rho} + \frac{20 \mu q d_H}{d_{Pe}^2 g \Delta \rho} \quad \text{.... P.1}$$

where V_{Pe} is the volume of the exit drop, d_{Pe} the diameter of exit drop and F' is the Harkins-Brown correlation factor.

The term d_{Pe} is negligible when the continuous phase viscosity is less than 1×10^{-2} Nms^{-2} and Harkins-Brown correlation factor = 1.0 [27]. Then $V_{Pe} = 3.098 \times 10^{-9}$ m^3 and the predicted exit drop size $d_{Pe} = 1.8086 \times 10^{-3}$ m or $d_{Pe} \approx 1.8$ mm. The experimental exit drop size was 0.83 mm.

APPENDIX Q

DERIVATION OF QUEUE LENGTH EQUATION

The following steps were used in the derivation of the queue length, Lq, equation.

Let $n+1 = k$, then for $0<n<c$, the difference equation becomes [225],

$$P_k = \frac{1}{k}[(\rho + (k-1))P_{k-1} - \rho P_{k-2}],\ 2 \le k \le c \qquad \text{.... Q.1}$$

Also the difference equation corresponding to $n \ge c$ becomes [225]:

$$P_k = \frac{1}{c}[(\rho + c)P_{k-1} - \rho P_{k-2}],\ k \ge c+1 \qquad \text{.... Q.2}$$

These two equations, together with the difference equation for n=o, can now be used in the induction procedure.

The value of P_o is determined from

$$\sum_{n=o}^{\infty} P_n = 1 \qquad \text{.... Q.3}$$

which gives [151],

$$P_o = \left[\sum_{n=o}^{c-1} \frac{\rho^n}{n!} + \frac{\rho^c}{c!}\sum_{n=c}^{\infty} \frac{\rho^{n-c}}{c^{n-c}}\right]^{-1} \qquad \text{.... Q.4}$$

$$P_o = \left[\sum_{n=o}^{c-1} \frac{\rho^n}{n!} + \frac{\rho^c}{c!}\left(\frac{1}{1-\rho/c}\right)\right]^{-1},\ \frac{\rho}{c} < 1 \qquad \text{.... Q.5}$$

The expression for Lq is obtained as follows [225]:

$$Lq = \sum_{n=c}^{\infty}(n-c)Pn = \sum_{k=o}^{\infty} kP_{k+c} = \sum_{k=o}^{\infty} \frac{k\rho^{k+c}}{c^k c!} P_o \qquad \text{.... Q.6}$$

Then,

$$Lq = P_o \frac{\rho^c}{c!} \frac{\rho}{c} \sum_{k=o}^{\infty} k \left(\frac{\rho}{c}\right)^{k-1} = Po \frac{\rho^c}{c!} \frac{\rho}{c} \left(\frac{1}{(1-\rho/c)^2}\right) \quad \text{.... Q.7}$$

Finally,

$$Lq = \left[\frac{\rho^{c+1}}{(c-1)!\,(c-\rho)^2}\right] P_o = \left(\frac{c\rho}{(c-\rho)^2}\right) P_c \quad \text{.... Q.8}$$

APPENDIX R

Computer program for Evaluation of

i) Tabulation of Experimental Single Phase Pressure Drop Data

ii) Mean and standard deviation of Superficial Velocity

iii) Mean and standard deviation of Single Phase Pressure Drop

iv) Correlation Coefficient for (ii) and (iii)

```
C THIS PROGRAM FOR ANALYSIS OF SINGLE PHASE PRESSURE DROP DATA:
C ============================================================
C
C
C
      DIMENSION X(999),PR1(999),Y(999),DC(999),BD(999)
      REAL N,NBAD,MEANX,MEANY
      INTEGER EXPN
       PRINT 35
  35  FORMAT(9X,' SINGLE-PHASE PRESSURE DROP EXPERIMENTAL',
     @' DATA',/,9X,46('-')///)
C
C
       READ *,L
        READ *,(DC(KK),BD(KK),KK=1,L)
         READ *,NPT
        READ *,(X(II),II=1,NPT)
C
C
       DO 2 K=1,L
        EXPN=K
        PRINT 210,EXPN
  210  FORMAT(6X,'EXPERIMENT NUMBER=',I4,'A',/,6X,28('-')/)
C
C
      PRINT 222,DC(K),BD(K)
 222  FORMAT(5X,'BALLOTINI PARTICLE DIAMETER (MICRONS)=',F6.1,//
     @,5X,'COALESCER BED DEPTH (MM.)=',F6.1,//)
C
C
       PRINT 211
  211  FORMAT(9X,'SUPERFICIAL VELOCITY(1/1000)  PRESSURE DROP',
     @'(KN/M**2)',/,9X,60('-'))
C
       READ *,(Y(NN),NN=1,NPT)
C
        DO 11 I=1,NPT
        PR1(I)=Y(I)
C
        PRINT 150,X(I),PR1(I)
  150  FORMAT(10X,F10.3,20X,F10.3)
  11     CONTINUE
C
      SUMX=0.0
      SUMY=0.0
      SUMXSQ=0.0
      SUMYSQ=0.0
      SUMXY=0.0
      N=0.0
       DO 15 I=1,NPT
        SUMX=SUMX+X(I)
        SUMY=SUMY+Y(I)
        SUMXSQ=SUMXSQ+X(I)**2.0
        SUMYSQ=SUMYSQ+Y(I)**2.0
```

```
        SUMXY=SUMXY+X(I)*Y(I)
         N=N+1.0
  15   CONTINUE
C
C
C COMPUTER TENTATIVE DISTRIBUTION OFF BAD ONES FROM SUMS
C
      MEANX=SUMX/N
      MEANY=SUMY/N
      SDEVX=SQRT(N*SUMXSQ-SUMX**2)/N
      SDEVY=SQRT(N*SUMYSQ-SUMY**2)/N
       I=1
       NBAD=0.0
C
C CHECK ALL DATA POINTS,SUBTRACTION OFF BAD ONES FROM SUMS
C
  30   IF(ABS(X(I)-MEANX).LT.3.0*SDEVX.AND.ABS(Y(I)-MEANY)
     @.LT.3.0*SDEVY) THEN
       GO TO 40
       ELSE
        SUMX=SUMX-X(I)
        SUMY=SUMY-Y(I)
        SUMXSQ=SUMXSQ-X(I)**2.0
        SUMYSQ=SUMYSQ-Y(I)**2.0
        SUMXY=SUMXY-X(I)*Y(I)
          NBAD=NBAD+1.0
         ENDIF
  40    I=I+1
        AI=I
        IF(AI.LE.N) THEN
         GO TO 30
         ELSE
C   CHECK WHETHER THERE WERE TOO MANY ERRORS
C
         IF (NBAD.LT.(0.03*N)) THEN
          GO TO 50
           ELSE
          PRINT 200,NBAD
 200    FORMAT(6X,I3,'ERROR FOUND',//)
        ENDIF
         ENDIF
         STOP
C
C
  50  N=N-NBAD
C
C  COMPUTE ALL VALUE
C  =================
C
          MEANX=SUMX/N
          MEANY=SUMY/N
          XFACTR=SQRT(N*SUMXSQ-SUMX**2)
          YFACTR=SQRT(N*SUMYSQ-SUMY**2)
          SDEVX=XFACTR/N
```

```
          SDEVY=YFACTR/N
          CORRLN=(N*SUMXY-SUMX*SUMY)/(XFACTR*YFACTR)
C
       PRINT 300,N,MEANX,MEANY,SDEVX,SDEVY,CORRLN
 300   FORMAT(/,9X,'NUMBER OF (GOOD) DATA POINTS=',F5.0,//,
     @9X,'MEAN OF X DISTRIBUTION=',F14.6,//,
     @9X,'MEAN OF Y DISTRIBUTION=',F14.6,//,
     @9X,'STANDARD DEVIATION OF X DISTRIBUTION=',F14.6,//,
     @9X,'STANDARD DEVIATION OF Y DISTRIBUTION=',F14.6,//,
     @9X,'CORRELATION COEFFICIENT=',F14.6,//)
  5    CONTINUE
  2     CONTINUE
       STOP
        END
```

SINGLE-PHASE PRESSURE DROP EXPERIMENTAL DATA

EXPERIMENT NUMBER= 1A

BALLOTINI PARTICLE DIAMETER (MICRONS)= 146.0

COALESCER BED DEPTH (MM.)= 20.0

SUPERFICIAL VELOCITY(1/1000)	PRESSURE DROP(KN/M**2)
0.000	0.000
0.800	0.844
1.030	1.182
1.500	1.520
2.500	2.533
3.050	3.039
3.600	3.546
4.750	4.728
6.000	5.910

NUMBER OF (GOOD) DATA POINTS= 9.

MEAN OF X DISTRIBUTION= 2.581111

MEAN OF Y DISTRIBUTION= 0.766667

STANDARD DEVIATION OF X DISTRIBUTION= 1.857917

STANDARD DEVIATION OF Y DISTRIBUTION= 0.536967

CORRELATION COEFFICIENT= 0.999675

EXPERIMENT NUMBER= 2A

BALLOTINI PARTICLE DIAMETER (MICRONS)= 146.0

COALESCER BED DEPTH (MM.)= 30.0

SUPERFICIAL VELOCITY(1/1000)	PRESSURE DROP(KN/M**2)
0.000	0.000
0.800	1.013
1.030	1.182
1.500	1.688
2.500	2.870
3.050	3.546

3.600	4.052
4.750	5.572
6.000	6.923

NUMBER OF (GOOD) DATA POINTS= 9.

MEAN OF X DISTRIBUTION= 2.581111

MEAN OF Y DISTRIBUTION= 0.883333

STANDARD DEVIATION OF X DISTRIBUTION= 1.857917

STANDARD DEVIATION OF Y DISTRIBUTION= 0.635085

CORRELATION COEFFICIENT= 0.999647

EXPERIMENT NUMBER= 3A

BALLOTINI PARTICLE DIAMETER (MICRONS)= 146.0

COALESCER BED DEPTH (MM.)= 40.0

SUPERFICIAL VELOCITY(1/1000)	PRESSURE DROP(KN/M**2)
0.000	0.000
0.800	1.182
1.030	1.351
1.500	2.026
2.500	3.208
3.050	3.883
3.600	4.559
4.750	5.910
6.000	7.598

NUMBER OF (GOOD) DATA POINTS= 9.

MEAN OF X DISTRIBUTION= 2.581111

MEAN OF Y DISTRIBUTION= 0.977778

STANDARD DEVIATION OF X DISTRIBUTION= 1.857917

STANDARD DEVIATION OF Y DISTRIBUTION= 0.683988

CORRELATION COEFFICIENT= 0.999658

EXPERIMENT NUMBER= 4A

BALLOTINI PARTICLE DIAMETER (MICRONS)= 266.0

COALESCER BED DEPTH (MM.)= 10.0

SUPERFICIAL VELOCITY(1/1000)	PRESSURE DROP(KN/M**2)
0.000	0.000
0.800	0.507
1.030	0.675
1.500	1.182
2.500	1.857
3.050	2.364
3.600	2.702
4.750	3.546
6.000	4.390

NUMBER OF (GOOD) DATA POINTS= 9.

MEAN OF X DISTRIBUTION= 2.581111

MEAN OF Y DISTRIBUTION= 0.566667

STANDARD DEVIATION OF X DISTRIBUTION= 1.857917

STANDARD DEVIATION OF Y DISTRIBUTION= 0.410961

CORRELATION COEFFICIENT= 0.998989

EXPERIMENT NUMBER= 5A

BALLOTINI PARTICLE DIAMETER (MICRONS)= 266.0

COALESCER BED DEPTH (MM.)= 20.0

SUPERFICIAL VELOCITY(1/1000)	PRESSURE DROP(KN/M**2)
0.000	0.000
0.800	0.675
1.030	0.844
1.500	1.351
2.500	2.195
3.050	2.702
3.600	3.208
4.750	4.221
6.000	5.234

NUMBER OF (GOOD) DATA POINTS= 9.

MEAN OF X DISTRIBUTION= 2.581111

MEAN OF Y DISTRIBUTION= 0.672222

STANDARD DEVIATION OF X DISTRIBUTION= 1.857917

STANDARD DEVIATION OF Y DISTRIBUTION= 0.485976

CORRELATION COEFFICIENT= 0.999772

EXPERIMENT NUMBER= 6A

BALLOTINI PARTICLE DIAMETER (MICRONS)= 266.0

COALESCER BED DEPTH (MM.)= 30.0

SUPERFICIAL VELOCITY(1/1000)	PRESSURE DROP(KN/M**2)
0.000	0.000
0.800	0.844
1.030	1.013
1.500	1.520
2.500	2.364
3.050	2.870
3.600	3.546
4.750	4.559
6.000	5.741

NUMBER OF (GOOD) DATA POINTS= 9.

MEAN OF X DISTRIBUTION= 2.581111

MEAN OF Y DISTRIBUTION= 0.738889

STANDARD DEVIATION OF X DISTRIBUTION= 1.857917

STANDARD DEVIATION OF Y DISTRIBUTION= 0.523757

CORRELATION COEFFICIENT= 0.999628

EXPERIMENT NUMBER= 7A

BALLOTINI PARTICLE DIAMETER (MICRONS)= 266.0

COALESCER BED DEPTH (MM.)= 40.0

SUPERFICIAL VELOCITY(1/1000)	PRESSURE DROP(KN/M**2)
0.000	0.000
0.800	1.013
1.030	1.351
1.500	1.688

2.500	2.702
3.050	3.377
3.600	4.052
4.750	5.234
6.000	6.416

NUMBER OF (GOOD) DATA POINTS= 9.

MEAN OF X DISTRIBUTION= 2.581111

MEAN OF Y DISTRIBUTION= 0.850000

STANDARD DEVIATION OF X DISTRIBUTION= 1.857917

STANDARD DEVIATION OF Y DISTRIBUTION= 0.585947

CORRELATION COEFFICIENT= 0.999106

EXPERIMENT NUMBER= 8A

BALLOTINI PARTICLE DIAMETER (MICRONS)= 266.0

COALESCER BED DEPTH (MM.)= 50.0

SUPERFICIAL VELOCITY(1/1000)	PRESSURE DROP(KN/M**2)
0.000	0.000
0.800	1.182
1.030	1.520
1.500	2.195
2.500	3.377
3.050	4.052
3.600	4.897
4.750	6.247
6.000	7.936

NUMBER OF (GOOD) DATA POINTS= 9.

MEAN OF X DISTRIBUTION= 2.581111

MEAN OF Y DISTRIBUTION= 1.033333

STANDARD DEVIATION OF X DISTRIBUTION= 1.857917

STANDARD DEVIATION OF Y DISTRIBUTION= 0.716860

CORRELATION COEFFICIENT= 0.999572

EXPERIMENT NUMBER= 9A

BALLOTINI PARTICLE DIAMETER (MICRONS)= 364.0

COALESCER BED DEPTH (MM.)= 20.0

SUPERFICIAL VELOCITY(1/1000)	PRESSURE DROP(KN/M**2)
0.000	0.000
0.800	0.675
1.030	0.844
1.500	1.182
2.500	2.026
3.050	2.364
3.600	2.870
4.750	3.883
6.000	4.728

NUMBER OF (GOOD) DATA POINTS= 9.

MEAN OF X DISTRIBUTION= 2.581111

MEAN OF Y DISTRIBUTION= 0.611111

STANDARD DEVIATION OF X DISTRIBUTION= 1.857917

STANDARD DEVIATION OF Y DISTRIBUTION= 0.437021

CORRELATION COEFFICIENT= 0.999500

EXPERIMENT NUMBER= 10A

BALLOTINI PARTICLE DIAMETER (MICRONS)= 364.0

COALESCER BED DEPTH (MM.)= 30.0

SUPERFICIAL VELOCITY(1/1000)	PRESSURE DROP(KN/M**2)
0.000	0.000
0.800	0.675
1.030	1.013
1.500	1.351
2.500	2.364
3.050	2.702
3.600	3.377
4.750	4.390
6.000	5.403

NUMBER OF (GOOD) DATA POINTS= 9.

MEAN OF X DISTRIBUTION= 2.581111

MEAN OF Y DISTRIBUTION= 0.700000

STANDARD DEVIATION OF X DISTRIBUTION= 1.857917

STANDARD DEVIATION OF Y DISTRIBUTION= 0.501110

CORRELATION COEFFICIENT= 0.999262

EXPERIMENT NUMBER= 11A

BALLOTINI PARTICLE DIAMETER (MICRONS)= 364.0

COALESCER BED DEPTH (MM.)= 40.0

SUPERFICIAL VELOCITY(1/1000)	PRESSURE DROP(KN/M**2)
0.000	0.000
0.800	0.844
1.030	1.182
1.500	1.688
2.500	2.702
3.050	3.208
3.600	3.883
4.750	4.897
6.000	6.247

NUMBER OF (GOOD) DATA POINTS= 9.

MEAN OF X DISTRIBUTION= 2.581111

MEAN OF Y DISTRIBUTION= 0.811111

STANDARD DEVIATION OF X DISTRIBUTION= 1.857917

STANDARD DEVIATION OF Y DISTRIBUTION= 0.568027

CORRELATION COEFFICIENT= 0.999502

EXPERIMENT NUMBER= 12A

BALLOTINI PARTICLE DIAMETER (MICRONS)= 487.0

COALESCER BED DEPTH (MM.)= 30.0

SUPERFICIAL VELOCITY(1/1000)	PRESSURE DROP(KN/M**2)
0.000	0.000
0.800	0.507

1.030	0.844
1.500	1.182
2.500	1.857
3.050	2.364
3.600	2.702
4.750	3.715
6.000	4.559

NUMBER OF (GOOD) DATA POINTS= 9.

MEAN OF X DISTRIBUTION= 2.581111

MEAN OF Y DISTRIBUTION= 0.583333

STANDARD DEVIATION OF X DISTRIBUTION= 1.857917

STANDARD DEVIATION OF Y DISTRIBUTION= 0.422953

CORRELATION COEFFICIENT= 0.999204

EXPERIMENT NUMBER= 13A

BALLOTINI PARTICLE DIAMETER (MICRONS)= 615.0

COALESCER BED DEPTH (MM.)= 30.0

SUPERFICIAL VELOCITY(1/1000)	PRESSURE DROP(KN/M**2)
0.000	0.000
0.800	0.507
1.030	0.675
1.500	1.013
2.500	1.688
3.050	2.026
3.600	2.364
4.750	3.039
6.000	3.883

NUMBER OF (GOOD) DATA POINTS= 9.

MEAN OF X DISTRIBUTION= 2.581111

MEAN OF Y DISTRIBUTION= 0.500000

STANDARD DEVIATION OF X DISTRIBUTION= 1.857917

STANDARD DEVIATION OF Y DISTRIBUTION= 0.355121

CORRELATION COEFFICIENT= 0.999651

APPENDIX S

Two Computer Programs for Tabulating Experimental Data of Transient Two-Phase Pressure Drop and Steady-State Two-Phase Pressure drop.

```
C THIS COMPUTER PROGRAM FOR TABULATING EXPERIMENTAL DATA
C ======================================================
C OF TRANSIENT TWO-PHASE PRESSURE DROP.
C ====================================
C
C
      DIMENSION X(999),PR2(999),Y(999),DC(999),BD(999)
     @,PHR(999),D21(999),U(999)
      INTEGER EXPN
       PRINT 35
  35  FORMAT(10X,' TRANSIENT TWO-PHASE PRESSURE DROP EXPERIMENTAL',
     @' DATA',/,10X,50('-'),//)
C
        PRINT 40
 40     FORMAT(10X,'  TOLUENE-WATER LIQUID SYSTEM :',/10X,28('-')//)
C
       READ *,L
       READ *,(DC(M),BD(M),PHR(M),D21(M),U(M),M=1,L)
         READ *,NPT
        READ *,(X(II),II=1,NPT)
C
       DO 2 K=1,L
        EXPN=K
        PRINT 210,EXPN
  210  FORMAT(6X,'EXPERIMENT NUMBER=',I4,'B1',/,6X,28('-')/)
C
      PRINT 222,DC(K),BD(K),PHR(K),D21(K),U(K)
 222  FORMAT(5X,'BALLOTINI PARTICLE DIAMETER (MICRONS)=',F6.1,/,
     @5X,'COALESCER BED DEPTH (MM.)=',F6.1,/,
     @5X,'INLET PHASE RATIO (% V/V)=',F6.1,/,
     @5X,'MEAN INLET DROP SIZE (MICRONS)=',F6.1,/,
     @5X,'SUPERFICIAL VELOCITY (1/1000,M/S)=',F6.1,//)
C
       PRINT 211
  211  FORMAT(9X,'  TIME (SECONDS)          TRANSIENT PRESSURE DROP',
     @'(KN/M**2)',/,9X,60('-'))
C
       READ *,(Y(NN),NN=1,NPT)
        DO 11 I=1,NPT
        PR2(I)=Y(I)
C
        PRINT 150,X(I),PR2(I)
  150  FORMAT(10X,F10.3,20X,F10.3)
  11     CONTINUE
         PRINT 300
 300     FORMAT(10X,//)
  2       CONTINUE
           STOP
           END
```

TRANSIENT TWO-PHASE PRESSURE DROP EXPERIMENTAL DATA

TOLUENE-WATER LIQUID SYSTEM :

EXPERIMENT NUMBER= 1B1

BALLOTINI PARTICLE DIAMETER (MICRONS)= 146.0
COALESCER BED DEPTH (MM.)= 20.0
INLET PHASE RATIO (% V/V)= 2.0
MEAN INLET DROP SIZE (MICRONS)= 27.0
SUPERFICIAL VELOCITY (1/1000,M/S)= 3.0

TIME (SECONDS)	TRANSIENT PRESSURE DROP(KN/M**2)
60.000	5.065
120.000	5.572
300.000	6.247
600.000	7.091
1200.000	8.105
1800.000	8.780
2400.000	9.118
3000.000	9.286
3600.000	9.286
4200.000	9.286
4800.000	9.286

EXPERIMENT NUMBER= 2B1

BALLOTINI PARTICLE DIAMETER (MICRONS)= 146.0
COALESCER BED DEPTH (MM.)= 30.0
INLET PHASE RATIO (% V/V)= 1.0
MEAN INLET DROP SIZE (MICRONS)= 27.0
SUPERFICIAL VELOCITY (1/1000,M/S)= 3.0

TIME (SECONDS)	TRANSIENT PRESSURE DROP(KN/M**2)
60.000	6.416
120.000	7.260
300.000	7.936
600.000	8.611
1200.000	9.118
1800.000	9.455
2400.000	9.962
3000.000	10.300

3600.000	10.468
4200.000	10.468
4800.000	10.468

EXPERIMENT NUMBER= 3B1

BALLOTINI PARTICLE DIAMETER (MICRONS)= 146.0
COALESCER BED DEPTH (MM.)= 30.0
INLET PHASE RATIO (% V/V)= 2.0
MEAN INLET DROP SIZE (MICRONS)= 27.0
SUPERFICIAL VELOCITY (1/1000,M/S)= 1.5

TIME (SECONDS)	TRANSIENT PRESSURE DROP(KN/M**2)
60.000	5.910
120.000	6.585
300.000	7.091
600.000	7.767
1200.000	8.442
1800.000	9.118
2400.000	9.455
3000.000	9.793
3600.000	9.962
4200.000	9.962
4800.000	9.962

EXPERIMENT NUMBER= 4B1

BALLOTINI PARTICLE DIAMETER (MICRONS)= 146.0
COALESCER BED DEPTH (MM.)= 30.0
INLET PHASE RATIO (% V/V)= 2.0
MEAN INLET DROP SIZE (MICRONS)= 27.0
SUPERFICIAL VELOCITY (1/1000,M/S)= 3.0

TIME (SECONDS)	TRANSIENT PRESSURE DROP(KN/M**2)
60.000	9.793
120.000	10.637
300.000	11.144
600.000	11.819
1200.000	12.495
1800.000	13.170
2400.000	13.339
3000.000	13.676
3600.000	13.845
4200.000	14.014

4800.000	14.014

EXPERIMENT NUMBER= 5B1

BALLOTINI PARTICLE DIAMETER (MICRONS)= 146.0
COALESCER BED DEPTH (MM.)= 30.0
INLET PHASE RATIO (% V/V)= 2.0
MEAN INLET DROP SIZE (MICRONS)= 27.0
SUPERFICIAL VELOCITY (1/1000,M/S)= 6.0

TIME (SECONDS)	TRANSIENT PRESSURE DROP(KN/M**2)
60.000	17.560
120.000	18.066
300.000	18.742
600.000	19.417
1200.000	19.755
1800.000	20.261
2400.000	20.937
3000.000	21.274
3600.000	21.612
4200.000	21.781
4800.000	21.781

EXPERIMENT NUMBER= 6B1

BALLOTINI PARTICLE DIAMETER (MICRONS)= 146.0
COALESCER BED DEPTH (MM.)= 40.0
INLET PHASE RATIO (% V/V)= 2.0
MEAN INLET DROP SIZE (MICRONS)= 27.0
SUPERFICIAL VELOCITY (1/1000,M/S)= 3.0

TIME (SECONDS)	TRANSIENT PRESSURE DROP(KN/M**2)
60.000	11.481
120.000	12.663
300.000	13.170
600.000	13.845
1200.000	14.183
1800.000	14.690
2400.000	15.196
3000.000	15.534
3600.000	15.703
4200.000	15.703
4800.000	15.703

EXPERIMENT NUMBER= 7B1

BALLOTINI PARTICLE DIAMETER (MICRONS)= 266.0
COALESCER BED DEPTH (MM.)= 10.0
INLET PHASE RATIO (% V/V)= 2.0
MEAN INLET DROP SIZE (MICRONS)= 27.0
SUPERFICIAL VELOCITY (1/1000,M/S)= 1.5

TIME (SECONDS)	TRANSIENT PRESSURE DROP(KN/M**2)
60.000	2.195
120.000	2.533
300.000	3.039
600.000	3.377
1200.000	3.546
1800.000	3.715
2400.000	3.883
3000.000	3.883
3600.000	3.883
4200.000	3.883
4800.000	3.883

EXPERIMENT NUMBER= 8B1

BALLOTINI PARTICLE DIAMETER (MICRONS)= 266.0
COALESCER BED DEPTH (MM.)= 10.0
INLET PHASE RATIO (% V/V)= 2.0
MEAN INLET DROP SIZE (MICRONS)= 27.0
SUPERFICIAL VELOCITY (1/1000,M/S)= 3.0

TIME (SECONDS)	TRANSIENT PRESSURE DROP(KN/M**2)
60.000	3.039
120.000	4.052
300.000	4.559
600.000	4.897
1200.000	5.403
1800.000	5.741
2400.000	5.910
3000.000	5.910
3600.000	5.910
4200.000	5.910
4800.000	5.910

EXPERIMENT NUMBER= 9B1

BALLOTINI PARTICLE DIAMETER (MICRONS)= 266.0
COALESCER BED DEPTH (MM.)= 20.0
INLET PHASE RATIO (% V/V)= 1.0
MEAN INLET DROP SIZE (MICRONS)= 27.0
SUPERFICIAL VELOCITY (1/1000,M/S)= 1.5

TIME (SECONDS)	TRANSIENT PRESSURE DROP(KN/M**2)
60.000	2.702
120.000	3.377
300.000	3.883
600.000	4.052
1200.000	4.390
1800.000	4.728
2400.000	4.897
3000.000	4.897
3600.000	4.897
4200.000	4.897
4800.000	4.897

EXPERIMENT NUMBER= 10B1

BALLOTINI PARTICLE DIAMETER (MICRONS)= 266.0
COALESCER BED DEPTH (MM.)= 20.0
INLET PHASE RATIO (% V/V)= 1.0
MEAN INLET DROP SIZE (MICRONS)= 27.0
SUPERFICIAL VELOCITY (1/1000,M/S)= 3.0

TIME (SECONDS)	TRANSIENT PRESSURE DROP(KN/M**2)
60.000	3.546
120.000	4.390
300.000	4.897
600.000	5.403
1200.000	6.078
1800.000	6.416
2400.000	6.923
3000.000	7.091
3600.000	7.091
4200.000	7.091
4800.000	7.091

TRANSIENT TWO-PHASE PRESSURE DROP EXPERIMENTAL DATA

CLAIRSOL-WATER LIQUID SYSTEM :

EXPERIMENT NUMBER= 1B2

BALLOTINI PARTICLE DIAMETER (MICRONS)= 266.0
COALESCER BED DEPTH (MM.)= 30.0
INLET PHASE RATIO (% V/V)= 1.0
MEAN INLET DROP SIZE (MICRONS)= 27.0
SUPERFICIAL VELOCITY (1/1000,M/S)= 1.5

TIME (SECONDS)	TRANSIENT PRESSURE DROP(KN/M**2)
60.000	4.728
120.000	5.910
300.000	6.754
600.000	7.260
1200.000	7.936
1800.000	8.105
2400.000	8.442
3000.000	8.611
3600.000	8.611
4200.000	8.611
4800.000	8.611

EXPERIMENT NUMBER= 2B2

BALLOTINI PARTICLE DIAMETER (MICRONS)= 266.0
COALESCER BED DEPTH (MM.)= 30.0
INLET PHASE RATIO (% V/V)= 1.0
MEAN INLET DROP SIZE (MICRONS)= 27.0
SUPERFICIAL VELOCITY (1/1000,M/S)= 3.0

TIME (SECONDS)	TRANSIENT PRESSURE DROP(KN/M**2)
60.000	7.767
120.000	9.624
300.000	10.300
600.000	11.144
1200.000	11.819
1800.000	12.326
2400.000	12.832
3000.000	13.001

3600.000	13.339
4200.000	13.339
4800.000	13.339

EXPERIMENT NUMBER= 3B2

BALLOTINI PARTICLE DIAMETER (MICRONS)= 266.0
COALESCER BED DEPTH (MM.)= 30.0
INLET PHASE RATIO (% V/V)= 1.0
MEAN INLET DROP SIZE (MICRONS)= 27.0
SUPERFICIAL VELOCITY (1/1000,M/S)= 6.0

TIME (SECONDS)	TRANSIENT PRESSURE DROP(KN/M**2)
60.000	16.209
120.000	17.898
300.000	18.742
600.000	19.586
1200.000	19.924
1800.000	23.469
2400.000	20.261
3000.000	20.430
3600.000	20.430
4200.000	20.599
4800.000	20.599

EXPERIMENT NUMBER= 4B2

BALLOTINI PARTICLE DIAMETER (MICRONS)= 266.0
COALESCER BED DEPTH (MM.)= 30.0
INLET PHASE RATIO (% V/V)= 2.0
MEAN INLET DROP SIZE (MICRONS)= 42.0
SUPERFICIAL VELOCITY (1/1000,M/S)= 3.0

TIME (SECONDS)	TRANSIENT PRESSURE DROP(KN/M**2)
60.000	9.793
120.000	10.637
300.000	11.650
600.000	12.157
1200.000	12.326
1800.000	13.001
2400.000	13.170
3000.000	13.339
3600.000	13.676
4200.000	13.676

4800.000	13.676

EXPERIMENT NUMBER= 5B2

BALLOTINI PARTICLE DIAMETER (MICRONS)= 266.0
COALESCER BED DEPTH (MM.)= 30.0
INLET PHASE RATIO (% V/V)= 2.0
MEAN INLET DROP SIZE (MICRONS)= 27.0
SUPERFICIAL VELOCITY (1/1000,M/S)= 0.8

TIME (SECONDS)	TRANSIENT PRESSURE DROP(KN/M**2)
60.000	2.533
120.000	3.039
300.000	3.377
600.000	3.715
1200.000	4.052
1800.000	4.390
2400.000	4.728
3000.000	4.897
3600.000	4.897
4200.000	4.897
4800.000	4.897

EXPERIMENT NUMBER= 6B2

BALLOTINI PARTICLE DIAMETER (MICRONS)= 266.0
COALESCER BED DEPTH (MM.)= 30.0
INLET PHASE RATIO (% V/V)= 2.0
MEAN INLET DROP SIZE (MICRONS)= 27.0
SUPERFICIAL VELOCITY (1/1000,M/S)= 1.0

TIME (SECONDS)	TRANSIENT PRESSURE DROP(KN/M**2)
60.000	3.546
120.000	4.897
300.000	5.403
600.000	5.910
1200.000	6.247
1800.000	6.416
2400.000	6.585
3000.000	6.585
3600.000	6.585
4200.000	6.585
4800.000	6.585

EXPERIMENT NUMBER= 7B2

BALLOTINI PARTICLE DIAMETER (MICRONS)= 266.0
COALESCER BED DEPTH (MM.)= 30.0
INLET PHASE RATIO (% V/V)= 2.0
MEAN INLET DROP SIZE (MICRONS)= 27.0
SUPERFICIAL VELOCITY (1/1000,M/S)= 1.5

TIME (SECONDS)	TRANSIENT PRESSURE DROP(KN/M**2)
60.000	5.403
120.000	6.247
300.000	7.260
600.000	7.767
1200.000	8.611
1800.000	9.118
2400.000	9.455
3000.000	9.624
3600.000	9.624
4200.000	9.624
4800.000	9.624

EXPERIMENT NUMBER= 8B2

BALLOTINI PARTICLE DIAMETER (MICRONS)= 266.0
COALESCER BED DEPTH (MM.)= 30.0
INLET PHASE RATIO (% V/V)= 2.0
MEAN INLET DROP SIZE (MICRONS)= 27.0
SUPERFICIAL VELOCITY (1/1000,M/S)= 2.5

TIME (SECONDS)	TRANSIENT PRESSURE DROP(KN/M**2)
60.000	7.429
120.000	8.105
300.000	9.286
600.000	10.131
1200.000	11.313
1800.000	11.819
2400.000	11.988
3000.000	12.157
3600.000	12.157
4200.000	12.157
4800.000	12.157

EXPERIMENT NUMBER= 9B2

BALLOTINI PARTICLE DIAMETER (MICRONS)= 266.0
COALESCER BED DEPTH (MM.)= 30.0
INLET PHASE RATIO (% V/V)= 2.0
MEAN INLET DROP SIZE (MICRONS)= 27.0
SUPERFICIAL VELOCITY (1/1000,M/S)= 3.0

TIME (SECONDS)	TRANSIENT PRESSURE DROP(KN/M**2)
60.000	9.793
120.000	10.975
300.000	11.650
600.000	12.157
1200.000	12.663
1800.000	13.170
2400.000	13.508
3000.000	14.014
3600.000	14.183
4200.000	14.352
4800.000	14.352

EXPERIMENT NUMBER= 10B2

BALLOTINI PARTICLE DIAMETER (MICRONS)= 266.0
COALESCER BED DEPTH (MM.)= 30.0
INLET PHASE RATIO (% V/V)= 2.0
MEAN INLET DROP SIZE (MICRONS)= 27.0
SUPERFICIAL VELOCITY (1/1000,M/S)= 3.6

TIME (SECONDS)	TRANSIENT PRESSURE DROP(KN/M**2)
60.000	11.650
120.000	12.663
300.000	13.508
600.000	14.014
1200.000	14.690
1800.000	15.196
2400.000	15.534
3000.000	15.871
3600.000	16.378
4200.000	16.547
4800.000	16.547

```
C THIS COMPUTER PROGRAM FOR TABULATING EXPERIMENTAL DATA OF
C ============================================================
C STEADY-STATE TWO-PHASE PRESSURE DROP.
C ======================================
C
      DIMENSION X(999),PR2(999),Y(999),DC(999),BD(999)
     @,PHR(999),D21(999)
      INTEGER EXPN
       PRINT 35
  35  FORMAT(10X,'  STEADY-STATE TWO-PHASE PRESSURE DROP',
     @' EXPERIMENTAL  DATA',/,10X,60('-'),//)
C
        PRINT 40
 40      FORMAT(10X,'  TOLUENE-WATER LIQUID SYSTEM :',/10X,28('-')//)
       READ *,L
       READ *,(DC(M),BD(M),PHR(M),D21(M),M=1,L)
         READ *,NPT
        READ *,(X(II),II=1,NPT)
       DO 2 K=1,L
        EXPN=K
        PRINT 210,EXPN
  210  FORMAT(6X,'EXPERIMENT NUMBER=',I4,'C1',/,6X,28('-')/)
C
      PRINT 222,DC(K),BD(K),PHR(K),D21(K)
 222  FORMAT(5X,'BALLOTINI PARTICLE DIAMETER (MICRONS)=',F6.1,/,
     @5X,'COALESCER BED DEPTH (MM.)=',F6.1,/,
     @5X,'INLET PHASE RATIO (% V/V)=',F6.1,/,
     @5X,'MEAN INLET DROP SIZE (MICRONS)=',F6.1,//)
C
       PRINT 211
  211  FORMAT(4X,' SUPERFICIAL VELOCITY (1/1000,M/S)  TWO-PHASE ',
     @'PRESSUR DROP(KN/M**2)',/,9X,60('-'))
C
       READ *,(Y(NN),NN=1,NPT)
        DO 11 I=1,NPT
        PR2(I)=Y(I)
C
        PRINT 150,X(I),PR2(I)
  150  FORMAT(10X,F10.3,20X,F10.3)
  11     CONTINUE
C
         PRINT 300
 300     FORMAT(10X,//)
  2       CONTINUE
           STOP
           END
```

STEADY-STATE TWO-PHASE PRESSURE DROP EXPERIMENTAL DATA

TOLUENE-WATER LIQUID SYSTEM :

EXPERIMENT NUMBER= 1C1

BALLOTINI PARTICLE DIAMETER (MICRONS)= 146.0
COALESCER BED DEPTH (MM.)= 20.0
INLET PHASE RATIO (% V/V)= 2.0
MEAN INLET DROP SIZE (MICRONS)= 42.0

SUPERFICIAL VELOCITY (1/1000,M/S)	TWO-PHASE PRESSUR DROP(KN/M**2)
0.800	3.208
1.030	5.234
1.500	6.247
2.500	7.936
3.050	8.780
3.600	10.975
4.750	13.676
6.000	15.534

EXPERIMENT NUMBER= 2C1

BALLOTINI PARTICLE DIAMETER (MICRONS)= 146.0
COALESCER BED DEPTH (MM.)= 20.0
INLET PHASE RATIO (% V/V)= 2.0
MEAN INLET DROP SIZE (MICRONS)= 27.0

SUPERFICIAL VELOCITY (1/1000,M/S)	TWO-PHASE PRESSUR DROP(KN/M**2)
0.800	3.546
1.030	5.572
1.500	6.585
2.500	8.780
3.050	9.286
3.600	11.650
4.750	14.352
6.000	16.378

EXPERIMENT NUMBER= 3C1

BALLOTINI PARTICLE DIAMETER (MICRONS)= 146.0
COALESCER BED DEPTH (MM.)= 20.0
INLET PHASE RATIO (% V/V)= 2.0
MEAN INLET DROP SIZE (MICRONS)= 22.0

SUPERFICIAL VELOCITY (1/1000,M/S)	TWO-PHASE PRESSUR DROP(KN/M**2)
0.800	3.715
1.030	6.247
1.500	6.923
2.500	9.118
3.050	9.962
3.600	12.326
4.750	15.196
6.000	17.053

EXPERIMENT NUMBER= 4C1

BALLOTINI PARTICLE DIAMETER (MICRONS)= 146.0
COALESCER BED DEPTH (MM.)= 30.0
INLET PHASE RATIO (% V/V)= 0.5
MEAN INLET DROP SIZE (MICRONS)= 27.0

SUPERFICIAL VELOCITY (1/1000,M/S)	TWO-PHASE PRESSUR DROP(KN/M**2)
0.800	4.390
1.030	6.585
1.500	7.260
2.500	9.455
3.050	10.468
3.600	13.001
4.750	19.079
6.000	20.768

EXPERIMENT NUMBER= 5C1

BALLOTINI PARTICLE DIAMETER (MICRONS)= 146.0
COALESCER BED DEPTH (MM.)= 30.0
INLET PHASE RATIO (% V/V)= 1.0
MEAN INLET DROP SIZE (MICRONS)= 27.0

SUPERFICIAL VELOCITY (1/1000,M/S)	TWO-PHASE PRESSUR DROP(KN/M**2)
0.800	4.390
1.030	6.585

1.500	7.260
2.500	9.455
3.050	10.468
3.600	13.170
4.750	19.079
6.000	20.768

EXPERIMENT NUMBER= 6C1

BALLOTINI PARTICLE DIAMETER (MICRONS)= 146.0
COALESCER BED DEPTH (MM.)= 30.0
INLET PHASE RATIO (% V/V)= 2.0
MEAN INLET DROP SIZE (MICRONS)= 42.0

SUPERFICIAL VELOCITY (1/1000,M/S)	TWO-PHASE PRESSUR DROP(KN/M**2)
0.800	4.559
1.030	6.585
1.500	7.598
2.500	9.793
3.050	10.806
3.600	13.676
4.750	17.560
6.000	21.106

EXPERIMENT NUMBER= 7C1

BALLOTINI PARTICLE DIAMETER (MICRONS)= 146.0
COALESCER BED DEPTH (MM.)= 30.0
INLET PHASE RATIO (% V/V)= 2.0
MEAN INLET DROP SIZE (MICRONS)= 27.0

SUPERFICIAL VELOCITY (1/1000,M/S)	TWO-PHASE PRESSUR DROP(KN/M**2)
0.800	4.897
1.030	7.936
1.500	9.962
2.500	11.988
3.050	14.014
3.600	16.716
4.750	20.093
6.000	21.781

EXPERIMENT NUMBER= 8C1

BALLOTINI PARTICLE DIAMETER (MICRONS)= 146.0
COALESCER BED DEPTH (MM.)= 30.0
INLET PHASE RATIO (% V/V)= 2.0
MEAN INLET DROP SIZE (MICRONS)= 22.0

SUPERFICIAL VELOCITY (1/1000,M/S)	TWO-PHASE PRESSUR DROP(KN/M**2)
0.800	5.234
1.030	8.273
1.500	10.468
2.500	13.001
3.050	14.352
3.600	17.053
4.750	22.119
6.000	23.638

EXPERIMENT NUMBER= 9C1

BALLOTINI PARTICLE DIAMETER (MICRONS)= 146.0
COALESCER BED DEPTH (MM.)= 30.0
INLET PHASE RATIO (% V/V)= 2.0
MEAN INLET DROP SIZE (MICRONS)= 17.0

SUPERFICIAL VELOCITY (1/1000,M/S)	TWO-PHASE PRESSUR DROP(KN/M**2)
0.800	5.572
1.030	8.611
1.500	10.975
2.500	13.339
3.050	14.521
3.600	18.911
4.750	24.820
6.000	26.678

EXPERIMENT NUMBER= 10C1

BALLOTINI PARTICLE DIAMETER (MICRONS)= 146.0
COALESCER BED DEPTH (MM.)= 30.0
INLET PHASE RATIO (% V/V)= 2.0
MEAN INLET DROP SIZE (MICRONS)= 13.0

SUPERFICIAL VELOCITY (1/1000,M/S)	TWO-PHASE PRESSUR DROP(KN/M**2)

0.800	5.910
1.030	8.949
1.500	11.313
2.500	14.183
3.050	15.703
3.600	19.755
4.750	26.846
6.000	28.197

EXPERIMENT NUMBER= 11C1

BALLOTINI PARTICLE DIAMETER (MICRONS)= 146.0
COALESCER BED DEPTH (MM.)= 30.0
INLET PHASE RATIO (% V/V)= 4.0
MEAN INLET DROP SIZE (MICRONS)= 42.0

SUPERFICIAL VELOCITY (1/1000,M/S)	TWO-PHASE PRESSUR DROP(KN/M**2)
0.800	5.741
1.030	7.936
1.500	10.300
2.500	13.508
3.050	14.014
3.600	17.222
4.750	20.261
6.000	22.625

EXPERIMENT NUMBER= 12C1

BALLOTINI PARTICLE DIAMETER (MICRONS)= 146.0
COALESCER BED DEPTH (MM.)= 30.0
INLET PHASE RATIO (% V/V)= 4.0
MEAN INLET DROP SIZE (MICRONS)= 27.0

SUPERFICIAL VELOCITY (1/1000,M/S)	TWO-PHASE PRESSUR DROP(KN/M**2)
0.800	5.403
1.030	8.611
1.500	10.806
2.500	13.339
3.050	14.690
3.600	17.222
4.750	22.456
6.000	24.483

STEADY-STATE TWO-PHASE PRESSURE DROP EXPERIMENTAL DATA

CLAIRSOL-WATER LIQUID SYSTEM :

EXPERIMENT NUMBER= 1C2

BALLOTINI PARTICLE DIAMETER (MICRONS)= 146.0
COALESCER BED DEPTH (MM.)= 30.0
INLET PHASE RATIO (% V/V)= 1.0
MEAN INLET DROP SIZE (MICRONS)= 27.0

SUPERFICIAL VELOCITY (1/1000,M/S)	TWO-PHASE PRESSUR DROP(KN/M**2)
0.800	4.390
1.030	6.754
1.500	7.936
2.500	9.962
3.050	11.144
3.600	14.014
4.750	19.755
6.000	21.274

EXPERIMENT NUMBER= 2C2

BALLOTINI PARTICLE DIAMETER (MICRONS)= 146.0
COALESCER BED DEPTH (MM.)= 30.0
INLET PHASE RATIO (% V/V)= 2.0
MEAN INLET DROP SIZE (MICRONS)= 42.0

SUPERFICIAL VELOCITY (1/1000,M/S)	TWO-PHASE PRESSUR DROP(KN/M**2)
0.800	5.403
1.030	8.780
1.500	11.144
2.500	13.339
3.050	14.858
3.600	17.391
4.750	22.456
6.000	24.483

EXPERIMENT NUMBER= 3C2

BALLOTINI PARTICLE DIAMETER (MICRONS)= 146.0
COALESCER BED DEPTH (MM.)= 30.0
INLET PHASE RATIO (% V/V)= 2.0
MEAN INLET DROP SIZE (MICRONS)= 27.0

SUPERFICIAL VELOCITY (1/1000,M/S)	TWO-PHASE PRESSUR DROP(KN/M**2)
0.800	4.897
1.030	8.105
1.500	9.624
2.500	12.326
3.050	14.352
3.600	17.560
4.750	20.430
6.000	22.119

EXPERIMENT NUMBER= . 4C2

BALLOTINI PARTICLE DIAMETER (MICRONS)= 146.0
COALESCER BED DEPTH (MM.)= 30.0
INLET PHASE RATIO (% V/V)= 2.0
MEAN INLET DROP SIZE (MICRONS)= 22.0

SUPERFICIAL VELOCITY (1/1000,M/S)	TWO-PHASE PRESSUR DROP(KN/M**2)
0.800	5.403
1.030	8.780
1.500	10.806
2.500	13.339
3.050	14.690
3.600	17.560
4.750	22.456
6.000	23.976

EXPERIMENT NUMBER= 5C2

BALLOTINI PARTICLE DIAMETER (MICRONS)= 146.0
COALESCER BED DEPTH (MM.)= 30.0
INLET PHASE RATIO (% V/V)= 4.0
MEAN INLET DROP SIZE (MICRONS)= 27.0

SUPERFICIAL VELOCITY (1/1000,M/S)	TWO-PHASE PRESSUR DROP(KN/M**2)
0.800	5.572
1.030	9.118

1.500	11.144
2.500	13.508
3.050	15.027
3.600	17.898
4.750	22.794
6.000	24.145

EXPERIMENT NUMBER= 6C2

BALLOTINI PARTICLE DIAMETER (MICRONS)= 266.0
COALESCER BED DEPTH (MM.)= 20.0
INLET PHASE RATIO (% V/V)= 2.0
MEAN INLET DROP SIZE (MICRONS)= 27.0

SUPERFICIAL VELOCITY (1/1000,M/S)	TWO-PHASE PRESSUR DROP(KN/M**2)
0.800	3.208
1.030	4.897
1.500	6.247
2.500	8.273
3.050	9.286
3.600	10.637
4.750	12.663
6.000	14.014

EXPERIMENT NUMBER= 7C2

BALLOTINI PARTICLE DIAMETER (MICRONS)= 266.0
COALESCER BED DEPTH (MM.)= 30.0
INLET PHASE RATIO (% V/V)= 0.5
MEAN INLET DROP SIZE (MICRONS)= 27.0

SUPERFICIAL VELOCITY (1/1000,M/S)	TWO-PHASE PRESSUR DROP(KN/M**2)
0.800	4.390
1.030	6.247
1.500	8.611
2.500	11.313
3.050	13.339
3.600	15.365
4.750	18.066
6.000	20.599

EXPERIMENT NUMBER= 8C2

BALLOTINI PARTICLE DIAMETER (MICRONS)= 266.0
COALESCER BED DEPTH (MM.)= 30.0
INLET PHASE RATIO (% V/V)= 1.0
MEAN INLET DROP SIZE (MICRONS)= 27.0

SUPERFICIAL VELOCITY (1/1000,M/S)	TWO-PHASE PRESSUR DROP(KN/M**2)
0.800	4.390
1.030	6.247
1.500	8.611
2.500	11.313
3.050	13.339
3.600	15.365
4.750	18.066
6.000	20.599

EXPERIMENT NUMBER= 9C2

BALLOTINI PARTICLE DIAMETER (MICRONS)= 266.0
COALESCER BED DEPTH (MM.)= 30.0
INLET PHASE RATIO (% V/V)= 2.0
MEAN INLET DROP SIZE (MICRONS)= 42.0

SUPERFICIAL VELOCITY (1/1000,M/S)	TWO-PHASE PRESSUR DROP(KN/M**2)
0.800	4.559
1.030	6.416
1.500	8.780
2.500	11.481
3.050	13.676
3.600	15.871
4.750	18.404
6.000	21.443

EXPERIMENT NUMBER= 10C2

BALLOTINI PARTICLE DIAMETER (MICRONS)= 266.0
COALESCER BED DEPTH (MM.)= 30.0
INLET PHASE RATIO (% V/V)= 2.0
MEAN INLET DROP SIZE (MICRONS)= 27.0

SUPERFICIAL VELOCITY (1/1000,M/S)	TWO-PHASE PRESSUR DROP(KN/M**2)

0.800	4.897
1.030	6.585
1.500	9.624
2.500	12.157
3.050	14.352
3.600	16.547
4.750	19.248
6.000	21.950

EXPERIMENT NUMBER= 11C2

BALLOTINI PARTICLE DIAMETER (MICRONS)= 266.0
COALESCER BED DEPTH (MM.)= 30.0
INLET PHASE RATIO (% V/V)= 2.0
MEAN INLET DROP SIZE (MICRONS)= 22.0

SUPERFICIAL VELOCITY (1/1000,M/S)	TWO-PHASE PRESSUR DROP(KN/M**2)
0.800	5.403
1.030	7.936
1.500	10.300
2.500	12.832
3.050	15.871
3.600	18.066
4.750	21.443
6.000	24.820

EXPERIMENT NUMBER= 12C2

BALLOTINI PARTICLE DIAMETER (MICRONS)= 266.0
COALESCER BED DEPTH (MM.)= 30.0
INLET PHASE RATIO (% V/V)= 2.0
MEAN INLET DROP SIZE (MICRONS)= 17.0

SUPERFICIAL VELOCITY (1/1000,M/S)	TWO-PHASE PRESSUR DROP(KN/M**2)
0.800	5.910
1.030	9.286
1.500	11.650
2.500	15.703
3.050	18.235
3.600	20.937
4.750	24.483
6.000	27.184

APPENDIX T

Multi-Linear Regression Analysis Computer Program for the Analysis of Experimental Pressure Drop Data

```
C THIS PROGRAM FOR MULTIPLE LINEAR REGRESSION ANALYSIS:
C ======================================================
C
C
C
C      MAIN PROGRAM
C     -------------
C
C
      DIMENSION X(87,5),Y(87),A(25),B(5),XBAR(5),YHAT(87),
     @AA(5,5),W(87),H(87),T(87),P1(87),P2(87)
     @,C(87),DP(87),DC(87)
C
C
      READ *,NB,NX,M
C
        NN=NB*NB
       IF(NB.LE.0) THEN
        GO TO 555
          ELSE
       DO 1 K=1,M
        READ *,DC(K),H(K),C(K),DP(K),W(K)
         X(K,1)=ALOG(DC(K)*0.000001)
         X(K,2)=ALOG(H(K)*0.001)
         X(K,3)=ALOG(C(K)*0.01)
         X(K,4)=ALOG(DP(K)*0.000001)
         X(K,5)=ALOG(W(K)*0.001)
C
  1          CONTINUE
C
C
C
         READ *,CMU,DMU
           DO 3 I=1,M
          READ *,P1(I),P2(I)
           T(I)=(P2(I)*CMU)/(P1(I)*DMU)
           Y(I)=ALOG(T(I))
  3        CONTINUE
C
C
       CALL LESQ(X,Y,NB,M,A,B,XBAR,YHAT,AA,NN)
 555         STOP
             ENDIF
             END
C
C
C
C
      SUBROUTINE LESQ(X,Y,N,M,A,B,XBAR,YHAT,AA,N2)
C
      DIMENSION X(M,N),Y(M),A(N2),B(N),XBAR(N),YHAT(M),AA(N,N)
C
C
         PRINT 101
```

```
 101    FORMAT(10X,'MULTIPLE LINEAR REGRESSION ANALYSIS',/10X,40('-')//)
C
      PRINT 113
 113  FORMAT(10X,'FOR TOLUENE-WATER LIQIUD SYSTEM.',/10X,30('-')//)
C
C
C CALCULATE AVERAGE X AND Y VALUES
C
C
        DO 8 I=1,N
         SUMX=0.0
        DO 13 J=1,M
  13     SUMX=SUMX+X(J,I)
   8     XBAR(I)=SUMX/FLOAT(M)
         SUMY=0.0
        DO 15 K=1,M
  15     SUMY=SUMY+Y(K)
        YBAR=SUMY/FLOAT(M)
       PRINT 180
 180   FORMAT(//,6X,'VARIABLE AVERAGE VALUES',/,6X,23('-')/)
       PRINT 240,(II,XBAR(II),II=1,N)
 240   FORMAT(3(3X,'XBAR(',I1,')=',F10.3)/2(3X,'XBAR(',I1,')=',
     @F10.3)/)
        PRINT 260,YBAR
 260   FORMAT(6X,'YBAR=',1PE10.3,/)
C
C
C   CALCULATE REGRESSION MATRICES
C   =============================
C
C
      KK=1
      DO 25 I=1,N
      DO 25 J=1,N
      SUMA=0.0
      SUMB=0.0
       DO 30 K=1,M
      SUMA=SUMA+(X(K,I)-XBAR(I))*(X(K,J)-XBAR(J))
 30    SUMB=SUMB+(Y(K)-YBAR)*(X(K,I)-XBAR(I))
      AA(I,J)=SUMA
      A(KK)=SUMA
        KK=KK+1
 25   B(I)=SUMB
      PRINT 310
 310  FORMAT(//,10X,' A MATRIX',/,10X,9('-')/)
       DO 55 II=1,N
  55   PRINT 360,(AA(II,JJ),JJ=1,N)
 360   FORMAT(/,50(2X,E10.4))
       PRINT 410
 410   FORMAT(//,6X,'B MATRIX',/,6X,9('-')/)
       PRINT 440,(B(KK),KK=1,N)
 440   FORMAT(/,50(2X,E10.4))
C
C
```

```
C  SOLVE REGRESSION MATRICES FOR COEFFICIENTS
C  ==========================================
C
C
      CALL STMG(A,B,N,KS,N2)
       SUMX=0.0
       DO 60 I=1,N
 60    SUMX=SUMX+B(I)*XBAR(I)
       AZERO=YBAR-SUMX
       PRINT 460
 460   FORMAT(//,10X,'VALUES OF THE REGRESSION COEFFICIENTS',/,
     @10X,40('-')/)
       PRINT 470,(JJ,B(JJ),JJ=1,N)
 470   FORMAT(5(6X,'AHAT(',I2,')=',1PE16.8,/))
       PRINT 480,AZERO
 480   FORMAT(6X,' AZERO=',1PE16.8,/)
C
         AHAT0=EXP(AZERO)
        PRINT 490,AHAT0
 490   FORMAT(6X,' AHAT(0)=',1PE16.8,/)
C
C
C
C    CALCULATE S AND R VALUES
C ============================
C

C
      STEST=0.0
      DO 80 J=1,M
      SUMS1=0.0
      DO 90 K=1,N
  90   SUMS1=SUMS1+B(K)*X(J,K)
      YHAT(J)=AZERO+SUMS1
      DIFF=(Y(J)-YHAT(J))**2
  80  STEST=STEST+DIFF
      SUMST=0.0
      DO 92 I=1,M
  92  SUMST=SUMST+(Y(I)-YBAR)**2
      SUMSR=SUMST-STEST
      RTEST=SUMSR/SUMST
       PRINT 520
 520  FORMAT(////,6X,'EXPERIMENTAL VALUES',11X,'REGRESSION VALUES',
     @/,6X,50('-'))
C
C
      DO 115 KK=1,M
 115  PRINT 555,KK,Y(KK),KK,YHAT(KK)
 555  FORMAT(/7X,'Y(',I2,')=',1PE16.6,12X,'YHAT(',I2,')=',1PE16.6)
C
       PRINT 560,SUMST,STEST,RTEST
 560   FORMAT(///,6X,'SUMST=',1PE16.8,/,6X,'STEST=',1PE16.6,/,
     @6X,'RTEST=',1PE16.6,/)
C
```

```
        RETURN
        END
C
C
C
C
      SUBROUTINE STMG(A,B,N,KS,NS)
       DIMENSION A(NS),B(N)
       TOL=0.0
       KS=0
       JJ=-N
       DO 65 J=1,N
       JY=J+1
       JJ=JJ+N+1
       BIGA=0.0
        II=JJ-J
      DO 33 I=J,N
C
C
C   SEARCH FOR MAXIMUM COEFFICIENT IN COLUMN:
C   =========================================
C
       IJ=II+I
       IF((ABS(BIGA)-ABS(A(IJ))).GE.0.0) THEN
        GO TO 33
         ELSE
        BIGA=A(IJ)
        IMAX=I
             ENDIF
  33    CONTINUE
C
C  TEST FOR PIVOT LESS THAN TOLERANCE
C
        IF((ABS(BIGA)-TOL).GT.0.0) THEN
         GO TO 40
          ELSE
        KS=1
        RETURN
C
C   INTERCHANGE ROWS IF NECESSARY
C   =============================
C
  40   I1=J+N*(J-2)
          ENDIF
       II=IMAX-J
        DO 51 K=J,N
       I1=I1+N
       I2=I1+II
       SAVE=A(I1)
       A(I1)=A(I2)
       A(I2)=SAVE
C
C    DIVIDE EQUATION BY LEADING COEFFICIENT
C
```

```
 51     A(I1)=A(I1)/BIGA
       SAVE=B(IMAX)
       B(IMAX)=B(J)
       B(J)=SAVE/BIGA
C
C     ELIMINATE NEXT VARIABLE
C
          IF((J-N).EQ.0) THEN
        GO TO 70
         ELSE
        IQS=N*(J-1)
           ENDIF
        DO 65 IX=JY,N

        IXJ=IQS+IX
        II=J-IX
        DO 61 JX=JY,N
        IXJX=N*(JX-1)+IX
        JJX=IXJX+II
 61     A(IXJX)=A(IXJX)-(A(IXJ)*A(JJX))
        B(IX)=B(IX)-(B(J)*A(IXJ))
 65         CONTINUE
C
C
C      BACK SOLUTION
C
   70    NY=N-1
         II=N*N
          DO 81 J=1,NY
          IA=II-J
          IB=N-J
          IC=N
         DO 81 K=1,J
          B(IB)=B(IB)-A(IA)*B(IC)
          IA=IA-N
   81      IC=IC-1
           RETURN
            END
```

MULTIPLE LINEAR REGRESSION ANALYSIS

FOR TOLUENE-WATER LIQUID SYSTEM.

VARIABLE AVERAGE VALUES

XBAR(1)= -8.240 XBAR(2)= -3.535 XBAR(3)= -3.829
XBAR(4)= -10.530 XBAR(5)= -6.052

YBAR= 2.050E+00

A MATRIX

0.1734E+02	-.1254E+01	-.4573E+01	0.9477E+00	0.1569E+01
-.1254E+01	0.8561E+01	0.1157E+01	-.3069E+00	0.9212E+00
-.4573E+01	0.1157E+01	0.3718E+02	0.1742E+00	0.2746E+01
0.9477E+00	-.3069E+00	0.1742E+00	0.6370E+01	0.1048E+00
0.1569E+01	0.9212E+00	0.2746E+01	0.1048E+00	0.4082E+02

B MATRIX

0.1818E+01	0.2171E+01	0.3526E+01	-.1981E+01	-.9512E+01

VALUES OF THE REGRESSION COEFFICIENTS

AHAT(1)= 2.00699873E-01
AHAT(2)= 2.80978713E-01
AHAT(3)= 1.31155341E-01
AHAT(4)= -3.26702507E-01
AHAT(5)= -2.55053888E-01

AZERO= 2.16076773E-01

AHAT(0)= 1.24119770E+00

EXPERIMENTAL VALUES		REGRESSION VALUES	
Y(1)=	1.879978E+00	YHAT(1)=	1.942456E+00
Y(2)=	2.095940E+00	YHAT(2)=	2.022351E+00
Y(3)=	2.061380E+00	YHAT(3)=	1.993382E+00
Y(4)=	1.736959E+00	YHAT(4)=	1.728294E+00
Y(5)=	1.627512E+00	YHAT(5)=	1.768486E+00
Y(6)=	1.761159E+00	YHAT(6)=	1.672763E+00
Y(7)=	1.827474E+00	YHAT(7)=	1.746407E+00
Y(8)=	1.772878E+00	YHAT(8)=	1.753729E+00
Y(9)=	2.249386E+00	YHAT(9)=	2.351871E+00
Y(10)=	2.569796E+00	YHAT(10)=	2.375061E+00
Y(11)=	2.353230E+00	YHAT(11)=	1.986964E+00
Y(12)=	2.081032E+00	YHAT(12)=	2.001024E+00
Y(13)=	2.018154E+00	YHAT(13)=	2.017213E+00
Y(14)=	2.128873E+00	YHAT(14)=	2.059161E+00
Y(15)=	1.997132E+00	YHAT(15)=	1.746148E+00
Y(16)=	1.967163E+00	YHAT(16)=	1.830911E+00
Y(17)=	2.085102E+00	YHAT(17)=	2.411727E+00
Y(18)=	2.377842E+00	YHAT(18)=	2.126201E+00
Y(19)=	2.154165E+00	YHAT(19)=	1.976887E+00
Y(20)=	1.969697E+00	YHAT(20)=	1.990947E+00
Y(21)=	1.984058E+00	YHAT(21)=	2.007136E+00
Y(22)=	2.028165E+00	YHAT(22)=	1.988853E+00
Y(23)=	2.070879E+00	YHAT(23)=	1.985056E+00
Y(24)=	1.885551E+00	YHAT(24)=	1.911744E+00
Y(25)=	1.857695E+00	YHAT(25)=	2.492559E+00
Y(26)=	1.867056E+00	YHAT(26)=	1.803642E+00

Y(27)=	1.734716E+00	YHAT(27)=	1.852113E+00
Y(28)=	1.580941E+00	YHAT(28)=	1.788732E+00
Y(29)=	1.509931E+00	YHAT(29)=	1.774957E+00
Y(30)=	1.589220E+00	YHAT(30)=	1.679233E+00
Y(31)=	1.452978E+00	YHAT(31)=	1.752877E+00
Y(32)=	1.621578E+00	YHAT(32)=	1.760200E+00
Y(33)=	2.203505E+00	YHAT(33)=	2.298112E+00
Y(34)=	2.432066E+00	YHAT(34)=	2.286838E+00
Y(35)=	2.197328E+00	YHAT(35)=	1.978980E+00
Y(36)=	2.141372E+00	YHAT(36)=	1.915599E+00
Y(37)=	2.001639E+00	YHAT(37)=	1.888884E+00
Y(38)=	2.049127E+00	YHAT(38)=	1.913505E+00
Y(39)=	1.825050E+00	YHAT(39)=	1.722457E+00
Y(40)=	1.847015E+00	YHAT(40)=	1.807220E+00
Y(41)=	2.306273E+00	YHAT(41)=	2.388036E+00
Y(42)=	2.647411E+00	YHAT(42)=	2.402911E+00
Y(43)=	2.657546E+00	YHAT(43)=	2.399583E+00
Y(44)=	2.197290E+00	YHAT(44)=	1.977074E+00
Y(45)=	2.130187E+00	YHAT(45)=	2.070704E+00
Y(46)=	2.162044E+00	YHAT(46)=	2.095325E+00
Y(47)=	2.070783E+00	YHAT(47)=	2.010893E+00
Y(48)=	2.048805E+00	YHAT(48)=	2.018216E+00
Y(49)=	2.014106E+00	YHAT(49)=	2.311052E+00
Y(50)=	2.293605E+00	YHAT(50)=	2.193161E+00
Y(51)=	2.253795E+00	YHAT(51)=	2.241632E+00
Y(52)=	2.326561E+00	YHAT(52)=	2.178251E+00
Y(53)=	2.083475E+00	YHAT(53)=	2.151537E+00

Y(54)=	1.732620E+00	YHAT(54)=	1.990129E+00
Y(55)=	1.730751E+00	YHAT(55)=	1.865988E+00
Y(56)=	1.636591E+00	YHAT(56)=	1.950751E+00
Y(57)=	2.263247E+00	YHAT(57)=	2.531567E+00
Y(58)=	1.988687E+00	YHAT(58)=	2.395241E+00
Y(59)=	1.559025E+00	YHAT(59)=	1.888626E+00
Y(60)=	1.756719E+00	YHAT(60)=	1.784470E+00
Y(61)=	1.623397E+00	YHAT(61)=	1.886532E+00
Y(62)=	1.700116E+00	YHAT(62)=	1.882735E+00
Y(63)=	1.746579E+00	YHAT(63)=	1.847154E+00
Y(64)=	2.256237E+00	YHAT(64)=	2.088333E+00
Y(65)=	2.156143E+00	YHAT(65)=	2.228717E+00
Y(66)=	2.075603E+00	YHAT(66)=	2.079403E+00
Y(67)=	2.017238E+00	YHAT(67)=	2.093463E+00
Y(68)=	2.179038E+00	YHAT(68)=	2.109652E+00
Y(69)=	2.312968E+00	YHAT(69)=	2.151599E+00
Y(70)=	2.242201E+00	YHAT(70)=	2.168538E+00
Y(71)=	1.962018E+00	YHAT(71)=	1.961081E+00
Y(72)=	2.829239E+00	YHAT(72)=	2.528169E+00
Y(73)=	2.119679E+00	YHAT(73)=	2.256112E+00
Y(74)=	2.177696E+00	YHAT(74)=	2.304583E+00
Y(75)=	1.978524E+00	YHAT(75)=	1.970069E+00
Y(76)=	1.838990E+00	YHAT(76)=	2.010261E+00
Y(77)=	1.779337E+00	YHAT(77)=	1.914537E+00
Y(78)=	2.029146E+00	YHAT(78)=	1.988181E+00
Y(79)=	2.089923E+00	YHAT(79)=	1.995504E+00
Y(80)=	2.677709E+00	YHAT(80)=	2.533416E+00

Y(81)=	2.603115E+00	YHAT(81)=	2.522142E+00
Y(82)=	2.392636E+00	YHAT(82)=	2.147192E+00
Y(83)=	2.105474E+00	YHAT(83)=	2.057096E+00
Y(84)=	2.018112E+00	YHAT(84)=	1.961372E+00
Y(85)=	2.087997E+00	YHAT(85)=	2.035016E+00
Y(86)=	2.205896E+00	YHAT(86)=	2.066342E+00
Y(87)=	2.717204E+00	YHAT(87)=	2.633430E+00

SUMST= 7.21358694E+00
STEST= 2.702921E+00
RTEST= 6.253014E-01

APPENDIX U

Computer Program for Analysis of Malvern Particle Size Analyser Experimental Data

```
C  THIS PROGRAM FOR ANALYSING THE INLET DROP SIZE DISTRIBUTION
C  ============================================================
C  DATA (MALVERN PARTICLE SIZE ANALYSER DATA).
C  ===========================================
C
C
      DIMENSION D1(100),D2(100),D(100),FN(100),CFB(100),DT(100)
     @,ANORM(100),ALONM(100),SQRNOM(100),UPLIM(100),DNM(100),DLN(100)
     @,DSR(100),DUL(100),DW(100),FNW(100),SLOP(1),CINT(1),FNEW(100)
     @,DJ(100),CFBJ(100),CFBJL(100),DJL(100),CFBJLL(100),DACT2(100)
     @,FNEWD(100),CTF(100),DMX(100),DWD(100),CFAB(100)
     @,COVF(100),FN2(100),CFB2(100),V(100),VN(100),VNT(100)
     @,NKKJ(100),FWR1(100),FWRR(100),DR(100),DACT1(100)
     @,CFBJ1(100),CTF2(100),CTF1(100),CFB1(100),FN1(100),DN(100)
C
        READ *,NNNN

      READ *,NMK
      READ *,(D1(I),D2(I),CFB1(I),FN1(I),I=1,NMK)
C
C
      DO 5 M=1,NMK
      DN(M)=(D1(M)+D2(M))/2.0
  5   CONTINUE
      PRINT 923
 923  FORMAT(12X,'DATA FROM LAZER PARTICLE-SIZER (MALVERN):',
     +/12X,41('='))
C
       PRINT 12,NNNN
  12   FORMAT(13X,'AT EMULSIFICATION PUMP SPEED (R.P.M)=',I5/)
       PRINT 100
  100 FORMAT(13X,'   SIZE BAND          CUMULATIVE WT.(%)',
     @'  AVERAGE',
     @/13X,' UPPER   LOWER      BELOW      IN BAND   DIAMETER',
     @/13X,'-------------------------------------------')
      PRINT 125,(D1(I),D2(I),CFB1(I),FN1(I),DN(I),I=1,NMK)
 125  FORMAT(12X,F6.2,3X,F6.2,3X,F8.2,3X,F8.2,3X,F7.2)
C
C
          DO 6 K=1,NMK
          IF (DN(K).GE.4.0) THEN
               GO TO 6
               ELSE
               CFBLE=CFB1(K)
                ENDIF
  6            CONTINUE
      PRINT 963,CFBLE
  963 FORMAT(/,15X,'CUMULATIVE WT% OF IMPURITIES PARTICLES (NOT DROPS)=',
     +F6.2)
C
      NL=0
      DO 7 L=1,NMK
      IF(DN(L).LE.4.0) THEN
       NL=NL+1
```

```
          GO TO 7
          ELSE
          NK=L-NL
           FN(NK)=FN1(L)
          D(NK)=DN(L)
          CFB(NK)=(CFB1(L)-CFBLE)
            DACT1(NK)=D1(L)
            DACT2(NK)=D2(L)
                ENDIF
  7        CONTINUE
C
           N=NK
C
C
       PRINT 945,N
 945   FORMAT(15X,'THE ACTUAL NUMBER OF DATA POINTS (EXP.DATA)=',I2/)
C
        PRINT 939
 939   FORMAT(12X,'REAL DATA OF INLET DROP SIZE DIST.(BY WEIGHT%):',
      +/,12X,47('='))
C
C
       PRINT 943
 943   FORMAT(13X,'    SIZE BAND           CUMULATIVE WEIGHT',
      +'       AVERAGE',
      +/13X,'UPPER        LOWER     WT% BELOW  WT% IN BAND  DIAMETER',
      +/13X,'-------------------------------------------------------')
C
C
       PRINT 988,(DACT1(M),DACT2(M),CFB(M),FN(M),D(M),M=1,N)
 988   FORMAT(12X,F6.2,7X,F6.2,4X,F8.2,4X,F8.2,5X,F7.2)
C
             PRINT 1011
 1011         FORMAT(12X)
C
           DO 144 KK=1,N
           IF(FN(KK).LE.0.15) THEN
            FN(KK)=0.0
             ELSE
            FN(KK)=FN(KK)
            ENDIF
 144         CONTINUE
C
        CALL FREQNU(N,FN,D,FN2,CFB2,V,VN,VNT,CFAB)
C
       PRINT 932
 932   FORMAT(12X,'REAL INLET DROP SIZE DIST.DATA (BY NUMBER OF DROPS%):',
      +/12X,52('='))
C
          PRINT 946
 946   FORMAT(13X,'AVERAGE   DROPS NO.PER   CUM.DROPS NUMBER FRQ.OCC.(%)',
      +/13X,'DIAMETER  100 MM**3 VO.   BELOW     IN BAND      ABOVE ',
      +/13X,'-------------------------------------------------------')
       PRINT 947,(D(M),VN(M),CFB2(M),FN2(M),CFAB(M),M=1,N)
```

```
 947    FORMAT(12X,F6.2,7X,E8.3,4X,F8.2,3X,F8.2,3X,F7.2)
C
         PRINT 948
 948      FORMAT(5X,//)
C
       FNMX=0.0
       DO 2 IL=1,N
        FNMX=AMAX1(FNMX,FN(IL))
  2     CONTINUE
        II=1
  3     IF(FN(II).EQ.FNMX) THEN
        PRINT 150,D(II),FN(II)
 150    FORMAT(15X,'MOST FREQUENT DIAMETER(MODE DIAMETER)=',F7.3,
     +//15X,'AT WEIGHT% IN BAND=',F7.3/)
          DFR=D(II)
            ELSE
          II=II+1
          GO TO 3
           ENDIF
C
C
         SUMFN=0.0
         SUMDFN=0.0
          DO 10 IN=1,N
         SUMFN=FN(IN)+SUMFN
         SUMDFN=D(IN)*FN(IN)+SUMDFN
  10       CONTINUE
         DAM=SUMDFN/SUMFN
         PRINT 200,DAM
  200    FORMAT(15X,'ARITHMATIC MEAN DIAMETER=',F7.3/)
C
              PI=3.14159
C  SURFACE FACTOR FOR SPHERE=3.14
C  VOLUME FACTOR FOR SPHERE=0.52
C
       DPRJS=DAM*((3.14/PI)**0.5)
C
       DPRJV=DAM*(((0.52*6.0)/PI)**0.33333)
C
       PRINT 203,DPRJS,DPRJV
 203   FORMAT(15X,'EQUIVALENT PROJECTED DIAMETER(BY SURFACE FACTOR)=',F1
     @0.3,2(/),15X,'EQUIVALENT PROJECTED DIAMETER(BY VOLUME FACTOR)=',
     @F7.3/)
          SUMST=0.0
         NM=0.0
         DO 17 L=1,N
         IF(FN(L).EQ.0.0) THEN
         NM=NM+1
         GO TO 17
           ELSE
         SUMST=SUMST+(D(L)-DAM)**2.0
          NMN=L-NM
         ENDIF
  17       CONTINUE
```

```
          SN=(SUMST/NMN)**0.5
        PRINT 103,SN,NMN
 103    FORMAT(15X,'LINEAR STANDARD DEVIATION=',F7.3//15X,
     @'NUMBER OF DATA SHOULD BE USED IN THE CALCULATION=',I3/)
C
C
        SUMFN=0.0
        SUMLOF=0.0
         DO 20 IM=1,N
          SUMFN=FN(IM)+SUMFN
          SUMLOF=(ALOG(D(IM)))*FN(IM)+SUMLOF
 20        CONTINUE
         ALDGM=SUMLOF/SUMFN
          DGM=EXP(ALDGM)
          PRINT 250,DGM
 250     FORMAT(15X,'GEOMETRIC MEAN DIAMETER=',F7.3/)
C
C
C
         SUMFN=0.0
         SUMHMF=0.0
         DO 30 IK=1,N
         SUMFN=FN(IK)+SUMFN
         SUMHMF=(FN(IK)/D(IK))+SUMHMF
  30       CONTINUE
         DHM=SUMFN/SUMHMF
         PRINT 300,DHM
 300     FORMAT(15X,'HARMONIC MEAN DIAMETER=',F7.3/)
C
C
       READ *,MN,(CTF1(JI),DT(JI),JI=1,MN)
C
       DO 18 KI=1,MN
        CTF(KI)=(CTF1(KI)-CFBLE)
  18    CONTINUE
C
C
        FN50=50.0
        CALL INTPDM(CTF,DT,MN,FN50,DM)
          PRINT 600,DM
 600     FORMAT(15X,'MEDIAN DIAMETER(DM)=',F7.3/)
C
C
          READ *,MN,(CTF2(JJ),DT(JJ),JJ=1,MN)
C
          DO 19 KN=1,MN
        CTF(KN)=(CTF2(KN)-CFBLE)
  19    CONTINUE
C
C
          FN84=84.14
          CALL INTPDM(CTF,DT,MN,FN84,D84)
C
            SG=D84/DM
```

```
C
            PRINT 991,D84,SG
 991    FORMAT(15X,'AT 84.14% DIAMETER OF DROPS=',F7.3//15X,
     @'GEOMETRIC STANDARD DEVIATION (SG)=',F7.3/)
C
C
C
C  MEAN DIAMETER BASED UPON NUMBER,SURFACE,VOLUE AND WEIGHT.
C ------------------------------------------------------------
C
      PRINT 1022
 1022 FORMAT(//,12X,'MEAN DIAMETER BASED UPON NUMBER,SURFACE',
     @',VOLUME AND WEIGHT ',/,12X,57('-')//)
C
C
       FN2MX=0.0
       DO 22 IL=1,N
        FN2MX=AMAX1(FN2MX,FN2(IL))
  22    CONTINUE
C
        LL=1
 712      IF (FN2(LL).EQ.FN2MX) THEN
          PRINT 232,D(LL),FN2(LL)
 232   FORMAT(15X,'MODE DIAMETER(BASED UPON NUMBER OF DROPS)=',
     @F7.3,//15X,'AT NUMBER OF DROP SIZE% IN BAND=',F7.3/)
C
       DNFR=D(LL)
         ELSE
        LL=LL+1
        GO TO 712
         ENDIF
C
C
C
         SUM12=0.0
         SUM13=0.0
         DO 32 II=1,N
          SUM12=(1.0/(D(II)**2.0))*FN(II)+SUM12
          SUM13=(1.0/(D(II)**3.0))*FN(II)+SUM13
  32       CONTINUE
C
C
           D10=SUM12/SUM13
C
        PRINT 323,D10
 323    FORMAT(15X,'LINEAR MEAN DIAMETER (D10)=',F7.3/)
C
C
         SUM11=0.0
         DO 40 J=1,N
          SUM11=(1.0/(D(J)))*FN(J)+SUM11
 40       CONTINUE
        D20=(SUM11/SUM13)**0.5
        PRINT 350,D20
```

```
 350    FORMAT(15X,'SURFACE MEAN (D20)=',F7.3/)
C
C
C
          SUM00=0.0
        DO 50 JI=1,N
        SUM00=FN(JI)+SUM00
 50       CONTINUE
         D30=(SUM00/SUM13)**0.33333
        PRINT 400,D30
 400    FORMAT(15X,'VOLUME MEAN (D30)=',F7.3/)
C
C
C
          D31=(SUM00/SUM12)**0.5
          PRINT 500,D31
500       FORMAT(15X,'VOLUME DIAMETER (D31)='F7.3/)
C
C
          D32=SUM00/SUM11
        PRINT 550,D32
 550    FORMAT(15X,'VOLUME-SURFACE DIAMETER (SAUTER-D32)='F7.3/)
C
C
            SUM01=0.0
           DO 51 K=1,N
           SUM01=(D(K)*FN(K))+SUM01
  51         CONTINUE
C
            D43=SUM01/SUM00
C
         PRINT 602,D43
 602    FORMAT(15X,'MOMENT-WEIGHT DIAMETER (D43)=',F7.3//)
C
C
            D21=SUM11/SUM12
C
            PRINT 450,D21
 450     FORMAT(15X,'SURFACE DIAMETER (D21)=',F7.3//)
C
C
C      DISTRIBUTION FUNCTIONS
C     ------------------------
C
         LJ=0.0
         DO 73 LK=1,N
         IF(FN(LK).EQ.0.0) THEN
          LJ=LJ+1
          GO TO 73
         ELSE
         LJL=LK-LJ
         FNW(LJL)=FN(LK)
         DMX(LJL)=DACT1(LK)
          ENDIF
```

```
 73     CONTINUE
        DMAX=DMX(LJL)
C
        PRINT 610,DMAX
 610    FORMAT(15X,'MAXIMUM DIAMETER IN THE DATA=',F7.3//)
           PRINT 111
 111   FORMAT(15X,'Note:','Units of Diameters above are in Microns.',
     +/15X,'====',//)
C
C
C
         PRINT *,'              NORMAL DISTRIBUTION RESULTS:'
         PRINT *,'              ---------------------------'
          PRINT 810
 810      FORMAT(12X,'DROP DIAMETER      WT% IN NORMAL DIST.',
     @/12X,38('-'))
       DO 82 JK=1,N
       ANORM(JK)=(EXP(-((D(JK)-DAM)/(2.0*(SN**2.0)))))
     @*(1.0/(((2.0*PI)**0.5)*SN))*100.0
        DNM(JK)=D(JK)
  82      CONTINUE
        DO 183 L=1,N
        PRINT 120,DNM(L),ANORM(L)
 120    FORMAT(13X,F7.3,14X,F7.3)
 183     CONTINUE
C
C
          PRINT *,'        '
C
       PRINT *,'              LOG-NORMAL DISTRIBUTION RESULTS:'
       PRINT *,'              -------------------------------'
C
       PRINT 820
 820   FORMAT(12X,'DROP DIAMETER      WT% IN LOG-NORMAL DIST.',
     @/12X,42('-'))
          DO 84 JL=1,N
       ALONM(JL)=(EXP(-((((ALOG(D(JL)))-(ALOG(DGM)))**2.0)/(2.0*((ALOG
     @(SG))**2.0)))))*(1.0/(((2.0*PI)**0.5)*(ALOG(SG))))*100.0
       DLN(JL)=D(JL)
  84      CONTINUE
C
        DO 511 LL=1,N
        PRINT 512,DLN(LL),ALONM(LL)
 512    FORMAT(13X,F7.3,14X,F7.3)
 511    CONTINUE
C
          PRINT *,'        '
C
       PRINT *,'              SQUARE ROOT NORMAL DIST. RESULTS:'
C
       PRINT *,'              --------------------------------'
       PRINT 830
 830  FORMAT(12X,'DROP DIMETER    WT% IN SQUARE ROOT NOR. DIST.',
     +/12X,47('-'))
```

```
          DO 86 LL=1,N
         SQRNOM(LL)=(EXP(-(((D(LL)**0.5)-(DGM**0.5))**2.0/
     @(2.0*SG))))*(1.0/(((2.0*PI*SG)**0.5)*2.0))*100.0
        DSR(LL)=D(LL)
  86      CONTINUE
C
       DO 514 NL=1,N
       PRINT 516,DSR(NL),SQRNOM(NL)
 516   FORMAT(13X,F7.3,14X,F7.3)
 514    CONTINUE
C
        PRINT *,'           '
C
       PRINT *,'             UPPER LIMIT DISTRIBUTION RESULTS:'
       PRINT *,'              ------------------------------'
       PRINT 840
 840  FORMAT(12X,'DROP DIAMETER       WT% IN UPPER LIMIT DIST.',
     +/12X,44('-'))
C
          KN=0.0
       DO 88 KK=1,N
          IF(FN(KK).EQ.0.0.OR.D(KK).GE.DMAX) THEN
            KN=KN+1
          GO TO 88
           ELSE
          KNK=KK-KN
      UPLIM(KNK)=(EXP(-(((ALOG(((DMAX-D(KK))/DGM)))**2.0)/
     @(2.0*((ALOG(SG))**2.0)))))*(1.0/(((2.0*PI)**0.5)*(ALOG(SG))))*100
        DUL(KNK)=D(KK)
            ENDIF
 88       CONTINUE
C
C
       DO 518 JL=1,KNK
        PRINT 519,DUL(JL),UPLIM(JL)
 519    FORMAT(13X,F7.3,14X,F7.3)
 518     CONTINUE
C
         PRINT 521
 521       FORMAT(5X,/)
C
C
       PRINT *,'              REAL EXPERIMENTIAL DIST.DATA:'
C
      PRINT *,'              ------------------------------'
      PRINT 860
860   FORMAT(12X,'DROP DIAMETER       WT% FROM EXPERIMENTAL DATA',
     @/12X,46('-'))
         ML=0.0
         DO 99 LN=1,N
         IF(FN(LN).EQ.0.0) THEN
          ML=ML+1
          GO TO 99
           ELSE
```

```
          MLM=LN-ML
          FNW(MLM)=FN(LN)
          DW(MLM)=D(LN)
             ENDIF
  99         CONTINUE
C
C
        DO 223 KN=1,N
        IF(FN(KN).EQ.FNW(MLM)) THEN
         FNW(MLM+1)=FN(KN+1)
            DW(MLM+1)=D(KN+1)
          ELSE
         GO TO 223
         ENDIF
 223     CONTINUE
C
          DO 523 KL=1,MLM+1
          PRINT 524,DW(KL),FNW(KL)
 524      FORMAT(13X,F7.3,14X,F7.3)
 523        CONTINUE
C
C
         PRINT 1112
 1112    FORMAT(2X,/)
C
C   CALCULATION OF THE DEVELOPED DISTRIBUTION FUNCTION.
C   ---------------------------------------------------
C
C
         READ *,JJ,(DJ(J),CFBJ1(J),J=1,JJ)
C
          DO 23 MK=1,N
          CFBJ(MK)=(CFBJ1(MK)-CFBLE)
  23       CONTINUE
C
C
        DO 265 KL=1,JJ
        DJL(KL)=ALOG(DJ(KL)/DFR)
        CFBJL(KL)=ALOG(100.0/(100.0-CFBJ(KL)))
        CFBJLL(KL)=ALOG(CFBJL(KL))
 265     CONTINUE
C
         CALL SLOINT(JJ,DJL,CFBJLL,SLOP,CINT)
C
         SLOPE=SLOP(1)
           B1=SLOPE
           CINT1=EXP(CINT(1))
            C1=CINT1
C
          IF (C1.GT.0.95) THEN
           B=B1*1.35
               C=1.0
            ELSE
C
```

```
            IF (C1.LT.0.5) THEN
               C=0.5
            B=B1*1.15
             ELSE
              C=C1
                 B=B1
               ENDIF
              ENDIF
C
C
          X=1.0
        Z=C*B*(X**(B-1.0))*(EXP(-C*(X**B)))
       PRINT 989,B1,C1,B,C,Z
 989   FORMAT(/,15X,'SLOPE=',F7.3/15X,
     @'INTERCEPT=',F7.3/15X,
     @'BETA (B)=',F7.3/15X,
     @'ALPHA (C)=',F7.3/15X,
     @'CONSTANT (Z)=',F7.3)
       DO 63 MK=1,NMK
              IF (DN(MK).GT.5.0) THEN
       FNEW(MK)=(FNMX/Z)*C*B*((X*DN(MK)/DFR)**(B-1.0))*
     @(EXP(-C*(X*DN(MK)/DFR)**(1.0*B)))
                ELSE
            FNEW(MK)=0.0
             ENDIF
 63      CONTINUE
C
C
C
        LL=0
        DO 69 LK=1,NMK
        IF(DN(LK).GE.DMAX) THEN
         LL=LL+1
          GO TO 69
           ELSE
          LLM=LK-LL
         FNEWD(LLM)=FNEW(LK)
         DWD(LLM)=DN(LK)
           ENDIF
  69        CONTINUE
C
C
          PRINT *,'              THEORETICAL DIST. RESULTS:'
          PRINT *,'              -------------------------'
        PRINT *,'            DROP DIAMETER      WT% IN(THEORETICAL) '
C
       PRINT 973
 973     FORMAT(12X,40('-'))
C
C
          DO 527 LLL=1,LLM
          PRINT 528,DWD(LLL),FNEWD(LLL)
 528      FORMAT(13X,F7.3,14X,F7.3)
 527        CONTINUE
```

```
C
C
C
C
          PRINT 1211
 1211     FORMAT(3X,//)
C  CALCULATION OF ROSIN-RAMMLER DISTRIBUTION FUNCTION:
C ------------------------------------------------
C
C
         READ *,KL,(COVF(JL),DT(JL),JL=1,KL)
C
C
        FV36=36.8
        CALL INTPDM(COVF,DT,KL,FV36,DRR)
        PRINT 917,DRR
 917    FORMAT(15X,'ROSIN-RAMMLER DIAMETER=',F7.3)
      DO 191 KLL=1,N
        FWR1(KLL)=100.0*EXP(-((D(KLL)/DRR)**B1))
 191     CONTINUE
C
        DO 192 LLL=1,N
        FWRR(LLL)=(FWR1(LLL)-FWR1(LLL+1))
        DR(LLL)=D(LLL)
 192     CONTINUE
C
C
C
        PRINT *,'              ROSIN-RAMMLER DIST. RESULTS:'
        PRINT *,'              ---------------------------'
        PRINT 910
 910  FORMAT(12X,'DROP DIAMETER      WT.% BY ROSIN-RAMMLER',
     @/12X,40('-'))
C
         DO 531 KK=1,N
         PRINT 532,DR(KK),FWRR(KK)
 532      FORMAT(13X,F7.3,14X,F7.3)
 531      CONTINUE
C
        PRINT 1121
 1121   FORMAT(5X,/)
C
C
         G1=(1.0+((-1.0)/B1))
        GAMM1=((G1**G1)*(EXP(-G1))*((3.0*PI)/G1)**0.5)*(1.0+(1.0/
     @(228.0*(G1**2.0)))+(1.0/(5184*(G1**3.0))))
         G2=(1.0+((-2.0)/B1))
        GAMM2=((G2**G2)*(EXP(-G2))*((2.0*PI)/G2)**0.5)*(1.0+(1.0/
     @(228.0*(G2**2.0)))+(1.0/(5184*(G2**3.0))))
C
C
C
          DM21=(DFR/(C1**(1.0/B1)))*(GAMM1/GAMM2)
C
```

```
C
C
        DEVT=((DM21-D21)*100.0)/DM21
      PRINT 978,GAMM1,GAMM2,DM21,DEVT
 978   FORMAT(15X,'GAMMA(1)=',F7.3/15X,'GAMMA(2)=',F7.3/15X,
     @'THEORETICAL SURFACE MEAN DIAMETER(D21)=',F10.4/15X,
     @'DEVIATION OF THEORETICAL D21 FROM EXP. D21 (%)=',F8.3/)
C
C
      CALL OPEN
      CALL UNIT(10.0)
      CALL SCALE2(1.4,1.4)
      CALL CHASIZ(0.25, 0.3)
      CALL SHIFT2(2.3,2.3)
      CALL AXIPOS(0,0.0,0.0,12.0,1)
      CALL AXIPOS(0,0.0,0.0,10.0,2)
      CALL AXISCA(3,10,0.0,50.0,1)
      CALL AXISCA(3,10,0.0,100.0,2)
      CALL AXIDRA(1,1,1)
      CALL AXIDRA(-1,-1,2)
      CALL PENSEL(1,0.1,1)
      CALL GRASYM(DW,FNW,MLM,1,0)
      CALL GRACUR(DW,FNW,MLM)
      CALL PENSEL(2,0.1,1)
      CALL GRASYM(DNM,ANORM,NKN,2,0)
      CALL GRACUR(DNM,ANORM,NKN)
      CALL PENSEL(3,0.1,1)
      CALL GRASYM(DLN,ALONM,NLN,3,0)
      CALL GRACUR(DLN,ALONM,NLN)
      CALL PENSEL(4,0.1,1)
      CALL GRASYM(DSR,SQRNOM,LNL,4,0)
      CALL GRACUR(DSR,SQRNOM,LNL)
      CALL PENSEL(1,0.1,1)
        CALL GRASYM(DUL,UPLIM,KNK,5,0)
      CALL GRACUR(DUL,UPLIM,KNK)
      CALL GRACUR(DUL,UPLIM,KNL)
      CALL PENSEL(2,0.1,1)
      CALL GRASYM(DWD,FNEWD,LLM,6,0)
      CALL GRACUR(DWD,FNEWD,LLM)
      CALL PENSEL(3,0.1,1)
      CALL GRASYM(DR,FWRR,MLM,7,0)
      CALL GRACUR(DR,FWRR,MLM)
       CALL MOVTO2(4.0,-1.3)
     CALL CHAHOL(27HDROPLET DIAMETER(MICRONS)*.)
       CALL MOVTO2(-1.1,1.3)
     CALL CHAANG(90.0)
     CALL CHAHOL(42HWEIGHT FREQUENCY OCCURENCE OF DROPLET(%)*.)
      P=10.0
      S=10.0
      DO 186 J=1,7,1
      READ(62,-) (NKKJ(JJ),JJ=1,10)
      CALL MOVTO2(P,S)
      CALL CHAANG(0.0)
      CALL SYMBOL(J)
```

```
      CALL MOVTO2(P+0.35,S-0.35)
      CALL CHAHOL(5H = *.)
      CALL ASCII(NKKJ,10)
        S=S-0.7
 186    CONTINUE
       CALL DEVEND
C
C
        STOP
C
       END
C
C
C
C THIS SUBROUTINE PERFORMS LAGRANGIAN INTERPOLATION WITHIN A
C SET OF (FN,D2)PAIRS TO GIVE THE DM VALUE CORRESPONDING TO FN%
C DEGREE OF INTERPOLATING POLYNOMIAL IS :(N-1).
C
C
      SUBROUTINE INTPDM(X,Y,N,XINT,YOUT)
C
       DIMENSION X(100),Y(100)
       YOUT=0.0
      DO 11 I=1,N
       TERM=Y(I)
       DO 9 J=1,N
       IF(I.EQ.J)  GO TO 9
     IF(X(I).EQ.X(J)) GO TO 9
         TERM=TERM*((XINT-X(J))/(X(I)-X(J)))
  9      CONTINUE
        YOUT=YOUT+TERM
 11      CONTINUE
         RETURN
          END
C
C
C
C SUBROUTINE FOR CALCULATION THE SLOPE AND INTERCEPT:
C
C
C CALL SUBROUTINE (G02CAF) FROM THE NAG LIBRARY.
C
C
      SUBROUTINE SLOINT(N,X,Y,SLOP,CINT)
      REAL X(N),Y(N),SLOP(1),CINT(1),RES(20),COR(1)
      INTEGER N,IFAIL
C
      IFAIL=0
      CALL G02CAF(N,X,Y,RES,IFAIL)
C
      SLOP(1)=RES(6)
      CINT(1)=RES(7)
      COR(1)=RES(5)
C
```

```
        PRINT 956,COR(1)
 956    FORMAT(15X,'CORRELATION COFFICIENT=',F10.3)
        RETURN
         END
C
C
C
C THIS SUBROUTINE FOR CALCULATION THE DENSITY DISTRIBUTION DATA:
C
C
      SUBROUTINE DENDIS(M,DE,W,DWDD)
C
       DIMENSION DE(100),W(100),WT(100),WL(100),DWDD(100)
C
         WT(0)=0.0
        DO 31 I=1,M
        WT(I)=WT(I-1)+W(I)
  31     CONTINUE
C
        WTOL=WT(M)
        DO 32  J=1,M
        WL(J)=WT(J)/WTOL
  32     CONTINUE
C
        WL(0)=0.0
        DE(0)=0.0
        DO 34 K=1,M
        DWDD(K)=(WL(K)-WL(K-1))/(DE(K)-DE(K-1))
  34     CONTINUE
C
         DO 183 L=1,M
        PRINT 120,DE(L),W(L),DWDD(L)
 120    FORMAT(13X,F10.3,14X,F10.3,9X,F10.3)
 183          CONTINUE
         PRINT 121
 121     FORMAT(15X)
C
          RETURN
          END
C
C
C
C
C
C THIS SUBROUTINE  FOR CALCULATION THE PERCENT OF ACTUAL FREQ.
C OCCURENCE OF DROP SIZE NUMBER AND PERCENT OF ACCUMULATION OF
C DROP SIZES FREQ. OCCUR IN THE SYSTEM .
C
C
C
      SUBROUTINE FREQNU(K,FNF,D,FN,CFB,V,VN,VNT,CFAB)
        DIMENSION FNF(50),D(50),FN(50),CFB(50),V(50),VN(50),VNT(50)
     +,CFAB(50)
C
```

```
          VNT(0)=0.0
        DO 501 I=1,K
          V(I)=3.14159*((D(I)/1000.0)**3.0)/6.0
         VN(I)=FNF(I)/V(I)
         VNT(I)=VN(I)+VNT(I-1)
 501     CONTINUE
C
C
        VTOL=VNT(K)
C
C
         DO 503 II=1,K
         FN(II)=VN(II)*100.0/VTOL
         CFB(II)=VNT(II)*100.0/VTOL
 503      CONTINUE
C
             DO 507 LL=1,K
              CFAB(LL)=100.0-CFB(LL)
 507           CONTINUE
              RETURN
          END
```

DATA FROM LAZER PARTICLE-SIZER (MALVERN):

AT EMULSIFICATION PUMP SPEED (R.P.M)= 3500

SIZE BAND UPPER	SIZE BAND LOWER	CUMULATIVE WT.(%) BELOW	CUMULATIVE WT.(%) IN BAND	AVERAGE DIAMETER
1.50	1.20	7.90	3.70	1.35
1.90	1.50	11.60	2.70	1.70
2.40	1.90	14.20	0.00	2.15
3.00	2.40	14.20	0.00	2.70
3.90	3.00	14.20	0.00	3.45
5.00	3.90	14.20	0.00	4.45
6.40	5.00	14.20	1.30	5.70
8.20	6.40	15.50	0.80	7.30
10.50	8.20	16.30	8.00	9.35
13.60	10.50	24.30	10.90	12.05
17.70	13.60	35.20	20.40	15.65
23.70	17.70	55.70	24.40	20.70
33.70	23.70	80.10	14.60	28.70
54.90	33.70	94.70	4.50	44.30
118.40	54.90	99.20	0.80	86.65
118.40	118.40	100.00	0.00	118.40

CUMULATIVE WT% OF IMPURITIES PARTICLES (NOT DROPS)= 14.20
THE ACTUAL NUMBER OF DATA POINTS (EXP.DATA)=11

REAL DATA OF INLET DROP SIZE DIST.(BY WEIGHT%):

SIZE BAND UPPER	SIZE BAND LOWER	CUMULATIVE WEIGHT WT% BELOW	CUMULATIVE WEIGHT WT% IN BAND	AVERAGE DIAMETER
5.00	3.90	0.00	0.00	4.45
6.40	5.00	0.00	1.30	5.70
8.20	6.40	1.30	0.80	7.30
10.50	8.20	2.10	8.00	9.35
13.60	10.50	10.10	10.90	12.05
17.70	13.60	21.00	20.40	15.65
23.70	17.70	41.50	24.40	20.70
33.70	23.70	65.90	14.60	28.70
54.90	33.70	80.50	4.50	44.30
118.40	54.90	85.00	0.80	86.65
118.40	118.40	85.80	0.00	118.40

REAL INLET DROP SIZE DIST.DATA (BY NUMBER OF DROPS%):

AVERAGE DIAMETER	DROPS NO.PER 100 MM**3 VO.	CUM.DROPS NUMBER FRQ.OCC.(%) BELOW	IN BAND	ABOVE
4.45	.000E+01	0.00	0.00	100.00
5.70	.134E+08	20.75	20.75	79.25
7.30	.393E+07	26.82	6.08	73.18
9.35	.187E+08	55.75	28.92	44.25
12.05	.119E+08	74.16	18.41	25.84

15.65	.102E+08	89.89	15.73	10.11
20.70	.525E+07	98.02	8.13	1.98
28.70	.118E+07	99.84	1.83	0.16
44.30	.989E+05	100.00	0.15	0.00
86.65	.235E+04	100.00	0.00	0.00
118.40	.000E+01	100.00	0.00	0.00

MOST FREQUENT DIAMETER(MODE DIAMETER)= 20.700

AT WEIGHT% IN BAND= 24.400

ARITHMATIC MEAN DIAMETER= 20.203

EQUIVALENT PROJECTED DIAMETER(BY SURFACE FACTOR)= 20.198

EQUIVALENT PROJECTED DIAMETER(BY VOLUME FACTOR)= 20.157

LINEAR STANDARD DEVIATION= 25.056

NUMBER OF DATA SHOULD BE USED IN THE CALCULATION= 9

GEOMETRIC MEAN DIAMETER= 18.179

HARMONIC MEAN DIAMETER= 16.482

MEDIAN DIAMETER(DM)= 19.652

AT 84.14% DIAMETER OF DROPS= 50.189

GEOMETRIC STANDARD DEVIATION (SG)= 2.554

MEAN DIAMETER BASED UPON NUMBER,SURFACE,VOLUME AND WEIGHT

MODE DIAMETER(BASED UPON NUMBER OF DROPS)= 9.350

AT NUMBER OF DROP SIZE% IN BAND= 28.925

LINEAR MEAN DIAMETER (D10)= 11.288

SURFACE MEAN (D20)= 12.396

VOLUME MEAN (D30)= 13.631

VOLUME DIAMETER (D31)= 14.979

VOLUME-SURFACE DIAMETER (SAUTER-D32)= 16.482

MOMENT-WEIGHT DIAMETER (D43)= 20.203

SURFACE DIAMETER (D21)= 13.613

MAXIMUM DIAMETER IN THE DATA=118.400

Note:Units of Diameters above are in Microns.

NORMAL DISTRIBUTION RESULTS:

DROP DIAMETER	WT% IN NORMAL DIST.
4.450	1.612
5.700	1.611
7.300	1.609
9.350	1.606
12.050	1.603
15.650	1.598
20.700	1.592
28.700	1.581
44.300	1.562
86.650	1.510
118.400	1.472

LOG-NORMAL DISTRIBUTION RESULTS:

DROP DIAMETER	WT% IN LOG-NORMAL DIST.
4.450	13.793
5.700	19.799
7.300	26.502
9.350	33.090
12.050	38.648
15.650	42.010
20.700	42.143
28.700	37.790
44.300	27.096
86.650	10.630
118.400	5.776

SQUARE ROOT NORMAL DIST. RESULTS:

DROP DIMETER	WT% IN SQUARE ROOT NOR. DIST.
4.450	5.032
5.700	6.266
7.300	7.743
9.350	9.390
12.050	11.038
15.650	12.253
20.700	12.284
28.700	9.876

44.300	4.071
86.650	0.086
118.400	0.002

UPPER LIMIT DISTRIBUTION RESULTS:

DROP DIAMETER	WT% IN UPPER LIMIT DIST.
5.700	6.407
7.300	6.599
9.350	6.856
12.050	7.213
15.650	7.724
20.700	8.518
28.700	9.989
44.300	13.841
86.650	35.651

REAL EXPERIMENTIAL DIST.DATA:

DROP DIAMETER	WT% FROM EXPERIMENTAL DATA
5.700	1.300
7.300	0.800
9.350	8.000
12.050	10.900
15.650	20.400
20.700	24.400
28.700	14.600
44.300	4.500
86.650	0.800
118.400	0.000

CORRELATION COFFICIENT= 0.965

SLOPE= 2.970
INTERCEPT= 0.610
BETA (B)= 2.970
ALPHA (C)= 0.610
CONSTANT (Z)= 0.984

THEORETICAL DIST. RESULTS:

DROP DIAMETER	WT% IN(THEORETICAL)
1.350	0.000
1.700	0.000
2.150	0.000
2.700	0.000
3.450	0.000
4.450	0.000
5.700	3.494
7.300	5.607

9.350	8.859
12.050	13.687
15.650	19.842
20.700	24.400
28.700	17.095
44.300	0.584
86.650	0.000

ROSIN-RAMMLER DIAMETER= 18.132

ROSIN-RAMMLER DIST. RESULTS:

DROP DIAMETER	WT.% BY ROSIN-RAMMLER
4.450	1.636
5.700	3.322
7.300	6.568
9.350	12.654
12.050	21.872
15.650	29.700
20.700	20.715
28.700	2.002
44.300	0.000
86.650	0.000
118.400	0.000

GAMMA(1)= 1.495

GAMMA(2)= 2.299

THEORETICAL SURFACE MEAN DIAMETER(D21)= 15.9013

DEVIATION OF THEORETICAL D21 FROM EXP. D21 (%)= 14.391

APPENDIX V

Polynomial Regression Analysis Computer Program for Analysis of Mean Inlet Drop Size Data

```
C THIS PROGRAM FOR POLYNOMIAL REGRESSION ANALYSIS OF MEAN INLET DROP SIZES.
C ==========================================================================
C
C
      DIMENSION N(10),M(10),M1(10),X(50),Y(50),A(50),Z(50),S(50),
     @T(50),H(10)
C
       DO 3 LL=1,3
      READ *,N(LL)
      READ *,(X(I),Y(I),I=1,N(LL))
       READ *,M(LL),M1(LL)
      CALL E02ACF(X,Y,N,A,M1,REF)
      PRINT *,'                CURVE FITTING RESULTS: '
        PRINT *,'                ----------------------'
      PRINT *,'                POLYNOMIAL COEFFICIENTS :'
          DO 15 I=1,M1(LL)
          PRINT 16,A(I)
  16     FORMAT(40X,E15.6)
  15      CONTINUE
C
        PRINT 222
 222    FORMAT(10X,/)
C
         PRINT 22
  22   FORMAT(15X,'   X          Y          FIT          RESIDUAL ')
          PRINT 23
  23     FORMAT(14X,46('-'))
       DO 10 J=1,N(LL)
        Z(J)=X(J)
        S(J)=A(M(LL)+1)
        I=M(LL)
  20    S(J)=S(J)*Z(J)+A(I)
        IF(I-1) 30,30,40
 40      I=I-1
        GO TO 20
 30     T(J)=Y(J)
        H(LL)=S(J)-T(J)
        PRINT 100,Z(J),T(J),S(J),H(LL)
 100    FORMAT(14X,F7.1,3X,F10.6,2X,F10.6,2X,F10.6)
  10    CONTINUE
       PRINT 12
 12    FORMAT(//,14X,50('-'),14X,//)
  3     CONTINUE
      CALL OPEN
      CALL UNITS(10.0)
      CALL SCALE2(0.6,0.6)
      CALL CHASIZ(0.25,0.3)
      CALL SHIFT2(4.0,4.0)
      CALL AXIPOS(0,0.0,0.0,10.0,1)
      CALL AXIPOS(0,0.0,0.0,10.0,2)
      CALL AXISCA(3,10,0.0,6.0,1)
        CALL AXISCA(3,5,0.0,6.0,2)
      CALL AXIDRA(1,1,1)
      CALL AXIDRA(-1,-1,2)
```

```
      CALL MOVTO2(3.0,-2.5)
      CALL CHAHOL(17HPUMP SPEED(RPM)*.)
      CALL MOVTO2(-2.5,2.5)
      CALL CHAANG(90.0)
     CALL PENSEL(2,0.1,1)
      CALL CHAHOL(22HINLET DROP SIZE(D21)*.)
      CALL CHAANG(0.0)
        DO 6 NN=1,3
      CALL GRASYM(Z,T,N(NN),1,0)
     CALL PENSEL(3,0.1,1)
      CALL POLTO2(Z,S,N(NN))
6      CONTINUE
      CALL DEVEND
         STOP
         END
```

CURVE FITTING RESULTS:

POLYNOMIAL COEFFICIENTS :

0.825147E+02
-0.273947E-01

X	Y	FIT	RESIDUAL
1250.0	47.622000	48.271333	0.649333
1500.0	42.072000	41.422667	-0.649333
2000.0	27.076000	27.725333	0.649333

CURVE FITTING RESULTS:

POLYNOMIAL COEFFICIENTS :

0.470213E+02
-0.993700E-02

X	Y	FIT	RESIDUAL
2000.0	27.067000	27.147250	0.080250
2500.0	22.259000	22.178750	-0.080250
3000.0	17.130000	17.210250	0.080250
3500.0	13.187000	12.241750	-0.945250
4000.0	10.082000	7.273250	-2.808750

CURVE FITTING RESULTS:

POLYNOMIAL COEFFICIENTS :

0.179497E+02
-0.200500E-02

X	Y	FIT	RESIDUAL
4000.0	10.082000	9.929650	-0.152350
4500.0	8.774800	8.927150	0.152350
5000.0	8.077000	7.924650	-0.152350

APPENDIX W

Computer Program for Evaluation of Capture Mechanism Contributions

```
C       ================================================
C       COMPUTER PROGRAM FOR EVALUATION OF "CAPTURE
C       MECHANISM CONTRIBUTION" IN COALESCENCE OF
C       OIL/WATER SECONDARY DISPERSIONS.
C       ================================================
C
C
C
      DIMENSION DC(50),V(50),DP(50),CAPM(50),E(50),RC(50)
         REAL K
      PARAMETER(PI=3.14159, CD=1000.0,CV=0.001,DD=860.0,
     +Q=0.401E-20,DA=105.0E-06,K=0.138048E-22,T=293.0,GR=9.81)
C
C
      PRINT 95
 95   FORMAT(10X,'EVALUATION OF CAPTURE MECHANISM CONTRIBUTIONS'/
     +10X,46('*'))
C
          READ*,N,M,J
                READ*,(DC(I),I=1,N)
          READ *,(E(IN),IN=1,N)
C
                     READ*,(V(II),II=1,M)
                       READ*,(DP(IJ),IJ=1,J)
                DO 2 I=1,N
                  PRINT 100,DC(I)
 100       FORMAT(///5X,'PARTICLE DIAMETER=',3PE10.4/5X,19('_')/)
                DO 3 II=1,M
                  PRINT 110,V(II)
 110     FORMAT(//7X,'SUPERFICIAL VELOCITY =',1PE10.4/7X,21('='))
          PRINT 105
 105      FORMAT(5X,//
     +5X,'  INLET DROP    SIGNIFICANT     MECHANISM TOTAL  %RELATIVE',/
     +5X,'  SIZE(METER)   MECHANISMS      EFFICIENCY  EFF. CONTRIBUTION',
     +/5X,62('-'))
                DO 4 IJ=1,J
                 PRINT 120,DP(IJ)
 120    FORMAT(5X,2PE13.5)
C
C               CALCULATE THE DIMENSIONLESS GROUP
C               ---------------------------------
C
              RD=DP(IJ)/DC(I)
          RDII=DP(IJ)/DA
            RE=DC(I)*V(II)*CD/CV
         CAM=(1.0-E(I))**0.3333
         AS=(2.0*(1-CAM**5))/(2.0-(3*CAM)+(3*(CAM**5))-(2*(CAM**6)))
C
C
         SKT=((DP(IJ)**2)*CD*V(II))/(9*CV*DC(I))
C
         G=(((DP(IJ)/2)**2)*2.0*(DD-CD)*GR)/(9*CV*V(II))
C
```

```
      AD=(Q*((DC(I)/2)**2))/(9*PI*CV*V(II)*AS*((DP(IJ)/2)**4))
C
      PE=(12*PI*(DC(I)/2)*(DP(IJ)/2)*V(II)*CV)/(K*T)
C
C
C              CALCULATION OF CAPTURE MECHANISM EFFICIENCIES
C              =============================================
C
C
         CAPM(1)=1.5*(RD**2.0)
C
C
           IF(RDII.GE.1.0) THEN
        CAPM(2)=1.0
           ELSE
        CAPM(2)=0.0
           ENDIF
C
           IF(RE.LE.10.0) THEN
       CAPM(3)=0.0
         ELSE
      CAPM(3)=(SKT**3)/((SKT**3)+0.77*(SKT**2)+0.22)
          ENDIF
C
               IF(G.GE.0.0001) THEN
            CAPM(4)=G
               ELSE
            CAPM(4)=0.0
               ENDIF
C
       CAPM(5)=2.0*AS*(RD**2)*((9.0*AD/5.0)**0.3333)
        CAPM(6)=4.04/(PE**0.6667)
C
C
             CAPET=CAPM(1)+CAPM(2)+CAPM(3)+CAPM(4)+CAPM(5)+CAPM(6)
C
             DO 7 IN=1,6
              RC(IN)=CAPM(IN)*100.0/CAPET
C
C
       IF(RC(IN).LT.0.000001) GO TO 7
C
C
             IF(IN.EQ.1) THEN
         PRINT 150,CAPM(1),CAPET,RC(1)
 150  FORMAT(18X,'INDIRCT INTERCEP.',F10.7,1X,F8.4,1X,F9.3)
                ELSE
C
                  IF(IN.EQ.2) THEN
            PRINT 155,CAPM(2),CAPET,RC(2)
 155    FORMAT(18X,' DIRECT INTERCEP.',F10.7,1X,F8.4,1X,F9.3)
                  ELSE
C
                  IF(IN.EQ.3) THEN
```

```
            PRINT 160,CAPM(3),CAPET,RC(3)
 160    FORMAT(18X,' INERTIAL IMPACT.',F10.7,1X,F8.4,1X,F9.3)
                    ELSE
C
                      IF(IN.EQ.4) THEN
                PRINT 165,CAPM(4),CAPET,RC(4)
 165      FORMAT(18X,'   SEDIMENTATION  ',F10.7,1X,F8.4,1X,F9.3)
                     ELSE
C
                        IF(IN.EQ.5) THEN
              PRINT 170,CAPM(5),CAPET,RC(5)
 170    FORMAT(18X,'LONDON-VAN FORCES',F10.7,1X,F8.4,1X,F9.3)
C
                         ELSE
C
                    IF(IN.EQ.6) THEN
           PRINT 175,CAPM(6),CAPET,RC(6)
 175   FORMAT(16X,'  DIFFUSION      ',2X,F10.7,1X,F8.4,1X,F9.3)
C
C
               ENDIF
                ENDIF
                 ENDIF
                  ENDIF
                   ENDIF
                    ENDIF
C
C

   7       CONTINUE
   4       CONTINUE
   3       CONTINUE
   2       CONTINUE
         STOP
           END
```

EVALUATION OF CAPTURE MECHANISM CONTRIBUTIONS
****

PARTICLE DIAMETER=266.00E-06

SUPERFICIAL VELOCITY =8.0000E-04

INLET DROP SIZE(METER)	SIGNIFICANT MECHANISMS	MECHANISM EFFICIENCY	TOTAL EFF.	%RELATIVE CONTRIBUTION
47.0000E-06				
	INDIRCT INTERCEP.	0.0468300	0.0714	65.607
	LONDON-VAN FORCES	0.0245000	0.0714	34.324
	DIFFUSION	0.0000495	0.0714	0.069
42.0000E-06				
	INDIRCT INTERCEP.	0.0373961	0.0602	62.141
	LONDON-VAN FORCES	0.0227297	0.0602	37.770
	DIFFUSION	0.0000533	0.0602	0.089
27.0000E-06				
	INDIRCT INTERCEP.	0.0154545	0.0325	47.617
	LONDON-VAN FORCES	0.0169295	0.0325	52.162
	DIFFUSION	0.0000716	0.0325	0.221
22.0000E-06				
	INDIRCT INTERCEP.	0.0102606	0.0251	40.861
	LONDON-VAN FORCES	0.0147686	0.0251	58.812
	DIFFUSION	0.0000821	0.0251	0.327
17.0000E-06				
	INDIRCT INTERCEP.	0.0061267	0.0187	32.833
	LONDON-VAN FORCES	0.0124358	0.0187	66.644
	DIFFUSION	0.0000975	0.0187	0.522
13.0000E-06				
	INDIRCT INTERCEP.	0.0035827	0.0141	25.413
	LONDON-VAN FORCES	0.0103989	0.0141	73.760
	DIFFUSION	0.0001166	0.0141	0.827
10.0000E-06				
	INDIRCT INTERCEP.	0.0021200	0.0110	19.292
	LONDON-VAN FORCES	0.0087299	0.0110	79.444
	DIFFUSION	0.0001389	0.0110	1.264
80.0000E-07				
	INDIRCT INTERCEP.	0.0013568	0.0090	15.007
	LONDON-VAN FORCES	0.0075230	0.0090	83.211
	DIFFUSION	0.0001611	0.0090	1.782

SUPERFICIAL VELOCITY =1.0300E-03

INLET DROP SIZE(METER)	SIGNIFICANT MECHANISMS	MECHANISM EFFICIENCY	TOTAL EFF.	%RELATIVE CONTRIBUTION
47.0000E-06				
	INDIRCT INTERCEP.	0.0468300	0.0694	67.485
	LONDON-VAN FORCES	0.0225210	0.0694	32.454
	DIFFUSION	0.0000418	0.0694	0.060
42.0000E-06				
	INDIRCT INTERCEP.	0.0373961	0.0583	64.106
	LONDON-VAN FORCES	0.0208937	0.0583	35.817
	DIFFUSION	0.0000451	0.0583	0.077
27.0000E-06				
	INDIRCT INTERCEP.	0.0154545	0.0311	49.730
	LONDON-VAN FORCES	0.0155620	0.0311	50.076
	DIFFUSION	0.0000605	0.0311	0.195
22.0000E-06				
	INDIRCT INTERCEP.	0.0102606	0.0239	42.921
	LONDON-VAN FORCES	0.0135756	0.0239	56.788
	DIFFUSION	0.0000694	0.0239	0.290
17.0000E-06				
	INDIRCT INTERCEP.	0.0061267	0.0176	34.731
	LONDON-VAN FORCES	0.0114313	0.0176	64.802
	DIFFUSION	0.0000824	0.0176	0.467
13.0000E-06				
	INDIRCT INTERCEP.	0.0035827	0.0132	27.060
	LONDON-VAN FORCES	0.0095589	0.0132	72.196
	DIFFUSION	0.0000985	0.0132	0.744
10.0000E-06				
	INDIRCT INTERCEP.	0.0021200	0.0103	20.658
	LONDON-VAN FORCES	0.0080248	0.0103	78.198
	DIFFUSION	0.0001173	0.0103	1.143
80.0000E-07				
	INDIRCT INTERCEP.	0.0013568	0.0084	16.136
	LONDON-VAN FORCES	0.0069153	0.0084	82.244
	DIFFUSION	0.0001362	0.0084	1.619

SUPERFICIAL VELOCITY =1.5000E-03

INLET DROP SIZE(METER)	SIGNIFICANT MECHANISMS	MECHANISM EFFICIENCY	TOTAL EFF.	%RELATIVE CONTRIBUTION
47.0000E-06				
	INDIRCT INTERCEP.	0.0468300	0.0667	70.177
	LONDON-VAN FORCES	0.0198689	0.0667	29.774
	DIFFUSION	0.0000325	0.0667	0.049
42.0000E-06				
	INDIRCT INTERCEP.	0.0373961	0.0559	66.941
	LONDON-VAN FORCES	0.0184333	0.0559	32.996
	DIFFUSION	0.0000351	0.0559	0.063
27.0000E-06				
	INDIRCT INTERCEP.	0.0154545	0.0292	52.870

	LONDON-VAN FORCES	0.0137294	0.0292	46.969
	DIFFUSION	0.0000471	0.0292	0.161
22.0000E-06				
	INDIRCT INTERCEP.	0.0102606	0.0223	46.029
	LONDON-VAN FORCES	0.0119770	0.0223	53.729
	DIFFUSION	0.0000540	0.0223	0.242
17.0000E-06				
	INDIRCT INTERCEP.	0.0061267	0.0163	37.643
	LONDON-VAN FORCES	0.0100852	0.0163	61.964
	DIFFUSION	0.0000641	0.0163	0.394
13.0000E-06				
	INDIRCT INTERCEP.	0.0035827	0.0121	29.627
	LONDON-VAN FORCES	0.0084333	0.0121	69.739
	DIFFUSION	0.0000767	0.0121	0.634
10.0000E-06				
	INDIRCT INTERCEP.	0.0021200	0.0093	22.817
	LONDON-VAN FORCES	0.0070798	0.0093	76.200
	DIFFUSION	0.0000913	0.0093	0.983
80.0000E-07				
	INDIRCT INTERCEP.	0.0013568	0.0076	17.938
	LONDON-VAN FORCES	0.0061010	0.0076	80.661
	DIFFUSION	0.0001060	0.0076	1.401

SUPERFICIAL VELOCITY =2.5000E-03

INLET DROP SIZE(METER)	SIGNIFICANT MECHANISMS	MECHANISM EFFICIENCY	TOTAL EFF.	%RELATIVE CONTRIBUTION
47.0000E-06				
	INDIRCT INTERCEP.	0.0468300	0.0636	73.619
	LONDON-VAN FORCES	0.0167584	0.0636	26.345
	DIFFUSION	0.0000232	0.0636	0.036
42.0000E-06				
	INDIRCT INTERCEP.	0.0373961	0.0530	70.601
	LONDON-VAN FORCES	0.0155475	0.0530	29.352
	DIFFUSION	0.0000250	0.0530	0.047
27.0000E-06				
	INDIRCT INTERCEP.	0.0154545	0.0271	57.095
	LONDON-VAN FORCES	0.0115801	0.0271	42.781
	DIFFUSION	0.0000335	0.0271	0.124
22.0000E-06				
	INDIRCT INTERCEP.	0.0102606	0.0204	50.295
	LONDON-VAN FORCES	0.0101019	0.0204	49.517
	DIFFUSION	0.0000384	0.0204	0.188
17.0000E-06				
	INDIRCT INTERCEP.	0.0061267	0.0147	41.739
	LONDON-VAN FORCES	0.0085063	0.0147	57.950
	DIFFUSION	0.0000456	0.0147	0.311
13.0000E-06				
	INDIRCT INTERCEP.	0.0035827	0.0108	33.327
	LONDON-VAN FORCES	0.0071130	0.0108	66.166

	DIFFUSION	0.0000545	0.0108	0.507
10.0000E-06				
	INDIRCT INTERCEP.	0.0021200	0.0082	25.992
	LONDON-VAN FORCES	0.0059714	0.0082	73.212
	DIFFUSION	0.0000650	0.0082	0.796
80.0000E-07				
	INDIRCT INTERCEP.	0.0013568	0.0066	20.626
	LONDON-VAN FORCES	0.0051459	0.0066	78.228
	DIFFUSION	0.0000754	0.0066	1.146

SUPERFICIAL VELOCITY =3.0500E-03

INLET DROP SIZE(METER)	SIGNIFICANT MECHANISMS	MECHANISM EFFICIENCY	TOTAL EFF.	%RELATIVE CONTRIBUTION
47.0000E-06				
	INDIRCT INTERCEP.	0.0468300	0.0625	74.887
	LONDON-VAN FORCES	0.0156837	0.0625	25.080
	DIFFUSION	0.0000203	0.0625	0.032
42.0000E-06				
	INDIRCT INTERCEP.	0.0373961	0.0520	71.959
	LONDON-VAN FORCES	0.0145504	0.0520	27.999
	DIFFUSION	0.0000219	0.0520	0.042
27.0000E-06				
	INDIRCT INTERCEP.	0.0154545	0.0263	58.715
	LONDON-VAN FORCES	0.0108374	0.0263	41.174
	DIFFUSION	0.0000293	0.0263	0.111
22.0000E-06				
	INDIRCT INTERCEP.	0.0102606	0.0197	51.957
	LONDON-VAN FORCES	0.0094541	0.0197	47.873
	DIFFUSION	0.0000336	0.0197	0.170
17.0000E-06				
	INDIRCT INTERCEP.	0.0061267	0.0141	43.367
	LONDON-VAN FORCES	0.0079608	0.0141	56.350
	DIFFUSION	0.0000399	0.0141	0.283
13.0000E-06				
	INDIRCT INTERCEP.	0.0035827	0.0103	34.826
	LONDON-VAN FORCES	0.0066569	0.0103	64.709
	DIFFUSION	0.0000478	0.0103	0.464
10.0000E-06				
	INDIRCT INTERCEP.	0.0021200	0.0078	27.300
	LONDON-VAN FORCES	0.0055885	0.0078	71.967
	DIFFUSION	0.0000569	0.0078	0.733
80.0000E-07				
	INDIRCT INTERCEP.	0.0013568	0.0062	21.748
	LONDON-VAN FORCES	0.0048159	0.0062	77.194
	DIFFUSION	0.0000660	0.0062	1.058

SUPERFICIAL VELOCITY =3.6000E-03

INLET DROP SIZE(METER)	SIGNIFICANT MECHANISMS	MECHANISM EFFICIENCY	TOTAL EFF.	%RELATIVE CONTRIBUTION
47.0000E-06				
	INDIRCT INTERCEP.	0.0468300	0.0617	75.913
	LONDON-VAN FORCES	0.0148405	0.0617	24.057
	DIFFUSION	0.0000182	0.0617	0.029
42.0000E-06				
	INDIRCT INTERCEP.	0.0373961	0.0512	73.062
	LONDON-VAN FORCES	0.0137682	0.0512	26.900
	DIFFUSION	0.0000196	0.0512	0.038
27.0000E-06				
	INDIRCT INTERCEP.	0.0154545	0.0257	60.051
	LONDON-VAN FORCES	0.0102548	0.0257	39.847
	DIFFUSION	0.0000263	0.0257	0.102
22.0000E-06				
	INDIRCT INTERCEP.	0.0102606	0.0192	53.339
	LONDON-VAN FORCES	0.0089459	0.0192	46.504
	DIFFUSION	0.0000301	0.0192	0.157
17.0000E-06				
	INDIRCT INTERCEP.	0.0061267	0.0137	44.736
	LONDON-VAN FORCES	0.0075328	0.0137	55.003
	DIFFUSION	0.0000358	0.0137	0.261
13.0000E-06				
	INDIRCT INTERCEP.	0.0035827	0.0099	36.100
	LONDON-VAN FORCES	0.0062990	0.0099	63.469
	DIFFUSION	0.0000428	0.0099	0.431
10.0000E-06				
	INDIRCT INTERCEP.	0.0021200	0.0075	28.422
	LONDON-VAN FORCES	0.0052880	0.0075	70.895
	DIFFUSION	0.0000509	0.0075	0.683
80.0000E-07				
	INDIRCT INTERCEP.	0.0013568	0.0060	22.716
	LONDON-VAN FORCES	0.0045570	0.0060	76.295
	DIFFUSION	0.0000591	0.0060	0.990

SUPERFICIAL VELOCITY =4.7500E-03

INLET DROP SIZE(METER)	SIGNIFICANT MECHANISMS	MECHANISM EFFICIENCY	TOTAL EFF.	%RELATIVE CONTRIBUTION
47.0000E-06				
	INDIRCT INTERCEP.	0.0468300	0.0604	77.564
	LONDON-VAN FORCES	0.0135308	0.0604	22.411
	DIFFUSION	0.0000151	0.0604	0.025
42.0000E-06				
	INDIRCT INTERCEP.	0.0373961	0.0500	74.844
	LONDON-VAN FORCES	0.0125531	0.0500	25.124
	DIFFUSION	0.0000163	0.0500	0.033
27.0000E-06				
	INDIRCT INTERCEP.	0.0154545	0.0248	62.251

	LONDON-VAN FORCES	0.0093498	0.0248	37.661
	DIFFUSION	0.0000218	0.0248	0.088
22.0000E-06				
	INDIRCT INTERCEP.	0.0102606	0.0184	55.637
	LONDON-VAN FORCES	0.0081564	0.0184	44.227
	DIFFUSION	0.0000250	0.0184	0.136
17.0000E-06				
	INDIRCT INTERCEP.	0.0061267	0.0130	47.040
	LONDON-VAN FORCES	0.0068680	0.0130	52.732
	DIFFUSION	0.0000297	0.0130	0.228
13.0000E-06				
	INDIRCT INTERCEP.	0.0035827	0.0094	38.271
	LONDON-VAN FORCES	0.0057431	0.0094	61.349
	DIFFUSION	0.0000356	0.0094	0.380
10.0000E-06				
	INDIRCT INTERCEP.	0.0021200	0.0070	30.356
	LONDON-VAN FORCES	0.0048213	0.0070	69.038
	DIFFUSION	0.0000423	0.0070	0.606
80.0000E-07				
	INDIRCT INTERCEP.	0.0013568	0.0056	24.399
	LONDON-VAN FORCES	0.0041548	0.0056	74.717
	DIFFUSION	0.0000491	0.0056	0.884

SUPERFICIAL VELOCITY =6.0000E-03

INLET DROP SIZE(METER)	SIGNIFICANT MECHANISMS	MECHANISM EFFICIENCY	TOTAL EFF.	%RELATIVE CONTRIBUTION
47.0000E-06				
	INDIRCT INTERCEP.	0.0468300	0.0594	78.891
	LONDON-VAN FORCES	0.0125172	0.0594	21.087
	DIFFUSION	0.0000129	0.0594	0.022
42.0000E-06				
	INDIRCT INTERCEP.	0.0373961	0.0490	76.283
	LONDON-VAN FORCES	0.0116128	0.0490	23.688
	DIFFUSION	0.0000139	0.0490	0.028
27.0000E-06				
	INDIRCT INTERCEP.	0.0154545	0.0241	64.067
	LONDON-VAN FORCES	0.0086494	0.0241	35.856
	DIFFUSION	0.0000187	0.0241	0.077
22.0000E-06				
	INDIRCT INTERCEP.	0.0102606	0.0178	57.555
	LONDON-VAN FORCES	0.0075454	0.0178	42.325
	DIFFUSION	0.0000214	0.0178	0.120
17.0000E-06				
	INDIRCT INTERCEP.	0.0061267	0.0125	48.991
	LONDON-VAN FORCES	0.0063535	0.0125	50.805
	DIFFUSION	0.0000254	0.0125	0.203
13.0000E-06				
	INDIRCT INTERCEP.	0.0035827	0.0089	40.138
	LONDON-VAN FORCES	0.0053129	0.0089	59.521

DIFFUSION	0.0000304	0.0089	0.341
10.0000E-06			
INDIRCT INTERCEP.	0.0021200	0.0066	32.041
LONDON-VAN FORCES	0.0044602	0.0066	67.411
DIFFUSION	0.0000362	0.0066	0.548
80.0000E-07			
INDIRCT INTERCEP.	0.0013568	0.0052	25.881
LONDON-VAN FORCES	0.0038436	0.0052	73.317
DIFFUSION	0.0000421	0.0052	0.802

APPENDIX X

Computer Program To Calculate Initial Drop Capture Rate In Coalescer

```
C COMPUTER PROGRAM FOR CALCULATION OF RATE OF DROP CAPTURE.
C ==========================================================
C
C
C
C
      DIMENSION D(100),BD(100),U1(10),E(150),F(150)
C
         REAL N(100)
C
        READ *,NPT
C
       READ *,DC,AC,AS,C1,CV,CD,DD,G1,Q,CK,T,E1
C
C
C
      PRINT 101
 101  FORMAT(///10X,'RATE OF NOT CAPTURED DROPS RESULTS',
     @/,10X,33('-')//)
C
       READ *,(U1(MM),MM=1,NPT)
         READ *,(BD(JJ),JJ=1,5)
C
C
        DO 3 M=1,NPT
C
C
C
           PRINT 102,U1(M)
  102  FORMAT(10X, 'SUPERFICIAL VELOCITY=',F10.6,1X,'M/S',/)
C
        DO 4 J=1,5
C
         PRINT 155,BD(J)
 155  FORMAT(//,10X,'BED DEPTH=',F10.5,'METER',/,10X,10('-')//)
C
C
       PRINT 166
 166   FORMAT(5X,' I   D2     FNW(D2)    D(I)       N(I)       F3',
     @/5X,55('-'))
        D2=2
       F1=U1(M)*AC*Q
        W1=FNW(D2)
C
          F3=0.0
C
           DO 5 I=1,25
           W2=FNW(D2)
       F2=0.01*(W1-W2)*F1
       D(I)=(D2-1)*0.1E-05
       N(I)=6.0*F2/(3.14159*(D(I)**3))
C
C
C
```

```
      AD=(Q*((DC/2)**2))/(9*3.14159*CV*U1(M)*AS*((D(I)/2)**4))
C
      E(I)=1+1.622*AS*(AD**0.333)+2.223*((AS*CK*T*AD/Q)**0.667)
C
C
      N(I)=N(I)*EXP(-0.75*((1-E1)/AC)*E(I)*BD(J))
C
       F3=F3+N(I)*3.14159*(D(I)**3)/6
        F4=F3*100/F1
C
         PRINT 201,I,D2,W2,D(I),N(I),F3
 201   FORMAT(5X,I3,1X,F4.1,1X,4(1PE10.3,1X))
C
         D2=D2+2
C
   5      CONTINUE
C
        PRINT 177,F4
 177  FORMAT(/,10X,'TOTAL UNCAPTURED DROPS RATE (F4)=',F10.3,'%',/)
        PRINT 200
 200    FORMAT(//,7X,60('-')//)
   4     CONTINUE
   3     CONTINUE
C
         STOP
         END
C
C
C
C
         FUNCTION FNW(D)
         FNW=113.525-3.44*D
C
         RETURN
         END
```

RATE OF NOT CAPTURED DROPS RESULTS

SUPERFICIAL VELOCITY= 0.000800 M/S

BED DEPTH= 0.01800METER

I	D2	FNW(D2)	D(I)	N(I)	F3
1	2.0	1.066E+02	1.000E-06	0.000E+00	0.000E+00
2	4.0	9.977E+01	3.000E-06	1.392E-30	0.000E+00
3	6.0	9.289E+01	5.000E-06	2.714E-21	1.776E-37
4	8.0	8.600E+01	7.000E-06	3.779E-18	6.789E-34
5	10.0	7.913E+01	9.000E-06	1.131E-16	4.385E-32
6	12.0	7.225E+01	1.100E-05	7.383E-16	5.584E-31
7	14.0	6.537E+01	1.300E-05	2.306E-15	3.211E-30
8	16.0	5.849E+01	1.500E-05	4.812E-15	1.171E-29
9	18.0	5.161E+01	1.700E-05	7.891E-15	3.201E-29
10	20.0	4.473E+01	1.900E-05	1.111E-14	7.190E-29
11	22.0	3.785E+01	2.100E-05	1.412E-14	1.404E-28
12	24.0	3.096E+01	2.300E-05	1.674E-14	2.470E-28
13	26.0	2.409E+01	2.500E-05	1.888E-14	4.014E-28
14	28.0	1.721E+01	2.700E-05	2.053E-14	6.130E-28
15	30.0	1.033E+01	2.900E-05	2.173E-14	8.905E-28
16	32.0	3.445E+00	3.100E-05	2.255E-14	1.242E-27
17	34.0	-3.435E+00	3.300E-05	2.303E-14	1.676E-27
18	36.0	-1.031E+01	3.500E-05	2.324E-14	2.197E-27
19	38.0	-1.720E+01	3.700E-05	2.324E-14	2.814E-27
20	40.0	-2.408E+01	3.900E-05	2.307E-14	3.530E-27
21	42.0	-3.096E+01	4.100E-05	2.277E-14	4.352E-27
22	44.0	-3.784E+01	4.300E-05	2.237E-14	5.283E-27
23	46.0	-4.472E+01	4.500E-05	2.189E-14	6.328E-27
24	48.0	-5.160E+01	4.700E-05	2.137E-14	7.489E-27
25	50.0	-5.848E+01	4.900E-05	2.081E-14	8.771E-27

TOTAL UNCAPTURED DROPS RATE (F4)= 59.959%

BED DEPTH= 0.02000METER

I	D2	FNW(D2)	D(I)	N(I)	F3
1	2.0	1.066E+02	1.000E-06	0.000E+00	0.000E+00
2	4.0	9.977E+01	3.000E-06	8.993E-33	0.000E+00
3	6.0	9.289E+01	5.000E-06	2.072E-22	1.356E-38
4	8.0	8.600E+01	7.000E-06	6.898E-19	1.239E-34
5	10.0	7.913E+01	9.000E-06	3.172E-17	1.223E-32
6	12.0	7.225E+01	1.100E-05	2.660E-16	1.976E-31
7	14.0	6.537E+01	1.300E-05	9.770E-16	1.322E-30
8	16.0	5.849E+01	1.500E-05	2.281E-15	5.352E-30
9	18.0	5.161E+01	1.700E-05	4.059E-15	1.579E-29
10	20.0	4.473E+01	1.900E-05	6.078E-15	3.762E-29
11	22.0	3.785E+01	2.100E-05	8.111E-15	7.695E-29
12	24.0	3.096E+01	2.300E-05	9.993E-15	1.406E-28
13	26.0	2.409E+01	2.500E-05	1.163E-14	2.358E-28
14	28.0	1.721E+01	2.700E-05	1.298E-14	3.695E-28
15	30.0	1.033E+01	2.900E-05	1.405E-14	5.489E-28
16	32.0	3.445E+00	3.100E-05	1.485E-14	7.805E-28
17	34.0	-3.435E+00	3.300E-05	1.541E-14	1.071E-27
18	36.0	-1.031E+01	3.500E-05	1.577E-14	1.425E-27
19	38.0	-1.720E+01	3.700E-05	1.596E-14	1.848E-27
20	40.0	-2.408E+01	3.900E-05	1.602E-14	2.346E-27
21	42.0	-3.096E+01	4.100E-05	1.596E-14	2.921E-27
22	44.0	-3.784E+01	4.300E-05	1.581E-14	3.580E-27
23	46.0	-4.472E+01	4.500E-05	1.559E-14	4.324E-27
24	48.0	-5.160E+01	4.700E-05	1.532E-14	5.157E-27
25	50.0	-5.848E+01	4.900E-05	1.501E-14	6.082E-27

TOTAL UNCAPTURED DROPS RATE (F4)= 41.574%

BED DEPTH= 0.03000METER

I	D2	FNW(D2)	D(I)	N(I)	F3
1	2.0	1.066E+02	1.000E-06	0.000E+00	0.000E+00
2	4.0	9.977E+01	3.000E-06	0.000E+00	0.000E+00
3	6.0	9.289E+01	5.000E-06	5.378E-28	0.000E+00
4	8.0	8.600E+01	7.000E-06	1.397E-22	2.509E-38
5	10.0	7.913E+01	9.000E-06	5.501E-20	2.102E-35
6	12.0	7.225E+01	1.100E-05	1.614E-18	1.146E-33
7	14.0	6.537E+01	1.300E-05	1.333E-17	1.648E-32
8	16.0	5.849E+01	1.500E-05	5.455E-17	1.129E-31
9	18.0	5.161E+01	1.700E-05	1.462E-16	4.889E-31
10	20.0	4.473E+01	1.900E-05	2.984E-16	1.560E-30
11	22.0	3.785E+01	2.100E-05	5.070E-16	4.019E-30

12	24.0	3.096E+01	2.300E-05	7.577E-16	8.846E-30
13	26.0	2.409E+01	2.500E-05	1.032E-15	1.729E-29
14	28.0	1.721E+01	2.700E-05	1.313E-15	3.082E-29
15	30.0	1.033E+01	2.900E-05	1.585E-15	5.106E-29
16	32.0	3.445E+00	3.100E-05	1.839E-15	7.975E-29
17	34.0	-3.435E+00	3.300E-05	2.068E-15	1.187E-28
18	36.0	-1.031E+01	3.500E-05	2.269E-15	1.696E-28
19	38.0	-1.720E+01	3.700E-05	2.441E-15	2.343E-28
20	40.0	-2.408E+01	3.900E-05	2.584E-15	3.146E-28
21	42.0	-3.096E+01	4.100E-05	2.699E-15	4.120E-28
22	44.0	-3.784E+01	4.300E-05	2.790E-15	5.281E-28
23	46.0	-4.472E+01	4.500E-05	2.859E-15	6.645E-28
24	48.0	-5.160E+01	4.700E-05	2.907E-15	8.226E-28
25	50.0	-5.848E+01	4.900E-05	2.938E-15	1.004E-27

TOTAL UNCAPTURED DROPS RATE (F4)= 6.860%

BED DEPTH= 0.04000METER

I	D2	FNW(D2)	D(I)	N(I)	F3
1	2.0	1.066E+02	1.000E-06	0.000E+00	0.000E+00
2	4.0	9.977E+01	3.000E-06	0.000E+00	0.000E+00
3	6.0	9.289E+01	5.000E-06	1.396E-33	0.000E+00
4	8.0	8.600E+01	7.000E-06	2.830E-26	0.000E+00
5	10.0	7.913E+01	9.000E-06	9.539E-23	3.641E-38
6	12.0	7.225E+01	1.100E-05	9.798E-21	6.864E-36
7	14.0	6.537E+01	1.300E-05	1.818E-19	2.161E-34
8	16.0	5.849E+01	1.500E-05	1.305E-18	2.522E-33
9	18.0	5.161E+01	1.700E-05	5.264E-18	1.606E-32
10	20.0	4.473E+01	1.900E-05	1.465E-17	6.867E-32
11	22.0	3.785E+01	2.100E-05	3.170E-17	2.224E-31
12	24.0	3.096E+01	2.300E-05	5.746E-17	5.884E-31
13	26.0	2.409E+01	2.500E-05	9.161E-17	1.338E-30
14	28.0	1.721E+01	2.700E-05	1.327E-16	2.706E-30
15	30.0	1.033E+01	2.900E-05	1.789E-16	4.990E-30
16	32.0	3.445E+00	3.100E-05	2.278E-16	8.543E-30
17	34.0	-3.435E+00	3.300E-05	2.775E-16	1.377E-29
18	36.0	-1.031E+01	3.500E-05	3.264E-16	2.109E-29
19	38.0	-1.720E+01	3.700E-05	3.731E-16	3.099E-29
20	40.0	-2.408E+01	3.900E-05	4.167E-16	4.393E-29
21	42.0	-3.096E+01	4.100E-05	4.566E-16	6.041E-29
22	44.0	-3.784E+01	4.300E-05	4.924E-16	8.091E-29
23	46.0	-4.472E+01	4.500E-05	5.240E-16	1.059E-28
24	48.0	-5.160E+01	4.700E-05	5.515E-16	1.359E-28

25	50.0	-5.848E+01	4.900E-05	5.749E-16	1.713E-28

TOTAL UNCAPTURED DROPS RATE (F4)= 1.171%

BED DEPTH= 0.05000METER

I	D2	FNW(D2)	D(I)	N(I)	F3
1	2.0	1.066E+02	1.000E-06	0.000E+00	0.000E+00
2	4.0	9.977E+01	3.000E-06	0.000E+00	0.000E+00
3	6.0	9.289E+01	5.000E-06	3.624E-39	0.000E+00
4	8.0	8.600E+01	7.000E-06	5.732E-30	0.000E+00
5	10.0	7.913E+01	9.000E-06	1.654E-25	0.000E+00
6	12.0	7.225E+01	1.100E-05	5.946E-23	4.144E-38
7	14.0	6.537E+01	1.300E-05	2.481E-21	2.895E-36
8	16.0	5.849E+01	1.500E-05	3.121E-20	5.804E-35
9	18.0	5.161E+01	1.700E-05	1.896E-19	5.457E-34
10	20.0	4.473E+01	1.900E-05	7.191E-19	3.128E-33
11	22.0	3.785E+01	2.100E-05	1.981E-18	1.274E-32
12	24.0	3.096E+01	2.300E-05	4.357E-18	4.049E-32
13	26.0	2.409E+01	2.500E-05	8.131E-18	1.070E-31
14	28.0	1.721E+01	2.700E-05	1.342E-17	2.454E-31
15	30.0	1.033E+01	2.900E-05	2.018E-17	5.031E-31
16	32.0	3.445E+00	3.100E-05	2.821E-17	9.432E-31
17	34.0	-3.435E+00	3.300E-05	3.725E-17	1.644E-30
18	36.0	-1.031E+01	3.500E-05	4.696E-17	2.698E-30
19	38.0	-1.720E+01	3.700E-05	5.704E-17	4.211E-30
20	40.0	-2.408E+01	3.900E-05	6.722E-17	6.299E-30
21	42.0	-3.096E+01	4.100E-05	7.723E-17	9.086E-30
22	44.0	-3.784E+01	4.300E-05	8.689E-17	1.270E-29
23	46.0	-4.472E+01	4.500E-05	9.606E-17	1.729E-29
24	48.0	-5.160E+01	4.700E-05	1.046E-16	2.297E-29
25	50.0	-5.848E+01	4.900E-05	1.125E-16	2.990E-29

TOTAL UNCAPTURED DROPS RATE (F4)= 0.204%

SUPERFICIAL VELOCITY= 0.001500 M/S

BED DEPTH= 0.01800METER

I	D2	FNW(D2)	D(I)	N(I)	F3
1	2.0	1.066E+02	1.000E-06	0.000E+00	0.000E+00
2	4.0	9.977E+01	3.000E-06	1.551E-26	0.000E+00
3	6.0	9.289E+01	5.000E-06	3.156E-19	2.065E-35
4	8.0	8.600E+01	7.000E-06	9.278E-17	1.668E-32
5	10.0	7.913E+01	9.000E-06	1.305E-15	5.149E-31
6	12.0	7.225E+01	1.100E-05	5.505E-15	4.351E-30
7	14.0	6.537E+01	1.300E-05	1.299E-14	1.929E-29
8	16.0	5.849E+01	1.500E-05	2.232E-14	5.873E-29
9	18.0	5.161E+01	1.700E-05	3.178E-14	1.405E-28
10	20.0	4.473E+01	1.900E-05	4.021E-14	2.849E-28
11	22.0	3.785E+01	2.100E-05	4.706E-14	5.131E-28
12	24.0	3.096E+01	2.300E-05	5.220E-14	8.457E-28
13	26.0	2.409E+01	2.500E-05	5.578E-14	1.302E-27
14	28.0	1.721E+01	2.700E-05	5.801E-14	1.900E-27
15	30.0	1.033E+01	2.900E-05	5.916E-14	2.655E-27
16	32.0	3.445E+00	3.100E-05	5.944E-14	3.583E-27
17	34.0	-3.435E+00	3.300E-05	5.908E-14	4.694E-27
18	36.0	-1.031E+01	3.500E-05	5.823E-14	6.001E-27
19	38.0	-1.720E+01	3.700E-05	5.703E-14	7.514E-27
20	40.0	-2.408E+01	3.900E-05	5.558E-14	9.240E-27
21	42.0	-3.096E+01	4.100E-05	5.397E-14	1.119E-26
22	44.0	-3.784E+01	4.300E-05	5.226E-14	1.336E-26
23	46.0	-4.472E+01	4.500E-05	5.049E-14	1.577E-26
24	48.0	-5.160E+01	4.700E-05	4.870E-14	1.842E-26
25	50.0	-5.848E+01	4.900E-05	4.693E-14	2.131E-26

TOTAL UNCAPTURED DROPS RATE (F4)= 77.695%

BED DEPTH= 0.02000METER

I	D2	FNW(D2)	D(I)	N(I)	F3
1	2.0	1.066E+02	1.000E-06	0.000E+00	0.000E+00
2	4.0	9.977E+01	3.000E-06	2.632E-28	0.000E+00
3	6.0	9.289E+01	5.000E-06	3.812E-20	2.495E-36
4	8.0	8.600E+01	7.000E-06	2.254E-17	4.050E-33
5	10.0	7.913E+01	9.000E-06	4.479E-16	1.750E-31
6	12.0	7.225E+01	1.100E-05	2.312E-15	1.786E-30
7	14.0	6.537E+01	1.300E-05	6.216E-15	8.937E-30
8	16.0	5.849E+01	1.500E-05	1.170E-14	2.961E-29

9	18.0	5.161E+01	1.700E-05	1.780E-14	7.539E-29
10	20.0	4.473E+01	1.900E-05	2.368E-14	1.604E-28
11	22.0	3.785E+01	2.100E-05	2.881E-14	3.001E-28
12	24.0	3.096E+01	2.300E-05	3.298E-14	5.102E-28
13	26.0	2.409E+01	2.500E-05	3.615E-14	8.059E-28
14	28.0	1.721E+01	2.700E-05	3.840E-14	1.202E-27
15	30.0	1.033E+01	2.900E-05	3.985E-14	1.711E-27
16	32.0	3.445E+00	3.100E-05	4.066E-14	2.345E-27
17	34.0	-3.435E+00	3.300E-05	4.094E-14	3.115E-27
18	36.0	-1.031E+01	3.500E-05	4.080E-14	4.031E-27
19	38.0	-1.720E+01	3.700E-05	4.036E-14	5.101E-27
20	40.0	-2.408E+01	3.900E-05	3.968E-14	6.334E-27
21	42.0	-3.096E+01	4.100E-05	3.883E-14	7.735E-27
22	44.0	-3.784E+01	4.300E-05	3.785E-14	9.311E-27
23	46.0	-4.472E+01	4.500E-05	3.680E-14	1.107E-26
24	48.0	-5.160E+01	4.700E-05	3.569E-14	1.301E-26
25	50.0	-5.848E+01	4.900E-05	3.457E-14	1.514E-26

TOTAL UNCAPTURED DROPS RATE (F4)= 55.184%

BED DEPTH= 0.03000METER

I	D2	FNW(D2)	D(I)	N(I)	F3
1	2.0	1.066E+02	1.000E-06	0.000E+00	0.000E+00
2	4.0	9.977E+01	3.000E-06	3.695E-37	0.000E+00
3	6.0	9.289E+01	5.000E-06	9.801E-25	0.000E+00
4	8.0	8.600E+01	7.000E-06	1.905E-20	3.422E-36
5	10.0	7.913E+01	9.000E-06	2.132E-18	8.171E-34
6	12.0	7.225E+01	1.100E-05	3.021E-17	2.187E-32
7	14.0	6.537E+01	1.300E-05	1.562E-16	2.016E-31
8	16.0	5.849E+01	1.500E-05	4.627E-16	1.019E-30
9	18.0	5.161E+01	1.700E-05	9.802E-16	3.541E-30
10	20.0	4.473E+01	1.900E-05	1.675E-15	9.558E-30
11	22.0	3.785E+01	2.100E-05	2.479E-15	2.158E-29
12	24.0	3.096E+01	2.300E-05	3.318E-15	4.271E-29
13	26.0	2.409E+01	2.500E-05	4.131E-15	7.651E-29
14	28.0	1.721E+01	2.700E-05	4.877E-15	1.268E-28
15	30.0	1.033E+01	2.900E-05	5.532E-15	1.974E-28
16	32.0	3.445E+00	3.100E-05	6.086E-15	2.923E-28
17	34.0	-3.435E+00	3.300E-05	6.539E-15	4.154E-28
18	36.0	-1.031E+01	3.500E-05	6.895E-15	5.702E-28
19	38.0	-1.720E+01	3.700E-05	7.164E-15	7.602E-28
20	40.0	-2.408E+01	3.900E-05	7.356E-15	9.886E-28
21	42.0	-3.096E+01	4.100E-05	7.481E-15	1.259E-27

22	44.0	-3.784E+01	4.300E-05	7.548E-15	1.573E-27
23	46.0	-4.472E+01	4.500E-05	7.568E-15	1.934E-27
24	48.0	-5.160E+01	4.700E-05	7.547E-15	2.344E-27
25	50.0	-5.848E+01	4.900E-05	7.495E-15	2.806E-27

TOTAL UNCAPTURED DROPS RATE (F4)= 10.230%

BED DEPTH= 0.04000METER

I	D2	FNW(D2)	D(I)	N(I)	F3
1	2.0	1.066E+02	1.000E-06	0.000E+00	0.000E+00
2	4.0	9.977E+01	3.000E-06	0.000E+00	0.000E+00
3	6.0	9.289E+01	5.000E-06	2.520E-29	0.000E+00
4	8.0	8.600E+01	7.000E-06	1.611E-23	2.893E-39
5	10.0	7.913E+01	9.000E-06	1.014E-20	3.875E-36
6	12.0	7.225E+01	1.100E-05	3.948E-19	2.790E-34
7	14.0	6.537E+01	1.300E-05	3.926E-18	4.795E-33
8	16.0	5.849E+01	1.500E-05	1.830E-17	3.714E-32
9	18.0	5.161E+01	1.700E-05	5.398E-17	1.760E-31
10	20.0	4.473E+01	1.900E-05	1.185E-16	6.017E-31
11	22.0	3.785E+01	2.100E-05	2.133E-16	1.636E-30
12	24.0	3.096E+01	2.300E-05	3.338E-16	3.762E-30
13	26.0	2.409E+01	2.500E-05	4.720E-16	7.624E-30
14	28.0	1.721E+01	2.700E-05	6.194E-16	1.401E-29
15	30.0	1.033E+01	2.900E-05	7.678E-16	2.381E-29
16	32.0	3.445E+00	3.100E-05	9.110E-16	3.802E-29
17	34.0	-3.435E+00	3.300E-05	1.044E-15	5.767E-29
18	36.0	-1.031E+01	3.500E-05	1.165E-15	8.383E-29
19	38.0	-1.720E+01	3.700E-05	1.272E-15	1.176E-28
20	40.0	-2.408E+01	3.900E-05	1.364E-15	1.599E-28
21	42.0	-3.096E+01	4.100E-05	1.441E-15	2.119E-28
22	44.0	-3.784E+01	4.300E-05	1.505E-15	2.746E-28
23	46.0	-4.472E+01	4.500E-05	1.556E-15	3.488E-28
24	48.0	-5.160E+01	4.700E-05	1.596E-15	4.356E-28
25	50.0	-5.848E+01	4.900E-05	1.625E-15	5.357E-28

TOTAL UNCAPTURED DROPS RATE (F4)= 1.953%

BED DEPTH= 0.05000METER

I	D2	FNW(D2)	D(I)	N(I)	F3
1	2.0	1.066E+02	1.000E-06	0.000E+00	0.000E+00
2	4.0	9.977E+01	3.000E-06	0.000E+00	0.000E+00
3	6.0	9.289E+01	5.000E-06	6.478E-34	0.000E+00
4	8.0	8.600E+01	7.000E-06	1.362E-26	0.000E+00
5	10.0	7.913E+01	9.000E-06	4.828E-23	1.843E-38
6	12.0	7.225E+01	1.100E-05	5.160E-21	3.614E-36
7	14.0	6.537E+01	1.300E-05	9.866E-20	1.171E-34
8	16.0	5.849E+01	1.500E-05	7.241E-19	1.397E-33
9	18.0	5.161E+01	1.700E-05	2.973E-18	9.044E-33
10	20.0	4.473E+01	1.900E-05	8.388E-18	3.917E-32
11	22.0	3.785E+01	2.100E-05	1.835E-17	1.282E-31
12	24.0	3.096E+01	2.300E-05	3.358E-17	3.421E-31
13	26.0	2.409E+01	2.500E-05	5.394E-17	7.834E-31
14	28.0	1.721E+01	2.700E-05	7.866E-17	1.594E-30
15	30.0	1.033E+01	2.900E-05	1.066E-16	2.955E-30
16	32.0	3.445E+00	3.100E-05	1.364E-16	5.082E-30
17	34.0	-3.435E+00	3.300E-05	1.668E-16	8.221E-30
18	36.0	-1.031E+01	3.500E-05	1.969E-16	1.264E-29
19	38.0	-1.720E+01	3.700E-05	2.258E-16	1.863E-29
20	40.0	-2.408E+01	3.900E-05	2.528E-16	2.648E-29
21	42.0	-3.096E+01	4.100E-05	2.777E-16	3.650E-29
22	44.0	-3.784E+01	4.300E-05	3.001E-16	4.900E-29
23	46.0	-4.472E+01	4.500E-05	3.200E-16	6.427E-29
24	48.0	-5.160E+01	4.700E-05	3.374E-16	8.261E-29
25	50.0	-5.848E+01	4.900E-05	3.523E-16	1.043E-28

TOTAL UNCAPTURED DROPS RATE (F4)= 0.380%

APPENDIX Y

Computer Program for Calculation of Number of Channels Inside the Coalescer using The Model for The Simulation of Channeling In A Random Bed of Spherical Packing

```
C     PACKED BED SIMULATION PROGRAM:
C     ==============================
C
C
C
C
C
      DIMENSION H(999),NCHI(999),AI(999),CT(999),B(999)
C
        REAL G05DAF
        COMMON/SET1/NS
C
        CALL G05CBF(0)
C
C  GENERAL PACKING BED PROGRAM
C ---------------------------
C
      DO 1 K=1,150
      H(K)=0.0
      NCHI(K)=0.0
      AI(K)=0.0
      CT(K)=0.0
      B(K)=0.0
  1    CONTINUE
C
C BED SIMULATION PROGRAM
C
C
C
        READ *,EE,HMAX
       WID=10.0
      AREA1=3.14159*((WID/2)**2)
      VOL1=AREA1*HMAX
      DC=0.226
      AREA2=0.121*(DC**2)
      PRINT 100,HMAX,AREA1,VOL1,DC,AREA2
 100  FORMAT(//10X,'BED DIMENSION',/10X,14('-')/,
     @10X,'BED DEPTH=',F8.3/10X,'BED AREA=',F8.3,/,
     @10X,'BED VOLUME=',F12.3,//20X,'CHANNELS DIMENSION',/,
     @20X,19('-')//,10X,'MINIMUM HEIGTH=',E12.5,/10X,
     @'CROSS SECTION AREA=',E12.5,///,10X,
     @'BED SIMULATION:',/,10X,15('-')/)
C
C
        AMIN=0.266
        AMAX=1.414*AMIN
        PI=4.0*ATAN(1.0)
        PIT=PI/2
        HI=0.0
        AI2=0.0
        VOLC=0.0
         II=1
        PRINT 200
  200     FORMAT(6X,/)
C
```

```
      PRINT 300
 300  FORMAT('CHANNEL NO.  NO.OF PASS  CHANNEL LENGHT(MM)',
     @'  CUM.CHANNEL VOL(MM**3)  BED VOIDAGE',/79('-'))
C
   4  I=0
      HI=0.0
      H1=0.0
   5  I=I+1
C
C
C  PASS LENGTH
C  ===========
C
C
          AI1=G05DAF(AMIN,AMAX)
          IF(II.EQ.1) AI(I)=AI1
C
C   INCLINATION ANGLE
C   -----------------
C
C
          CT1=G05DAF(0.0,PI)
          IF(II.EQ.1) CT(I)=CT1
          AI2=AI1+AI2
          IF(CT1.LT.PIT)  GO TO 6
            IF(CT1.EQ.PIT) GO TO 7
          CT2=PI-CT1
C
C
C    ACCUMULATION BED DEPTH
C
C
            HI=HI+SIN(CT2)*AI1
            HA=SIN(CT2)*AI1
               GO TO 8
   6      HI=HI+SIN(CT1)*AI1
          HA=SIN(CT2)*AI1
              GO TO 8
   7        HI=HI+AI1
                HA=AI1
   8      HI=HI
        IF(II.EQ.1) H(I)=H1
        IF(II.EQ.1)B(I)=H1/HMAX
         IF(HI.LT.HMAX) GO TO 9
          IF(II.EQ.HMAX) GO TO 10
        HI=HMAX
        H1=HMAX
          IF(II.EQ.1) H(I)=HMAX
          IF (II.EQ.1) B(I)=1.0
           IF(II.EQ.1) AI(I)=SIN(CT1)/(HMAX-H(I-1))
           GO TO 10
   9      GO TO 5
C
C   TOTAL NUMER OF PASS
```

```
C
  10      NCHI(II)=I
C
C
C       FREE BED VOLUME
C       ---------------
C
C
            VOL=AI2*(0.226**2.0)
           VOLO=VOLO+VOL
           E=VOLO/VOL1
           PRINT 400,II,NCHI(II),AI2,VOLO,E
 400    FORMAT(2X,I6,8X,I3,8X,F12.4,8X,F10.3,8X,F10.4)
       T=EE-E
           IF(T.LT.0.0)  GO TO 11
           II=II+1
         AI2=0.0
         GO TO 4
 11       PRINT 500
 500     FORMAT(10X,///)
C
C
         AREATOL=3.14*((76.2/2.0)**2.0)
C
             TOLNUM=II*(AREATOL/AREA1)
C
           PRINT 524,TOLNUM
 524     FORMAT(5X,'TOLTAL NUMBER OF CHANNELS=',F10.1,//)
C
          DC=0.266
          PRINT 600,DC,EE
 600    FORMAT(10X,'PACKED BED DIAMETER=',F10.4,2X,'MM.',/,
      @10X,'BED VOIDAGE=',F10.4,///)
C
C
              STOP
              END
```

BED DIMENSION

BED DEPTH= 30.000
BED AREA= 78.540
BED VOLUME= 2356.192

CHANNELS DIMENSION

MINIMUM HEIGTH= 0.22600E+00
CROSS SECTION AREA= 0.61802E-02

BED SIMULATION:

CHANNEL NO.	NO.OF PASS	CHANNEL LENGHT(MM)	CUM.CHANNEL VOL(MM**3)	BED VOIDAGE
1	145	47.0498	2.403	0.0010
2	151	48.8748	4.899	0.0021
3	142	45.8423	7.241	0.0031
4	139	44.8825	9.533	0.0040
5	148	47.1325	11.941	0.0051
6	139	44.6292	14.220	0.0060
7	151	48.7685	16.711	0.0071
8	154	49.2047	19.224	0.0082
9	162	51.9497	21.878	0.0093
10	159	50.2339	24.443	0.0104
11	150	48.3588	26.913	0.0114
12	142	45.7935	29.252	0.0124
13	153	48.7532	31.742	0.0135
14	139	44.7875	34.030	0.0144
15	158	50.6689	36.618	0.0155
16	144	45.8118	38.958	0.0165
17	150	48.3042	41.425	0.0176
18	156	49.6498	43.961	0.0187
19	149	47.6714	46.396	0.0197
20	135	42.9830	48.591	0.0206
21	140	44.8905	50.884	0.0216
22	152	49.0906	53.391	0.0227
23	157	49.9880	55.945	0.0237
24	147	47.6979	58.381	0.0248
25	152	48.8189	60.874	0.0258
26	151	48.5763	63.355	0.0269
27	140	44.8743	65.647	0.0279
28	148	47.4588	68.071	0.0289
29	142	45.1475	70.377	0.0299
30	146	47.1331	72.785	0.0309
31	143	46.6256	75.166	0.0319
32	152	48.1080	77.623	0.0329

33	137	43.9863	79.870	0.0339
34	142	45.3731	82.187	0.0349
35	152	48.9449	84.687	0.0359
36	140	44.9883	86.985	0.0369
37	147	46.7052	89.371	0.0379
38	141	45.3396	91.686	0.0389
39	151	48.2180	94.149	0.0400
40	142	45.5027	96.473	0.0409
41	156	49.9909	99.027	0.0420
42	157	50.0056	101.581	0.0431
43	152	49.2137	104.094	0.0442
44	148	47.4880	106.520	0.0452
45	154	48.5780	109.001	0.0463
46	147	47.4699	111.426	0.0473
47	150	47.7113	113.862	0.0483
48	147	46.8055	116.253	0.0493
49	148	46.9862	118.653	0.0504
50	152	48.9066	121.151	0.0514
51	152	48.6097	123.634	0.0525
52	149	47.8382	126.077	0.0535
53	153	49.0412	128.582	0.0546
54	136	44.0482	130.832	0.0555
55	146	46.3999	133.202	0.0565
56	138	43.9871	135.448	0.0575
57	144	45.4381	137.769	0.0585
58	161	50.5528	140.351	0.0596
59	143	46.1221	142.707	0.0606
60	141	44.7817	144.994	0.0615
61	148	47.5228	147.421	0.0626
62	150	48.3679	149.892	0.0636
63	162	51.7933	152.537	0.0647
64	147	47.2443	154.950	0.0658
65	147	47.3429	157.368	0.0668
66	153	48.7806	159.860	0.0678
67	156	50.2823	162.428	0.0689
68	143	45.9887	164.777	0.0699
69	149	47.7035	167.214	0.0710
70	131	41.9873	169.358	0.0719
71	149	48.4429	171.832	0.0729
72	150	47.4826	174.258	0.0740
73	145	46.3913	176.627	0.0750
74	158	50.1384	179.188	0.0760
75	146	47.2157	181.600	0.0771
76	161	51.7700	184.244	0.0782
77	152	48.9645	186.745	0.0793
78	140	44.6751	189.026	0.0802
79	144	46.9270	191.423	0.0812
80	146	46.6736	193.807	0.0823
81	135	43.4313	196.026	0.0832
82	154	48.9604	198.526	0.0843
83	144	46.5226	200.902	0.0853
84	150	47.7856	203.343	0.0863
85	153	48.5553	205.823	0.0874
86	154	49.8676	208.370	0.0884

87	140	45.1807	210.678	0.0894
88	152	48.7155	213.166	0.0905
89	150	47.8483	215.610	0.0915
90	152	48.4616	218.085	0.0926
91	159	50.7372	220.677	0.0937
92	154	49.5564	223.208	0.0947
93	142	46.0777	225.561	0.0957
94	157	50.6418	228.148	0.0968
95	145	46.7950	230.538	0.0978
96	152	48.5508	233.018	0.0989
97	144	46.2163	235.378	0.0999
98	149	47.5003	237.804	0.1009
99	150	48.5921	240.286	0.1020
100	153	48.5995	242.768	0.1030
101	135	42.9313	244.961	0.1040
102	156	50.6085	247.546	0.1051
103	148	47.1928	249.957	0.1061
104	143	45.9708	252.305	0.1071
105	134	43.3995	254.521	0.1080
106	147	47.3849	256.941	0.1090
107	146	46.9897	259.341	0.1101
108	144	46.5214	261.718	0.1111
109	148	47.3622	264.137	0.1121
110	141	44.5794	266.414	0.1131
111	142	45.7053	268.748	0.1141
112	149	47.8157	271.190	0.1151
113	138	44.3711	273.457	0.1161
114	145	46.4807	275.831	0.1171
115	142	46.5650	278.209	0.1181
116	149	47.8181	280.651	0.1191
117	139	44.9023	282.945	0.1201
118	157	50.3160	285.515	0.1212
119	144	46.0669	287.868	0.1222
120	147	46.9305	290.265	0.1232
121	146	46.9229	292.661	0.1242
122	145	46.3249	295.027	0.1252
123	142	45.5337	297.353	0.1262
124	145	46.0358	299.704	0.1272
125	157	50.8374	302.301	0.1283
126	142	45.3059	304.615	0.1293
127	155	49.8141	307.159	0.1304
128	147	46.7412	309.547	0.1314
129	149	47.7834	311.987	0.1324
130	151	47.8664	314.432	0.1334
131	135	43.2015	316.639	0.1344
132	159	50.4460	319.215	0.1355
133	136	43.4712	321.436	0.1364
134	151	47.7281	323.873	0.1375
135	148	47.2300	326.286	0.1385
136	151	48.1660	328.746	0.1395
137	143	46.0643	331.099	0.1405
138	156	49.5529	333.629	0.1416
139	150	48.0052	336.081	0.1426
140	149	47.7296	338.519	0.1437

141	155	49.3222	341.038	0.1447
142	152	48.8143	343.532	0.1458
143	149	47.5499	345.960	0.1468
144	141	45.0602	348.262	0.1478
145	142	44.9811	350.559	0.1488
146	137	44.1577	352.815	0.1497
147	146	46.6864	355.199	0.1508
148	138	44.9595	357.496	0.1517
149	146	47.2148	359.907	0.1527
150	143	46.2462	362.269	0.1538
151	156	50.3553	364.841	0.1548
152	148	47.8397	367.285	0.1559
153	144	46.9227	369.681	0.1569
154	143	45.9358	372.027	0.1579
155	153	49.3697	374.549	0.1590
156	146	46.9796	376.949	0.1600
157	141	45.5039	379.273	0.1610
158	157	50.5702	381.856	0.1621
159	143	45.5822	384.184	0.1631
160	149	47.9454	386.633	0.1641
161	142	45.4537	388.954	0.1651
162	147	47.1167	391.361	0.1661
163	140	45.4510	393.682	0.1671
164	147	47.5116	396.109	0.1681
165	154	49.5685	398.641	0.1692
166	142	45.8809	400.984	0.1702
167	149	47.7231	403.422	0.1712
168	152	49.0666	405.928	0.1723
169	147	47.0098	408.329	0.1733
170	144	46.2903	410.693	0.1743
171	150	48.2218	413.156	0.1753
172	152	48.5716	415.637	0.1764
173	141	45.3674	417.954	0.1774
174	143	45.9665	420.302	0.1784
175	149	47.9287	422.750	0.1794
176	154	50.2160	425.315	0.1805
177	142	45.7962	427.654	0.1815
178	150	47.7501	430.093	0.1825
179	148	46.9008	432.488	0.1836
180	150	48.3237	434.956	0.1846
181	152	48.8269	437.450	0.1857
182	153	49.0431	439.955	0.1867
183	145	46.1683	442.313	0.1877
184	147	47.5194	444.740	0.1888
185	167	53.2768	447.462	0.1899
186	143	45.8146	449.802	0.1909
187	149	47.8304	452.245	0.1919
188	150	48.0355	454.698	0.1930
189	152	48.9731	457.199	0.1940
190	145	46.9751	459.599	0.1951
191	154	49.6365	462.134	0.1961
192	143	46.0732	464.487	0.1971
193	136	43.7133	466.720	0.1981
194	151	48.4504	469.195	0.1991

195	156	50.6409	471.781	0.2002
196	145	46.9705	474.180	0.2012
197	148	47.1948	476.591	0.2023
198	161	51.2518	479.208	0.2034
199	145	46.0737	481.562	0.2044
200	145	46.7190	483.948	0.2054
201	147	47.2093	486.359	0.2064
202	145	46.4572	488.732	0.2074
203	147	46.8307	491.124	0.2084
204	133	43.4758	493.344	0.2094
205	145	46.7342	495.731	0.2104
206	156	50.2071	498.296	0.2115
207	140	45.2606	500.608	0.2125
208	157	50.5265	503.188	0.2136
209	142	45.6178	505.518	0.2145
210	145	46.2743	507.882	0.2156
211	157	49.3712	510.403	0.2166
212	157	50.1517	512.965	0.2177
213	147	46.8289	515.357	0.2187
214	152	49.1700	517.868	0.2198
215	143	45.9478	520.215	0.2208
216	142	45.9568	522.562	0.2218
217	135	43.3441	524.776	0.2227
218	148	48.0685	527.231	0.2238
219	150	48.5935	529.713	0.2248
220	139	44.7716	532.000	0.2258
221	158	50.3619	534.572	0.2269
222	143	45.8468	536.914	0.2279
223	142	46.1148	539.269	0.2289
224	141	45.5094	541.594	0.2299
225	140	44.6418	543.874	0.2308
226	144	46.5109	546.250	0.2318
227	151	48.1612	548.709	0.2329
228	142	46.0982	551.064	0.2339
229	155	49.1359	553.574	0.2349
230	142	45.3393	555.889	0.2359
231	139	45.1719	558.197	0.2369
232	148	48.4038	560.669	0.2380
233	148	47.8627	563.113	0.2390
234	148	47.7531	565.552	0.2400
235	153	48.9615	568.053	0.2411
236	153	49.0991	570.561	0.2422
237	147	47.1161	572.968	0.2432
238	153	48.7680	575.458	0.2442
239	148	47.2363	577.871	0.2453
240	148	47.1599	580.280	0.2463
241	150	48.2160	582.742	0.2473
242	146	46.7474	585.130	0.2483
243	152	48.7215	587.619	0.2494
244	156	49.5846	590.151	0.2505
245	147	47.2773	592.566	0.2515
246	137	43.8573	594.806	0.2524
247	146	46.2395	597.168	0.2534
248	142	45.6446	599.499	0.2544

249	149	47.6773	601.934	0.2555
250	151	47.8619	604.379	0.2565
251	144	46.4040	606.749	0.2575
252	149	47.4849	609.174	0.2585
253	157	51.0003	611.779	0.2596
254	147	47.2854	614.194	0.2607
255	143	45.8498	616.536	0.2617
256	150	48.4095	619.009	0.2627
257	145	46.4343	621.380	0.2637
258	150	48.2214	623.843	0.2648
259	138	44.3367	626.108	0.2657
260	141	46.1112	628.463	0.2667
261	152	48.4802	630.939	0.2678
262	142	46.4033	633.309	0.2688
263	145	46.9479	635.707	0.2698
264	148	47.7101	638.144	0.2708
265	138	44.7432	640.429	0.2718
266	142	45.5620	642.757	0.2728
267	150	48.0768	645.212	0.2738
268	151	49.1811	647.724	0.2749
269	145	45.8121	650.064	0.2759
270	147	47.3444	652.482	0.2769
271	139	44.6207	654.761	0.2779
272	140	45.5975	657.090	0.2789
273	144	46.8402	659.483	0.2799
274	153	49.8768	662.030	0.2810
275	136	43.6820	664.261	0.2819
276	156	50.6278	666.847	0.2830
277	143	46.0816	669.201	0.2840
278	149	47.4376	671.624	0.2850
279	138	44.2381	673.883	0.2860
280	140	44.9923	676.181	0.2870
281	146	46.5011	678.556	0.2880
282	148	47.5385	680.984	0.2890
283	142	45.2701	683.297	0.2900
284	139	44.7729	685.583	0.2910
285	140	44.6468	687.864	0.2919
286	152	48.7225	690.352	0.2930
287	148	47.9137	692.800	0.2940
288	145	46.9322	695.197	0.2951
289	144	46.9664	697.595	0.2961
290	141	45.6456	699.927	0.2971
291	145	46.3464	702.294	0.2981
292	145	45.9176	704.639	0.2991
293	143	45.6519	706.971	0.3000
294	145	46.5455	709.348	0.3011
295	146	47.0154	711.750	0.3021
296	152	47.9883	714.201	0.3031
297	143	46.3109	716.566	0.3041
298	144	46.3706	718.935	0.3051
299	143	46.4698	721.308	0.3061
300	147	46.9251	723.705	0.3072
301	164	52.7193	726.398	0.3083
302	151	48.6388	728.882	0.3093

303	156	50.4576	731.459	0.3104
304	141	45.1591	733.766	0.3114
305	140	44.7708	736.052	0.3124
306	140	44.9310	738.347	0.3134
307	138	44.6114	740.626	0.3143
308	151	49.0540	743.131	0.3154
309	149	47.4382	745.554	0.3164
310	166	52.6999	748.246	0.3176
311	151	48.8423	750.741	0.3186
312	152	48.5910	753.222	0.3197
313	152	48.9089	755.720	0.3207
314	139	44.4049	757.988	0.3217
315	147	46.6053	760.369	0.3227
316	158	49.9604	762.921	0.3238
317	163	52.6935	765.612	0.3249
318	151	48.6496	768.097	0.3260
319	146	46.7563	770.485	0.3270
320	148	47.3327	772.903	0.3280
321	153	49.0847	775.410	0.3291
322	151	48.7791	777.901	0.3302
323	147	47.1800	780.311	0.3312
324	139	44.3155	782.574	0.3321
325	139	44.4627	784.845	0.3331
326	155	49.6151	787.379	0.3342
327	152	48.3153	789.847	0.3352
328	138	44.6598	792.128	0.3362
329	150	48.0410	794.582	0.3372
330	132	42.0741	796.731	0.3381

TOLTAL NUMBER OF CHANNELS= 19151.6

PACKED BED DIAMETER= 0.2660 MM.
BED VOIDAGE= 0.3380

APPENDIX Z

Computer Program for Queuing Drop Model

```
C
C          COMPUTER  PROGRAM  FOR  QUEUEING  LENGTH
C          ========================================
C
C
C
                DIMENSION P(999)
C
C
              M=48
             PTOL=0.00001
  5         IF(III.GT.4) THEN
            GO TO 500
             ELSE
C
C
              READ *,XLAM,XMU,C,XN,XK
C
             NC=C
             N=XN
             K=XK
              RHO=XLAM/XMU
             ELAM=XLAM
             PRINT 701,NC,N,K
            IF(K.LT.99999.AND.K.GT.M.AND.N.GT.M) THEN
              GO TO 350
             ELSE
              NN=M
             RC=RHO/C
             PZ=1.0
             DO  10  I=1,NN
  10           P(I)=0.0
                IF(NC.GT.1) THEN
                 GO TO 60
                ELSE
               IF(K.LT.99999) THEN
                  GO TO 30
                ELSE
                IF  (RC.GT.1.0.AND.N.EQ.99999)  THEN
                   GO TO 350
                 ELSE
C         (M/M/1):(GD/*/*)
C         ================
C
                   PZ=PZ-RHO
               IF(N.LT.99999) THEN
                 PZ=PZ/(1.0-RHO**(N+1))
                 ELSE
                P(1)=PZ*RHO
                DO 20 I=2,NN
                  P(I)=P(I-1)*RHO
  20            CONTINUE
                     I=NN+1
                 GO TO 150
C          (M/M/1):(GD/N/*)
```

```
C       ================
 30          P(1)=XK*RHO
             PZ=PZ+P(1)
            DO 40 I=2,NN
C
             IX=K-I+1
             P(I)=P(I-1)*IX*RHO
             PZ=PZ+P(I)
 40         CONTINUE
 45          PZ=1.0/PZ
                DO 50 I=1,NN
                P(I)=PZ*P(I)
 50           CONTINUE
                  I=NN+1
 51                LL=I-1
                  QL=0.0
                  DO 52 J=NC,LL
                   IX=J-NC
 52                QL=QL+IX*P(J)
                    R=C*PZ
                   IF(I.GE.NC) THEN
                     GO TO 56
                  DO 53 J=1,NC
 53                P(J)=0.0
 56               DO 57 J=1,NC
                      IX=NC-J
 57              R=R+IX*P(J)
                      ELAM=XMU*(C-R)
                      GO TO 160
  60                IF(NC.LT.99999) THEN
                      GO TO 80
                        ELSE
C       (M/M/*):(GD/*/*)
C       ================
                  PZ=EXP(-RHO)
                  P(1)=PZ*RHO
                    DO 70 I=2,NN
                  IX=I
                  P(I)=P(I-1)*RHO/IX
  70              CONTINUE
                I=NN+1
                QL=0.0
              GO TO 160
  80         IF(K.LT.99999) THEN
               GO TO 120
               ELSE
              IF(RC.GT.1.0.AND.N.EQ.99999) THEN
               GO TO 350
                ELSE
C       (M/M/C):(GD/*/*)
C       ================
                 P(1)=RHO
               DO 90 I=2,NC
              IX=I
```

```
            P(I)=P(I-1)*RHO/IX
  90       PZ=PZ+P(I-1)
            X=P(NC)/(1.0-RC)
C       (M/M/C):(GD/N/*)
C       ================
C
             IF(N.LT.99999) THEN
              X=X*(1.0-RC**(N-NC+1))
              ELSE
              PZ=PZ+X
              PZ=1.0/PZ
              DO 100 I=1,NC
              P(I)=PZ*P(I)
 100            CONTINUE
                DO 110 I=NC,NN
               P(I)=P(I-1)*RC
 110            CONTINUE
                 I=NN+1
                  GO TO 150
C            CM/M/R):(GD/K/K)
C            ================
   120         P(1)=XK*RHO
                DO 130 I=2,NC
                 IX=I
              IY=K-I+1
              P(I)=P(I-1)*RHO*IY/IX
 130         PZ=PZ+P(I-1)
             DO 140 I=NC,NN
             IX=K-I+1
              P(I)=P(I-1)*RC*IX
 140          PZ=PZ+P(I)
               GO TO 45
 145          P(NC)=0.0
 150       QL=RC*P(NC)/(1.0-RC)**2.0
            IF(N.LT.9999) THEN
            QL=QL*(1.0-RC**(N-NC)-(XN-C)*RC**(N-NC)*(1.0-RC))
             ELSE
              ELAM=XLAM*(1.0-P(NN))
 160            SL=QL+ELAM/XMU
                  WS=SL/ELAM
                WQ=QL/ELAM
 200          MAX=I-1
               PRINT 702,XLAM,ELAM,XMU,RHO
               PRINT 703,WS,WQ,SL,QL
               PRINT 704,MAX,(P(I),I=1,MAX)
                       ENDIF
                     ENDIF
                   ENDIF
                 ENDIF
               ENDIF
               ENDIF
                 ENDIF
                   ENDIF
                     ENDIF
```

```
                    ENDIF
                      ENDIF
              III=III+1
                    GO TO 5
C
  350       PRINT 702,XLAM,ELAM,XMU,RHO
C
 701    FORMAT(22X,'(M/M/',I3,'):(GD/',I3,'/',I3,')',/21X,25('=')//)
C
 702    FORMAT(2X,'LAMBDA=',E12.5,5X,'LAMBDA EFF.=',E12.5,/,
     @5X,'MU=',E12.5,10X,'RHO=',E12.5,//)
C
 703   FORMAT(2X,'WS=',E12.5,3X,'WQ=',E12.5,5X,'LS=',E12.5,3X,'LQ=',
     @E12.5/)
C
 704    FORMAT(6X,'VALUES OF P(N) FOR N=0 TO',I4,1X,'OTHERWISE P(N)=',
     @'0.0,',//,8(2X,6E10.3,/)//)
                PRINT *,'       INVALID INPUT DATA'
                    GO TO 5
  500       STOP
           ENDIF
                    END
```

(M/M/255):(GD/***/***)

LAMBDA= 0.10000E+02 LAMBDA EFF.= 0.10000E+02
MU= 0.30500E+01 RHO= 0.32787E+01

WS= 0.32787E+00 WQ= 0.00000E+01 LS= 0.32787E+01 LQ= 0.00000E+01

VALUES OF P(N) FOR N=0 TO 48 OTHERWISE P(N)=0.0,

0.124E+00 0.203E+00 0.221E+00 0.181E+00 0.119E+00 0.650E-01
0.304E-01 0.125E-01 0.455E-02 0.149E-02 0.444E-03 0.121E-03
0.306E-04 0.717E-05 0.157E-05 0.321E-06 0.619E-07 0.113E-07
0.195E-08 0.319E-09 0.498E-10 0.743E-11 0.106E-11 0.145E-12
0.190E-13 0.239E-14 0.290E-15 0.340E-16 0.384E-17 0.420E-18
0.444E-19 0.455E-20 0.452E-21 0.436E-22 0.409E-23 0.372E-24
0.330E-25 0.285E-26 0.239E-27 0.196E-28 0.157E-29 0.122E-30
0.933E-32 0.695E-33 0.507E-34 0.361E-35 0.252E-36 0.172E-37

(M/M/299):(GD/***/***)

LAMBDA= 0.20000E+02 LAMBDA EFF.= 0.20000E+02
MU= 0.30500E+01 RHO= 0.65574E+01

WS= 0.32787E+00 WQ= 0.00000E+01 LS= 0.65574E+01 LQ= 0.00000E+01

VALUES OF P(N) FOR N=0 TO 48 OTHERWISE P(N)=0.0,

0.931E-02 0.305E-01 0.667E-01 0.109E+00 0.143E+00 0.157E+00
0.147E+00 0.120E+00 0.877E-01 0.575E-01 0.343E-01 0.187E-01
0.945E-02 0.443E-02 0.193E-02 0.793E-03 0.306E-03 0.111E-03
0.385E-04 0.126E-04 0.394E-05 0.117E-05 0.335E-06 0.914E-07
0.240E-07 0.605E-08 0.147E-08 0.344E-09 0.778E-10 0.170E-10
0.360E-11 0.737E-12 0.146E-12 0.282E-13 0.529E-14 0.964E-15
0.171E-15 0.295E-16 0.496E-17 0.812E-18 0.130E-18 0.203E-19
0.309E-20 0.461E-21 0.672E-22 0.958E-23 0.134E-23 0.183E-24

(M/M/330):(GD/***/***)

LAMBDA= 0.30000E+02 LAMBDA EFF.= 0.30000E+02
MU= 0.30500E+01 RHO= 0.98361E+01

WS= 0.32787E+00 WQ= 0.00000E+01 LS= 0.98361E+01 LQ= 0.00000E+01

VALUES OF P(N) FOR N=0 TO 48 OTHERWISE P(N)=0.0,

0.526E-03 0.259E-02 0.848E-02 0.209E-01 0.410E-01 0.673E-01
0.945E-01 0.116E+00 0.127E+00 0.125E+00 0.112E+00 0.916E-01
0.693E-01 0.487E-01 0.319E-01 0.196E-01 0.114E-01 0.620E-02
0.321E-02 0.158E-02 0.740E-03 0.331E-03 0.141E-03 0.580E-04
0.228E-04 0.863E-05 0.314E-05 0.110E-05 0.375E-06 0.123E-06
0.390E-07 0.120E-07 0.357E-08 0.103E-08 0.290E-09 0.793E-10
0.211E-10 0.546E-11 0.138E-11 0.338E-12 0.812E-13 0.190E-13
0.435E-14 0.972E-15 0.213E-15 0.454E-16 0.951E-17 0.195E-17

(M/M/321):(GD/***/***)

LAMBDA= 0.40000E+02 LAMBDA EFF.= 0.40000E+02
MU= 0.30500E+01 RHO= 0.13115E+02

WS= 0.32787E+00 WQ= 0.00000E+01 LS= 0.13115E+02 LQ= 0.00000E+01

VALUES OF P(N) FOR N=0 TO 48 OTHERWISE P(N)=0.0,

0.264E-04 0.173E-03 0.758E-03 0.248E-02 0.652E-02 0.142E-01
0.267E-01 0.437E-01 0.637E-01 0.836E-01 0.997E-01 0.109E+00
0.110E+00 0.103E+00 0.900E-01 0.738E-01 0.569E-01 0.415E-01
0.286E-01 0.188E-01 0.117E-01 0.699E-02 0.398E-02 0.218E-02
0.114E-02 0.576E-03 0.280E-03 0.131E-03 0.593E-04 0.259E-04
0.110E-04 0.449E-05 0.179E-05 0.689E-06 0.258E-06 0.940E-07
0.333E-07 0.115E-07 0.387E-08 0.127E-08 0.406E-09 0.127E-09
0.386E-10 0.115E-10 0.336E-11 0.957E-12 0.267E-12 0.729E-13

(M/M/335):(GD/***/***)

LAMBDA= 0.50000E+02 LAMBDA EFF.= 0.50000E+02
MU= 0.30500E+01 RHO= 0.16393E+02

WS= 0.32787E+00 WQ= 0.00000E+01 LS= 0.16393E+02 LQ= 0.00000E+01

VALUES OF P(N) FOR N=0 TO 48 OTHERWISE P(N)=0.0,

0.124E-05 0.102E-04 0.558E-04 0.229E-03 0.749E-03 0.205E-02
0.479E-02 0.982E-02 0.179E-01 0.293E-01 0.437E-01 0.597E-01
0.753E-01 0.882E-01 0.964E-01 0.987E-01 0.952E-01 0.867E-01
0.748E-01 0.613E-01 0.479E-01 0.357E-01 0.254E-01 0.174E-01

0.114E-01 0.718E-02 0.436E-02 0.255E-02 0.144E-02 0.789E-03
0.417E-03 0.214E-03 0.106E-03 0.512E-04 0.240E-04 0.109E-04
0.484E-05 0.209E-05 0.877E-06 0.359E-06 0.144E-06 0.561E-07
0.214E-07 0.797E-08 0.290E-08 0.103E-08 0.361E-09 0.123E-09

NOMENCLATURE

The symbols have the following meanings except where specifically included in the text:-

a	-	specific surface area (surface area per unit volume of particle (m^2/m^3))
a	-	arrival distribution in queueing drop model
A	-	hydrodynamic function of flow (-)
A_c	-	surface area of coalescer (m^2)
A_{cap}	-	area of capillary available for flow (m^2)
A_f	-	parameter of characteristic of neighbour in fibres on the flow field near an individual fibre (Happel's cell flow parameter for assembly of cylinders) (-)
A_s	-	flow parameter characterising influence of neighbouring spherical collectors (Happel's cell flow parameter for assembly of spheres) (-)
b	-	radius of equivalent spherical particle (-)
b	-	departure distribution in queuing drop model (-)
B	-	permeability coefficient to the bed (m^2)
c	-	fractional concentration of dispersion (-)
c	-	number of parallel channels in the system in queuing drop model
C	-	concentration of dispersion v/v (-)
C_a	-	fractional concentration of dispersion (-)
C_{in}	-	phase ratio of inlet dispersion (-)
C_r	-	correlation coefficient (-)
C_m	-	Gunningham's correction factor (-)
d	-	service discipline in queuing drop model (-)
d	-	channel diameter (m)
d_a	-	aperture diameter (m)

d_{am} - arithmetic mean diameter (m)

d_c - particle diameter or collector diameter (m)

d_{ce} - effective collector diameter (m)

d_e - diameter of equivalent spherical drop (m)

d_f - fibre diameter (m)

d_{fe} - effective fibre diameter (m)

d_{fr} - most frequency mean diameter or mode (m)

d_{gm} - geometric mean diameter (m)

d_{hm} - harmonic mean diameter (m)

d_H - hydraulic mean diameter (m)

d_m - median diameter (m)

d_{max} - maximum drop diameter (m)

d_n - nozzle diameter (m)

d_o - orifice diameter (m)

d_p - inlet drop diameter (m)

d_{pe} exit drop diameter (m)

d_{PJ} - equivalent projected diameter (m)

d_{10} - linear mean diameter (m)

d_{20} - mean-surface mean diameter (m)

d_{21} - surface-linear mean diameter (m)

d_{30} - mean-volume mean diameter (m)

d_{31} - volume-linear mean diameter (m)

d_{32} - volume-surface mean diameter or Sauter mean diameter (m)

d_{43} - moment-weight mean diameter (m)

d_s - distance between centres of two drops (m)

D - diameter of coalescer (m)

D_{BM} - diffusion coefficient ($=K'T/3\pi\mu_c d_p$) (m^2/s)

D_c - diffusion parameter ($=1/N_{Pc}$) (-)

D_F - Molecular diffusion coefficient (m^2/s)

e - voidage fraction or porosity of filter (-)

e - maximum number allowed in the system in queuing drop model (-)

E - internal energy of the system (J)

E_a - axial secondary dispersion coefficient (m^2/s)

E_r - raidal secondary dispersion coefficient (m^2/s)

E_s - efficiency of collection by a single fibre (-)

f - calling sources in queuing drop model (-)

f - friction factor (-)

$f_n(d)$ - number frequency of drops (percentage of number of drop in each size interval) (-)

f(s) - dispersed phase saturation function (-)

f_w - correction factor for wall effect (-)

fw(d) - weight frequency of drops (percentage of weight of drops in each size interval) (-)

F - mass transfer rate (m^3/s)

F_a - force of attraction (N)

F_{Ad} - adhesion force (N)

F^* - dimensionless number ($= \frac{2G\mu(d_p/2)}{\gamma}$) (-)

g,gc - acceleration due to gravity = 9.81 (m/s^2)

G - shear rate (s^{-1})

h - film thickness or drop/collector separation (m)

I - mass capture rate (m^3/s) r rate of drop collection by single collector (drops/s)

j - rate of drop capture per unit sphere length (n_o/ms)

K_D - constant (-)

K_p - constant (-)

K - Kozeny constant (-)

K' - Boltzman's constant = 1.380×10^{-21} (kgm/s^2K^o)

K_a - inertial parameter (-)

K_A - aerosol collection coefficient (m^3/s)

K_B - Brownian diffusion coefficient ($= \frac{2K'T}{3\mu_c}$) (m^3/s)

K_G - gradient coagulation constant (m^3/s)

K_I - impaction-interception coagulation constant (m^3/s)

K_m - constant (=53.5) (-)

K_e - elastic modulus (-)

K_o - shape factor (-)

K_V - volume coefficient (-)

l - distance into coalescing bed from inlet face (m)

L - bed depth (m)

Lq - length of queue (m)

L_s - length of service channels in queuing system (-)

M - number of service channels in queuing system (-)

n - number of units in queueing system (-)

no - number of drops entering interval 1 from inlet face (-)

n1 - number of drops leaving interval 1 from inlet face (-)

N - pump speed (rpm)

N_{Ad} - adhesion number $= \frac{4Q}{g \pi N_R^2} \cdot \frac{1}{\mu_c U d_p^2 A_s}$ (-)

N_G - gravity number $= \frac{d_p^2 (\rho_d - \rho_c)}{18 \mu_c U}$ (-)

N_L - number of layers (-)

N_{Pe} - Peclet number $= \frac{d_c U}{D_{BM}}$ (-)

N_R - indirect interception number $\left(= \frac{d_p}{d_c} \right)$ (-)

N_{Rd} - direct interception number $\left(\frac{d_p}{d_a} \right)$ (-)

N_{Re} - Reynold's number $\left(= \frac{d_c U \rho_c}{\mu_c} \right)$ (-)

$N_{Re'}$ - Modified Reynold's number $\left(= \frac{d_c U \rho_c}{\mu_c (1-e_1)} \right)$ (-)

N_{Sh} - Sherwood number ($= \frac{I}{\pi d_c D_F C_a}$) (-)

N_{stk} - Stoke's number ($= \frac{d_p^2 \rho_c U}{q \mu_c d_c}$) (-)

P - Pressure (N/m^2)

ΔP - Pressure drop (N/m^2)

q - flow rate of dispersion (m^3/s)

Q - London -van der Waal constant or Hamaker constant (N)

Q_M - quantity of diffusing dispersion (m^3)

r - radial co-ordinate (-)

r - radius of droplet (m)

r_f - equivalent radius of deformed film (m)

r_n - radius of the discharge weir in the centrifuge (m)

r_{22} - inter-molecular distance (m)

S_d - average oil saturation or average saturation of dispersed phase (-)

S_c - average saturation of continuous phase (-)

S_e - effective saturation (-)

S_G - geometric standard deviation (-)

S_f - fixed saturation eleminated from flow (-)

S_m - average of total saturation of dispersed phase (-)

S_N - standard deviation (-)

S_r - residual saturation in bed (-)

ΔS - entropy (J/kg)

t - time (s)

T - absolute temperature (K^{O})

T_e - tortuosity factor (-)

U - superficial velocity (m/s)

U_{cr} - critical superficial velocity (m/s)

U_{cap} - interstitial velocity (m/s)

v - volume (m^3)

v_i - cumulative volume (m^3)

v_T - total volume (m^3)

V - velocity (m/s)

V_o - critical velocity (m/s)

V_s - settling velocity (m/s)

w - impeller speed of centrifuge (rps)

x - axial co-ordinate

x - pass length (m)

Y - the ratio of outlet to inlet drop densities (-)

Greek Letters

α and β parameters in the Weibull distribution function (-)

β - the fraction of collisions between drops that results in coalescence (-)

γ - interfacial tension (N/m)

ε - dielectric constant of continuous phase (-)

ε' - dielectric constant of outside medium (-)

ϑ - surface tension (N/m)

η - drops capture efficiency

η_c - coalescence efficiency

η_{exp} - experimental efficiency

μ	-	viscosity (Ns/ m^2)
μ	-	service rate in queuing system (s^{-1})
ρ	-	density (kg/m^3)
ρ	-	utilisation factor in queuing systems = λ/μ (-)
λ	-	arrival rate in queuing system
λ_c	-	theoretical filter coefficient (m^{-1})
λ_e	-	experimental filter coefficient (m^{-1})
υ	-	kinematic viscosity (m^2/s)
ψ	-	sphericity (-)
θ	-	contact angle (rad)
$\emptyset_H$	-	Hold-up of the bed (-)

Subscripts

1	-	single phase flow
2	-	two phase flow
c	-	continuous phase
d	-	dispersed phase
f	-	bed of fibres
s	-	bed of spheres
D	-	diffusion
DI	-	direct interception
G	-	gravity or sedimentation
GI	-	settling - interception
I	-	indirect interception
II	-	inertial impaction
L	-	London -van der Waal's forces
T	-	total

REFERENCES

1 Davies GA, Jeffreys GV, and Pryce Bayley D, (Knitmesh DC Coalescer Co.), British Patent, 1, 409, 045, (1981).

2 Bikenman, J Coll Interfac Sci., Ind Eng Chem., 57, (1), 56-62, (1965).

3 Ford RE and Furmidge CGL, J Coll Interfac Sci, 22, 331-341, (1966).

4 Sumner C.G, J Appl Chem, 7, 504 (1957).

5 Davies SS, and Smith A, "Theory and Practice of Emulsion Technology", Proceeding of a Symposium organised by the Soc of Chem Ind, Brunel University, Sept 16-18 1974, Academic Press, London (1976).

6 Bennett KE, Hatfield JC, Davies HT, Macosko CW, and Scriven LE, "Microemulsions", Proceeding of a Conference on the Physical Chemistry of Microemulsions, organised on behalf of the Industrial Sub-committee of the Faraday Division of the Chemical Society, Sept 15-16 1980, Cambridge, England, Plenum Press, New York and London (1982).

7 Becher P and Yudenfreund MN, "Emulsions, Latices and Dispersions", A symposium held as apart of the 51st Colloid and Surface Science symposium held at Grand Isle, June 1977, Marcel Dekker, New York (1978).

8 Sherman P, "Emulsion Science", Academic Press, London (1968).

9 Lissant KJ, J Coll Interfac Sci, 22, 462-468, (1966).

10 Allak AMA, PhD Thesis, University of Aston in Birmingham (1973).

11 Cockbain EG and Mcrobert TS, J Coll Interfac Sci, 8, 440-451 (1953).

12 Doxastakis G and Sherman P, Colloid Polymer Sci, 262, (11), 902-905, (1984).

13 Hodgson TD and Lee JC, J Coll Interfac Sci, 30, (1), 94-108, May (1969).

14 Nielson LE, Wall R, and Adams C, J Coll Interfac Sci, 13, 441-458, (1958).

15 Science Reserch Council (UK), Science Board Chemistry Committee, "Report on the Science of Colloidal Dispersions", Jan (1972).

16 Austin DG, PhD Thesis, University of Aston in Birmingham, (1979).

17 Attarzadeh GR, PhD Thesis, University of Aston in Birmingham (1979).

18 Saito H and Shinoda K, J Coll Interfac Sci, 24, 10-15, (1967).

19 Shinoda K, J Coll Interfac Sci, 24, 4-9, (1967).

20 Jeffreys GV and Hawksley JL, J Appli Chem, 12, 329-336, Aug (1962).

21 Hermanie PHJ and Van der Waarden MJ, J Coll Interfac Sci, 21, 513, (1966).

22 Richardson EG, J Coll Interfac Sci, 5, 404-413, (1950).

23 Rumscheidt FD and Mason SG, J Coll Interfac Sci, 16, 238-261, (1961).

24 Taylor GI, Proc Roy Soc (London), A146, 501-523, (1934).

25 Gupta SK, Saraf DN and Pandey BP, Colloid and Polymer Sic, 257, 663-669, (1979).

26 Polichronakis CI, MSc Thesis, University of Aston in Birmingham, (1972).

27 Baez Poleo S, PhD Thesis, University of Aston in Birmingham, (1983).

29 Prince LM, J Coll Interfac Sci,23,165-173, (1967).

29 Messener HP and Chertow B, Ind Eng Chem, 38, (8), 859, (1946).

30 Wood RW, and Loomis AI, Philosophical Magazine and Journal of Science, 4, (22), 417-436, Sept (1927).

31 Murkes J, Filt and Sep, 200-204, May/June (1983).

32 Hayes JC, Hayes LA and Wood HS, Chem Eng Prog, 45, 235-240, April (1949).

33 Hill JB, Ind Eng Chem, 31, 1361-1363, (1939).

34 Kirkup WM, Filt and Sep, 259-266, May/June (1977)

35 Smith GJ, PhD Thesis, University of Southamption, (1969).

36 Bloess JJ, US Pat 4, 430, 202, Feb 7, (1984).

37 Hazlett RN and Corhart HW, Filt and Sep, 456-464, July/Aug, (1972).

38 Osterman JW, Filt and Sep, 127-132, March/April, (1966).

39 Curtis BG, Filt and Sep, 35-43, Jan/Feb, (1964).

40 Belk TE, Chem Eng Prog, 61, (10), 72-76, October, (1965).

41 Blaschta, Dietrich; Neubert, Leopold; Schwarz, Detlef, (VEB Petrol-chemisches Kombinat Schwedt), Ger (East) 206, 907, Feb 8, (1984), Appl 234, 009, Oct 12, (1981). CA P57552q.

42 Franklin JS, Effluent and Water Treatment Journal, 655-657, October, (1973).

43 Farly R and Valentin FHH, AIChemE - IChemE Symposium Series No 1, 1:39-1:48, (1965)

44 Lindenhofen HE, Filt and Sep, 317-321, July/Aug (1968).

45 Cabriel JC, and Parry G, Filt and Sep, 253-256, May-June (1977).

46 GarrettWD, and Barger WR, Environmental Sci and Tech, 4, (2), 123-127, Feb

(1970).

47 Bennett H,"Practical Emulsions", Brooklyn, Chemical Pub Co, (1943).

48 Atkinson E and Freshwater DC, British Chem Eng, 554-562, Oct (1958).

49 Landis DM, Chem Eng Progress, 61 (10), 58-63, Oct (1965).

50 Sullivan FE, Chem Eng Progress, 52, (21), 83-84, Feb (1955).

51 Wang LK, Yang JY, and Dhan DB, Chemistry and Industry, 13, (5), 562-564, July (1975).

52 Waterman, LC, Chem Eng Progress, 61, (10), 51-57, Oct (1965).

53 Pontello AP, Filt and Sep, 561-623, Nov/Dec (1976).

54 Anisimov BF, Emelyanchenko VG, Kolloidn ZH, 528-534, 39, (3), (1977), Russ, CA 107031J.

55 Graham D, (Davy Corp Ltd) US Pat 4, 283, 290, 11th Aug (1981).

56 Abadie A and Roques H (D Young Co), British Patent, 1, 347, 755, 19 April (1971).

57 Shalhoub N, PhD Thesis, University of Aston in Birmingham, (1975).

58 Luthy RG, Selleck RE and Galloway FR, J Water Pollution Control Fed, 50 (2), 331-346, Feb (1978).

59 Al-Taweel AM, Farag HA, Fadaly O and Mackey GD, Can J Chem Eng, 61, 534-540, Aug (1983).

60 Jackson ID, Filt and Sep, 67, Jan/Feb (1978).

61 Clayton R, Hiebenthal D and Illmer M, Ind Chem Eng Symp, Manchester, Nov (1977).

62 Rohlich GA, Ind Eng chem, 46, 304 (1954).

63 Outlook - 'Waste Water Treatment with Air Flotation', Proces Engineering, 7, (11), 996, (1973).

64 Calyton R, Hiebenthal D and Illmer M, Filt and Sep, 68, Jan/Feb (1978).

65 Kaiser R, Colton CK, Miskolezy G and Mir L, AIChemE Symp series 68, (124), 115, (1971).

66 Jorden GV, Chem Eng Prog, 61, (10), 64-71, Oct (1965).

67 Najmi AI, PhD Thesis, University of Aston in Birmingham, (1979).

68 Davies GA and Jeffreys GV, Filt and Sep, 349-354, July/Aug (1969).

69 Yu TS, "Naval Ship Research and Development Lab Report", 3191, oct (1969).

70 Wolfe NH, US Patent 3, 554, 906, (1971).

71 Redmon OC, Chem Eng Prog, 59, (9), 87-90, Sept (1963).

72 Bartle JW, Filt and Sep, 404-413, Sept/Oct (1966).

73 Wilkinson D, Mumford CJ, and Jeffreys GV, AIChemEJ, 21, (5), 910, (1975).

74 Thomas RJ and Mumford CJ, Proceeding ISEC, 1, (50), 400-417, (1971).

75 Langdon WM, Naik PP, Wasan DT, Envir Sci Tech, 6, (10), 905-910, Oct (1972).

76 Gammon H, Filt and Sep, 409, July/Aug (1973).

77 Spielman, LA and Goren SL, Ind Eng Chem Fund, 11, (1), 73-83, (1972).

78 Burtis, TA and Kirkbride CG, Tran AIChemEJ, 42, (3), 413, (1946).

79 Bitten JF, J Coll Interfac Sci, 37, (2), 272, (1971).

80 Bird RB, Stewart WE and Lightfoot EN, "Transport Phenomena", Chapter 6, John Wiley, New York, (1960).

81 Sareen SS, Rose PM, Gudesen RC and Kintner RC, AIChemEJ, 12, (6), 1045, (1966).

82 Vinson GG and Churchill SW, Chem Eng J, 1, 110-119, (1970).

83 Voyuskii SS, Kalyanova KA, Panick R and Doiman N, Doki Nauk SSSR, 91, 1155, 1953, CA, 12053d, (1955).

84 Hazlett RN, Ind Eng Chem Fund, 8,(4), 625, (1969).

85 Spielman LA, and Goren SL, Ind Eng Chem Fund, 11, (1), 66-72, (1972).

86 Ronsenfeld JI, and Wasan DT, Can J Chem Eng, 52, (3), Feb (1974).

87 Rushton A and Griffiths P, Trans Inst Chem Eng, 49, 49-59, (1971).

88 Jeater P, Rushton E and Davies GA, Filt and Sep, 129-133, March/April (1980).

89 De-Koning WG, Ger Often, 2, 914, 816, 18 Oct 1979, CA 217217k, (1980).

90 Jeater P, Rushton E and Davies GA, World Filt Congr, 605-615 (1979).

91 Langdon WM, Petro Chem Eng, 34, (1963).

92 Davies GA, Jeffreys GV, and Smith DV, Proceeding ISEC, 1 , (35),385, (1971).

93 Hazlett RN, Ind Eng Chem Fund, 9, 520 (1970).

94 Spielman LA, PhD Thesis, University of California, Berkely, (1969).

95 Wilkinson D, PhD Thesis, University of Aston in Birmingham, (1974).

96 Osterman LRB, Douglas E and Walsh T, Trans Inst Mar Eng, 72, 409, (1960).

97 Greenkorn RA, "Flow Phenomena in Porous Media", Marcel Dekker Inc, New York and Brasel (1983).

98 Spielman LA and Goren SL, Ind Eng Chem Fund, 16, (2), 272 (1977).

99 Krneger DL, US Patent 3, 951, 814, 20th April (1976).

100 Pontello AP, Filt and Sep, 561, (1976).

101 Schniedegger AE, "The Physics of Flow Through Porous Media", Macmillan, New York, (1957).

102 Schwartz AM, Ind Eng Chem, 61, (1), 10, (1969).

103 Wasan DT, Mcnanara JJ, Shah SM and Sampath K, J Rheology, 32, (2), 181-207, (1979).

104 Ibrahim SY, MSc Thesis, University of Aston in Birmingham, (1981).

105 Kidher FAA, PhD Thesis, University of Manchester-Institute of Science and Technology (UMIST) , (1984).

106 Al-Meshan MAF, PhD Thesis, University of Aston in Birmingham, (1985).

107 Gutkowski B, Mydlarczyh S, Kowalska M, Stud Envir Sci, 23, 285-293, (1984).

108 Douglas E, and Elliot IG, Trans Inst Mar Eng, 74, 164, (1962).

109 Heidenreich E, Kidher FA and Davies GA, World Filtration Congress III, 688-695, (1982).

110 Austin DG, Mumford CJ, and Jeffreys GV,Unpublished Work, University of Aston in Birmingham, (1976).

111 Sherony DF and Kintner RC, Can J Chem Eng, 49, 314, (1971).

112 Bitten JF and Fochtman EG, J Coll Interfac Sci, 37, (2), 312-317, (1971).

113 Scheele GF and Clark DB, Chem Eng Commun, 5, (3), (1980).

114 Coulson JM and Richardson JF,"Chemical Engineering", Vol 2, Third Edition, Fergamon Press, Oxford, (1978).

115 Shah D, Langdon W and Wasan D, Envir Sci and Tech, 11, (2), 167, (1977).

116 Davies GA and Jeffreys GV, Filt and Sep, 546-550, Sept/Oct (1970).

117 Vinson CG, "Doctoral Dissertation", University of Michigan, Michigan, (1965).

118 Lindenhofen HE, Filt and Sep, 567, Sept/Oct (1969).

119 Ridgeway K and Tarbuck KJ, British Chem Eng, 12, 384 (1967).

120 Gutkokwski B, Mydlarczyh S, Kodwalska M and Hypka J, Stud Envir Sci, 23, 285-293 (1984).

121 Davies GA, and Jeffreys GV, Ind Chem Eng Fund, 9, (3), 519, (1970).

122 Hsu, GC and Kintner RC, J Chem Eng Data, 14, 67, (1969).

123 Collins RE,. "Flow of Fluids Through Porous Materials", Reinhold, New York (1961).

124 Singhal AK and Dranchuk PM, Can J Chem Eng, 53, 3-8, (1975)

125 Fowkes FM, Anderson FW and Berger JE, Envir Sic and Tech, 4, (9), 510, (1970).

126 Wenzel RN, Ind Chem Eng, 28, 988, (1935).

127 Ludvikson V and Lightfoot EN, AIChemEng, 6, (14), 674, (1968).

128 Rose W and Heins RW, J Coll Interfac Sci, 17, 39, (1962).

129 Holland L "The Properties of Glass Surfaces", Chapman & Hall, London, (1964).

130 Bartell FE and Sherphard JW, J Phys Chem, 57, 455, (1953).

131 Davies JT and Rideal EK, "Interfacial Phenomena", Academic Press, New York, (1961).

132 Fowkes FM and Harkins WD, JA Chem Soc, 62, 3372, (1940).

133 Borgin K, Norsk Skogind, 13, 429, (1959).

134 Hitit HA, PhD Thesis, University of Aston in Birmingham, (1972).

135 Kowoski K, J Coll Interfac Sci, 17, 167, (1962).

136 Gayler R and Pratt HRC, Trans Inst Chem Eng, 31, 69, (1953).

137 Hair ML, "Clean Surfaces", Marcel Dekker Inc, New York, (1970).

138 Bascon WE and Singleterry CR, J AChem Soc, 66, 236-242, (1962).

139 Bitten JF, J Coll Interfac Sci, 33, (2), 265, (1970).

140 Ghosh MM, and Brown WP, J Water Pollution Control Fed, 47, (8), 2101-2113, (1975).

141 Ronsenfeld JI and Wasan DT, ISEC Lyons, 74, 319, (1974).

142 Austin DG and Jeffreys GV, J Chem Biotechnol, 31, 475-488, (1981).

143 Emi H, Okuyama K and Yoshioka N, J Chem Eng Japan, 6, (4), 349-354, (1973).

144 Langmuir I, OSRD Report, 825, Sept, (1942).

145 Rajagopalan R and Tien C, Can J Chem Eng, 55, 246-255, Jun (1977).

146 Soo H and Radke CJ, J Coll Interfac Sci, 102, (2), 462-476, 91984).

147 Bradie JK, PhD Thesis, Heriot Watt University, Edinburgh, (1969).

148 Redman OC, Chem Eng Prog, 59, 87, (1963).

149 Spielman LA and Goren SL, Envir Sic and Tech, 4,(2), 135, (1970).

150 Spielman LA and Fitzpatrick JA, J Coll Interfac Sci, 42, (3), 607-621, March (1973).

151 Hamaker HC Physica, 5, (10), 105-1078, Nov (1937).

152 Fowkes FM, Ind Eng Chem, 56, (12), 40-52, Dec (1964).

153 Sherony DF and Kintner RC, AIChemEng J, 17, (2), 291-294, March (1971).

154 Prieve DC and Ruckenstein E, AIChem Eng J, 20, (16), 1178-1186, Nov (1974).

155 Happel J, AIChem Eng, 4, 97, (1958).

156 Pich J, 'Aerosol Science', Chapters 9 and 10, Academic Press, New york (1966).

157 Friedlander SK, J Coll Interfac Sci, 23, 157, (1967).

158 Lawson GB, Chemical and Process Eng, 45-60, May (1967).

159 Rosenfeld JI, Phd Thesis, Illinois Institution of Technology, Chicago (1973).

160 Fiedlander SK, Ind Eng Chem, 50, 1161, (1958).

161 Ramskill EA and Anderson WL, J Coll Interfac Sci, 5, 416 (1951).

162 Dorman RG, "Filtration in Aerosol Science", Academic Press, New York (1966).

163 Landahl H and Herman K, J Coll Interfac Sci, 4, 103, (1949).

164 Levich VG, Physicochemical Hydrodynamics, Prentice Hall, Englewood Cliffs, New Jersey, (1962).

165 Sherony DF, PhD Thesis, Illinois Institute of Technology, Chacago (1969).

166 Spielman LA and Goren SL, Envir Sci and Tech, 2, (4), 279, April (1968).

167 Spielman LA and Goren SL, Ind Eng Fund, 62, 10, (1970).

168 Carman PC, J Soil Sci, 52, (10), (1941).

169 Leonard RA and Lemlich R, Chem Eng Sci, 20, 790, (1955).

170 Mason GJ, J Coll Interfac Sci, 35, 286, (1971).

171 Brown R, "A Microphographic Study of Water Coalescece", Fort Belvior, Virgnina , (1966).

172 Rowe EL, J Pharm Sci, 54, (21), 260-264, (1965).

173 Coulter Counter Model ZB - Instruction Manual, Coulter Electronics Ltd, Dunstable, England (1975).

174 Matthews BA, Can J Phar Soc,m 6 (2), 89 (1971).

175 Allen T, Proc Particle Size Analysis Conf, Loughborough Soc for Analytical Chem, 110 (1967).

176 Irani RR and Callis CF,"Particle Size Measurement, Interpretation and Application", John Wiley, New York (963).

177 Trolinger JD, Optical Engineering, 14, (5), 383, (1975).

178 Thompson BJ, J Phys Eng (Scientific Instruments), 7, 781, 91974).

179 Thompson BJ, Appl Optics, 6, (3), 519 (1967).

180 Kunkel BA, J appl Meteorology, 10, 482, June (1971).

181 Bachalo WD, "Laser Velocimetry and Particle Sizing", Proceeding of the third International Workshop on Laser Velocimetry, Purdue University, 506-517, July (1978).

182 Malvern Electronics - Malvern Particle Sizer 2200, Instruction Manual, Malvern, England, (1981).

183 Manual on Recommended Particles in Spectrophotometry, By ASTM Committee, American Soc for Testing and Materials, Feb (1966).

184 Meithes, L, "Handbook of Analytical Chemistry", First Edition, McGraw-Hill, New York, (1963).

185 Ergun S, Chem Eng Prog, 48, 98, (1952).

186 Macdonald, IF, Ind Eng Chem Fund, 18, 199 (1979).

187 Dullien FAL, "Porous Media', Academic Press, London (1979).

188 Rumf H and Gupta AR, Chem Ind Tech, 43, 367, (1971).

189 Carmen PC, J Soc Chem Ind Trans, 15, 150, (1937).

190 Kozeny J, Royal Academic of Science, Proc Class I, 136, 271, Vienna (1927).

191 Scheidegger AE, "The Physics of Flow Through Porous Media", University of Toronto Press, Toronto (1974).

192 Millington RJ, Quirk K, JP, Trans Faraday Soc, 57, 1200 (1961).

193 Marshall TJ, J Soil Sci, 9, 1 (1958).

194 Morcon AR, Trans Inst Chem Eng, 24, 30, (1946).

195 Chilton TH and Colburn AP, Trans American Inst Chem Eng, 26, 178 (1931).

196 Brown GG, "Unit Operation", Chapter 16, John Wiley, New York (1950).

197 Martin JJ, PhD Thesis, Caragic Institute of Technology, Caragic (1948).

198 Bear J, "Dynamics of Fluids in Porous Media", American Elsevier, New york, (1972).

199 Sullivan RR and Hartel KL, Advances in Colloid Sciences, 1, 37, 91942).

200 Muskat M and Botsen HG, Physics, 1, 27, (1931).

201 Coulson JM, Trans Inst Chem Eng, 27, 237 (1949).

202 Bartell FG and Osterhof HJ, J Phys Chem, 32, 1553 (1928).

203 Hitchcock DI, J Ger Physiol, 9, 755, (1926).

204 Rose HE and Rizk AMA, Proc Inst Mech Eng, 160, 493 (1949).

205 Masters K, "Spray Drying Hand Book", Third Edition, Chapter 2, John Wiley, New York (1979).

206 Clyde Orr JR, "Particulate Technology" Macmillan Co, New York (1966).

207 Weast RC, Astle MJ and Beyer WH, "Handbook of Chemistry and Physics", 64th Editions, CRC Press, (1983).

208 Allen T, "Particle Size Measurement", 2nd Edition, Champman and Hall, London (1974).

209 Cadle RD, "Particle Size Determination", Interscience publishers, New York (1955).

210 Giles JW, Hanson C and Marsland JG, Proceeding ISEC, 1, 94-111, (1971).

211 Nelson PA and Steven WF, AIChem EngJ, 7, (1), 80-87, 1961.

212 Walpole RE aned Hyers RH, "Probability and Statistics for Engineers and Scientists", Macmillan Co, New York (1972).

213 Mugele RA and Evans HD, Ind Eng Chem, 43, (6), 1317-1324, (1951).

214 Spiegel MR, "Probability and Statistics", Scham's Outline Series, McGraw-Hill, New York (1975).'

215 Saraf DH, and Fatt I, Soc Petrol Eng J, 7, 235 (1967).

216 Josendal VA, Sandiford BB, Wilson JW, Trans AIME, 195, 65 (1952).

217 Jones PJ, World Oil, 129, (2), 170, (1949).

218 Perry HJ and Chilton CH, "Chemical Engineer's Handbook", Fifth Edition, McGraw-Hill, Tokyo (1973).

219 Gerald CF, "Applied Numerical Analysis" Second Edition, Addison-Wesley Co, London, (1978).

220 Grank J, "Mathematics of Diffusion", Clarendon Press, Oxford (1956).

221 Barrer RM, "Diffusion In and Through Solids", Cambridge University Press, Cambridge, England, (1951).

222 Carberry JJ and Bertton RH, AIChemEng J, 4, (3), 367 (1958).

223 Mickley HS, Sherwood TS and Reed CE, "Applied Mathematics in Chemical Engineering", Second Edition, McGraw-Hill, New Dehli (1975).

224 Leonard RA and Lemlich R, AIChemEngJ, 11, 18 (1965).

225 Taha HA, "Operation Research", Chapter 13, Second Edition, Collier Macmillan Publishers, London (1971).

226 Lee A, "Applied Queuing Theory", Macmillan, Toronto (1966).

227 Parzen E, "Stochastic processes", Holden-Day, San Francisco (1962).

228 Morse P, "Queues, Inventories and Maintenance", John Wiley, New York (1958).

229 NAGFLIB:801/715:MK5:NOV 74, G02 - Correlation and Regression Analysis File, Computer Centre, The University of Aston in Birmingham.

230 Hildebrand FB, "Advanced Calculus for Application", Second Edition, Prentice-Hall, Englewood Cliffs, New Jersey (1976).

231 Stephenson G, "Mathematical Methods for Science Students", Second Edition, Longman Group Ltd, London (1973).

232 Scheele GF, Meister BJ, AIChemEngJ, 14, (1), 9, (1968).